Flinders University

Development of Ferroptosis-Inducing Liposomes to Target Multiple Myeloma

By

Ali Habib
BMedSci (Hons)

Thesis

Submitted to Flinders University
for the degree of
Doctor of Philosophy

College of Medicine and Public Health
15th October 2025

TABLE OF CONTENTS

ABSTRACT

Multiple myeloma (MM) is an incurable malignancy, characterised by the uncontrolled proliferation of clonal plasma cells, usually in the bone marrow. MM accounts for 10% of all haematological malignancies diagnosed worldwide and has a significant impact on both patients and healthcare systems. The poor outcome of patients with MM highlights the urgent need for novel treatment strategies that overcome resistance to more conventional apoptosis-based regimens.

Ferroptosis is a recently characterised form of non-apoptotic programmed cell death. Phospholipids (PLs) containing polyunsaturated fatty acids (PUFAs) play a crucial role as ferroptosis substrates as they are readily oxidised to form toxic lipid reactive oxygen species (ROS). Despite evidence suggesting ferroptosis may represent a novel approach for the treatment of cancer, targeting tumour cells while minimising off-target effects, is a significant challenge. One way in which this has been achieved is through the development of monoclonal antibodies raised against proteins expressed by the tumour cells, which by themselves or by directing therapeutics to the tumour cells, result in greater tumour cell death whilst minimising toxicities. Regimens incorporating monoclonal antibodies have proven highly effective for a range of cancers, including MM.

In this study, ferroptosis was induced by treating cells with RSL3, which inhibits glutathione peroxidase 4 (GPX4), a key enzyme in the primary lipid antioxidant system within cells. Ferroptosis was confirmed as the mechanism of cell death by using the synthetic antioxidant, liproxstain-1. Using a range of scientific techniques, we identified a strong correlation between the PL profile of MM and diffuse large B cell lymphoma (DLBCL) cells and their sensitivity to ferroptosis. Our findings demonstrate that DLBCL cells, which contain high proportions of PLs containing PUFAs are sensitive to ferroptosis-mediated cell death, while MM cells, which generally contain high proportions of PLs containing monounsaturated fatty acids (MUFAs), are relatively resistant.

Altering the lipidome of MM cells through exogenous supplementation with PL-PUFAs identified by our lipidome profiling was sufficient to induce ferroptosis-mediated cell death and sensitise the cells to RSL3. Liposomes, predominantly comprised of the same PL-PUFAs, were subsequently manufactured and loaded with RSL3. Uptake, cytotoxicity and lipid ROS studies showed these novel liposomes were readily taken up and triggered ferroptosis-mediated cell death of MM cells. Furthermore, liposomes containing RSL3 were significantly more effective at inducing ferroptosis than empty liposomes or free RSL3; IC_{50} values for RSL3 were on average between 7.1 and 14.5-fold

lower in the liposomal formulation compared to free RSL3, representing a reduction from a micromolar to a nanomolar effective dose range.

In order to specifically target MM cells, the liposomes were modified to enable conjugation to the FDA-approved anti-CD38 monoclonal antibody, daratumumab. These functionalised liposomes were readily taken up by MM cells but interestingly and moreover, importantly, the presence of daratumumab reduced uptake and cytotoxic effects of the liposomes against the FH9 healthy B cell line, suggesting a potential reduction in the effects of the liposomes against healthy, non-CD38 expressing cells.

The findings of this study significantly increase our understanding of the mechanisms associated with the resistance of MM cells to ferroptosis. The data presented are proof of the concept that antibody-conjugated liposomes may represent an effective and targeted means of delivering key substrates and drugs to trigger ferroptosis in cancers that are insensitive to this form of programmed cell death, such as MM.

DECLARATION

I certify that this thesis:

1. does not incorporate without acknowledgment any material previously submitted for a degree or diploma in any university

2. and the research within will not be submitted for any other future degree or diploma without the permission of Flinders University; and

3. to the best of my knowledge and belief, does not contain any material previously published or written by another person except where due reference is made in the text; and

4. This thesis has been completed without the use of generative artificial intelligence tools.

Signed: Ali Habib

Date: 6/10/2025

ACKNOWLEDGEMENTS

I would like to begin by thanking Flinders University for making it possible for me to complete my studies, and the help of all the staff and peers that have helped along the way.

My development as a researcher would not have been possible without the support and guidance of my supervisors, to Professor Craig Wallington-Gates, thank you for picking me up during my honours and supporting, guiding and instilling me with so much knowledge over the last 5 years. Craig's support as a supervisor has helped shape me into the person and researcher I am today. To Dr Giles Best thank you for your constant guidance and support, and the countless hours of Flow tech support (and sorry for breaking your equipment!). I would also like to thank Professor Clive Prestidge for his instrumental role in the last few years of the work, his guidance and wisdom were greatly appreciated.

Thank you to the many scientists who have helped shape this research and myself as a researcher. I would like to especially thank Professor Marten Snel, Dr Paul Trim, Professor Stuart Pitson, Dr Manjun Li, Ms Isabella Revesz and Ms Kara Paxton for all of their help with the project. I would also like to thank the people that have trained, provided equipment or shared spaces with our group, especially Professor Harald Janovjak, Professor Janni Petersen, Professor Luke Selth, Associate Professor Michael Michael, Dr Nick Eyre and Dr Joshua Dubowsky. Thank you to both of my assessors during my candidature, Dr Lauren Thurgood and Dr Pramod Nair, for your input and feedback.

Thank you to all members of the Multiple Myeloma Translational Research Laboratory and the Haematology laboratory, Dr Lauren Thurgood, Dr Charlotte Toomes, Dr Rachel Mynott, Ms Joanna Cole, Ms Alana White, Ms Olivia Burling, Mr Mulugeta Melku Gobezie and Mr Ben Davies. Your support has been important and has helped shape the project. I want to particularly thank Rachel for helping me to transition into the scientist I am today, all of your finicky habits (especially data presentation!) have helped immensely. I am also grateful for the friendships I have developed through my PhD, particularly Rahkesh, Josh, Daniel and Razia, which have been invaluable.

I am grateful for the opportunity provided by the Flinders Foundation who financially supported my project through the Jane Ramsey Scholarship. To Jane and Bill, I hope this research would have made you proud. This research is also supported by the Australian Government Research Training Program (RTP) fee offset.

Finally, I would like to thank my parents for instilling me with the highest of aspirations and nurturing my desire for knowledge, this PhD is a testament to all of your hard work, sacrifice and support. To my wife, Parya, I would not have been able to do this without you, the unwavering support and love you have provided me over the past 5 years has made it possible for me to complete my studies.

PUBLICATIONS AND PRESENTATIONS

Peer reviewed publications

Habib, A.; Best, O. G.; Toomes, C. E.; Wallington-Gates, C. T. The instrumental role of lipids in governing the sensitivity of multiple myeloma to ferroptosis. *Discov Oncol*. 2025, 16, 1612. https://doi.org/10.1007/s12672-025-03444-9

Habib, A.; Mynott, R.L.; Best, O.G.; Revesz, I.A.; Prestidge, C.A.; Wallington-Gates, C.T. Novel (1S,3R)-RSL3-Encapsulated Polyunsaturated Fatty Acid Rich Liposomes Sensitise Multiple Myeloma Cells to Ferroptosis-Mediated Cell Death. *Int. J. Mol. Sci*. 2025, 26, 6579. https://doi.org/10.3390/ijms26146579

Mynott, R.L.; Habib, A.; Best, O.G.; Wallington-Gates, C.T. Ferroptosis in Haematological Malignancies and Associated Therapeutic Nanotechnologies. *Int. J. Mol. Sci.* 2023, 24, 7661. https://doi.org/10.3390/ijms24087661

Presentations

Habib, A.; Mynott, R.L.; Best, O.G.; Wallington-Gates, C.T 2024. Phospholipid deficiencies and tailored liposome development drive ferroptosis sensitivity in multiple myeloma (oral presentation). FHMRI cancer symposium. Adelaide, Australia

Habib, A.; Mynott, R.L.; Best, O.G.; Wallington-Gates, C.T 2024. Phospholipid composition drives ferroptosis sensitivity in Multiple Myeloma (poster presentation). Iron, Reactive Oxygen Species & Ferroptosis in Life, Death & Disease. Suzhou, China.

Habib, A.; Mynott, R.L.; Best, O.G.; Wallington-Gates, C.T 2024. Phospholipid composition drives ferroptosis sensitivity in Multiple Myeloma (poster presentation). Blood Meeting. Brisbane, Australia.

Habib, A.; Mynott, R.L.; Best, O.G.; Wallington-Gates, C.T 2023. Development of precision liposomes to induce ferroptosis in multiple myeloma (oral presentation). Emerging leaders showcase. Adelaide, Australia.

Habib, A.; Mynott, R.L.; Best, O.G.; Wallington-Gates, C.T 2023. Supplementation with Phospholipids Sensitises Multiple Myeloma Cells to Ferroptosis (oral presentation). FerrOZtosis. Melbourne, Australia.

Habib, A.; Mynott, R.L.; Best, O.G.; Wallington-Gates, C.T 2022. Ferroptosis in aggressive B cell malignancies (poster presentation). Blood Meeting. Sydney, Australia.

LIST OF FIGURES

ABBREVIATIONS

AA	Arachidonic acid
ACSL4	Acyl-CoA synthetase long-chain family member 4
ADC	Antibody-drug conjugates
ADCC	Antibody-dependent cellular cytotoxicity
AML	Acute myeloid leukemia
BCA	Bicinchoninic acid
BCMA	B-cell maturation antigen
BMME	Bone marrow microenvironment
CAR-T	Chimeric antigen receptor expressing T cell
CD38	Cluster of differentiation 38
CFSE	Carboxyfluorescein succinimidyl ester
CHO	Chinese hamster ovary cells
CML	Chronic myeloid leukemia
CoQ10	Ubiquinone
CoQ10-H2	Ubiquinol
CRC	Colorectal cancer
DLBCL	Diffuse large B cell lymphoma
DLS	Dynamic light scattering
DOX	Doxorubicin
DSPC	1,2-distearoyl-sn-glycero-3-phosphocholine
DSPE-PEG200 glycol)-2000]	1,2-distearoyl-sn-glycero-3-phosphoethanolamine-N- [amino (polyethylene
EBV	Epstein-Barr virus
ELISA	Enzyme-linked immunosorbent assay
FA	Fatty acid
FDPS	Farnesyl diphosphate synthase
FTH1	ferritin heavy chain 1
FTL	Ferritin light chain
FPP	Farnesyl phosphate
FSC	Forward scatter
FSP1	Ferroptosis suppressor protein 1

GPX4	Glutathione peroxidase 4
GSH	Glutathione
HEK293t	Human embryonic kidney cells
HD	Hyperdiploid
HDL	High-density lipoprotein
HO-1	Heme oxygenase-1
HPLC	High-performance liquid chromatography
HSC	Hematopoietic stem cell
IC_{50}	Half-maximal inhibitory concentration
IPP	Isopentenyl pyrophosphate
LC-MS	Liquid chromatography-mass spectrometry
LncRNA	Long non-coding RNA
LOX	Lipoxygenases
LPCAT3	Lysophosphatidylcholine acyltransferase 3
LPE	Lysophosphatidylethanolamine
LPL	Lysophospholipid
mAb	Monoclonal antibody
MADP	Monash Antibody Discovery Platform
MBOAT	Membrane-bound O-acyltransferase
MDA	Malonyl dialdehyde
MDD	Mevalonate diphosphate decarboxylase
MGUS	Monoclonal gammopathy of undetermined significance
MM	multiple myeloma
MMP2	Matrix metalloproteinase 2
MTT	3-(4,5-dimethylthiazol-2-yl)-2,5-diphenyltetrazolium bromide assay
MT1DP	Metallothionein 1D pseudogene
MUFA	Monounsaturated fatty acid
NADPH	Nicotinamide adenine dinucleotide phosphate
NHD	Non-hyperdiploid
NHS	N-Hydroxysuccinimide
NSCLC	Non-small cell lung cancer
PA	Phosphatidic acid
PDI	Polydispersity index

PBS	Phosphate buffered saline
PDGFB	Platelet-derived growth factor subunit
PC	Phosphatidylcholine
PCD	Programmed cell death
PE	Phosphatidylethanolamine
PE	R-Phycoerythrin
PG	Phosphatidylglycerol
PI	Proteasome inhibitor
PL	Phospholipid
PLOO-	Lipid peroxyl radicals
PL-PUFA-OH	Phospholipid alcohol
PL-PUFA-OOH	Phospholipid hydroperoxides
PS	Phosphatidylserine
PUFA	Polyunsaturated fatty acid
RhB	Rhodamine B
ROS	Reactive oxygen species
RSL3	(1S,3R)-RSL3
SFA	Saturated fatty acid
SLC3A2	Solute carrier family 3 member 2
SLC7A11	Solute carrier family 7 member 11
SMM	Smouldering multiple myeloma
SSC	Side scatter
TFA	Trifluoroacetic acid
TfR	Transferrin receptor
TXNRD1	Thioredoxin reductase 1
WBC	White blood cell
WT	Wild type

CHAPTER 1. INTRODUCTION

1.1 Multiple Myeloma

Multiple Myeloma (MM) is characterised by the clonal proliferation of plasma cells and is currently incurable (1). It is the second most common haematological malignancy, accounting for 10% of all blood cancers worldwide with 106,000 recorded deaths in 2018 alone (2). Approximately 2,500 people are diagnosed with MM annually in Australia and 1,009 deaths from MM were recorded in 2020, with 1,100 deaths estimated for 2022 (3). Due to a median age of 70 at diagnosis, frailty and comorbidities often limit the use of many chemotherapeutic agents (3).

All of the cell types present in the blood are derived from primitive multipotent hematopoietic stem cells (HSCs) (Figure 1) (4). HSCs are self-renewing and are present in various haemopoietic tissues within the body, including the peripheral blood, bone marrow and in umbilical cord blood (4). HSCs can differentiate into myeloid or lymphoid stem cells, which mature further in either myeloid or lymphoid lineages, losing their self-renewal ability in the process (Figure 1) (5). Plasma cells are terminally differentiated B-lymphocytes (5) that produce antibodies and play a key role in the adaptive immune system, as they are the main cells responsible for humoral immunity (1, 6). Short lived plasma cells proliferate and have a life span of 3-5 days, whereas long lived plasma cells are unable to proliferate but have a life span of months to years (6).

The uncontrolled proliferation of plasma cells in MM causes an array of painful symptoms and clinically significant effects, most notably hypercalcemia, renal failure, anaemia, and bone destruction.

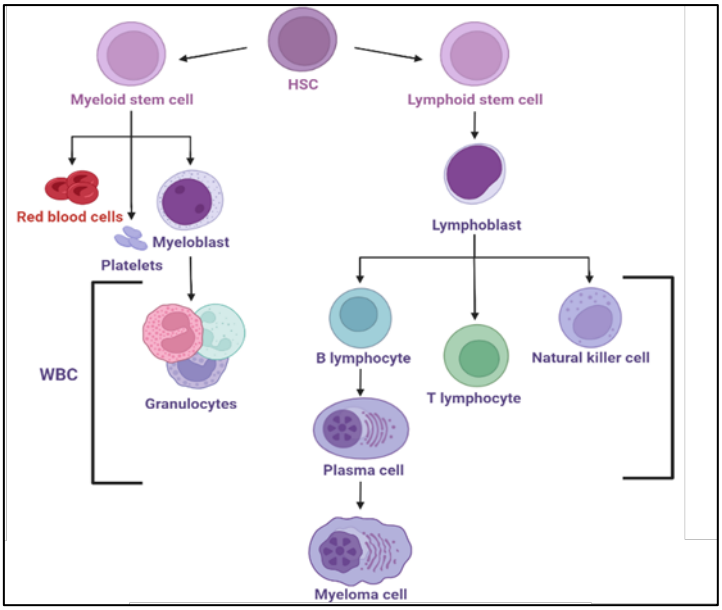

Figure 1. Schematic of the hematopoietic tree and the differentiation of haematopoietic stem cells (HSC) to cancerous myeloma cells

HSC, haematopoietic stem cells; WBC, white blood cells.

1.1.2 MM diagnosis and precursor states

Certain clinical features are used to define MM, including high blood calcium, renal impairment, anaemia, and bone lytic lesions, referred to by the acronym CRAB. In most MM cases, the malignant plasma cells overproduce a monoclonal immunoglobulin (antibody), known as a paraprotein; levels of paraprotein in the serum are often used as an indicator of treatment response and disease progression. However, 3-5% of all MM patients present with disease classified as non-secretory MM, which means the clonal expansion of plasma cells does not result in the overproduction of paraprotein (7).

A diagnosis of MM is confirmed when the clonal bone marrow plasma cells exceed 10% and a myeloma defining event (i.e. one or more CRAB criteria), or a biomarker of disease is identified. These biomarkers include greater than or equal to 60% clonal plasma cells in the bone marrow, a serum free light chain (FLC) ratio ≥100 or more than 1 focal bone marrow lesion identified by magnetic resonance imaging (MRI). Notably, healthy individuals typically have serum ratios of immunoglobulin light chains (κ or λ) of between 0.26 and 1.25 (8).

Two asymptomatic, pre-malignant plasma cell disorders often precede MM; monoclonal gammopathy of undetermined significance (MGUS) and smouldering multiple myeloma (SMM). MGUS is characterised by serum paraprotein concentrations of less than 30 g/L, less

than 10% clonal plasma cells in the bone marrow and the absence of CRAB criteria or biomarkers of disease. MGUS is identified in 2-3% of individuals over 50 and 5% of individuals over 70 years of age (9). The annual rate of progression to MM among individuals diagnosed with MGUS is approximately 1%. Current recommendations are that individuals with MGUS are not treated but are monitored for progression to MM (9). SMM is also described as an asymptomatic clonal plasma cell disorder, characterised by serum paraprotein concentrations of greater than 30 g/L, 10% – 60% clonal bone marrow plasma cells and the absence of MM defining events (10). In contrast to MGUS, the risk of progression to MM among patients with SMM is significantly higher, at approximately 10% in the first 5 years, 3% over the subsequent 5 years and 1% in subsequent years. SMM is also significantly less common than MGUS, with approximately 0.3% (11) of the population identified with the condition (10, 12).

1.1.3 MM biology

High risk multiple myeloma can be characterised based on genetic abnormalities associated with poor clinical outcomes. MM is a highly heterogenous disease, but patients can be broadly categorised into two main pathological groups based on the initiating chromosomal events (13). Hyperdiploid (HD) MM is characterised by multiple trisomies of the odd numbered chromosomes, whereas non-hyperdiploid (NHD) MM patients present with chromosomal translocations, typically leading to overexpression of certain oncogenes (13). The NHD MM group also contains hypodiploid (≤44 chromosomes), pseudodiploid (45-46 chromosomes) and tetraploid (>75 chromosomes) subtypes. Importantly, the key genetic drivers associated with the NHD MM subtype are primary translocations that involve the immunoglobulin heavy chain gene (IGH) locus on chromosome 14 (14). The two patient subsets also differ in terms of prognosis and survival outcomes, with HD MM patients typically having a better prognosis than NHD MM (15, 16). Approximately 10% of all MM patients have both translocations and trisomies involving the *IgH*, which are associated with significantly worse outcomes (17). Certain abnormalities can have some value as prognostic markers in MM, which lead to the classification of some patients as having high risk disease. These include the translocations between chromosomes 4 and 14, 14 and 16 or 14 and 20, which are described as t(4;14) (*IgH:FGFR3/MMSET*), t(14;16) (*IgH:MAF*), or t(14;20) (*IgH:MAFB*), respectively. Deletions of 17p (del(17p)) and gains of the 1q arm are also associated with a worse prognosis (18). Deletion of 17p is observed in 7-8% of MM patients and is the strongest indication of poor

prognosis among patients with MM, with a median overall survival of just 22 months in transplant-eligible patients (19). Patients with the translocation t(4;14), which is observed in 10-15% of cases have an overall survival of 40 months (19). Recent studies have also shown that MM patients presenting with chromosome 1p deletion have poor response to autologous stem cell transplantation, with a poor overall survival or 22 month (20). The deletion of 1p and associated poor prognosis lies within the loss or inactivation of tumour suppressor genes (20). *TP53* dysregulation is another established high risk prognosis marker in MM, with the dysregulation of this gene through deletion (del17p), mutation or inactivation associated with poor prognosis (21). Incidence of TP53 dysregulation is approximately 5% at diagnosis and rises to 25% in late-stage relapse (22). Two or more high risk features are defined as double-hit or triple-hit MM and are associated with higher disease burden, a more aggressive disease pattern and shorter progression free survival and overall survival (23).

These studies aid in identifying patients who are likely to have a more aggressive disease course and for whom novel precision therapeutic approaches are most urgently required. Interestingly, an extra copy of a chromosome, known as a trisomy, can also influence the MM disease course. Trisomies of chromosomes 3 and 5 were associated with a significant increase in overall survival time, while trisomy of chromosome 21 significantly reduced overall survival (18). This highlights the heterogeneity among MM patients and why tailored treatment approaches may need to be considered for MM patients. There is also an increasing awareness of patients with 'functional high-risk' myeloma who exhibit poor responses to therapy or experience rapid relapses that are independent of genetic risk factors. Interestingly, it has been suggested that MM should not be considered a single disease and that the array of molecular abnormalities means MM is more likely a group of diseases (13).

A recent study also demonstrated that even in a single MM patient there may be significant differences between tumour cells, known as intra-tumoral heterogeneity (24). Spatial genomic heterogeneity, defined as distinct genetic variations observed in MM cells across different bone marrow sites, has been observed in more than 75% of patients (24). The existence of different clones in different marrow sites further increases the complexity of treating the disease, as different regions may harbour cells with different mutations. Longitudinal studies have now shown that the presence of these clones drives relapse and genomic evolution in MM (25-27). However, the exact mechanisms of how this clonal

diversity arises and its impact on disease relapse and drug resistance are still being investigated (28). Temporal heterogeneity or genetic evolution, which is defined as changes in the genetic aberrations in tumour cells over time, has also been documented in MM (29). In some cases, the genetic lesions remain mostly unchanged, this is referred to as stable evolution (29). In contrast to clonal evolution, stable evolution results in genomically stable MM cells, which are typically more predictable in their drug response (30). The heterogeneity between MM patients and between MM cells in the same patient are likely significant contributing factors in the incurable nature of the disease (30). Another major factor that can drive drug resistance in MM is the bone marrow microenvironment (BMME), which is a collective term for the various bone marrow cellular components, including other immune cells, the extracellular matrix and stromal cells and an array of soluble factors, such as cytokines and growth factors (31).

The BMME is an interactive dynamic system that regulates myeloma cell behaviour through different mechanisms. Bone marrow stromal cells are key components of the BMME, and produce factors, including interleukin-6, B-cell activating factor (BAFF) and a proliferation-inducing ligand (APRIL), that can promote the survival, proliferation and migration of MM cells (31). Immune cells in the BMME can also influence disease progression, with both myeloid derived suppressor cells and regulatory T cells in the BMME creating an immunosuppressive environment that can enable MM cell survival and proliferation (31). Factors secreted into the BMME, including interleukin-6 and interleukin-10, have also been shown to enhance MM cell survival and prevent cytotoxicity induced by chemoimmunotherapy, contributing to drug resistance (31). Heterogeneity in the BMME between patients may also impact its effects on MM cells and can contribute to drug resistance. For example, expression of the key immune checkpoint molecule, PD-L_1, correlates with a poor prognosis in relapsed or refractory MM (32). These studies suggest that therapies that account for the role of the BMME may improve patient outcomes.

As mentioned above, a common clinical feature of MM is immunosuppression, which significantly increases the infection risk among patients. MM cells exert an immunosuppressive effect by secreting soluble factors that inhibit the function of immune effector cells while also recruiting immunosuppressive cells, including regulatory T cells, myeloid-derived suppressor cells, and tumour-associated macrophages (33). Infections are

not only a significant cause of morbidity but are also currently the primary cause of death among MM patients, with one study suggesting that 45% of all early deaths among MM patients (within 6 months of diagnosis) were due to infections (33-35). All these factors contribute to the significant rate of disease relapse and high incidence of refractory disease among MM patients and highlights the currently unmet need for novel, personalised, and targeted therapeutic approaches for this cancer.

1.1.4 MM treatment

MM is still considered to be incurable, despite treatment advances over several decades. Until the turn of the century, MM was poorly treated, with 5-year survival rates of less than 35% before 2000 (36). Research and development of novel therapies has significantly improved the quality and duration of the lives of people diagnosed with MM. However, the 5-year progression free survival for high-risk patients is as low as 17% (37) and survival among older MM patients (>65 years) has stagnated over the last 20 years (38).

The introduction of immunomodulatory drugs (IMiDs), proteasome inhibitors (PIs) and monoclonal antibodies (mAbs) has significantly changed the landscape of MM treatment, and when combined with autologous stem cell transplantation, have significantly improved treatment outcomes (39). Despite the improvement in treatment efficacy, the 5-year survival rate for MM is only approximately 50% with a median overall survival of 5.5 years (3). On-going development and trials of next generation agents in these classes will likely continue to improve survival rates (36, 39).

The IMiD class of drugs are believed to act both directly against MM cells and indirectly by modulating the immune system against the cancer. The first of the IMiDs, thalidomide, was developed in the 1950s and was available as an over-the-counter sleep aid and anti-emetic in Australia (40). However, after significant birth defects were observed among pregnant women who took the drug, its use was discontinued and only re-introduced for the treatment of leprosy. The use of thalidomide was authorised in 5 patients with end stage MM on a compassionate use protocol and unexpectedly one of the patients experienced a significant response, despite being refractory to prior lines of therapy. This sparked a phase II clinical trial of 84 patients, in which 29% of patients achieved a 50% decrease in their paraprotein levels and two patients achieved a complete response (40). In subsequent years the second

and third generation IMiDs, lenalidomide and pomalidomide, were developed and trialled as part of treatment regimens for MM demonstrating significant efficacy (40).

Proteasome inhibitors (PI) are a class of drug that target the cellular system that functions to degrade damaged or misfolded proteins. Inhibition of the proteasome induces an accumulation of these proteins, leading to cell death through endoplasmic reticular stress (41). Bortezomib, which was the first approved PI for the treatment of MM, is now commonly used in multiple treatment regimens, and has shown response rates of 66-90% and complete response rates of 15-21%, when combined with the corticosteroid, dexamethasone (41). The next generation PI carfilzomib now approved in many countries, including Australia, is associated with improvements in overall response rates and complete response rates compared to bortezomib-containing regimens (41-43). The next generation oral PI ixazomib has been shown to have comparable safety and efficacy data to bortezomib when combined with lenalidomide and dexamethasone, with markedly lower rates of neurotoxicity (44).

The corticosteroids, dexamethasone and prednisone bind cytosolic glucocorticoid receptors, which then translocate into the nucleus and modulate gene expression (45). Corticosteroids have broad anti-inflammatory and immunosuppressive effects, caused by the transactivation and indirect repression of target genes via their effects on the activity of transcription factors (45). Corticosteroids are now a staple in frontline treatment for MM and are associated with high response rates when paired with other agents, such as proteasome inhibitors and Immunotherapeutics (45).

The recent introduction of therapeutic monoclonal antibodies (mAbs) has significantly improved and revolutionised the treatment of MM (46). mAbs, which are discussed in detail below, are highly specific, synthesised antibodies that recognise a specific epitope in target proteins (Figure 2)(47). The mAb, daratumumab, exerts direct anti-tumour and immunomodulatory activity by binding to CD38, a type II transmembrane glycoprotein that mediates signal transduction via enzymatic signalling (catalysing the conversion of NAD^+) and receptor mediated signalling by associating with other membrane proteins (46). Daratumumab was deemed so effective that it was granted a breakthrough-therapy designation by the United States Food and Drug Administration (FDA) as a monotherapy for MM (46), following the GEN501 and SIRIUS clinical trials, in which patients treated with daratumumab demonstrated an overall response rate of 36% (46, 48, 49). Daratumumab, in

combination with lenalidomide and dexamethasone (POLLUX) or bortezomib and dexamethasone (CASTOR), has also been shown to increase progression free survival and decrease the risk of disease progression in clinical trials (46, 50, 51). The next generation anti-CD38 mAb, isatuximab, has also shown efficacy in terms of increased progression free survival durations (46, 52). Elotuzumab is another mAb used in MM therapy that has demonstrated promising results (53) and is now approved for treatment of Australian patients. Elzotizumab binds to CD319 on NK and MM cells, which activates the NK cells, and tags the MM cells for destruction by the activated NK cells (54). Therapeutic mAbs have also been developed against the B-cell maturation antigen (BCMA), which is a highly expressed surface protein on MM cells, which will be discussed in more detail below. In addition, bispecific antibodies and antibody drug conjugates (ADCs) have also been developed, with the results of trials suggesting these may further improve response rates and patient outcomes (46).

Bispecific antibodies are engineered molecules that are specifically developed to recognise and target two completely different antigens/epitopes (Figure 2)(55). The dual targeting capacity of these antibodies provides several key advantages over conventional mAbs, including the ability to bring immune cells in close proximity to tumour cells, enhanced selectivity and reduced off target toxicity (55). In 2022 and 2023 teclistamab, elranatamab, and talquetamab were all approved for use in the US, after promising results in clinical trials (56). Teclistamab and elranatamab simultaneously bind BCMA on MM cells and CD3 on endogenous T cells, bringing together the cancer and immune cells (56). Talquetamab also binds CD3 on T cells and is targeted towards G protein–coupled receptor, class C, group 5, member D (GPRC5D), a highly expressed receptor in MM (56). All three have received approval as 5th line therapies, providing an option for patients with complex and difficult to treat disease.

One of the emerging novel and effective uses of mAbs for cancer treatment is in drug delivery in the form of antibody-drug conjugates (ADCs). Antibody-conjugated drugs are comprised of mAbs that are covalently bound by a chemical linker to cytotoxic drugs, referred to as prodrugs, which are inactive derivates of drug molecules that can be enzymatically reactivated once inside cells (Figure 2)(57). ADCs are designed to deliver cytotoxic payloads specifically to the target cancer cells, thus reducing the potential for off-target and toxicity of the drug (57). The specificity of the antibody ensures binding and internalisation of the drug

into the cancer cell being targeted, thereby limiting off target effects (58). Belantamab Mafodotin, a BCMA targeted ADC, is the only FDA approved ADC for treatment of MM and will be further discussed below. However, this ADC has now been withdrawn from the US and European markets (59), suggesting ADCs may have efficacy in MM but that further development of drugs in this class is required.

Chimeric antigen receptor (CAR)-expressing T cell therapies are another relatively new form of cancer treatment that involves engineering T-cells to express cell surface proteins known as CARs, that are specific to antigens on the surface of the tumour cells (60). CAR-T cell therapies harness the cytotoxic capacity of activated T cells and the ability of the CAR to effectively induce cell death of cancer cells (60). There are currently only two FDA approved CAR-T-cell therapies that both target BCMA, which will be further discussed below.

Personalised medicine approaches are revolutionising the treatment of a range of different cancers. Personalised medicine describes health care that involves personalised approaches that enable providers to investigate and discover unique information that informs medical decisions (61). Although personalised medicine is being investigated as an approach for MM, to date there are no FDA approved therapies for the various molecular sub-types of MM (62). A subset of MM patients have a translocation between chromosomes 11 and 14 [t(11;14)], which results in increased expression of the anti-apoptotic protein, BCL-2 (62). Venetoclax is an oral therapeutic that inhibits BCL-2 and is now being investigated in this subset of MM patients (62). Clinical trials with venetoclax have shown promising results, with increased overall response rates and median time to progression among patients with t(11;14) (63), highlighting the potential of precision therapies for patients with MM. Although the clinical and biological heterogeneity of MM means treatment is challenging, identifying the susceptibility of different MM patient subgroups to particular therapies may represent an effective approach. As many MM therapeutics target or modulate the immune system, it is important to appreciate and review key immunology concepts that underpin these approaches

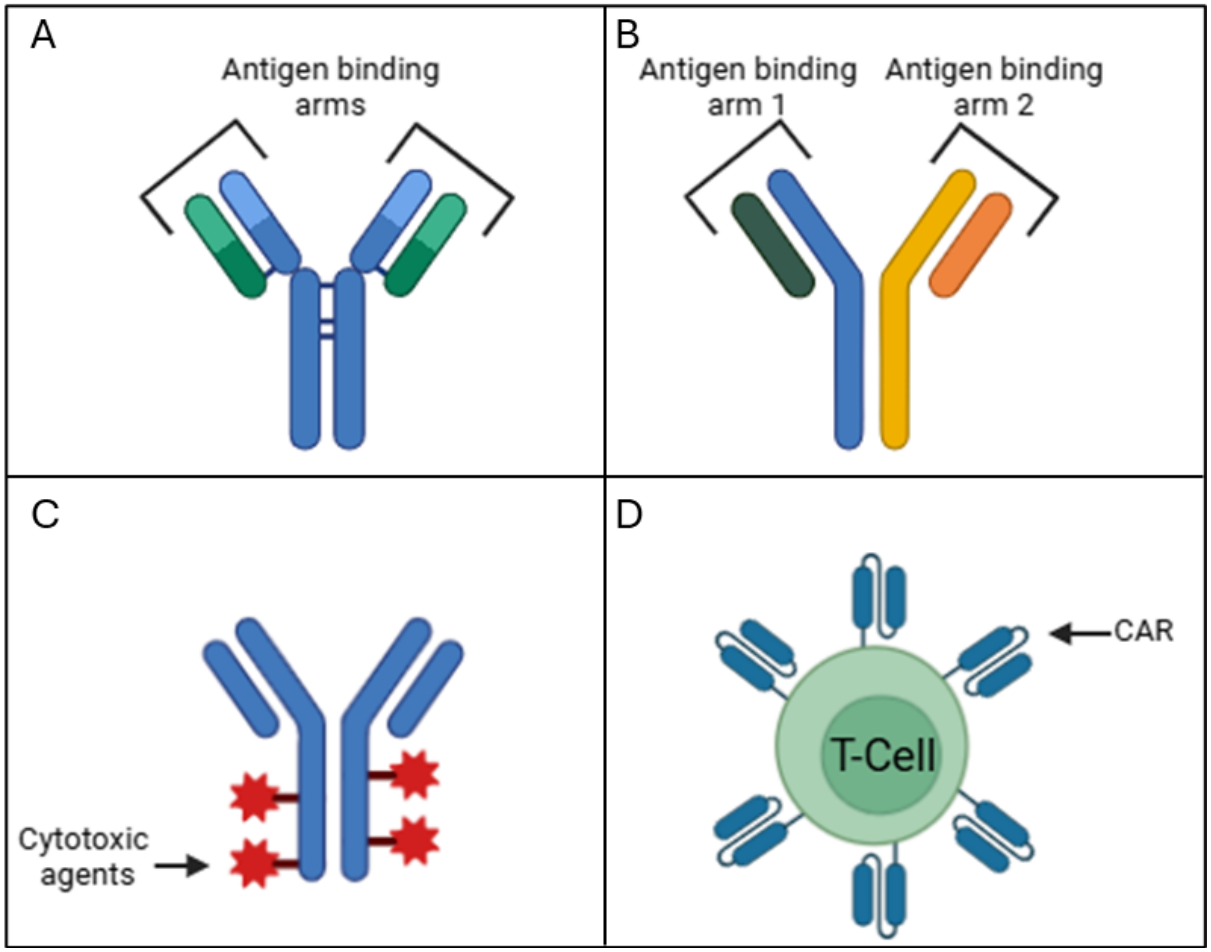

Figure 2. Different classes of MM drugs.

(A) Monoclonal antibody with antigen binding site specific to a single antigen. **(B)** Bispecific antibody with two antigen binding arms, each specific to a single antigen. **(C)** Antibody drug conjugate loaded with cytotoxic agents. **(D)** Chimeric antigen receptor (CAR) T-cell.

1.3 Immunology

The immune system is a complex biological system comprised of many different cell types and organs, that primarily functions to protect the body from infections caused by foreign antigens. The immune system also has two primary lines of defence, known as the innate and adaptive immune systems. The innate immune system is comprised of four unique barriers, the anatomic barrier, physiologic barrier, endocytic and phagocytic barrier, and an inflammatory barrier. Innate immunity is present in the body at birth, with characteristics that are inherited from parents, and acts in a non-specific manner to rapidly defend against any foreign antigens (64). Once a foreign antigen has been recognised by the innate immune

system the immunity is present for life, although the potency of the reaction decreases with repeated exposure to the same pathogen (64). The adaptive immune system mounts a more sophisticated response to foreign pathogens and when required it can work hand in hand with the innate immune system to protect the body from infection. The adaptive immune system is a highly specific and potent defence system that acts slowly (1-2 weeks) to ward off infections that cannot be eradicated solely by the innate immune system and is primarily responsible for the production of antibodies (64).

1.3.1 Antibodies

Antibodies are proteins that are produced by plasma cells in response to foreign antigens, to induce an adaptive immune response. Antibodies occur naturally in healthy immune systems and consist of both heavy chain and light chain regions, which form unique antigen binding sites (Figure 2) (65). Antibody production begins when B-cells recognise pathogens in secondary lymphoid organs, such as lymph nodes, which leads to B-cell differentiation into memory B-cells and plasma cells. Memory B-cells remain in the body to mount a response against subsequent attacks from the same pathogen, whereas plasma cells produce specific antibodies against the pathogen (65). Antibodies can be classed into five groups, each with their own specialised functions (65). The five immunoglobin classes (isotypes) of antibodies found in serum are IgM, IgG, IgA, IgE, and IgD. After encountering a foreign antigen, IgM is the first antibody produced by plasma cells and acts as a B-cell surface immunoglobulin. Complex signalling pathways are then activated in the B-cells that induce isotype switching to yield the optimal immunoglobulin for recognition of the specific pathogen (65). IgG is mostly synthesised as a secondary immune response to pathogens, particularly against encapsulated bacteria, while also being the only immunoglobulin that can cross the placenta to protect the neonate from infectious diseases (66). IgA is the major secretory antibody in the body, found in saliva, tears, the intestinal and genital tracts and respiratory secretions, and protects the epithelial surfaces of the respiratory and digestive systems (66). IgE is the most important antibody involved in host defence against parasitic infections. This antibody also binds to high affinity receptors on mast cells and basophils and is the primary antibody involved in allergic reactions (66). The function of the last of the immunoglobulin classes, IgD, is less clearly defined, but has been associated with antigen triggered lymphocyte differentiation (66).

Antibodies are also classed as either polyclonal or monoclonal (mAbs) (Figure 2). Polyclonal antibodies are a mixture of structurally heterogenous antibodies that are typically secreted by different B-cell clones in the body. Polyclonal antibodies have a high affinity to the antigen; however, the differences in their structure mean they recognise different regions or epitopes of the antigen, resulting in non-specific interactions with the antigen as well as an increased chance that the antibody will cross react with other antigens.

1.3.2 Antibody production

Methods for antibody production differ depending on whether polyclonal or monoclonal antibodies are required. However, both forms of antibody have been used extensively in both research and clinical applications. Polyclonal antibodies are easier to produce and purify than mAbs, as they do not originate from a single clone (67). In contrast, mAbs are antibodies that are secreted during the expansion of a single clone of antibody-producing plasma cells. These antibodies have a high affinity for the specific epitope within the antigen to which they were raised (67). Polyclonal antibody production is performed completely *in vivo*. An immunocompetent animal (most commonly rabbits, mice and goats) is injected with a specific immunogen to elicit an immune response and then samples are collected when sufficiently high titres of the desired antibody are present in the serum (68). The antibody is then purified from all other serum proteins (68).

The initial steps involved in mAb production are identical to those for polyclonal antibody production, however antigen responsive splenic B-cells, rather than serum, are removed from the immunised animals. The B-cells are then fused *in vitro* with a histocompatible myeloma cell line (Figure 3) (47). These myeloma cells are unique in that they have a hypoxanthine guanine phosphoribosyltransferase (HGPRT) enzyme deficiency. HGPRT is vital in the salvage pathway of nucleotide biosynthesis, meaning that these myeloma cells can only synthesise nucleotides through the *de novo* pathway. The cells formed by the fusion of the primary splenic B-cells to myeloma cells are known as hybridomas, and are cultured in a selective medium containing hypoxanthine, aminopterin, and thymidine (HAT) to remove any unfused myeloma cells (Figure 3). The aminopterin in the HAT medium blocks the *de novo* nucleotide synthesis pathway, the only available pathway for HGPRT deficient myeloma cells, effectively killing them (Figure 3) (47). The newly formed hybridomas survive because the HGPRT enzyme

is present in the splenic B-cells. The next stage of mAb production is the screening process, which identifies and selects the hybridoma clones that are producing antibodies with the desired specificity. Rapid primary screening is performed, which evaluates the hybridoma culture supernatant for antibody reactivity and specificity, to eliminate non-specific hybridomas as early as possible (47). Qualitative and quantitative testing of the antibodies from the different clones is performed to test for antigen binding capacity using flow cytometry or an enzyme-linked immunosorbent assay (ELISA). The selected hybridoma clone(s) can then be cultured further to produce higher antibody titres or may be cryopreserved for later experiments. After the initial screening process, hybridomas can be further refined to achieve a pure clonal population, if required. This process is called sub-cloning and is performed to isolate individual cells and establish a monoclonal cell line. In this way, cells can be cloned, screened and re-cloned until a monoclonal cell line is established (47). The selected cell lines can then be cryopreserved until required. Antibody purification from the supernatant of hybridomas can be performed by protein A or G chromatography to yield pure mAbs. If required, hybridomas can also be used to generate chimeric or humanized antibodies to reduce undesirable immune responses.

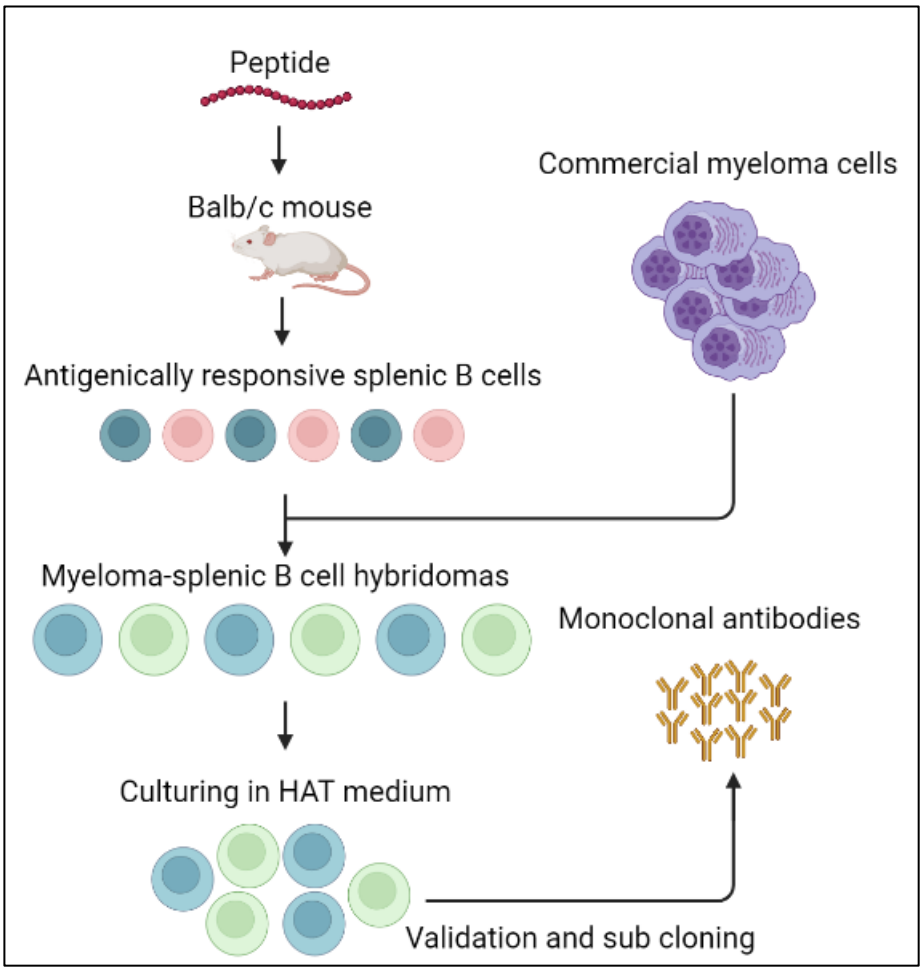

Figure 3. Process of monoclonal antibody production through immunisation of mice

HAT, hypoxanthine, aminopterin, and thymidine.

1.3.2 Clinical and research applications of monoclonal antibodies

Antibodies have become a valuable resource in the diagnosis and treatment of a range of diseases. mAbs have quickly become crucial in a wide range of clinical laboratory diagnostic tests due to their high specificity and restricted reactivity, allowing precise characterisation and identification of pathogens. The diagnosis of protozoal (malaria) and parasitic infections (tapeworms) has significantly improved with the development of mAb technologies, since these have overcome the limitations associated with polyclonal antibodies discussed earlier.

MAbs have also proven to be very effective as therapeutic agents, by directly binding to specific proteins on the target cell, resulting in cell death, inhibition of cell growth, blockade of specific ligand binding sites, or through the potentiation of other drugs (69). A wide array

of drugs have also been developed based on mAb technology, easily identifiable as all their names end with the suffix 'mab.'

1.3.3 B-cell maturation antigen

BCMA, also commonly known as tumour necrosis factor receptor superfamily member 17 (TNFRS17) is a member of the tumour necrosis factor (TNFR) superfamily. The *BCMA* gene encodes a 184 amino acid protein with a short 54 amino acid extracellular domain (Figure 4). BCMA is a type III transmembrane protein that contains an intracellular TNF receptor associated factor binding domain, a transmembrane domain, and an extracellular cysteine rich binding domain (Figure 4) (70). BCMA, as well as B-cell activation factor receptor (BAFF-R) and the transmembrane activator and calcium modulator and cyclophilin ligand interactor (TACI) are critical regulators of B-cell proliferation and survival (70). Two ligands for BCMA have been identified, B-cell activator of the TNF family (BAFF) and a proliferation inducing ligand (APRIL), which activate intracellular pro-survival signals after binding to BCMA (71). The multiple growth and survival pathways activated include the canonical nuclear factor kappa B (NF-κB) signalling pathway, the protein kinase B (AKT) pathway, the MEK/ERK pathway, c-Jun N-terminal kinases (JNK), ELK-1 and p38 Kinase (70-72). Importantly, elevated levels of soluble BCMA (sBCMA) have been observed in the serum of MM patients and has been associated with poor treatment response rates (58). Additionally, elevated levels of sBCMA in patients with smouldering myeloma correlate with progression to MM (58). The rationale for targeting BCMA as a therapeutic approach for MM was based on several factors. BCMA is highly expressed on the surface of mature B lymphocytes, while it is only minimally expressed on hematopoietic stem cells or non-hematopoietic tissue. BCMA is essential for the survival of long-lived bone marrow plasma cells but is not required for B-cell homeostasis (73). MM cells universally express BCMA on their cell surface, and expression has been shown to be elevated on malignant plasma cells compared to either normal plasma cells or other bone marrow cell subsets (73).These findings suggest that BCMA-targeted therapies may be less likely to result in off target effects in MM, and that BCMA may serve as a valuable biomarker for assessing response to therapy in MM.

Currently, there are three types of BCMA-targeted therapies that have been trialled for MM patients. However, research is expected to lead to an increase in the number of BCMA-

targeted therapies. As already discussed, antibody-drug conjugates (ADC) are therapeutic agents comprised of a mAb bound to a cytotoxic agent. The specificity of the antibody results in binding and internalisation of the drug into the cancer cell being targeted, thereby limiting off target effects (58). The anti-BCMA ADC, belantamab mafodotin gained FDA approval in 2020 after promising initial clinical trial results. However, this agent was later withdrawn from both the US and European markets, primarily because the confirmatory DREAMM-3 trial did not meet its primary endpoint (59). The phase III clinical trial, DREAMM-8, is currently evaluating if the ADC has any synergistic potential when combined in other regimens (59). The results from DREAMM-7 and DREAMM-8 (both investigating belantamab mafodotin in combination regimens) have led to the drug being accepted for review by the FDA for use in relapsed/refractory multiple myeloma, with a decision expected in 2025 (74). This identifies a gap in the market for ADCs in MM.

The BCMA bi-specific antibodies teclistamab and elranatamab bind to both BCMA on the tumour cell and CD3-expressing T cells, which brings cytotoxic T-cells in close proximity to the tumour cells and promotes killing of the tumour cells by the T-cells (58). Both of these bispecific antibodies are currently used to treat MM patients. A trial published in 2022 investigating BCMA-targeted CAR-T cell therapy in MM showed promising results with a significant improvement in treatment response rates (75). As of 2024, two BCMA-targeted CAR-T cell therapies had been FDA approved for the treatment of MM, ciltacabtagene autoleucel and idecabtagene vicleucel (76). These two therapies are approved for use in relapsed and refractory MM and have demonstrated effective targetability (77). BCMA CAR-T cell therapy is not without issues and addressing the challenges of scalability and feasibility are important for more widespread implementation of this form of therapy (78).

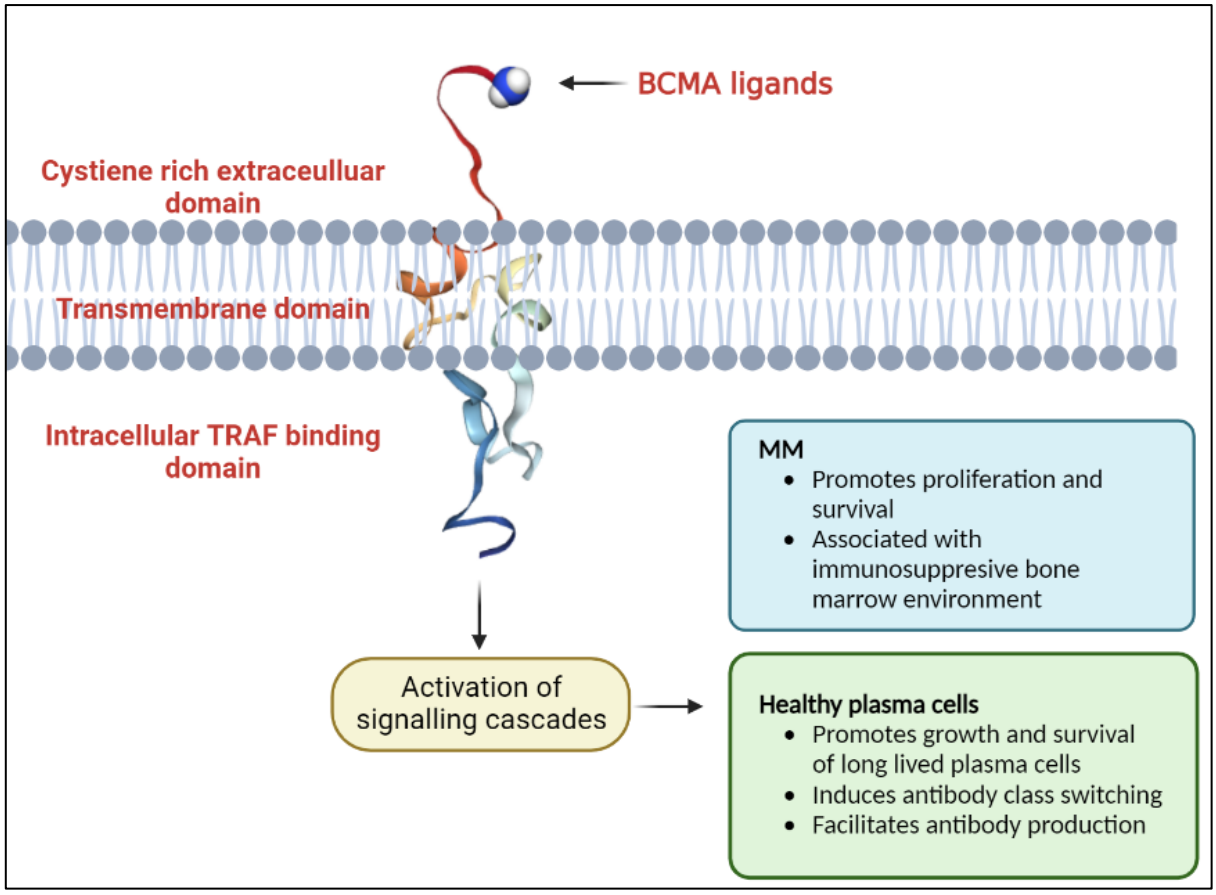

Figure 4. B-cell maturation antigen domains and activation in MM and healthy plasma cells.

BCMA ligands APRIL, a proliferation-inducing ligand and BAFF, B-cell-activating factor; MM, multiple myeloma; TRAF, TNF receptor associated factor.

1.3.4 Cluster of differentiation 38 (CD38) and daratumumab

CD38 is an enzyme that is normally expressed at low levels on the plasma membrane of human immune and endothelial cells. CD38 is expressed at higher levels on a range of tumour cells, including MM plasma cells. Biologically, CD38 acts as a NADase catalysing the synthesis of nicotinamide and ADP-ribose using nicotinamide adenine dinucleotide as a substrate. Nicotinamide adenine dinucleotide is a cofactor that plays an important role in energy metabolism and other vital cellular processes, suggesting that CD38 is a negative regulator of the cofactor (79). CD38 can also mediate the production of a range of cytokines by attaching to CD31, including but not limited to IL-12 and IL-6 (80), which are important in mediating immune responses (79). Importantly, CD38 is highly expressed on MM cells, hence the rationale for the development and clinical implementation of anti-CD38 therapeutics, such as daratumumab,

Daratumumab is an FDA approved monoclonal antibody that targets a specific epitope of the human CD38 molecule (79). Early testing *in vitro* found that daratumumab induced complement dependant cytotoxicity, antibody dependant cell mediated cytotoxicity and antibody-dependent cellular phagocytosis (81, 82). *In vivo* studies in mouse xenograft models found that daratumumab was effective at inhibiting tumour growth (81). Interestingly, daratumumab has also been suggested to directly induce apoptosis, specifically through Fc gamma receptor I mediated cross-linking and can amplify the effects of MM chemotherapeutics (83, 84). Depending on the country, daratumumab is available as first line, second line and subsequent lines of therapy, in combination with other agents.

1.4 Regulated cell death

Cell death is a fundamental physiological process that ensures cell survival, integrity and homeostasis. Cell death can generally be classified into two main forms, unprogrammed or programmed cell death (PCD) (85). Unprogrammed cell death occurs in a non-regulated manner, typically in response to overwhelming chemical or physical stimuli (85, 86). In contrast, PCD is a tightly regulated process of cell death that is essential for tissue homeostasis and protection against viruses and disease(86) . Various forms of PCD have now been established and researched, including but not limited to apoptosis, pyroptosis, necroptosis and ferroptosis (Table 1) (86). Apoptosis is a caspase-dependant form of PCD, acting as a homeostatic mechanism to control cell populations, and a mechanism that protects the body from cells damaged by disease or noxious gases (87). Apoptosis is characterised morphologically by cell shrinkage, membrane blebbing due to cytoskeletal degradation and subsequent fragmentation into membrane-bound apoptotic bodies (88). The efficacy of most cancer therapies is dependent on apoptosis-mediated cell death. Since drug resistance is often associated with dysregulation of apoptosis, targeting alternate forms of regulated cell death may be an effective approach for the treatment of cancers, including MM.

Pyroptosis is a necrotic and inflammation-dependant form of PCD that is induced by inflammatory caspases in response to offending agents (89). Morphologically, pyroptosis is associated with cell swelling and membrane rupture, with an ensuing release of the cytoplasmic contents from the cell (89). Necroptosis is a form of necrotic cell death that is mediated by death receptors and primarily acts against pathogen-mediated infections (90).

Necroptosis is unique in that it requires the inhibition of caspase-8 (a caspase involved in apoptosis), suggesting that necroptosis is a program of cell death that kills cells that have been inhibited from undergoing apoptosis (90). Morphologically, necroptosis is similar to pyroptosis, in that it is characterised by cell swelling and membrane rupture (90). The plethora of research that has been conducted on the forms of PCD highlights how fundamental these processes are (Table 1).

Table 1. Distinct forms of programmed cell death

Cell death	Defining characteristics	Morphology	References
Apoptosis	Caspase-dependant form of cell death that mediates cell population and protects body from damaged cells	Cell shrinkage, membrane blebbing, nuclear condensation, DNA fragmentation and fragmentation into membrane bound apoptotic bodies	(86)
Ferroptosis	Iron and poly unsaturated fatty acid (PUFA) dependant form of cell death induced by the accumulation of lipid ROS	Ballooning phenotype consisting mainly of cytoplasm, mitochondrial condensation, lack of mitochondrial cristae and rupture of outer mitochondrial membrane	(91)
Pyroptosis	Necrotic and inflammatory form of cell death induced by inflammatory caspases	Nuclear condensation, DNA fragmentation, cell swelling and membrane rupture	(89)
Necroptosis	Induced by death receptors in response to pathogen mediated infections and requires the inhibition of caspase 8	Cell and organelle swelling, loss of membrane integrity and membrane rupture (Dhuriya and Sharma, 2018)	(90)
Paraptosis	PCD leading to cellular necrosis, mediated by large potassium channels, and initiated by ROS	Cytoplasmic vacuolation, dilated endoplasmic reticulum and mitochondria.	(92)

Autophagy	Lysosomal catabolic process that removes and recycles intracellular endogenous and exogenous components	Double membrane vesicles that contain cytosol, large autophagic vesicles and presence of lysosomes	(93)
Necrosis	Uncontrollable/unprogrammed cell death induced by pathological circumstances (e.g., infection or trauma)	Membrane swelling of the organelles, oncosis, DNA degradation and the release of cytoplasmic content inducing an inflammatory response	(94)
Entosis	Cells in suspension integrate or are engulfed by a neighbour cell, causing the cell to program cell death within the phagosome	Entotic vacuole, crescent nuclear shape of the outer cell and no membrane fusion	(95)

1.5 Ferroptosis

Ferroptosis is a form of non-apoptotic PCD, that has relatively recently been characterised as being dependent on lipid peroxidation and iron dependence (96). Ferroptosis is associated with distinct morphological, genetic, and mechanistic characteristics, which can be used to distinguish ferroptosis from other forms of PCD (Figure 5) (96). The potential of ferroptosis as a target for novel therapies is due to the accumulation of cellular reactive oxygen species (ROS) in cells undergoing this form of PCD. Cancer cells proliferate at a greater rate than healthy cells, which requires increased metabolic rates, leading to higher levels of cellular ROS than in healthy cells. Since ferroptosis is triggered by increased ROS levels, some cancer cells may only require a relatively small perturbation in cellular ROS levels before they undergo ferroptosis.

Lipid peroxidation is a hallmark of ferroptosis and is characterised by chain reactions that result in the oxidative degradation of lipids, yielding highly toxic peroxyl radicals (ROO•) (97). The active degradation of lipids and the resulting formation of peroxyl radicals irreversibly compromises membrane integrity and leads to cell death (98). The role of iron and lipid peroxides in ferroptosis is further highlighted by the unique fact that iron chelators and synthetic antioxidants can inhibit this form of cell death (99). Iron chelators reduce cellular iron levels, which is a crucial co-factor in ferroptosis, while synthetic antioxidants inhibit ferroptosis by scavenging free radicals that would otherwise propagate lipid peroxidation (99). Interestingly, ferroptosis cannot be inhibited by potent inhibitors of either apoptosis or necrosis inhibitors, highlighting the distinction between ferroptosis and these other forms of PCD (Publication 1 in the Appendix) (96). MM cells are often resistant to apoptosis and have dysregulated lipid profiles (Publication 1 and 3 in Appendix) which suggest ferroptosis may be a viable therapeutic target. Preliminary research in our lab observed that MM cells could be forced to undergo ferroptosis when cultured with the ferroptosis inducer RSL3, however at much higher concentrations than diffuse large B cell lymphoma (DLBCL) cells. This led us to investigate the factors that dictate ferroptosis sensitivity in MM to help develop novel therapeutics.

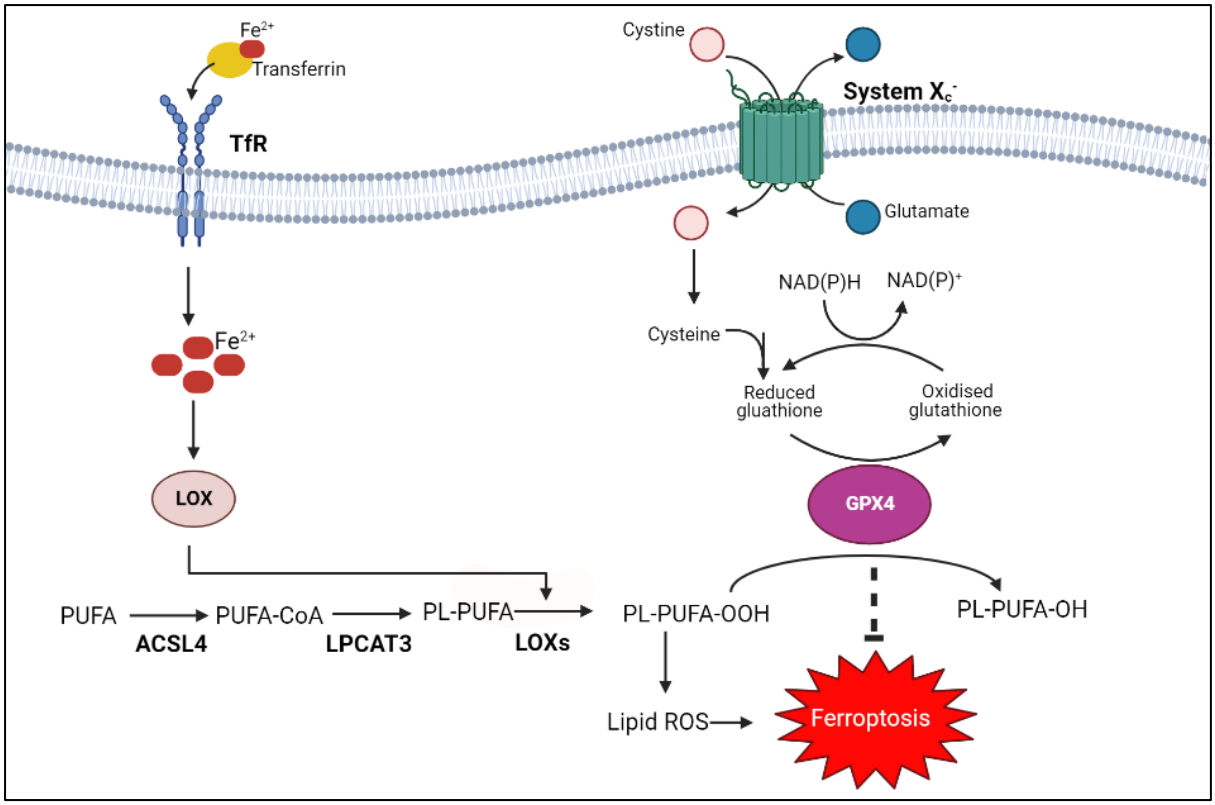

Figure 5. Biochemical pathways involving system Xc- and GPX4 that regulate ferroptosis inhibition.

ACSL4, acyl-CoA synthetase long-chain family member 4; Fe2+, ferrous iron; GPX4, glutathione peroxidase 4; LOXs, lipoxygenases; LPCAT3, lysophosphatidylcholine acyltransferase 3; PL, phospholipid; PL-PUFA-OH, phospholipid alcohol; PL-PUFA-OOH, phospholipid hydroperoxides; PUFA, polyunsaturated fatty acid; ROS, reactive oxygen species; TfR, transferrin receptor.

1.5.1 The role of system X_c^- and GPX4 in ferroptosis

System X_c^- is a plasma membrane-bound amino acid antiporter that is comprised of two subunits: the functional subunit, solute carrier family 7 member 11 (SLC7A11) and the regulatory subunit, solute carrier family 3 member 2 (SLC3A2). System X_c^- is an important regulatory component of ferroptosis, facilitating the exchange of intracellular glutamate for extracellular cystine, which is then rapidly converted to cysteine by thioredoxin reductase 1 (TXNRD1) (Figure 5) (100). Production of cysteine is the rate limiting step in the biosynthesis of glutathione (GSH), an important antioxidant and enzyme substrate. Once reduced, GSH activates the catalytic domain of glutathione peroxidase 4 (GPX4) (100). GPX4 is a selenoprotein, that facilitates the conversion of toxic lipid peroxides into neutral alcohols, inhibiting the propagation of lipid peroxidation and the eventual induction of ferroptosis

(Figure 5) (100, 101). A better understanding of the role of system X_c^- in the regulation of GPX4 is crucial for determining how this pathway may be targeted for the development of novel therapeutic approaches.

GPX4 can also be directly targeted to induce ferroptosis with the inhibitor (1S,3R)-RSL3 (referred to as RSL3). RSL3 is a small molecule inhibitor that binds to the active domain of GPX4, rendering the protein permanently inactive, leading to its degradation within the cell (102). The potent ferroptosis-inducing effects of RSL3 have been demonstrated in a variety of cancers *in vitro*, including colorectal, lung and pancreatic cancer cells (102-104).

1.5.2 Ferroptosis suppressor protein 1 and the Mevalonate Pathway

Antioxidant systems, independent of GPX4, also exist, which suppress ferroptosis. One of these systems is the ferroptosis suppressor protein 1 (FSP1)/mevalonate pathway, a system very adept at supressing ferroptosis (105). The mevalonate pathway is a multifaceted biological pathway that leads to the production of isopentenyl pyrophosphate (IPP) as well as CoQ (Figure 6). The mevalonate pathway involves the reduction of acetyl-CoA to mevalonate through a series of reactions, which is then converted to IPP (106). IPP is also involved in the maturation of selenocysteine, an amino acid required for GPX4 translation (107, 108) and can be converted to farnesyl pyrophosphate, which is an important upstream substrate in the generation of CoQ (106). CoQ is a naturally occurring quinone that is vital to cell and tissue health in most aerobic organisms (109). CoQ is primarily involved as a co-factor in the electron transport chain, functioning as a high-energy transfer molecule (109). The biosynthesis of CoQ begins and ends in the mitochondria, facilitated by a protein complex, which has not been fully elucidated (110). CoQ is comprised of a benzoquinone ring derived from tyrosine (amino acid) that is chemically linked to 10 isoprenoid units (synthesised by the mevalonate pathway) (111). Ferroptosis suppressor protein 1 (FSP1) catalyses the regeneration of CoQ and reduces CoQ to CoQ_{10}-H_2 (ubiquinol), initiating a radical trapping system (Figure 6) (105). FSP1 functions independently, is not involved in the canonical ferroptosis pathway, is only protective against ferroptosis inducing agents and not pro-apoptotic agents and does not appear to be regulated by p53 (105). Interestingly, expression of FSP1 has been shown to directly correlate with sensitivity to ferroptosis-inducing compounds, including RSL3, while

genetic knockdown of *FSP1* results in increased sensitivity to ferroptosis-inducing compounds in a range of cancer cell lines (105).

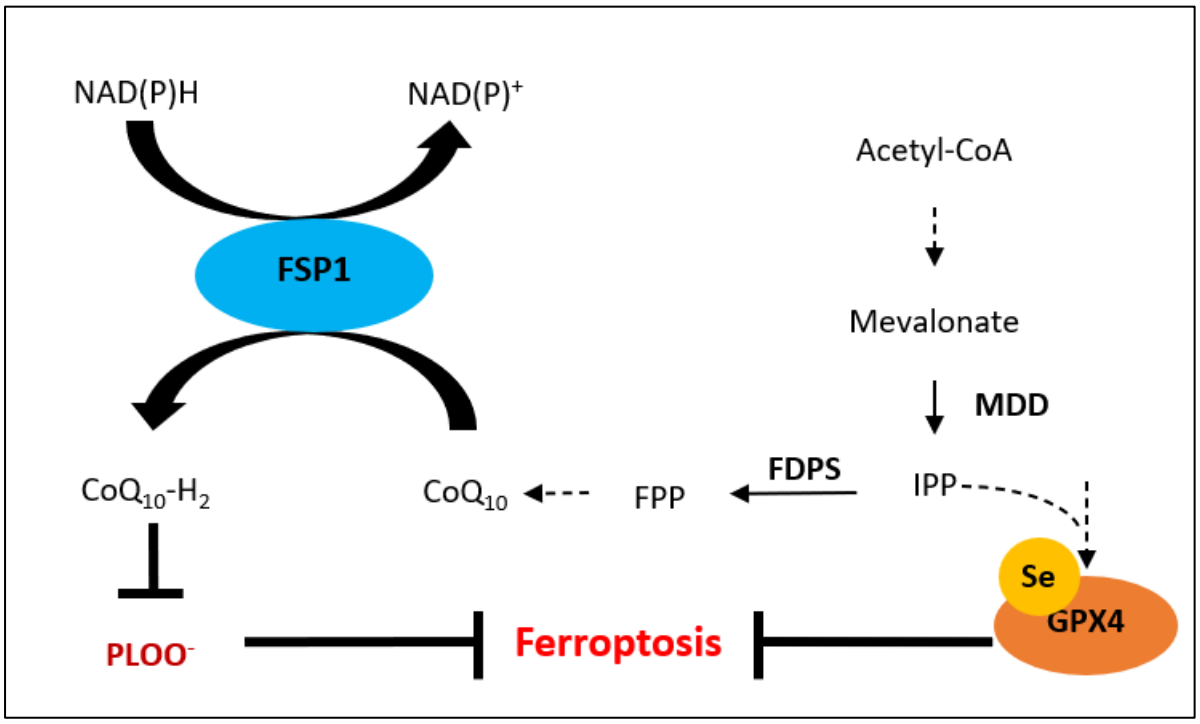

Figure 6. Biochemical pathways involving the mevalonate pathway involved in inhibition of ferroptosis.

CoQ10, ubiquinone; CoQ10-H2, ubiquinol; FDPS, farnesyl diphosphate synthase; FPP, farnesyl phosphate; FSP1, ferroptosis suppressor protein 1; GPX4, glutathione peroxidase 4; IPP, isopentenyl phosphate; MDD, mevalonate diphosphate decarboxylase; PLOO-, lipid peroxyl radicals; Se, selenocysteine. Dotted arrows represent multiple steps within a pathway.

1.5.3 Iron dependency in ferroptosis

Iron is an essential metal involved in cellular homeostasis and in the programmed cell death mechanism known as ferroptosis (112). The role of Iron in ferroptosis is multifaceted but has primarily been shown to drive ferroptosis. Intracellular iron levels, in particular the labile iron pool, has been shown to play an important role in ferroptosis. Labile iron can react with intracellular hydrogen peroxide yielding highly reactive hydroxyl radicals, as part of the Fenton reaction (113). These hydroxyl radicals are destructive oxidising agents that can attack organic material, including phospholipids, and have been shown to initiate lipid peroxidation (Figure 5) (113). The iron dependence of ferroptosis is further demonstrated by the ferroptosis inhibitory capacity of iron chelators (114).

In addition to iron's role in the Fenton reaction, it is also involved in ferroptosis through lipoxygenases, which are iron-containing enzymes that regulate lipid peroxidation by catalysing the oxidation of PUFAs in lipids, contributing to the production of lipid hydroperoxides (108). Lipoxygenase overexpression has been shown to sensitise HEK293 cells to RSL3-induced ferroptosis (115), while the specific knockdown of 15-lipoxygenase-1 (ALOX15-1) prevents both RSL3 and erastin induced ferroptosis in HT1080 cells (116). While iron plays an important role in ferroptosis induction, polyunsaturated fatty acid containing phospholipids are the primary substrates of ferroptosis and serve as key targets of lipid peroxidation, that ultimately lead to cell death.

1.6 Lipids

Lipids are a diverse group of organic molecules and are among the most essential building blocks of life. Lipids make up the structural composition of cell membranes, play important roles as signalling molecules and are a critical energy repository (117). Lipids can be loosely categorised into fatty acids, glycerides, nonglyceride lipids and complex lipids, which can be further classified into more distinct lipid groups. In the context of ferroptosis, phospholipids (PLs) or more specifically glycerophospholipids, are understood to be important in the initiation and propagation of lipid peroxidation (117).

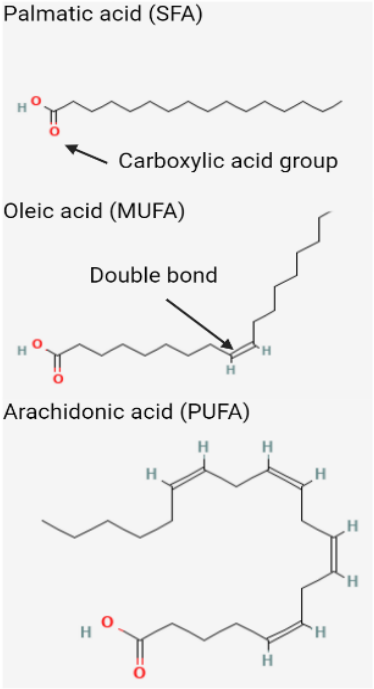

Figure 7. Types of fatty acids. SFA; saturated fatty acid; MUFA, monounsaturated fatty acid; PUFA, polyunsaturated fatty acid

Glycerophospholipids are diglycerides that contain any derivative of glycerophosphoric acid residue attached to the glycerol moiety and are synthesised from glycerol-3-phosphate in the *de novo* pathway (118, 119). Ester linkages are formed with the phosphate group to the glycerol backbone, with the long-chained hydrocarbons (fatty acids) also forming ester linkages to glycerol (Figure 9). The two fatty acids that are chemically attached to the glycerol molecule have hydrophobic properties, while the polar head consisting of the phosphate group attached to the third carbon has hydrophilic properties. Glycerophospholipids are

amphipathic (both hydrophilic and hydrophobic) in nature due to their hydrophobic tail and hydrophilic head (118). Glycerophospholipids are a major component of the lipid membrane and are usually organised with the polar hydrophilic heads oriented outwards towards the aqueous environment and the non-polar hydrophobic tails oriented inwards (119). Glycerophospholipids represent a diverse species of lipids that have slightly differing structural characteristics with the most basic being phosphatidic acid, an extremely important intermediate species (120). All glycerophospholipids are derivatives of this lipid species and are formed when an additional head group is attached to the phosphate group, allowing for the formation of many phosphoglycerides (phospholipids).

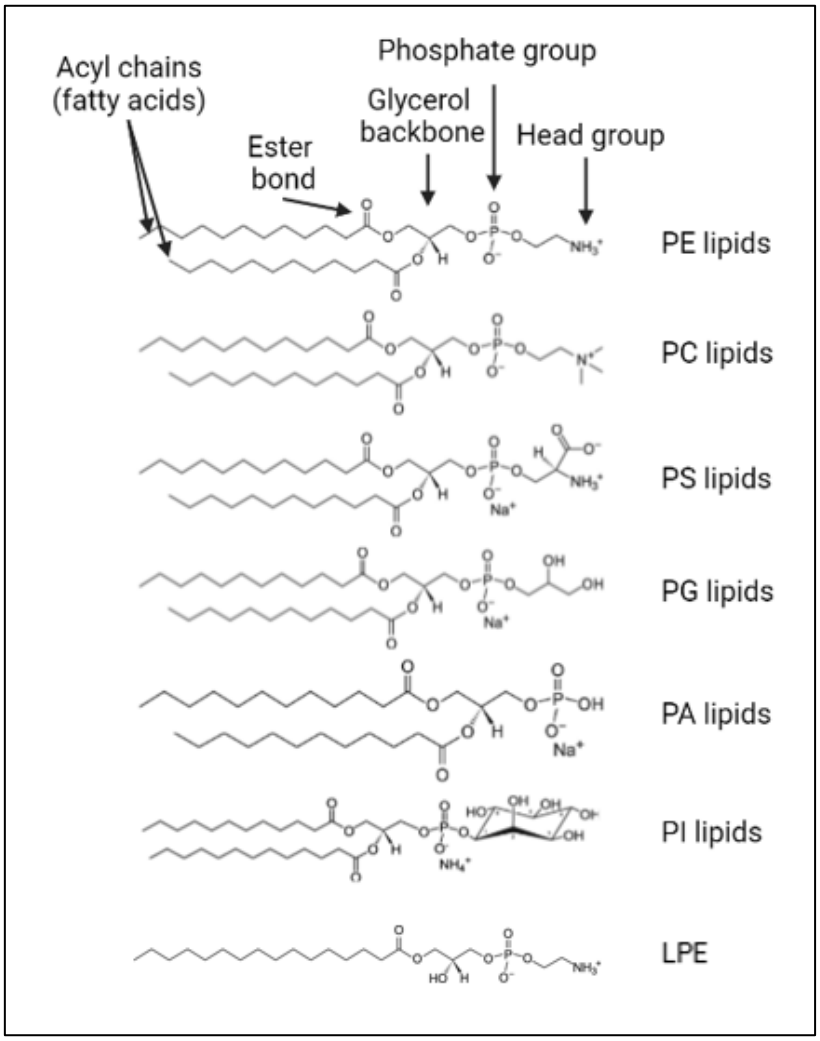

Figure 8. Different phospholipid species.

LPE, lysophosphatidylethanolamine; PC, phosphatidylcholine; PE, phosphatidylethanolamine; PS, phosphatidylserine; PG, phosphatidylglycerol; PA, phosphatidic acid; PI, phosphatidylinositol.

PLs are characterised according to the 'head' group as phosphatidylcholine (PC), phosphatidylethanolamine (PE), phosphatidylserine (PS), phosphatidylinositol (PI), phosphatidylglycerol (PG) or phosphatidic acid (PA) (Figure 8). These PLs contain different head groups and are characterised accordingly, with the different head groups being associated with unique roles within the cell. PC is the most abundant PL in mammalian membranes and makes up to 40-50% of total cellular lipids, primarily within the inner leaflet of the membrane (121). PC is essential in the formation and secretion of low-density lipoproteins (cholesterol) and also plays a key role in bile salt mediated micelle formation. PE is the second most abundant PL in mammalian membranes, making up to 30% of total cellular PLs. PE is enriched within the mitochondrial membrane and is vital for the growth and stability of these organelles and for insertion of proteins into the mitochondrial membrane (122). PS is most abundant within the inner leaflet of plasma membranes, accounting for approximately 10% of the lipids within the membrane. Newly synthesised PS is a precursor for PC and PE, whereas membrane-bound PS plays an important role in the signalling mechanisms that mediate blood clotting and the phagocytosis of apoptotic cells (122). Although PI levels in the mammalian membrane are low (≤2%), they have been shown to play an important role in mediating the role of proteins within the plasma membrane (122). PG is another lipid that is present at low levels in mammalian cells (1-2% of total PLs). However, PG is an essential precursor for mitochondrial cardiolipin, which is required for normal electron transport and oxidative phosphorylation (123). PA is another minor component of the total cellular PLs; however, it plays an important role as a second messenger in intracellular signalling pathways and a precursor for the biosynthesis of many lipids (124). While PLs are an important factor to consider in the context of ferroptosis, the fatty acid acyl chains are the key determinates of their potential for oxidation.

Fatty acids are carboxylic acids with an aliphatic chain, comprised of oxygen, carbon, and hydrogen atoms. They can be categorised into three distinct groups, saturated fatty acids (SFA), monounsaturated fatty acids (MUFA) and polyunsaturated fatty acids (PUFA). SFAs are defined by the lack of double bonds present between the carbons within their hydrocarbon chain, MUFA contain only one double bond in the hydrocarbon chain, while PUFA are fatty acids with more than one double bond in the hydrocarbon chain (Figures 8-9). Fatty acids have a multitude of roles that include, but are not limited to, involvement in signal

transduction pathways and protein modification, energy depositaries and important components of hormones and lipids (125). Fatty acids, particularly PUFA containing PLs, are pivotal in ferroptosis, necessary for the initiation and propagation of lipid peroxidation. PUFAs are more readily oxidised within the cell and are hence an important substrate for lipid peroxidation. Interestingly, free fatty acids are not an essential substrate of lipid peroxidation and hence are not readily involved in ferroptosis (126). The lipid in which the fatty acids are contained also plays an important role in dictating their peroxidation potential.

The initiation of lipid peroxidation in ferroptosis is primarily associated with the formation of potent oxidising agents, particularly hydroxyl radicals (•OH) produced by the Fenton reaction. Hydroxyl radicals are extremely destructive oxidising agents that indiscriminately and instantaneously attack organic material within a 5-nanometre radius. Once formed, hydroxyl radicals are able to remove a bis-allylic hydrogen atom from the PUFA within PLs (PUFA-PL) (127). Bis-allylic hydrogen atoms contain two allene groups, which form the weakest bond within the PUFA-PL complex (127). The removal of this hydrogen atom results in the formation of carbon-centred PLs, which then react with free oxygen, forming the highly potent PL peroxyl radical (ROO•). PL peroxyl radicals are then able to remove hydrogen atoms from PUFA-PL, which subsequently form PL hydroperoxides (ROOH). PL hydroperoxides and lipid-free radicals, including alkoxyl PL radicals (RO•) and peroxyl radicals, propagate the removal of hydrogen atoms from PUFA-PLs further driving the cascade of lipid peroxidation. The breakdown of cellular PUFA-PLs and formation of PL hydroperoxides may result in eventual loss of cell membrane integrity and organelle and cell membrane rupture (128). PL hydroperoxides may also drive the cascade of lipid peroxidation by reacting with ferrous (Fe^{2+}) and ferric (Fe^{3+}) ions, generating peroxyl free radicals and alkoxyl PL radicals (129). Inhibiting the cascade of lipid peroxidation is complex and involves many different mechanisms, including the antioxidant systems mediated by FSP1 and GPX4.

Ferroptosis sensitivity may correlate with the number of bis-allylic hydrogen atoms in PUFA-PLs and the proportion of PUFA-PLs (Publication 2 in the Appendix). Not only are PUFA-PLs required for the induction and execution of ferroptosis, but these lipids may also serve as biomarkers for ferroptosis sensitivity. Research concerning the role of PUFA-PL in ferroptosis is rapidly expanding and may provide information regarding the importance of cellular lipid composition in this form of PCD. Several studies that have examined the *in vitro* effects of

specific exogenous PUFAs such as AA, eicosapentaenoic acid, docosahexaenoic acid, have shown that *in vitro* supplementation of cells is associated with increased sensitivity to ferroptosis and in some cells, can directly induce ferroptosis (Publication 2 in the Appendix)(126, 130, 131). PLs containing MUFA and other less reactive lipid species within the lipidome (such as SFA) have been associated with an increased resistance to ferroptosis (100, 108, 132). Mechanistically, the literature suggests that over time, MUFAs can displace PUFAs from PLs in the lipid membrane and other areas of the cell (132).

1.6.1 Lysophospholipids

Lysophospholipids (LPL), which are characterised by a polar head group and a singular carbon chain (acyl chain), represent a relatively minor component of the total lipid species within cells. The lysolipid structure of the bioactive molecules exhibit increased hydrophilicity and versatility, in comparison to their corresponding PLs (133). LPLs are typically recognised as extracellular mediators and, in some cases, mediators of intracellular signal transduction (133). LPLs are most commonly formed when the ester bonds of PLs are enzymatically hydrolysed by phospholipase A; given that the acyl chains are bound by ester bonds, the products of this cleavage are LPL and a free fatty acid chain (134). Research into the role of lipids in ferroptosis has identified that LPL levels significantly increase in ferroptotic cells, whereas levels of the corresponding PUFA-PL decrease (135, 136). These changes in LPL expression are associated with oxidised acyl chains being the preferred substrate of specific lipases, in particular phospholipase A (136). Interestingly, inhibiting phospholipase A can rescue inducible GPX4 null cells from ferroptosis, suggesting that cleaved and oxidised PUFAs are actively involved in the induction of membrane damage and cell death (136). The results of these studies suggest that cleaved and oxidised PUFAs play an important role in ferroptosis, and increased levels of LPL may represent an indication of impending ferroptosis-mediated cell death.

1.6.2 Cholesterol

Cholesterol is a major structural component of cell membranes, comprised of a hydrocarbon tail, a centre sterol nucleus, and a hydroxyl group (137). The role of cholesterol in cell membranes is to provide stability and fluidity, while also being a major component of regions in the membrane called lipid rafts (137). Cholesterol also plays an important role as a

precursor in the synthesis of steroid hormones, vitamin D and bile acids (137). In the context of ferroptosis, the role of cholesterol has largely been hypothesised, however recent studies have shown that cholesterol supplementation can induce a state of ferroptosis resistance in human epithelial cells, with results akin to ferrostatin-1 (Publication 3 in the Appendix)(138). The mechanism of ferroptosis suppression in these cells was shown to be related to an increase in squalene and CoQ, both of which known to inhibit ferroptosis (138). Squalene is a lipophilic metabolite that alters the lipid profile of cells, protecting them from oxidative stress and cell death (139).

A recent study published in 2023 also revealed that long-term hematopoietic stem cells from C57BL/6 mice, which were fed a high-cholesterol diet, had significantly lower levels of lipid peroxidation, decreased levels of Fe^{2+} and increased levels of GSH compared to controls (140). Furthermore, freshly isolated long-term hematopoietic stem cells were significantly more resistant to erastin *ex vivo* than cells from control mice (140). The underlying mechanism of this resistance was suggested to be due to dampening of intracellular signalling pathways that trigger ferroptosis and upregulation of SLC7A11/GPX4 expression (140).

1.6.3 Potential determinants of ferroptosis sensitivity

Defining the factors that determine cellular sensitivity to ferroptosis is vital in understanding how ferroptosis can be harnessed as a therapeutic approach. In addition to the mechanisms that regulate ferroptosis that have already been discussed, including system X_c^-, GPX4, iron and lipids, there are a number of other factors that also govern ferroptosis. Nicotinamide adenine dinucleotide phosphate (NADPH) is a critical reductant, involved in a plethora of different pathways, most notably in anabolic reactions and redox balance. NADPH also plays a key role in the inhibition of ferroptosis, actively donating electrons to glutathione reductase, which subsequently catalyses the conversion of oxidised GSH to reduced GSH. This led to the suggestion that intracellular NADPH levels may represent a potential biomarker for ferroptosis (141). The role of GSH as an activator of GPX4 suggests that any factor that affects the activity of the GSH enzyme may also serve as a potential biomarker. Selenium is an essential element required for the biosynthesis of the amino acid selenocysteine, a critical component of GPX4, suggesting that selenium depletion or supplementation can increase or decrease ferroptosis sensitivity, respectively (142).

1.7 Clinical applications of ferroptosis

1.7.1 Ferroptosis and cancer

There have been many challenges in the development of effective cancer treatments and despite significant improvements, disease relapse and drug resistance remain extremely common for most forms of cancer. Many of the conventional cancer therapies aim to induce death of tumour cells, while sparing healthy, untransformed cells. Unfortunately, this is not possible in many patients or the case for many of the treatments used, as patients often develop cancers that are non-responsive to treatment or the treatment regimens are toxic towards healthy cells and tissues.

A growing number of studies suggest that induction of ferroptosis may have potential as a novel approach for the treatment of cancer, which may avoid or overcome resistance to more conventional therapies, that are generally reliant on apoptosis (143). Studies also suggest that induction of ferroptosis may act in synergy with more conventional anticancer agents, such as cisplatin; for example, the system X_c^- inhibitor sulfasalazine acted in synergy with cisplatin to suppress the tumour growth in a cisplatin-resistant mouse model of head and neck cancer (144). Furthermore, ferroptosis may play an innate role in tumour suppression, protecting against tumorigenesis. Cancer cells may be capable of overcoming ferroptosis-mediated cell death by increasing their antioxidant capacity, potentially through upregulation of system X_c^-. This is supported by the observation that upregulation of system X_c^- almost always correlates with poor survival and drug resistance among cancer patients, due to the associated increase in antioxidant capacity (145). However, the link between ferroptosis and tumour growth and why some cancers have an underlying sensitivity to ferroptosis, are yet to be fully elucidated.

1.7.2 Ferroptosis in MM

Advances in therapy in the last 20 years have significantly improved the survival of MM patients. Unfortunately, as with most conventional anti-cancer therapies, primary or acquired resistance is common among MM patients. Novel targeted therapies that are effective against apoptosis-resistant disease may represent an innovative approach in the treatment of

relapsed or refractory MM. There is a growing literature concerning ferroptosis in MM, however further research is required to determine how to effectively induce ferroptosis in MM cells (Publication 1 and 2 in the Appendix).

Ferroptosis of MM cell lines was first demonstrated by Yang *et al* in 2014, who showed that MM cell lines were significantly less sensitive to the ferroptosis-inducing drug erastin than DLBCL cell lines (136). Subsequent research demonstrated that iron supplementation triggers MM cell death through induction of lipid ROS, which can be augmented by the addition of bortezomib *in vitro* and *in vivo* (146). This study also found that iron inhibits proteasome function, thereby interfering with redox potential and protein homeostasis (146). The study proposed that iron levels may impact the efficacy of current MM therapies and increasing levels in patients may improve response rates, particularly in elderly un-fit patients (146).

Drug screens have led to a rapid increase in the number of compounds that have the potential to induce ferroptosis and may have important clinical applications. FTY720, which was developed by structurally modifying the antibiotic myriocin, has immunosuppressive effects and is currently FDA approved for the treatment of multiple sclerosis (147). A study suggests that FTY720 can also induce apoptosis and autophagy of MM cells, however the results were inconclusive. More recently, FTY720 was found to induce ROS accumulation and cell death of MM cells, which was partially preventable by ferrostatin-1 (147). FTY720 treatment also reduced GPX4 and SLC7A11 expression both at the mRNA and protein levels *in vitro,* supporting the idea that ferroptosis, rather than apoptosis, may be the mechanism of cell death induced by this compound in MM cells (147). The study concluded that FTY720 likely induces both ferroptosis and autophagy through the protein phosphatase 2A/AMP-activated protein kinase pathway (147).

Recent research into ferroptosis in MM has uncovered a relationship between ferroptosis induction and subsequent DNA changes (148). Induction of ferroptosis in MM cells results in the upregulation of a multitude of key genes involved in cellular stress, cell death pathways, inflammation, and fatty acid metabolism. Expression of the ferroptosis-related genes, *ferritin heavy chain 1 (FTH1), ferritin light chain (FTL), HO-1* and *SLC7A11* increases upon induction of ferroptosis in MM cells (148). Interestingly, this study also showed that changes in the expression of 95 of the 616 differentially expressed genes identified could be prevented by pre-treatment with ferrostatin-1 (148), suggesting that these 95 genes may play a role in

ferroptosis. These included genes that encoded zinc finger proteins, and proteins with roles in metal binding, nuclear receptor signalling and chromatin remodelling (148). A review article published by our group, summarising studies of ferroptosis in the context of MM is included in the appendix (Publication 1 in the Appendix).

1.7.3 Ferroptosis in other haematological malignancies

The literature regarding ferroptosis as a therapeutic target in haematological malignancies is expanding at an exponential rate. This will be discussed in this section and in the published review article in the appendix (Publication 1 in the Appendix).

A recent study investigating an association between cholesterol uptake during ferroptosis in DLBCL, follicular lymphoma, and Burkitt's lymphoma found that treating cell lines with high-density lipoprotein (HDL)-like nanoparticles that bind to scavenger receptor type B1 and reduce cholesterol uptake into the cells, resulted in cell death through mechanisms consistent with ferroptosis (149). Follicular lymphoma is a slow-growing cancer of transformed follicular centre B-cells, whereas Burkitt's lymphoma is a highly aggressive B-cell lymphoma, commonly associated with Epstein-Barr virus (EBV) infections (149, 150). These findings not only reinforce the notion that ferroptosis is a highly regulated process and that B-cell malignancies have an innate sensitivity to ferroptosis but also identify another pathway that may be manipulated to induce ferroptotic cell death.

Acute myeloid leukemia (AML) is a haematological malignancy characterised by the clonal expansion of immature blast cells, primarily in the bone marrow and peripheral blood (151). AML is a relatively rare disease, with 1,143 cases diagnosed in Australia in 2018 (152). AML in adults is a difficult cancer to cure and with a 5-year survival rate of just 27.4%, alternative treatments are needed (152). A recent study conducted by Yusuf *et al*., showed that ferroptosis induced in AML cells by inhibition of GPX4 is associated with decreased levels of aldehyde dehydrogenase 3a2, an enzyme involved in the conversion of aldehydes into carboxylic acids (153). The results of this study suggest that aldehyde dehydrogenase 3a2 protects AML cells from undergoing ferroptotic cell death and raises the possibility that targeting this protective mechanism may be a novel therapeutic approach in this disease (153).

Data from a study by Akiyama *et al*., also demonstrate that ferroptosis can be induced in AML cells, in this case using ML210, a covalent GPX4 inhibitor (154). Gene expression analysis of tumour cells from AML patients showed that high expression of the ferroptosis-related proteins, SLC7A11 and GPX4, was associated with significantly shorter rates of overall survival (154).

APR-246, which targets p53, has also been investigated as a potential therapy for patients with AML by Birsen *et al*., (155). The study showed that early cell death of AML cells exposed to APR-246 is suppressed by inhibitors of lipid peroxidation. The authors concluded that cell death induced by APR-246 was not due to apoptosis and more likely ferroptosis-mediated due to the increase in cellular ROS levels and iron dependence observed (155). The study went on to demonstrate that inhibition of GPX4 had only modest effects on AML cell lines, but that inhibitors of aldehyde dehydrogenase 3a2 and GPX4 were synergistic, both *in vitro* and *in vivo* (155).

Lung and breast cancer are the two leading causes of cancer-related mortality in women and although recent advances in treatment have improved outcomes, novel therapies are required to treat patients with apoptosis-resistant disease (156). Recent studies suggest that breast cancer cells are susceptible to ferroptosis, induced either by erastin or RSL3 (157, 158). Ferroptosis has also been shown to target breast cancer stem cells, which are typically refractory to standard treatment and their persistence leads to disease relapse (159). The results of these studies suggest that induction of ferroptosis may represent a therapeutic approach that has greater efficacy than current treatment options for patients with breast cancer, particularly those patients who experience relapsed/refractory disease.

Small-cell lung cancer is an aggressive cancer with a typically poor prognosis, and poor response rates to current therapies (160). Research concerning ferroptosis in small cell lung cancer has shown promising results; a study by Lida *et al*., demonstrated that inhibition of system X_c^-, with sulforaphane, induces ferroptosis in small-cell lung cancer cells *in vitro* (160). Other studies in small-cell lung cancer have also identified that non-neuroendocrine differentiation plays an important role in determining ferroptosis sensitivity, through lipid remodelling, more specifically due to the upregulation of ether lipid synthesis (161). This study further supports the role of ether lipids as crucial factors of ferroptosis sensitivity in cancer.

A study of the novel ferroptosis inducer, talaroconvolutin A, demonstrates the potential efficacy of ferroptosis-targeted therapies for colorectal cancer (CRC) (162). Xia *et al*. have shown that talaroconvolutin A induces ferroptosis in CRC cells through downregulation of SLC7A11 with concomitant upregulation of arachidonate lipoxygenase 3, both *in vitro* and *in vivo* (162). CRC is a collective term for cancers of the colon or rectum, and with approximately one million new cases diagnosed annually worldwide, is one of the most commonly diagnosed cancers (163).

The efficacy of ferroptosis-targeted therapies shown by these studies, in a wide range of both haematological malignancies and solid tumours, highlights the potential for novel therapeutic strategies that harness this form of PCD. However, it is also apparent that further studies are required to better understand the mechanisms that regulate ferroptosis in different cancer cell types. A combination of ferroptosis-inducing drugs and emerging nanotechnologies may also augment the effects shown by the extremely promising data presented in the studies discussed. For example, encapsulating otherwise toxic ferroptosis-inducing substrates or compounds into nanoparticles that are functionalised to specifically target cancer cells, may represent a viable approach for treating cancers by inducing ferroptosis.

1.8 Nanotechnology

The term nanotechnology refers to the study and engineering of functional systems at the molecular scale, ranging from only a few to several hundred nanometres (164). The study of nanotechnologies is multidisciplinary and aims to address many complex issues within the medical, physics, electronics, and aerospace fields (164). The engineering and synthesis of nanomaterials is a complicated and intricate process but can generally be approached in one of two ways: the top-down or bottom-up approaches. The top-down approach uses macroscopic materials and integrates smaller-scale details into the original material. The best example of implementation of the top-down approach is the photolithography technique applied in the semiconductor industry, where complex patterns are etched into silicon wafers to generate integrated circuits (165). The bottom-up approach takes a slightly different approach and begins by designing and synthesising custom-made molecules that have unique properties that allow them to self-assemble into higher order mesoscale and macroscale structures (165). An example of this in the medical field is the growth of artificial bone

biomimetics by inducing the formation of organoapatite on implanted titanium structures (165). It is theorised that the capture and nucleation of tiny embryonic crystals leads to the growth of apatite on the titanium implant (165). The potential of nanotechnologies is limitless and is a rapidly expanding field of research, with the expectation that nanotechnologies will soon impact almost every aspect of life.

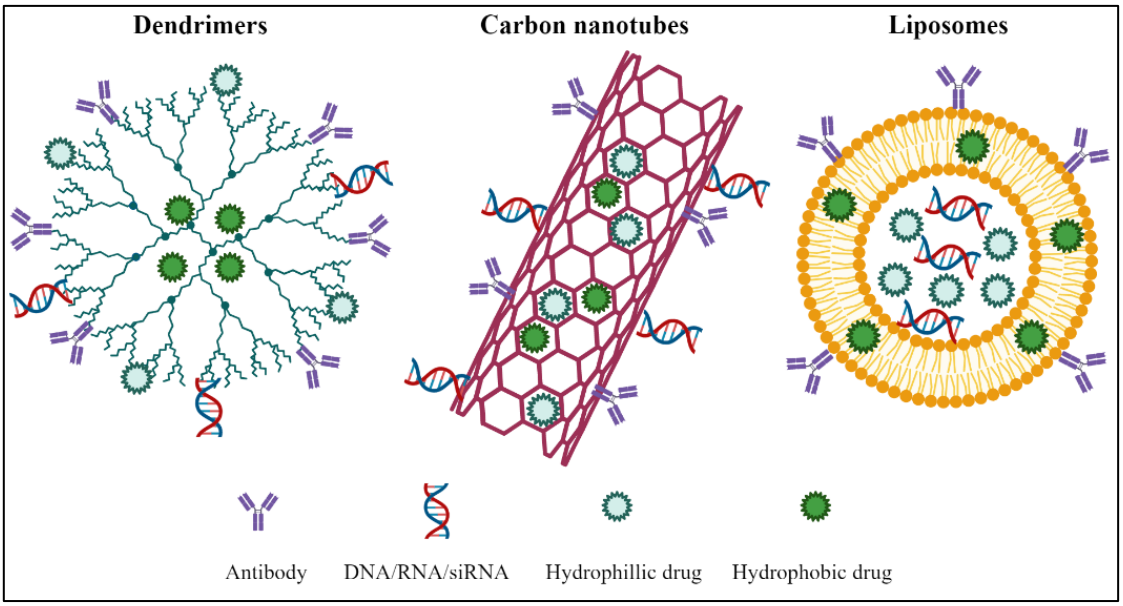

Figure 9. Examples of nanotechnological structures and potential ways in which these particles can be functionalised.

1.8.1 Nanotechnology in medicine

The philosophy behind Nanotechnology in medicine is that they represent a promising way in which to improve the efficacy of treatment, through the synthesis of nano drugs or engineering of targeted nanocarriers (166). Nanotechnologies are likely to become a large component of modern-day medicine, revolutionising the way treatment, diagnosis and health monitoring is conducted (166). The applications of nanomedicine can primarily be broken into two subgroups, nano-diagnosis, and nano-therapy (167).

The use of nanotechnology in diagnosis is based on the ability to alter the optical, electrical, and magnetic properties of particles to be used in the diagnosis of diseases at an early stage and at low levels (167). The application of nanotechnologies in diagnosis is rapidly expanding and to date has been studied in the context of cancer, Alzheimer's, HIV, hepatitis B, and

tuberculosis. Nanotechnologies enable a faster and more precise diagnosis of disease, which is vital in the battle against cancer.

Nano-therapy describes technologies that are being designed to improve the efficiency of drug targeting and delivery systems, improve safety and compatibility, and improve the pharmacokinetics of treatment (168). Initial efforts to develop nanodrugs involved the re-engineering of already available therapeutic and diagnostic agents (168). However, nanotechnology proponents have recently started to develop and apply new therapeutic and diagnostic systems (168). Drug delivery has been an important aspect in the development of any new cancer treatment and, in some cases, has limited further clinical development. In particular, large molecules pose many issues in terms of drug delivery, including poor solubility, poor absorption, off target binding and *in vivo* stability, all of which contribute to many potential treatments never making it past pre-clinical phases of testing. Developing new delivery systems that target specific cells (e.g., cancer cells) may resolve some of these issues, highlighting the potential of nano-based drug delivery systems that combine the biological and physical sciences (169). Nanotechnology is a relatively new sector in the field of medical research that has already been implemented in a wide array of areas, including as biosensors, microfluidics, and drug delivery systems (169, 170). Nanoparticle and nanomaterial technologies, using nanoparticles such as carbon nanotubes, dendrimers, and liposomes, are also being developed for applications in medicine (Figure 9) (170).

Carbon nanotubes are nanoscale cylindrical molecules comprised of rolled up sheets of carbon atoms (Figure 9) (170). Carbon nanotubes have high external surface areas, and therefore high loading capacities as drug carriers (170). In addition to being an efficient drug carrier, the optical, mechanical, and electrical properties of carbon nanotubes mean they have potential applications as contrast agents for medical imaging and as biological sensors (171). Dendrimers are a type of spherical synthetic polymer that has a structure comprised of repeated branching chains expanding from a central core (Figure 9). The branching chains also typically contain exterior functional groups (170). Therapeutic cargos can then be encapsulated within the inner space of the dendrimer or bound to the functional groups on the exterior of the polymer. These characteristics make dendrimers highly bioavailable and biodegradable, both of which are very important qualities for an efficient drug delivery system (170).

Table 2. Recent advancements in liposomal technologies that induce ferroptosis in cancer.

Liposome functionalisation/contents	Malignancy	Findings	Ferroptosis measure	Reference
Folate-modified LPs encapsulating erastin and MT1DP (lncRNA that represses antioxidation) (E/M@FA-LPs)	Human NSCLC	E/M@FA-LPs more effective than erastin and MT1DP alone – decrease cell viability *in vitro* and reduced tumour volume/weight *in vivo*.	GSH depletion *in vitro* and increased MDA *in vitro* & *in vivo.*	(172)
LP rich in unsaturated lipids, containing iron and GSH-responsive DOX prodrug (LipoDSSSD)	Murine melanoma	LipoDSSSD effectively killed tumour cells, but not healthy cells *in vitro*; more effective than other treatment groups at reducing tumour volume/weight in mice.	Increase in oxidised C11-BODIPY & depletion of GSH *in vitro.*	(173)
Ultrasmall active catalysts (UACs, $Cu_xFe_{3-x}O_4$), camptothecin and DOX coated with pH-sensitive LP (LFCCD)	Murine colorectal cancer (*in vitro* and *in vivo*)	Ferroptosis induced by UACs synergised with apoptosis induced by the two chemotherapeutic agents resulting in inhibited tumour growth in mice.	Increase in oxidised C11-BODIPY & depletion of GSH *in vitro.*	(174)
PDGFB-targeted, iron-platinum nanoLP containing glucose oxidase (pLFePt-GOx)	Triple negative breast cancer	The pLFePt-GOx treatment group exhibited the lowest tumour volume in a mouse xenograft model.	Decreased GPX4 expression, increased ROS production *in vitro.*	(175)
CuO_2 & artemisinin loaded LP (Lipo-ART@CPNs)	Murine lung cancer	Lipo-ART@CPNs significantly reduced tumour burden compared to control and	Increase in oxidised C11-BODIPY *in vitro*.	(176)

		when combined with ultrasound irradiation, was the most effective treatment group.	GPX4 protein downregulation *in vitro* and *in vivo.*	
Unsaturated fatty acid-rich phosphatidylcholine LPs loaded with ferric ammonium citrate (LPOgener)	Human breast cancer & murine mammary carcinoma	LPOgener effectively killed breast cancer cells, with some toxicity to normal liver cells while FAC and empty LPs had no effect. A similar trend was seen in a mouse model and no damage to any organs was observed.	Small mitochondria with condensed membranes *in vitro*. Increase in oxidised C11-BODIPY *in vitro* and *in vivo*.	(177)
LPs loaded with nanoprobes and superparamagnetic iron oxide (L1/C-Lipo/DS), and LPs with GOx and DOX (L2/C-Lipo/GD)	Murine mammary carcinoma	The combination of the two LPs had a great antitumour effect in a metastatic breast cancer mouse model compared to other treatment groups.	Increase in oxidised C11-BODIPY and cell death prevented by ferrostatin-1 *in vitro*.	(178)

$ATB^{0,+}$, amino acid transporter $B^{0,+}$; DOX, doxorubicin; GSH, glutathione; lncRNA, long non-coding RNA; LP, liposome; MDA, malonyl dialdehyde; MMP2, matrix metalloproteinase 2; MT1DP, metallothionein 1D pseudogene; NSCLC, non-small cell lung cancer PDGFB, platelet-derived growth factor subunit B; WT, wild type.

1.8.3 Liposomes

Liposomes are extremely versatile spherical vesicles that primarily consist of lipids and range from 30 nm to a few microns in size (Figure 10) (170). The lipid-rich nature of these nanoparticles enables hydrophilic agents to be encapsulated inside the aqueous core, which is surrounded by a hydrophobic lipid bilayer. Although small vesicles such as liposomes are typically taken up by cells via endocytosis, uptake can be modified and improved by controlling the lipid composition of the liposomes (179). The versatility of liposomes is in the ability to modify the surface of the vesicles with polymers, antibodies, and proteins. Adding components, or functionalising the surface of liposomes, with these modifications may significantly expand the possible therapeutic applications of liposomes, by enabling delivery of macromolecular drugs or genetic therapies (e.g., siRNA) in a highly targeted manner.

Liposomes represent a safe and effective method of drug delivery, as they are comprised of lipids that resemble the plasma membrane. Liposome generation has historically been a complicated process to control with a low degree of reproducibility, due to the techniques involved (180). However, new laboratory technologies have been developed which synthesise uniform and reproducible liposomes. Instruments, such as the NanoAssemblr® Ignite™ designed by precision Nanosystems, automates liposome synthesis and is now being widely used in genomic medicine and vaccine development.

An example of where liposomes are currently being investigated is in the delivery of a peptide vaccine against colorectal cancer, in a mechanism that involves activation of the immune system against the malignant cells (Naciute *et al*., 2021). These biohybrid vaccines have demonstrated efficacy, leading to a reduction in tumour growth and increased lymphocytic infiltration *in vivo* (Naciute *et al*., 2021).

The ability to modify the surface of liposomes has also prompted research into whether they may be used as biomimetics for applications within the nervous system (181). In a recent study, Zinger *et al*., described humanized biomimetic neural nanovesicles that can specifically target neural cells *in vitro* (181). Although these liposomes are in an early stage of development, the study demonstrates the potential of liposomal nanovesicles as a novel approach for delivery of therapeutic cargos in the treatment of neurological diseases (181).

1.8.4 Liposomes in ferroptosis

Although the literature concerning liposomal-based therapies for haematological malignancies is limited, it is a promising avenue for research and will play a vital role in ferroptosis-mediated treatments. Further information regarding the use of liposomes to induce ferroptosis in MM can be found in the published review article in the appendix.

Nanotechnologies have been used to induce ferroptosis in non-small lung cancer (NSCLC), breast cancer, colon cancer, colorectal cancer, ovarian cancer and skin cancers (Table 2) (154, 176, 182-185). Many of these studies focused on iron-containing, ferroptosis-inducing nanotechnologies, and although few studies have used liposomes to induce ferroptosis, recent studies have shown promising results (Table 2). Interestingly, some of these studies have utilised liposomes as 'dual executioners', encapsulating compounds that induce both ferroptosis and apoptosis within nanoparticles with the aim of overcoming drug resistance (Table 2) (186, 187).

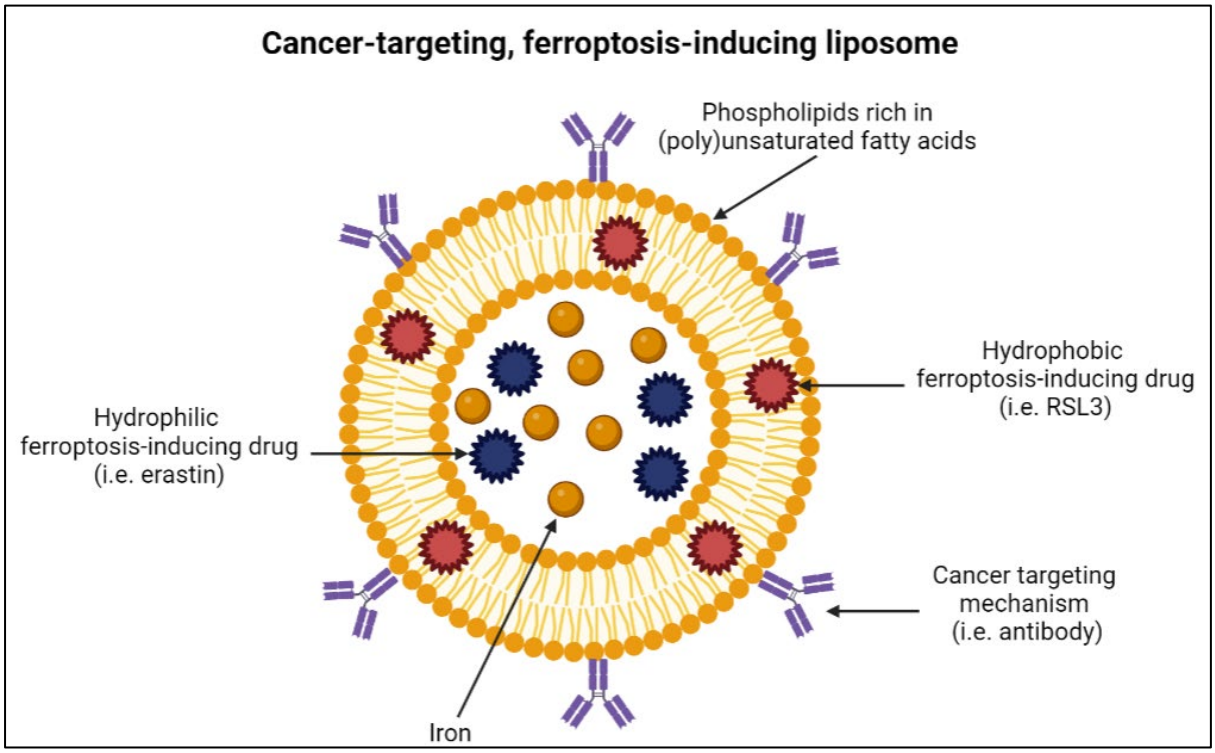

Figure 10. Potential functionalisation and drug encapsulation within liposomes.

In another recent study, Yang *et al*., generated ferroptosis-inducing liposomes containing unsaturated lipids, iron, and doxorubicin (DOX) to target melanoma cells (173). Unsaturated lipids and iron are key factors for ferroptosis induction, and interestingly the addition of DOX

was found to increase the generation of H_2O_2, which feeds into the Fenton reaction. DOX is a chemotherapy drug that induces apoptosis through various mechanisms (188), supporting the idea that nanoparticles comprised of combinations of ferroptosis and apoptosis-inducing agents or substrates may have significant anti-cancer effects. The liposomes developed by Yang *et al*., showed efficacy both *in vitro* and *in vivo,* and were shown to significantly prolong the circulation of the prodrugs, while the prodrugs relieved any adverse toxicity caused by liposome accumulation, compared to mice that were administered the drugs in a non-liposomal form (173).

Similarly, another study investigated the efficacy of inducing both ferroptosis and apoptosis as a treatment for breast cancer. Dual functional liposomes were generated containing sorafenib (System X_c^- inhibitor) and DOX and were tested both *in vitro* and *in vivo* (186). Although some toxicity was observed in the breast cancer mouse models, tumour burden was significantly decreased in mice administered the liposomes, compared to mice in the control group and those treated with DOX and DOX plus sorafenib in a non-liposomal form (186).

There is growing interest in liposomal technologies as potential cancer treatments, particularly given the ability to functionalise these nanoparticles with a wide range of targeted molecules. Targeted liposomes with the optimal lipid composition for different cancer types or for each patient, that encapsulate ferroptosis substrates or drugs, may represent a highly effective, precision medicine for the treatment of cancers, including MM.

1.9 Conclusions

This introductory chapter describes our current knowledge of MM, antibody production, ferroptosis and nanotechnologies, and provide the rationale for the study presented in this thesis. In summary, MM is an incurable plasma cell malignancy that affects thousands of Australians every year, who are faced with a 50% 5-year survival rate with current therapies. Despite improved survival rates in the last few decades, the prognosis for patients that present with high-risk disease or who are elderly, is extremely poor. Relatively new therapies, such as the antibody, daratumumab, and the antibody-drug conjugate, belantamab mafodotin, have shown some efficacy but a significant proportion of patients will still relapse with refractory disease.

Ferroptosis is a non-apoptotic mechanism of programmed cell death that has potential to overcome resistance to more conventional, apoptosis-dependent therapies. Nanotechnologies, such as lipid nanoparticles, or liposomes, which are functionalised to specifically target cancer cells and deliver ferroptosis-inducing drugs or substrates, may represent an effective treatment option for MM. This project aims to better understand the key lipids that trigger ferroptosis in MM cells and use this information to develop a novel therapeutic approach to kill MM cells.

HYPOTHESIS AND AIMS

Hypothesis: A novel class of lipid nanoparticles induce ferroptosis of multiple myeloma cells in a targeted and precise manner.

Project Aims:

Aim 1: Determine whether sensitivity of multiple myeloma cells to ferroptosis correlates with cellular lipid composition and identify the key lipid species involved.

This aim focuses on determining differences in the lipidomes of ferroptosis-sensitive diffuse large B-cell lymphoma (DLBCL) and ferroptosis resistant multiple myeloma (MM) cells and will include the following investigations:

A. A lipidomic analysis of 11 cell lines (5 MM, 5 DLBCL, and a normal B-cell line) using mass spectrometry, to define differences in lipid composition.
B. An analysis of the changes in lipid composition in MM cells (KMS-11, OPM-2) that occur following treatment with the GPX4 inhibitor and ferroptosis-inducing drug RSL3, or culture with the ferroptosis substrates, ferric ammonium citrate and arachidonic acid.
C. Experiments to determine the significance of the specific polyunsaturated fatty acids (PL-PUFA) identified in A and B in relation to the sensitivity of MM cells to ferroptosis.

Aim 2: Development of novel B-cell maturation antigen (BCMA)-directed monoclonal antibodies.

Aims 2 and 3 will exploit the fact that MM cells express high levels of BCMA to develop a targeted drug delivery system. In aim 2, antibodies against a novel epitope within the extracellular domain of the BCMA protein will be developed. The steps in this aim will be as follows:

A. Supernatants from hybridomas generated from the B-cells of immunized mice will be screened for anti-BCMA antibodies using MM and DLBCL cell lines and a BCMA-negative chronic myeloid leukemia (CML) cell line. Specificity of the serum antibodies will also be confirmed using BCMA-knockout MM cell lines.

B. The functional effects of the culture supernatants containing BCMA antibodies will be tested against MM cell lines. Possible cytotoxic and anti-proliferative effects of the antibodies will be assessed using a range of methods, including flow cytometry and MTT assays. Antibody-dependent cellular cytotoxicity (ADCC) and phagocytosis will also be investigated using appropriate in vitro methodologies.
C. Next, anti-BCMA antibodies will be purified from the hybridoma supernatants that demonstrated efficacy in A and B, by sub-cloning from the relevant hybridomas. The binding and functional effects of the resulting anti-BCMA monoclonal antibodies will be assessed against MM cell lines and the BCMA-negative K562 cell line to confirm the specificity of the antibodies.

Aim 3: Generation and testing of functionalised ferroptosis-inducing liposomes

Aim 3 will use an innovative approach to develop a novel, targeted drug delivery system. Using our data concerning the lipid composition of MM cells and our novel anti-BCMA antibody, we will generate liposomes that are comprised of ferroptosis substrates (PL-PUFA) and functionalised with a BCMA antibody. The aim is to develop nanoparticles that specifically target MM cells and deliver lipids that sensitise MM cells to ferroptosis-mediated cell death.

A. Liposomes tailored to MM cell lines will be manufactured using a NanoAssemblr® Ignite™ instrument. A fluorescently conjugated lipid within the liposomes will be used to confirm uptake into the MM cells. The effects of the liposomes on cell viability, oxidised lipids and ferroptosis induction will be assessed using Annexin V/PI, C11-BODIPY, and Liproxstatin-1 via flow cytometry, respectively.
B. The liposomes will then be developed further by encapsulating ferroptosis-inducing compounds, including ferric ammonium citrate and/or RSL3. Ferroptosis-mediated cell death of MM cells will then be assessed as described in stage A of this aim. The effects of these liposomes will be compared to those of liposomes that do not contain ferroptosis-inducing compounds.
C. The final stage will be to test whether functionalising liposomes with an antibody increases their specificity and effects against MM cells. Analyses will include those described in stages A and B towards MM cell lines, and a cell line derived from healthy cells, FH9.

CHAPTER 2. MATERIALS AND METHODS

2.1 Materials

2.1.1 Cell lines and cell culture

The human MM cell line, RPMI-8226 (ATC CCL-155), was purchased from the American Type Culture Collection (ATCC, Manassas, VA, USA). The KMS-11 (JCRB1179) human MM cell line was purchased from CellBank Australia (Sydney, Australia). The LP-1 (ACC 41) and OPM-2 (ACC 50) human MM cell lines were purchased from the Leibniz Institute DSMZ—German Collection of Microorganisms and Cell Cultures GmbH (Braunschweig, Germany). The NCI-H929 line was kindly provided by Prof. Andrew Spencer (Monash University, Victoria, Australia), and KMS-18 cells were kindly provided by Prof. Junia Melo (South Australia Pathology, Adelaide, Australia). The DLBCL cell lines SU-DHL-8, OCI-Ly19, Farage, U-2932 and HBL-1 were supplied by Dr Giles Best (Flinders University). All cells were cultured in RPMI-1640 (Gibco, Waltham, MA, USA) supplemented with 10% foetal bovine serum, 50 units/mL penicillin, 0.25 mg/mL streptomycin, 2 mM L-glutamine and 15 mM HEPES buffer (all Gibco). Cells were maintained at 37°C in 5% CO_2. All cell lines were genetically authenticated by the Australian Genome Research Facility (AGRF; Adelaide, Australia) and determined mycoplasma-free using the MycoStrip™ - Mycoplasma Detection Kit (InvivoGen, San Diego, CA, USA).

2.1.2 Drugs, chemicals, and other reagents

(1S,3R)-RSL3 (RSL3) and liproxstatin-1 were purchased from Selleck Chemicals (Houston, TX, USA). The lipids, 16:0 PE, 16:0-18:1 PE, 16:0-18:2 PE, 16:0-20:4 PE, 16:0-22:6 PE, 1,2-distearoyl-sn-glycero-3-phosphoethanolamine-N- [amino (polyethylene glycol)-2000] (DSPE-PEG2000 Amine), Carboxy NHS, 1,2-distearoyl-sn-glycero-3-phosphoethanolamine-N-[carboxy(polyethylene glycol)-2000, NHS ester] (DSPE-PEG(2000) Carboxy NHS), 1,2-distearoyl-sn-glycero-3-phosphocholine (DSPC) and cholesterol were purchased from Sigma-Aldrich (St. Louis, MO, USA). FITC-conjugated Annexin V and Annexin V Binding Buffer were purchased from Becton Dickinson Biosciences (Franklin Lakes, NJ, USA). Propidium iodide was purchased from Sigma-Aldrich. BODIPY™ 581/591 C11 (D3861) and goat anti-human IgG Fc

secondary antibody, PE were purchased from Thermo Fisher Scientific (Waltham, MA, USA). Carboxyfluorescein succinimidyl ester (CFSE) was purchased from Jomar Life Research (Mulgrave, Victoria, Australia).

2.1.3 Antibodies and reagents

GPX4 anti-human polyclonal antibody (52455S) and TNFRSF17/BCMA anti-human polyclonal antibody were purchased from Cell Signalling Technology (Danvers, Massachusetts, USA). Goat anti-rabbit and anti-mouse IgG and peroxidase conjugated secondary antibodies were purchased from Cell Signalling Technology. Anti-actin clone C4 (MAB1501) was purchased from Merk Millipore (Burlington, MA, USA). cOmplete EDTA-free Protease Inhibitor Cocktail was purchased from Sigma Aldrich. Precision Plus Protein All Blue and Kaleidoscope Pre-stained Protein Standards molecular weight ladders were purchased from Bio-Rad (Hercules, California, USA).

2.2 Cell biology

2.2.1 Cell counts and viability

Viable cells were enumerated by mixing 10 µL of cell suspension in a 1:1 ratio with 0.4% trypan blue (Life Technologies, Carlsbad, CA, USA) and counted using a haemocytometer.

2.2.2 Live cell imaging

50 µl poly-L-ornithine (Sigma Aldrich) was added to each well of a 96 well plates and incubated for 1 hour at ambient temperature, the solution was then removed from the wells and then plates were dried for 1 hour. 5,000-10,000 cells with or without treatment were added to each well. Images were obtained every hour for up to 24 hours using an IncuCyte® S3 Live-Cell Analysis System (Sartorius AG, Gottingen, Germany) at 20x magnification.

2.2.3 Assessment of cell proliferation

Cell proliferation was assayed using the thiazolyl blue tetrazolium bromide (MTT) assay. Cells were cultured at a density of 3 x 10^5 cells/mL with or without treatment for 20 hours at 37 °C, in a final volume of 100 µL. 10 µL of MTT was then added at a final concentration of 5 mg/mL

before plates were incubated for 4 hours at 37 °C. 100 µL of solubilisation solution was then added and the plates incubated overnight at 37 °C. Absorbance was recorded the following day at a 570 nm using a CLARIOstar plus microplate reader (BMG Labtech, Ortenberg, Germany).

Cell proliferation was confirmed using carboxyfluorescein succinimidyl ester (CFSE) assay. Cells were washed in serum free RPMI-1640 media and stained with 1 µM of CFSE for 15 minutes at 37 °C. Cells were then washed in serum free RPMI-1640 media and resuspended in complete culture media. 2 x 10^4 cells/mL cells were then plated in 96 well plates with or without treatment and incubated at 37 °C. Cells were harvested and readings taken every 24 hours at excitation/emission wavelengths of 488/525 nm using a CytoFLEX SRT (Beckman Coulter, Brea, CA, USA) flow cytometer.

2.3 Flow cytometry

2.3.1 Assessment of cell viability

Cells were initially cultured at a cell density of 3 x 10^5 cells/mL with or without treatment for up to 24 hours. Liproxstatin-1 was added to the cell culture simultaneously with other treatments. Cells were washed in phosphate buffered saline (PBS) before staining with 0.27 µg/mL FITC- conjugated Annexin V and 0.4 µg/mL propidium iodide (PI) in 1X Annexin V Binding Buffer for 10 minutes in the dark at room temperature. Intact cells were gated based on their size (forward scatter, FSC) and internal complexity (side scatter, SSC). Doublets were excluded by area scaling of the FSC area and height properties. Data from a minimum of 10,000 intact single cells was acquired either on a CytoFLEX S or CytoFlex SRT flow cytometer (Beckman Coulter), with analysis performed using CytExpert Software (Beckman Coulter). Cells negative for both Annexin V and propidium iodide were considered viable.

2.3.2 Assessment of lipid ROS

Cells were cultured with or without treatment for 24 hours at 37 °C. 30 minutes prior to the end of the treatment, a final concentration of 400 nM C11 BODIPY-FITC was added to relevant wells before a further 15 min incubation. Cells were then washed twice with PBS and re-suspended in fresh PBS prior to analysis by flow cytometry, as described above.

2.3.3 Nano-Flow cytometry

Antibody conjugated liposomes, produced according to the methods described below, were assessed using a CytoFLEX nano flow cytometer (Beckman Coulter). The presence of the humanised anti-CD38 antibody, daratumumab, on the surface of the liposomes was assessed by incubating the liposomes with a phycoerythrin (PE)-conjugated, goat anti-human IgG Fc secondary antibody, at a final concentration of 1 μg/mL for 30 minutes. The liposomes were then diluted 4-fold in Milli-Q ultrapure water. Data acquisition and analysis was kindly performed by Dr. Giles Best using CytExpert Nano Software (Beckman Coulter).

2.3.4 Western blot assay

4 x 10^6 cells were cultured with the drugs of interest for the times indicated in the relevant figures. The cells were then harvested and lysates prepared as follows: cells were washed twice in cold PBS, and 150 µL ice cold lysis buffer (10 mM Tris/HCl pH 7.4, 137 mM NaCl, 10 % glycerol, 1 % NP40, 1M β-glycerophosphate, 200 mM sodium fluoride and cOmplete EDTA free protease inhibitor cocktail) added to the cell pellet with vortexing. Cells were kept on ice for 10 minutes before centrifugation at 14,000 x g to clarify the lysate. The supernatant was then removed and stored at -20 °C until required. The bicinchoninic acid (BCA) assay (Pierce BCA Protein Assay Kit) (ThermoFisher, Massachusetts, USA) was used to quantify the protein content of lysates, as per the manufacturers recommendations, with absorbance readings at 570 nm on a Packard Bioscience Fusion Microplate Reader (PerkinElmer, Waltham, Massachusetts, USA). Cell lysates containing 30 µg of protein were made up to a final volume of 20 µL by addition of 4 µL 5X sample buffer (50 mM Tris/HCl pH 8, 5 mM EDTA, 100 mM DTT, 5% SDS (w/v), 50 % glycerol and 0.1 % bromophenol blue) and ultrapure water. The samples were then boiled at 100°C for 5 minutes before being loaded onto MiniPROTEAN TGX Precast Gels (Bio-Rad, California, USA), together with a molecular weight ladder (Bio-Rad). Gels were then run at 250 volts/ 300 mA in the Mini-PROTEAN Tetra Cell immunoblotting tanks for 25 minutes or until the dye front reached the bottom of the gel. The gels were then removed from their cassettes and placed into transfer stacks. Proteins were transferred from the gels onto nitrocellulose membranes using the Trans-Blot Turbo Transfer System (Bio-Rad) under conditions specified by the manufacturer. Non-specific binding of antibodies was inhibited by incubating the membranes in blocking solution, which was comprised of 5% non-

fat dairy milk powder dissolved in 1X Tris-buffered saline solution with Tween-20 (TBST; 50 mM Tris (pH 7.4), 1.5 M NaCl and 1% Tween20). Blocking was performed at room temperature, with gentle rocking for two hours. Membranes were then incubated with primary antibodies, which were diluted 1:1000 (1:5000 for anti-actin) in blocking solution. Membranes were then washed 3 times in 1X TBST for 5 minutes per wash, before being incubated in horse radish peroxidase (HRP)-conjugated secondary antibody diluted 1:15,000 in blocking solution, for 2 hours at room temperature. After another three, 5-minute washes in 1X TBST, membranes were incubated for 5 minutes in Clarity Western ECL Substrate (Bio-Rad) according to the manufactures recommendations, before being imaged on a ChemiDoc MP (Bio-Rad) using the Chemi High Sensitivity blot protocol for an appropriate exposure time. Image Lab Software (Bio-Rad) was used for densitometric analysis of Western blot images.

2.4 Lipidomics

2.4.1 Lipidomics sample preparation

Cells were cultured at a density of 3 x 10^5 cells/mL with or without treatment for 4 hours. Cell suspensions were washed in PBS and stored as dry pellets at -80°C before processing. Subsequent sample processing and analysis by liquid chromatography/mass spectrometry was performed in the Lipidomics and Metabolomics core facility at the South Australian Health and Medical Research Institute (SAHMRI, Adelaide, Australia). All samples were prepared in duplicate and protein concentrations determined using the bicinchoninic acid (BCA) assay (Thermo Fisher Scientific), as per the manufacturer's instructions. An extraction buffer consisting of acetonitrile/isopropanol/splash mix (99:99:2, v/v) was made fresh and 100 µL added to the equivalent of 10 µg of protein from each sample. Samples were then sonicated for 10 minutes and incubated at –20 °C for one hour. Samples were centrifuged at 16,000 *x g* for 15 minutes and the supernatant transferred to a glass vial. A pooled quality control sample was prepared by combining 10 µL of supernatant from all samples in a glass vial. Samples were then run on a XEVO G2-XS QTOF liquid chromatography/mass spectrometer (Waters Corporation, Milford, MA, USA) according to a lipidomics assay protocol established at SAHMRI (33). Sample data were processed and analysed using Skyline Targeted Mass Spec Environment (34), MetaboAnalyst (Wishart Research Group, Alberta, Canada) and Microsoft Excel. Heatmaps and Volcano plots were generated using

MetaboAnalyst. Data were normalised to the median, log10 transformed, auto-scaled (mean-centred) and divided by the standard deviation of each variable.

2.5 Monoclonal antibody screening

2.5.1 Supernatant screening: cell surface binding

A total of 70 supernatants were received from the Monash Antibody Discovery Platform (MADP). To assess for the presence of anti-BCMA antibodies in the supernatants, MM and CML cells were washed in 1X PBS and cell pellets incubated with 100 µL of undiluted hybridoma supernatant. Cells were incubated at a cell density of 1 x 10^6 cells/mL at room temperature, in the dark for 30 minutes. Cells were then washed with PBS and the cell pellets stained with 1:50 R-Phycoerythrin (PE) conjugated AffiniPure goat anti-mouse IgG (Stratech Scientific, Cambridgeshire, UK) at room temperature, in the dark, for 30 minutes. Samples were then washed and resuspended in PBS and assessed for antibody binding by flow cytometry.

2.6 Transformation and transfection

2.6.1 Transforming and culturing bacteria for DNA amplification

Competent *Escherichia coli* (XL-10 gold cells) was kindly donated by the Janovjak lab (Flinders University). BCMA cDNA ORF Clone, Human, C-GFPSpark® tag and pCMV3-C-GFPSpark Control Vector (C-terminal GFPSpark-tagged) were purchased from Jomar Life Research. XL-10 bacteria were thawed on ice for 5 minutes, and 1 µL DNA added to the cells and mixed gently by stirring. The cells were then incubated on ice for 20 minutes and then plated on LB agar plates with 50 µg/mL kanamycin (Sigma Aldrich) using a sterile spreader. Plates were incubated overnight at 30°C. The following day, single colonies were picked using a toothpick and added to 2 mL of broth culture before being incubated overnight on a shaker at 37°C. Stocks of the bacteria were prepared the following day by adding 500 µL of cells in broth to 500 µL 80% glycerol stock (ChemSupply, Adelaide, Australia). DNA extraction was performed using a Monarch Plasmid Miniprep kit (New England BioLabs, Ipswich, Massachusetts, USA). DNA purity and concentration were assessed using a NanoDrop 8000 instrument (ThermoFisher).

2.6.2 Digesting and running DNA on gel

Cut smart (New England Biolabs), DNA, nuclease free H_2O and XbaI and KpnI restriction enzyme (kindly donated by Professor Janni Peterson) were added to an Eppendorf tube and incubated in a heat block at 37°C, for between 20 minutes and 2 hours. Digested samples were mixed with loading buffer (kindly donated by Professor Janni Peterson) at a ratio of 1:5 and added to appropriate wells of the agarose gel (Agarose powder, TAE and GelGreen). A DNA ladder (New England BioLabs) was also added in a separate well. The gel was run at 120 volts/ 200 mA for 20-30 minutes and imaged using a ChemiDoc MP imager (Bio-Rad).

2.6.3 Sanger sequencing

DNA and specific primers for BCMA (Merk Millipore, Massachusetts, USA) were provided at relevant concentrations to GNOMIX sequencing team (Adelaide, Australia). Sequencing results were analysed using Benchling (Benchling, San Francisco, USA).

2.6.4 Transfection

One day prior to transfection, 0.4 – 0.6 x 10^5 human embryonic kidney (HEK293t) or Chinese hamster ovary (CHO) cells were plated in a 6 well plate in 2 mL of growth medium, without antibiotics. These cell densities resulted in 80-90% confluency after 24 hours. For a single reaction, 10 µL of Lipofectamine™ 2000 Transfection Reagent (ThermoFisher) was diluted in 240 µL of Opti-MEM (ThermoFisher) and incubated for 5 minutes at room temperature. At the same time, 4 µg of plasmid DNA was also diluted in 240 µL Opti-MEM and incubated for 5 minutes at room temperature. The samples containing the diluted Lipofectamine™ 2000 Transfection Reagent and DNA were then combined, mixed gently, and incubated at room temperature for 20 minutes. 500 µL of the lipofectamine/DNA complex was then added to appropriate wells containing the HEK293t or CHO cells and mixed by gently rocking the plates. Cells were then incubated for 48-72 hours at 37°C. Transfection efficiency was assessed using an EVOS M5000 Imaging System (ThermoFisher), and flow cytometry on a CytoFLEX S instrument (Beckman Coulter). GFP-positive were then isolated using a FACSAria™ Fusion instrument (Becton Dickinsons, Franklin Lakes, NJ, USA).

2.7 Liposome preparation

2.7.1 Micro-fluidics synthesis

A Nanoassemblr® ignite system (Precision Nanosystems, Vancouver, BC, Canada) was used to prepare all formulations using the following parameters: total flow rate = 12mL/min, flow ratio = 3:1 (aqueous: organic), total volume = 4mL, start and end waste = 0.01mL. Lipids were dissolved in 1mL of ethanol as the organic phase to produce a final lipid concentration of 1mg/mL. Drug free liposomes were prepared using PBS (pH = 7.4) as the aqueous phase. Liposomes were prepared in an organic phase consisting of PE (16:0_22:6): DSPE-PEG2000 at ratios of 98:2 (w/w%). Synthesised liposomes were dried under N_2 gas to remove excess solvent. Liposomes containing a Rhodamine B-conjugated lipid at a concentration of 1 µg/mL were also synthesised to enable liposome uptake to be assessed by flow cytometry.

2.7.2 Liposome characterisation

The various liposome formulations were characterised by dynamic light scattering (DLS) using a Malvern Zetasizer Nano ZS at 25°C (Malvern Panalytical, Worcestershire, UK). Samples were diluted 10-fold with Milli-Q ultrapure water (Merck Millipore) for all size measurements. Results were reported as a mean hydrodynamic diameter ± standard deviation, and polydispersity index (PDI). Zeta potential, which is a measure of liposome charge was also measured using the Malvern Zetasizer. Undiluted samples were used for zeta potential measurements, with results reported as the average zeta potential ± standard deviation. A Nanosight NS300 instrument (Malvern Panalytical) was used to assess the size and the number of liposomes present. For these measurements, samples were diluted 200-fold with Milli-Q ultrapure water.

2.7.3 Assessment of liposome uptake

Cells were cultured, with or without, liposomes containing the PE (18:1) (lissamine rhodamine B sulfonyl)-conjugated lipid (approximately 1 µg/mL in 1 mg/mL liposome concentration) at concentrations of up to 50 µg/mL, for 24 hours at 37 °C. Cells were then washed with PBS and resuspended in fresh PBS. The proportion of cells containing the fluorochrome-tagged lipid was determined by flow cytometry, as described above.

2.7.4 Assessment of liposome RSL3 encapsulation

Liposomes were prepared, with or without, varying concentrations of RSL3. Ultrafiltration using an Ultracell Ultrafiltration system fitted with a PES 5 kDa membrane filter (Merck Millipore) was then used to remove free RSL3. The liposome solutions were weighed before and after filtration to account for volume lost during filtration before dilution at a 1:1 ratio in the mobile phase and analysis, as described below.

2.7.5 High-performance liquid chromatography

High-performance liquid chromatography (HPLC – Shimadzu Nexera XR) and a Phenomenex Luna 5 µm C18(2) 100 Å, LC Column 250 x 4.6 mm (Phenomenex, Torrance, CA, USA) HPLC column were used to determine the concentration of RSL3 encapsulated within the liposomes. Conditions were as per manufacturer's instructions and are described below, with alterations to account for equipment variability. The column oven was set to 25°C, with a wavelength of 280 nm and flow rate of 0.8 mL/min. Mobile phase A consisted of H_2O and 0.1 % trifluoroacetic acid (TFA), while mobile phase B was composed of acetonitrile and 0.1 % TFA. Naphthalene was used as an internal standard at a concentration of 100 µg/mL. The injection volume was 10 µL and the isocratic method used was 10 % mobile phase A/90 % mobile phase B. RSL3 standards, ranging from 5 µg/mL – 250 µg/mL, and unknown samples were prepared in mobile phase B. Peaks were detected at a retention time of 1.9 minutes. All samples were measured in triplicate with a minimum of three biological replicates.

2.7.6 Antibody conjugated liposomes

Liposomes were synthesised as described above but DSPE-PEG(2000) was substituted for DSPE-PEG(2000) Carboxy NHS in the liposomal formulation at the same ratios. Liposomes were then incubated with daratumumab at a 1:5 molar ratio of antibody to NHS-containing liposomes. The mixture was then incubated for 4 hours at room temperature on a shaker and then characterised using DLS and analysed as described above using the CytoFLEX nano flow cytometer (Beckman Coulter).

2.8 Statistical analysis

Statistical analyses were performed using a student's t-test for two-group comparisons and two-way ANOVA for comparison of more than two groups, using GraphPad Prism software (GraphPad Software, Boston, MA, USA). A P-value of < 0.05 was considered statistically significant, with differing degrees of statistical significance indicated as follows: *P < 0.05, **P < 0.01, ***P < 0.001, ****P < 0.0001. The fractional product method was used to determine synergy, with values of <0.1 indicative of synergy (189). This method determines whether the combination of drugs/agents act in synergy or have additive or antagonistic effects. Synergy is defined as two agents that exert a greater effect, we used in combination than the product of their individual effects. GraphPad Prism was used to fit 4- parameter logistic (4PL) sigmoidal dose-response models for cell viability data to determine IC_{50} values.

CHAPTER 3. PHOSPHOLIPID COMPOSITION DRIVES FERROPTOSIS SENSITIVITY IN MULTIPLE MYELOMA

3.1 Introduction

The overarching aim of this chapter is to determine the underlying factors that confer ferroptosis resistance in MM cells and to assess whether it is possible to sensitise them to this form of cell death. Yang *et al* have previously shown in a study published in 2014, that DLBCL cell lines are sensitive to ferroptotic cell death induced by erastin, an inhibitor of system X_c^-, while MM cell lines were significantly more resistant to this inhibitor. Research in our lab supports this, showing that DLBCL cell lines are more sensitive to the GPX4 inhibitor RSL3, than MM cell lines (Figure 11A). The factors that determine ferroptosis sensitivity are currently being investigated, as understanding these mechanisms is critical for developing new ferroptosis-mediated treatments. Lipids play an important role in ferroptosis, serving as key substrates for the generation of toxic peroxyl radicals. Among these, glycerophospholipids containing the functional head groups ethanolamine (phosphatidylethanolamine) and choline (phosphatidylcholine) have been shown to be particularly important in ferroptosis. The functional head group of phospholipids (PLs) influence their susceptibility to peroxidation through indirect mechanisms such as cellular localisation. Some studies suggest that the overall saturation of the lipids, more specifically, fatty acid saturation, plays a more significant role in dictating peroxidation sensitivity than the functional head groups (190, 191).

Fatty acid chains play an important role in the cell, including as key components of the plasma membrane, energy repositories and key cell signalling molecules. Polyunsaturated fatty acids (PUFA) are a type of fatty acid with more than one double bond in their carbon chain and play an important role as ferroptosis substrates (117, 191). The double bonds in the carbon chain create areas of high electron density that are sensitive to peroxidation. Importantly, free fatty acids do not appear to play a prominent role in ferroptosis (192). However, ACSL4 converts free PUFA into acyl-CoA esters and LPCAT3 then incorporates acyl-CoA into LPL, forming PLs containing PUFA (192). Both ACSL4 and LPCAT3 have been shown to regulate ferroptosis, with

knockout of either enzyme resulting in ferroptosis resistance (Figure 5) (192-195). PUFA incorporation into PLs makes it a target for either enzymatic or non-enzymatic peroxidation, both of which are catalysed by LOX (Figure 5). This peroxidation yields the highly potent PL peroxyl radicals, which trigger a chain reaction of lipid peroxidation, leading to membrane damage and eventual ferroptotic cell death. These studies highlight the importance of PUFA regulation within the cell, and mechanisms by which PUFA are primed as ferroptosis substrates through incorporation into PLs.

Monounsaturated fatty acids (MUFAs) are fatty acids that contain one double bond in the carbon chain and play an important role as inhibitors of lipid peroxidation and therefore ferroptosis (100, 108, 132). MUFAs are more stable and less prone to oxidation than PUFAs, making them less suitable as substrates for ferroptosis (100, 108, 132). The primary mechanism by which MUFAs reduce lipid peroxidation is by outcompeting PUFAs in the plasma membrane, thereby decreasing the availability of ferroptosis substrates (132). The enzyme ACLS3, which plays an important role in fatty acid incorporation into phospholipids by activating them, preferentially targets, MUFAs. This increases the proportion of these FAs in the lipidome, which leads to increased membrane fluidity, integrity, and capacity to withstand lipid peroxidation. Interestingly, new research investigating the role of membrane-bound O-acyltransferase (MBOAT) family 1 and 2 demonstrated that these enzymes preferentially incorporate MUFA into LPL, supressing ferroptosis in a GPX4 and FSP1 independent manner (196). Both endogenous and exogenous MUFAs were incorporated into LPL by MBOAT2, resulting in remodelling of the phospholipidome and a decrease in ferroptosis sensitivity. The study demonstrated that overexpression of MBOAT2 in the human fibrosarcoma cell line, HT1080, overexpression of MBOAT2 decreased the proportion of PE-PUFA and increased PE-MUFA (196). Downregulation of the MBOAT1 and MBOAT2 enzymes resulted in increased ferroptosis sensitivity of breast and prostate cancer cells, respectively (196). This work highlights the effects of changes in PL levels on ferroptosis sensitivity and the role of different fatty acids, especially MUFAs, in ferroptosis resistance.

Our knowledge concerning the role of saturated fatty acids (SFA) in ferroptosis is expanding, with most research suggesting that SFAs play an important role in lipotoxicity but not ferroptosis (197). However, other studies suggest that SFAs, such as palmitic acid, are actively involved in ferroptosis (198). GPX4 overexpression and ferrostatin-1 were able to protect

against palmitic acid-induced lipid ROS, but not against cell death (198). In contrast, the SFA, stearic acid, has been shown to protect cardiomyocytes from ferroptosis, by displacing PUFAs with SFAs, which are less prone to oxidation (199). Although SFAs are mainly associated with lipotoxicity, there is growing evidence that SFAs can act as both inhibitors and promoters of ferroptosis, suggesting that they may have a complex and context-dependent role in ferroptosis.

The current study sought to determine the role of PUFAs and MUFAs in ferroptosis of MM cells. The proportions of MUFAs and PUFAs were investigated in cell lines from two haematological cancers, MM and DLBCL, using untargeted lipidomics analysis. DLBCL cell lines were chosen for comparison to the MM cell lines as we and others have shown that they are significantly more sensitive to ferroptosis, induced by indirect and direct inhibition of GPX4, than MM cells. MM cancer cell lines were cultured with PE lipids with varying degrees of unsaturation (SFA, MUFA, PUFA), with and without the GPX4 inhibitor, RSL3. A lipidomics analysis was performed after addition of the PE lipids, to investigate changes in the phospholipidome. The effects of PE supplementation on cell viability and lipid ROS were also investigated. It was hypothesised that cell lines containing a higher proportion of unsaturated PLs would be more sensitive to ferroptosis induced by RLS3. A large body of this work has now been peer review and published (Publication 2 in the Appendix).

3.2 Results

3.2.1 Multiple myeloma cells typically display resistance to ferroptosis induction via GPX4 inhibition while diffuse large B cell lymphoma cells display sensitivity

GPX4 catalyses the reduction of PL hydroperoxides into their corresponding alcohols, decreasing lipid ROS levels and inhibiting ferroptosis (113). A previous study has shown that indirect inhibition of GPX4 with the cysteine antiporter X_C^- inhibitor, erastin, induces ferroptosis in DLBCL and that MM cell lines are significantly less sensitive to the inhibitor (136). Data by PhD student Rachel Mynott demonstrated similar effects in MM and DLBCL cells using RSL3, a small molecule inhibitor that directly inhibits GPX4 by binding to the catalytic selenocysteine residue of the enzyme (Figure 11A). Cell death was observed in all 5 of the DLBCL cell lines tested, with an average IC_{50} value of 354.41 ± 170.04 nM. With the exception of OPM-2 cells, the MM lines were significantly less sensitive to RSL3, with an average IC_{50} value of 4722.50 ± 1741.65 nM(Figure 11A). Expression of GPX4 was examined by Western blotting to determine if this was related to the sensitivity of the cells to RSL3. While differences in GPX4 expression were observed between the lines, no correlation between sensitivity to RSL3 and GPX4 expression were observed (Figure 11A-C). Much of the work in this figure was data generated by past PhD student Rachel Mynott.

Ferroptosis is associated with characteristic changes in cell morphology, including a “ballooning” of the cytoplasm. Using an IncuCyte® S3 Live-Cell Analysis System, we observed morphological changes that are consistent with ferroptosis in both the MM and DLBCL cells, with the RSL3 sensitive OPM-2 (MM) cell line displaying the ferroptotic morphology when cultured with the relatively low dose of 200 nM RSL3 for 24 hours (Figure 11D). The effects of RSL3 on cell viability (200) and morphology were inhibited by the synthetic antioxidant, liproxstatin-1, which supports the assertion that the changes observed were associated with ferroptosis.

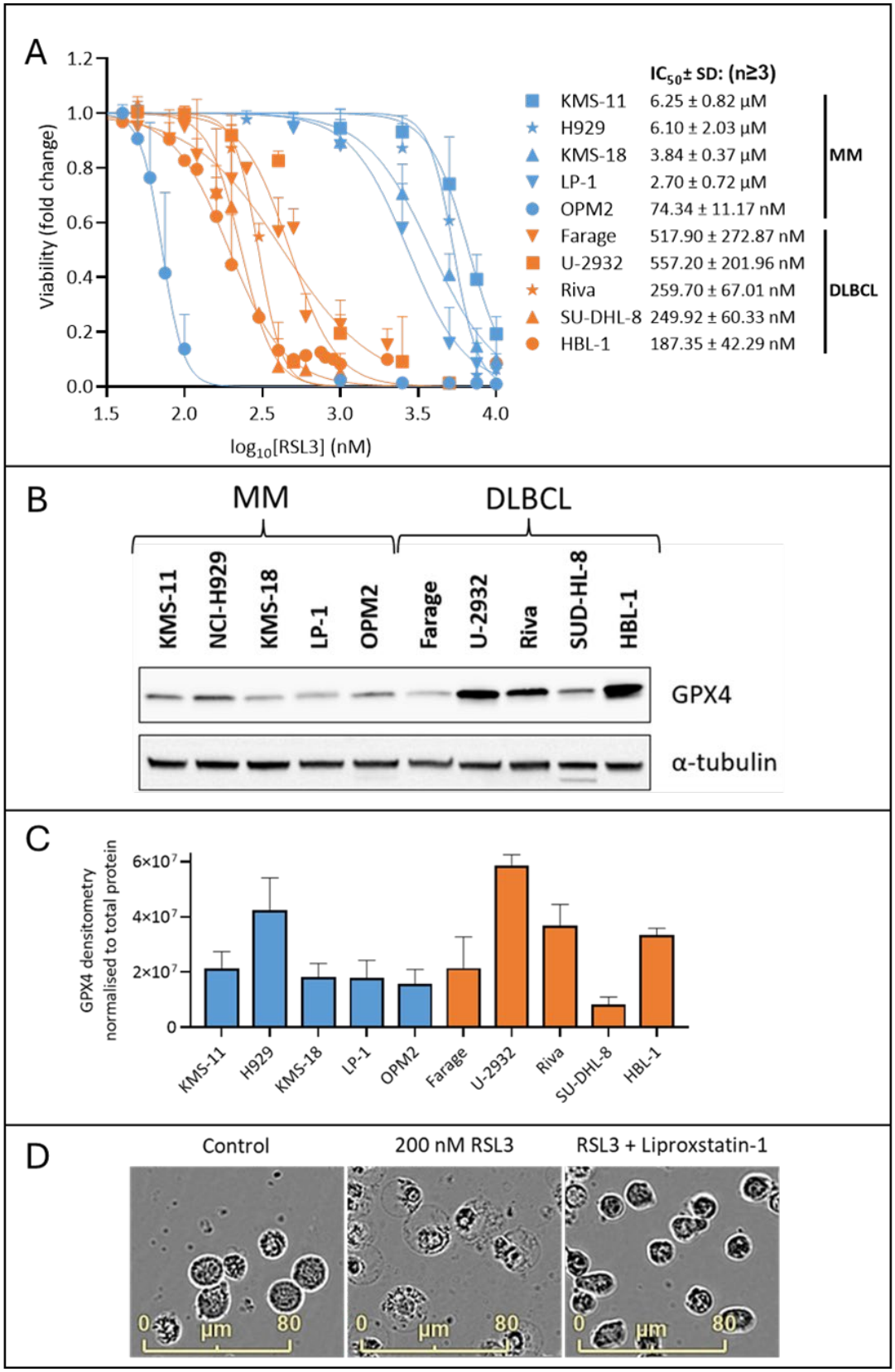

Figure 11. MM cell lines, with the exception of OPM2 cells, are significantly less sensitive to RSL3 than DLBCL cell lines.

(A) Cell viability was assessed by annexin V/PI staining and flow cytometry in the 5 MM and 5 DLBCL cell lines indicated, following treatment with RSL3 for 24 hours. Dual annexin V/PI negative cells were

considered viable. The mean ± standard deviation of duplicate measurements are shown from at least 3 independent experiments. **(B)** Western blot for GPX4 expression in untreated MM and DLBCL cells. Alpha tubulin expression was assessed as a loading control. **(C)** Western blot densitometry data are mean (normalised to total protein) ± standard deviation from a minimum of three independent experiments. **(D)** Untreated OPM-2 cells, OPM-2 cells cultured with 200 nM RSL3, and OPM-2 cells cultured with 200 nM RSL3 and 2 µM liproxstatin-1, for 24 hours. Images were captured at 20x magnification using an IncuCyte S3 live cell analysis instrument.

3.2.2 Differential lipid expression in MM and DLBCL cells may be associated with sensitivity to ferroptosis

PLs containing PUFAs (more than one double bond in the fatty acid chain) play an important role as ferroptosis substrates, with peroxidation of these lipids being a crucial step in ferroptosis (131). In contrast, PLs containing MUFA (one double bond in the fatty acid chain) have been shown to inhibit ferroptosis (191). The phospholipidome of 5 MM and 5 DLBCL cell lines was assessed by liquid chromatography-mass spectrometry (LC-MS). The resulting data were first analysed using MetaboAnalyst, a publicly available lipidomics processing software, to generate heatmaps comparing the lipid profiles of the MM and DLBCL cell lines.

The heatmap generated from MetaboAnalyst revealed the top 25 differentially expressed lipids when the MM and DLBCL cell lines were grouped. The trend in the data showed that the DLBCL cells were composed of a higher proportion of PE and PC lipids containing PUFAs than the MM cells (Figure 12). Interestingly, many of the highly expressed lipids containing PUFAs in the DLBCL lines were ether lipids. Ether lipids are a unique class of lipids with an ether bond (O-) found between the glycerol backbone and a fatty acid chain and have been shown to play an important role in ferroptosis susceptibility (201). Two of the most differentially expressed lipids in the dataset were ether lipids, with the DLBCL cell lines exhibiting higher levels compared to the MM cell lines (Figure 13A). In contrast, MM cell lines were found to contain higher levels of PL-MUFAs than the DLBCL cells (Figure 12). In contrast to the DLBCL lines, the PLs expressed at high levels in the MM cell lines mainly contained ester, not ether bonds. The two most differentially expressed lipids between the MM and DLBCL lines were MUFAs containing phosphatidylinositol lipids (Figure 13A-B).

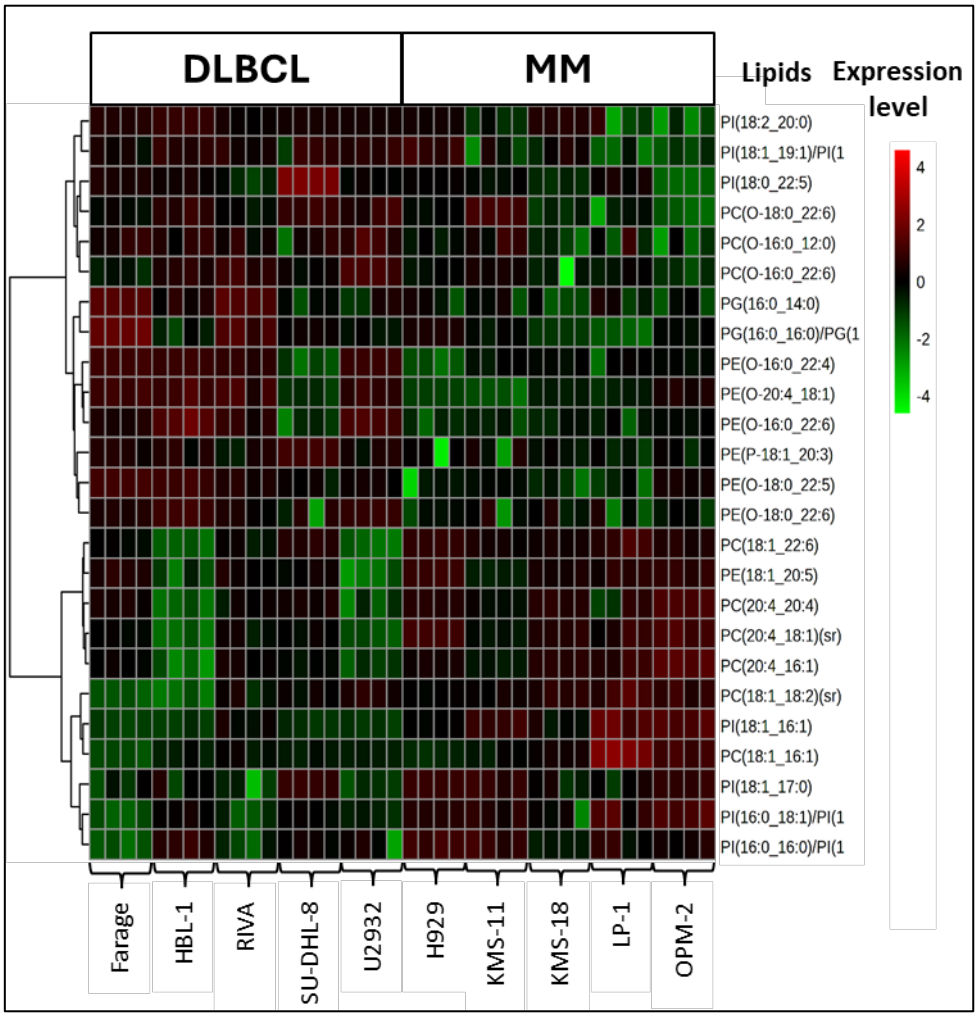

Figure 12. MM cell lines have a higher proportion of PL-MUFA, whereas PL-PUFA were higher in the DLBCL cell lines.

Heatmap of the 25 most differentially expressed lipids between the MM and DLBCL lines. Data presented are from 4 biological replicates per cell line.

PC: phosphatidylcholines, PE: phosphatidylethanolamine, PG: phosphatidylglycerol, PI: phosphatidylinositol.

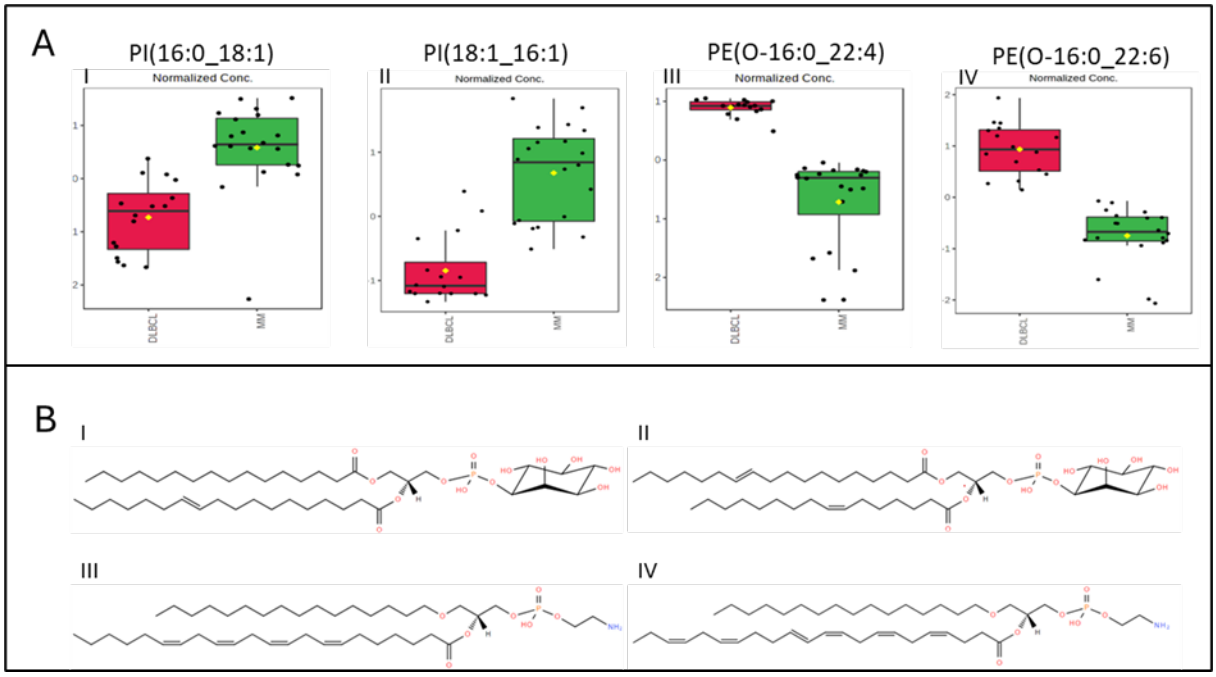

Figure 13. Comparative Analysis of Lipid Expression and Chemical Structures of Lipids in MM and DLBCL Cell Lines.

(A) Boxplots showing levels of the highly expressed lipids in MM and DLBCL cell lines identified from data presented in Figure 12. Data are the median and the interquartile range from a minimum of 4 biological replicates per cell line. **(B)** Chemical structures of the phospholipids identified in (A). PC: phosphatidylcholines, PE: phosphatidylethanolamine, PG: phosphatidylglycerol, PI: phosphatidylinositol.

3.2.3 Phospholipid proportions may dictate ferroptosis sensitivity in DLBCL and MM

To examine the acyl chains within the PLs in more detail, the PLs were grouped as follows: 1) PLs with completely saturated acyl chains (SFA), 2) PLs containing a combination of SFA and MUFA (MUFA), 3) PLs containing both MUFA and PUFA (MUFA/PUFA), or 4) PLs containing a combination of SFA and PUFA (PUFA). Due to their low abundance, phospholipids containing SFA/MUFA or MUFA/MUFA were grouped together and those containing SFA/PUFA or PUFA/PUFA were also grouped together. PLs typically contain a SFA in the *sn1* position, whereas the *sn2* position can contain SFA, MUFA or PUFA (202). PLs that contain both ferroptosis substrate (PUFAs) and a known ferroptosis inhibitor (MUFAs) are not well understood in the literature, suggesting that these lipids may have unique roles in ferroptosis that may be worthwhile investigating in the future.

The most notable difference between the two cancer types appears to be in the proportions of PLs containing PUFA or MUFA (Figure 14A). The DLBCL cell lines were found to contain significantly ($P<0.01$) higher levels of PL-PUFA (38.52% ± 2.72% of the total phospholipidome) in comparison to the MM cell lines (33.76% ± 6.20%) (Figure 14A). In contrast, the MM cell lines had significantly ($P<0.0001$) higher levels of PL-MUFA, which constituted up to 49.36% ± 7.58% of their total PL content, compared to 39.35 ± 6.62% in the DLBCL cells (Figure 14A-B). There was also a significant ($P<0.001$) difference between DLBCL and MM lines in the levels of PLs containing SFA only, however SFA levels were under 10% in all the lines from both cancers (Figure 14A). There was no significant difference in the levels of MUFA/PUFA PLs between the MM and DLBCL lines (Figure 14A). In addition to distinct differences between the two cancers, differences in the PL composition between each of the cell lines were also observed (Figure 12 and Appendix Figure 2). Interestingly, among the specific PUFA containing lipids in the MM and DLBCL cell lines, docosahexaenoic acid (22:6) stood out; in the DLBCL cell lines, PLs containing docosahexaenoic acid made up 7.17% of the lipidome, while significantly less ($P<0.001$) was detected in the MM lines, at 5.52% of the lipidome.

Next, we compared the phospholipidome of the ferroptosis sensitive and resistant MM cell lines, OPM-2 and KMS-11, respectively (Figure 14A). A higher proportion (40.12% ± 8.44%) of PUFAs were identified in the OPM-2 cells compared to MUFA (36.57 ± 11.91%) (Figure 14A).

In contrast, the lipid profile of KMS-11 cells was almost the reverse, with the largest proportion of lipids identified as MUFAs (53.36 ± 4.20%), with a significantly ($P<0.0001$) smaller proportion of PUFAs (33.65 ± 2.62%) (Figure 14B). There was also a statistically significant difference in MUFA ($P<0.001$) and PUFA ($P<0.05$) between the two cell lines (Figure 14A). Interestingly, the OPM-2 cell line had significantly greater proportions of SFA ($P<0.01$) and MUFA/PUFA ($P<0.001$) than the KMS-11 cell line (Figure 14B). Some studies suggest that SFA plays a role in promoting ferroptosis induction, while others suggest that they play a role in protecting against ferroptosis, suggesting that the effects of SFAs may be context dependent (Publication 3 in the Appendix). The role of PLs containing both MUFA and PUFA has yet to be fully elucidated but there is some evidence suggesting they may influence ferroptosis sensitivity.

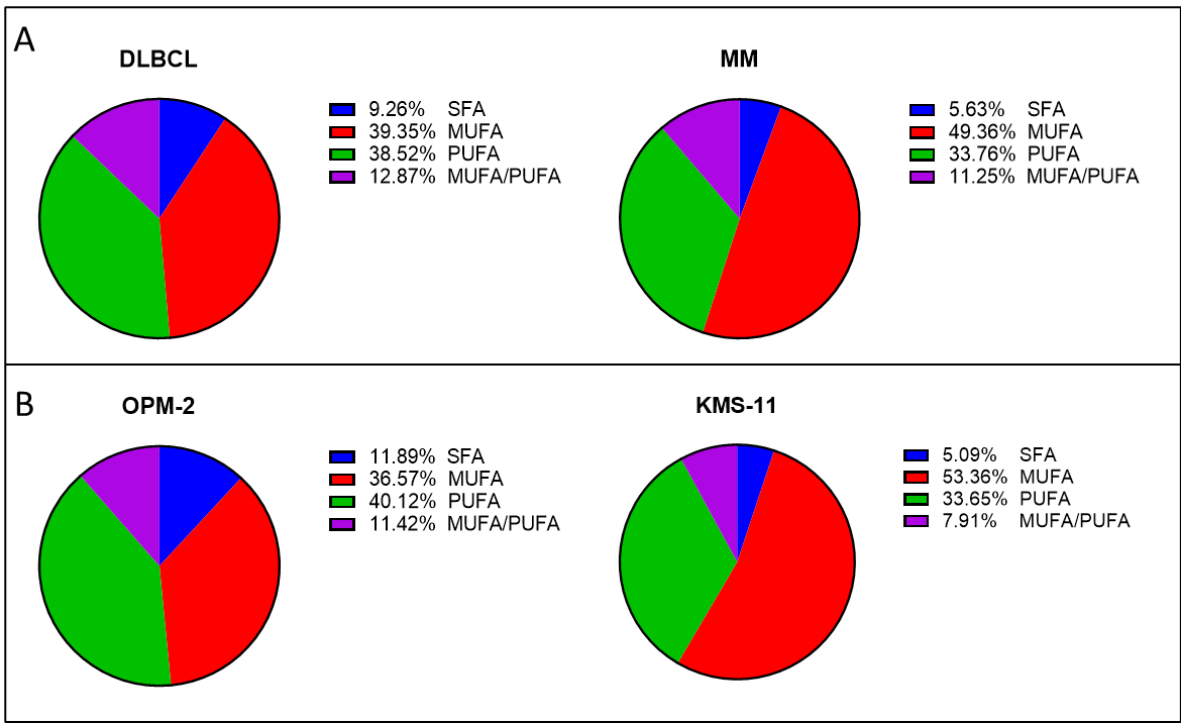

Figure 14. Distinct differences in the phospholipid composition of MM and DLBCL cells

(A) Analysis of data pooled from the MM (excluding ferroptosis-sensitive OPM-2) and DLBCL lines showing the proportions of each PL acyl chain. Proportions were calculated from LC-MS data as the peak area of each acyl chain relative to the total PL peak area. Data are the mean of a minimum of 4 biological replicates per cell line. **(B)** PL composition in the OPM-2 and KMS-11 MM lines showing the proportions of each PL acyl chain. Data are the mean from a minimum of 12 biological replicates per cell line. All statistical analyses were performed using the Student's t-test on data from a minimum of 4 biological replicates. MUFA, monounsaturated fatty acid; PUFA, polyunsaturated fatty acid; SFA, saturated fatty acid.

3.2.4 Phospholipid proportions before and after culturing with ferroptosis substrates

Iron plays an important role in ferroptosis, and although not the primary focus of this chapter, was investigated in context of ferroptosis in the MM cell lines. Ferrous ion (Fe^{2+}) catalyses lipid peroxidation through the Fenton reaction, producing highly reactive hydroxyl radicals (142). Studies have shown that iron supplementation can sensitise resistant cell lines to ferroptosis, highlighting its importance as a ferroptosis substrate (203). MM cells (KMS-11 and OPM-2) were treated with iron and PUFA and changes in the lipidome assessed by LC-MS, as described earlier. These cell lines were selected due to the significant difference in

their sensitivity to RSL3. The cells lines were cultured with iron, PUFA (arachidonic acid) or RSL3 and the various combinations of these compounds, for 4 hours before being prepared for lipidomic analyses.

These compounds, alone and in combination, resulted in significant changes in the lipid composition of the OPM2 cells. The addition of arachidonic acid (AA) decreased the total proportion of PUFA in the lipidome but did not actually change the proportion of AA in the cells (Figure 15A). This observation will be discussed further below; however, this may be due to the short incubation time (four hours), dynamic shifting of the lipidome or mechanistic factors not incorporating PUFA into PLs (ACLS4). The addition of iron (ferric ammonium citrate; FAC) or RSL3 significantly decreased the proportion of PUFA in the cells, suggesting that they were being utilised as ferroptosis substrates (Figure 15A). The addition of iron and AA had a greater effect on the proportion of PUFA than iron alone, with similar results to those observed with AA alone (Figure 15A). Interestingly the decrease in PUFA proportion observed when the cells were cultured with iron and RSL3 was not greater than RSL3 alone, while the effects of AA and RSL3 in combination were similar to those of AA alone (Figure 15A).

The addition of PUFA in the form of AA had marginal effects on the lipidome of the KMS-11 cell line, inducing a non-significant increase in the proportion of PUFA (Figure 15B). Addition of iron or RSL-3 had no observable effect on the lipidome of KMS-11 cells (Figure 15B). Although iron and AA had a minor effect on the lipidome, the response was almost identical to the effects of AA alone. Since the effects of RSL3 and AA in combination were similar to those of iron and AA, it was likely that the effects on the lipidome were being induced by AA alone (Figure 15B). This is supported by the fact that treating KMS-11 cells with RSL3 and iron had little impact on the lipidome. Future experiments may investigate whether varying the treatment time may help to elucidate whether the ferroptosis-related compounds effect changes in the lipidome.

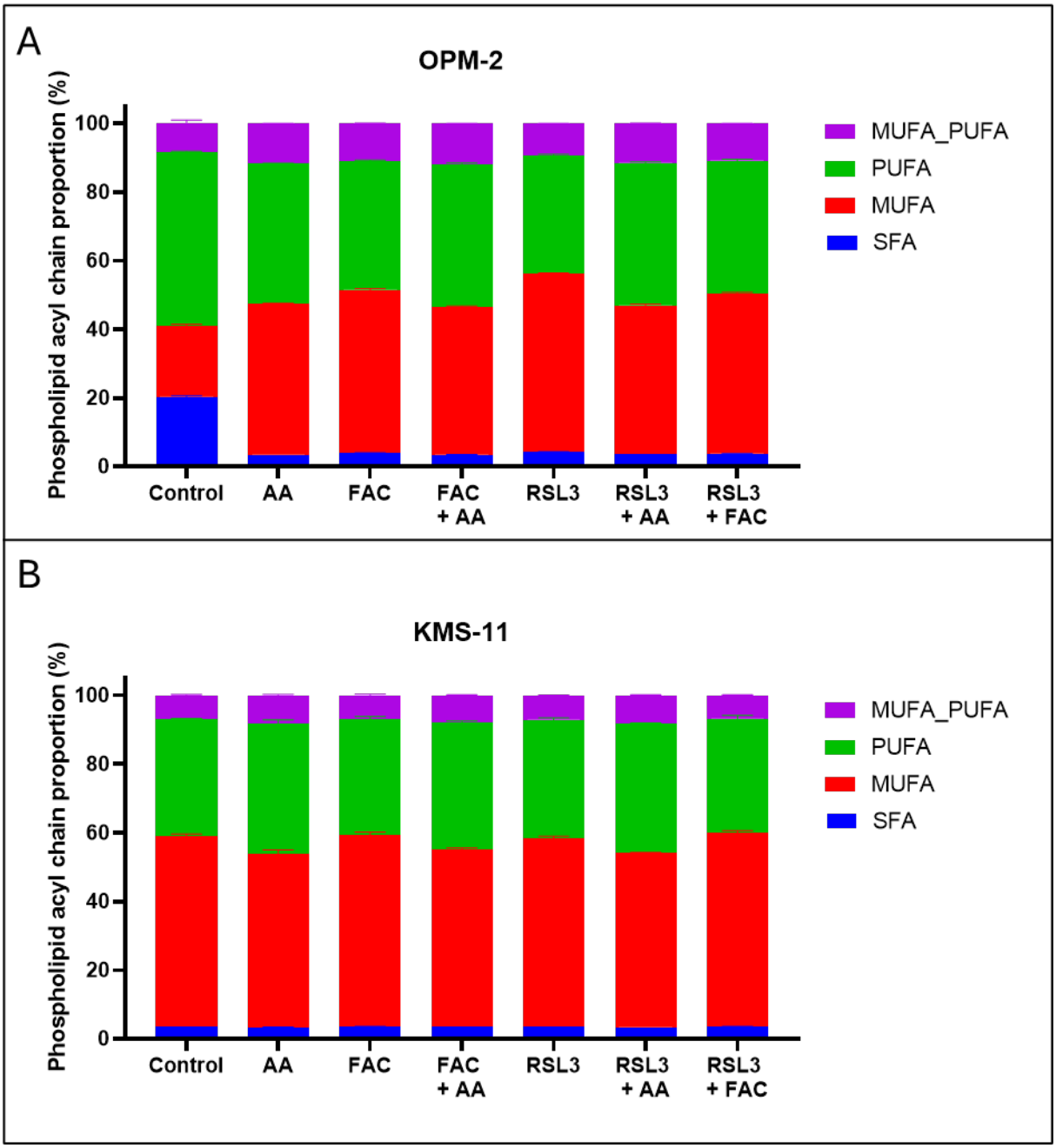

Figure 15. Ferroptosis compounds induce changes in the lipidome of OPM-2, but not KMS-11 MM cells.

(A) OPM-2 and (**B)** KMS-11 cells were cultured with 20 µM AA, 100 µM FAC or 100 nM (OPM-2) or 500 nM RSL3 (KMS-11), alone or in combination, for 4 hours. The relative proportions of each phospholipid acyl chain are shown. Data are the mean and standard deviation from a minimum of 4 biological replicates per cell line. AA, arachidonic acid; FAC, ferric ammonium citrate.

3.2.5 PE-PUFA induces ferroptotic cell death in MM cell lines independent of GPX4 inhibition

PE is an important phospholipid in cells and has been shown to be extremely relevant in the context of ferroptosis (191). We determined that PE lipids, particularly ether PE lipids, are highly expressed in the DLBCL cell lines (Figure 12). Given the importance of these lipids as ferroptosis substrates (191) and our earlier data, which showed that MM cells (excluding OPM-2), contain lower levels of PLs comprised of PUFA (Figure 14A), we hypothesised that increasing the proportion of PUFA in the lipidome of MM cells may sensitize them to ferroptosis (Figure 14). This was investigated in the RSL3 sensitive OPM-2 MM cell line and the RSL3 resistant KMS-11 MM cell line, which were cultured with PE lipids with varying degrees of unsaturation. PLs containing SFA, MUFA and PUFA were utilised in these next sections. All lipids were purchased with the same sn-1 fatty acid, while the sn-2 fatty acid was either a SFA, MUFA or PUFA. Cells were not cultured with PE-MUFA alone in this section, but this lipid species was used in the subsequent experiments.

Both cell lines demonstrated the capacity to take up the four lipids studied, as demonstrated by the significant increase in the levels of these lipids in lysates analysed by LC-MS from cells treated with the lipids (Figure 16A). However, uptake of the lipids varied between the two cell lines. Addition of PE (16:0_16:0) resulted in an 80.1 ± 31.4-fold increase in the intracellular levels of the PL in the OPM-2 cell line, while a fold change increase of 540.3 ± 156.9 was observed in KMS-11 cells (Figure 3A). Uptake of PE (16:0_18:2) was observed in both cell lines, with a 95.4 ± 34.8-fold increase in OPM-2 cells and a 65.5 ± 38.1-fold increase in KMS-11 cells (Figure 16A). Uptake of PE (16:0_20:4) was also observed in the two lines, with fold changes of 39.3 ± 33.3 and 58.8 ± 26.0 in the OPM-2 and KMS-11 cells, respectively. Following the addition of PE (16:0_22:6), we observed a 248.2 ± 41.0-fold increase in this lipid in OPM-2 cells, compared to a 439.3 ± 161.4-fold change in KMS-11 cells (Figure 16A).

Interestingly, both OPM-2 and KMS-11 cells were found to contain significantly higher levels of the lysophospholipids, lysophosphatidylethanolamine (LPE) (16:0) and LPE (22:6), following treatment with PE (16:0_22:6) (Figure 16B). Lysophospholipids are characterised by a polar head group and a single carbon chain and are typically a minor component of the total lipid composition of cells. However, studies have shown that levels of lysophospholipids significantly increase during ferroptosis, with a concomitant decrease in the corresponding

PUFA-containing PL (9, 46). In OPM-2 cells, LPE (16:0) and LPE (22:6) increased by 65.9 ± 17.0 and 4.9 ± 1.3-fold, respectively, while in KMS-11 cells, the same lipids increased by 45.2 ± 12.4 and 2.9 ± 0.6-fold, respectively (Figure 16B). No significant change in the levels of these lysophospholipids was observed in either cell line following culture with the other lipids. These findings suggest PE (16:0_22:6) may be consumed during ferroptosis, resulting in the formation of the corresponding lysophospholipids.

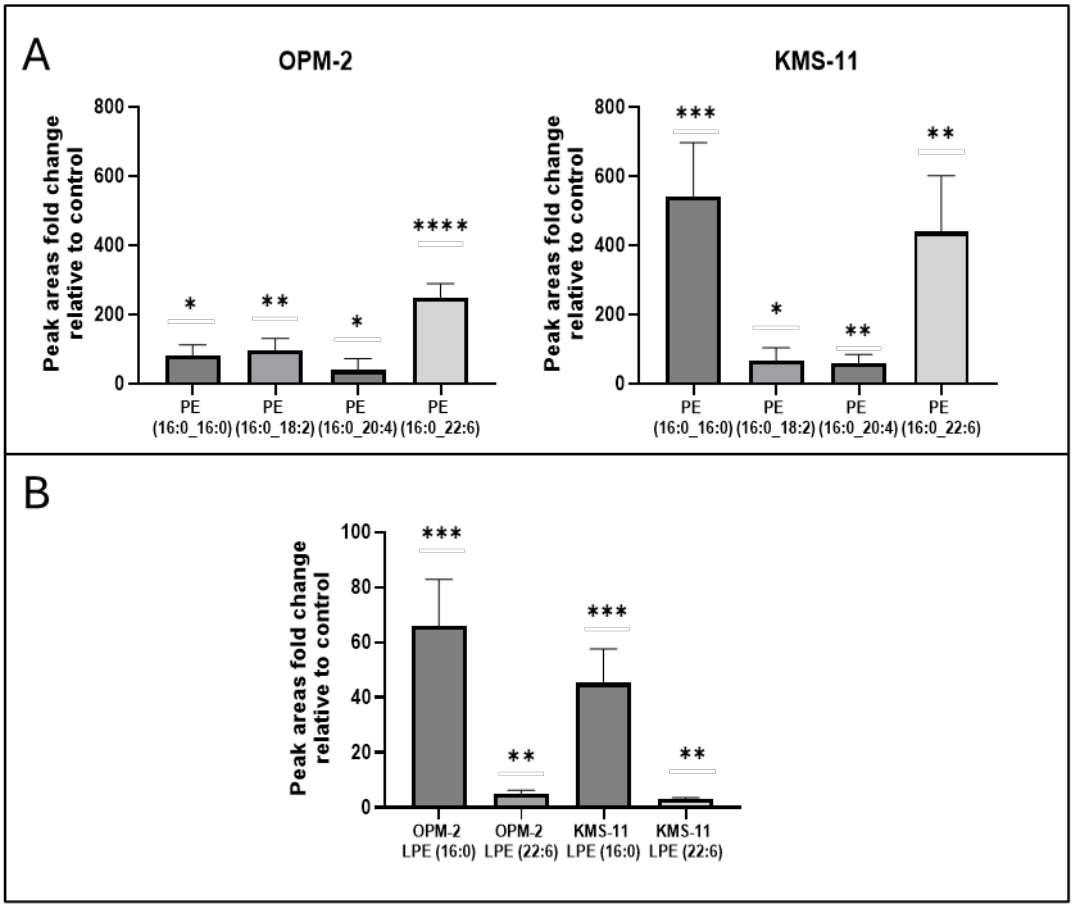

Figure 16. Significant lipid uptake was observed in both the OPM-2 and KMS-11 cells following addition of PE (16:0_22:6), with a significant increase in lysophospholipids.

(A) OPM-2 and KMS-11 cells were cultured with 20 µM of the lipids indicated for 4 hours. Lipid uptake was assessed by LC-MS. Data are presented as mean fold changes from 3 biological replicates. **(B)** OPM-2 and KMS-11 MM cells were cultured with 20 µM PE (16:0_22:6) for 4 hours. LPE levels were determined by LC-MS. Data are presented as mean fold changes from 3 biological replicates. LPE, lysophosphatidylethanolamine; PE, phosphatidylethanolamine. Data are presented as mean fold changes relative to unmanipulated cell lines ± standard deviation from 3 independent experiments and statistical analyses performed using the student's t-test for statistical analysis (*P<0.05, **P<0.01, ***P<0.001, **** P<0.0001).

The effects of adding exogenous PUFA to cells has been well studied in the literature, showing that addition of PUFA in the form of AA, or another PUFA, can sensitise and even induce ferroptosis in some cases (130, 194, 204-209). Prior research in our group has shown that the addition of AA to MM cells, in combination with RSL3, induces significant ferroptotic cell death. Limited literature is available that demonstrates the use of PUFA containing PLs to sensitise cells to ferroptosis. As shown in Figure 15, addition of free AA does not significantly alter the proportions of PUFA in either the KMS-11 or the OPM-2 cell lines but does decrease SFA levels in OPM-2 cells. The exact mechanism of this decrease in SFA was unclear and repetitions may be necessary with different conditions (concentration of AA and time points) to discern these changes. To investigate whether exogenous lipids would act differently, the phospholipid profile of the OPM-2 and KMS-11 cells cultured with the four PE lipids described above, was analysed.

Addition of exogenous PE (16:0_16:0) to the OPM-2 and KMS-11 MM cell lines resulted in a statistically significant ($p > 0.0001$) increase in the proportion of SFA in the lipidome (Figure 17). OPM-2 control cells had mean SFA proportion of 6.65%, which increased to 22.9% following culture with PE (16:0_16:0) (Figure 17A). The KMS-11 control cells were comprised of 5.65% SFA, which increased to 27% with the addition of PE (16:0_16:0) (Figure 18B). Addition of PE (16:0_18:2) resulted in a statistically significant ($P<0.05$), 8% increase in the proportion of PUFA in the OPM-2 cell line, while no significant increase in PUFA was observed in the KMS-11 cells (Figure 17). The addition of PE (16:0_20:4) significantly ($P<0.05$) increased the proportion of PUFA in the OPM-2 cell line, by 12%. However, again no significant increase in the proportion of PUFA was observed in the KMS-11 cell line (Figure 18). The addition of exogenous PE (16:0_22:6) significantly increased the proportion of PUFAs in both the KMS-11 ($P<0.05$) and OPM-2 ($P<0.01$) cells. An increase of 25.5% was observed in the OPM-2 cells, with the proportion increasing from 37.1 to 62.6% (Figure 17A). KMS-11 control cells had a PUFA proportion of 30.0%, which increased to 45.3% following addition of PE (16:0_22:6), (increase of 15.3%) (Figure 17B).

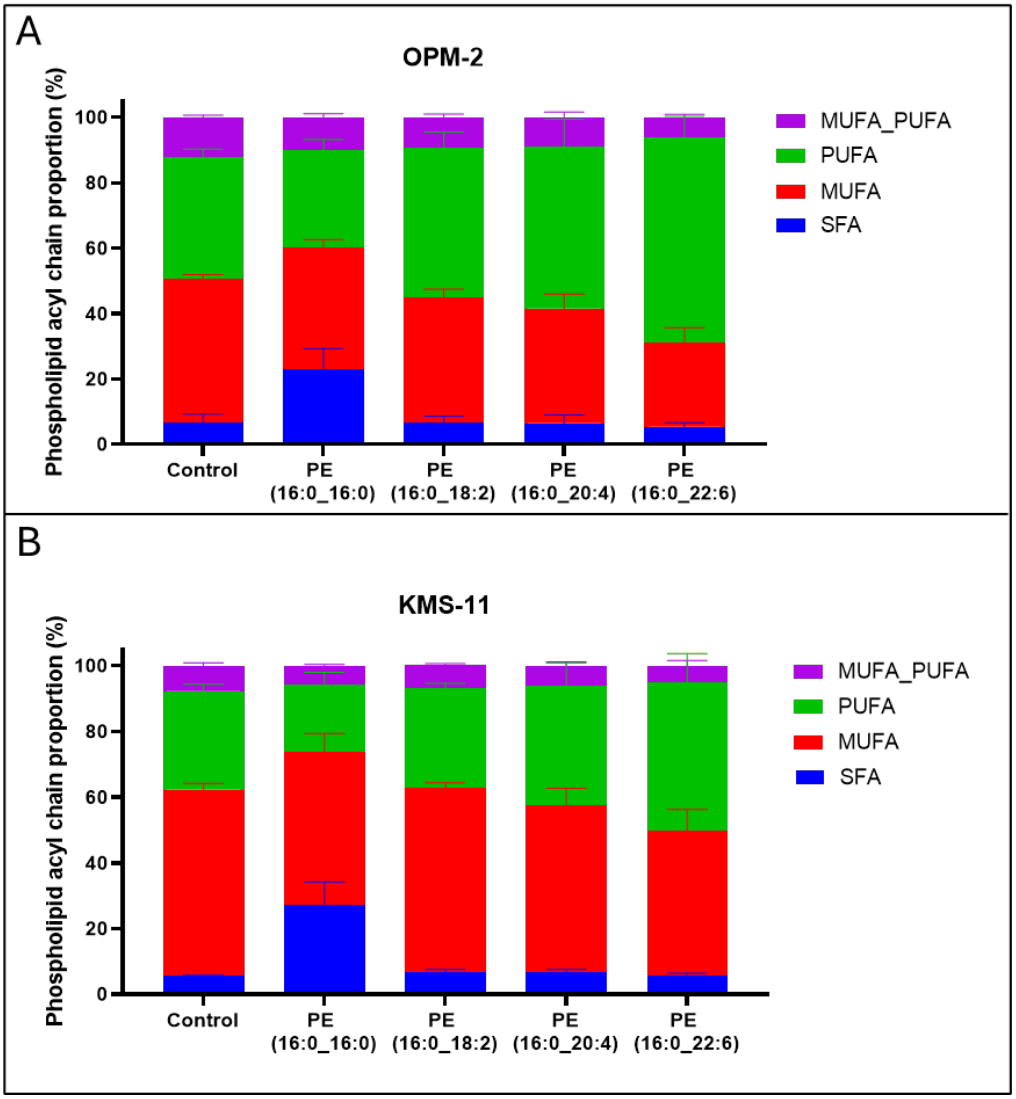

Figure 17. Exogenous phospholipids can be employed to effectively modulate the phospholipidome of KMS-11 and OPM-2.

(A) OPM-2 and **(B)** KMS-11 cells were cultured with 20 µM of the lipids indicated for 4 hours. Lipid uptake was assessed by LC-MS. Relative proportions of each phospholipid acyl chain are presented. Data are the mean and standard deviation from a minimum of 3 biological replicates per cell line. (Statistical analysis performed using T-test of a minimum of 3 biological replicates. *P<0.05, **P<0.01, ***P<0.001, **** P<0.0001). PE, phosphatidylethanolamine.

PE (16:0_20:4) and PE (16:0_22:6) induced cell death of both cell lines, with IC_{50} values of 53.61 ± 5.62 µM and 33.99 ± 15.34 µM for OPM-2 cells, and 54.19 ± 2.51 µM and 37.33 ± 9.03 µM for KMS-11 cells, respectively (Figure 18A). The cytotoxic effects of these lipids in both cell lines were inhibited by the synthetic antioxidant, liproxstatin-1, suggesting the cell death observed was due to ferroptosis (Figure 18A). In contrast, no cytotoxic effects of PE (16:0_16:0) or PE (16:0_18:2) were observed (Figure 18A). The cytotoxic effects of these lipids

towards both cell lines were inhibited by the synthetic antioxidant, liproxstatin-1, again confirming that the cell death was due to ferroptosis (Figure 18B).

Treatment of OPM-2 and KMS-11 cells with PL-PUFA increased lipid ROS levels, as demonstrated by oxidised C11 BODIPY staining; fold changes of >2 were observed in both OPM-2 and KMS-11 cells following treatment with 40 μM PE (16:0_20:4) or PE (16:0_22:6) (Figure 18C). A significant increase in levels of oxidised C11 BODIPY, without a decrease in cell viability, was also observed in OPM-2, but not KMS-11, cells following treatment with PE (16:0_18:2). Treatment with PE (16:0_16:0) had no significant effect on lipid ROS levels or cell viability in either cell line. In all cases, increases in the levels of lipid ROS were prevented by liproxstatin-1 (Figure 18C).

Next, we examined the effects of the lipids on the morphology of MM cells. OPM-2 cells were cultured with PE (16:0_22:6) and images captured over a 24-hour period on an Incucyte live cell imaging instrument (Figure 18D). The images show, that in response to the lipid, the cells underwent morphological changes characteristic of ferroptotic cell death, including cytoplasmic 'ballooning.'

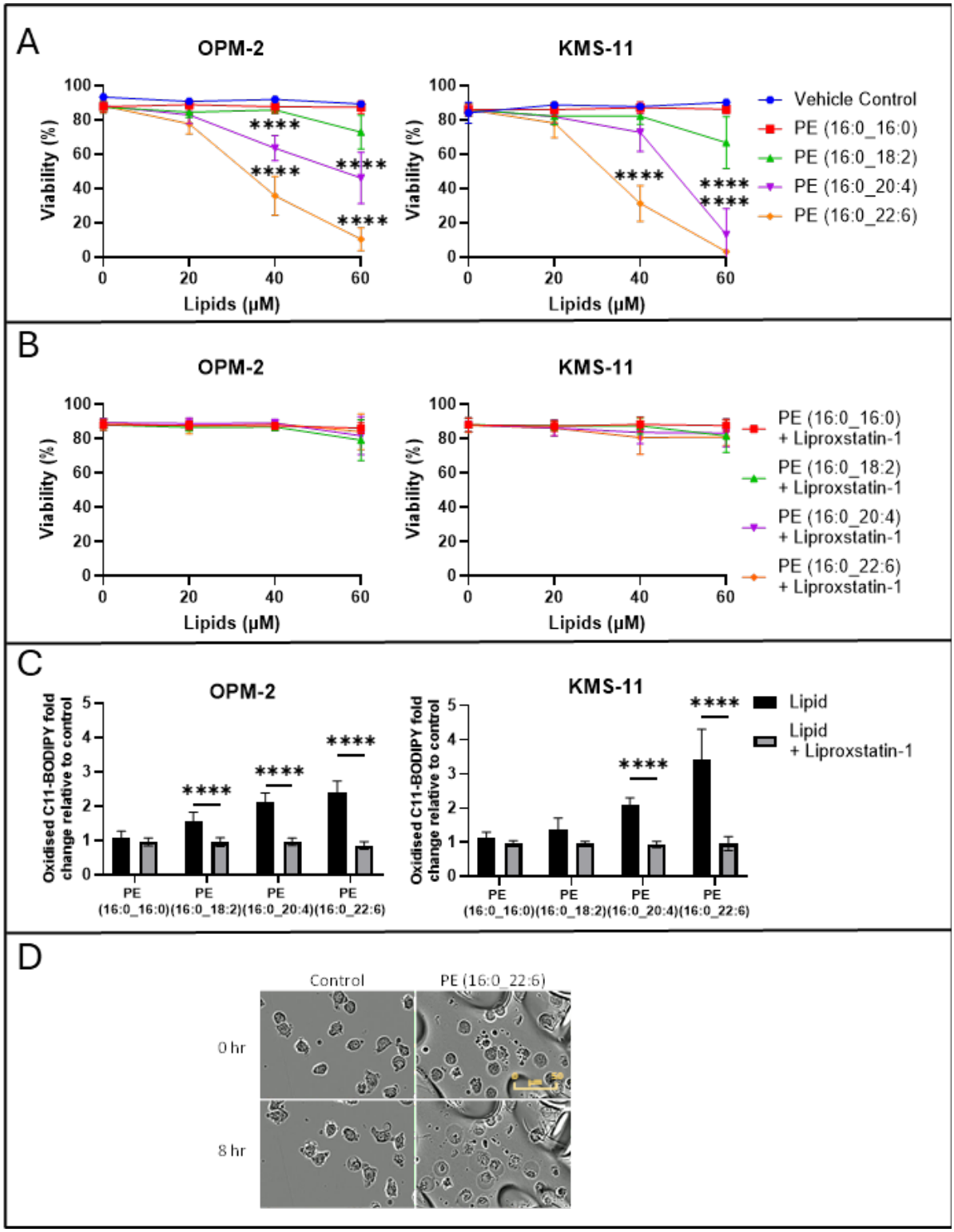

Figure 18. Ferroptosis induced by exogenous PL-PUFA correlates with the degree of acyl chain saturation.

(A) OPM-2 and KMS-11 MM cells were cultured with the concentrations of the PE lipids indicated for 24 hours and cell viability assessed by flow cytometry. **(B)** OPM-2 and KMS-11 MM cells were cultured with the concentrations of the PE lipids indicated and 2 μM liproxstatin-1 for 24 hours. Cell viability was assessed by flow cytometry following staining with annexin V and PI. Dual annexin V/PI negative

cells were considered viable. **(C)** OPM-2 and KMS-11 MM cells were cultured with 40 µM of the PE lipids, ±liproxstatin-1, as indicated. Lipid ROS levels were assessed by flow cytometry in cells stained with oxidised C11 BODIPY. Data are the mean and standard deviation from a minimum of 3 biological replicates per cell line. **(D)** OPM-2 cells were cultured with or without 60 µM PE (16:0_22:6). Images were acquired at the 0 and 8-hour time points on an IncuCyte live cell analysis system at 20x magnification. PE, phosphatidylethanolamine. Statistical analysis performed using two-way ANOVA and T-test of a minimum of 3 biological replicates. *P<0.05, **P<0.01, ***P<0.001, **** P<0.0001.

3.2.6 Exogenous PE-PUFA can inhibit proliferation of MM cells

PLs play an important role in the overall function of a cell, including in their proliferation (210). Changes in lipid metabolism have been shown in MM cells, which may drive cancer progression (211). To investigate the effects of lipids on MM cell proliferation, cells from 5 MM lines were cultured with concentration of exogenous PE-PUFA that were previously shown not to have an effect on cell viability after 24 hours. In three of the MM cell lines, KMS-11, OPM-2 and H929, there was a reduction in cellular proliferation compared to the vehicle control after 24h (Figure 19). Only PE (16:0_22:6) statistically significantly reduced in proliferation in the 3 MM cell lines, while PE (16:0_20:4) reduced the proliferation in the OPM-2 and H929 cell lines (Figure 19). PE-PUFAs did not reduce proliferation in LP-1 and KMS-18 cells.

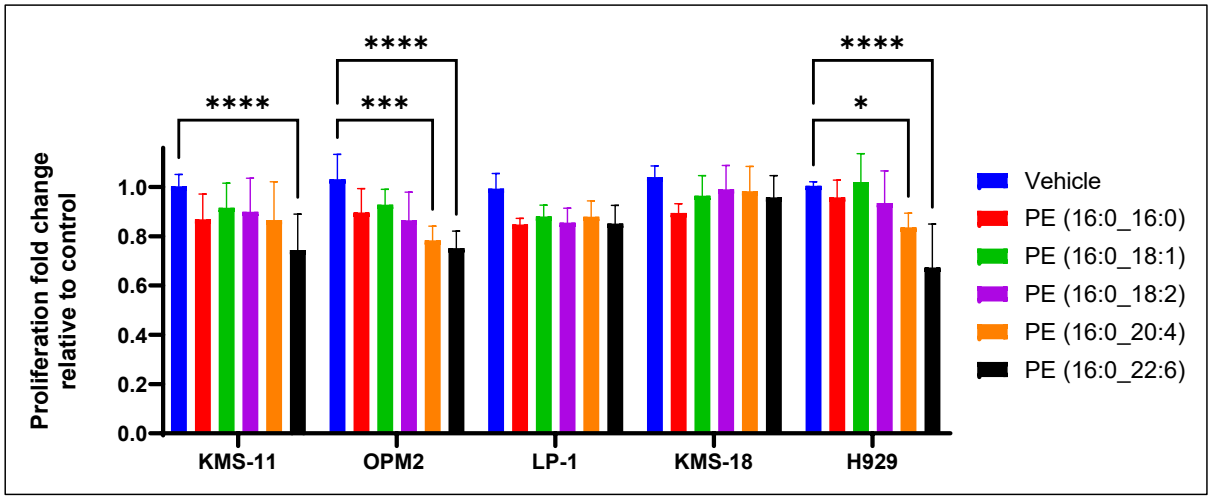

Figure 19. Exogenous PE-PUFA, but not PE-SFA or PE-MUFA, induces a decrease in cell proliferation in some MM cell lines.

MM cell lines were cultured with 20 µM of the lipids indicated for 24 hours. Cell proliferation was assessed by MTT cell proliferation assay. Data are the mean and standard deviation from a minimum

of 3 biological replicates per cell line. PE, phosphatidylethanolamine. Statistical analysis performed using two-way ANOVA of a minimum of 3 biological replicates. *P<0.05, **P<0.01, ***P<0.001, **** P<0.0001.

3.2.7 Exogenous PE supplementation can be used to manipulate MM cell response to RSL3

The role of exogenous PE-PUFA as a sole agent was investigated in the previous section of the chapter, showing that PE-PUFA can induce ferroptotic cell death in MM cell lines, independent of GPX4 inhibition (Figure 18). Next, we sought to investigate the response of the cell lines to the lipid ferroptosis substrates in combination with the GPX4 inhibitor, RSL3. It was hypothesised that altering the lipid composition of MM cells may sensitise these cells to the GPX4 inhibitor, RSL3.

MM cell lines were cultured with exogenous PE-PUFA or MUFA containing lipids and RSL3 for 24 hours. The effects of MUFAs were investigated as they are less readily oxidised during ferroptosis and studies suggest that MUFA can inhibit ferroptotic cell death by multiple mechanisms, including by displacing PUFA from the lipid bilayer (197).

Combinations of RSL3 and PE (16:0_20:4) or PE (16:0_22:6) were found to synergise with one another, in terms of their cytotoxic actions, against OPM-2 MM cells; in combination with PE (16:0_20:4) or PE (16:0_22:6) the IC_{50} values for RSL3 were 43.59 ± 5.24 nM and 34.11 ± 6.54 nM, respectively, compared to an IC_{50} of 74.34 ± 11.17 nM for RSL3 alone (Figures 11A and 20A). In KMS-11 cells, PE (16:0_20:4) and PE (16:0_22:6) significantly increased the sensitivity of the cells to RSL3; IC_{50} values for RSL3 in combination with the lipids were 4.86 ± 2.05 µM and 2.13 ± 0.69 µM, respectively while the IC_{50} value for RSL3 alone was 6.25 ± 0.82 µM (Figures 11A and 20A). Synergistic cell death with RSL3 was observed for both PE (16:0_20:4) and PE (16:0_22:6), with fractional products of -0.3 and -0.75 for the two lipids, respectively (Figure 20A, fractional products of < -0.1 are indicative of synergy). In both OPM-2 and KMS-11 cells, addition of liproxstatin-1 prevented the cell death induced by combinations of RSL3 and the lipids, consistent with a ferroptosis-mediated mechanism of cell death (Figure 20B).

Combining RSL3 and PE (16:0_22:6) augmented lipid ROS generation in both the OPM-2 and KMS-11 cell lines (Figure 20C), suggesting that increasing cellular PL-PUFA content increases the availability of substrates for lipid ROS generation. The increase in lipid ROS generation in

cells treated with PE (16:0_22:6) and RSL3 was also inhibited by liproxstatin-1 in both cell lines (Figure 20C).

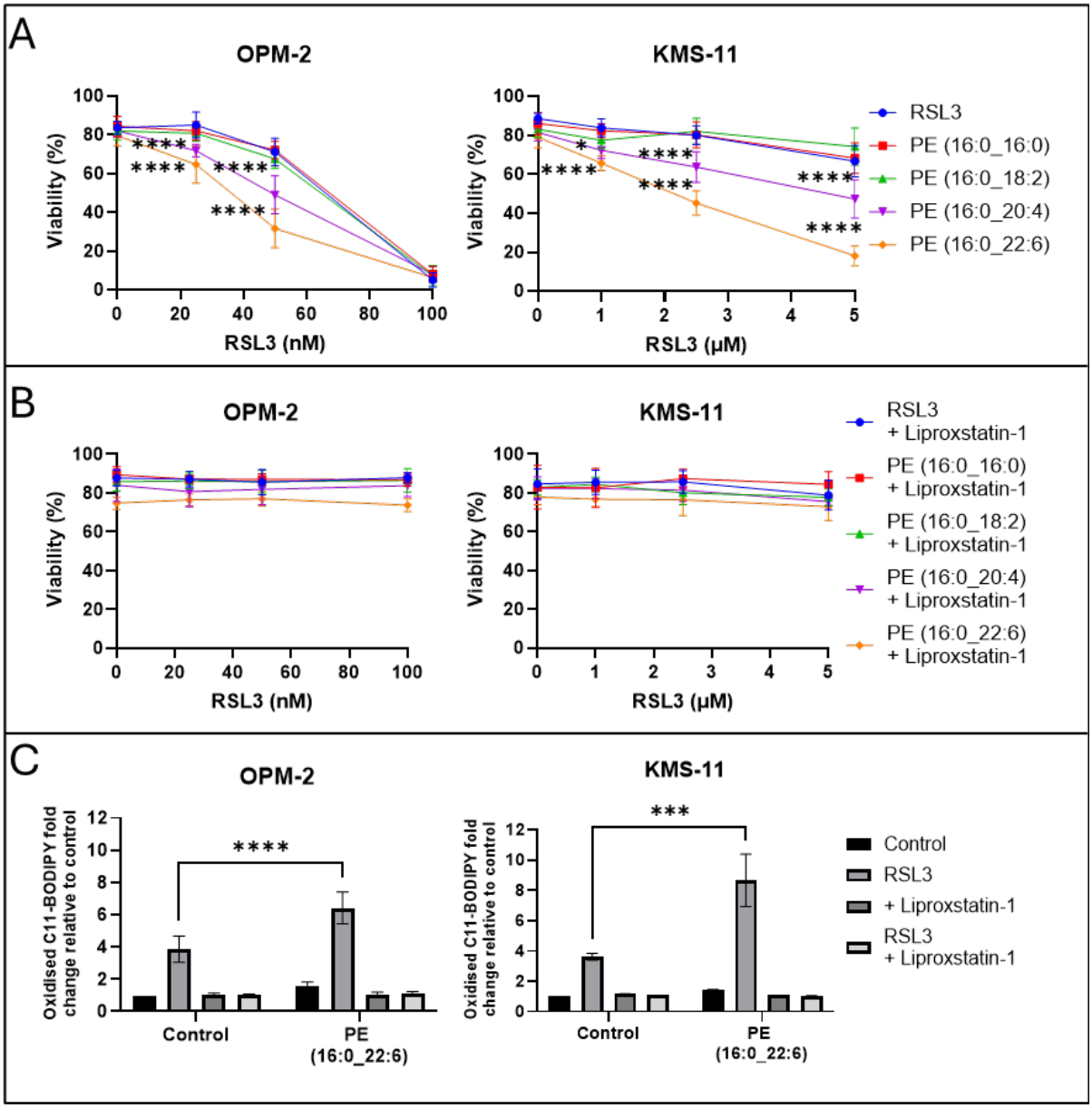

Figure 20. PUFA and RSL3 induce synergistic cell death in OPM2 and KMS-11 cells.

(A) OPM-2 and KMS-11 cells were cultured with 20 µM of the indicated lipids and RSL3 for 24 hours. Cell viability was assessed using annexin V/PI staining and flow cytometry. **(B)** OPM-2 and KMS-11 cells were cultured with 20 µM of the indicated lipids, RSL3 and 2 µM liproxstatin-1 for 24 hours. Cell viability was assessed using annexin V/PI staining and flow cytometry. Data are the mean and standard deviation from a minimum of 3 biological replicates per cell line. **(C)** OPM-2 and KMS-11 were cultured with 1 µM or 50 nM (OPM-2) RSL3 for 24 hours, with or without 20 µM PE (16:0_22:6) and liproxstatin-1 for 24 hours. Lipid ROS levels were assessed by flow cytometry using oxidised C11 BODIPY**.** Data are

the mean and standard deviation from a minimum of 3 biological replicates per cell line. Statistical analysis performed using two-way ANOVA of a minimum of 3 biological replicates. *P<0.05, **P<0.01, ***P<0.001, **** P<0.0001.

As discussed earlier, PE-MUFA plays an important role in reducing sensitivity to ferroptosis, as they displace PUFAs, which are far more readily oxidised. MM cell lines OPM-2 and KMS-11 were cultured with PE (16:0_18:1) and RSL3 for 24 hours. No viable OPM-2 cells remained after a 24-hour treatment with 100 nM RSL3 (Figure 21A). In contrast, the combination of PE (16:0_18:1) and RSL3 had no effect on cell viability compared to controls at 24 hours, suggesting that the PE-MUFA completely blocked the ferroptosis induced by the GPX4 inhibitor (Figure 21A). Liproxstatin-1 also completely blocked the cytotoxic effects of RSL3 (Figure 21A). Treatment of KMS-11 cells with PE (16:0_18:1) in combination with the doses of RSL3 indicated had no effect on cell viability, as RSL3 alone at these concentrations did not induce significant cell death (Figure 21A).

RSL3 alone induced lipid ROS generation in KMS-11 cells, with a 3.6-fold increase in levels of oxidised C11-BODIPY following treatment with 1 μM RSL3 (Figure 21B). The synthetic antioxidant, liproxstatin-1, completely attenuated lipid ROS generation at this concentration of RSL3 (Figure 21B). Similarly, addition of PE (16:0_18:1) also significantly reduced the levels of lipid ROS generated in KMS-11 cells. The effects of PE (16:0_18:1) in OPM-2 cells were again similar to those of liproxstatin-1, with a complete inhibition of the lipid ROS generated in response to RSL3 (Figure 21B).

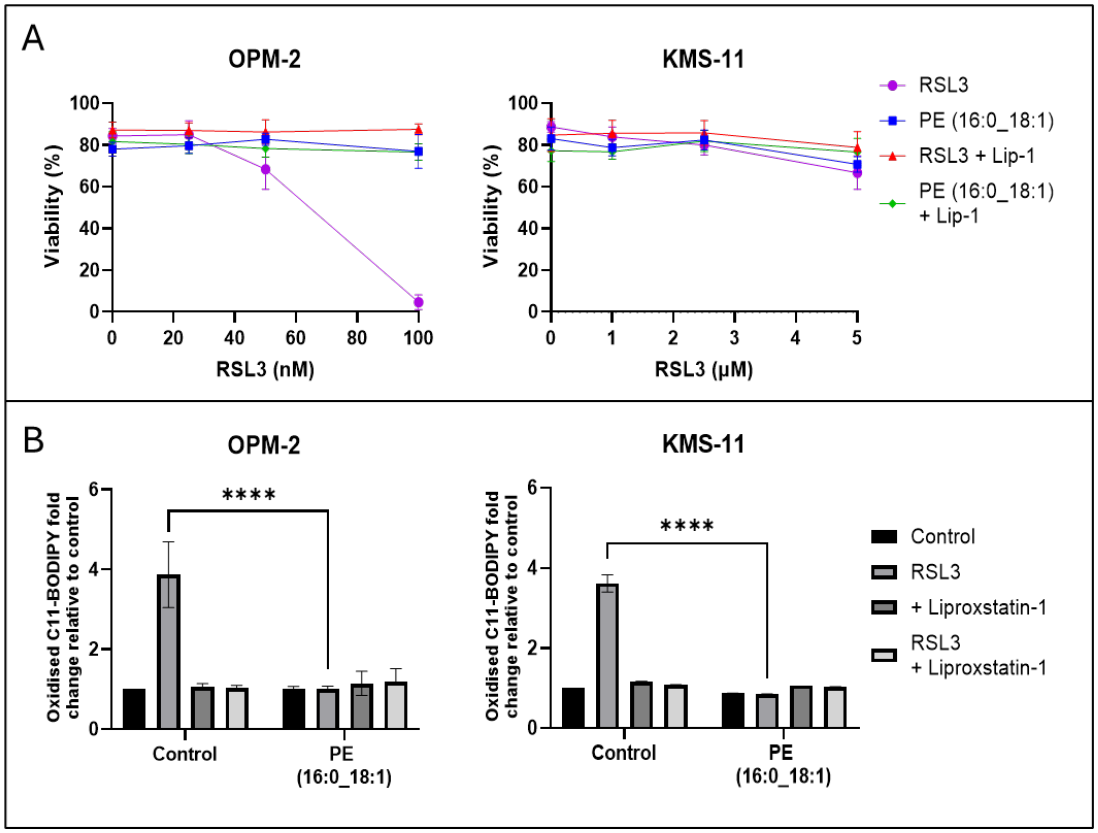

Figure 21. PE-MUFA can inhibit cell death and lipid ROS induced by RSL3.

(A) OPM-2 and KMS-11 cells were treated with 20 μM PE (16:0_16:0) or PE (16:0_18:1), RSL3 and liproxstatin-1 for 24 hours. Cell viability was assessed by flow cytometry in cells stained with annexin V and PI. **(B)** OPM-2 and KMS-11 were cultured with 1 μM or 50 nM (OPM-2) RSL3 for 24 hours, with or without 20 μM PE (16:0_18:1) and liproxstatin-1 for 24 hours. Lipid ROS levels were assessed by flow cytometry in cells stained with oxidised C11 BODIPY. Data are the mean and standard deviation from a minimum of 3 biological replicates per cell line. Statistical analysis performed using two-way ANOVA of a minimum of 3 biological replicates. *P<0.05, **P<0.01, ***P<0.001, **** P<0.0001.

To study the effects of PE-PUFA and PE-MUFA on MM cells in more detail, three additional MM cell lines were treated with RSL3 and either PE-PUFA or PE-MUFA. The MM cell lines LP-1, H9292 and KMS-18, while all more sensitive to RSL3 that KMS-11, still displayed ferroptosis resistance, with micromolar IC_{50}s, especially when compared to the OPM-2 and DLBCL cell lines. The primary focus of testing these MM cell lines was to investigate whether manipulating the lipidome of all available MM cell lines could dictate ferroptosis susceptibility, or if it was cell line dependant. Cell lines were cultured with PE-PUFA and RSL3 for 24 hours and cell viability assessed. Remarkably, all of the MM cell lines displayed significant cell death

when cultured with PE-PUFA and RSL3 (Figure 22A). The KMS-18 cell line that displayed minimal decrease in cell viability at 5 μM, was no longer viable once PE (16:0_22:6) was added (Figure 24 B). The LP-1 and H929 cell lines that did respond to RSL3 as seen by the reductions in cell viability, were also sensitised by the addition of PE (16:0_22:6) (Figure 22A-B). Also consistent with our earlier findings, we observed synergy between RSL3 and PE (16:0_22:6) in the LP-1 (-0.37), H929 (-0.52) and KMS-18 (-0.48) cell lines, thereby suggesting this effect is not cell line dependant.

Another important reason the range of cells was expanded was to test if changes in cell viability in response to higher concentration of RSL3 would be inhibited by exogenous PE-MUFA. Consistent with our findings from the OPM-2 cell line, treatment of LP-1 and H929 cells with RSL3 in combination with PE (16:0_18:1), led to a significant reduction in cell death, comparable to the addition of liproxstatin-1 (Figure 22A-B). However, this effect was not observed in the KMS-18 cell line as the cell line did not display a decrease in cell viability in response to the chosen concentration of RSL3.

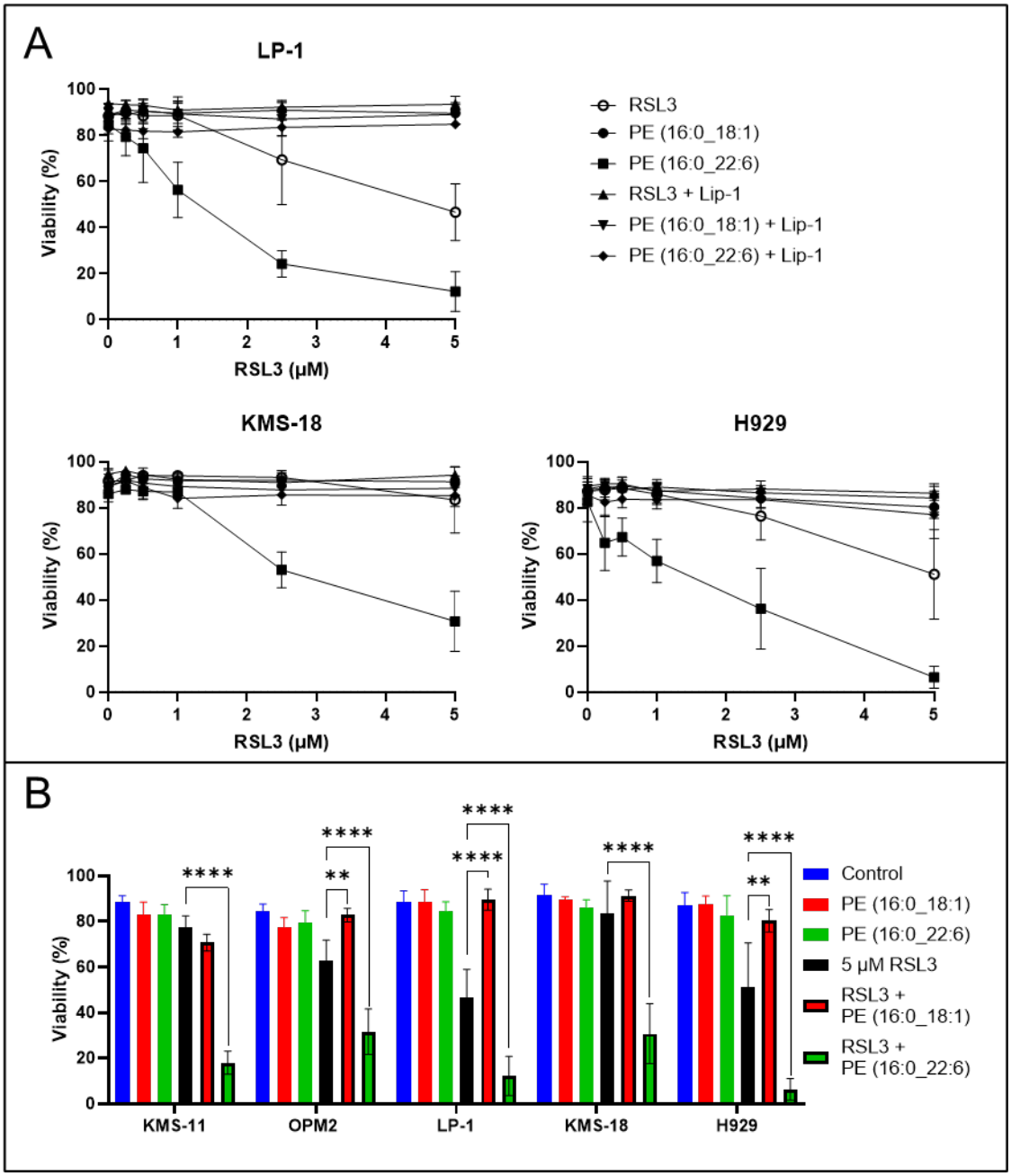

Figure 22. PUFA and RSL3 induce synergistic cell death while MUFA protects MM cells from ferroptosis-mediated cell death.

(A) LP-1, KMS-18 and H929 cells were cultured with 20 μM PE (16:0_18:1) or PE (16:0_22:6), RSL3 and liproxstatin-1 for 24 hours. Cell viability was assessed by flow cytometry in cells stained with annexin V and PI. **(B)** MM cell lines were cultured with 5 μM or 50nM (OPM-2) RSL3 for 24 hours, with or without 20 μM PE (16:0_18:1) or PE (16:0_22:6). Cell viability was assessed by flow cytometry following staining with annexin V and PI. Data are the mean and standard deviation from a minimum of 3 biological replicates per cell line. Statistical analysis was performed using two-way ANOVA of a minimum of 3 biological replicates. *P<0.05, **P<0.01, ***P<0.001, **** P<0.0001.

As mentioned earlier, the mechanism by which MUFA inhibits ferroptosis is thought to involve the displacement of PUFA and a subsequent reduction in the availability of ferroptosis substrates in the lipidome (197). Interestingly, LC-MS analysis did not show a significant increase in PE (16:0_18:1) in cells treated with this lipid. However, it appeared that levels of other oleic acid (18:1)-containing PLs were increased throughout the phospholipidome of both OPM-2 and KMS-11 cells, while the proportion of PL-PUFA decreased (Figure 23 and Appendix Figure 3). Cells can take up and metabolise exogenous PLs, such as PE (16:0_18:1), breaking them down into free fatty acids, allowing them to be incorporated into other PLs (132, 212). This may explain why oleic acid, and not specifically PE (16:0_18:1) levels increased in the treated samples. Further experiments would be required to determine if this explains the fate of this lipid in MM cells.

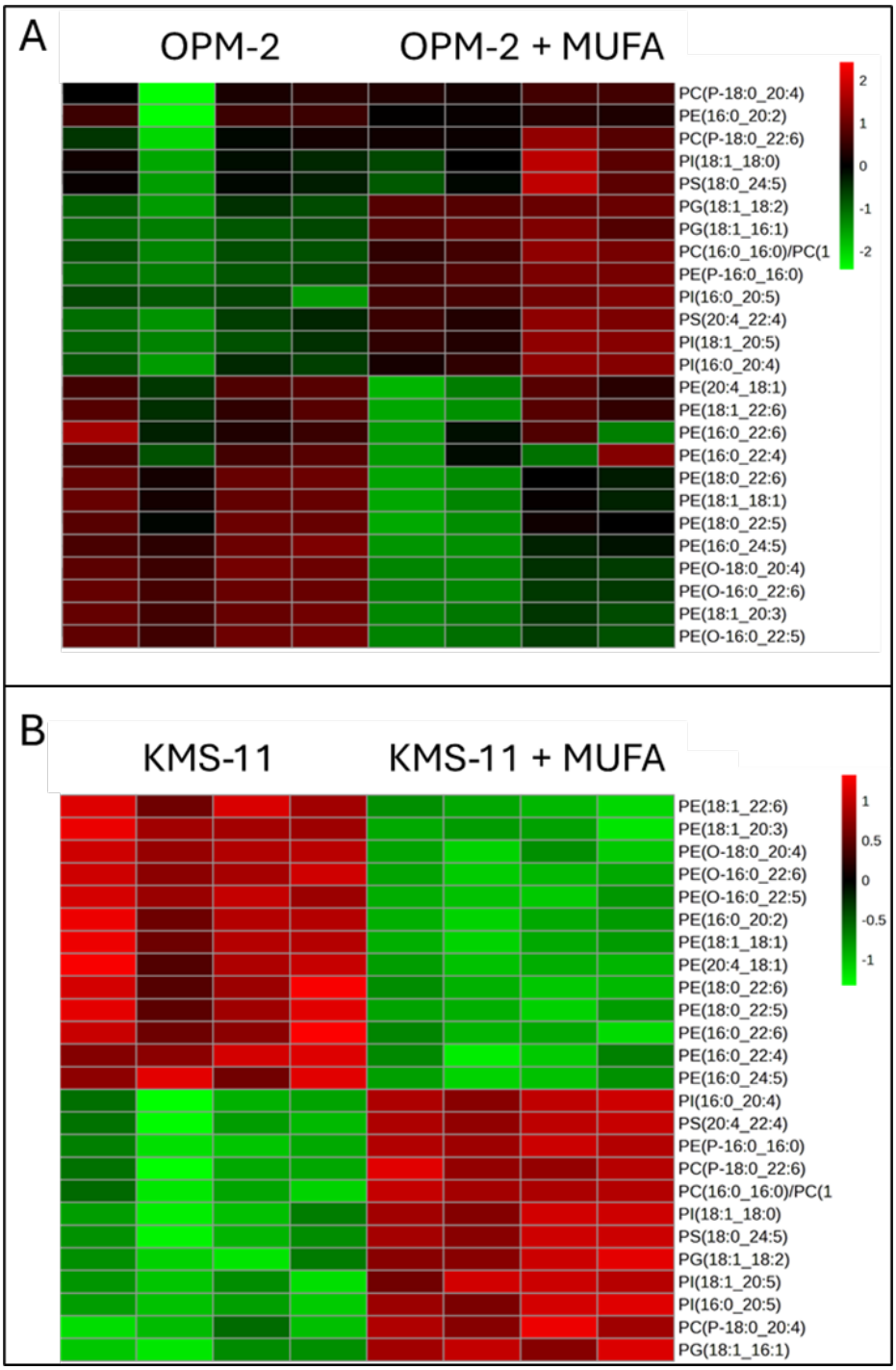

Figure 23. Oleic acid appears to displace PUFA in phospholipids in OPM-2 and KMS-11 cells.

(A) Heatmap of the 25 most differentially expressed lipids in OPM-2 cells, cultured with or without PE (16:0_18:1) for 4 hours. Oleic acid is denoted as 18:1. PUFA have been defined in this chapter as lipids with 1 or more fatty acid chains that contain more than one double bond (PE 16:0_22:6) **(B)** Heatmap of the 25 most differentially expressed lipids in KMS-11 cells, cultured with or without PE (16:0_18:1) for 4 hours. Data are the mean and standard deviation from a minimum of 3 biological replicates per cell line.

3.2.8 Precision lipids and the role of acyl chain saturation in ferroptosis in MM cells.

To further understand how different PLs impact the sensitivity of MM cells to ferroptosis and whether identifying deficiencies in specific lipids might be harnessed for the development of precision therapies, differences in the lipid composition of MM and DLBCL cells were investigated in greater detail. An analysis was performed comparing the KMS-11, LP-1 and KMS-18 cell lines to the DLBCL cell lines using the MetaboAnalyst software to identify whether the effects of PUFA-containing PLs, other than the ones studied earlier, were also worth testing. Many limitations were found during this screening, mostly around the commercial availability of PLs. From this screen, two lipids were identified as being in relatively low abundance in the aforementioned MM cell lines, including PC (16:0_22:6) in all three cell lines and PC (16:0_20:5) in the KMS-11 cell line (Appendix Figure 4). These lipids were then tested against the OPM-2, KMS-11, LP-1 and KMS-18 cell lines, in combination with RSL3 and liproxstatin-1.

Interestingly, the cell death observed in response to the PLs in combination with RSL3 in all 4 cell lines was largely double bond dependant; the higher the number of double bonds in the sn-2 position of the PL, the more effective the lipid was at sensitising cells to RSL3 (Figure 24). This correlation was also independent of the head group. For example, similar effects were observed with PE (16:0_22:6) or PC (16:0_22:6) in combination with RSL-3 in all four cell lines (Figure 24A). The KMS-11 ($P<0.001$) and LP-1 ($P<0.001$) cell lines were both significantly more sensitive to RSL3 when cultured with PE (16:0_22:6) than with PC (16:0_20:5). In the OPM-2 and KMS-18 cell lines, no significant difference in RSL3 sensitivity was observed when the cells were cultured with PC (16:0_20:5), PC (16:0_22:6) or PE (16:0_22:6). Importantly, the OPM-2 ($P<0.001$), KMS-11 ($P<0.0001$), LP-1 ($P<0.0001$) and KMS-18 ($P<0.001$) cell lines were significantly more sensitive to RSL3 when cultured with PE (16:0_22:6) than with PE (16:0_20:4). In all cases, the cytotoxic effects of the lipids in combination with RSL-3 were inhibited by liproxstatin-1, meaning the effects are consistent with ferroptosis (Figure 25). These findings suggest that ferroptotic cell death in response to lipids in combination with RSL-3 is largely governed by the saturation of the FAs in the PLs, rather than the functional group of the PLs.

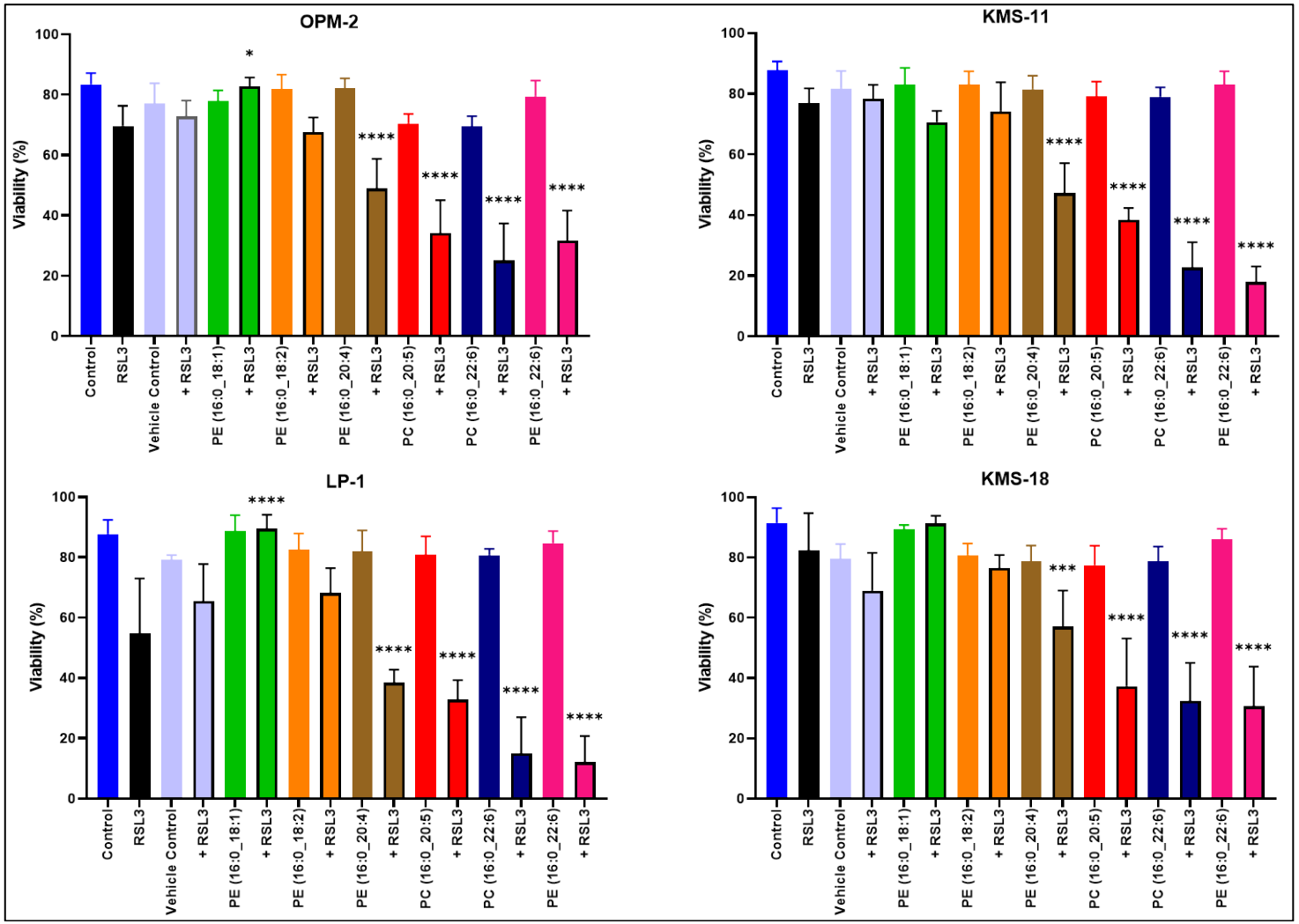

Figure 24. The ability of PLs to sensitise MM cells to RSL3 induced ferroptosis is double bond dependant.

MM cell lines were cultured with 5 µM or 50nM (OPM-2) RSL3 for 24 hours, with or without 20 µM of the indicated lipid. Cell viability was assessed using flow cytometry following staining with annexin V and PI. Data are the mean and standard deviation from a minimum of 3 biological replicates per cell line. Statistical analysis performed using one-way ANOVA of a minimum of 3 biological replicates with conditions compared to the RSL3-alone. *P<0.05, ***P<0.001, **** P<0.0001.

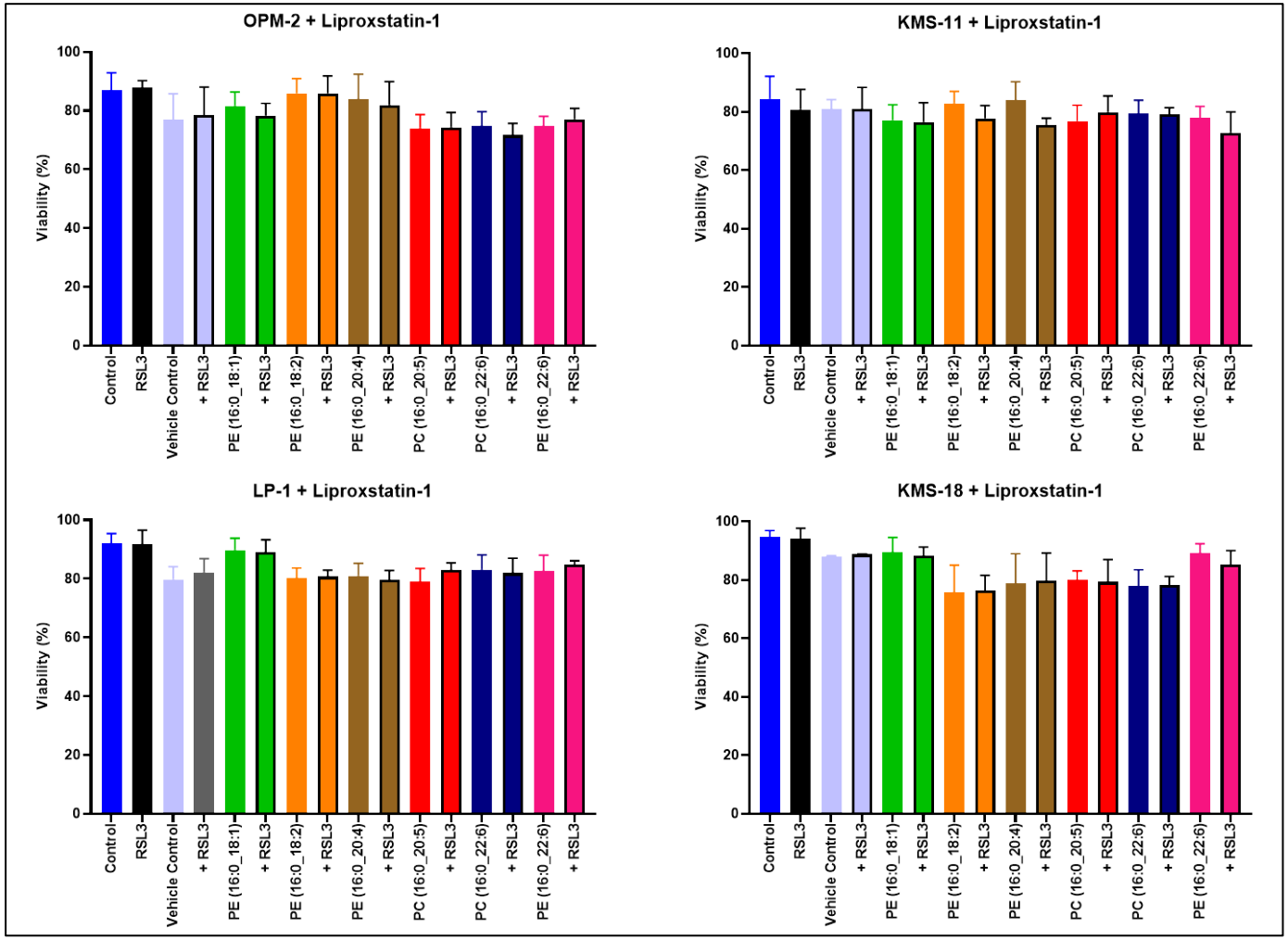

Figure 25. Liproxstatin-1 prevents cell death induced by combinations of different PLs and RSL3.

MM cell lines were cultured with 5 µM or 50nM (OPM-2) RSL3 for 24 hours, with or without 20 µM of the indicated lipid and liproxstatin-1. Cell viability was assessed using flow cytometry following staining with annexin V and PI. Data are the mean and standard deviation from a minimum of 3 biological replicates per cell line. Statistical analysis performed using one-way ANOVA of a minimum of 3 biological replicates with conditions compared to the RSL3-alone. *P<0.05, ***P<0.001, **** P<0.0001.

3.2.9 Phospholipid components of foetal calf serum and added media

Foetal calf serum (FCS) is an important component of most cell culture media. FCS contains large amounts of the nutrients required for cell growth and survival (213), including lipids and PLs. As the data presented in this study suggests that exogenous lipids play an important role in ferroptosis, the lipid composition of the FCS used for culturing the MM cells was investigated. FCS was diluted at a 1:10 ratio in RPMI-1640 base medium for MM cell culture. A lipidomics analysis was performed on neat FCS, neat RPMI-1640 and RPMI-1640 containing 10 % FCS. Results from this lipidomics analysis found that neat FCS contained almost equal proportions of PLs containing MUFAs and PUFAs (Figure 26). The FCS was also comprised of 20 % of PLs containing SFAs and 7 % containing both MUFAs and PUFAs (Figure 26). Relative to the neat FCS, RPMI-1640 contained low levels of lipids, suggesting that the majority of the lipids present in complete culture medium were contained within the FCS (Figure 26B).

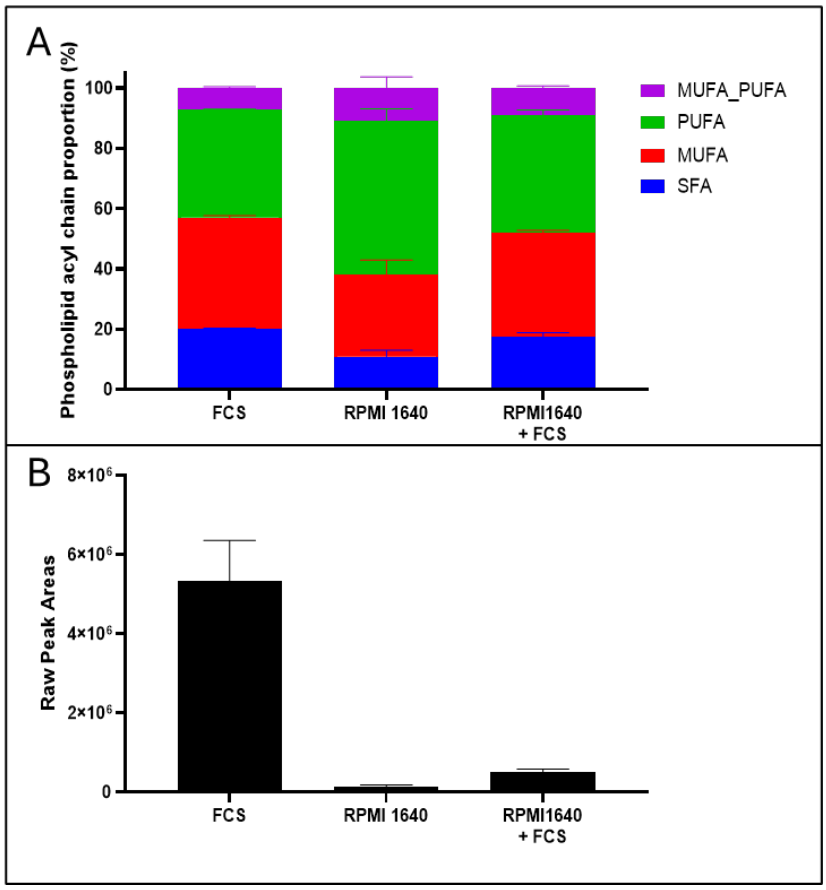

Figure 26. Phospholipid profile of FCS and RPMI 1640 medium.

(A) Lipid compositions were assessed by LC-MS. Relative proportions of each PL acyl chain are presented. **(B)** Raw peak areas derived from the lipidomic analysis. Data are the mean and standard deviation from a minimum of 3 biological replicates per cell line.

3.3 Discussion

3.3.1 MM cells are relatively insensitive to ferroptosis induction via GPX4 inhibition

Ferroptosis involves a complex cellular mechanism that involves lipid biology, ROS production and cell antioxidant systems. Past work by *Yang et. al* demonstrated that DLBCL but not MM cells were sensitive to the system X_c^- inhibitor erastin (136). Initially, we sought to replicate the data of Yang et al., but found that we could not induce ferroptotic cell death with erastin in the MM and DLBCL cell lines available to us (data not shown). Therefore, we began investigating the effects of RSL3, a direct inhibitor of GPX4. RSL3 binds to the active catalytic domain of GPX4, rendering it unable to neutralise toxic lipid ROS, leading to protein degradation (102). Following treatment of the MM and DLBCL cell lines with RSL3 for 24 hours we found the MM cell lines were generally less sensitive to RSL3 than DLBCL lines, with micromolar IC_{50}s (Figure 11A).The DLBCL cell lines were very sensitive to ferroptosis induced by the GPX4 inhibitor, with IC_{50}s for RSL-3 in a nanomolar range (Figure 11A). Interestingly, one of the MM cell lines, OPM-2, was a clear outlier in the study, as these cells were highly sensitive to RSL3, similar to the DLBCL cell lines (Figure 11A). This meant we had cell lines from different cancers and from MM cell lines themselves that were both sensitive and relatively resistant to RSL-3. Initially, we investigated if differences in expression of GPX4 might explain the differences in sensitivity to RSL3. Previous work in the field of ferroptosis has revealed that GPX4 inhibition can directly induce ferroptosis, as shown in the work in this study, while GPX4 upregulation can inhibit ferroptosis (214). Interestingly, cells that displayed comparably less GPX4 were more sensitive to ferroptosis induction (214). Given these results, we investigated the basal levels of GPX4 in 5 MM and 5 DLBCL cell lines. However, our results did not shed light on the reason for the differences in ferroptosis sensitivity between the cancer types or between the cell lines (Figure 11B-C). The OPM-2 MM cell line had comparable levels to the other MM cell lines, while displaying a significantly lower, nanomolar IC_{50} to RSL3. GPX4 expression in the DLBCL cell lines also did not correlate with ferroptosis sensitivity. These results lead to a few different hypotheses for why MM cells are relatively insensitive to ferroptosis. Our initial thoughts were that the MM cell lines have alternative mechanisms to overcome the lipid oxidation and ROS production, independent of GPX4 or that MM cells have alterations in iron metabolism. Building on ongoing research within the group, we focused on

investigating whether MM cells lack the necessary or optimal substrates for ferroptosis. As studies by other members of our group were exploring the possible role of alternative antioxidant systems and iron metabolism in the ferroptosis resistance of MM cells, the research detailed in this thesis focused specifically on the levels of ferroptosis substrates, with an emphasis on PLs.

3.3.2 MUFA-rich phospholipids drive MM cell ferroptosis resistance, while PUFA dominates in DLBCL

PLs are the primary substrate of ferroptosis and are essential in the production of toxic lipid peroxides and eventual cell death via ferroptosis (191). Importantly, PLs within the inner leaflet of the plasma membrane that contain PUFA are the most readily oxidised of these PLs and are the primary substrate of lipid peroxidation (191). MUFA on the other hand play an important role as inhibitors of ferroptosis, as they are not oxidised at the same rate as PUFA. Our initial studies concerning the lipidome of MM and DLBCL cell lines suggested that in general MM cell lines expressed a higher proportion of PLs containing MUFA than the DLBCL cell lines (Figure 12). As the RSL3 sensitive DLBCL cell lines expressed a higher proportion of PLs containing PUFA, we hypothesised that the levels of PUFA and MUFA could dictate ferroptosis sensitivity.

To further investigate this hypothesis, 5 MM and 5 DLBCL cell lines were subjected to lipidomics analysis by LC-MS. The data generated from this expanded panel of cell lines showed a similar trend, in that the RSL3 resistant MM cell lines generally contained a higher proportion of PLs containing MUFA (Figure 12). Two of the most differentially upregulated lipids in the panel of MM cell lines contained MUFA, with one of the lipids containing MUFA in both the sn-1 and sn-2 fatty acid positions (Figure 13A). This is consistent with the literature, which suggests that MUFA is associated with ferroptosis resistance (197). The DLBCL cell lines on the other hand expressed a higher proportion of lipids containing PUFA, particularly lipids containing AA (20:4) or docosahexaenoic acid (22:6) (Figures 12 and 13). Notably, many of the lipids identified as being upregulated in the DLBCL cells contained an ether bond in place of an ester bond, and while this piqued our interest, the limited literature and lack of commercial availability of the lipid, made it difficult to further investigate this observation. Ether lipids have recently been shown to play an important role in ferroptosis, by providing PUFA as a substrate for lipid peroxidation and by modulating iron uptake (201,

215). The literature concerning ether lipids in ferroptosis is still limited, however some of the published research does suggest it is important to consider ether lipids in the context of ferroptosis sensitivity. Furthermore, it would be interesting to investigate whether exogenous ether PLs are more effective at inducing ferroptosis that those with an ester bond, and if the ratio of these lipids has any function in determining ferroptosis sensitivity.

Analysis of lipid expression is generated from peak areas for each individual lipid in the library based on their known retention times. Using the peak areas, it was possible to calculate the proportions of different PL classes present in each cell line. Initially, lipids were assigned as either SFA, MUFA or PUFA, based on the fatty acids contained within the lipids. However, upon further analysis of the data a fourth group was created, which were PLs that contained both PUFA and MUFA. The role of these lipids in the literature has not been investigated and poses the interesting question, whether PLs that contain a MUFA and a PUFA can be oxidised. The position of the PUFA and the MUFA may play a role in determining whether these lipids are oxidisable or not, but due to time constraints and commercial availability, this group of lipids were not investigated further.

The proportions of lipids in 5 MM and 5 DLBCL cell lines were determined and the data grouped according to the particular cancer (Figure 14A). Notably, significant differences were observed in the PL profiles of the MM and DLBCL cell lines (Figure 14A). The MM cell lines had a significantly higher proportion of PLs containing MUFA, with a concomitantly lower proportion of PLs containing PUFA, compared to the DLBCL cell lines (Figure 14A). Despite the differences in the PL profile of the two cancers, no correlation between lipid proportions and RSL3 sensitivity was observed. This may be due to the stark differences in the IC_{50} values for RSL3, or because even small changes in the lipidome may be sufficient to render a cell line sensitive or resistant to ferroptosis (Figure 11A). Importantly, the PL profile of the RSL3 sensitive OPM-2 (MM) cell line closely resembled that of the DLBCL cell lines rather than the other MM lines (Figure 14A-B). When compared to the RSL3 resistant KMS-11 cell line, OPM-2 cells were found to contain a significantly higher proportion of PLs containing PUFA and significantly lower levels lipids containing MUFA (Figure 14B). Furthermore, differences in the proportion of MUFA were more statistically significant than proportions of PUFA between the cancer groups and the OPM-2 and KMS-11 cell lines (Figure 14). This suggests that MUFAs play a greater role in dictating ferroptosis susceptibility than PUFA in these cell lines. These

results align with the literature, suggesting that higher proportions of PUFA promote ferroptosis sensitivity, while higher levels of MUFA confer resistance (216).

Another group of lipids that were not a focus of the lipidomics data analysis were PLs that contained either two MUFA or two PUFA fatty acid chains, as these lipids were very low in abundance. A study published in 2024 found that PLs containing two PUFA promote ferroptosis and can induce ferroptotic cell death in cancer cell lines (217). In this study, Stockwell and colleagues found that PC lipids with two docosahexaenoic acids (PUFAs) were more potent inducers of ferroptosis than PC lipids containing only one of the PUFA (217). The study also suggested that the cell death induced by this lipid could not be explained by the presence of two PUFA only. PE and PG lipids with two docosahexaenoic acid fatty acids also induced significant cell death, but that this could not be prevented by ferrostatin-1. PC lipids with two PUFA were found to be more abundant in ferroptosis sensitive cell lines and to induce mitochondrial stress, leading to ferroptosis (217). The role of PLs that contain two MUFA remains largely unexplored in the literature and there is currently no evidence that these lipids have been studied in the context of ferroptosis.

Lipidome plasticity and the dynamic regulation of the lipidome are important in ferroptosis (218). These terms have been used to describe the response of the phospholipidome to ferroptosis inducers and substrates, and the regulation of pro-ferroptosis lipids. The MM cell lines, OPM-2 and KMS-11, were cultured with ferroptosis substrates AA and ferric ammonium citrate, as well as GPX4 inhibitor RSL3 (and various combinations of these compounds) to better understand the role of lipid plasticity in MM cells (Figure 15). Iron had minimal effects on either cell line, and given it has limited effects on cell viability as a single agent, may require other factors to induce any significant change in the lipidome (Figure 15). The addition of AA resulted in a slight increase in the proportion of PUFA in KMS-11 but not OPM-2 cells. ACLS4 and LPCAT3 are required for the integration of PUFA into PLs, and without these enzymes' lipids cannot be converted into substrates for ferroptosis (193, 195). Given the short incubation time of 4 hours and the intracellular mechanisms required to make PUFA available for lipid peroxidation, increased time or greater concentrations of AA may be required to observe and elucidate the response of cells to this lipid. While PUFA levels decreased in the OPM-2 cells following culture with AA, the proportion of AA-containing lipids in the cells did not decrease. This may indicate a dynamic shift in the lipidome of OPM-2 cells involving PUFA

depletion to avoid an increase in ferroptosis sensitivity. However, further work is necessary to fully elucidate how MM cells adapt to increased levels of exogenous PUFAs.

RSL3 and all combinations of RSL3 decreased PUFA levels in the OPM-2 but not KMS-11 cells (Figure 15). The KMS-11 cell line is not sensitive to RSL3 induced cell death, suggesting that the drug may have little effect on the levels of lipids in these cells (Figure 15). The decrease in PUFAs in the OPM-2 cell line we observed has been documented in previous studies, with an increase in the levels of oxygenated PLs and lysophospholipids and a decrease in the abundance of PLs containing PUFAs (131, 135).

3.3.3 Exogenous PE-PUFA can induce MM cell death and bring upon lipidome changes

Having identified that PUFA play an important role in dictating the sensitivity of MM and DLBCL cells to ferroptosis, the next step was to develop a method by which specific lipids can be delivered to MM cells to increase their sensitivity to ferroptosis. Previous studies have shown that the addition of specific PUFAs as free fatty acids can increase the sensitivity of cells to ferroptosis by increasing the intracellular pool of ferroptosis substrates. Supplementing the medium with PUFAs, including AA, docosahexaenoic acid, linoleic acid and eicosapentaenoic acid has been shown to sensitise cells to ferroptosis or even induce ferroptosis in some cell types (130, 194, 204-209). However, adding free fatty acids to cell media is reliant on the ability of the cells to take up the lipids uptake and on intracellular conversion of the free fatty acids into ferroptosis substrates (126). Mechanistically, ACSL4 and LPCAT3 are required to prime and insert fatty acids into PLs, suggesting that regulation of these enzymes or pathways may be crucial in how cancer cells resist ferroptosis-mediated cell death (192-195). We hypothesised that culturing cells with PLs rather than free fatty acids might represent an effective and rapid method of sensitising cells to ferroptosis that was not dependant on ACLS4 or LPCAT3. As mentioned earlier, PLs typically have two fatty acyl chains and a functional head group, and in the context of ferroptosis, PE containing PUFAs is the preferred substrate (131, 191).

The lipidomics study performed on our cell lines identified PE lipids, particularly ether lipids, as some of the most differentially expressed between DLBCL and MM (Figure 12). The DLBCL cell lines expressed higher amounts of PE lipids with a high degree of unsaturation in the sn-

2 fatty acid position, particularly docosahexaenoic acid, than the MM cells. Based on these results and the important roles of PE lipids highlighted by the literature, four PE lipids were purchased with various degrees of unsaturation in the sn-2 position. To confirm the uptake of exogenously adding ferroptosis substrates, lipidomics analysis was performed in the OPM-2 and KMS-11 cell lines after the addition of one of the four lipids. All four lipids resulted in a significant increase in the particular lipid in the PL profile of the cell lines, after four hours, however significant differences in the proportion of the different lipids were observed (Figure 16A). The addition of PE (16:0_22:6) resulted in a fold change increase of approximately 200 in both cell lines, which may explain the profound effects of this lipid on the viability of these cells (Figure 16A and 18A). Although a significant increase of 39.3 ± 33.3-fold change in the OPM-2 and 58.8 ± 26.0-fold change in the KMS-11 was observed following the addition of PE (16:0_20:4), this increase was not as profound as the effects of PE (16:0_22:6) (Figure 16).

An interesting and unexpected phenomenon was observed when MM cell lines were cultured with PE (16:0_22:6). The addition of this lipid resulted in an increase in the LPL species LPE, particularly LPE (16:0) (Figure 16B). As previously mentioned, LPL can play an important role in ferroptosis, primarily acting as an acceptor of fatty acids leading to the formation of PLs. LPL levels have been shown to significantly increase in ferroptotic cells, whereas the corresponding PUFA-containing PLs decrease (135, 136). This data suggest that the MM cells are internalising PE (16:0_22:6) and the lipid is being utilised as a ferroptosis substrate within four hours. Expanding on this research by performing a time course would help to determine if the increase in LPE observed correlates with ferroptotic cell death. To investigate the impact of the exogenous lipids on the lipidome of MM cell lines, the data from the lipidomics analysis were analysed in more detail.

The addition of PE (16:0_16:0) to OPM-2 and KMS-11 MM cells resulted in a significant increase in the proportion of SFAs in both lines, while addition of PE (16:0_18:2) only had significant effects on the lipidome of OPM-2 cells (Figure 17). Addition of PE (16:0_20:4) did significantly increase the proportion of PUFAs in the OPM-2 but not KMS-11 cells, while the addition of PE (16:0_22:6) significantly increased the proportion of PUFAs in both MM cell lines (Figure 17). Docosahexaenoic acid, as previously discussed, is expressed at significantly lower levels in the MM, compared to DLBCL cell lines, which may explain the efficacy of this lipid at sensitising MM cells to ferroptosis. After treatment with PE (16:0_22:6), the lipidome

of the KMS-11 cells resembled that of OPM-2 cells at baseline, suggesting that exogenous addition of this lipid is effective at modulating the lipidome.

Cell lines were cultured with the four lipids (PE (16:0_16:0), PE (16:0_18:2), PE (16:0_20:4) and PE (16:0_22:6), one of which contained only SFAs, to test the impact of the lipids on ferroptosis sensitivity. Intriguingly, cell death of the OPM-2 and KMS-11 cells appeared to be dependent on the double bonds within the lipids, with higher amounts of unsaturation correlating with a greater capacity to induce ferroptosis (Figure 18A). As expected, addition of PE (16:0_16:0) had no effect on cell viability. There is evidence in the literature that suggests palmitic acid uptake via CD36, leads to ER stress and an increase in intracellular iron, suggesting iron overload was the mechanism that induced ferroptosis (219, 220). Other studies have shown that SFA can promote apoptotic and not ferroptotic cell death, but it was apparent that this fatty acid had no effect on the viability of MM cells (Figure 18A) (221). Minimal effects of PE (16:0_18:2) were also observed and only at the higher concentrations (Figure 18A). Studies have shown that linoleic acid (18:2) can act as a substrate for ferroptosis in some cell types, but we observed low levels of lipid peroxidation in MM cells following culture with this lipid (Figure 18A) (207, 209). In contrast, culturing MM cells with AA did significantly increase lipid ROS levels and ferroptosis-mediated cell death (Figure 18A), which is consistent with previous studies concerning this lipid (194, 204, 206). Interestingly, addition of PE (16:0_22:6) resulted in the most significant decrease in cell viability and increase in lipid ROS generation in the MM cells (Figure 18A and C). The docosahexaenoic acid in this lipid has been investigated in the context of ferroptosis, although not as extensively as AA, and has been shown to promote ferroptosis (130, 204, 205, 217). The cell death observed in the MM cell lines was dependent on the number of double bonds, which is consistent with findings in a study on colon cancer and hypopharyngeal carcinoma in which the cytotoxic effects of free fatty acids were also found to correlate with the degree of saturation (204). Phospholipids containing DHA (PC (18:0_22:6)) have also been shown to induce ferroptosis in human ovarian cancer cell lines (217). This study also demonstrated greater lipid ROS generation when cells were cultured with PC and PE (18:0_22:6) than PC (18:0_20:4), further supporting our results (217).

MM cells cultured with the PE lipid containing docosahexaenoic acid, also clearly displayed morphological changes associated with ferroptosis (Figure 18D). In addition to the cytotoxic

effects, we found that PE (16:0_22:6) also inhibits the proliferation of cells from three MM lines (Figure 19), an effect that has also been shown in other cancers, including leukemia, breast cancer, neuroblastoma, colorectal cancer, prostate cancer and melanoma (222).

3.3.4 Ferroptosis substrate PE (16:0_22:6) and GPX4 inhibition induce synergistic dell death in MM cell lines

PLs containing PUFAs are well recognised as ferroptosis substrates in other cell types, but there is limited information concerning their role in ferroptosis of MM cells. A PE lipid comprised of docosahexaenoic acid was identified as having the most significant effect on MM cell viability and proliferation and caused the largest increase in the proportion of intracellular PUFAs. The role of docosahexaenoic acid as a free fatty acid has been studied in the context of ferroptosis but there are a limited number of studies of this lipid once it has been incorporated into PLs. This is also the case for AA, prompting us to investigate the effects of both fatty acids following their incorporation into PE lipids in MM cells. The results discussed in the previous section suggest that the capacity of lipids to induce ferroptosis of MM cells is dependent on the number of double bonds in the lipids. To further investigate the potential of these lipids to sensitise MM cells to ferroptosis we assessed the effects of culturing MM cells with PE lipids in combination with the GPX4 inhibitor, RSL3.

The OPM-2 and KMS-11 cell lines were cultured with 20 µM of all the PE lipids mentioned above and increasing concentrations of RSL3, for 24 hours. The addition of PE (16:0_16:0) had no effect on the viability of the cells (Figure 20A). Palmitic acid has been shown to promote ferroptosis in a non-canonical manner, utilising CD36 to induce ER stress and disrupt the balance of intracellular iron (219, 220). CD36 is a long chain fatty acid transporter that is not generally expressed in MM, which might explain why palmitic acid does not promote ferroptosis in MM cells (223). Addition of the PUFA, PE (16:0_18:2) (linoleic acid) also had minimal effect on cell viability when combined with RSL3. Linoleic acid has been shown to promote ferroptosis in a range of cancer cells, by increasing the pool lipids that are available as ferroptosis substrates. However, this was not evident in MM cells in our study (Figure 20A) (207, 209).

AA has been extensively studied in the context of ferroptosis and has emerged as an essential ferroptosis substrate (194, 204, 206). The addition of a PE lipid containing AA (PE (16:0_20:4)

did result in a significant increase in the proportion of PUFAs in the OPM-2 but not the KMS-11 cells, despite its ability to augment the effects of RLS3 in both cell lines (Figure 18 and 20). This result was not unexpected, particularly given the prior research in our group, which showed that free arachidonic acid can increase the sensitivity of MM cells to ferroptosis and the literature, which suggests AA is an important ferroptosis substrate. Notably, the combination of PE (16:0_20:4) and RSL3 did not result in cell death of all KMS-11 cells, even at the highest concentration of RSL3, suggesting that either a longer time of treatment may be necessary or this combination may not be effective at fully sensitising this resistant cell line to RSL3 (Figure 20 A). However, this result supports the notion that optimal ferroptosis-mediated cytotoxic effects may be achieved by tailoring the lipids to the MM cells. Although our results demonstrate that MM and DLBCL cells analysed express similar levels of PLs containing AA, the MM cells had a significant deficiency in PLs containing docosahexaenoic acid.

As discussed earlier, the role of docosahexaenoic acid in ferroptosis has been investigated and has been shown to promote ferroptosis by increasing the levels of intracellular PUFAs (130, 204, 205). PE (16:0_22:6) in combination with RSL3 had a significant impact on the viability of KMS-11 cells, decreasing cell viability to approximately 20 % at the highest concentration of RSL3 (Figure 20A). The effects of the lipid and GPX4 inhibitor against KMS-11 cell line were also confirmed as synergistic. A marked increase in the sensitivity of OPM-2 cells to RSL3 was also observed with the addition of the lipid, an effect that again was confirmed to be synergistic (Figure 20A). Interestingly, synergy in terms of ROS generation was also observed in both cell lines in response to PE (16:0_22:6) in combination with RSL3 (Figure 20C). These results were subsequently confirmed in three other MM cell lines, H929, KMS-18 and LP-1 (Figure 22B). In all three cell lines the combination of PE (16:0_22:6) and RSL3 induced synergistic cell death, which was preventable by treatment with liproxstatin-1. This result is significant as it suggests that MM cell lines can be sensitised to ferroptosis irrespective of the basal levels of ferroptosis substrates in the cells. The addition of PE (16:0_22:6) can not only sensitise RSL3 resistant MM cells but can further sensitise already sensitive cells (OPM-2) to ferroptosis. These results suggest that although cell lines may be deficient in specific lipids, as shown by the lipidomics data, culturing MM cells with a PUFA PL with a high degree of unsaturation will sensitise the cells to ferroptosis. These results were

confirmed when additional lipids were tested in the OPM-2, KMS-11, LP-1 and KMS-18 cell lines (Figure 24). The results of these experiments showed that the efficacy of PUFA PLs to sensitise cells to ferroptosis were largely dependent on the number of double bonds in the PL, particularly evident in cells cultured with RSL3 and PE (16:0_22:6), compared to RSL3 and PE (16:0_20:4) (Figure 24). Importantly, no significant increase (or decrease) in sensitivity to RSL3 was observed when the cells were cultured with PC (16:0_22:6) compared to PE (16:0_22:6), suggesting that the head group of the PL was not as important as degree of PL saturation (Figure 24).

3.3.5 PE-MUFA is an effective inhibitor of ferroptosis

MUFAs have been extensively studied in the context of ferroptosis and have been shown to play a pivotal role in ferroptosis resistance (224-226). Using MUFAs to promote ferroptosis resistance has been demonstrated in other cancers, but not in MM. The high proportion of MUFAs in most of the MM cell lines tested, prompted us to investigate the effects of exogenous MUFAs on the ferroptosis sensitivity of MM cells. Viability of cells from all five of the MM cell lines was assessed following a 24 h culture with RSL3 and PE (16:0_18:1) (Figure 25B). Remarkably, in all the cell lines (OPM-2, LP-1 and H929) that responded to treatment with RSL3 alone, addition of PE (16:0_18:1) completely attenuated the cell death, in a manner comparable to liproxstatin-1 (Figure 25). Furthermore, lipid ROS generated in KMS-11 and OPM-2 cells in response to treatment with RSL3 was completely inhibited by the addition of MUFAs (Figure 21B).

A lipidomics analysis was performed after culturing the cells with PE (16:0_18:1) for 4 hours. Intriguingly, no significant increase in the lipid in the MM cell lines was observed, nor was there a significant change in the lipidome of either of the cell lines. However, oleic acid was more prominent in generated heatmaps and volcano plots in samples cultured with PE (16:0_18:1), while PL-PUFA appeared to be displaced (Figure 23 and Appendix Figure 3). This may indicate that the cells only require a small shift in their lipid composition, with displacement of PUFAs by oleic acid to resist ferroptosis. While the uptake of PE (16:0_18:1) and the increase in oleic acid requires further investigation, the results demonstrate that MUFAs play a key role in determining the sensitivity of MM cells to ferroptosis, which is consistent with findings in other cancers (217, 224, 225).

3.3.6 Conclusions

This chapter has focused primarily on elucidating the mechanisms by which MM cells can be sensitised to ferroptosis. Previous research within our group and in the literature has demonstrated that MM and AML cells are more resistant to ferroptosis than other aggressive haematological malignancies, such as DLBCL (136). Lipids, particularly PLs containing PUFA, have been shown to be important ferroptosis substrates and may play a key role in dictating ferroptosis sensitivity (117, 191). The data presented in this chapter demonstrate that, in general, MM cells are comprised of significantly higher proportions of MUFAs, which confer ferroptosis resistance, and significantly lower proportions of PUFAs, than the DLBCL cells analysed. Notably, the RSL3 sensitive MM cell line, OPM-2, has a similar PL profile to the sensitive DLBCL cell lines, suggesting that the lipid composition of cells may be useful in determining their sensitivity to ferroptosis. Importantly, the data demonstrate that supplementing MM cells with PLs containing PUFAs can remodel the PL composition of the cells and increase the proportion of PUFAs. This significantly increased the sensitivity of all the MM cell lines to RSL3, while addition of exogenous MUFA had the opposite effect, increasing their resistance to the GPX4 inhibitor. These data represent an important step towards a better understanding of the factors that dictate ferroptosis sensitivity of cells and may aid in identifying novel, ferroptosis-mediated treatment approaches designed to treat apoptosis resistant cancers.

The work presented in this chapter also represents a foundation for the final aim of this project, which was to develop targeted ferroptosis inducing liposomes. It was intended that data from the lipidomics analyses presented in this chapter could be used to determine the specific lipid or lipids that render each MM cell line sensitive to ferroptosis and that liposomes tailored to each cell line could then be manufactured. However, throughout the course of this project we gained a better understanding of the role of lipids in ferroptosis, through our own work and from emerging research from other groups. It became apparent that rather than specific lipids being important for each cell line, PE lipids with a high degree of unsaturation represent important ferroptosis substrates, regardless of the cell line. This suggests that precision liposomes tailored to an individual cell line or patient MM cells may be less effective than liposomes composed of lipids with the highest oxidation capacity.

The next chapters describe the results of work aimed at developing a novel antibody for targeting MM cells and the manufacture of novel liposomes that induce ferroptosis of MM cells.

CHAPTER 4. DEVELOPMENT OF NOVEL B-CELL MATURATION ANTIGEN (BCMA)-TARGETED MONOCLONAL ANTIBODIES

4.1 Introduction

The overarching aim of this chapter was to develop a novel monoclonal antibody (mAb) targeted to the B cell maturation antigen (BCMA). BCMA is a type III transmembrane protein, which plays a critical role in B-cell proliferation and survival (70). The important pro-survival signalling pathways downstream of BCMA, which include NF-κB signalling pathway, the protein kinase B (AKT) pathway, the MEK/ERK pathway, c-Jun N-terminal kinases (JNK), ELK-1 and p38 Kinase, mean targeting BCMA represents a promising therapeutic strategy, particularly for B-cell malignancies (70-72). BCMA is preferentially expressed on the surface of plasma cells and a subset mature B lymphocytes, while it is minimally expressed on hematopoietic stem cells or non-hematopoietic tissue. MM cells consistently express BCMA on their cell surface, and studies have demonstrated that the expression of BCMA is higher on malignant plasma cells compared to either normal plasma cells or other bone marrow cell subsets (73). BCMA is essential for the survival of long-lived bone marrow plasma cells but is not required for B-cell homeostasis (73). This highlights the potential of BCMA as a target for precision therapy of MM and as a biomarker for assessing response to therapy in this disease.

MAbs have become increasingly important for the diagnosis and treatment of many diseases. The high specificity and restricted reactivity of mAbs have made them crucial in a range of diagnostic tests, for identifying and characterising diseases and distinguishing cell populations. MAbs have also proven to be highly effective as therapeutic agents; by binding to specific proteins on target cells they can induce cell death, inhibit cell growth, block specific ligand binding sites, or potentiate the actions of other drugs (38). Given the specificity of mAbs and the elevated expression of BCMA on MM cells, new therapies have emerged that utilise BCMA to target MM cells. The novelty of developing a BCMA monoclonal antibody was in discovering antibodies that had unique properties, with greater binding affinity and anti-MM effects, compared to currently approved antibodies. There are currently no BCMA

antibodies that are used as single agents in MM, highlighting an important gap in MM treatment.

The primary focus of the work in this chapter was the development of a novel anti-BCMA monoclonal antibody, which could be used to functionalise the liposomes developed in the next chapter. Given the complexity of developing and screening monoclonal antibodies, anti-CD38 mAb, daratumumab, which is an FDA approved monoclonal antibody was also used in this chapter. The proven efficacy and safety of daratumumab, in addition to the well-defined pharmokinetics and pharmacodynamics, would make it a suitable comparison for our own novel antibody.

Daratumumab targets CD38, an extracellular and intracellular enzyme that is normally expressed at low levels on human immune cells and endothelial cells. CD38 is overexpressed on a range of tumour cells, including MM, making it a therapeutic target. Daratumumab is an immunoglobulin G1 kappa mAb that recognises a unique epitope of the human CD38 (79). While there is no research surrounding daratumumab and ferroptosis, the antibody has been hypothesised to directly induce apoptosis, specifically through $F_c\gamma$ receptor I mediated cross-linking (83). Daratumumab has been used both as a single agent and in combination with other agents, and is effective via antibody-dependant cellular cytotoxicity (ADCC), antibody dependant cellular phagocytosis (ADCP), complement dependant cytotoxicity (CDC) and direct cellular apoptosis (49, 50, 81, 82, 227). The combination of the commonly used MM drug lenalidomide and daratumumab resulted in enhanced anti-cancer affects (84). Daratumumab is approved in Australia for MM patients experiencing their first relapse, in combination with bortezomib and dexamethasone (DaraVd) as published in the CASTOR trial (228). Daratumumab monotherapy showed promising efficacy in patients with MM who were heavily pretreated (median of 5 previous lines of therapy), with a 3-year survival of 36.5 % and no treatment related deaths (227). The final use for the antibody selected will be to functionalise the surface of novel liposomes, developed in the next chapter.

4.2 Results

4.2.1 MM cell lines variably express BCMA

BCMA is in an important cell surface antigen that is overexpressed on the surface of malignant plasma cells, promoting cell survival and proliferation, making it a useful therapeutic target for MM (58). Cell surface expression of BCMA was assessed on five MM cell lines and on the chronic myeloid leukemia (CML) line, K562, by flow cytometry and by western blotting using a commercial antibody (Figure 27).

Cells were stained with either the commercial BCMA antibody or an isotype control antibody, followed by a phycoerythrin (PE) conjugated secondary antibody. The mean fluorescence intensity (MFI) in the PE signal was then used to calculate the fold change in the BCMA to isotype signal as a measure of BCMA expression (Figure 27A-B). Strong BCMA expression was observed in all five of the MM cell lines, with the highest expression observed on the H929 MM cell line (Figure 27A). The lowest BCMA expression observed among the MM cell lines was on the KMS-18 cells. Importantly, no expression of BCMA was observed on the K562 (CML) cells. Western blotting was also used to examine BCMA expression in the cell lines (Figure 27C). The results obtained by Western blotting were consistent with those from flow cytometry, moreover, as the Western blotting was performed on whole cell lysates, these data also demonstrate that K562 cells do not express BCMA on their cell surface or internally. Also consistent with the flow cytometry results, the lowest level of expression was observed in the KMS-18 cell lysate with a relatively faint band corresponding to BCMA, while the highest expression was observed in the H929 lysate (Figure 27C).

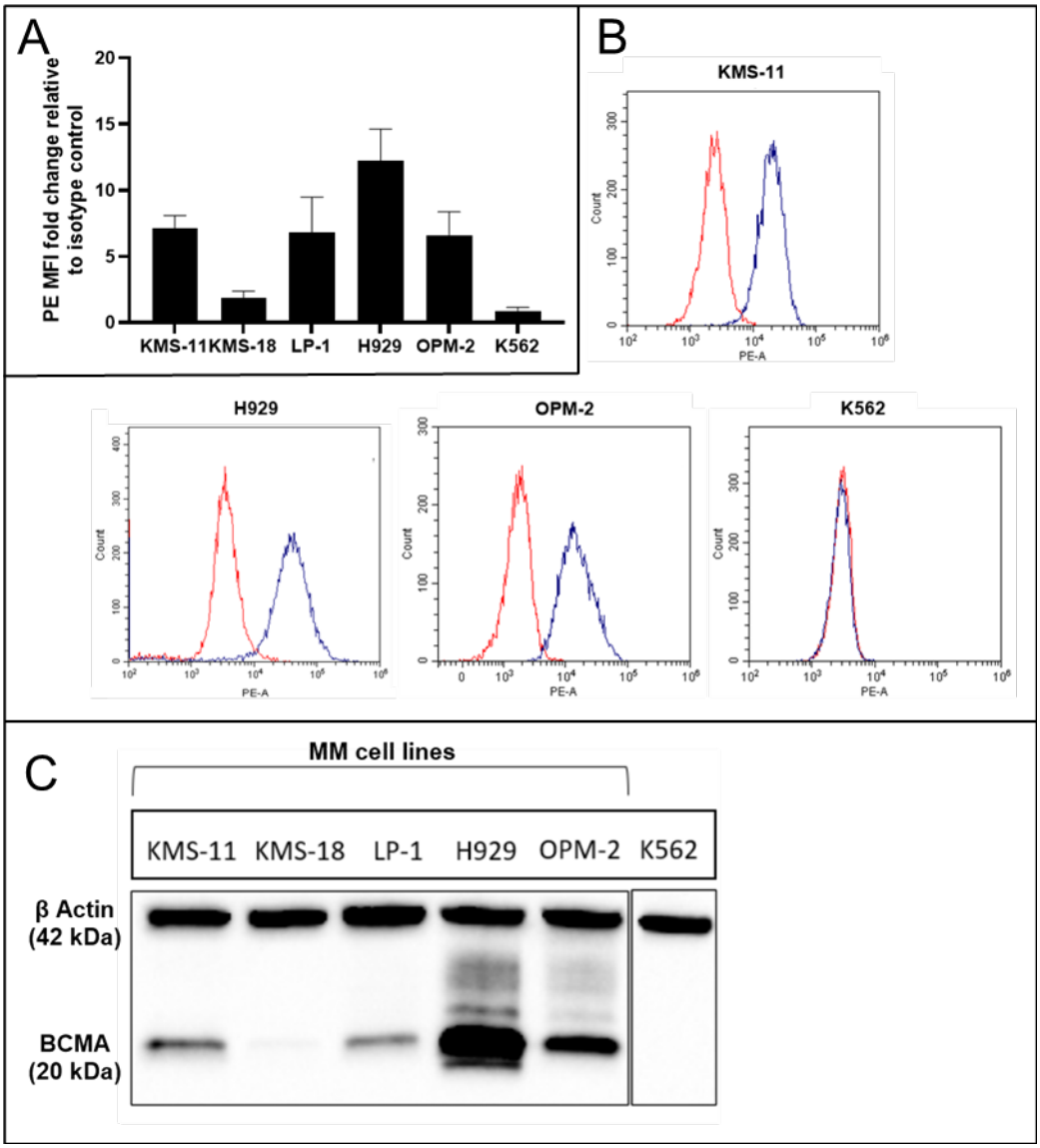

Figure 27. BCMA is expressed at varying levels in MM cell lines, whereas K562 (CML) cells do not express BCMA.

(A) MM cell lines and K562 (negative control) were incubated with either a commercial anti-BCMA antibody or an isotype control antibody for 30 minutes. Cells were then stained with a phycoerythrin (PE)-conjugated secondary antibody and analysed by flow cytometry. Expression of BCMA was assessed as the fold change in the mean fluorescence intensity (MFI) of cells stained with the BCMA antibody compared to cells incubated with the isotype control. Data are the mean and standard deviation from a minimum of 2 biological replicates per cell line. **(B)** Representative flow cytometry histograms of BCMA expression in the different MM and K562 cell lines. **(C)** BCMA expression was assessed by Western blotting in whole cell lysates from the MM and K562 cell lines. Expression of β-actin was used as a control for protein loading.

4.2.2 Hybridoma supernatants display surface binding capacity in MM but not CML cell line K562

A detailed description of antibody production can be found within the introduction in section 1.3.2 (Figure 3). To briefly summarise, we developed a novel 15 amino acid peptide that corresponds to an extracellular section of the BCMA domain based on its uniqueness to other BCMA antibodies, immunogenicity, and water solubility. Immunocompetent mice were injected with our novel peptide to elicit an immune response and screened for BCMA binding antibodies through ELISA, against our peptide. Splenic B cells were then removed to develop hybridoma cell lines, which are formed by the fusion of primary splenic B-cells to myeloma cells, which produce and secrete antibodies into the culture supernatant (68). These steps were performed by the Monash Antibody Discovery Platform (MADP).

These supernatants are then tested against cell lines that express the protein that the antibodies are raised against to confirm their ability to recognise the protein and their specificity for the protein. Due to the complexity of forming hybridomas and the subsequent subcloning of a cell line, screening is often performed after the hybridomas are formed and before subcloning occurs. This increases the possibility of developing a successful antibody that binds to its target. During this process, the cells secreting the antibodies are often not clonal, meaning that the antibodies secreted are polyclonal rather than monoclonal. The nomenclature given to the supernatants tested in the sections below refers to the well from which the hybridoma cells were grown.

Three different MM cell lines, OPM-2, KMS-11 and LP-1, and one CML cell line, K562, were initially used to screen the supernatants derived from the hybridoma cells. The MM cell lines were incubated with neat supernatant, washed and then incubated with a secondary anti-mouse PE-conjugated antibody. Our initial screens using the LP-1 and K526 cell lines identified supernatants that showed some degree of BCMA binding capacity to the MM cells, but not the K562 cell line (Figure 28A). Notably, supernatants 16B8 and 1D9 appeared to have the greatest binding capacity to the LP-1 cell line (Figure 28A). A further set of supernatants was then tested against the OPM-2 and KMS-11 cell lines to determine whether anti-BCMA antibodies were likely present. These two cell lines were subsequently used to perform the remainder of the antibody screening, as they had been determined as the two best candidates for testing in other aspects of the project. This second screen uncovered several more

supernatants that appeared to contain antibodies with BCMA binding capacities, notably supernatants 14C8, 4F10, 2B10 and 5G4 (Figure 28B and 29). From this initial screening, the top eight supernatants were selected for further testing against the KMS-11 and OPM-2 cell lines. The supernatants in Figure 29 all exhibited surface binding capacities, presumably to BCMA, by flow cytometry. The histograms for supernatants 4F10 and 5G4 (Figure 29 B-C) displayed a right-shift in the fluorescence signal compared to cells incubated only with the secondary antibody, indicating an increase in binding of the secondary antibody, likely due to the presence of a primary BCMA antibody. The supernatants selected were then screened for potential cytotoxic effects against the MM and CML cell lines, however no effect on the viability of any of the cell lines was observed following incubation with any of the supernatants (Figure 30).

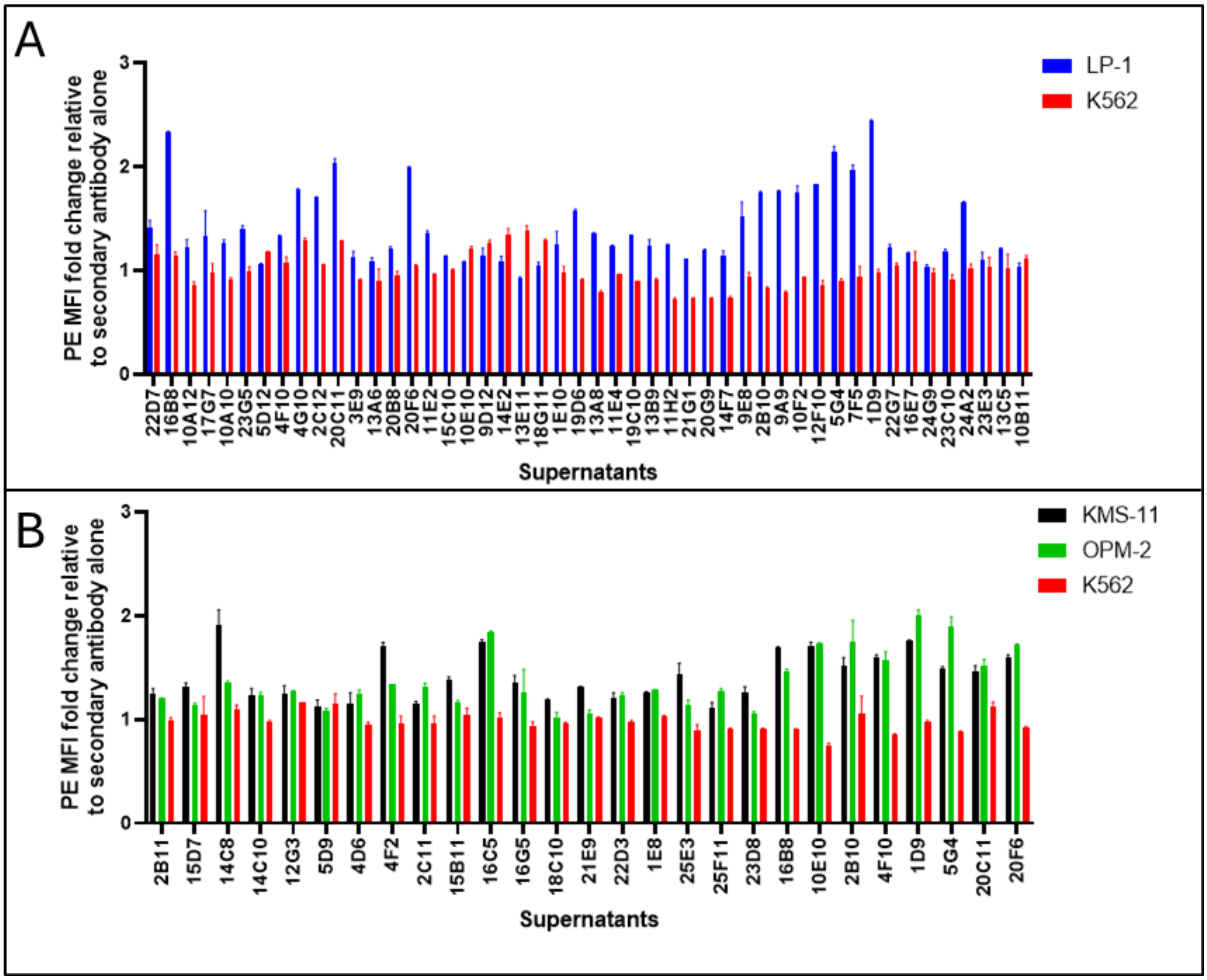

Figure 28. Supernatants derived from established hybridomas exhibit BCMA binding capacity.

(A) MM cell lines LP-1, **(B)** OPM-2 and KMS-11 and the CML cell line, K562, were incubated with neat hybridoma cell culture supernatant, washed and then stained with an anti-mouse PE-conjugated secondary antibody. BCMA binding capacity was assessed by flow cytometry. Data are the mean and standard deviation from a minimum of 2 technical replicates per cell line.

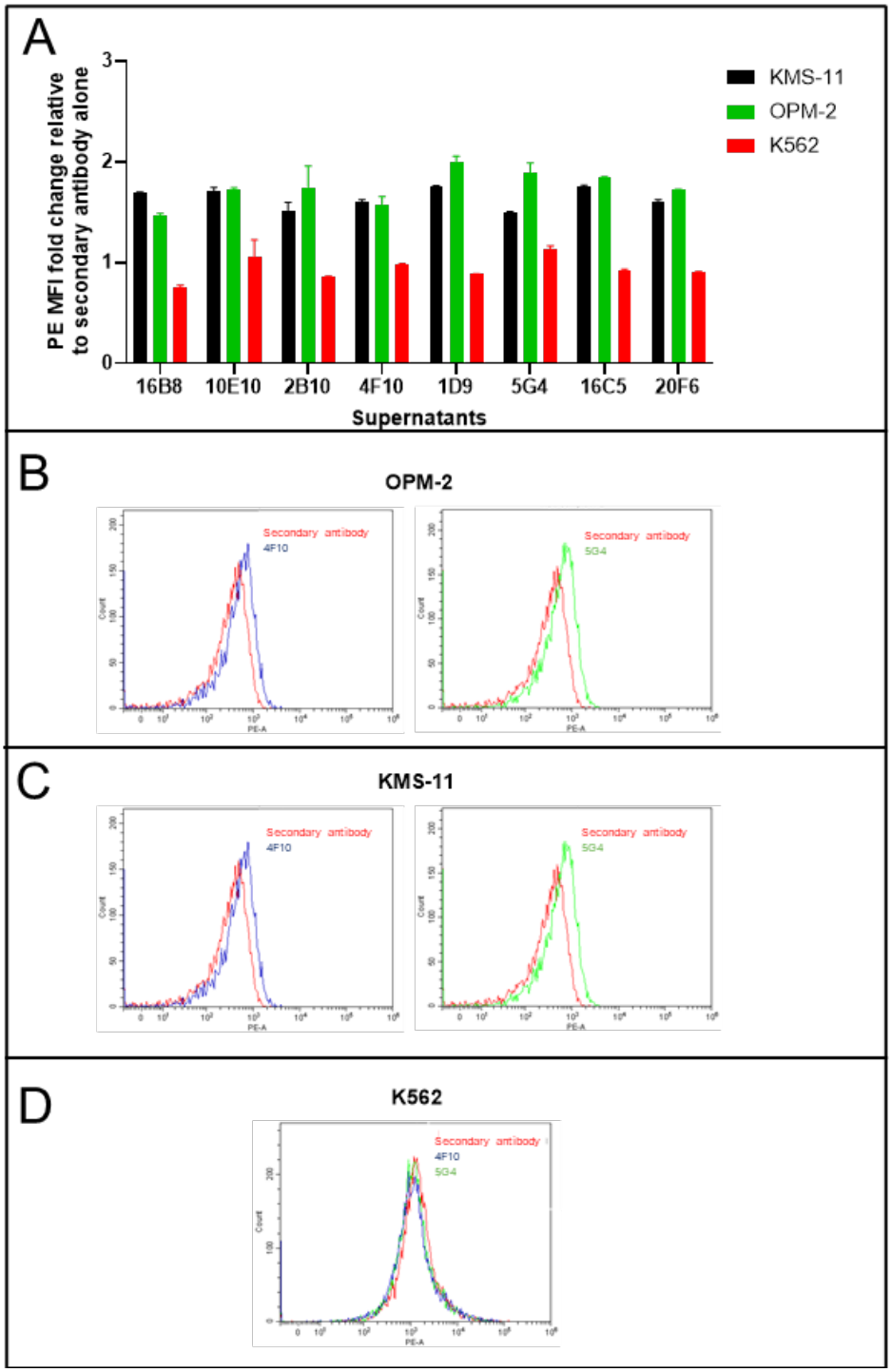

Figure 29. Top eight supernatants exhibit BCMA binding capacity to MM but not K562 cells.

(A) MM cell lines, OPM-2 and KMS-11 and the CML cell line K562 were incubated with neat supernatant, followed by staining with a PE-conjugated secondary antibody. BCMA binding capacity was assessed by flow cytometry. **(B)** to **(D)** Representative flow cytometry histograms of supernatants 4F10 and 5G4 against OPM-2, KMS-11 and K562 cells. Data are the mean and standard deviation from a minimum of 2 technical replicates per cell line.

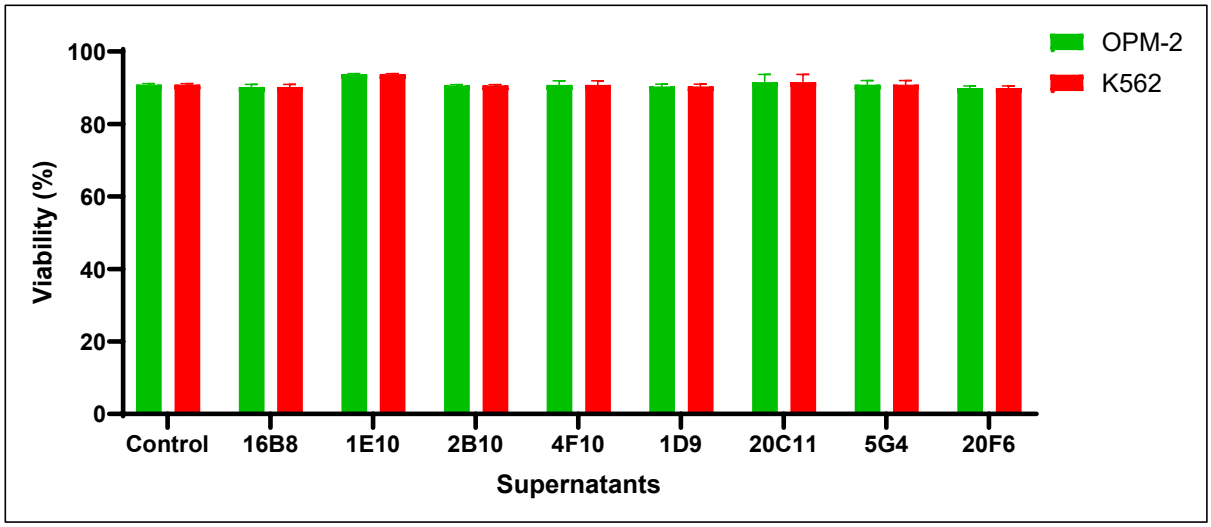

Figure 30. Supernatants that bind to BCMA do not induce cell death of OPM-2 or K562 cells.

OPM-2 and K562 were cultured with the hybridoma supernatant indicated for 24 hours. Cell viability was assessed by flow cytometry following staining with annexin V and PI. Data are the mean and standard deviation from a minimum of 2 technical replicates per cell line.

4.2.3 BCMA hybridoma supernatants can have anti-proliferative effects on MM cells

Given the role that BCMA plays in promoting MM cell proliferation and survival, we investigated the effects of the BCMA hybridoma supernatants on the survival and proliferation of OPM-2 (MM) and K562 (CML) cells (58). The effects of all of the supernatants received from MADP were screened by MTT assay. As shown in Figure 31, many of the supernatants had no functional effects on OPM-2 cells. However, some of the supernatants did have anti-proliferative effects against OPM-2, but not K562 cells, suggesting that the antibodies present in these samples do have effects on the ability of BCMA to promote MM cell proliferation (Figure 31). Of the supernatants that did decrease OPM-2 cell proliferation, the greatest effects were observed with samples 3E9, 4F10, 1D99, 5G4 and 5D12. Importantly, these supernatants had no effect on K562 cells (Figure 31).

To further confirm these functional effects, 6 supernatants that demonstrated the greatest effect on the OPM-2 cells (Figure 31) were selected for further testing against the KMS-11 and OPM-2 MM cell lines and the K562 cell line. From these experiments only two supernatants

induced a significant decrease in proliferation of the MM cell lines, 5G4 and 4F10 (Figure 32). Importantly, none of the six supernatants tested had any anti-proliferative effect on K562 cells (Figure 32). The anti-proliferative effects against OPM-2 cells were subsequently confirmed by staining the cells with carboxyfluorescein succinimidyl ester (CFSE) and by measuring the rate of decay of the CFSE signal by flow cytometry, with excitation and emission at 488 nm and 565 nm, respectively. Levels of CFSE fluorescence were recorded over a 72-hour time course. These data further confirmed those obtained by MTT assay, with significant reductions in proliferation observed in OPM-2, but not K562, cells incubated with 5G4, 2B10 and 4F10 (Figure 33). None of the supernatants had an effect on proliferation at 24 hours, and only sample (4F10) induced a significant decrease in cell proliferation at 48 hours (Figure 33).

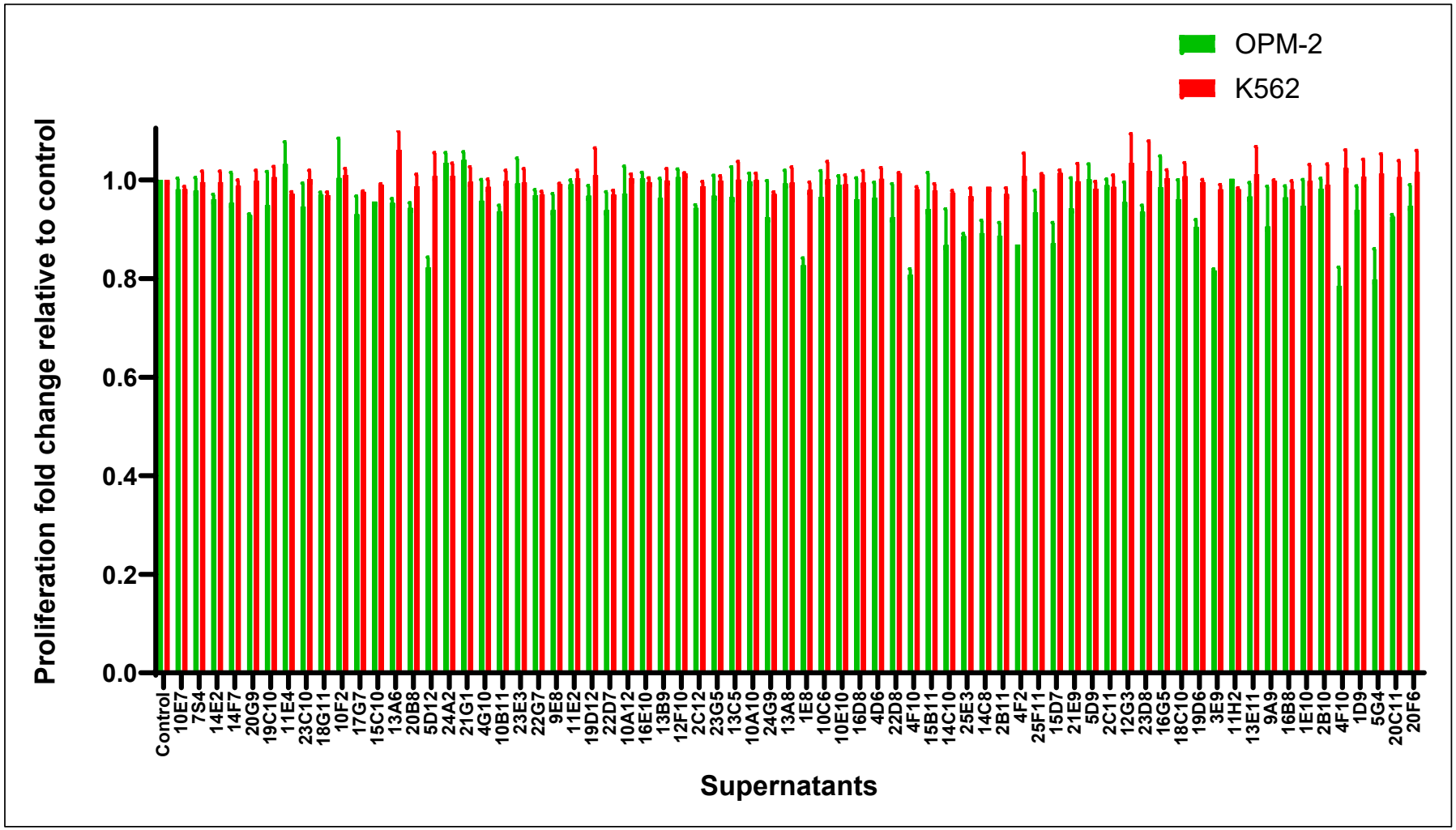

Figure 31. Some supernatants decrease proliferation of OPM-2 but not K562 cells.

OPM-2 and K562 cells were cultured for 24 hours in the presence of the supernatants indicated. Cell proliferation was assessed by MTT assay and compared to untreated control. Data are the mean and standard deviation of two technical replicates.

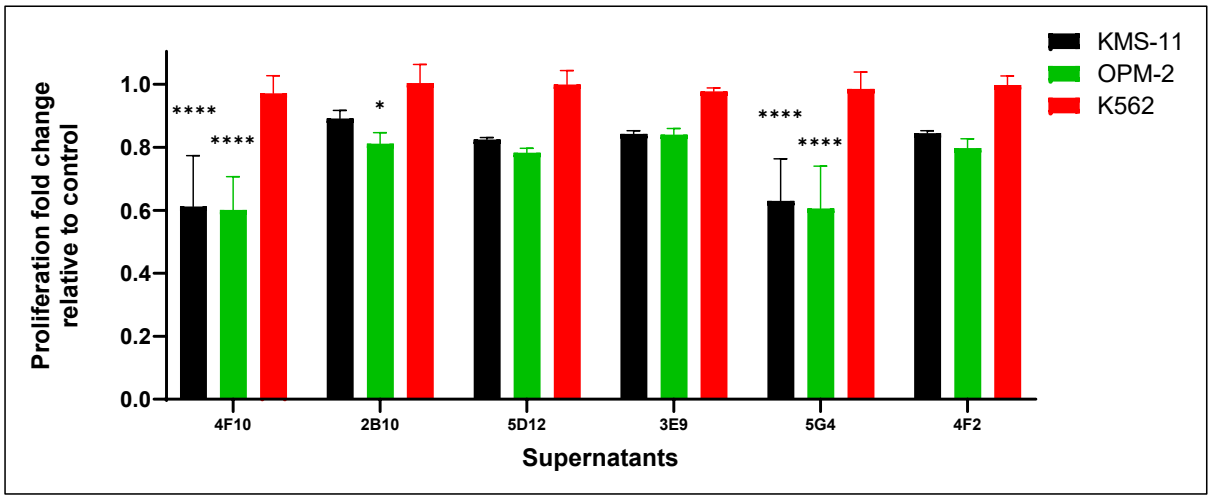

Figure 32. Supernatants from BCMA antibody supernatants induce a significant decrease in cell proliferation.

KMS-11, OPM-2 and K562 cells were cultured with neat supernatant for 24 hours. Cell proliferation was assessed by MTT cell proliferation assay and compared to untreated control. Data are the mean and standard deviation of two technical replicates. Statistical analysis performed using two-way ANOVA of a minimum of 3 biological replicates. *P<0.05, **P<0.01, ***P<0.001, **** P<0.0001.

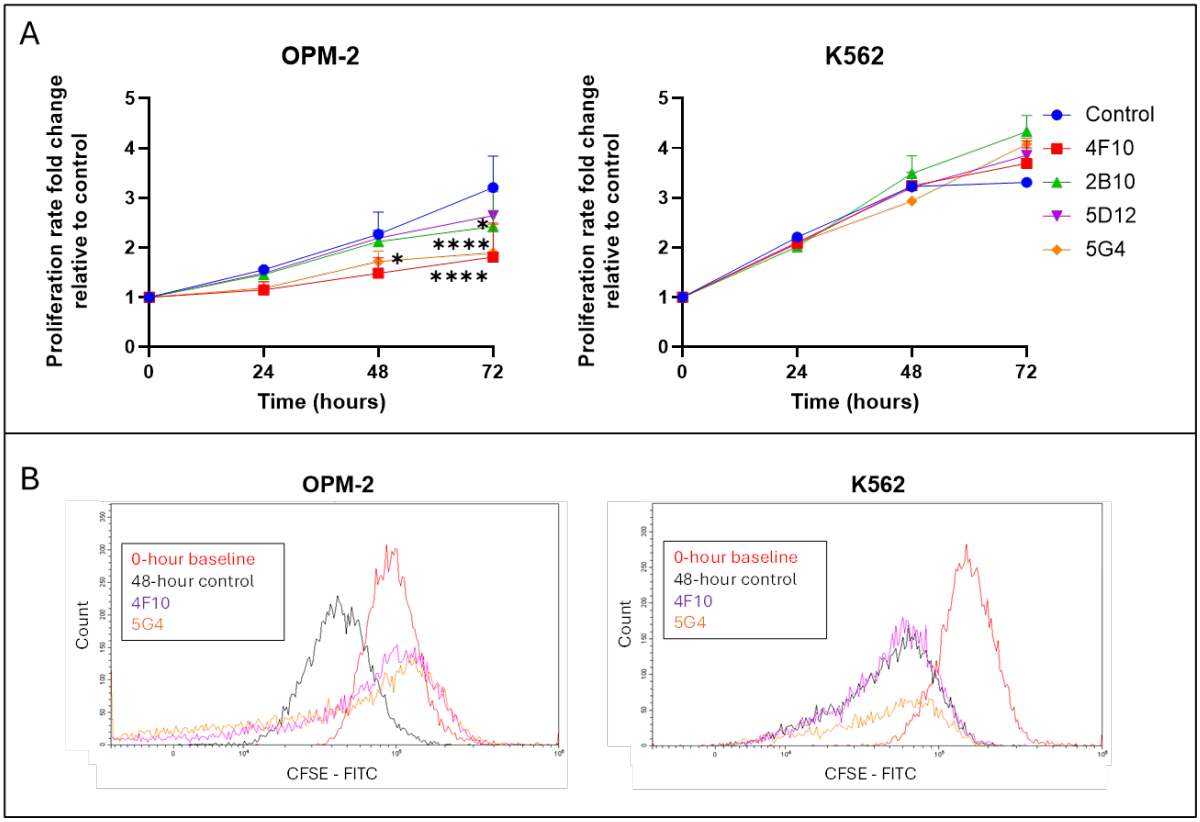

Figure 33. 4F10, 5G4 and 2B10 supernatants induce a significant decrease in cell proliferation in OPM-2, but not K562 cells.

OPM-2 and K562 cells were cultured with neat hybridoma supernatant for up to 72 hours. Cell proliferation was assessed by flow cytometry in cells stained with CFSE compared to untreated control. Data are the mean and standard deviation of 3 biological replicates. **(B)** Representative histograms of the OPM-2 and K562 cell lines. Statistical analysis performed using two-way ANOVA of a minimum of 3 biological replicates: *P<0.05, **P<0.01, ***P<0.001, **** P<0.0001.

4.2.4 5G4 and 4F10 as suitable supernatant for subcloning and the production of monoclonal antibodies

Hybridoma supernatants 5G4 and 4F10 were shown to rank among the top 8 supernatants in terms of surface binding to the OPM-2 and KMS-11 cell lines, but not K562 cells, when compared to untreated control (Figure 29). The results presented earlier also suggest that these two supernatants had the greatest effect on cellular proliferation against the MM cell lines, both by MTT and CFSE assays (Figures 32 and 33). These results were confirmed in three additional MM cell lines, with significant decreases in proliferation in all three cell lines at 24 hours following treatment with the 4F10 and 5G4 supernatants (Figure 34B). To confirm that the reduction in proliferation was not due to cell death, we assessed cell viability and showed that the supernatants had no significant cytotoxic effect against any of the 4 cell lines (Figure 34A).

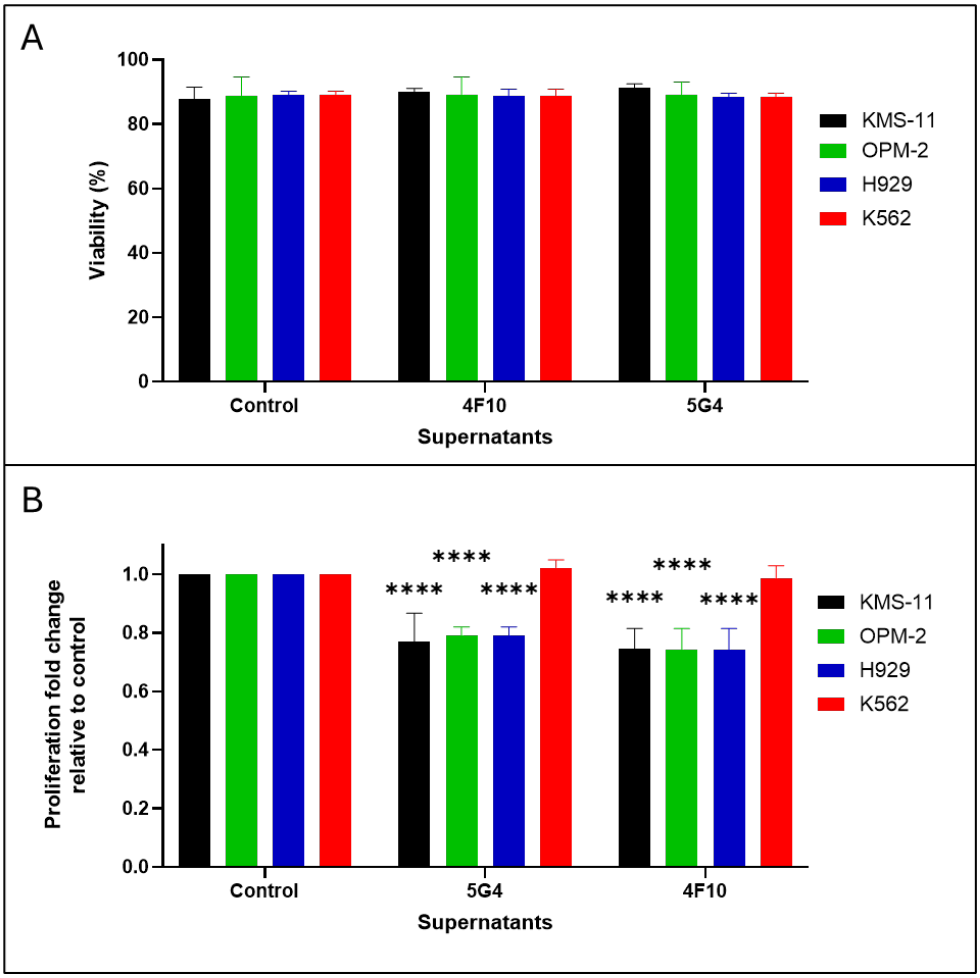

Figure 34. Hybridoma supernatants 5G4 and 4F10 induced a significant decrease in cell proliferation of MM cell lines, with no change in viability.

(A) KMS-11, OPM-2, H929 and K562 were cultured with neat supernatant for 24 hours. Cell viability was assessed by flow cytometry following staining with annexin V and PI. **(B)** KMS-11, OPM-2, H929 and K562 cells were cultured with neat supernatant for 24 hours. Cell proliferation was assessed by MTT cell proliferation assay. Data are the mean and standard deviation from a minimum of 3 biological replicates per cell line. Statistical analysis performed using two-way ANOVA of a minimum of 3 biological replicates. *P<0.05, **P<0.01, ***P<0.001, **** P<0.0001.

Next, BCMA knockout cell lines were developed in collaboration with the Molecular Therapeutics Laboratory at the Centre for Cancer Biology (CCB), Adelaide, to further confirm that binding and the effect of the supernatants on MM cell proliferation were mediated via BCMA expression on the MM cell surface. BMCA knockout construct were successfully transduced into KMS11 and OPM-2 cells using a CRISPR knock out guide RNA 1 and 2. BCMA knockout in the cell lines was confirmed by flow cytometry, in comparison to control BCMA-expressing cell lines (Figure 35A). BCMA expression was also confirmed by Western blot, but with interesting results. A distinct band at the expected molecular weight (20 kDa) was observed in control KMS-11 cells, however a higher molecular weight

band was evident in the two knockout cell lines (Figure 35B). This was also observed in one of the OPM-2 knock out lines, while no evidence of BCMA at the expected molecular weight or the higher molecular weight protein was observed in the other OPM-2 knockout line (Figure 35B). Possible explanations for the higher molecular weight band in the knockout cells will be discussed later in the chapter. These cell lines were developed to confirm the effects of the supernatants were BCMA specific. Figure 35C clearly demonstrates binding of a component of the 5G4 and 4F10 hybridoma supernatants to the two control MM cell lines and minimal binding to the BCMA knockout cell lines. The 5G4 and 4F10 supernatants also significantly reduced the proliferation of the vector control OPM-2 and KMS-11 cells but had no effect on the BCMA knockout cell lines (Figure 35D).

Given the results described above, subcloning of the 5G4 and 4F10 supernatants was attempted by staff at the MADP facility. Unfortunately, subclones derived from the hybridomas that produced the 5G4 and 4F10 supernatants did not yield any high affinity anti-BCMA antibodies that had binding against the OPM-2 or KMS-11 cell lines (Figure 36A). The products from the subcloned cells also had no effect on the proliferation of the MM cell lines (Figure 36B), while the BCMA binding capacity and antiproliferative effects of the parent supernatants 5G4 and 4F10 remained consistent (Figure 36). After multiple rounds of subcloning were unsuccessful, it was decided that another approach for developing a BCMA monoclonal antibody would be attempted.

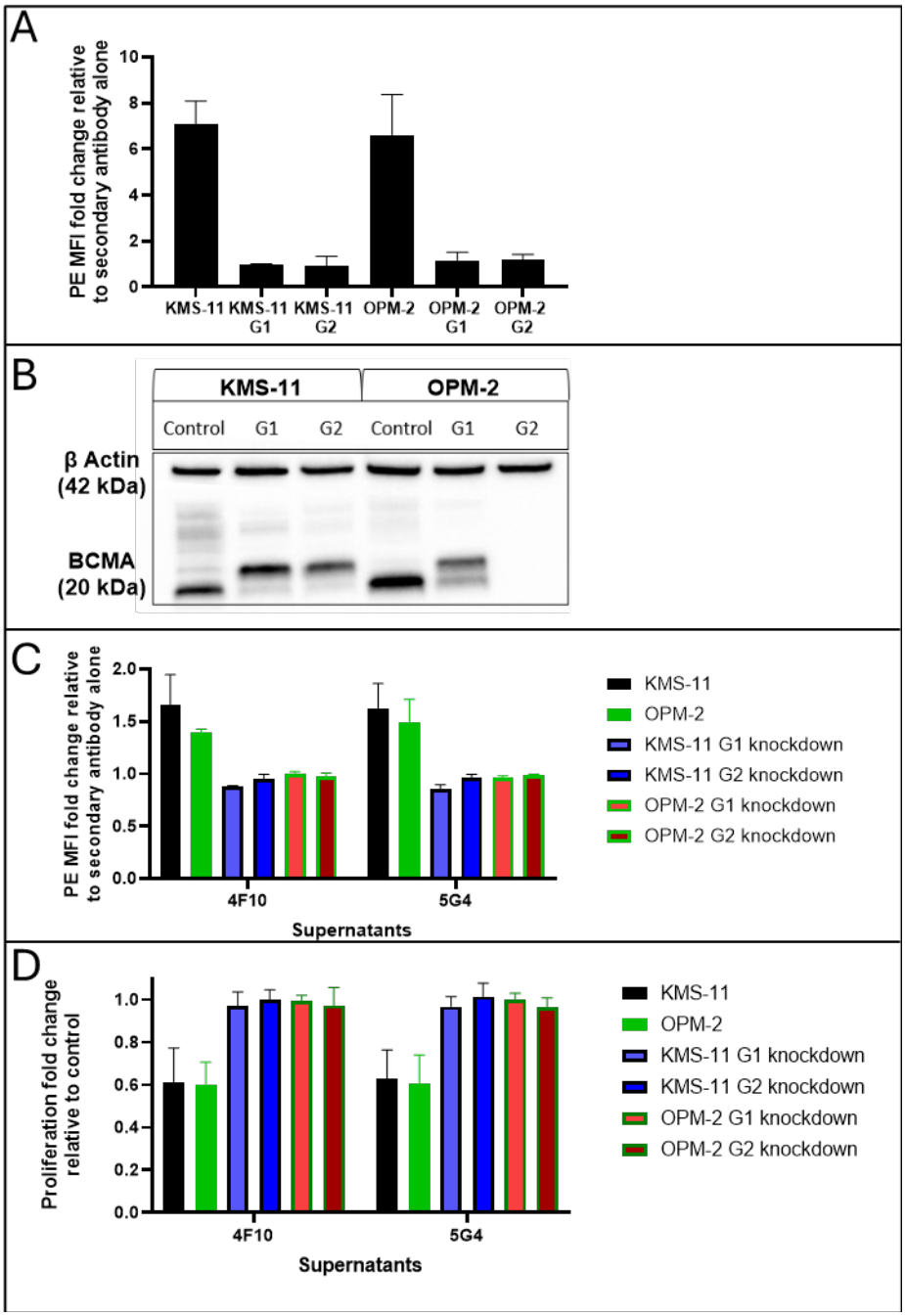

Figure 35. 5G4 and 4F10 supernatants do not bind to or impact proliferation of BCMA knockout KMS-11 and OPM-2 cells.

(A) KMS-11 and OPM-2 cells transduced with a control vector, BCMA guide RNA 1 (G1) and BCMA guide RNA 2 (G2) were incubated for 30 mins with a commercial BCMA antibody, followed by a PE-conjugated secondary antibody. BCMA expression was assessed by flow cytometry. Data are the mean and standard deviation from a minimum of 2 biological replicates per cell line. **(B)** BCMA expression in KMS-11, OPM-2 and corresponding BCMA knockout cell lysates was assessed by Western blot. **(C)** KMS-11, OPM-2 and corresponding BCMA knockout cell lines were incubated with neat supernatant. BCMA binding capacity was assessed by flow cytometry. Data are the mean and standard deviation from a minimum of 2 technical replicates per cell line. **(D)** KMS-11, OPM-2 and corresponding BCMA knockout cell lines were cultured with neat supernatant for 24

hours. Cell proliferation was assessed by MTT cell proliferation assay. Data are the mean and standard deviation from a minimum of 3 biological replicates per cell line.

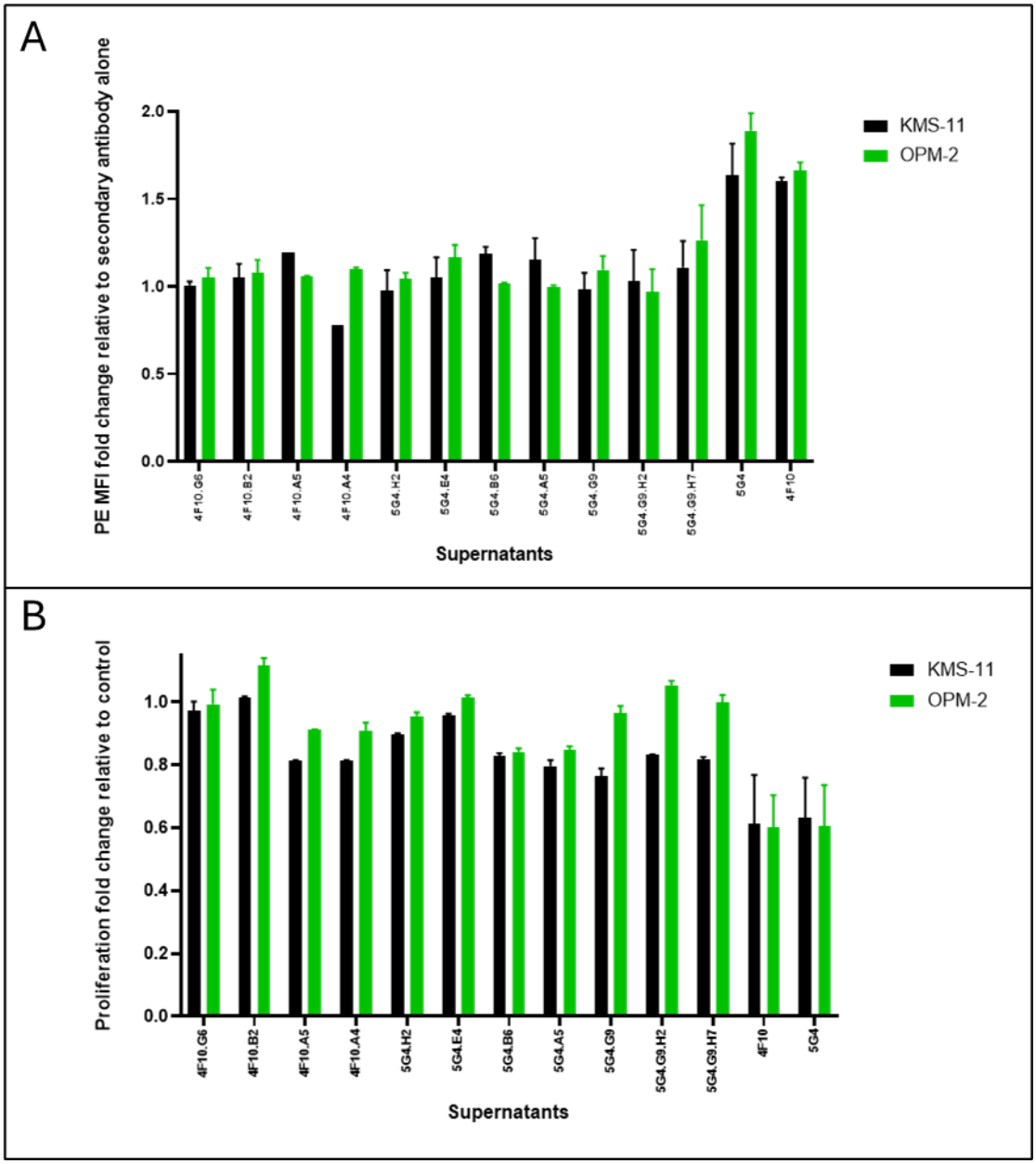

Figure 36. 5G4 and 4F10 subclones failed to bind BCMA or induce a significant reduction in cell proliferation of KMS-11 or OPM-2 cells.

(A) KMS-11 and OPM-2 cell lines were incubated with neat subclone supernatant from the hybridomas indicated. BCMA binding capacity was assessed by flow cytometry. **(B)** KMS-11 and OPM-2 cell lines were cultured with neat supernatant for 24 hours. Cell proliferation was assessed by MTT cell proliferation assay. Data are the mean and standard deviation from a minimum of 2 technical replicates per cell line.

4.2.4 Expression of BCMA in CHO and HEK293t cell lines

As subcloning of the hybridomas was unsuccessful, it was decided that a different approach would be attempted to generate a novel monoclonal BCMA antibody. The method suggested by the team at MADP involved purchasing a BCMA containing plasmid to express BCMA in two cell lines that do not normally express the protein (Appendix Figure 5A-B). One cell line would be used to immunise immunosuppressed mice, and the other cell line would be used to screen for BCMA binding antibodies secreted by the resulting hybridomas. We performed the first stage of this approach, involving transfection of CHO and HEK293t cells. Prior to transfection, the commercial plasmids were verified by agarose gel electrophoresis and Sanger sequencing (Appendix Figure 5C).

CHO and HEK293t cell lines were transfected with a commercially available BCMA-containing plasmid using the Fugene® transfection reagent. Initial experiments were promising in the HEK293t cell line, but we observed low transfection efficiency in the CHO cell line, as seen by the proportion of GFP-expressing cells (Figure 37). The GFP positive cells were then isolated by flow cytometry and cultured in media containing the selection agent, hygromycin B, at an appropriate concentration of 500 µg/mL (Figure 38). Although cell sorting and expansion was possible in these transfected cell lines, the number of GFP expressing cells present following transfection with the BCMA plasmid was low (Figure 38). We also believe that the transfected cells were eventually outgrown by wild type cells when hygromycin B was not present in the media, while cells cultured in hygromycin B did not remain viable or proliferate. We subsequently repeated the transfections using a Lipofectamine 2000-based methodology, which yielded GFP-positive cells, but again the cells that were transfected with the BCMA plasmid did not remain viable, leading to similar results to those shown earlier (Figures 37-39). Further development of BCMA-expressing cells was then performed by MADP.

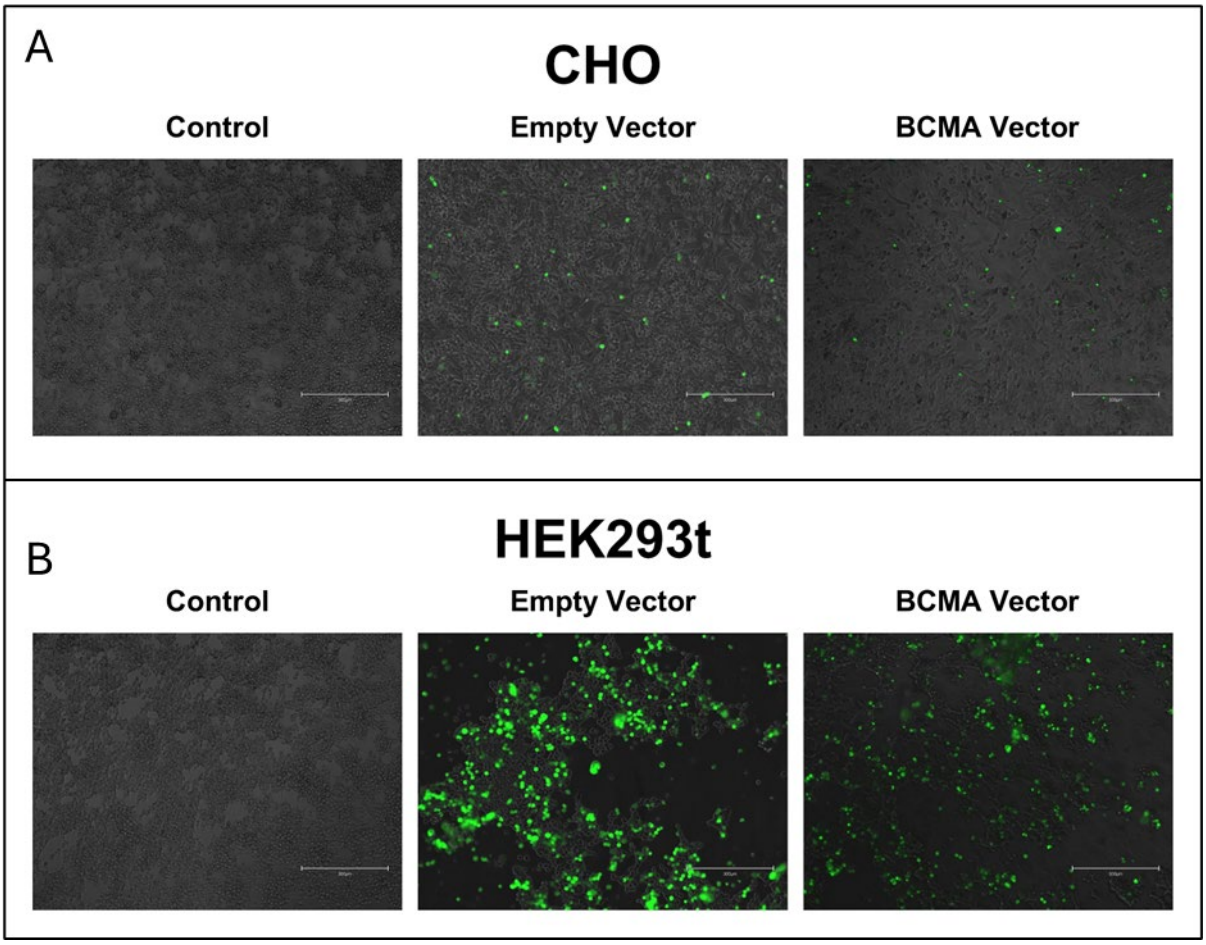

Figure 37. Commercial BCMA plasmids can be used to transfect CHO and HEK293t cell lines.

(A) CHO and **(B)** HEK293t cell lines were transfected with commercial plasmids using a Fugene-based methodology for 72 hours. Images were captured at 20x magnification using an EVOS M5000 Imaging System.

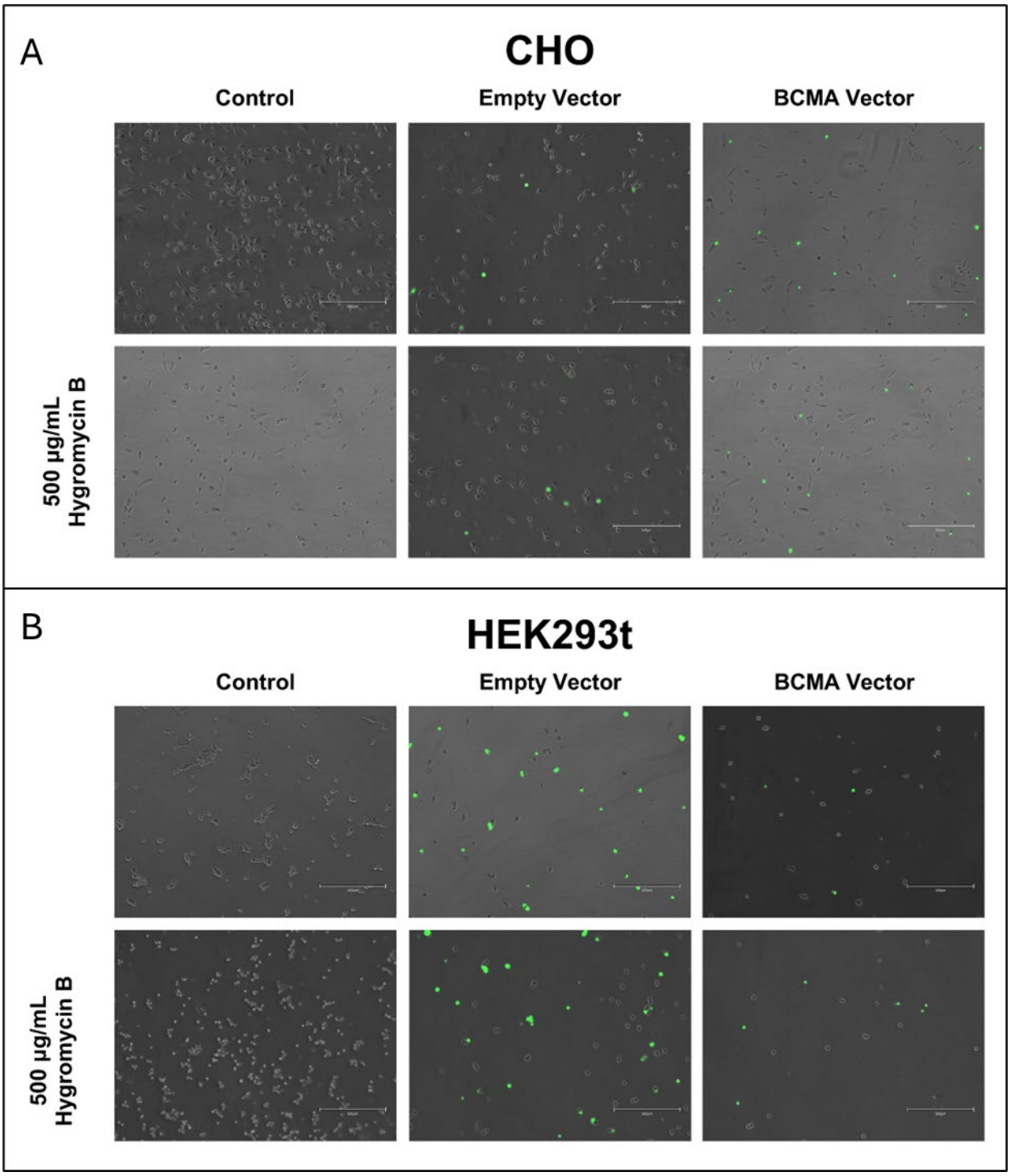

Figure 38. Flow cytometry can be used to identify and isolate GFP-expressing cells but selection using hygromycin B was not effective.

(A) CHO and **(B)** HEK293t cell lines transfected with commercial plasmids using a Lipofectamine 2000-based methodology for 72 hours were sorted by flow cytometry. Images show cells 24 hours after sorting with and without Hygromycin B. Images captured at 20x magnification using the EVOS M5000 Imaging System.

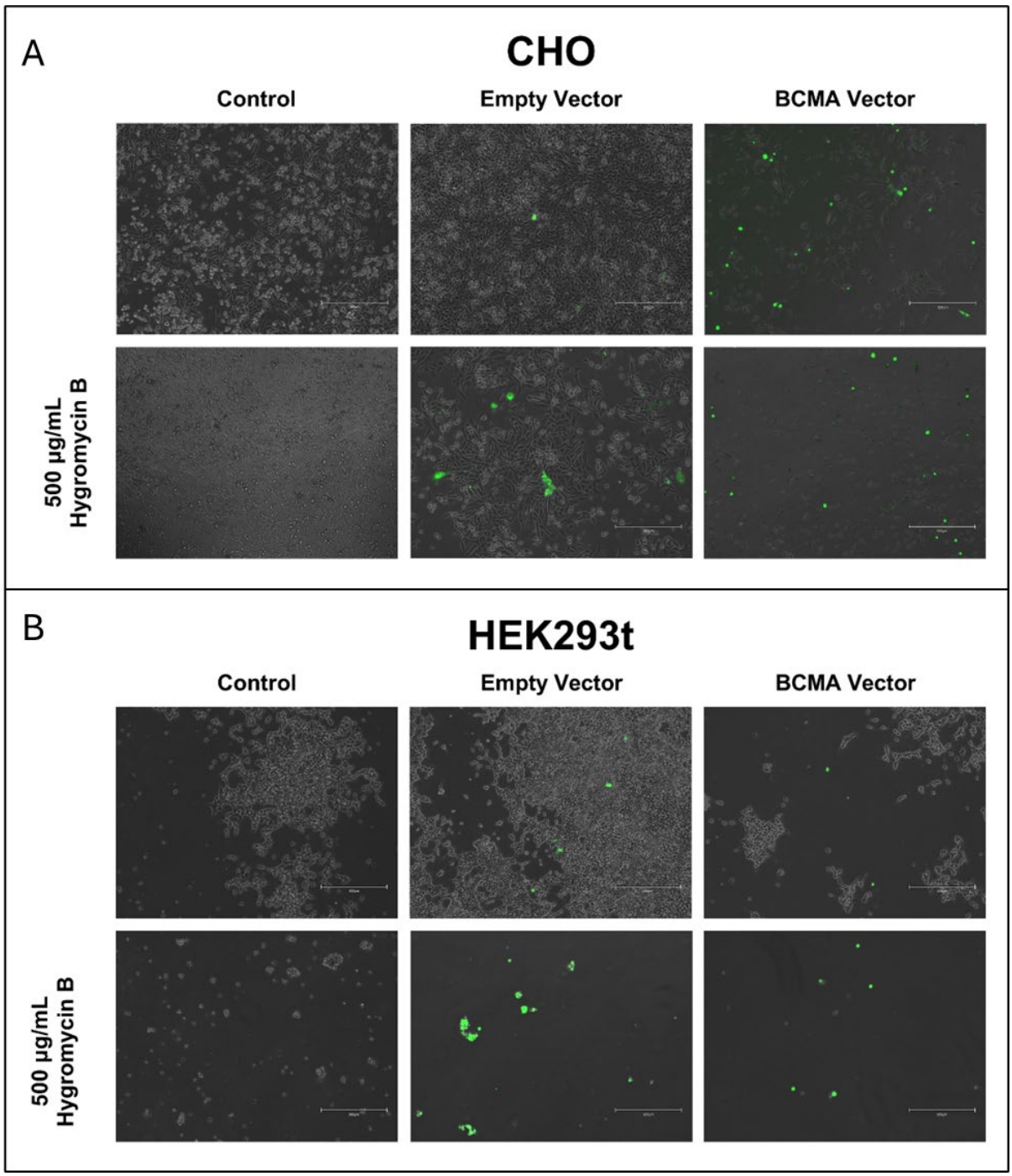

Figure 39. Hygromycin B selection was cytotoxic towards non-transfected HEK293t but not CHO cells.

(A) CHO and **(B)** HEK293t cell lines were transfected with commercial BCMA plasmids using a Lipofectamine 2000-based methodology for 72 hours. GFP-expressing cells were subsequently isolated by flow cytometry. Images show cells seven days post sorting, cultured with or without hygromycin B. Images were captured at 20x magnification using an EVOS M5000 Imaging System.

4.2.4 Transfecting CHO and HEK293t cell lines with BCMA containing plasmid

The team at the MADP have extensive knowledge and expertise in the development of knock in cell lines, hence the reason for engaging them in this aspect of the project. The CHO and COS7 cell lines and the same BCMA containing plasmid were used to develop two GFP-expressing cell lines, which were assumed to express the BCMA protein, although this was not checked. The GFP positive cells were isolated using a method similar to our in-house approach and the GFP-expressing CHO cell line was subsequently used to immunise the mice. The supernatants generated from the hybridomas derived from these mice were then screened using the GFP-expressing COS7 cell line. Several supernatants were identified that were thought to have antibodies that bound to the COS7 cells.

Unfortunately, the CHO and COS7 cell lines were not screened for BCMA surface expression prior to injection into the mice. We requested the cells be sent to Flinders University and we subsequently found that neither the CHO nor the COS7 cell line expressed BCMA (Figure 40A). This was confirmed using both flow cytometry and Western blotting, suggesting that the cells did not express BCMA, either on their cell surface or internally (Figure 40A-B). Interestingly, when the transfected COS7 cell line was cultured with supernatants derived from the hybridomas, a small, non-significant increase in the fold change for PE fluorescence was observed, indicative of some surface binding (Figure 40C-D). These results suggest that the binding capacity of the supernatants that were screened by the MADP was not specific to BCMA.

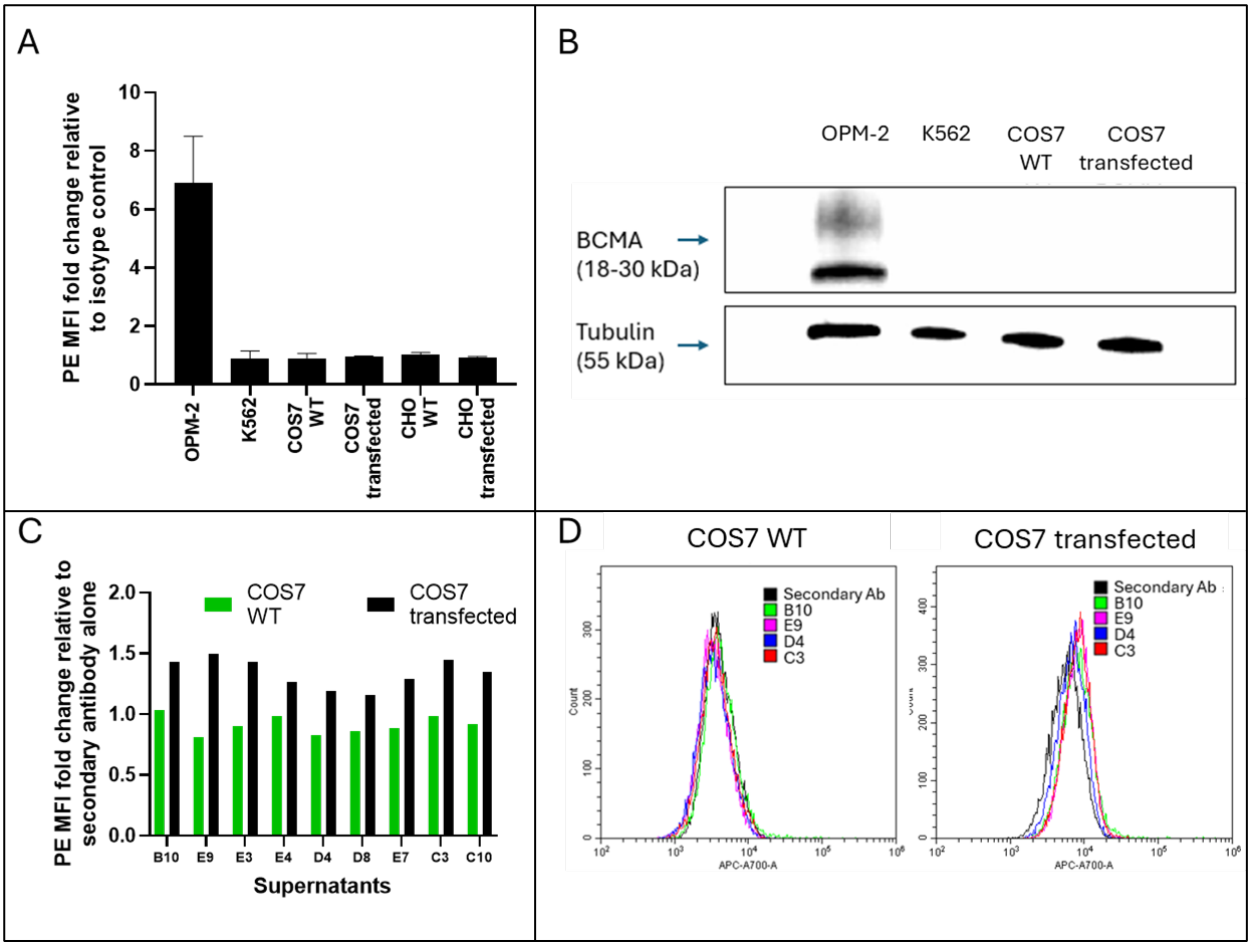

Figure 40. Transfected COS7 cells did not express BCMA but supernatants derived from hybridomas did show some binding to the cell line.

(A) OPM-2, K562, COS7 and CHO cell lines were stained with a commercial BCMA antibody for 30 minutes, followed by staining with a PE-conjugated secondary antibody. BCMA expression was assessed by flow cytometry as a fold change in PE fluorescence relative to cells incubated with secondary antibody alone. Data are the mean and standard deviation from a minimum of 2 biological replicates per cell line. **(B)** BCMA expression by Western Blot in OPM-2, K562, COS7 and CHO cell lysates. **(C)** COS7 wildtype and transfected, GFP positive cells were incubated with neat hybridoma supernatant. The binding capacity of the supernatants was assessed by flow cytometry. **(D)** Representative flow cytometry histograms showing minimal binding of components from the hybridoma supernatants to the COS7 transfected cell line.

4.2.5 FDA approved daratumumab as an alternative antibody for liposome conjugation

An aim of the project was always to test liposomes conjugated to a clinically approved antibody alongside the novel BCMA antibody that we had intended to develop. Daratumumab was chosen for this purpose, as it is also commercially available. Daratumumab is an anti-CD38 monoclonal antibody that is currently used in a range of highly effective treatment regimens for MM (227). CD38 is overexpressed on MM cells compared to most other immune cells (lymphoid and myeloid cells), making it an attractive target for therapy of MM.

Initially, we used daratumumab to assess CD38 expression and binding of the antibody to the MM cell lines, OPM-2, KMS-11 and KMS-18, the healthy B-cell, FH9 and the CLL cell line, OSU-CLL (Figure 41). As expected, CD38 expression was observed on the MM cell lines but not on the FH9, OSU-CLL or HEK293T cell lines, supporting the notion that CD38 represents a specific target on MM cells. Interestingly, we observed a higher fluorescent signal when daratumumab and a PE-conjugated secondary antibody was used, compared to the signal from a commercial anti-CD38 antibody (Becton Dickinson; Appendix Figure 6). The effects on cellular viability were then investigated against the OPM-2 and KMS-11 cell lines. No decrease in cell viability was observed in either cell line, following a 24h treatment with daratumumab (Figure 42A). Daratumumab also had no effect on cell proliferation in either of the two MM cell lines, OPM-2 and KMS-11 (Figure 42B). The lack of cytotoxic or anti-proliferative effects of daratumumab were not surprising given the absence of other immune cells. This will be discussed in more detail below.

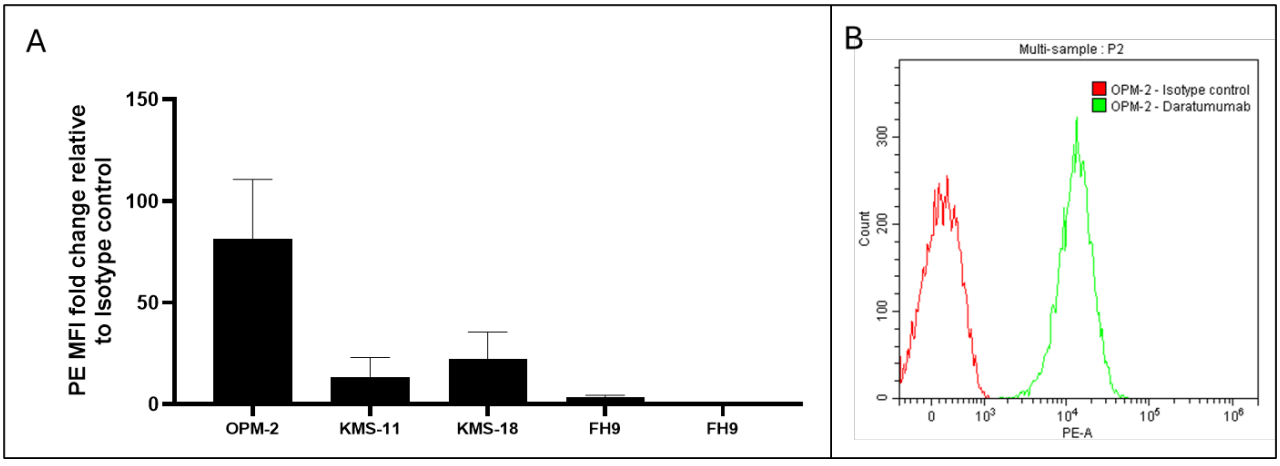

Figure 41. Daratumumab effectively binds CD38 on MM cell lines.

(A) OPM-2, KMS-11, KMS-18, FH9 (non-malignant B cells) and OSU-CLL cell lines were incubated with daratumumab or an isotype control antibody for 30 minutes, followed by staining with a PE-conjugated secondary antibody. CD38 expression was assessed by flow cytometry as a fold change in fluorescence

compared to the isotype control. Data are the mean and standard deviation from a minimum of 2 biological replicates per cell line**. (B)** Representative flow cytometry histograms of OPM-2 cells stained with daratumumab or isotype control and PE-conjugated secondary antibody.

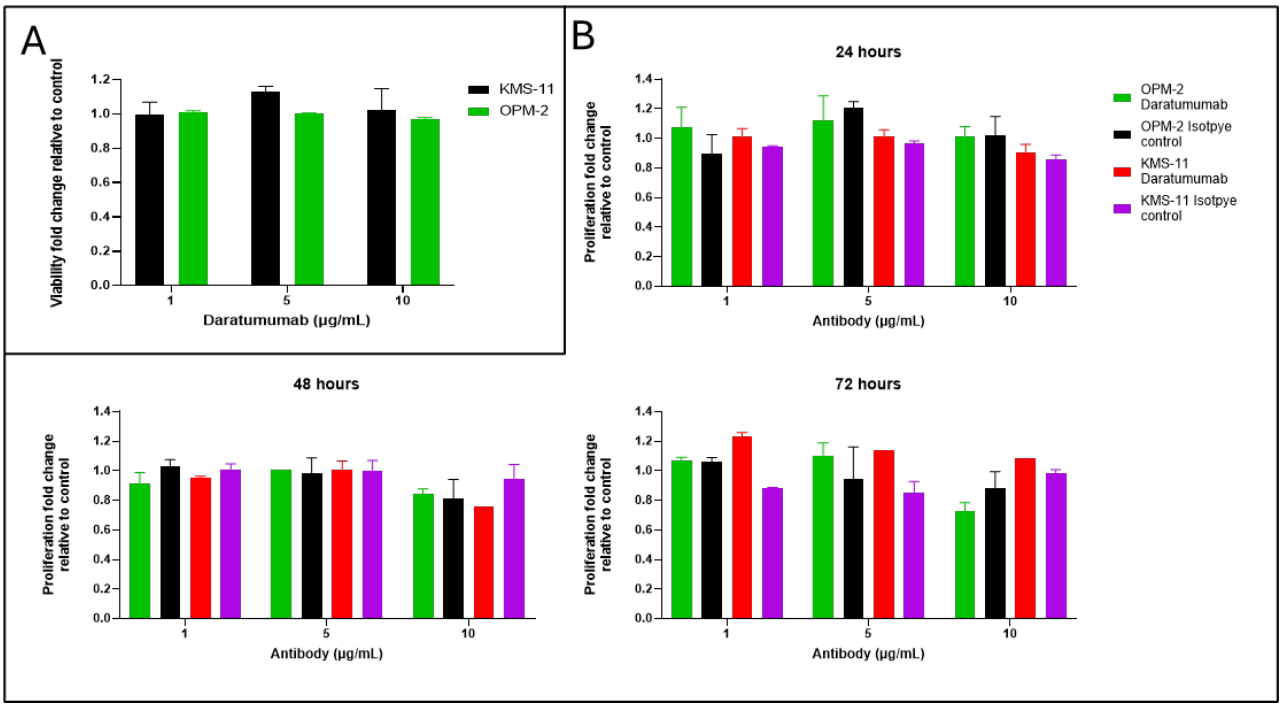

Figure 42. Daratumumab does not induce changes in the viability or proliferation of MM cell lines.

(A) OPM-2 and KMS-11 cell lines were cultured with the doses of daratumumab indicated for 24 hours. Cell viability was assessed by staining with annexin V and PI with analysis by flow cytometry. **(B)** OPM-2 and KMS-11 cell lines were cultured with the doses of daratumumab indicated for up to 72 hours. Cell proliferation was assessed by MTT cell proliferation assay and compared to untreated control. Data are the mean and standard deviation from a minimum of 1 independent experiment per cell line**.**

4.3 Discussion

4.3.1 Targeting BCMA in MM

The overarching aim of this chapter was to develop a novel BCMA-targeting antibody using a unique peptide, specifically designed to elicit an immune response in mice. BCMA is well established as a protein that is over-expressed on malignant (MM) plasma cells, compared to other healthy cells including plasma cells, making it a promising therapeutic target for MM. Targeting BCMA as a therapeutic strategy is not a novel concept in MM, with the ADC belantamab mafodotin showing promising efficacy as a single agent and in combination therapies (229). Belantamab mafodotin utilises a BCMA monoclonal antibody to deliver monomethyl auristatin F to MM cells, inducing cell cycle arrest and subsequent apoptosis (229). Belantamab mafodotin was FDA approved first in 2020, but was later withdrawn from both the US and European markets (59). It is now being reviewed again by the FDA for use in combination regimens, with an decision expected to be made in 2025 (74). Immunotherapies utilising BCMA as a target have also been developed in the last 5 years, with more than 10 BCMA-targeting CAR-T cell therapies approved for early phase clinical trials in 2020 (230). As of April 2024, the FDA has approved two BCMA CAR-T cell therapies for MM, Idecabtagene vicleucel and ciltacabtagene autoleucel, both of which have displayed promising results in clinical trials (77).

BCMA expression was investigated in a range of MM cells using both flow cytometry and Western blot analysis (Figure 27). All of the MM cell lines studied were found to express BCMA by both flow cytometry and Western blot, although expression varied between the different lines. H929 clearly demonstrated the highest expression of BCMA, while KMS-18 had minimal BCMA expression with either of the techniques (Figure 27). These results were consistent with the literature, which suggests that the majority of MM cells express BCMA (76). Additionally, the Raji (Burkitt's lymphoma) cell line, primary lymphomas and a subset of healthy mature B cells have been shown to express low levels of BCMA (76). This suggests that BCMA targeted therapeutics may be useful in more than just MM. Importantly, in the context of the current study, the CML cell line K562, which was used as a negative control, did not express BCMA.

4.3.2 Novel antibodies can bind BCMA on MM cell lines

Antibody production begins with the immunisation of immunocompetent mice with a suitable antigen. A 15 amino acid peptide, corresponding to an extracellular domain of BCMA was generated based on its uniqueness to other BCMA antibodies, immunogenicity, and water solubility (68). The

novelty of developing a new BCMA monoclonal antibody is within the unique epitope the antibody is generated against. The use of BCMA mAbs in ADC production is discussed above. BCMA targeting has also been implemented in CAR-T therapies (75) and as bispecific antibodies (70), however to date there are no unconjugated BCMA targeting monoclonal antibodies approved for use in MM. Unconjugated antibodies have been used in MM with great efficacy, including daratumumab (227), which suggests a therapeutic opportunity, leading us to develop a novel BCMA monoclonal antibody. Currently there are limited FDA approved BCMA targeting therapies for MM.

A key function of monoclonal antibodies is the capacity to bind its target and from our generated hybridomas we found that range of supernatants displayed surface binding by flow cytometry to MM cell lines but not the BCMA null K562 cell lines (Figure 28). Of the 70 supernatants screened, 8 supernatants stood out as clear candidates for further testing (Figure 29). The initial results were confirmed against the OPM-2 and KMS-11 cell lines, demonstrated by peak shifts in the fluorescence of the secondary, PE-conjugated antibody, compared to cells incubated with the secondary antibody alone. An isotype control antibody is a nonspecific antibody, that has a matching isotype (i.e. heavy chain), and fluorochrome conjugation (if applicable) to the primary antibody. As characterisation of the isotype(s) had not been performed on antibodies secreted by the hybridomas, it was not possible to use an isotype control for these assays. These antibodies generated against our novel 15 amino acid epitope displayed promising BCMA binding capacity.

4.3.3 Novel antibodies display functional effects in MM cell lines

Downregulation of BCMA is strongly associated with decreased viability of MM cells, and targeting the BCMA signalling pathway has proven to be a promising therapeutic strategy for the disease (231). To test the effects of BCMA binding on our MM cell lines, the cells were cultured for 24 hours with the hybridoma supernatants that we identified as having the greatest binding capacity; cell viability was assessed by flow cytometry. No change in viability was observed in the MM cell line, OPM-2, in response to any of the supernatants. Research has demonstrated that BCMA is also actively involved in the proliferation and survival of MM cells both *in vitro* and *in vivo* (231). More specifically the activation of BCMA by its ligand, a proliferation inducing ligand (APRIL), activates intracellular signalling via protein kinase B, MAPK and nuclear factor signalling, which collectively promote survival and growth (231). Therefore, blocking the binding of APRIL using an anti-BCMA antibody may disrupt this signalling and impact cell proliferation. To investigate this, MM cell lines were cultured with the hybridoma supernatants and cell proliferation was then assessed by MTT assay.

A screen was performed of all the supernatants, which narrowed down the supernatants to a panel of candidates deemed worthy of further testing (Figure 31). Interestingly, some of the supernatants tested had a notable impact on cell proliferation against the MM cell lines, in particular the supernatants 4F10 and 5G4. This was confirmed by MTT in the OPM-2, H929 and KMS-11 MM cell lines with a significant decrease in cell proliferation after 24 hours, with no impact on the CML cell line K562 (Figure 32 and 34). Cell viability assays were performed at the same time to investigate whether this change in proliferation correlated with a change in viability. Again, no effect of any of the supernatants was observed on cell viability. These results were recapitulated using another proliferation assay, based on the dilution of carboxyfluorescein succinimidyl ester (CFSE) over time. Both of the supernatants tested caused a significant decrease in cell proliferation in the OPM-2 but not the K562 cell line (Figure 32). These data suggest that some of the supernatants may have contained factors, possibly antibodies, with the ability to block the proliferation of MM cells. Although the presence of APRIL was not confirmed in the supernatants, it is possible that the anti-proliferative effects may have been mediated by a blockade of the binding site for the ligand on BCMA. This idea is consistent with previous studies that have shown antibodies can block the pro-survival or proliferative signalling of a receptor by occupying the binding site for the ligand (232). It was intended that questions regarding the mechanism by which the antibodies inhibited proliferation would be addressed following the production of a monoclonal anti-BCMA antibody.

4.3.4 Novel antibodies are BCMA specific and do not bind other MM surface proteins

Next, BCMA knockout OPM-2 and KMS-11 cell lines were developed, in collaboration with Professor Stuart Pitson at the Centre for Cancer Biology at the University of South Australia. Two models were developed in each of the MM cell lines using different guide RNAs. The cells were then assessed for BCMA expression by flow cytometry and Western blot. Flow cytometry was used to confirm the WT MM cell lines expressed BCMA on their surface, while the knockout lines did not (Figure 35A). Interestingly, protein bands were observed by Western blot in two of the KMS-11 and one of the OPM-2 knockout lines after incubation with the BCMA antibody (Figure 35B). However, these bands were larger than the size of the band expected for BCMA in both of the MM cell lines. These bands may be due to non-specific binding or BCMA knockout resulting in the removal of a region of the protein that localises it to the plasma membrane, rather than a complete knockout of the protein. Given that the knockout models did not express BCMA on their surface no further experiments were performed to examine BCMA expression or determine what the higher molecular weight protein

was in these cells. These knockout models were then used to investigate the specificity of the antibodies contained within supernatants 5G4 and 4F10. No increase in the PE signal from the secondary antibody was observed following incubation of the knockout cells with the hybridoma supernatants, indicating that surface binding did not occur in these cells (Figure 35C). Similarly, when the knockout cells were cultured with the supernatants for 24 hours, no decrease in proliferation was observed (Figure 35D). Knockout cell lines are valuable for confirming specificity and validating functional activity as negative controls. Having shown efficacy in terms of binding and functional effects of the hybridoma supernatants with a range of controls and different assays, the corresponding hybridomas were subjected to subcloning.

4.3.5 Subcloned hybridomas do not yield effective antibodies

Subcloning is the process of isolating and expanding a single, antibody-producing hybridoma cell so that a single antibody clone can be generated. Hybridomas, as mentioned above, are typically a mix of multiple clones and therefore the antibodies produced are polyclonal. The identification of a hybridoma clone that produces a suitable antibody is followed by the expansion and storage of the now clonal cell line (65). A clonal population of hybridoma cells produce monoclonal antibodies that are theoretically more stable and consistent than the heterogenous antibodies secreted by a polyclonal population of cells (polyclonal antibodies) (65). The process of subcloning was performed by the MADP team, who also screened the supernatants produced by the resulting hybridoma by ELISA. The hybridoma supernatants that contained the desired antibodies were subsequently sent to us for further testing. Unfortunately, the supernatants derived from the subcloned hybridomas no longer elicited any BCMA surface binding by flow cytometry or functional effect on MM cell proliferation (Figure 36). The reason that this stage was not successful is unclear but may be due to loss of cells that produced the desired antibody due to heterogeneity or instability. Although less likely, clonal variation, culture conditions, detection issues or contamination may also have caused the loss of the positive signal. These issues can often be difficult to trouble shoot. Despite another round of subcloning where similar results were obtained (results not shown), so another approach was taken to develop the novel BCMA monoclonal antibody.

4.3.6 Utilising cell-based immunisation to develop a monoclonal antibody

A commercially available plasmid containing BCMA was transfected into HEK293t or CHO cell lines using one of two different methods, using either a Fugene® or a lipofectamine based method. The control vector and the BCMA containing vector were verified by agarose gel electrophoresis and

Sanger sequencing. Initial transfections resulted in GFP-expressing cells, however neither cell line was viable or stably expressed GFP, even after cell purification by fluorescent activated cell sorting (FACS) (Figures 37-39). As the cells did not remain viable, BCMA expression was not confirmed on the isolated GFP-expressing cells. After these initial problems with stable transfection and due to limited experience in this field, we engaged the MADP to continue the work using the same plasmid to develop their own BCMA expressing cell lines. The plan was then to immunise mice with one of the BCMA-expressing cell lines and utilise the other cell line to screen for the presence of anti-BCMA antibodies. While less commonly used, antigen-expressing cell lines can be used as a means of immunising mice for antibody production (233). This study is one example of this approach, where HEK293t cells presenting native viral proteins were used to rapidly develop a monoclonal antibody (233). In our study, the transfected CHO cells were used to immunise mice, and the fusion process for generation of hybridomas was repeated as previously described. Transfected COS7 cells were then used to screen for the presence of anti-BCMA antibodies in the supernatants. Initial screens did show some positive results in terms of binding to the transfected COS7 and not WT cells. However, when both lines were assessed for BCMA expression it was discovered that neither the WT nor BCMA-transfected CHO cell lines that were used to immunise the mice, nor the COS7 cell lines used to screen the hybridoma supernatants expressed BCMA (Figure 40). This was also confirmed in the COS7 cell line by Western blot (Figure 40B). Unfortunately, this meant that the hybridoma supernatants could not have contained antibodies that target BCMA. This could have been avoided if BCMA expression was assessed on these cell lines prior to immunisation of the mice. This meant that we proceeded with our back up approach, which was to use an antibody that is both commercially available and FDA approved for conjugation to the liposomes.

4.3.7 Daratumumab is effective for targeting MM cells

Daratumumab is an FDA approved monoclonal antibody that is now widely used to treat MM patients (227). While the initial plan of the current project was to develop a novel BCMA antibody, we understood that generating a novel monoclonal antibody can be technically difficult and there was no guarantee that the methods employed would lead to a suitable antibody. For this reason and to demonstrate proof-of-principle with a monoclonal antibody that is currently used in the clinic, we chose to investigate daratumumab as a potential conjugate for targeting our liposomes to MM cells. Initially, we assessed daratumumab binding to MM cells *in vitro*, which also provided an indication of the levels of CD38 expression on the surface of the MM cell lines. Daratumumab clearly bound to the surface of the OPM-2 and KMS-11 cells, supporting the fact that both cell lines express

CD38 (Figure 41A). Unlike the hybridoma supernatants investigated earlier in the chapter, daratumumab had no effect on either the survival or proliferation of MM cells (Figure 42). These results were expected, as previous studies have shown that the mechanisms of action of daratumumab require effector cells (e.g., NK cells) to induce cell death of MM cells (81). Studies suggest that daratumumab may also induce cell death via F_c receptor mediated crosslinking (83). As daratumumab has been extensively studied and due to the costs and time involved, we did not investigate antibody-dependent cellular cytotoxicity and complement-dependent cytotoxicity as mechanisms of action of daratumumab.

4.3.8 Conclusions

In conclusion, this chapter describes the steps and experiments required to develop a monoclonal antibody, from the use of a peptide or antigen-presenting cells to immunise mice to the subsequent screening that is necessary of the resulting hybridoma supernatants. The functional effects of the hybridoma supernatants were investigated and although some did appear to contain potential anti-BCMA antibody candidates that were worthwhile subcloning, we were unsuccessful at developing a single BCMA hybridoma clone. Despite this, the knowledge and skills gained from the experiments and techniques used during this process helped in many other aspects of the overall project. We were able to proceed with the anti-CD38 monoclonal antibody, daratumumab, in the next chapter, which focuses on the development of antibody-conjugated ferroptosis liposomes.

CHAPTER 5. SYNTHESIS OF ANTIBODY-FUNCTIONALISED LIPOSOMES

5.1 Introduction

This chapter describes the development of lipid-based nanoparticles, called liposomes, to effectively deliver ferroptosis substrates or ferroptosis-inducing drugs to MM cells. Liposomes are versatile spherical vesicles primarily composed of lipids, and in the case of this project, PLs. As the results from chapter 3 highlight, lipids and in particular PLs play an integral role in ferroptosis, with PLs containing PUFAs a key ferroptosis substrate. This led to the hypothesis that unique liposomes comprised of the lipids identified in chapter 3 would represent a novel method by which PLs can be delivered to cancer cells. The versatility of liposomes also refers to their ability to act as a mechanism for drug delivery, especially for drugs with poor pharmacokinetic and toxicity profiles, such as RSL3 (234). Liposomes can be used to delivery hydrophobic drugs within the lipid bilayer or hydrophilic drugs in the aqueous core. The overarching aim of this chapter was to develop liposomes capable of inducing ferroptosis-mediated cell death through the delivery of both ferroptosis substrates (PUFAs) and ferroptosis-inducing compounds (RSL3).

To date, there have been no published studies that have examined ferroptosis-targeting nanotechnologies in MM, however research on liposomes and apoptosis has yielded promising results. For example, liposomes containing bortezomib have proven effective against MM cells *in vitro* and *in vivo* (235, 236). Studies of liposomes in the context of ferroptosis in other haematological malignancies is also limited but another form of nanoparticle has been investigated as a drug delivery mechanism in lymphoma. Zhang *et al*., demonstrated that delivery of the erastin analogue (system X_c^- inhibitor), IKE, to lymphoma cells could be enhanced by using polyethylene glycol-poly (lactic-co-glycolic acid) (PEG-PLGA) nanoparticles (237). These nanoparticles induced ferroptotic cell death in lymphoma models and reduced the toxicity observed when mice were treated with free IKE (237). Similarly, another group found that high-density lipoprotein-like nanoparticles were able to induce cell death consistent with ferroptosis of Burkitt's lymphoma, DLBCL and T cell–rich B cell lymphoma cells (149).

The novelty and therapeutic potential of liposomes lie in the ability to modify their design and functionalise them as a drug delivery system. One of the most common techniques involved in

liposome synthesis is the thin-film method. This technique involves forming a thin film of lipids on the inside of a rotary evaporator flask, which is then rehydrated with an appropriate buffer while being vigorously shaken and simultaneously heated to an appropriate temperature (238). This method is highly reproducible but lacks the ability to produce liposomes that are uniform in size or in the amount of drug that is encapsulated. However, this method is relatively inexpensive and requires minimal equipment (238). Emerging technologies in the field of nanoparticle research have improved the processes involved in liposome synthesis, particularly through implementation of microfluidics. Microfluidics describes the processing or manipulation of small volumes of fluids within a network of channels that are typically embedded within a microfluidic chip. The introduction of microfluidics into the process of liposome synthesis has significant advantages, particularly as this has led to the ability to uniformly disperse liposomes, meaning their size and charge can be more accurately controlled (239). The downside of using microfluidics to synthesise liposomes is the cost associated with purchasing assembly systems and microfluidic cassettes, limitations on what buffers can be used due to the sensitivity of the chips and the rate at which liposomes can be synthesised (239). Despite these limitations, we employed microfluidic systems in the current study to synthesise and optimise liposomal formulations due to the significant advantages of reproducibility and efficiency.

While the techniques used for liposome synthesis are important, the formulation of liposomes is equally as important and can be the factor that determines whether manufactured liposomes are suitable for functional testing. The formulation of liposomes varies considerably between studies, but they will often be composed of lipids with strategic roles, including cholesterol, distearoylphosphatidylcholine (DSPC) and distearoylphosphatidylethanolamine polyethylene glycol 2000 (DSPE-PEG2000) (240, 241). Cholesterol plays an important role in the stability, fluidity and elasticity of the liposome membrane and can impact drug release (241). DSPC is often used to improve liposome stability and the efficiency of drug encapsulation, while DSPE-PEG2000 prolongs the amount of time liposomes can remain in the circulation, improves drug bioavailability and reduces side effects associated with the nanoparticle (240). The formulation of liposomes also dictates their capacity for functionalisation.

The ability to functionalise liposomes with ligands, peptides or antibodies mean that these nanoparticles have significant potential to act as a targeted drug delivery system in a wide range of diseases, including cancer, thereby limiting toxicity. Liposomes coupled to antibodies, or immunoliposomes, which are synthesised by chemically coupling antibodies to the surface of the

liposomes, have proven to be highly specific for cells expressing the target antigen (242). Interestingly, PEGylated liposomes may also be capable of enhancing both the permeability and retention of antitumor agents in cancer cells through a process known as passive targeting (242). Once the liposomes reach the target cell they can be taken up in four distinct ways, either by endocytosis, liposome fusion to the cell membrane, lipid exchange with the cell or through interactions with cell surface receptors (243). In the case of targeted liposomes, uptake can also occur through receptor-mediated endocytosis (243).

To date, there have been few studies on liposomes comprised of PLs in the context of ferroptosis and none on these liposomes as a potential therapeutic strategy for MM, highlighting the novelty of the current research. The aim of the research conducted in this chapter was to investigate the effects of uniquely formulated liposomes that encapsulate the ferroptosis inducer, RSL3, as a means of delivering both a ferroptosis substrate, namely PL-PUFAs, and a ferroptosis-inducing inhibitor of GPX4, specifically to MM cells. A large body of this work has now been peer review and published (Publication 2 in the Appendix).

5.2 Results

5.2.1 Liposomes containing cholesterol have unexpected results in MM

Liposome formulations can dictate the stability, loading capacity and circulation time of nanoparticles, and often contain specific lipids that aid in these functions (244). Cholesterol exerts a profound role on the structural stability, permeability and fluidity of liposomes and often makes up a high percentage of the total lipids in common liposome formulations (244). PEGylated lipids increase the circulation half-life of nanoparticles while also enhancing stability (245). Liposomes are typically formulated for the purpose of drug delivery and otherwise have minimal influence on the therapeutic benefit of the drug. In the current project the lipid composition of the liposomes was designed based on the data presented earlier in the thesis that demonstrated the importance of the lipids as ferroptosis substrates.

Initially, liposomes containing PE (16:0_22:6): cholesterol: DSPC: DSPE-PEG2000 at ratios of 40:48:10:2 (w/w/w/w%) were generated. This formulation was based on a standard recipe proposed by Prof Clive Prestidge. These liposomes had an average diameter of 220 nm with a polydispersity index (PDI) of less than 0.3, suggesting they were relatively uniform and were within a suitable size. PDI represents the size distribution of liposomes, with values under 0.30 suggesting nanoparticles of uniform size. The liposomes also had a near neutral charge.

Surprisingly, the initial liposomes had little effect on the viability of either OPM-2 or KMS-11 cells and did not sensitise either cell line to RSL3 (Figure 43A-B). No significant difference in the viability of OPM-2 cells was observed when cells were treated with unencapsulated RSL3 and the liposomes compared to liposomes alone, suggesting the liposomes had no effect on the sensitivity of the cells to ferroptosis (Figure 43A). The relatively small decrease in cell viability observed in the OPM-2 cell line following treatment with the highest dose of liposomes was prevented by liproxstatin-1 (Figure 43A). The results were similar against the KMS-11 cell line following treatment with liposomes alone, with no significant decrease in viability (Figure 43A). The combination of unencapsulated RSL3 and the liposomes did induce cell death in this cell line, reducing the viability to approximately 45% (Figure 43A). However, this reduction in cell viability was not completely preventable by liproxstatin-1, with a viability of approximately 60% following treatment with the combination of liposomes, RSL3 and liproxstatin-1 (Figure 43A). Given the results presented in Chapter 3, which showed that SFAs play a minimal role in ferroptosis, we decided to investigate the effect of decreased levels of cholesterol on the ferroptosis-sensitising capacity of the liposomes. Cholesterol and cholesterol

precursors have been shown to be actively involved in ferroptosis inhibition in several different models (138, 246-248).

Liposomes were synthesised containing PE (16:0_22:6): cholesterol: DSPC: DSPE-PEG2000 at ratios of 40:20:38:2 (w/w/w/w%). Cholesterol levels were halved in the second liposome formulation, while the level of DSPC was tripled. The average size, PDI and charge of the liposomes remained largely unchanged. However, the reduction in cholesterol levels did not improve the efficacy of the liposomes, either alone or in combination with unencapsulated RSL3, in either of the cell lines (Figure 43B). This led to further revisions of the liposome formulation and the investigations in the discussion of this chapter.

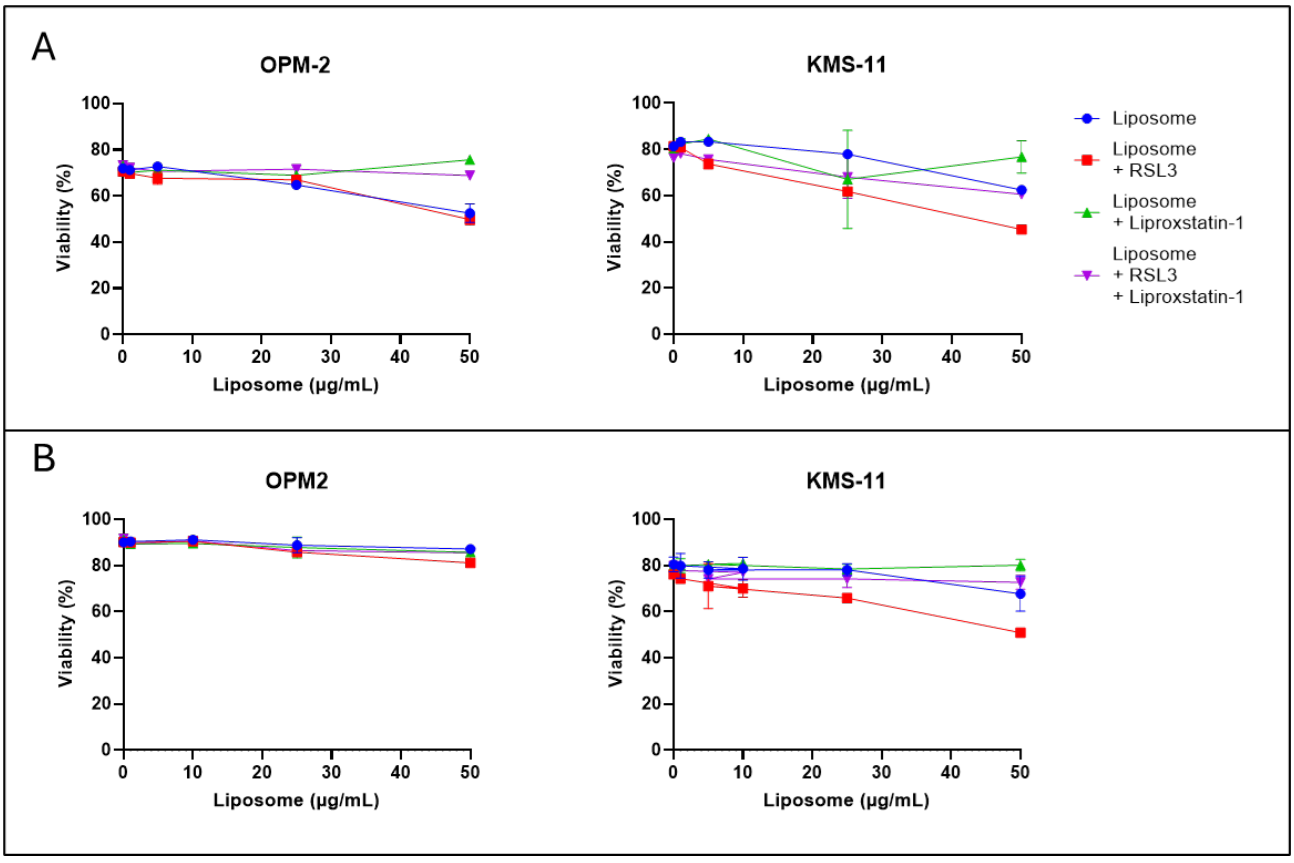

Figure 43. Cholesterol dampens the effect of liposomes containing PUFA

(A) OPM-2 and KMS-11 cells were cultured for 24 hours with the indicated amounts of liposomes comprised of PE (16:0_22:6): cholesterol: DSPC: DSPE-PEG2000 at ratios of 40:48:10:2 (w/w/w/w%), RSL3 (OPM-2 – 50 nM, KMS-11 – 2.5 µM) and liproxstatin-1. Cell viability was assessed by flow cytometry following staining with annexin V and PI. **(B)** OPM-2 and KMS-11 cells were cultured for 24 hours with the amounts indicated of liposomes comprised of PE (16:0_22:6): cholesterol: DSPC: DSPE-PEG2000 at ratios of 40:20:38:2 (w/w/w/w%), RSL3 (OPM-2 – 50 nM, KMS-11 – 2.5 µM) and liproxstatin-1. Cell viability was assessed by flow cytometry following staining with annexin V and PI. All data are the mean ± standard deviation of duplicate measurements from 1 independent experiments.

5.2.2 Liposomes devoid of cholesterol have powerful ferroptosis sensitising properties

Unfortunately, cholesterol is difficult to substitute in liposomal formulations, as liposomes that lack cholesterol often have poor stability, meaning a compromise had to be reached with the liposomes generated in the current study. Ultimately the goal of this chapter was to develop liposomes that can sensitise cells to ferroptosis and act as a delivery mechanism for RSL3. A new formulation was developed that did not contain cholesterol but instead contained a higher proportion of DSPC to aid in liposome stability. Liposomes were synthesised containing PE (16:0_22:6): cholesterol: DSPC: DSPE-PEG2000 at ratios of 49:0:49:2 (w/w/w/w%). As expected, these liposomes had different properties to the liposomes containing cholesterol. Liposomes with no cholesterol had an average diameter of 460 nm, with a PDI exceeding 0.3 and a neutral charge.

Liposome uptake into cells can be measured by including a fluorescently tagged lipid, such as PE (18:1) conjugated to lissamine rhodamine B sulfonyl (RhB) at dilutions of 1 in 1000 (249). Assessing liposome uptake into cells is reasonably straightforward and involves using flow cytometry to measure the cells that are positive for the fluorescence from the tagged lipid. Figure 44A shows that cells cultured with liposomes containing Rhodamine B (RhB) fluoresce following excitation with a yellow/green laser (561nm), emitting light at a similar wavelength to that of phycoerythrin (PE). Cells with higher fluorescence than unmanipulated cells were classified as RhB positive and were considered to have taken up the fluorescently tagged liposomes. The percentage of RhB positive cells increased in a dose-dependent manner, with greater than 80% of cells deemed to have taken up liposomes at the highest concentration (Figure 44A).

Although the liposomes were neither as small nor as uniform as the liposomes containing cholesterol, they displayed a profound capacity to sensitise MM cells to ferroptosis (Figure 44B). The liposomes alone did not induce ferroptosis in either of the MM cell lines, however the combination of unencapsulated RSL3 and the liposomes induced significant cell death (Figure 44B). The OPM-2 cell line displayed a liposome IC_{50} of 12.23 ± 5.00 µg/mL when combined with 50 nM unencapsulated RSL3 (Figure 44B). The KMS-11 cell line displayed a similar liposome IC_{50} of 12.82 ± 6.70 µg/mL when combined with unencapsulated RSL3 (2.5 µM) (Figure 44B). Unlike the OPM-2 cell line, the viability of the KMS-11 cells did not drop below 15% at the highest concentration of liposomes when combined with unencapsulated RSL3 (Figure 44B). Importantly, liproxstatin-1 was able to inhibit cell death induced by the liposomes, with or without unencapsulated RSL3 (Figure 44B).

Levels of lipid ROS, a key indication of ferroptosis, were also investigated in the two MM cell lines following treatment with the liposomes and unencapsulated RSL3. No significant increase in lipid ROS was observed in either the OPM-2 or KMS-11 cells following treatment with the liposomes alone (Figure 44C). However, it was clear that the combination of 10 μg/mL liposomes and unencapsulated RSL3 induced significantly higher levels of lipid ROS than RSL3 alone, in both the KMS-11 and OPM-2 cell lines. In the OPM-2 cell line, 50 nM RSL3 induced a 4-fold change increase in cellular lipid ROS, while the combination of liposomes and RSL3 induced a 13-fold increase in lipid ROS (Figure 44C). In the KMS-11 cell line, RSL3 alone induced a 3.5-fold increase, while the combination of RSL3 and liposomes induced an 8-fold increase in lipid ROS (Figure 44C). In both cell lines, liproxstatin-1 prevented the increases in lipid ROS induced by RSL3, with or without the liposomes (Figure 44C). Although it was evident that these liposomes were able to sensitise the cells to ferroptosis, there remained the issue regarding the size, uniformity and stability of this formulation. The next step was to investigate a new liposome formulation to test how different lipids influenced the liposome characteristics and capacity to sensitise the MM cells to ferroptosis.

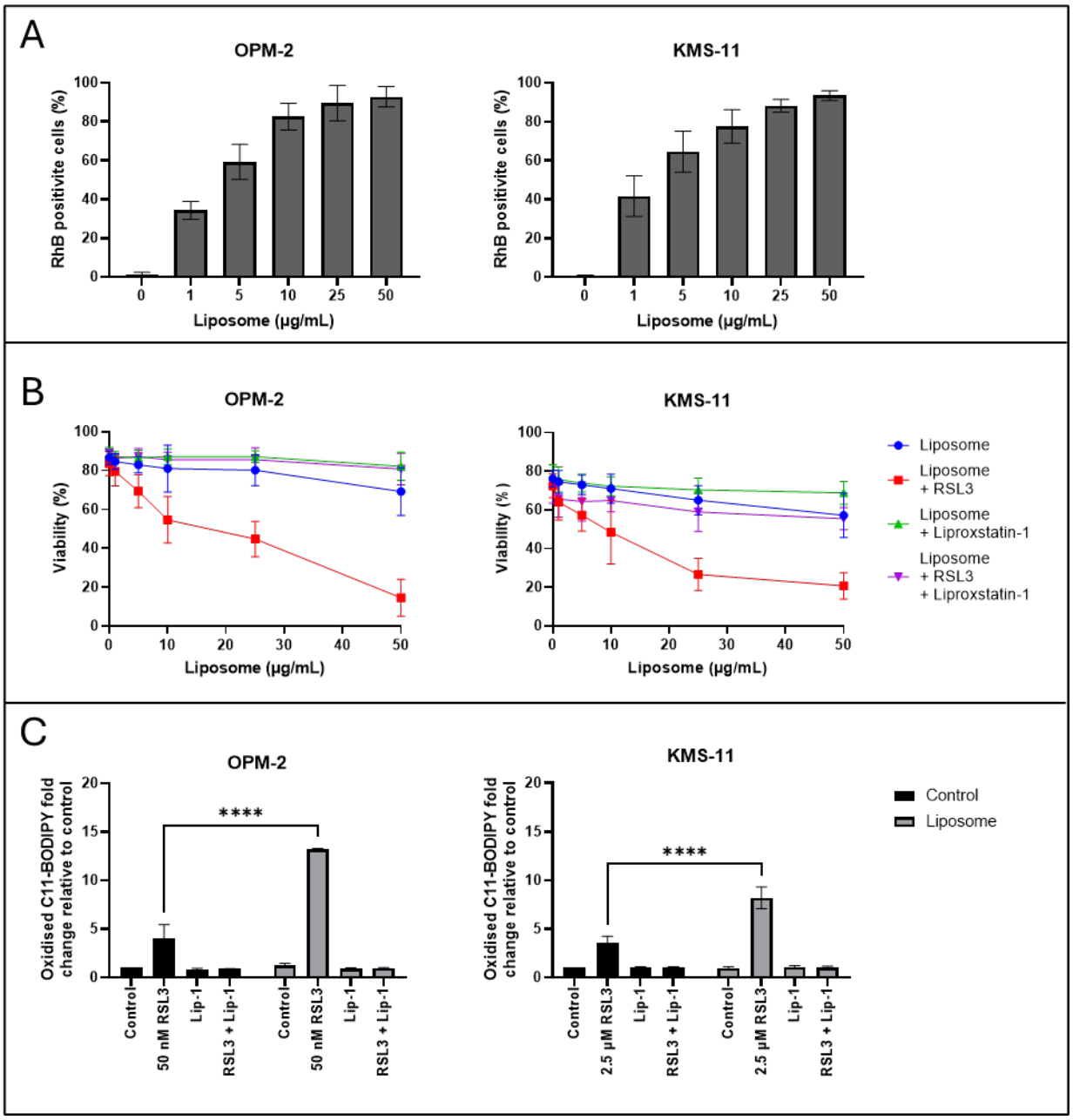

Figure 44. Liposomes containing PUFAs are readily taken up by MM cells and sensitise the cells to RSL3-induced cell death.

(A) OPM-2 and KMS-11 cells were cultured with liposomes containing a fluorescently tagged lipid for 24 hours. Uptake was assessed by flow cytometry. **(B)** OPM-2 and KMS-11 cells were cultured with liposomes with the formulation PE (16:0_22:6): cholesterol: DSPC: DSPE-PEG2000 at ratios of 48:0:48:2 (w/w/w/w%), RSL3 (OPM-2 – 50 nM, KMS-11 – 2.5 µM) and liproxstatin-1 for 24 hours. Cell viability was assessed by flow cytometry following staining with annexin V and PI. **(C)** OPM-2 and KMS-11 cells were cultured with 2.5 µM or 50 nM (OPM-2) RSL3, with or without liposomes and liproxstatin-1 for 24 hours. Lipid ROS levels were assessed by flow cytometry following staining with oxidised C11 BODIPY. All data are the mean ± standard deviation of duplicate measurements from 3 independent experiments. Statistical analysis was performed using two-way ANOVA of a minimum of 3 biological replicates. **** P<0.0001.

5.2.3 Optimised liposomes of a suitable size and uniformity increase the sensitivity of MM cells to ferroptosis

The specific lipids used in liposome formulations have a significant impact on the assembly of the nanoparticles, with different factors such as charge, head group and size affecting their assembly. To test how these factors impact the liposomes and their effects on MM cells, a range of liposomes were formulated with different compositions (data not shown) to determine how changing the proportion of the lipids affects the size and uniformity of the particles. A new formulation was developed that did not contain either cholesterol or DSPC, that was reliant only on DSPE-PEG2000 for stability. Liposomes were synthesised containing PE (16:0_22:6): cholesterol: DSPC: DSPE-PEG2000 at ratios of 98:0:0:2 (w/w/w/w%).

These novel liposomes were predominantly composed of PE (16:0_22:6) (98%), which is one of the lipids that induced ferroptosis-mediated cell death when added exogenously to the MM cells (Figure 20). The remaining 2% was a pegylated saturated fatty acid, DSPE-PEG2000, which was added to stabilise the liposomes. The mean diameter of the synthesised liposomes was 135 nm with a polydispersity index (PDI) of 0.06 and neutral charge of -2 mV (Appendix Figure 7). To assess their stability, liposomes were stored for 2 weeks at 4°C after synthesis; the mean diameter of the liposomes after 2 weeks was 131 nm with a PDI of 0.18, confirming they were stable within this time frame.

Initially, liposomes were synthesised with the lipid, PE (18:1) tagged to the fluorochrome lissamine rhodamine B sulfonyl, to enable their cellular uptake to be assessed. OPM-2 and KMS-11 cells were cultured with varying amounts of the liposomes for 24 hours and levels of the fluorescently tagged lipid in the cells were assessed by flow cytometry. Liposome uptake was similar in both the OPM-2 and the KMS-11 cells, with > 80% of the cells analysed deemed to be positive for the fluorescent lipid after a 24 hour treatment with 15 µg/mL of the liposomes (Figure 45A). The results also suggest that the uptake was dose-dependent, as the increase in fluorescence corresponding to the RhB fluorochrome increased as the concentration of liposomes was increased (Appendix Figure 8). In addition, imaging flow cytometry was used to visualise the locality of the RhB fluorescence within the cells. OPM-2 cells were cultured with 15 µg/mL liposomes with or without the RhB-conjugated lipid for 24 hours. As expected, no background fluorescence was observed in cells treated with either the control or blank liposomes (Appendix Figure 9). A clear fluorescent signal was observed in the majority of the cells treated with liposomes containing the RhB-tagged lipid, supporting the earlier data that the liposomes had been internalised into the cells (Appendix Figure 9).

Furthermore, the RhB lipid appeared to localise to the plasma membrane in many of the cells. Whether the RhB fluorochrome remained conjugated to the lipid is difficult to answer.

Next, varying amounts of the liposomes were added to OPM-2 and KMS-11 MM cells for 24 hours, with the result that dose dependent cell death was observed in both cell lines (Figure 45B). The IC_{50} values for the liposomes against the OPM-2 and KMS-11 cells were 36.80 ± 14.53 μg/mL and 33.28 ± 4.89 μg/mL, respectively (Figure 45B). A concomitant increase in levels of lipid ROS was also observed in cells treated with the liposomes, with a 1.6 ± 0.2-fold increase in the OPM-2 and a 1.7 ± 0.3-fold increase in the KMS-11 cells in response to a 15 μg/mL dose of the liposomes (Figure 45C). Addition of liproxstatin-1 prevented both the cell death and lipid ROS accumulation induced by the liposomes (Figure 45B-C).

Consistent with the results obtained using exogenous lipids and RSL3, addition of free RSL3 in combination with the liposomes significantly increased the cytotoxic effects of the nanoparticles. In combination with 50 nM or 2.5 μM RSL3, the IC_{50} values for the liposomes against the OPM-2 and KMS-11 cells were reduced to 10.61 ± 2.91 μg/mL and 8.44 ± 2.73 μg/mL, respectively (Figure 45B). Synergy between 15 μg/mL of the liposomes and RSL3 was confirmed, with fractional products of -0.54 for the OPM-2 cell line and -0.33 for the KMS-11 cell line (Figure 45B). RSL3 also significantly increased the levels of ROS induced by the liposomes in both cell lines; 15 μg/mL of liposomes in combination with RSL3 resulted in an 8.4 ± 1.1-fold increase of lipid ROS in the OPM-2 cells and a 15.8 ± 3.6-fold increase in the KMS-11 cells (Figure 45C).

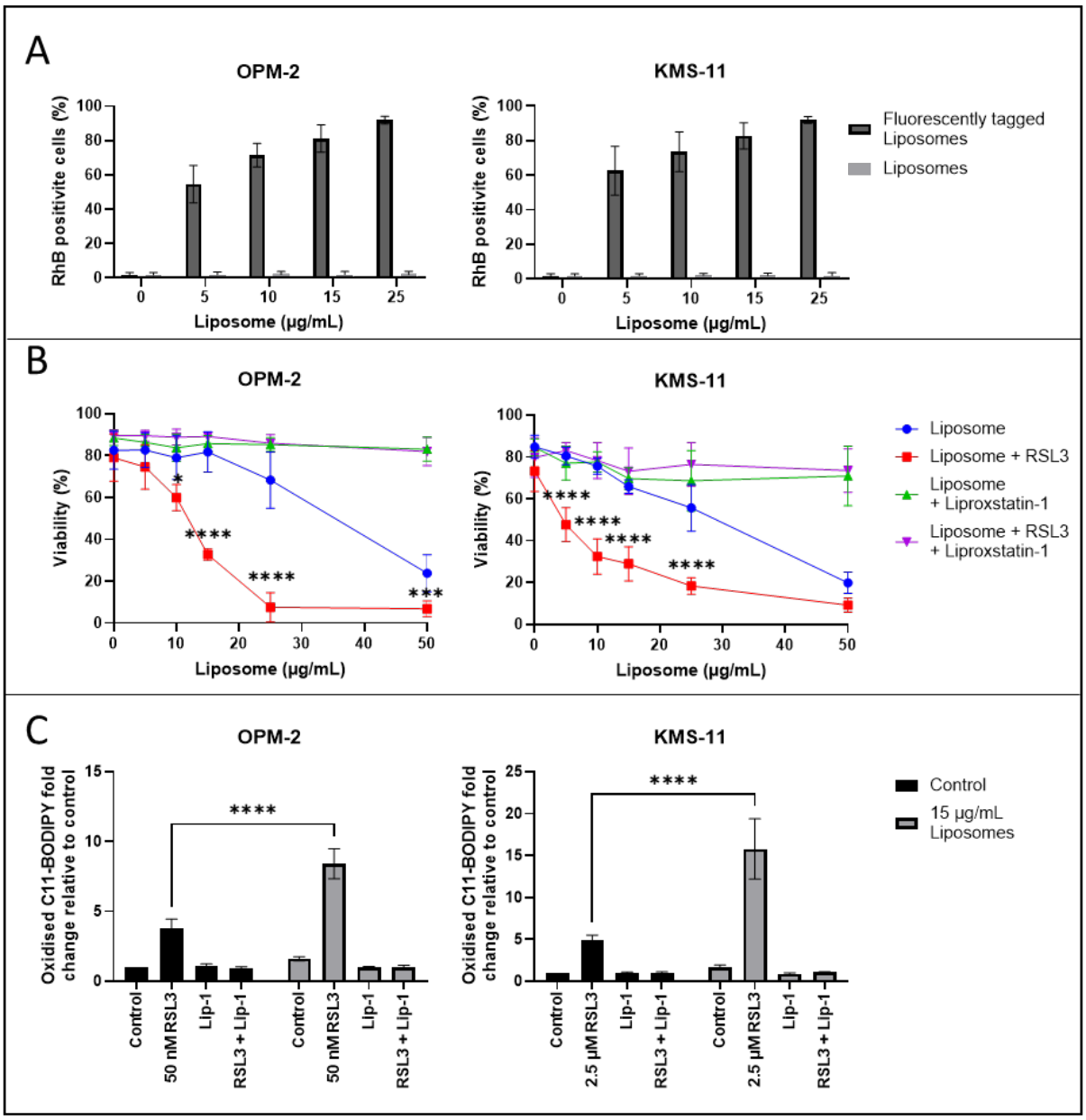

Figure 45.Optimised liposomes induce significant ferroptosis-mediated cell death in MM cells, enhanced by RSL3

(A) OPM-2 and KMS-11 cells were cultured for 24 hours with increasing concentrations of liposomes, that did or did not contain PE (18:1) (lissamine rhodamine B sulfonyl)-conjugated lipid at a 1 in 1000 dilution. The percentage of cells containing the fluorescently tagged lipid was assessed by flow cytometry. **(B)** OPM-2 and KMS-11 cells were cultured with increasing concentrations of liposomes, with or without 50 nM (OPM-2) or 2.5 µM (KMS-11) free RSL3 and with or without liproxstatin-1. Cell viability was assessed using annexin V/PI staining and flow cytometry. **(C)** OPM-2 and KMS-11 cells were cultured with 15 µg/mL liposomes, plus 50 nM or 2.5 µM RSL3, respectively ± liproxstatin-1. Lipid ROS levels were assessed by flow cytometry in cells stained with C11 BODIPY. All data are the mean ± standard deviation of duplicate measurements from 3 independent experiments using two-way ANOVA for statistical analyses. *P<0.05, **P<0.01, ***P<0.001, **** P<0.0001.

Another characteristic of ferroptotic cell death are the associated changes in morphology. Cells undergoing ferroptosis typically have an enlarged, ballooning cytoplasm, which previous results in this thesis have shown can be induced by PUFAs and RSL3. Cells were cultured with liposomes alone for 24 hours and the morphological changes visualised using an Incucyte live cell imaging system. The resulting images of OPM-2 cells clearly display morphological changes consistent with ferroptosis following treatment with 25 and 50 µg/mL of the liposomes (Figure 46). Liproxstatin-1 was able to inhibit the morphological changes induced by the liposomes in most of the cells, while the enlarged cytoplasm was still observed in some cells.

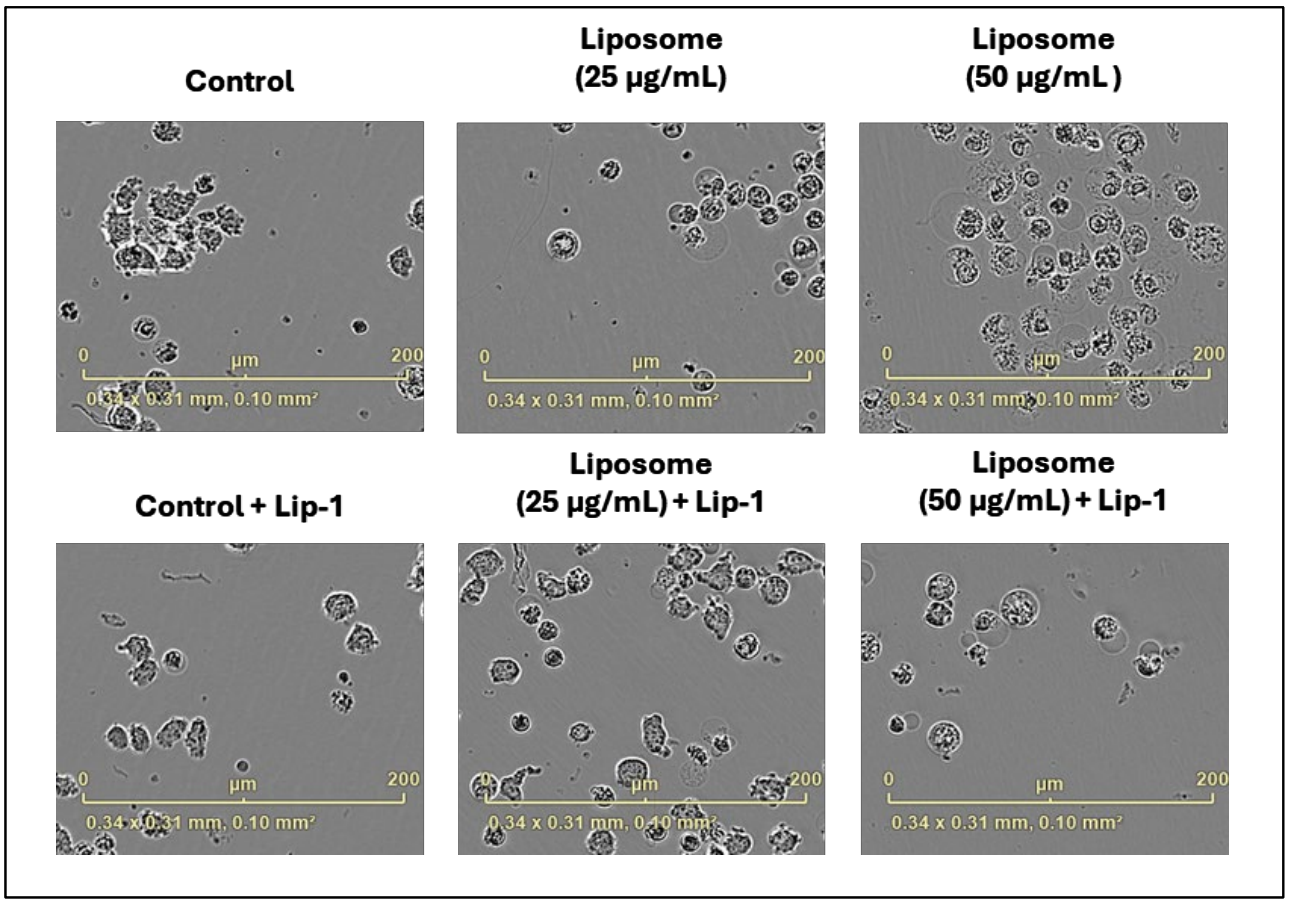

Figure 46. Liposomes induce morphological changes consistent with ferroptosis that can be largely inhibited by liproxstain-1 in OPM-2 MM cells.

OPM-2 cells were cultured with increasing concentrations of RSL3, with or without liproxstatin-1 for 24 hours. Images were captured at 20x magnification using an IncuCyte live cell analysis system. Lip-1: liproxstatin-1.

5.2.4 RSL3 encapsulation and quantification techniques

Drug delivery is one of the primary goals of liposomal technologies, aiming to deliver therapeutics that by themselves have poor pharmacokinetics or are toxic and cannot otherwise be used (250). RSL3 has both of these characteristics, as it has been shown to be toxic and has poor pharmacokinetics (234). Given that RSL3 is a potent inhibitor of GPX4, optimising delivery to the target cells could make RSL3 a very promising therapy for a range of diseases, including MM. RSL3 contains a large hydrophobic group which influences how the drug is incorporated into liposomes. Hydrophobic compounds are incorporated within the lipid bilayer of liposomes, which is often a limitation of liposomal formulations as this reduces the capacity of liposomes to carry the drug (250). This section of the chapter describes the development of a high-performance liquid chromatography (HPLC) method to determine the quantity of RSL3 in the liposomes and investigate methods to optimise RSL3 encapsulation within liposomes.

An HPLC method was developed based on the manufacturer's instructions for RSL3, with some slight differences (Appendix Figure 10). A column with similar properties was purchased for the HPLC instrument and all the conditions, including flow rate, temperature and wavelength were kept constant (Appendix Figure 10). The manufacturer used a binary gradient system with two mobile phases, an aqueous trifluoroacetic acid (TFA) containing mobile phase (mobile phase A) and a solvent phase comprised of acetonitrile and TFA (mobile phase B). Due to instrument availability an isocratic HPLC method with one mobile phase containing 90% mobile phase B and 10% mobile phase A was used. All standards and samples were made up in or diluted in this mobile phase.

RSL3 standards were analysed with an internal standard spiked into the samples. RSL3 had a retention time of 1.74 minutes, and the internal standard naphthalene had a retention time of 2.4 minutes (Appendix Figure 11). This also meant that the run time could be decreased significantly, compared to the 20-minute run time described in the method proposed by the manufacturer (Appendix Figures 10 and 11). The resulting ratio of RSL3 peak area to naphthalene peak area was used to calculate a standard curve (Figure 47B).

Drug encapsulation can be performed either passively or actively depending on the properties of the drug (251). Given the hydrophobicity of RSL3, the drug was loaded into the liposomes passively by adding the drug into the organic solvent containing the lipids prior to synthesis of the liposomes. Multiple methods were trialled to separate free RSL3 from the liposomes. Initially, centrifugation was used to separate unencapsulated RSL3 from the liposomes, but the drug also pelleted making

it impossible to separate free from the liposomes. Liquid-liquid extraction using organic solvents was then attempted, however RSL3 partitions into the same organic phase as the lipids, preventing separation via this method. Ultracentrifugation was then performed using the smallest filter available at the time (30 kDa), however the sheer stress led to partial rupture of the liposomes and lipids within the filtered sample.

Next, pressure ultrafiltration was trialled to separate unencapsulated RSL3 from the liposomes using nitrogen as the driving gas and a 5 kDa filter (Figure 47A). This method was much more efficient at separating the free RSL3 from the liposomes. DLS on the filtrate from the system confirmed that it did not contain any liposomes. The equation below was used to calculate encapsulation efficiency. Filtrate volume was also accounted for to ensure accurate calculations.

*Encapsulation efficiency = [(total RSL3 amount added – RSL3 amount in filtrate) / total RSL3 amount added] *100%* (252)

Liposomes were loaded with 50 µg/mL RSL3, which equates to 113.41 µM. The concentration of RSL3 loaded was influenced by two main factors. Firstly, we found this concentration of RSL3 did not disrupt the liposome bilayer, with 5% of the total liposome mass being an acceptable loading amount. Secondly, the RSL3 concentration needed to be biologically relevant in the MM cell lines. At 25 µg/mL of liposomes the RSL3 concentration was 2.8 µM, which is close to the 2.5 µM RSL3 used against the KMS-11 cell line in Figure 45. Unfortunately, due to the sensitivity of the OPM-2 cells to RSL3, the liposomes would need to be loaded with less than 5 µg/mL RSL3, which is below the detectable limit by HPLC. Ultimately, an RSL3 encapsulation efficiency of 67.45 ± 17.12% was achieved in the liposomes that were loaded with 50 µg/mL RSL3. Interestingly, when the liposomes were loaded with 100 µg/mL RSL3 the encapsulation efficiency was 96.50 ± 2.83%, but the corresponding concentration of the drug was deemed too high to use against the MM cells.

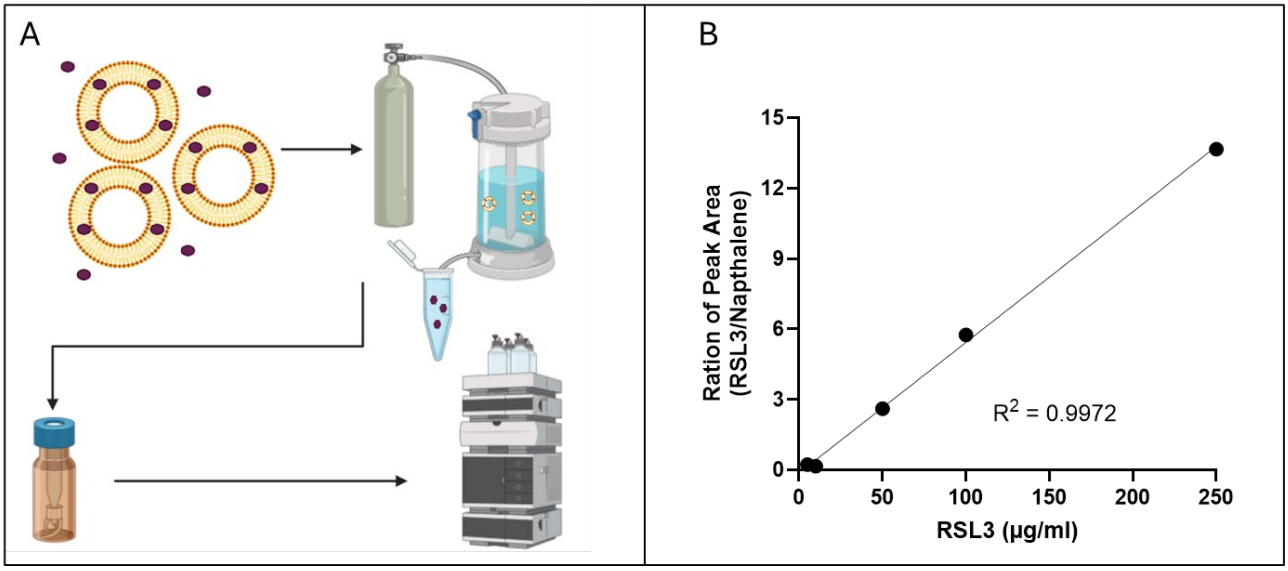

Figure 47. RSL3 encapsulation and quantification

(A) Flow diagram detailing the processes involved in generating liposomes encapsulated with RSL3 and assessment of RSL3 concentrations by HPLC analysis. Liposomes containing RSL3 were synthesised and pressure ultrafiltration was used to separate unencapsulated drug from the liposomes. Samples were then prepared and analysed using HPLC. (B) Representative standard curve generated using peak area ratios of RSL3 to naphthalene.

5.2.5 Liposomes loaded with RSL3 are potent ferroptosis inducers in MM cells

The previous section of this chapter demonstrated all the necessary steps required to reach this milestone, from optimisation of liposome formulation to RSL3 encapsulation. This section of the results will introduce these novel RSL3 and PUFA-containing liposomes as a means of inducing ferroptotic cell death in RSL3 insensitive MM cell lines. As mentioned above, it was not possible to examine the effects of the liposomes against OPM-2 cells as the appropriate concentration of RSL3 required for this cell line was below the detection limit for the HPLC.

RSL3 loading did not significantly impact the size or the PDI of the liposomes. The average diameter of RSL3 loaded liposomes was 131 nm with a PDI of 0.02. Separating unencapsulated RSL3 from liposomes was described in the previous section of the chapter and was found to be exceedingly difficult. Pressure ultrafiltration was successful in terms of separating unencapsulated drug from the liposomes and retrieving RSL3 in the filtrate, however retention of intact liposomes using this method was not possible. Next, dialysis was trialled as a means of separating unencapsulated RSL3 from the loaded liposomes, while maintaining integrity of the liposomes. Initial attempts at dialysis

using a 10 kDa membrane cassette showed that the PBS dialysate did not contain liposomes, suggesting that this method may be a potential option. However, the liposomes obtained using this method had minimal effects on the MM cells.

To investigate the reasons for the lack of efficacy of these liposomes, the NanoSight nanoparticle tracking analyser was used to measure the number of liposomes before and after dialysis. The concentration of liposomes prior to dialysis was 1.804E+11 particles per mL (Appendix Figure 12 – accounting for the 1/200 dilution). The concentration of liposomes after dialysis was 4.84E+10 (Appendix Figure 13 – accounting for the 1/200 dilution), which represents a liposome retention rate of only 27%. This meant this approach was neither experimentally nor financially viable. As we had exhausted the methods available to us and due to time constraints, the experiments in this section were performed with RSL3 dosing based on the total drug concentration loaded (50 μg/mL) rather than the concentration of encapsulated RSL3.

KMS-11, LP-1 and KMS-18 MM cell lines were cultured for 24 hours with increasing concentrations of liposomes, which did or did not contain RSL3. Liposomes containing RSL3 induced significantly more cell death than blank liposomes or RSL3 alone in all cell lines (Figure 48A and Appendix Figure 14). The IC_{50} values for the RSL3-encapsulated liposomes in the aforementioned cell lines were 3.80 ± 0.67 μg/mL, 3.35 ± 0.70 μg/mL and 4.05 ± 1.51 μg/mL, respectively, which are equivalent to RSL3 concentrations of 430.39 ± 76.13 nM (KMS-11), 379.84 ± 79.25 nM (LP-1) and 459.47 ± 171.52 nM (KMS-18) (Figure 48A). In comparison, the IC_{50} values for free RSL3 against these lines were 6.25 ± 0.82 μM, 2.70 ± 0.72 μM, and 3.84 ± 0.37 μM, respectively (Figure 11A), consistent with an average 7.1 to 14.5-fold decrease in the IC_{50}s by the RSL3-encapsulated liposomes, from the micromolar to the nanomolar range. Interestingly, when FH9 cells, a cell line derived from healthy B cells, were cultured with liposomes containing RSL3 they were found to be significantly less sensitive to ferroptosis than the MM cell lines (Appendix Figure 17). This suggests that the liposomes may have the ability to passively target MM cells, which will be further discussed below.

Morphological changes consistent with ferroptosis were observed in the MM cell lines after 24 hours of treatment with the RSL3-containing liposomes. Both the morphological changes and cell death induced by the liposomes were prevented by co-administration of liproxstatin-1 (Figure 48B and Appendix Figures 14 and 15). Additionally, increases in lipid ROS were also observed in cells from all three lines when cultured with liposomes containing RSL3 (Figure 48). The increase in lipid ROS were also prevented by liproxostatin-1, confirming ferroptosis as the mechanism of cell death (Figure 49).

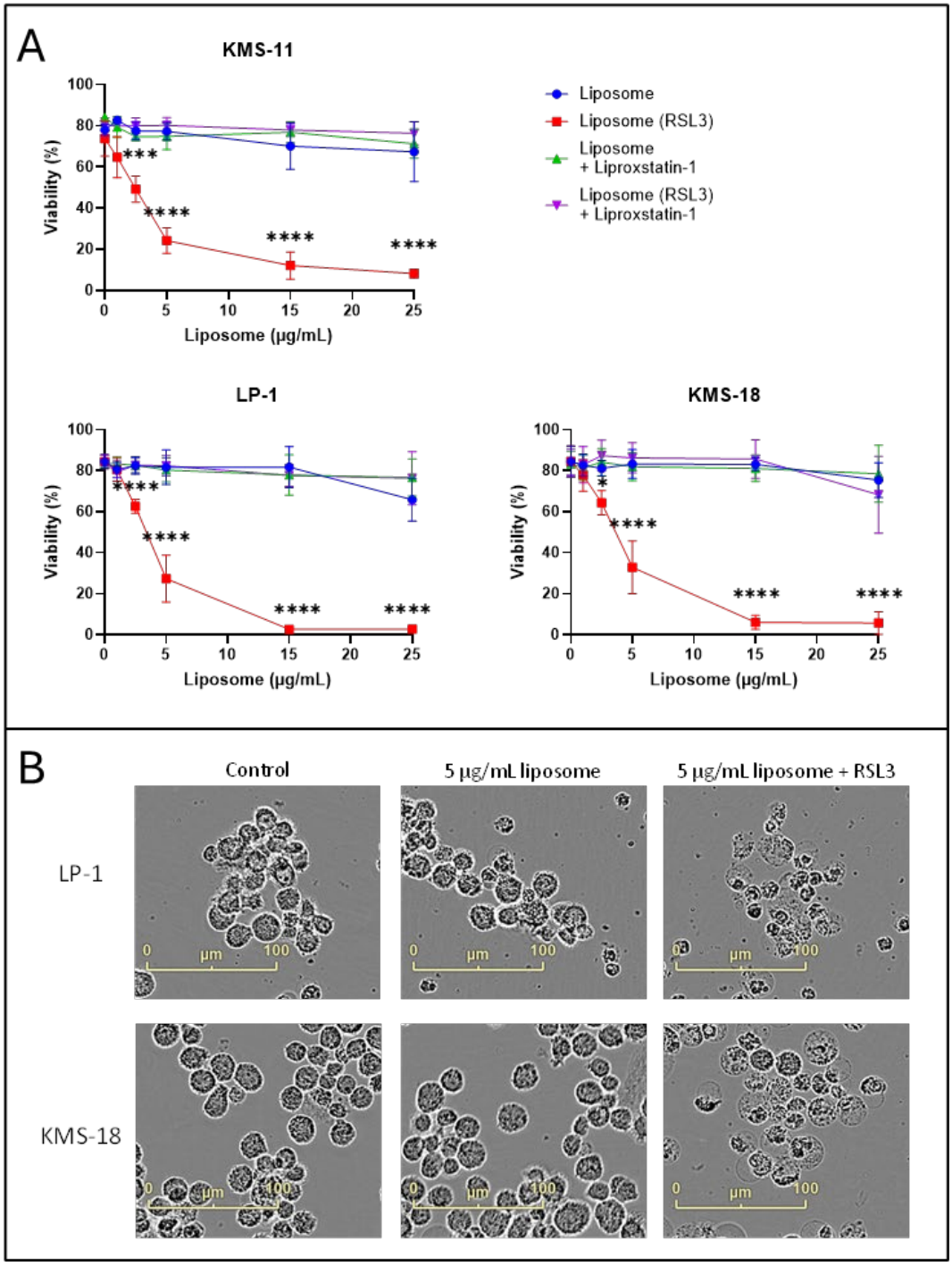

Figure 48. RSL3 encapsulation increases the MM cell killing capacity of liposomes.

(A) KMS-11, KMS-18 and LP-1 cells were cultured with liposomes with the formulation PE (16:0_22:6): DSPE-PEG2000 at ratios of 98:2 (w/w%), loaded with or without 50 µg/mL RSL3 and liproxstatin-1 for 24 hours. Cell viability was assessed by flow cytometry in cells stained with annexin V and PI. Data are the mean ± standard deviation from 3 independent experiments with statistical analyses performed by two-way ANOVA. *P<0.05, **P<0.01, ***P<0.001, **** P<0.0001. **(B)** MM cells were cultured for 24 hours with 5 µg/mL liposomes that either did or did not contain RSL3. Images were acquired after 24 hours of treatment using an IncuCyte S3 live cell analysis system at 20X magnification.

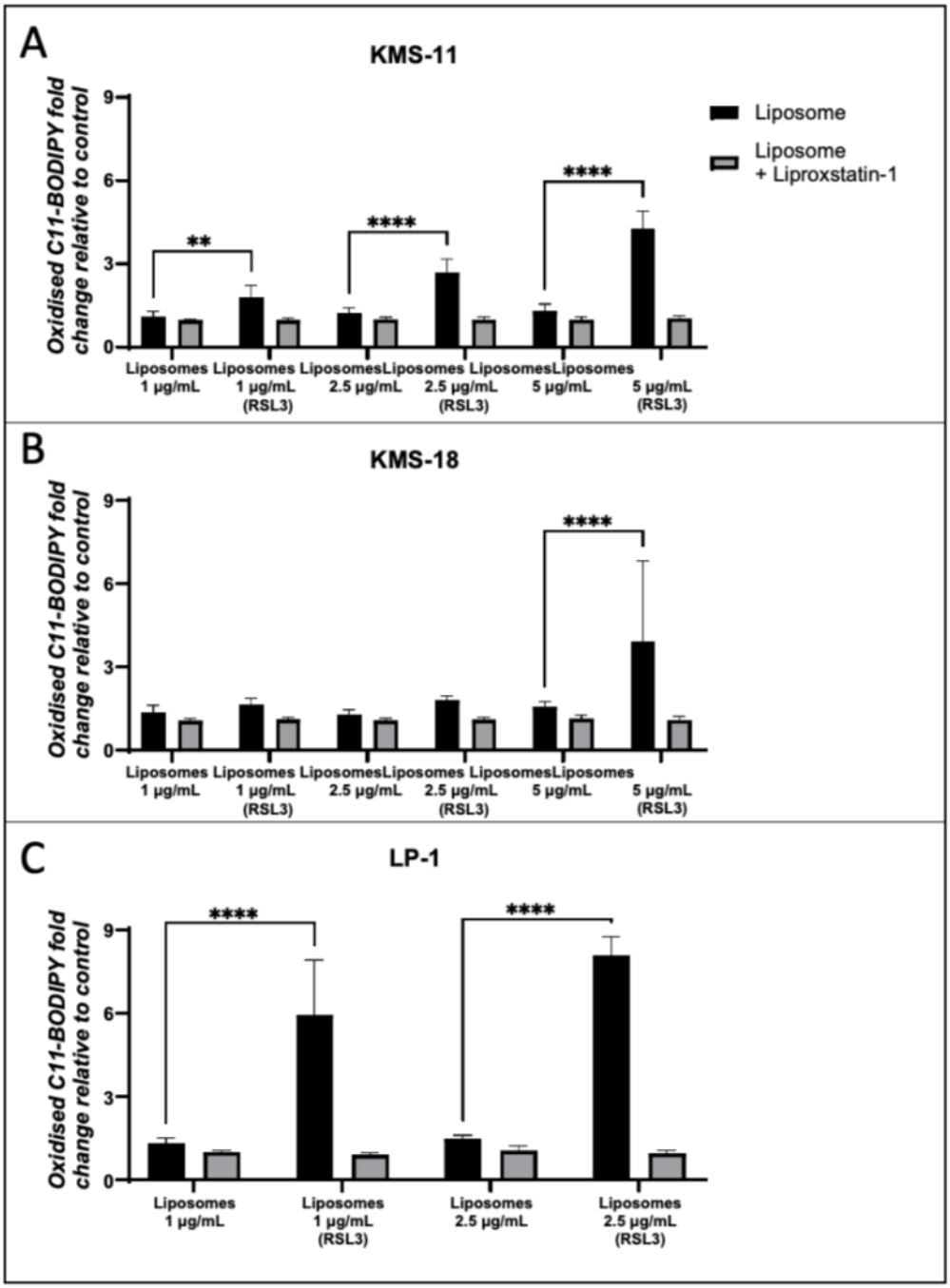

Figure 49. Liposomes containing RSL3 induce significantly higher levels of lipid ROS in MM cell lines than liposomes alone.

(A) KMS-11, **(B)** KMS-18 and **(C)** LP-1 MM cells were cultured for 24 hours with the indicated concentrations of either liposomes alone or liposomes containing RSL3. Lipid ROS levels were assessed by flow cytometry in cells stained with C11 BODIPY. Data are the mean ± standard deviation from 3 independent experiments using two-way ANOVA for statistical analysis. *P<0.05, **P<0.01, ***P<0.001, **** P<0.0001.

5.2.6 Conjugation of daratumumab to liposomes

The final part of this chapter describes the development of liposomes that specifically target MM cell lines. Daratumumab, an anti-CD38 monoclonal antibody introduced in chapter 4, was used to functionalise the surface of liposomes. This process required the adaptation of the liposome's formulation, with the replacement of DSPE-PEG2000 with DSPE-PEG2000 Carboxy NHS. The new liposome formulation was composed of PE (16:0_22:6): DSPE-PEG2000 Carboxy NHS at ratios of 98:2 (w/w%). These new liposomes were smaller than the liposomes previously described, with an average diameter 114.2 nm and a PDI of 0.05, well below the 0.3 threshold. The liposomes were then incubated with daratumumab at a molar ratio of 5:1 DSPE-PEG2000 Carboxy NHS to daratumumab, for 3 hours with continuous shaking. The liposomes were then assessed by DLS, which showed that the average size of the liposomes was larger than the control liposomes, with an average diameter of 116.3 and a PDI of 0.08.

To further characterise the daratumumab-conjugated liposomes a new method was developed using a CytoFLEX Nano flow cytometer (Beckman Coulter). A range of beads with known sizes were used to calibrate the instrument and to enable an assessment of the size of the liposomes. Similar to the results obtained by DLS, assessment by flow cytometry found the liposomes to be 121.2 ± 21.7 nm in size (Figure 50A and Appendix Figure 18). The mean size of the daratumumab-conjugated liposomes was also slightly larger than that of unconjugated liposomes, measuring 126.4 ± 17.7 nm in diameter (Figure 50 and Appendix Figure 18).

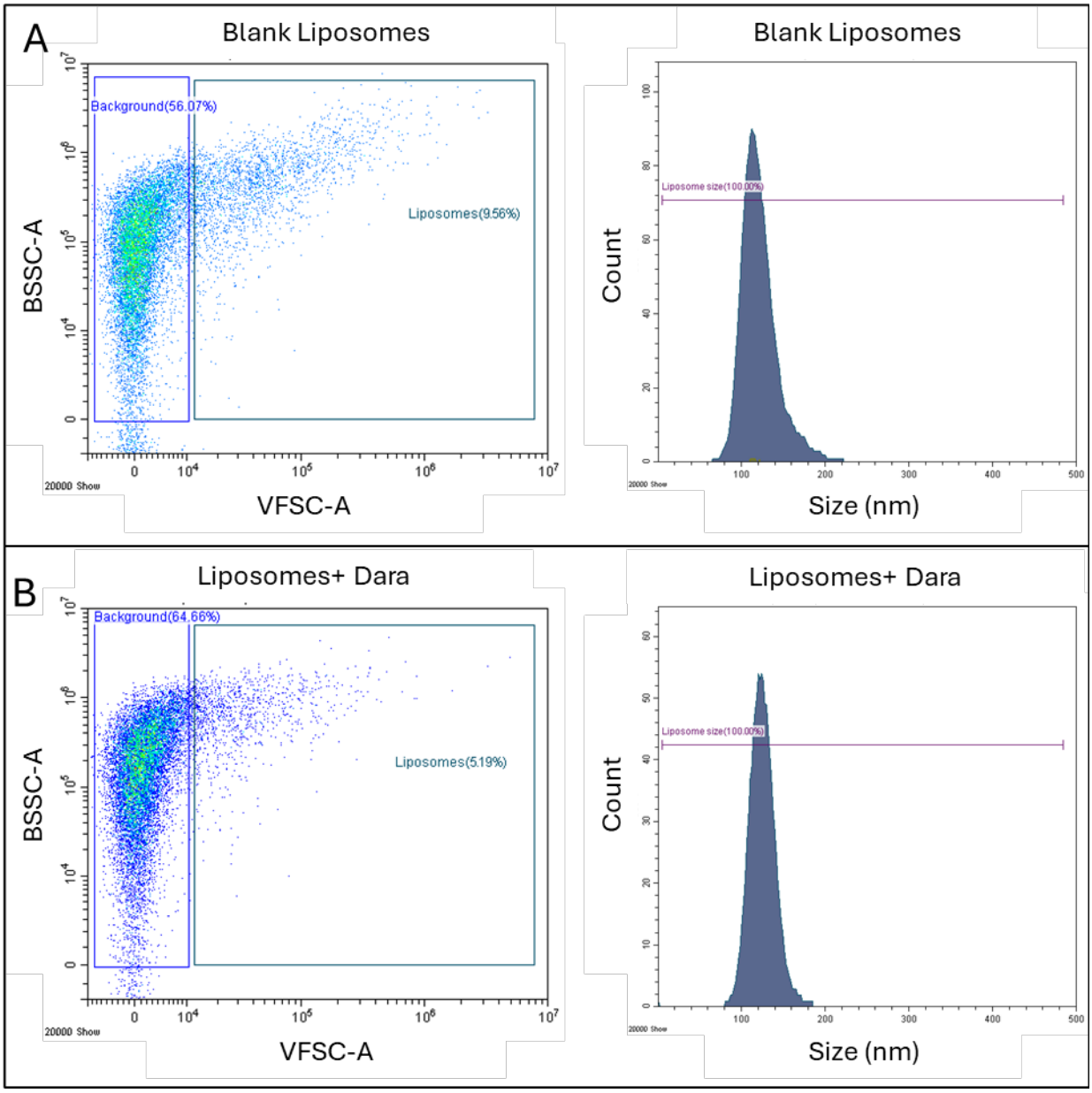

Figure 50. Assessment of liposome size using nano-scale flow cytometry.

The size distribution of **(A)** unconjugated liposomes and **(B)** daratumumab conjugated liposomes was assessed using a CytoFLEX Nano flow cytometer. BSSC-A, Blue Side Scatter Area; VFSC-A, Violet Forward Scatter Area.

The chemical process that resulted in the conjugation of the daratumumab monoclonal antibody is shown in Figure 51A. This process occurs via a reaction between the primary amine in the antibody and the NHS ester in the liposomes, forming a stable amine bond. This results in antibody-conjugated lipids and free NHS. Having shown that the antibody-conjugated liposomes were larger in size, expression of daratumumab on the surface of the liposomes was then assessed by incubating the liposomes with an anti-human, fluorochrome-conjugated, secondary antibody with analysis using the CytoFLEX Nano flow cytometer. Unconjugated liposomes incubated with the anti-human secondary antibody were used as a control (Figure 51B). The impressive results showed that the

conjugation efficiency was approximately 65% (Figure 51B-C). Interestingly, two peaks were observed in the flow cytometry histograms, which indicate daratumumab positive and negative populations (Figure 51B-C). Further analysis of the data also demonstrated that the size of the liposomes that were deemed positive for daratumumab were larger than the unconjugated liposomes. The daratumumab positive liposomes were 155.2 ± 35.9 nm in size, while the daratumumab negative liposomes in the same sample had a mean size of 122.9 ± 14.3 nm. The unconjugated, control liposomes were similar in size to the unconjugated liposomes in the sample at 123.7 ± 21.4 nm. These data suggest that functionalising liposomes with antibodies likely increases their size, which is an important factor to consider as it may influence the distribution, clearance and uptake of the liposomes.

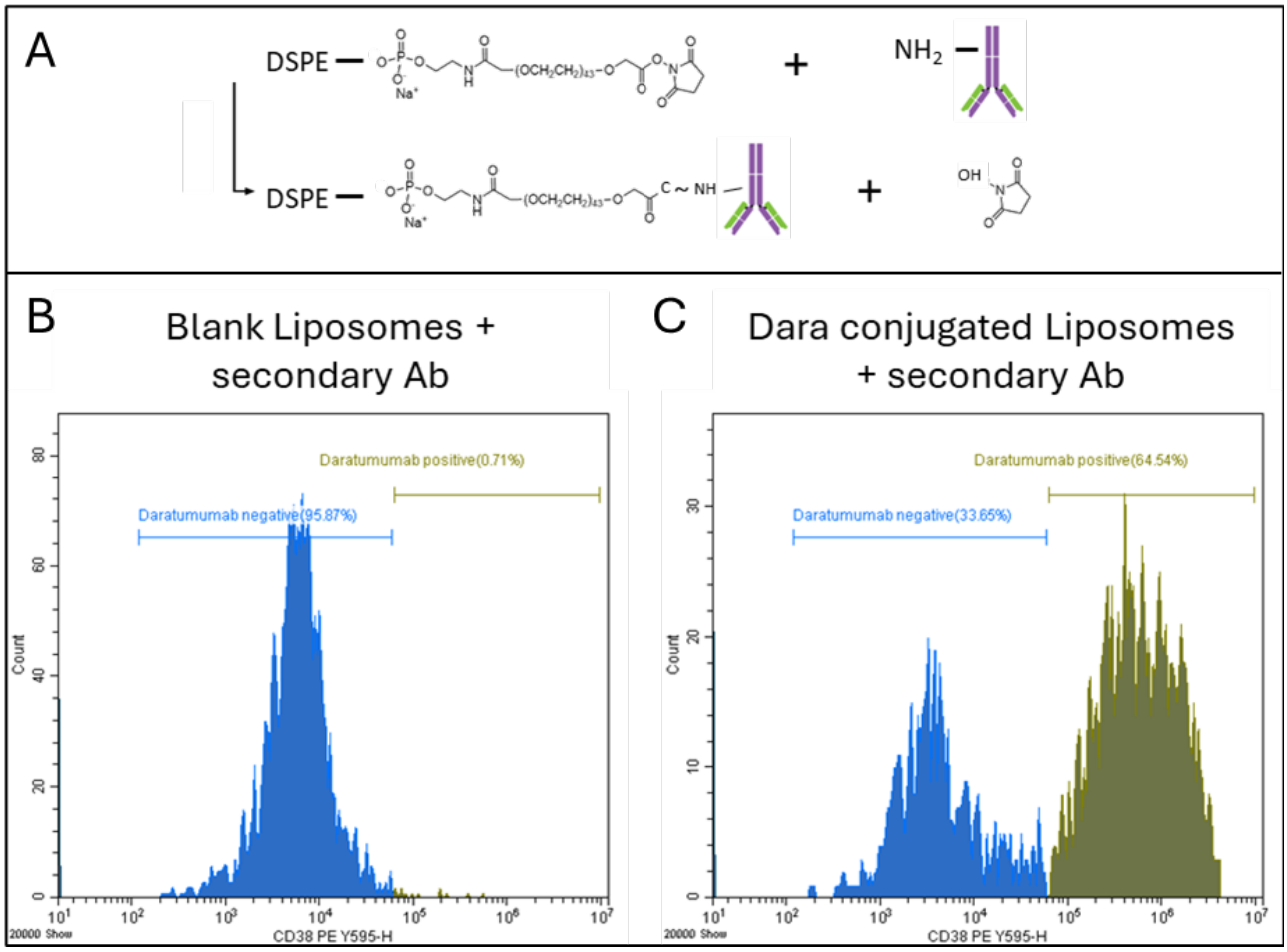

Figure 51. Conjugating daratumumab to liposomes.

(A) Diagram illustrating the chemical processes involved in antibody conjugation to DSPE-PEG2000 Carboxy NHS. **(B)** Unlabelled liposomes following incubation with an anti-human, PE-conjugated secondary antibody. **(C)** Daratumumab (Dara) labelled liposomes following incubation with an anti-human, PE-conjugated secondary. Representative flow cytometry plots generated using a CytoFLEX Nano flow cytometer.

5.2.7 Daratumumab conjugated liposomes induce targeted ferroptosis of MM cells

In the previous section of this chapter we were able to conjugate our novel liposomes to the monoclonal antibody, daratumumab, and confirm the conjugation using nano-flow cytometry. A large proportion of the liposomes were successfully conjugated with the antibody using the techniques described above. The final section of results in the current chapter will describe the functional properties of these novel liposomes, by investigating their uptake and capacity to induce ferroptosis in MM cells and the healthy B-cell line, FH9.

The MM cell lines, KMS-11, OPM-2 and KMS-18 and the FH9 line, which was derived from healthy B cells, were cultured with increasing concentrations of the daratumumab conjugated liposomes, containing the RhB-conjugated lipid. Intriguingly, daratumumab conjugation had no effect on liposome uptake into the MM cells. This result was not entirely unexpected given how efficiently the liposomes were passively taken up into MM cells (Figure 52A). The results in the FH9 cells were interesting, with relatively low liposome uptake at concentrations of 1 μg/mL and 5 μg/mL, regardless of whether the liposomes where functionalised with daratumumab or not (Figure 52A). This may be related to the ability of the liposomes to passively target the MM cells, which has been well-documented in the literature, and will be discussed in more detail below. Following culture with 5 μg/mL daratumumab-conjugated liposomes there was a trend towards a decrease in the liposome uptake into the FH9 cells compared to unconjugated liposomes (Figure 52A). This became more apparent following treatment with 15 μg/mL of the liposomes (Figure 52A); following culture with 15 μg/mL of unconjugated liposomes, approximately 60% of the FH9 cells were positive for RhB by flow cytometry. However, when the cells were cultured with the same concentration of the daratumumab conjugated liposomes, a significant decrease in uptake, to approximately 21%, was observed in the cells positive for the labelled lipid (Figure 52A). The meant that functionalising the liposomes with daratumumab reduced their uptake in the healthy B-cell line by almost 40% (Figure 53A).

Having shown no statistically significant difference in uptake of the unconjugated and daratumumab conjugated liposomes into MM cell lines, the results in Figure 52A were not unexpected. In the OPM-2 and KMS-11 cell lines, the unconjugated and daratumumab conjugated liposomes were equally as efficient at inducing ferroptotic cell death and sensitised the cell lines to unencapsulated RSL3. Importantly, this demonstrates that functionalisation with the antibody did not hinder the

utilisation of liposomes as a ferroptosis substrate (Figure 52B). Cell death was again prevented by liproxstatin-1 (Figure 52C).

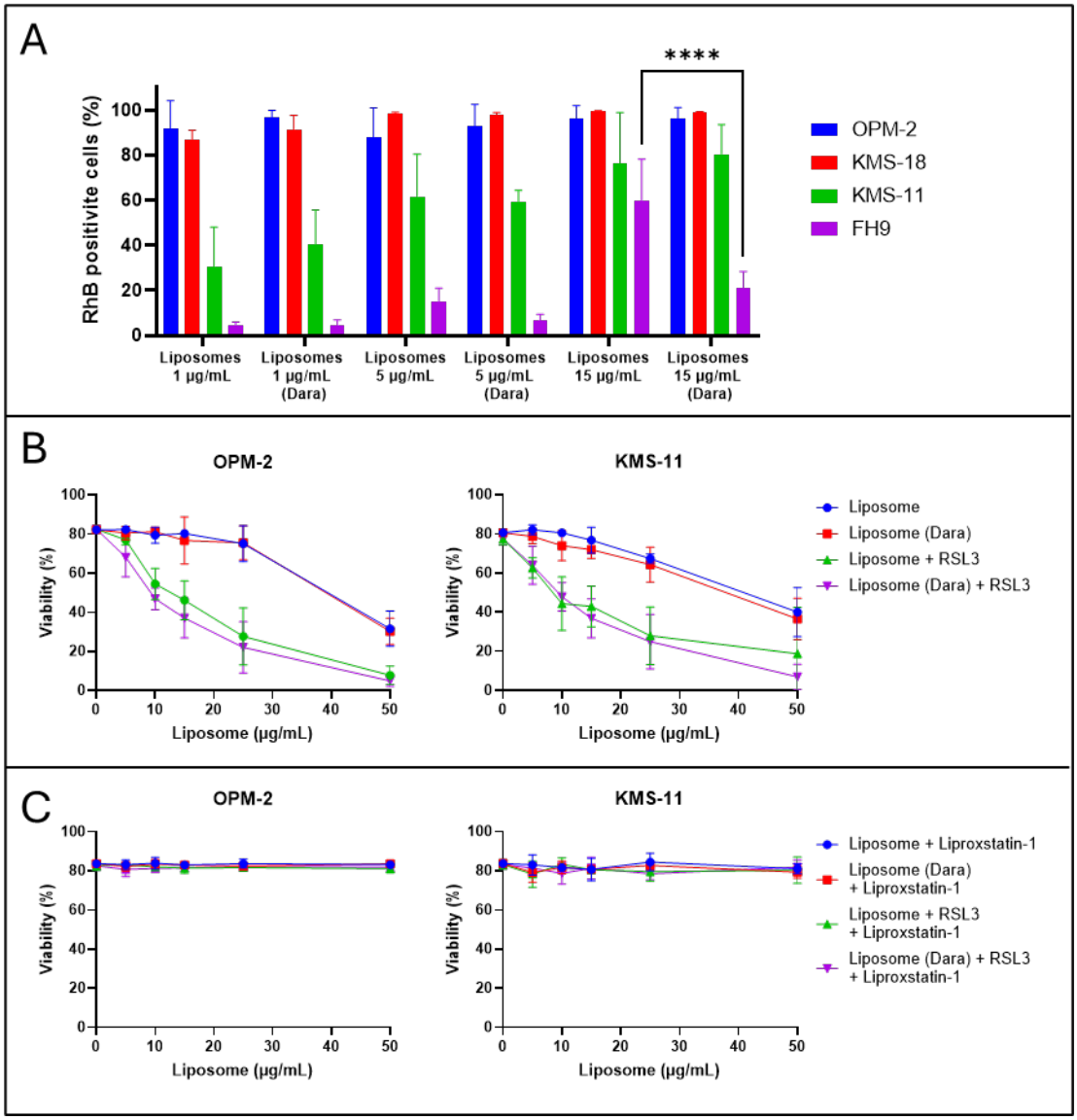

Figure 52. Conjugation of liposomes with daratumumab has no effect on their ferroptosis-inducing capacity in MM cells but reduces uptake into FH9, healthy B-cells.

(A) OPM-2, KMS-18, KMS-11 MM cells and FH9 cells (healthy B-cell line) were cultured for 24 hours with increasing concentrations of unconjugated and daratumumab-conjugated liposomes, containing the PE (18:1) (lissamine rhodamine B sulfonyl)-conjugated lipid at a 1 in 1000 dilution. The percentage of cells containing the fluorescently tagged lipid was assessed by flow cytometry. **(B)** OPM-2 and KMS-11 cells were cultured with increasing concentrations of liposomes, with or without 50 nM (OPM-2) or 2.5 µM (KMS-11) free RSL3. **(C)** OPM-2 and KMS-11 cells were cultured with increasing concentrations of liposomes, with or without 50 nM (OPM-2) or 2.5 µM (KMS-11) free RSL3 and liproxstatin-1. Cell viability was assessed using annexin V/PI staining and flow cytometry. All data are the mean ± standard deviation of duplicate measurements from 3 independent experiments using two-way ANOVA for statistical analyses. **** $P<0.0001$.

The results suggest that FH9 cells take up a significantly lower quantities of the liposomes once they are functionalised with daratumumab. The final step in the validation of these liposomes was to assess their cell killing capacity in the MM compared FH9 cells. Unconjugated liposomes containing RSL3 had an average diameter of 81.3 nm with a PDI of 0.11, while conjugated liposomes containing RSL3 had an average diameter of 83.8 nm and a PDI of 0.10. FH9 cells were cultured with an increasing concentration of unfunctionalized and functionalised liposomes that were loaded with 50 µg/mL RSL3. The encapsulation efficiency of these liposomes was not determined, primarily due to time constraints, and because these liposomes were subjected to shaking at room temperature for 3 hours during the antibody conjugation process, which would inevitably result in some release of RSL3 from the lipid membrane.

The healthy B cell line FH9 has demonstrated susceptibility to RSL3 induced cell death (Appendix Figure 19). KMS-11 cells were used to confirm the cell killing capacity of these liposomes. The IC_{50} values for the RSL3-encapsulated liposomes against the KMS-11 and FH9 cell lines were 4.67 ± 2.02 µg/mL and 5.28 ± 0.45 µg/mL for the unconjugated liposomes and 5.03 ± 1.54 µg/mL and 12.87 ± 2.05 µg/mL for the daratumumab functionalised liposomes (Figure 53A). There was no statistically significant difference between the IC_{50} values for the liposomes against the KMS-11 cells, but the IC_{50} was significantly higher for the conjugated liposomes against the FH9 cells (p=0.02) (Figure 53A). The above liposome concentrations correspond to RSL3 concentrations of 598.73 ± 50.77 nM and 1459.96 ± 232.45 nM in the FH9 cells, respectively, which is a 2.4-fold increase in RSL3 concentration for the daratumumab conjugated liposomes compared to unconjugated liposomes (Figure 53A). In the KMS-11 cells the liposome concentrations for the unconjugated liposomes corresponds to 529.25 ± 229.34 nM and 570.68 ± 170.50 nM for the daratumumab conjugated liposomes (Figure 53A). Cell death was largely prevented by co-culturing with liproxstatin-1 in both of the cell lines (Figure 53B).

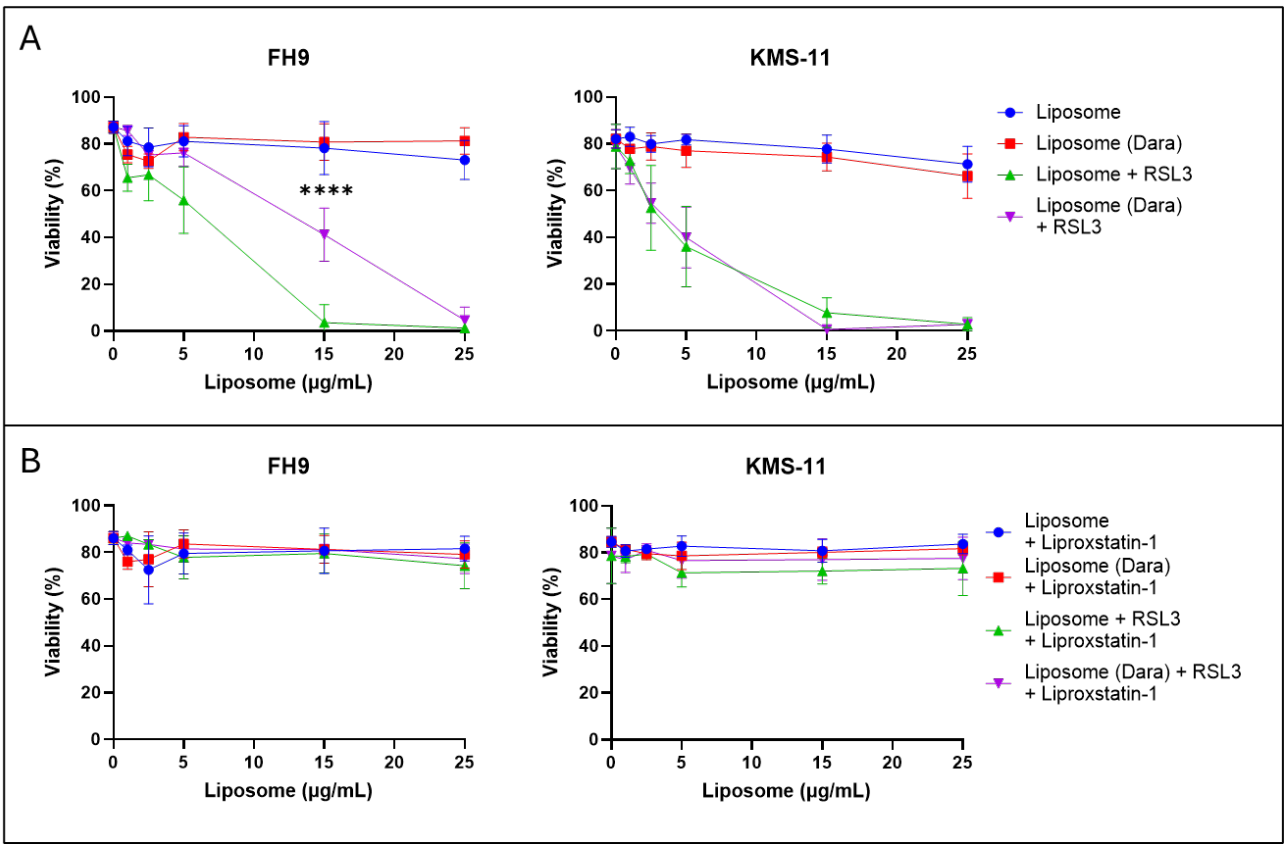

Figure 53. Daratumumab conjugated liposomes reduce cell death in FH9 cells while still killing MM cell line KMS-11.

(A) FH9 and KMS-11 cells were cultured with unconjugated and daratumumab-conjugated liposomes with the formulation PE (16:0_22:6): DSPE-PEG2000-NHS at ratios of 98:2 (w/w%) with or without 50 µg/mL encapsulated RSL3. **(B)** FH9 and KMS-11 cells were cultured with unconjugated and daratumumab conjugated liposomes with the formulation PE (16:0_22:6): DSPE-PEG2000-NHS at ratios of 98:2 (w/w%) loaded with or without 50 µg/mL RSL3 with liproxstatin-1. Cell viability was assessed using annexin V/PI staining and flow cytometry. All data are the mean ± standard deviation of duplicate measurements from 3 independent experiments using two-way ANOVA for statistical analyses. **** P<0.0001.

5.3 Discussion

The aim of this final results chapter was to develop an entirely new approach of inducing ferroptosis in MM cells and examine how this may represent a means of harnessing ferroptosis to target and eliminate MM cells. The first results chapter of this thesis described the importance of PUFAs as ferroptosis substrates and even went as far as to show that addition of exogenous PUFAs were sufficient to sensitise MM cells to ferroptosis. This chapter applied the novel findings from the first chapter to develop novel liposomes capable of triggering ferroptosis in MM cells. The concept of liposomes as nanoparticles was first demonstrated in 1964, in a study that found that hydrated PLs had self-assembled to form "multilamellar smectic mesophases" (253). Since this seminal work, the field of nanoparticles has grown rapidly, with the first FDA injectable liposomal formulation, DOXIL (doxorubicin loaded liposomes), approved in 1995 (253). Since then, liposomes have been used in a range of applications, including but not limited to cancer treatment, vaccines, and pain management (253, 254). Emerging research concerning ferroptosis has also recently begun to include studies on the potential of liposomes as a valuable tool against disease (Publication 1 and 2 in the Appendix). To date there is no literature published that describes using liposomes as a method to induce ferroptosis in MM. Although limited, there does exist literature in other haematological diseases that highlight the use of liposomes to induce ferroptosis (149, 255, 256). Additionally there have only been a few studies in which the liposomes have been comprised predominantly of PUFA-containing lipids, as substrates of ferroptosis, and no studies to date have focused on MM. Research on the potential of ferroptosis and liposomes in the context of haematological malignancies, although growing, remains sparse. Further research is required to uncover the potential role of ferroptosis in these diseases and to determine whether liposomes may represent a novel therapeutic tool.

5.3.1 Cholesterol and liposomes

Cholesterol is an integral part of liposomal formulations in which it provides and maintains structural stability and increases drug retention (241). Cholesterol is a lipid with a unique structure comprised of carbon, hydrogen and oxygen atoms and is classified as a sterol (257). Additionally, cholesterol is a vital component of cellular membranes and therefore is likely to play a role in lipid peroxidation and in turn ferroptosis. Cholesterol has been increasingly recognised as a key player in cancer progression by promoting the proliferation, invasive capacity, and migration of cancer cells (258). Importantly, in the context of ferroptosis, studies suggest that cholesterol may be involved in the inhibition of this form of programmed cell death. C57BL/6 mice fed a high-cholesterol diet had lower

basal levels of lipid ROS within their myeloid-based hematopoietic stem cells (259). The mechanism of the resistance induced by cholesterol appears to be cell dependent and triggers different pathways in different cells. One of these mechanisms may be mediated by the formation of lipid rafts. Cholesterol rich domains of the plasma membrane referred to as lipid rafts have been shown to restrict the rate of lipid peroxidation in melanoma cells (246). We recently published a review in which we described the current literature concerning cholesterol in the context of ferroptosis (Publication 3 in the Appendix). Ultimately, data in the current study and in the literature suggest it is important to consider the cholesterol content of liposome formulations as this may significantly impact the efficacy of these nanoparticles.

Despite the evidence suggesting cholesterol may inhibit ferroptosis, we initially generated and tested liposomes containing this lipid. We considered that it may be important for the liposomes to contain some cholesterol as too little may impact the stability and integrity of the nanoparticles, while too much cholesterol would counter their ferroptosis-inducing capacity. Liposomes were formulated with PE (16:0_22:6): cholesterol: DSPC: DSPE-PEG2000 at ratios of 40:48:10:2 (w/w/w/w%) and as expected these liposomes were uniform and small in size with an average diameter of 220 nm. This formulation was a well-established recipe for liposomes adapted from previous work, with a ratio of lipids that was known to produce stable liposomes. Unfortunately, these liposomes were not effective at sensitising the MM cells to ferroptosis, as minimal effects were observed when the liposomes were combined with RSL3 (Figure 43). To try and negate the effects of cholesterol, new liposomes were formulated that contained half the amount of cholesterol. The formulation for these liposomes was PE (16:0_22:6): cholesterol: DSPC: DSPE-PEG2000 at ratios of 40:20:38:2 (w/w/w/w%). However, similar effects against the MM cells were observed with these liposomes when combined with RSL3 (Figure 43). Although cholesterol has been demonstrated to inhibit ferroptosis in other cell types, its capacity to inhibit ferroptosis in MM cells was unexpected; even halving the cholesterol concentration within the liposomes did not improve their efficacy.

A study published in 2021 demonstrated that liposomes manufactured from PC lipids containing unsaturated fatty acids could be used to deliver iron and a prodrug to induce ferroptosis in the cancer cells in a mouse model of melanoma (173). These liposomes contained undisclosed PC lipids, cholesterol and DSPE-PEG2K at ratios of 90:10:10. Lipsoomes containing only iron had limited impact on cell viability, while liposomes containing the doxorubicin prodrug were more effective at killing the cells (173). The cytotoxicity was also found to be consistent with changes in lipid ROS

levels, with the liposomes containing iron found to induce a relatively small but significant increase in lipid ROS levels. This study used a combination of unsaturated lipids and iron to induce ferroptosis via the Fenton reaction while the doxuribicin induced apoptosis, providing proof-of-principle eveidence that liposomes may act as 'dual executioners' via the two distinct mechanisms of programmed cell death. While the unsaturated lipid nor the level of unsaturation within the lipid were disclosed in the study, the liposome formulation did contain cholesterol and the results included hallmarks of ferroptosis, including an increase in lipid ROS levels. However, the data presented in the current study suggest the liposomes manufactured by Logie *et al*., may have been more effective had the liposomes been synthesised without cholesterol. The effects of iron on ferroptosis sensitivity have been examined previously within our group, and suggested that alone, iron has a limited ability to induce ferroptosis in MM cells.

Although not discussed in the literature, it is important to consider that inhibitory factors may interfere with the capacity to sensitise cells to ferroptosis. This was clearly demonstrated in the current study, in which we found that the combination of exogenous PUFA and RSL3 were not able to overcome the resistance conferred by the cholesterol content within the liposomes (Figure 43) . While the initial liposomes manufactured were not effective at sensitising cells to ferroptosis, it was an important step in the optimisation process. Subsequent refinement of the liposomes focused on incorporating sufficient PE (16:0_22:6) and stabilising lipids, other than cholesterol (Figures 44 and 45).

5.3.2 Liposomes that lack cholesterol have poor structural qualities but are effective ferroptosis-sensitising agents

To combat the impact of cholesterol on ferroptosis, new liposomes were formulated without cholesterol. The role of cholesterol in membrane stability and integrity makes the synthesis of liposomes without cholesterol difficult, especially when the liposomes are designed for drug delivery. DPSC is a zwitterionic PL commonly used in combination with cholesterol in the synthesis of liposomes to enhance their stability and increase encapsulation efficiency (260). As expected, these liposomes were not as small nor as uniform as liposomes containing cholesterol. This was illustrated by their diameter, which was more than double the size of liposomes containing cholesterol and by a PDI greater than 0.3, which is associated with poor uniformity and spread of the liposomes. The obvious reason for this was the lack of cholesterol, despite the higher proportion of DSPC.

Although the liposomes were not ideal in terms of their size or uniformity, they were tested against MM cells, as a proof of concept as to whether liposomes could be used as a delivery mechanism for PUFA containing PLs. The formulation of the liposomes was PE (16:0_22:6): cholesterol: DSPC: DSPE-PEG2000 at ratios of 49:0:49:2 (w/w/w/w%). These liposomes were unable to induce ferroptosis alone. However, in combination with RSL3 a significant increase in cell death was observed in both the RSL3 resistant KMS-11 cells and the sensitive OPM-2 cell line (Figure 44). This cell death was concomitant with a significant increase in the levels of lipid ROS in the cell lines, which is a hallmark of ferroptosis. Interestingly, minimal increase in lipid ROS levels were observed in cells treated with the liposomes alone, suggesting that the cells were able to survive the increase in intracellular PUFAs, but that this was dependent on GPX4 activity.

The PL, DSPC, which is comprised of SFA only may also significantly impact the ability of these liposomes to sensitise cells to ferroptosis. SFAs have been shown to both inhibit and promote ferroptosis, but they are not believed to be as important as PUFAs or MUFAs and their effects are largely context dependent (100, 108, 132, 199, 219, 220). The fatty acid in DSPC, stearic acid, has been shown to confer resistance to ferroptosis in cardiomyocytes (199) and therefore it is possible this lipid may be dampening the capacity of the liposomes to induce ferroptosis in MM cells.

Uptake of these liposomes into MM cells was also analysed, with very promising results (Figure 44). These data suggest that liposome uptake was efficient making them a good candidate for drug delivery. Liposome uptake typically occurs through endocytosis, which involves the cells engulfing the liposomes through invaginations of the plasma membrane, leading to internalisation and subsequent release of their contents into the cytoplasm (243). Uptake can also occur through fusion of the liposomes with the lipid membrane of the cell. Interestingly, even the fusion of the liposomes with the cell membrane can be sufficient to allow exchange of lipids (243). These mechanisms often do not occur in isolation and uptake may be via a combination of these methods (243). Although we did not investigate the exact mechanism of liposome uptake into MM cells, future work could include examining the effects of endocytosis inhibitors or knockdown of endocytic proteins. Elucidating the mechanisms of liposome uptake may identify ways to increase the efficiency of uptake or alternate means of targeting the MM cells. Despite the efficiency of uptake and the ability of these liposomes to sensitise MM cells to RSL3, their relatively large size and lack of uniformity meant that further optimisation of the liposomes was necessary. Liposomes comprised of PE (16:0_22:6) and DSPE-PEG2000 only were subsequently manufactured.

5.3.3 Optimised liposomes induce ferroptosis in MM cells with and without RSL3

Next, we proposed to formulate liposomes, without either DPSC or cholesterol. Instead, we attempted to manufacture liposomes through the self-assembly of PE (16:0_22:6) and DSPE-PEG2000. DSPE is a zwitterionic PL, while the PEG2000 should confer some stability on the liposomes. The interaction between PLs in liposomal formulations are complex and it is often necessary to optimise the composition to decrease liposome size and increase uniformity. There is evidence in the literature suggesting that high proportions of SFAs, such as DSPE and DSPC, can increase the rigidity of the membranes (261). The removal of DSPC would, in theory, decrease membrane rigidity allowing for the synthesis of smaller liposomes. Prior research has also demonstrated that DSPC can form gel-phase domains, (262) and this may in turn affect the uniformity of the liposomes. However, more research would need to be conducted on these liposomes to better understand the effects of changes in the composition of liposomes.

PE (16:0_22:6), unlike DPSC, contains a highly unsaturated fatty acid (DHA, Docosahexaenoic acid, 22:6) that should increase membrane fluidity and decrease rigidity (261). This may help to form smaller and more unform liposomes. This was observed in the liposomes formed using PE (16:0_22:6): cholesterol: DSPC: DSPE-PEG2000 at ratios of 98:0:0:2 (w/w/w/w%), which were smaller than the liposomes containing cholesterol and DSPC, measuring 135.6 nm in diameter. These liposomes also had a mean PDI of 0.06, which is well below the acceptable value for uniformity. Not only were these liposomes smaller and more uniform than any of the previous liposomes tested, but they also contained a higher proportion of PE (16:0_22:6) than any of the liposomes manufactured previously.

Uptake of these liposomes was found to be higher than any of the previously synthesised liposomes, which may be due to their smaller size (Figure 45). Several studies have shown that smaller liposomes are more effectively taken up by cells than larger liposomes (263, 264). Uptake may also be affected by temperature, as demonstrated by one of these studies in a human colorectal adenocarcinoma cell line that showed that at 37°C, liposome uptake was largely mediated by endocytosis, while at 4°C uptake was primarily passive (263). The latest formulation of liposomes were also found to be highly effective at sensitising MM cells to ferroptosis (Figure 45). Strong synergistic cell death was observed when the liposomes were combined with unencapsulated RSL3 and significantly higher levels of lipid ROS were generated in the MM cell lines (Figure 45). Furthermore, the liposomes induced morphological changes in the MM cell lines that were

consistent with ferroptosis (Figure 46) and the effects were inhibited by the synthetic antioxidant, liproxstatin-1.

Previous studies have demonstrated that DHA is a potent promoter of ferroptosis when added exogenously as a free fatty acid (130, 204, 205). Our research builds on these findings, showing that delivery of DHA in a liposomal formulation is also highly effective. As previously mentioned, studies have shown that unsaturated lipids can be delivered in the form of liposomes, however these studies did not disclose the lipids used, making it difficult to compare the findings with our research (173).

In future, it would be valuable to develop a method that would allow for the comparison of the efficacy of exogenous free PUFA or PUFA containing PLs. Comparing the two may be difficult and would require complex and precise chemistry to determine the concentration of DHA within PLs. However, this may not be feasible, in the same way that comparing the effects of liposomes and free lipids is difficult due to differences in the physical state and organisation of the liposomes, as well as other lipid interactions.

5.3.4 RSL3 quantification methods and drug encapsulation

The overarching and final aim of this chapter was to develop liposomes that contain RSL3 and are targeted towards MM cells. The first steps were to develop liposomes manufactured from PL-PUFA ferroptosis substrates that can also act as a delivery system for RSL3. The results in this chapter demonstrate that liposomes with this ability were successfully developed and therefore we proceeded to investigate mechanisms for loading RSL3 into the nanoparticles. Loading drugs into liposomes is often a complicated process that may involve different methods to incorporate the drug into the appropriate region of the liposome.

Many factors can influence drug loading, including the aqueous solubility of the drug, chemical properties of the drug and lipid composition of the liposomes (251). RSL3 is a lipophilic drug meaning that incorporation of this drug would involve the lipid bilayer, further highlighting the importance of lipid composition. Studies suggest that loading hydrophobic drugs into liposomes can cause perturbations that lead to a decrease in the membrane stability and drug loading capacity of the nanoparticles (265). Furthermore, although loading hydrophobic drugs can result in incorporation efficiencies of up to 100%, even small changes in the environment surrounding the liposomes can alter the distribution of the drug (265). This may result in a decrease in the retention of the drug

following *in vivo* administration but before the liposomes reach their target, increasing the likelihood of off target effects (265).

Fortunately, the microfluidics used to synthesise liposomes in the current study made it relatively straightforward to load RSL3 into our liposomes. RSL3 was simply added to the organic lipid mixture and the liposomes were then synthesised using the methods described earlier. An HPLC-based method for measuring the quantity of RSL3 was developed, based on purity data provided by the manufacturer. By using solutions containing known concentrations of RSL3, in the presence or absence of liposomes, we were able to demonstrate that this method was extremely accurate. The main challenge in the next step was separating the liposomes from unencapsulated RSL3 to enable an assessment of the encapsulation efficiency. RSL3 and liposomes could not be separated using ultracentrifugation or liquid phase separation. Previous studies in which this has been attempted used HPLC coupled with a diode-array detector for separation (252), but unfortunately this was not a method that was available to us. Vakili-Ghartavol *et al*. used a complex dialysis technique using a 12-14 kDa molecular weight cut off against dextrose 5%, replacing the buffer four times for 8 hours each. Given the success of this method, we attempted a similar approach to purify the liposomes using a dialysis cassette with a 10 kDa filter.

The dialysis filtrate was checked for liposomes by DLS, and initial results suggested the liposomes had not passed through the membrane, as would be expected given the results from the pressure ultrafiltration. Recovering the liposomes was theoretically simple and just involved removing the solution from the cassette. However, the liposome recovery rate was poor with only 27% of the liposomes retained post dialysis (Appendix Figures 12 and 13). Regardless of their retention rate, the liposomes could in theory be retained, concentrated and used. Liposomes are typically formulated with relatively cheap lipids including cholesterol and DSPC. PE (16:0_22:6), which made up 98% of the total mass of our liposomes is expensive in comparison, at approximately 112 times more expensive than DSPC. While dialysis was found to be inefficient, other separation techniques such as column chromatographic separation would require large volumes of these relatively expensive liposomes. It became apparent that purifying the liposomes was going to be difficult both financially and experimentally, and it was decided that this should not be a priority within the project timeframe

Pressure ultrafiltration, which is well described in the literature (266), was subsequently determined to be the best method available to us to separate unencapsulated RSL3 from the liposomes, but

could not be used to retain the liposomes. This method allowed us to determine that the encapsulation efficiency of RSL3 was 67.5 ± 14.0 %. Previous studies have shown that encapsulation efficiencies of hydrophobic drugs vary, with an efficiency of 59.2% in one study (252), while another described 34-67% incorporation as highly efficient (267). Therefore, the data presented in the current study are well within the upper range for liposome encapsulation efficiencies documented in the relevant literature.

A study in which erastin was encapsulated within liposomes, demonstrated significant efficacy of the nanoparticles against non-small cell lung cancer *in vivo* (172). However, this study was performed without purifying the liposomes, likely due to the technical difficulties discussed above. In fact, many of the relevant published studies describing the basic properties of liposomes or proof of principle experiments involve liposomes that have not undergone any purification. Establishing an efficient purification procedure would be key in progressing the development of liposomes as a potential therapy, to avoid any potential off-target effects of unencapsulated drug.

5.3.5 Liposomes containing RSL3 induce mass ferroptosis in MM cell lines

The next step was to investigate the efficacy of the RSL3-encapsulating liposomes against MM cells. Liposomes loaded with 50 µg/mL RSL3 within their lipid membrane were synthesised. Cells were treated with quantities of liposomes based on the total concentration of RSL3 used during the assembly of the liposomes, as the purification steps described above had not been conducted at this point in time. All three MM cell lines tested displayed cell death at relatively low liposome concentrations. The three MM cell lines tested (KMS-11, KMS-18 and LP-1) all had RSL3 IC_{50} values that exceeded 2.5 µM. However, when RSL3 was encapsulated within the liposomes a significant decrease in the IC_{50} values were observed, to below 500 nM. The KMS-11 cell line, which was the least sensitive of all the MM cell lines, required unencapsulated concentrations of 2.5 µM RSL3 and >25 µg/mL liposomes to achieve close to total cell death. In comparison, similar effects were observed with 15 µg/mL liposomes containing half the amount of RSL3. Overall, the RSL3-containing liposomes had between 7.1-fold and 14.5-fold greater potency than RSL3 alone (Figure 48).

These results were not expected and rather surprising, given previous data generated within the group, showing that no other compound tested was capable of sensitising MM cells to such low concentrations of RSL3. The efficacy of the liposomes may be due to greater efficiency of their uptake compared to uptake of unencapsulated RSL3, resulting in higher intracellular concentrations

of the drug. RSL3 has poor solubility in aqueous solutions, including in cell culture media, meaning that its physical properties may impact its uptake into cells in culture.

Drugs encapsulated in liposomes are classified as new products, as the encapsulation often changes the pharmacokinetic properties and distribution of the drug (268). The study mentioned earlier clearly demonstrated greater efficacy of erastin-containing liposomes compared to free erastin in a mouse model of lung cancer and (172). Another study of liposomes encapsulating the topoisomerase inhibitor, irinotecan, in solid tumours demonstrates how liposomal drugs represent a significant advance as therapeutic options for patients (269). Compared to free irinotecan, the liposomal drug was shown to increase exposure of the cancer cells to the drug, prolong retention of the drug, and promote preferential uptake into the tumour cells (269). Our results are consistent with these published studies, demonstrating that liposomal drug delivery improves the anti-cancer efficacy.

5.3.6 Functionalisation of liposomal surface with daratumumab

Functionalisation of the liposomes was the final aim of this chapter, to develop liposomes capable of specifically targeting MM and not healthy cells. Liposome functionalisation with antibodies is not a simple process and often requires very complex chemistry to change the chemical structure of antibodies so that their orientation maintains their ability to bind the target protein. Maleimide reactions are commonly used in antibody conjugation and was therefore proposed as the first method to attempt conjugation of our liposomes (270). This reaction involves the introduction of thiol groups into the antibody, known as thiolation, which enable effective binding (270). However, this method comes with the risk of disrupting the structure of the antibody making it less effective or unable to bind its target.

Another method was proposed after searching the relevant literature, which involved using a lipid with an N-hydroxysuccinimide (NHS) ester group to bind the antibody to the liposomes. NHS esters are commonly used to label proteins such as antibodies and are commonly used in immunofluorescence and flow cytometry (271). This method has also been successfully used to conjugate antibodies to liposomes in the literature (272). The benefit of this method is that it does not involve modifying the antibody to facilitate its binding to the lipid. The processes involved in the conjugation are also relatively simple and only require a suitable buffer (PBS) and time. However, a limitation of this method was that the orientation of the antibody could not be controlled or assessed. Liposomes were synthesised with the DSPE-PEG2000 Carboxy NHS, after which the

antibody was added followed by incubation in a shaker for 3 hours. Liposome size was then confirmed by flow cytometry, showing that antibody conjugated liposomes were larger than unconjugated liposomes. The study mentioned earlier in which DSPE-PEG2000 NHS was used to functionalise liposomes found that antibody conjugation almost doubled liposome size from 134 nm to 240 nm (273). The study used a monoclonal antibody that was produced in their own lab, meaning it would be difficult to compare how different antibodies influence liposome size. Different conjugation methods could also influence how antibodies bind to the liposomes, which may in turn impact the size of the liposomes. Daratumumab is an IgG subclass of antibody, which are known to be between 10-15 nm in diameter. This would explain why an increase in the size of the liposomes was observed following antibody conjugation. After confirming the size of the liposomes, the next step was to develop a method to confirm the presence of antibody molecules on the liposomes.

To confirm surface binding of daratumumab, the liposomes were analysed using nano flow cytometry (CytoFLEX Nano; Beckman Coulter) and a fluorochrome-conjugated anti-human secondary antibody. The liposomes were incubated with the secondary antibody and the fluorescence of the PE fluorochrome compared between blank and daratumumab-conjugated liposomes to calculate the proportion of liposomes that had bound daratumumab (Figure 51). Impressively, approximately 65% of the conjugated liposomes had higher levels of fluorescence than the blank liposomes following incubation with the secondary antibody (Figure 51). Other studies have used similar methods, employing a secondary antibody to confirm antibody conjugation, albeit with fluorescence microscopy rather flow cytometry as a readout (273). This is likely due to the fact that the CytoFLEX Nano is a relatively new instrument and is unique in its ability to measure particles within a low nanometre range. The advantage of using flow cytometry rather than microscopy is that it enabled us to calculate a percentage of daratumumab positive liposomes.

Next, specificity of the liposomes for MM cells was investigated using the FH9 healthy B-cell line for comparison. Cells were cultured with unconjugated liposomes or liposomes conjugated to daratumumab with or without the RhB-tagged lipid used throughout this chapter.

5.3.7 Daratumumab functionalised liposomes as a targeted approach to killing MM cells

Liposome uptake was first measured in the MM and FH9 cell lines and clearly demonstrated that uptake was significantly more efficient in the MM cells compared to the FH9 cells (Figure 52A). This observation is supported by data in the literature, that suggest cancer cells have a greater affinity for liposomes than healthy cells. A study in a mouse model of melanoma found that the cancer cells had a significantly higher affinity for liposomes than mouse hepatocytes, irrespective of the phospholipid and cholesterol compositions of the liposomes (274). Although this is a relatively old study, it clearly demonstrates that cancer cells have a greater affinity for liposomal uptake than healthy cells *in vitro*. The mechanism behind this observation *in vitro* could be related to a multitude of different factors, including membrane permeability (275), lipid composition (liposomes and cellular lipid membrane) (260, 276) and charge (260). Further research would be necessary to elucidate why MM cells have a higher affinity for liposome uptake than FH9 cells. There is also evidence in the literature demonstrating that healthy cells are also spared from the effects of liposomes *in vivo*, possibly because liposomes passively target tumour cells due to their enhanced permeability and by retention inside these cells (277-279). Additionally, liposomes within a specific size range have been shown to localise in tumour tissues and are unable to exit the capillaries to affect healthy tissues. While not within the scope of this study, this does suggest one way in which liposomes may have benefits as a cancer drug delivery system (277, 280, 281).

Despite their potential, the preclinical development of targeted liposomes, especially antibody conjugated liposomes, has been challenging with few reaching clinical trials and no FDA approved therapies to date (282). There is evidence to suggest that coupling an entire antibody to a liposome can result in immunogenicity and a reduction in the mean residence time, which refers to the average time the liposomes remain in circulation before being cleared, of liposomes (283). However, recent advances in monoclonal antibody engineering have driven the concept that liposomes may be targeted to specific cell types using monoclonal antibody fragments, in which the antigen binding region of the antibody is preserved (284, 285). Alternate means of targeting liposomes to cancer cells should be a focus of research, especially for diseases that are currently considered incurable, such as multiple myeloma.

Antibody conjugated liposomes, often referred to as immunoliposomes, have a key advantage over other therapies, such as antibody drug conjugates (ADC) due to an increased capacity for drug loading (282). A study published in 2021 found that coating liposomes with an antibody against

CD147 significantly increased their uptake into melanoma cells, but not fibroblasts (286), demonstrating the potential of antibody conjugated liposomes as a targeted therapy for cancer (286). In another study published in 2023, researchers designed 'stealth' liposomes coated with PEG molecules and functionalised to target the human epidermal growth factor receptor 2 (HER2) which is overexpressed in breast cancer (283). The doxorubicin loaded functionalised liposomes were more effective at reducing tumour volume than naked liposomes, *in vitro* and *in vivo*, while also effectively reducing side effects in mice (283). Conjugation of our liposomes to daratumumab had no effect on their uptake into MM cell lines but significantly decreased uptake into a healthy B-cell line that expressed minimal levels of CD38 (FH9 cells) (Figure 52A). The reduction in uptake correlated with a decrease in the concentration of RSL3 payload to the FH9 cells and a significantly higher IC_{50} for the liposomes compared to MM cells. In the context of a novel treatment for MM patients, these data suggest the liposomes may be highly effective at inducing ferroptosis in the tumour cells, while at least partially sparing healthy cells (Figures 52-53).

These results represent proof-of-concept that daratumumab functionalisation of liposomes can improve uptake into MM compared to healthy cells. However, it is important to recognise the limitations of these liposomes, with emerging research suggesting that antibody fragments may be more effective than whole antibody molecules as they may improve bioavailability of the liposomes. This is an important future direction for research if these liposomes are to be progressed into animal models. In addition to optimising the processes involved in liposome purification, this is key to further the development of our immunoliposomes. Another novelty of our liposomes is that the coupling of an antibody is not limited to daratumumab, and in theory similar liposomes could be designed to target a range of cancers cells that express specific proteins on their surface. It is also important to note that it is likely that the healthy B-cell line, FH9, which was established at Flinders University, may not be an ideal model for healthy cells as they were immortalised. Experiments involving primary MM cells, alternate healthy controls and future directions for our research will be discussed in the next chapter.

5.4 Conclusions

This chapter builds upon the results presented in the previous two chapters, by integrating established and new methodologies to develop novel liposomes. The chapter described the optimisation of liposomes containing PUFAs and how different lipids, particularly cholesterol and DSPC can influence the size and uniformity of the product. Data generated suggest that liposomes

containing only PE (16:0_22:6) and DSPE-PEG2000 were smaller and more uniform than those that contained cholesterol or DSPC. The data also indicate the significant impact of cholesterol on the capacity of the liposomes to sensitise MM cells to ferroptosis and the ability of cholesterol to overcome the effects of RSL3 and PE (16:0_22:6). Our liposomes induced synergistic cell death when combined with unencapsulated RSL3. The ability of liproxstatin-1 to prevent the cell death, accumulation of lipid ROS and changes in morphology provides strong evidence that these effects were due to ferroptosis. Liposomes were then loaded with RSL3, and the results were compelling; these liposomes were more effective at inducing ferroptosis than any of the previous strategies tested against MM cells. The liposomes have IC_{50} values within a nanomolar range against the MM cell lines, which represented a significant increase in potency against all the three cell lines examined. These liposomes also induced morphological changes consistent with ferroptosis in the MM cell lines. The liposomes were then conjugated to daratumumab using an NHS ester group, to create liposomes capable of targeting MM cells. The efficiency of antibody conjugation was approximately 65% and resulted in effective targeting to MM cells but a reduction in uptake and cytotoxicity towards the healthy B-cell line, FH9. The overall result of the work presented in this thesis is the development of novel targeted, RSL3-loaded liposomes that are highly effective at inducing ferroptosis of MM cells.

CHAPTER 6 GENERAL DISCUSSION AND FUTURE DIRECTIONS

6.1 The unmet need for novel treatment strategies for patients with MM

Multiple myeloma (MM) remains an incurable malignancy, with current therapies offering more time but not a cure. MM represents a significant global burden, with estimates of 180,000 individuals living with the disease and 120,000 deaths in 2022 (287). Incidence rates are the highest in North America, Australia and New Zealand, with the highest mortality rates observed in Australian and New Zealand patient populations at ≥4 deaths per 100,000 population (287). New models based purely on population growth have predicted that these numbers will continue to rise, and by 2045 there will be estimated 320,000 MM patients worldwide, with 217,000 deaths due to the disease (287). While newer therapies, including the immunomodulatory drugs (IMiDs), proteasome inhibitors (PIs) and monoclonal antibodies (mAbs), have significantly improved response rates, MM patients will invariably relapse (39). This highlights the crucial need for novel, more effective therapies, that can overcome resistance to current therapies and offer a cure for this devastating disease.

6.2 Ferroptosis as an emerging programmed cell death mechanism

Ferroptosis is a relatively recently described form of programmed cell death, characterised by iron dependence and the accumulation of toxic lipid reactive oxygen species (ROS). Apoptosis is arguably the most well recognised and researched form of programmed cell death and is the key mechanism of action of many of the anti-cancer agents developed to date (87). Relapse and treatment refractory disease is common among MM patients and is predominantly driven by resistance to apoptosis-mediated cell death (288). From studies of treatment resistance in MM, it can be inferred that alternate mechanisms of cell death may be an effective treatment approach for patients who do not respond to conventional therapies. Emerging evidence suggests that MM cells can be forced to undergo ferroptosis via several different mechanisms (289). A previous study and our research demonstrate that MM cells are largely insensitive to ferroptosis, compared to cells from another aggressive B cell malignancy, diffuse large B-cell lymphoma (DLBCL) (136).More recently, a study has shown that the ability of erastin to induce ferroptosis is dependant on expression of SLC7A11, which was not observed in our work (200, 290). To combat this, we used the class II ferroptosis inducer RSL3, and demonstrated that MM cell lines are less sensitive to ferroptosis induced by this

compound than DLBCL cells, which was not driven by GPX4 expression (Figure 11A). This presents a challenege in developing ferroptosis based therapeutics in MM treatment, as ferroptosis inducers alone my not be sufficient to induce cell death.. This drove us to investigate other factors that could determine ferroptosis sensitivity, with a specific focus on identifying key substrates of ferroptosis.

6.3 Phospholipids dictate ferroptosis sensitivity in MM

The overarching aim of the third chapter of this thesis was to investigate the importance of phospholipids containing polyunsaturated fatty acids (PL-PUFA) as ferroptosis substrates and how they might be used to sensitise MM cells to ferroptosis. Studies in the literature suggest that PL-PUFA are important ferroptosis substrates and that the degree of unsaturation within these lipids correlates with their susceptibility to oxidation (190, 191). We first investigated levels of saturated, monounsaturated and polyunsaturated fatty acids in panels of MM and DLBCL cell lines (Figure 14A). While developing a method to class lipids, we identified an issue with how to classify lipids, as phospholipids contain two fatty acids, meaning it was possible for a phospholipid to contain both inhibitory MUFA and the ferroptosis substrate PUFA, which we addressed by creating a separate group. While this group of lipids represented a smaller proportion of the lipidome than either MUFA or PUFA-containing lipids, their potential impact on the sensitivity of the cells to ferroptosis may still be significant. However, as lipids containing both MUFAs and PUFAs are not commercially available, we were unable to investigate their role in any detail. Nevertheless, this is as an important gap in knowledge that should be addressed in the future.

Importantly, when we compared the composition of PUFAs and MUFAs between MM and DLBCL we observed significant differences between the two cancers (Figure 14A). The MM cell lines had a significantly ($P<0.0001$) higher proportion of PL-MUFA, which correlates with their relative insensitivity to ferroptosis, while the DLBCL had a significantly ($P<0.01$) higher proportion of PL-PUFAs, which correlates with their sensitivity to ferroptosis (Figure 14A). This trend was also apparent when we compared the OPM-2 and KMS-11 MM lines, which is important given that despite both being derived from patients with MM, are sensitive and insensitive to RSL3-induced ferroptosis, respectively (Figure 14B). These results indicate that while other factors likely dictate ferroptosis sensitivity, the phospholipidome of cells may be a critical determinant of their ferroptosis sensitivity. While our analysis grouped fatty acid according to their structure, a more in-depth analysis might involve scoring of the lipids based on their susceptibility to oxidation and therefore their potential as ferroptosis substrates. An open-source software, called LPP tiger

(https://www.lipidmaps.org/resources/tools/15?task=4.5), which has been developed by the Fedorova lab, represents one way that LC-MS data sets may be used to predict and identify phospholipid oxidation, and determine the susceptibility of specific lipids to oxidation (291). This approach may represent a more sensitive and informative analysis of the type of data generated in the current study. Importantly this data could be useful in disease stratification in MM, given that lipid dysregulation is observed in MM patients (Publication 3 in Appendix). Developing a method to understand and classify MM patients based on lipid profiles could uncover patient subgroups with profiles that align with ferroptosis sensitivity, providing much need non-apoptotic based treatment options.

We observed that PL-PUFAs (>2 double bonds) were able to induce ferroptosis and sensitise MM cells to ferroptosis induced by RSL3 (Figures 18, 20, 24 and 25). The capacity of these PL-PUFAs to sensitise the MM cells to RSL3 was found to be closely correlated with the degree of unsaturation in the FA, consistent with the literature (Figure 24-25) (131, 191). This would suggest that phospholipids containing two highly unsaturated fatty acids (e.g., PE 22:6_22:6) might be even more effective than the lipids tested in the current study, however, could not be tested due to commercial availability. The efficacy of adding exogenous lipids to MM cells also raises the question of diet and metabolism in cancer patients. Would a diet high in PUFA promote ferroptosis in cancer cells or would they feed into other pathways that could drive MM. While outside the scope of this research, dietetic studies in MM could aid in addressing the role of lipid consumption in MM treatment.

6.4 Liposomes rich in PL-PUFA can be used to deliver RSL3 to liposomes in a targeted manner

The aim of the final results chapter was to bring together all the knowledge and skills gathered during the project to develop a novel, targeted, drug delivery system. Liposomes are an established drug delivery mechanism and have been used in cancer medicine to delivery doxorubicin in the form of a pegylated liposome formulation (292). However, few studies have developed liposomes with a formulation that themselves represents a potential therapeutic agent. The therapeutic potential of the liposomes developed in this project lies in the significant role of PL-PUFAs as ferroptosis substrates, and the simultaneous inhibition of GPX4 by loading the nanoparticles with RSL3. Our novel liposomes were able to induce ferroptosis-mediated cell death, which was significantly augmented when RSL3 was encapsulated within the liposomes, displaying a 7.1-fold to 14.5-fold decrease in the IC_{50} values for RSL3 against the MM cell lines (Figure 48A). This was supported by

an *in vivo* glioma study that demonstrated that free RSL3 was rapidly cleared within the mice, while the nanoparticles had a significant effect on tumour growth (293).

Finally, to address the question of whether we could target the liposomes to MM cells using an antibody and their effects against healthy cells, we developed liposomes functionalised with daratumumab, an anti-CD38 monoclonal antibody currently used in the treatment of MM. Antibody conjugation proved to be relatively simple using a well-established antibody conjugation technique that has been previously used to functionalise liposomes (242). These functionalised liposomes were readily taken up by MM cells, with significantly ($P<0.0001$) lower levels of uptake observed in the FH9 healthy B-cell line, compared to unfunctionalised liposomes. Interestingly, conjugation of the liposomes to daratumumab reduced uptake and cytotoxicity towards FH9 cells but had no effect on the ability of the liposomes to induce ferroptosis in the KMS-11 cells (Figure 52). A study published in 2021 found that daratumumab functionalised immunopolymersomes, vesicles formed of polymers and functionalised with immune targeting elements, represented an effective and safe means of delivering vincristine sulfate to the tumour cells in a MM mouse model (294). Further investigation of our liposomes could include co-culture of MM and healthy cells (FH9 and MM cell lines or primary cells) in 2D or 3D models to determine whether there is preferential uptake when multiple cell types are present.

6.5 Future directions in ferroptosis inducing targeted liposomes

The novel liposomes developed in this study have the capacity to induce ferroptosis in a targeted manner, enhancing the potency of RSL3 in MM cells while appearing to spare healthy cells at certain doses. Future research should focus on investigating the effects of the liposomes against MM patient samples to validate the effects observed in the cell lines. It is also important to determine whether the efficacy of the liposomes is irrespective of molecular subtypes of MM that have defined low, intermediate and high-risk profiles correlating with progression-free and overall survival. These future directions aiming to test our novel functionalised nanoparticles in human MM patient samples would address many of the questions raised throughout the thesis. Importantly this would make it possible to address the specificity and toxicity of the liposomes when delivered to whole blood that contains MM cells and other blood cells. Theoretically it would be possible to assess the levels of liposome uptake in other blood cell types, assess viability and the efficacy after culturing with liposomes. Although patients sample experiments provide a great insight into specificity and

efficacy, they do not perfectly recapitulate the environment within the body, making *in vivo* experiments necessary to move forward.

The development of liposomes conjugated to a CD38 nanobody (295) may also prove worthwhile to prepare the liposomes for *in vivo* studies. This is important as functionalisation with intact antibodies has previously been shown to increase the immunogenicity and clearance rates of liposomes (283). Our proof of principle liposomes could potentially be further developed to utilise small peptides as the functionalisation agent, which may aid in reducing clearance, addressing a large limitation in the field.

An important aspect of future *in vivo* studies would be an assessment of the pharmacokinetics of these liposomes, particularly their drug release profile, which is a measure of the release of a substance from the nanoparticles over time (296). This would provide an indication of how the liposomes were behaving *in vivo* and potentially identify ways in which they might be modified to improve their drug release profile. Importantly, liposome stability, circulation time, safety and tolerability would need to be assessed, primarily to ensure that the liposomes are not immediately cleared or degraded after administration and whether they are causing any significant toxicity. The drug release profile of the liposomes would also aid in determining optimal administration times for *in vivo* studies.

The *in vivo* studies may also include an assessment of minimal residual disease (MRD) status as an endpoint in a MM mouse model. MRD negativity is a clinically validated endpoint which can indicate the depth of response and progression free survival, its inclusion would allow a better evaluation of whether our liposomes can achieve deep response (297). To increase their efficacy and to possibly achieve a greater rate of MRD negativity, liposomes that induce both ferroptosis and apoptosis could be developed. One example might be liposomes loaded with both RSL3 and a common MM therapeutic, such as doxorubicin or vincristine, either with both drugs in the same or separate liposomes. The ability to load both drugs into the same liposome will largely depend on whether the drugs interact with one another, loading capacity and the pharmacokinetics of the nanoparticles. This is not an entirely new concept as liposomes loaded with multiple drugs or compounds have been developed and have proven to be safe *in vivo* (298). Understanding the depth of response these liposomes can achieve will help establish how they can be used in current MM therapy, and whether they can be used to target apoptosis resistant relapsed or refractory disease or as a frontline therapy in combination with apoptosis-based therapies to achieve a deeper response.

Although studies of ferroptosis related to MRD status are limited, it is conceivable that liposomes containing both ferroptosis and apoptosis-inducing drugs or liposomes similar to the ones developed in the current study may represent a promising and much needed therapeutic option for MM patients.

6.6 Conclusions

This project has focused on investigating the role of phospholipids containing polyunsaturated fatty acids in ferroptosis, and how these lipids can be used to predict and modulate the ferroptosis sensitivity of MM cells. Lipidomic studies found that MM cell lines contain a higher proportion of inhibitory PL-MUFAs, while DLBCL cell lines contain more PL-PUFA, which correlates strongly with the sensitivity of these cells to ferroptosis. By increasing the proportion of PL-PUFAs, it was possible to significantly increase the sensitivity of MM cells to the GPX4 inhibitor RSL3. Interestingly, the opposite effect was observed using PL-MUFAs, which rescued cells from RSL3-induced ferroptosis. Liposomes developed from the PL-PUFAs identified and loaded with RSL3 were found to be highly effective at inducing ferroptosis in MM cells. Conjugating the anti-CD38 monoclonal antibody, daratumumab, to the liposomes was subsequently found to reduce both the uptake and cell killing capacity in the FH9, healthy B cell line, but not the KMS-11 MM cell line.

This research highlights the crucial role that PL-PUFAs play as ferroptosis substrates in MM cells and how this knowledge can be harnessed to develop liposomes that act both as a means of delivering a ferroptosis substrate and a drug to specific cells. Although MM is still considered incurable, the data presented herein highlight how targeted, ferroptosis-inducing nanotherapeutics may represent a novel therapeutic approach for the treatment of this devastating form of blood cancer.

APPENDIX

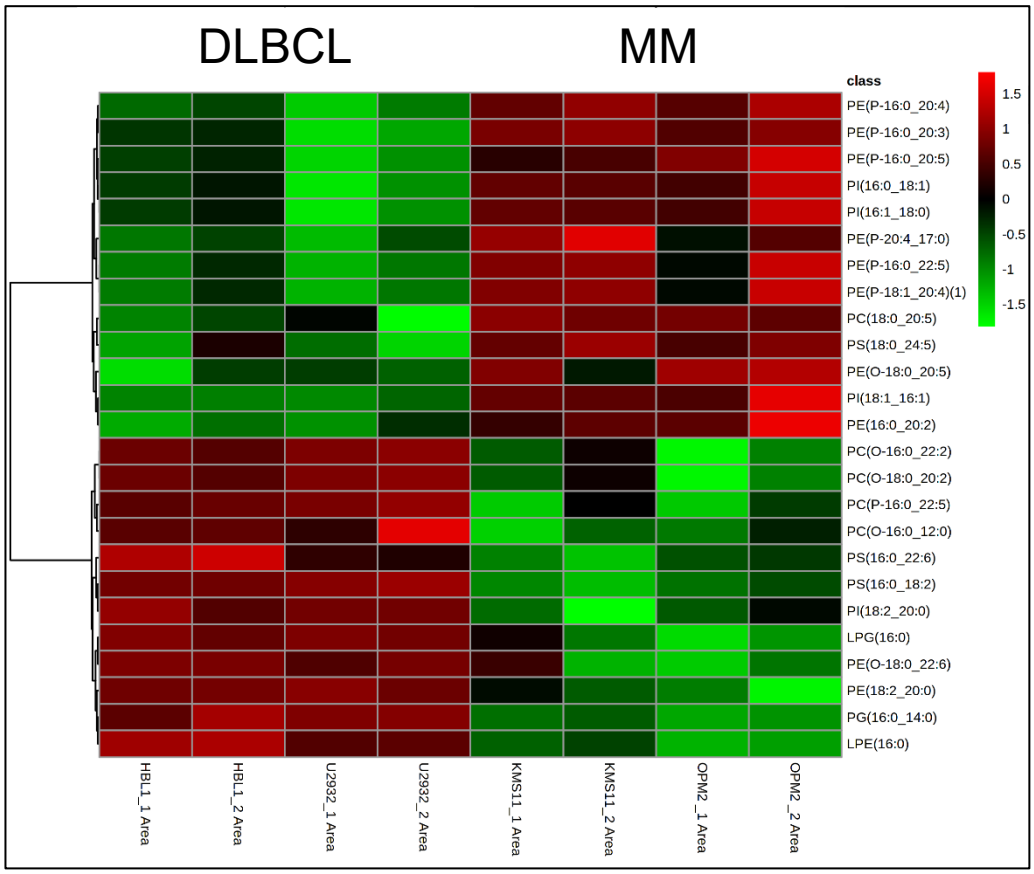

Appendix Figure 1. Heatmaps showing the results of a preliminary lipidomic screen of MM and DLBCL cell lines.

Heatmap of the 25 most differentially expressed lipids between the MM and DLBCL lines. Data presented from 2 biological replicates per cell line. LPE, Lysophosphatidylethanolamine; LPG, Lysophosphatidylglycerol; PC, phosphatidylcholines PE, phosphatidylethanolamine; PG, phosphatidylglycerol; PI, phosphatidylinositol.

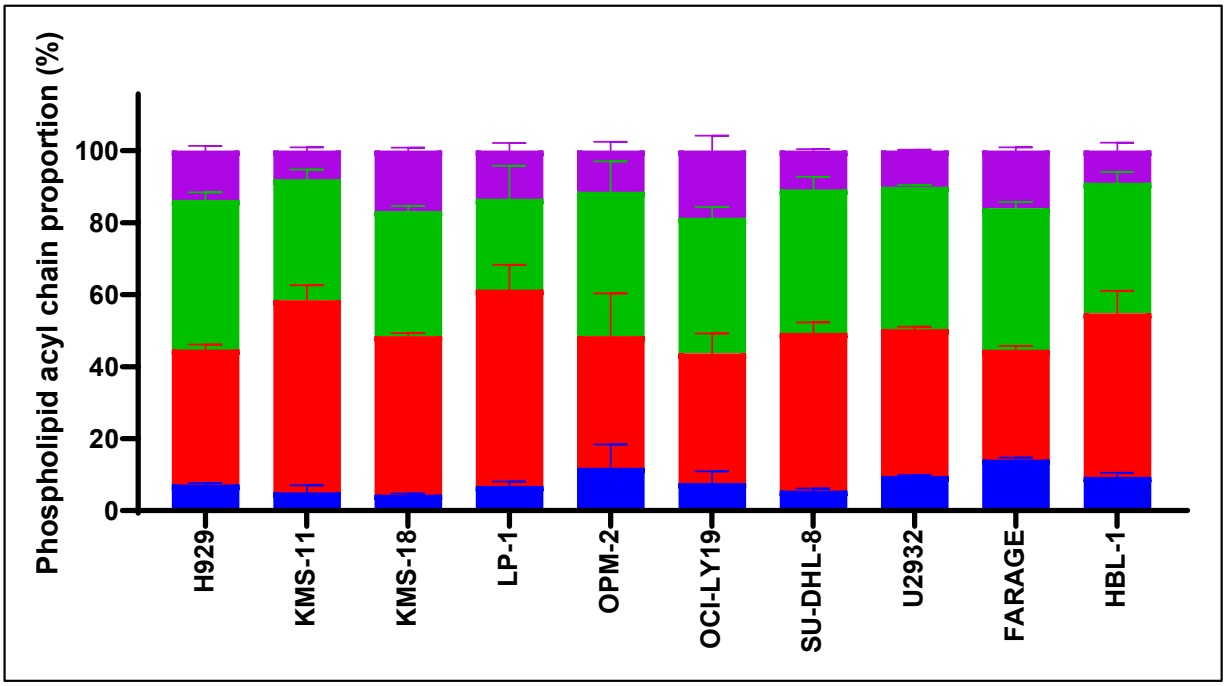

Appendix Figure 2. Variability of the phospholipidome of MM and DLBCL cell lines.

Relative proportions of each phospholipid acyl chain identified in the MM and DLBCL cell lines analysed. Data are the mean ± standard deviation of a minimum of 4 biological replicates.

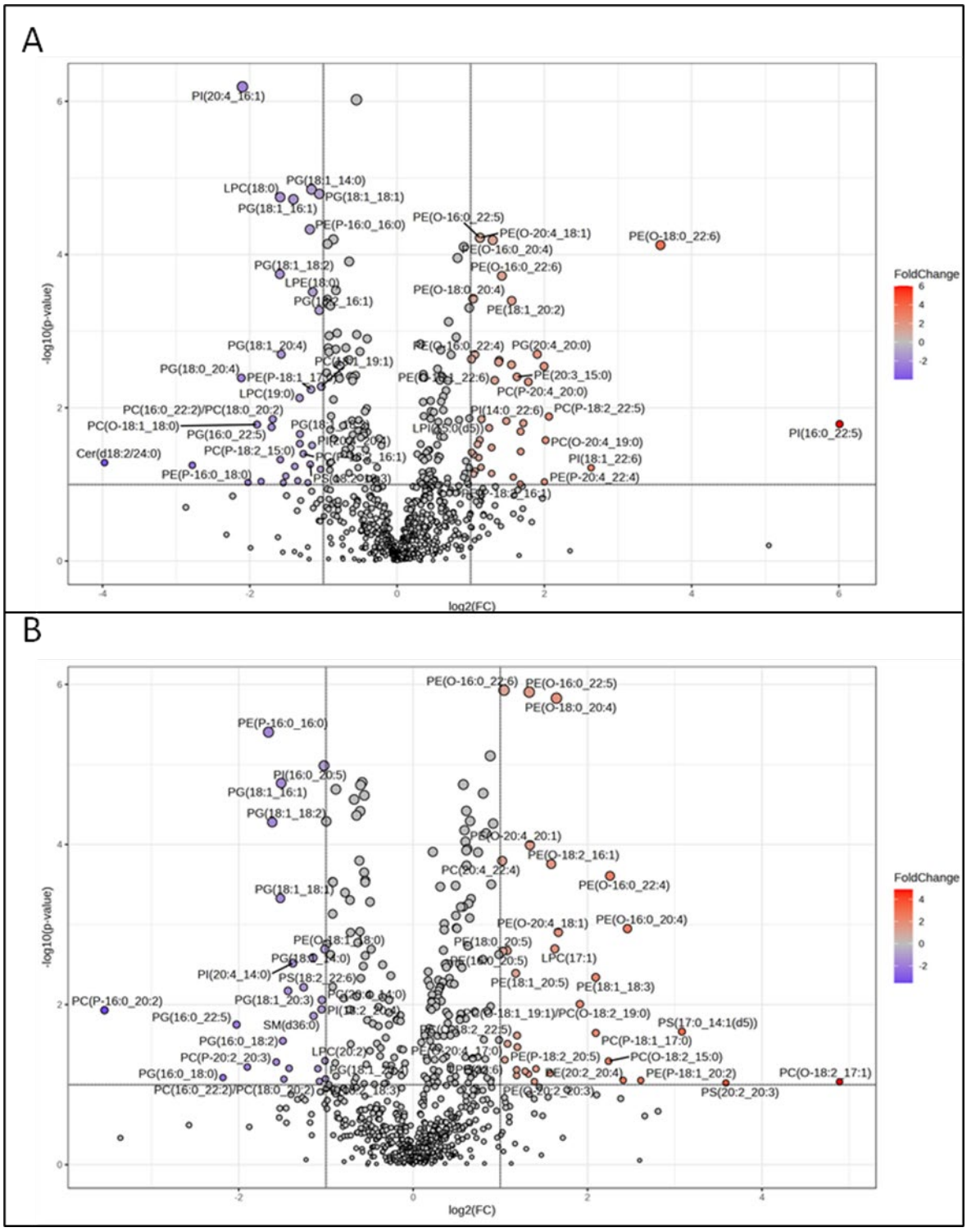

Appendix Figure 3. Changes in the lipidome of the OPM-2 and KMS-11 MM cell lines, induced by exogenous supplementation with MUFA.

(A) Volcano plot (direction of comparison OPM-2 + PE (16:0_18:1)/OPM-2) combining results from Fold Change (Threshold 2.0) Analysis and T-tests (P-value threshold 0.05) generated using MetaboAnalyst. **(B)** Volcano plot (direction of comparison KMS-11 + PE (16:0_18:1)/KMS-11) combining results from Fold Change (Threshold 2.0) Analysis and T-tests (P-value threshold 0.05) generated using MetaboAnalyst.

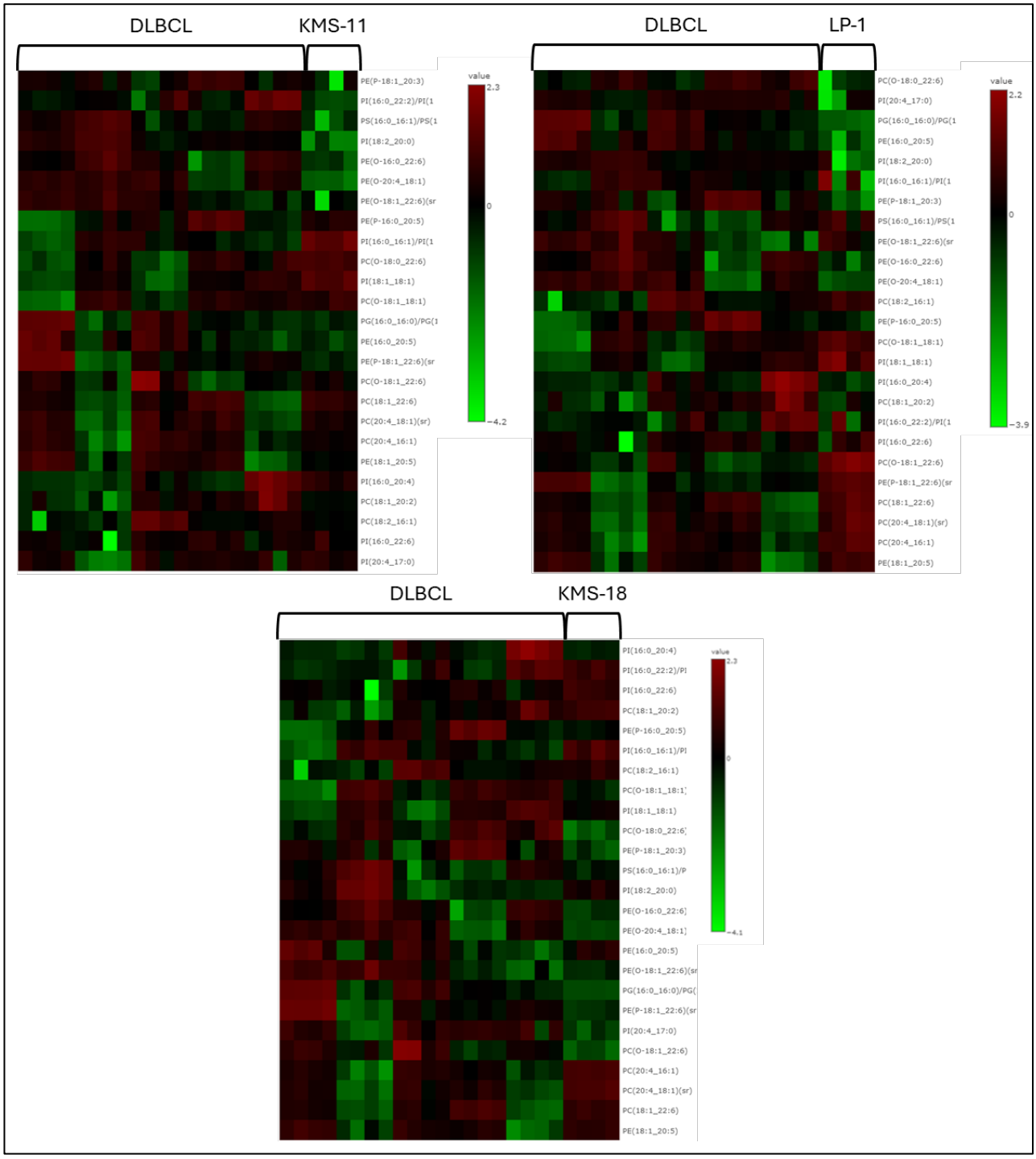

Appendix Figure 4. Lipidomic screen of MM and DLBCL cell lines.

Heatmap of the 25 most differentially expressed lipids between the KMS-11, LP-1 and KMS-18 and DLBCL lines. Data presented are from 4 biological replicates per cell line. LPE, Lysophosphatidylethanolamine; LPG, Lysophosphatidylglycerol; PC, phosphatidylcholines PE, phosphatidylethanolamine; PG, phosphatidylglycerol; PI, phosphatidylinositol.

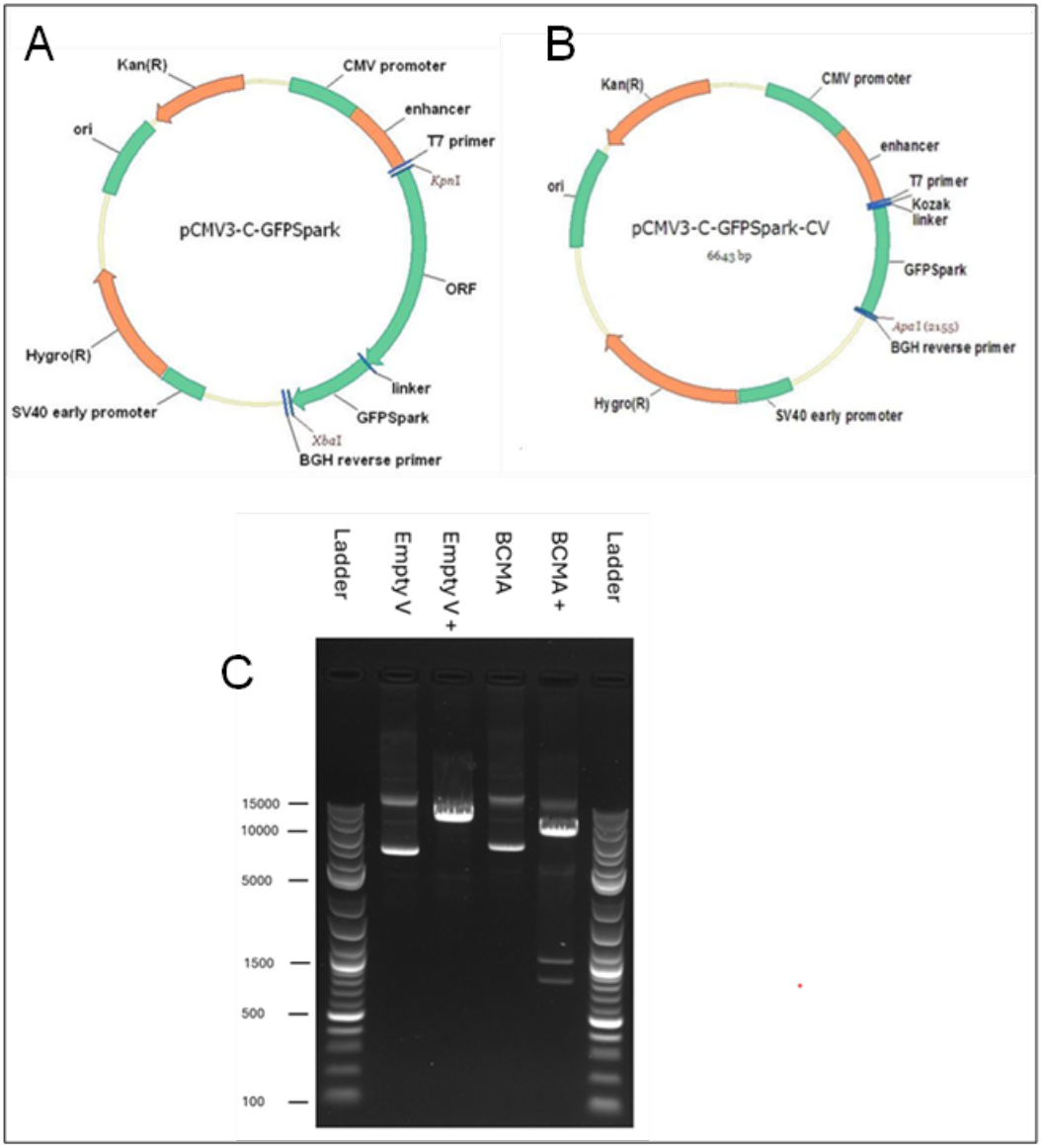

Appendix Figure 5. Plasmid maps and gel electrophoresis.

(A) Map of the BCMA-containing plasmid. **(B)** Map of the control plasmid. **(C)** Agarose gel electrophoresis of undigested plasmid B (lane 2) and restriction enzyme-digested plasmid B (lane 3), undigested plasmid A (lane 4) and restriction enzyme-digested plasmid A (lane 5) DNA. DNA ladders were run in lanes 1 and 2.

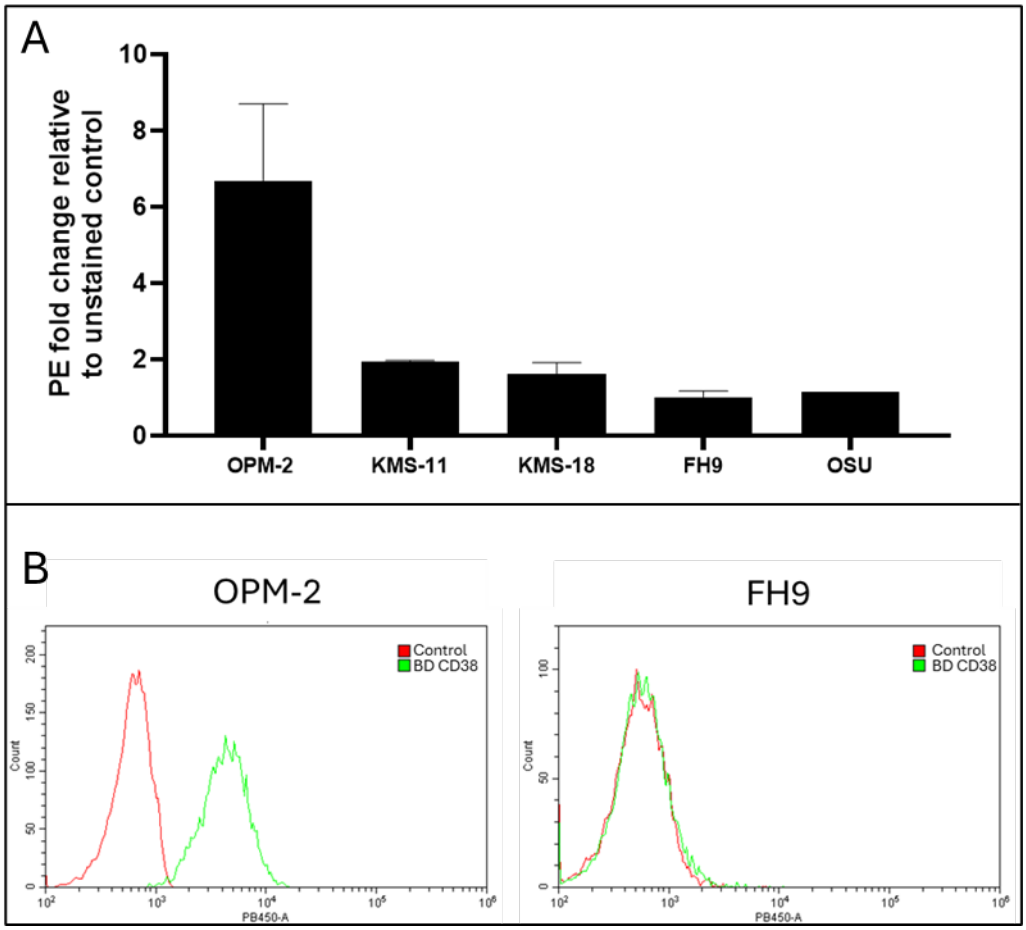

Appendix Figure 6. CD38 expression assessed using a commercial BD anti-CD38 antibody in MM, CLL and FH9 cell lines.

(A) OPM-2, KMS-11 and KMS-18 MM cell lines, OSU-CLL cell line and FH9 non-malignant B-cell line, were incubated with daratumumab or the relevant isotype control antibody for 30 minutes, followed by a fluorochrome-conjugated secondary antibody. CD38 expression was assessed by flow cytometry. Data are the mean and standard deviation from a minimum of 2 biological replicates per cell line**. (B)** Representative flow cytometry histograms of OPM-2 cells stained with daratumumab (green) or isotype control (red).

Sample Name:	Ali liposomes 10-05-24 98% new/new 2		
SOP Name:	mansettings.nano		
File Name:	blank liposomes_13-05-2022.mea	**Dispersant Name:**	Water
Record Number:	731	**Dispersant RI:**	1.330
Material RI:	1.59	**Viscosity (cP):**	0.8872
Material Absorbtion:	0.010	**Measurement Date and Time:**	Friday, 10 May 2024 1:59:09 I

Temperature (°C):	25.0	**Duration Used (s):**	60	
Count Rate (kcps):	301.9	**Measurement Position (mm):**	4.65	
Cell Description:	Disposable sizing cuvette	**Attenuator:**	7	

			Size (d.nm):	**% Intensity:**	**St Dev (d.nm):**
Z-Average (d.nm):	125.8	**Peak 1:**	134.6	100.0	36.16
PdI:	0.057	**Peak 2:**	0.000	0.0	0.000
Intercept:	0.943	**Peak 3:**	0.000	0.0	0.000
Result quality :	Good				

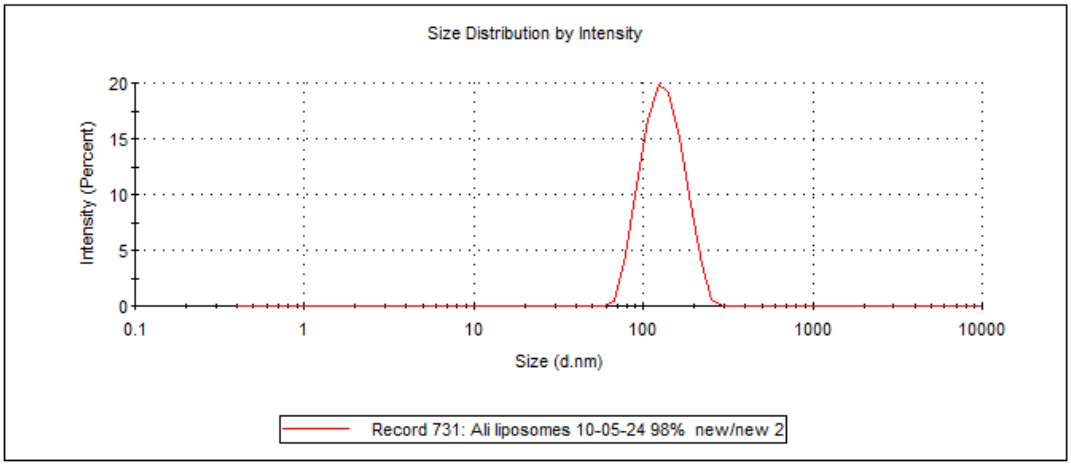

Appendix Figure 7. Representative DLS report of liposome size and distribution.

Liposomes were synthesised with PE (16:0_22:6): DSPE-PEG2000 at ratios of 98:2 (w/w%) and were analysed by DLS. The report generated by the Zetasizer software.

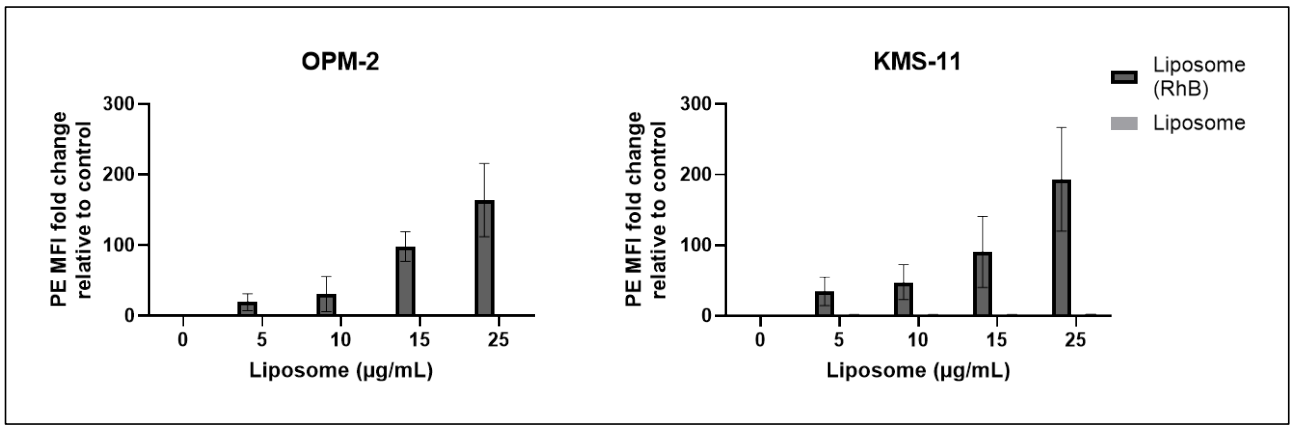

Appendix Figure 8. Liposome uptake into MM cells is dose dependent.

OPM-2 and KMS-11 cells were cultured with fluorescently tagged or blank liposomes for 24 hours and analysed by flow cytometry. Data are mean and standard deviation of 3 independent experiments.

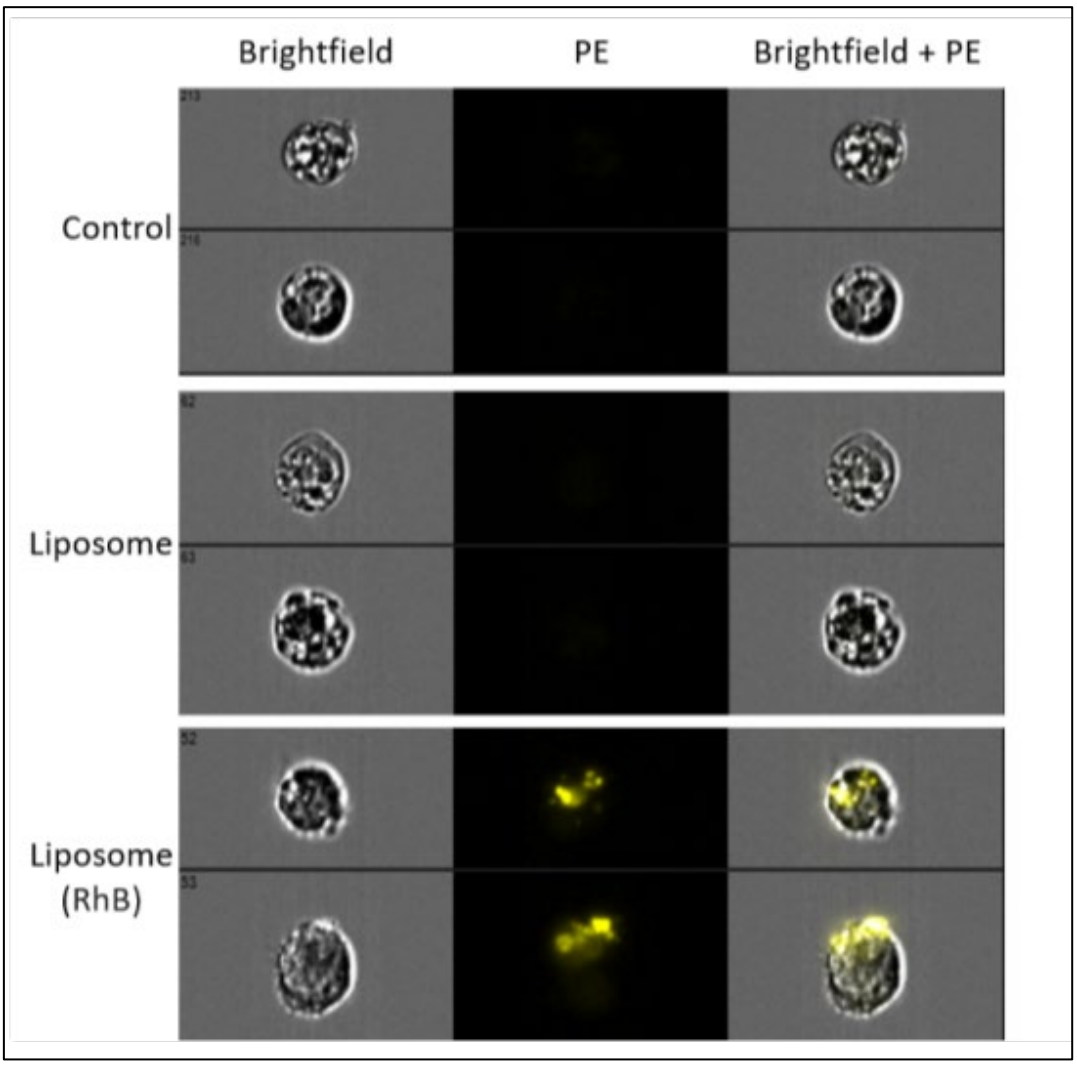

Appendix Figure 9. Liposome uptake into OPM-2 (MM) cells can be visualised by imaging flow cytometry.

OPM-2 cells were cultured with 15 µg/mL fluorescently tagged or blank liposomes for 24 hours. Images were generated using an imageStream X instrument at 40x magnification.

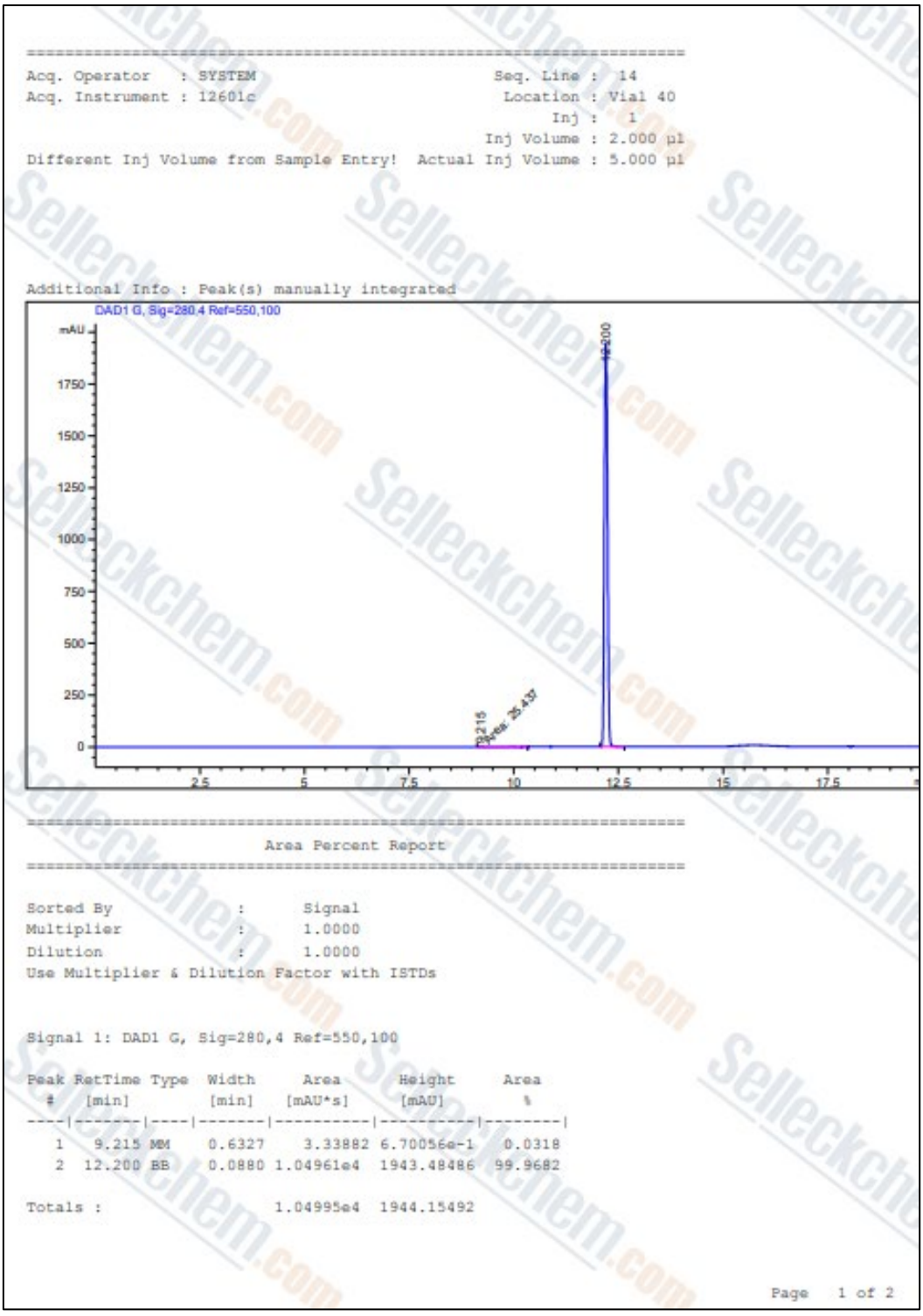

```
================================================================================
Acq. Operator   : SYSTEM                          Seq. Line :  14
Acq. Instrument : 1260ic                           Location : Vial 40
                                                       Inj :  1
                                                  Inj Volume : 2.000 µl
Different Inj Volume from Sample Entry!  Actual Inj Volume : 5.000 µl


Additional Info : Peak(s) manually integrated
```



```
================================================================================
                          Area Percent Report
================================================================================

Sorted By             :      Signal
Multiplier            :      1.0000
Dilution              :      1.0000
Use Multiplier & Dilution Factor with ISTDs


Signal 1: DAD1 G, Sig=280,4 Ref=550,100

Peak RetTime Type  Width     Area      Height     Area
  #   [min]        [min]   [mAU*s]     [mAU]       %
----|-------|----|-------|----------|----------|--------|
   1   9.215 MM    0.6327    3.33882 6.70056e-1   0.0318
   2  12.200 BB    0.0880 1.04961e4  1943.48486  99.9682

Totals :                  1.04995e4  1944.15492


                                                          Page   1 of 2
```

Appendix Figure 10. Manufacturers details regarding the analysis of RSL3 by HPLC.

Conditions and method for RSL3 detection by HPLC provided by Selleck Chemicals.

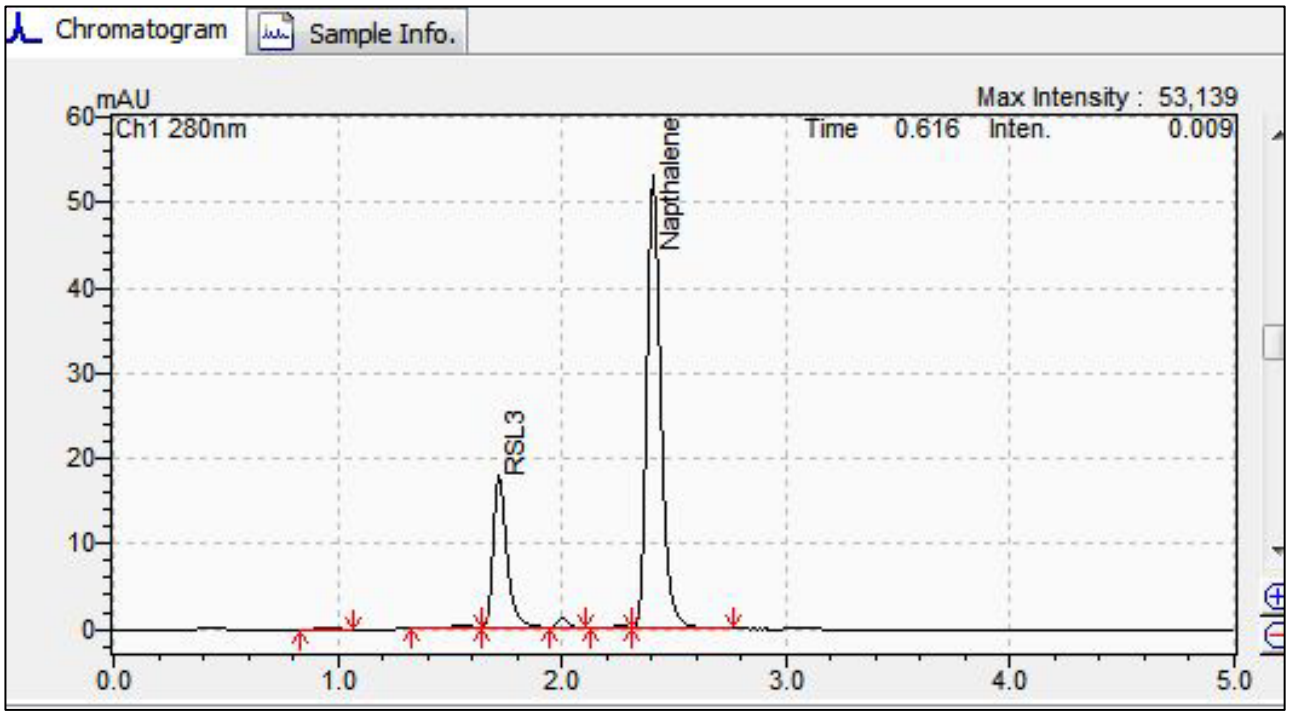

Appendix Figure 11. Representative HPLC chromatogram of RSL3 standard and the internal standard naphthalene

RSL3 standard was prepared in an appropriate mobile phase and spiked with naphthalene (10 μg/mL). The representative chromatogram shows the ratio of RSL3 to naphthalene, which was used to generate standard curves for determining RSL3 concentrations.

NANOSIGHT

liposomes 2025-01-15 13-29-40

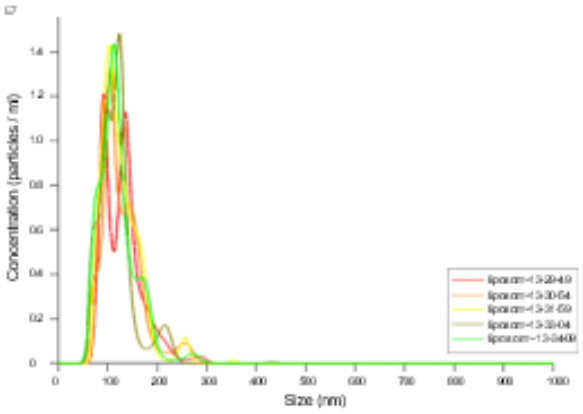

FTLA Concentration / Size graph for Experiment:
liposomes 2025-01-15 13-29-40

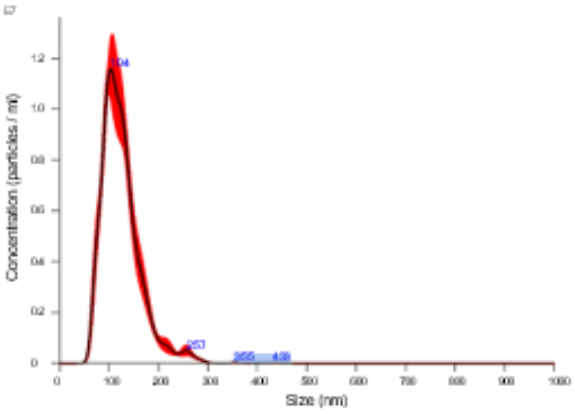

Averaged FTLA Concentration / Size for Experiment:
liposomes 2025-01-15 13-29-40
Error bars indicate + / -1 standard error of the mean

Included Files

liposomes 2025-01-15 13-29-49
liposomes 2025-01-15 13-30-54
liposomes 2025-01-15 13-31-59
liposomes 2025-01-15 13-33-04
liposomes 2025-01-15 13-34-09

Details

NTA Version:	NTA 3.4 Build 3.4.003
Script Used:	SOP Standard Measurement 01-29-35PM 15Jan2025.txt
Time Captured:	13:29:40 15/01/2025
Operator:	
Pre-treatment:	
Sample Name:	
Diluent:	
Remarks:	

Capture Settings

Camera Type:	sCMOS
Laser Type:	Blue405
Camera Level:	14
Slider Shutter:	1259
Slider Gain:	366
FPS	25.0
Number of Frames:	1498
Temperature:	21.2 - 21.3 °C
Viscosity:	(Water) 0.968 - 0.970 cP
Dilution factor:	Dilution not recorded
Syringe Pump Speed:	50

Analysis Settings

Detect Threshold:	8
Blur Size:	Auto
Max Jump Distance:	Auto: 12.2 - 12.8 pix

Results

Stats: Merged Data

Mean:	124.5 nm
Mode:	103.4 nm
SD:	39.4 nm
D10:	82.5 nm
D50:	117.7 nm
D90:	173.2 nm

Stats: Mean +/- Standard Error

Mean:	124.7 +/- 2.4 nm
Mode:	107.4 +/- 5.1 nm
SD:	39.2 +/- 0.7 nm
D10:	82.5 +/- 2.1 nm
D50:	118.7 +/- 2.5 nm
D90:	171.5 +/- 4.1 nm
Concentration (Upgrade):	9.02e+08 +/- 3.08e+07 particles/ml
	111.6 +/- 5.0 particles/frame
	144.2 +/- 7.5 centres/frame

Concentration measurements may require some caution due to noise
See summary file for more info

Appendix Figure 12. Representative report generated by a Nano tracker instrument showing details of one batch of liposomes containing RSL3.

Report generated from Nanosight NS300 software detailing the size, distribution and quantity of liposomes that were loaded with RSL3.

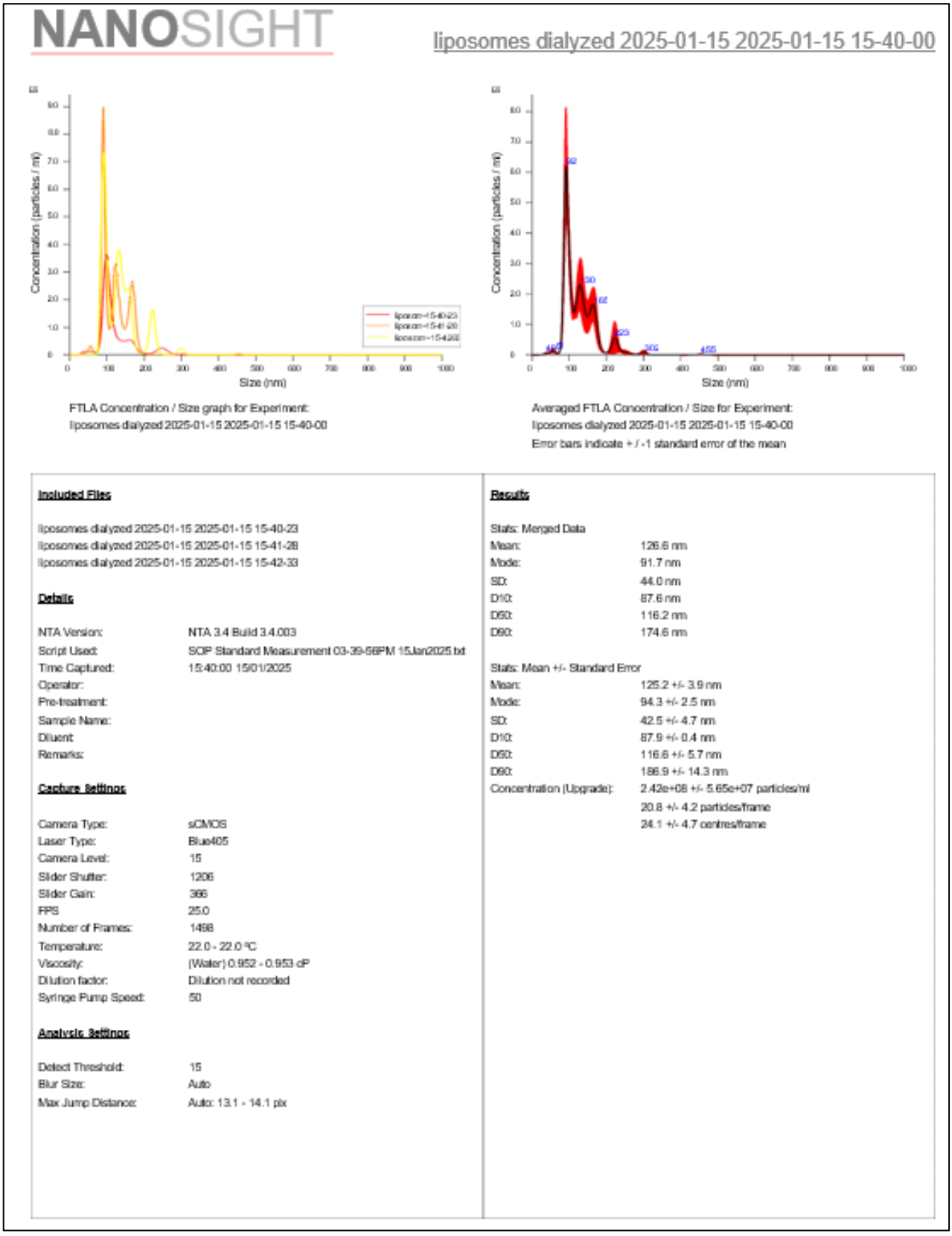

Appendix Figure 13. Representative report generated from a Nano tracker instrument regarding liposomes containing RSL3 following dialysis.

Report generated from Nanosight NS300 software detailing the size, distribution and quantity of liposomes loaded with RSL3 following dialysis.

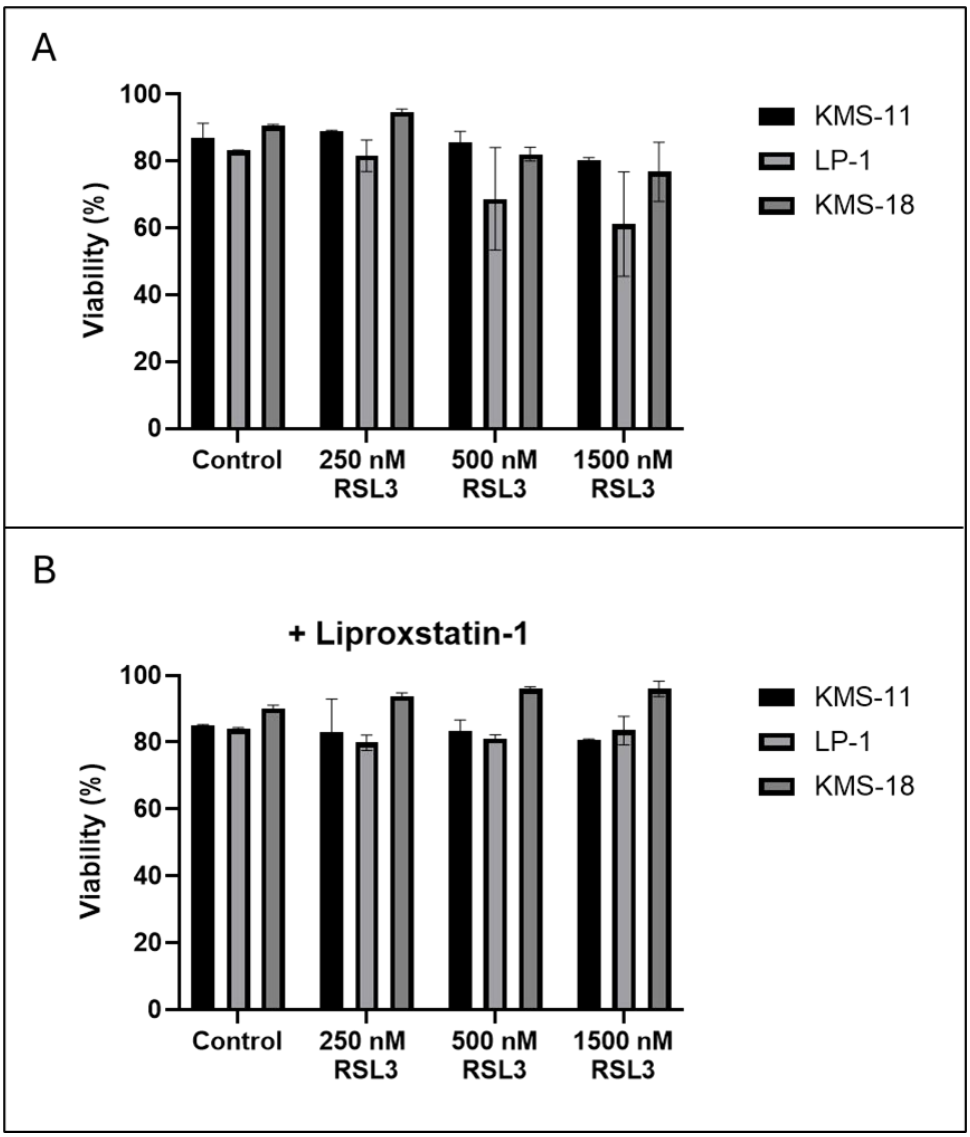

Appendix Figure 14. MM cells are insensitive to RSL3.

(A) MM cells were cultured with the indicated concentrations of RSL3 for 24 hours. **(B)** MM cells were cultured with indicated concentrations of RSL3 with liproxstatin-1 for 24 hours. Cell viability was assessed using annexin V/PI staining and flow cytometry. Data are the mean ± standard deviation of duplicate measurements from 3 independent experiments.

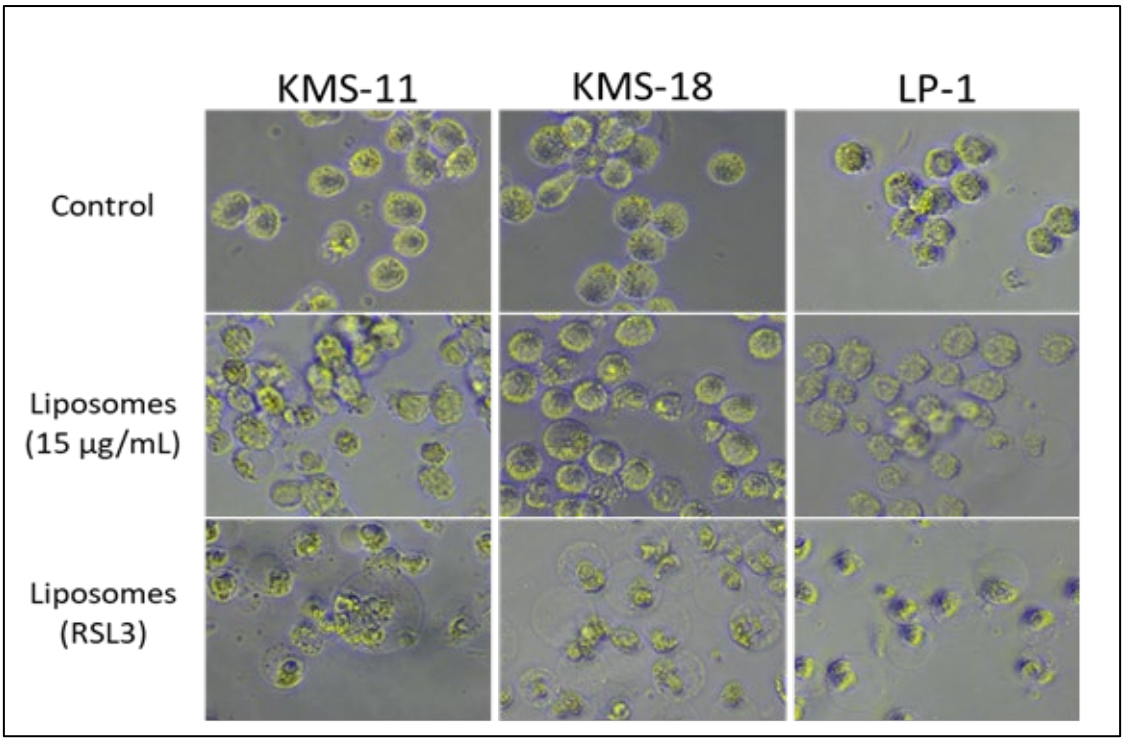

Appendix Figure 15. RSL3 containing liposomes induce ferroptosis in MM cell lines.

MM cells were cultured for 24 hours with 15 µg/mL liposomes that either did or did not contain RSL3. Images were acquired at 24 hours using an imaging microscope at 20X magnification.

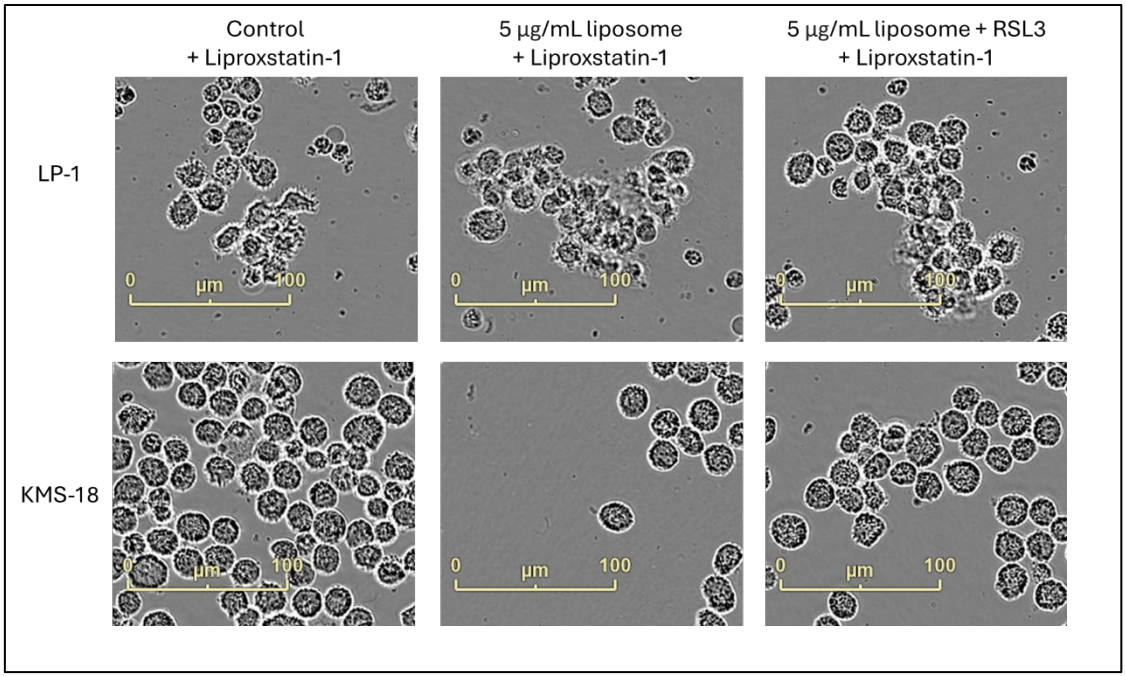

Appendix Figure 16. Cell death induced by liposomes containing RSL3 can be prevented by liproxstatin-1.

MM cells were cultured for 24 hours with 5 µg/mL liposomes that either did or did not contain RSL3, in addition to liproxstatin-1. Images were acquired at 24 hours using an IncuCyte S3 live cell analysis system at 20X magnification.

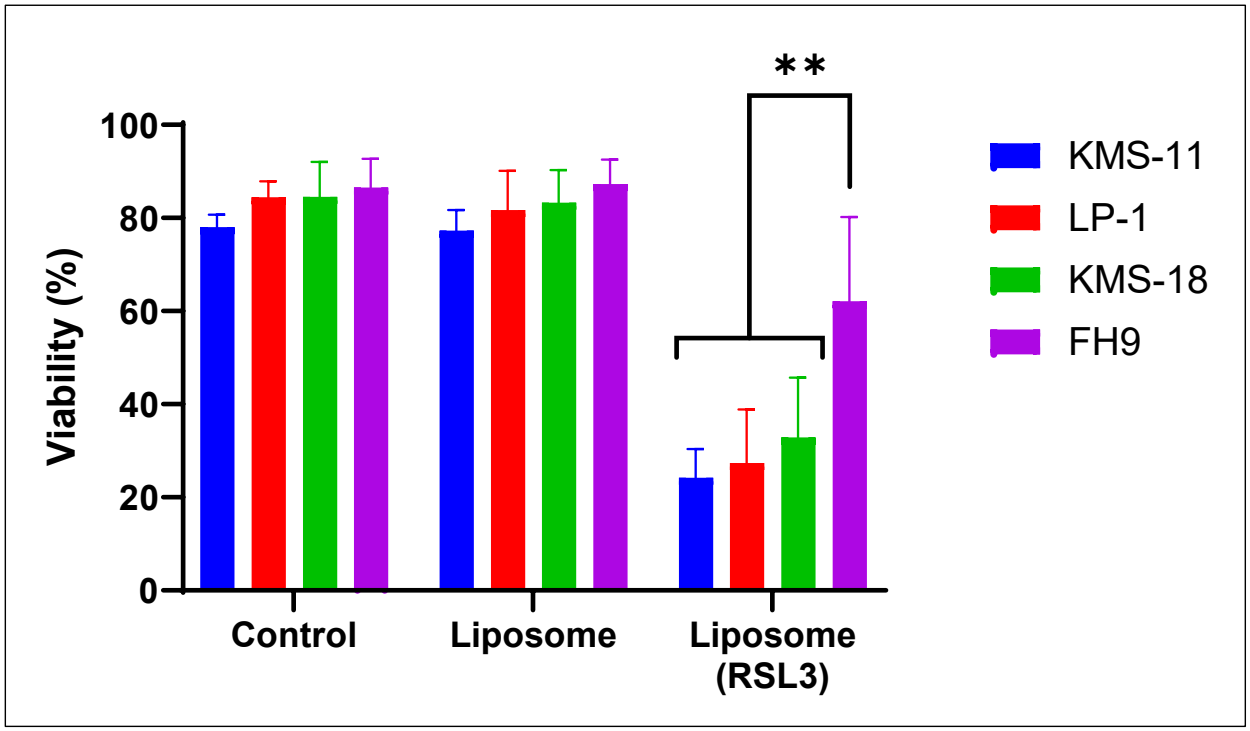

Appendix Figure 17. Liposomes containing RSL3 are more significantly effective at inducing cell death in MM cell lines than FH9 cells.

MM and FH9 cells were cultured for 24 hours with 5 μg/mL liposomes that either did or did not contain RSL3. Cell viability was assessed using annexin V/PI staining and flow cytometry. Data are the mean ± standard deviation of duplicate measurements from 3 independent experiments.

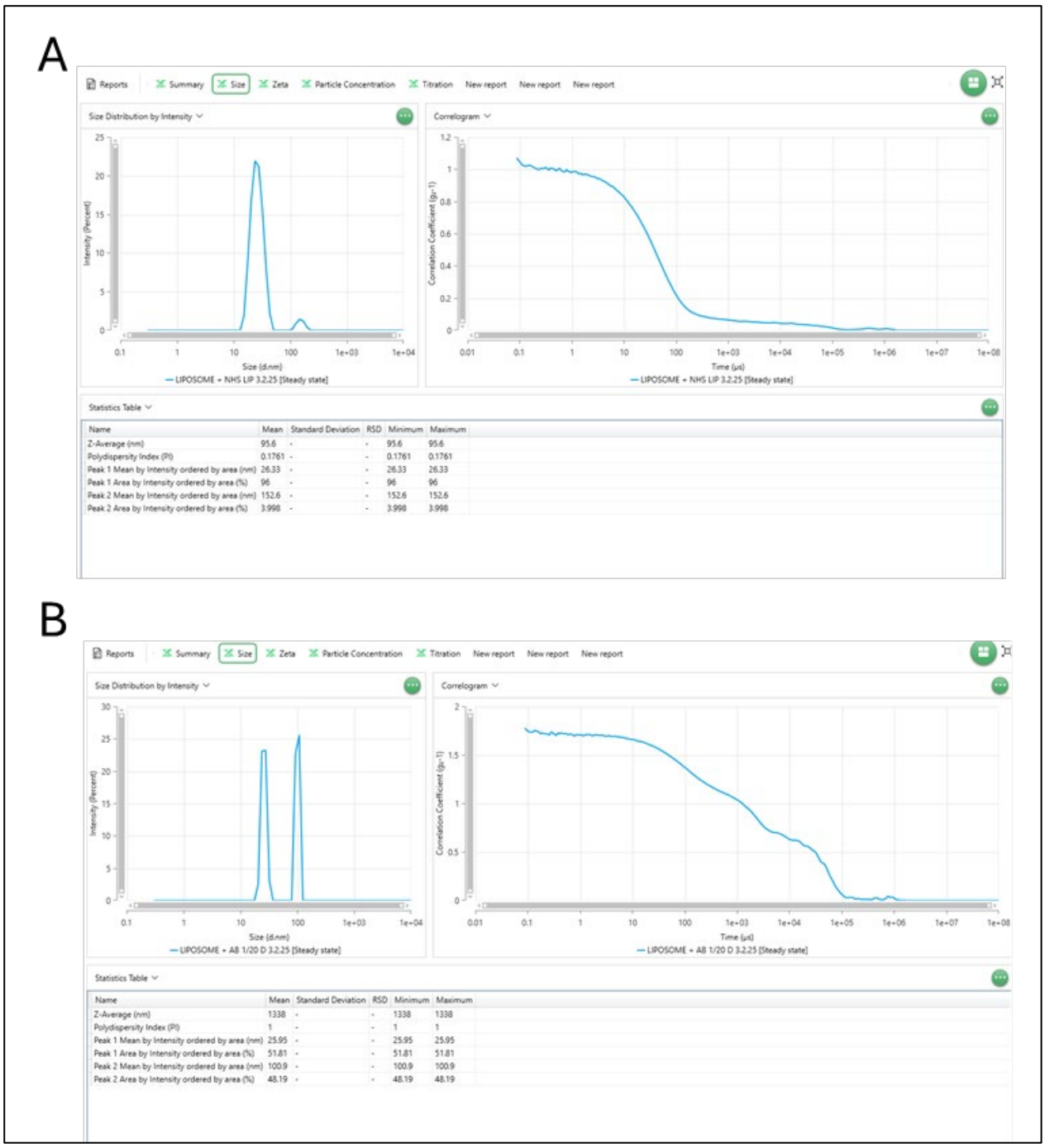

Appendix Figure 18. Representative DLS report regarding the size and PDI of liposomes that either were or were not conjugated to daratumumab.

(A) Control liposomes and **(B)** daratumumab-conjugated liposomes with the formulation PE (16:0_22:6): DSPE-PEG2000 carboxyl NHS at ratios of 98:2 (w/w%). Size and distribution were measured using DLS. Report generated from the Zetasizer software.

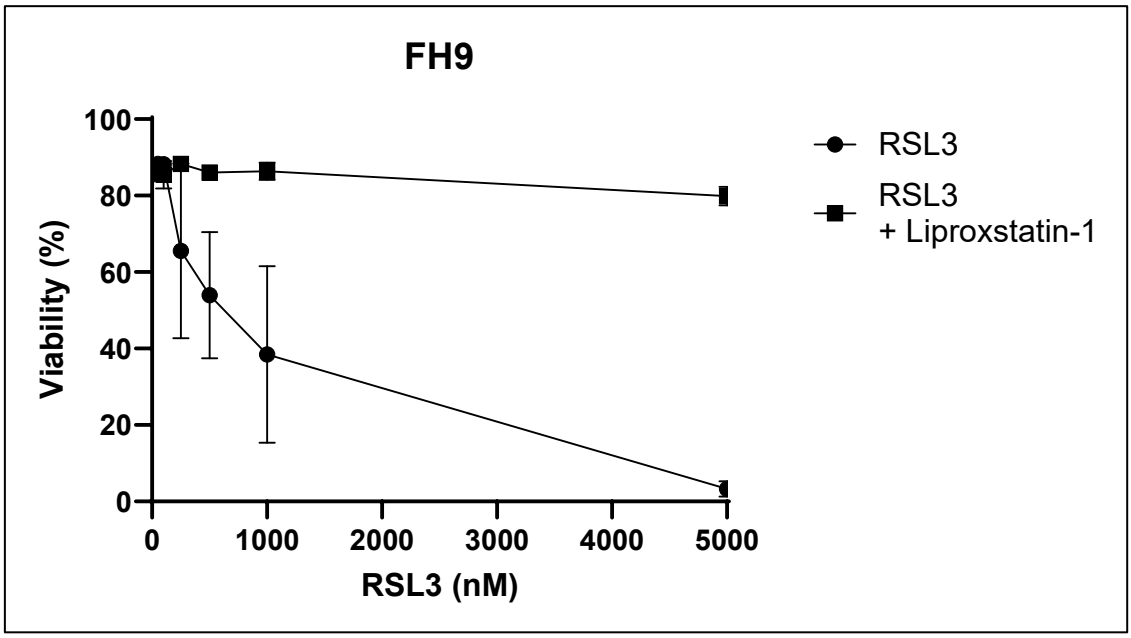

Appendix Figure 19. Healthy B cell line FH9 can undergo RSL3 induced ferroptosis.

FH9 cells were cultured for 24 hours with RSL3. Cell viability was assessed using annexin V/PI staining and flow cytometry. Data are the mean ± standard deviation of duplicate measurements from 2 independent experiments.

Publication 1

International Journal of
Molecular Sciences

MDPI

Review

Ferroptosis in Haematological Malignancies and Associated Therapeutic Nanotechnologies

Rachel L. Mynott [1], Ali Habib [1], Oliver G. Best [1] and Craig T. Wallington-Gates [1,2,*]

[1] Flinders Health and Medical Research Institute, College of Medicine & Public Health, Flinders University, Adelaide, SA 5042, Australia
[2] Flinders Medical Centre, Bedford Park, SA 5042, Australia
* Correspondence: craig.wallingtongates@flinders.edu.au

Abstract: Haematological malignancies are heterogeneous groups of cancers of the bone marrow, blood or lymph nodes, and while therapeutic advances have greatly improved the lifespan and quality of life of those afflicted, many of these cancers remain incurable. The iron-dependent, lipid oxidation-mediated form of cell death, ferroptosis, has emerged as a promising pathway to induce cancer cell death, particularly in those malignancies that are resistant to traditional apoptosis-inducing therapies. Although promising findings have been published in several solid and haematological malignancies, the major drawbacks of ferroptosis-inducing therapies are efficient drug delivery and toxicities to healthy tissue. The development of tumour-targeting and precision medicines, particularly when combined with nanotechnologies, holds potential as a way in which to overcome these obstacles and progress ferroptosis-inducing therapies into the clinic. Here, we review the current state-of-play of ferroptosis in haematological malignancies as well as encouraging discoveries in the field of ferroptosis nanotechnologies. While the research into ferroptosis nanotechnologies in haematological malignancies is limited, its pre-clinical success in solid tumours suggests this is a very feasible therapeutic approach to treat blood cancers such as multiple myeloma, lymphoma and leukaemia.

Keywords: ferroptosis; nanotechnology; nanomedicine; haematological malignancies

Citation: Mynott, R.L.; Habib, A.; Best, O.G.; Wallington-Gates, C.T. Ferroptosis in Haematological Malignancies and Associated Therapeutic Nanotechnologies. *Int. J. Mol. Sci.* **2023**, *24*, 7661. https://doi.org/10.3390/ijms24087661

Academic Editors: Sebastian Doll and Maceler Aldrovandi

Received: 27 March 2023
Revised: 19 April 2023
Accepted: 20 April 2023
Published: 21 April 2023

1. Introduction

Haematological malignancies comprise a large group of heterogeneous tumours that originate in blood-forming tissue, such as the bone marrow, or in the cells of the immune system. Broadly speaking, these tumours are grouped into those of myeloid or lymphoid origin and can be acute or chronic with regard to their natural history. Examples of bone marrow-derived malignancies include acute myeloid leukaemia, acute lymphoblastic leukaemia and chronic myeloid leukaemia, whilst chronic lymphocytic leukaemia, lymphomas and multiple myeloma are lymphoid malignancies originating outside the bone marrow in blood or lymphatic tissue. Given their biological heterogeneity, there are consequential differences in diagnostic, prognostic and therapeutic algorithms, with many being treatable but not curable.

The term ferroptosis was coined in 2012 to describe a new form of regulated cell death characterised by the iron-dependent accumulation of lipid-reactive oxygen species to lethal levels [1]. The sensitivity to ferroptosis is tightly linked to numerous biological processes, including the metabolism of amino acids, iron and polyunsaturated fatty acids, and the biosynthesis of glutathione and phospholipids. Ferroptosis has been implicated in the pathological cell death associated with degenerative diseases (e.g., Alzheimer's disease), stroke and traumatic brain injury; however, ferroptosis may also have a tumour-suppressive function that could be harnessed for cancer therapy [2]. Importantly, lipid metabolism is intimately involved in determining cellular sensitivity to ferroptosis, with

certain polyunsaturated phospholipids being susceptible to the iron-dependent lipid peroxidation necessary for its execution [3]. It is this dependence on certain phospholipids that paves the way for potential ferroptosis-inducing nanotechnologies, in particular those based on a liposome design, to be developed.

Cancer therapeutics have advanced tremendously over the past few decades, with firstly, a shift towards tumour-targeting mechanisms and, more recently, true patient-individualised or precision strategies [4,5]. An example of the former is the monoclonal antibody daratumumab, which targets CD38 on the surface of myeloma plasma cells, whilst a precision therapeutic could be the application of venetoclax in those myeloma patients whose plasma cells harbour t(11;14), which upregulates bcl-2, the target of venetoclax [6,7]. Thus, cancer drug classes have expanded to include traditional chemotherapeutics such as DNA damaging agents and mitotic spindle inhibitors, tumour-targeting small molecule inhibitors, tumour-targeting immunological agents (monoclonal antibodies, bi-specific antibodies, antibody-drug conjugates, CAR-T cells) and precision therapeutics, which may incorporate any one or more of the other therapeutic classes [4]. Nanotechnologies, on the other hand, are often seen as vehicles for existing cancer drugs in an effort to maximise cancer cell cytotoxicity through improved drug pharmacokinetics and pharmacodynamics [8]. This approach aims to not only increased tumour killing but also minimise both on-target and off-target related drug toxicities, particularly when incorporating tumour-targeting and precision principles.

In this review, we describe the major haematological cancers, ferroptosis and clinical applications thereof before providing an in-depth discourse on the use of ferroptosis-inducing nanotechnologies in cancer, focusing on those of haematological origin. We provide examples of dendritic mesoporous silica nanoparticles, iron oxide nanoparticles, micelles and liposomes, whether or not employing tumour-targeting or precision approaches. Throughout, we highlight the significance of liposome-based nanotechnologies given their importance in not only being drug carriers but also ferroptosis-inducing therapeutics in themselves by supplying relevant phospholipids to the cancer cell.

2. Multiple Myeloma

Multiple myeloma (MM) is a malignancy of antibody-producing plasma cells of the bone marrow [9]. In Australia, in 2018, 2247 people were diagnosed with MM at a median age of 71 years, with the overall survival at 5 years being 55% [10]. A diagnosis of MM is defined as the presence of more than 10% clonal plasma cells in the bone marrow, as well as one or more of the "CRAB" criteria: hypercalcaemia, renal insufficiency, anaemia or bone lytic lesions. Other diagnostic criteria have been recently introduced, including at least 60% clonal plasma cells in the bone marrow, one or more focal bone marrow lesions on magnetic resonance imaging (MRI) imaging (indicating bone marrow involvement) or an involved to uninvolved free immunoglobulin light chain ratio > 100 [9].

The median survival of patients with MM has significantly improved since the 1990s, predominantly due to the introduction of new therapeutic agents [11,12]. These novel therapies include proteasome inhibitors (e.g., bortezomib and carfilzomib), immunomodulatory drugs (e.g., lenalidomide and pomalidomide) and monoclonal antibodies (e.g., daratumumab and elotuzumab, which target the CD38 and SLAMF7 proteins, respectively) [11,13]. In practice, these drugs are not used alone but rather in combination; however, despite significant improvements in quality of life and overall survival in the last few decades, relapsed disease inevitably occurs.

3. Lymphomas

Lymphomas are a diverse group of haemopoietic malignancies that arise from the clonal proliferation of lymphocytes, usually in lymph nodes. Characterisation of lymphomas morphologically, immunophenotypically and genetically allows for the identification of many different subtypes with varying prognostic and treatment algorithms, however they are generally classified as either Hodgkin lymphomas (HL) or non-Hodgkin

lymphoma (NHL) [14]. HLs can be identified in lymph nodes by the presence of Reed–Sternberg cells admixed with variable numbers of B cells, T cells and other haemopoietic lineages. These lymphomas tend to be highly chemo-sensitive, with a 5-year survival rate exceeding 80% [15]. NHLs constitute a large group of diverse lymphoid tumours of either B or T-cell origin, with B-cell NHLs being more common than T-cell NHLs.

As an example, diffuse large B-cell lymphoma (DLBCL) is the most common non-Hodgkin lymphoma (NHL), accounting for 30–40% of all NHL cases and approximately one-third of all newly diagnosed lymphoma cases worldwide [16,17]. A treatment regimen consisting of cyclophosphamide, doxorubicin, vincristine and prednisone (CHOP) combined with the monoclonal antibody rituximab (R-CHOP) is the current frontline treatment for DLBCL [16]. While over 60% of patients can be cured with R-CHOP, those with either primary refractory disease or who relapse after a period of remission have poorer outcomes [16]. DLBCL can be further classified into two main molecular subtypes, activated B-cell (ABC) and germinal centre B-cell (GCB), the former being associated with significantly worse prognosis and complete remission (CR) rates of 30% and 70%, respectively [17]. In approximately 10% of cases, translocations involving *MYC* and *Bcl-2* and/or *Bcl-6* (double and triple hit DLBCL) are identified, which are also associated with less favourable clinical outcomes [18,19]. Furthermore, overexpression of *Bcl-2* and *MYC* ('double-expressor') can occur through mechanisms that do not involve chromosomal translocations [18,20]. It is for these patients with poorer clinical outcomes that novel therapeutics are urgently required.

4. Leukaemias

Leukaemias are a heterogenous group of diseases that arise from the clonal proliferation of immature or mature leukocytes [21]. It is estimated that 5202 people will be diagnosed with leukaemia in 2022 in Australia, with a 5-year survival rate of 64.4% [10]. Leukaemias can be characterised by the cell of origin (lymphoid or myeloid) and by the rate of proliferation (acute or chronic) [21]. The predominant subtypes of leukaemia and their prevalence in Australia are outlined in Table 1.

Table 1. Leukaemia statistics in Australia.

Leukaemia Subtype	Median Age at Diagnosis *	Incidence *	Deaths +	5-Year Survival Rate *
Acute lymphoblastic leukaemia (ALL)	15.1	382	90	74.5%
Acute myeloid leukaemia (AML)	69.1	1082	1169	26.4%
Chronic lymphocytic leukaemia (CLL)	71.5	1945	306	85.4%
Chronic myeloid leukaemia (CML)	61.4	392	84	83.4%

* Data extracted from 2018 Cancer data in Australia [10]. + Data extracted from 2020 Cancer data in Australia [10].

Chemotherapy, chemoimmunotherapy and stem cell transplantation are common treatment options for leukaemia, but with a better understanding of the mechanisms that drive these diseases, novel targeted agents are becoming more widely used. Response and outcome rates vary significantly between the different forms of leukaemia, but invariably a proportion of patients will relapse with refractory disease. Whilst survival rates among patients diagnosed with acute leukaemia have improved markedly in the last few decades, particularly for patients under the age of 50 [22], those diagnosed with acute lymphoblastic leukaemia (ALL) or acute myeloid leukaemia (AML) experience decreased survival with age with 5-year survival rates being as low as 12% and 4%, respectively, for people over the age of 80 at diagnosis [22].

Unlike patients with acute leukaemia, who generally require intensive treatment, patients with chronic leukaemia can often be managed with a 'watch and wait' approach with minimal to no treatment required for many years [21]. Approximately 30% of patients diagnosed with chronic lymphocytic leukaemia (CLL) never require treatment, whereas many CLL patients will have or will rapidly develop the symptomatic disease after diagnosis, requiring early intervention [23]. Chronic myeloid leukaemia (CML) is a slow-growing malignancy characterised by the Philadelphia chromosome formed by a reciprocal transloca-

tion of chromosomes 22 and 9 [24]. The resulting fusion oncogene (BCR-ABL) is effectively targeted by tyrosine kinase inhibitors such as imatinib, which have significantly improved survival rates among CML patients [24].

5. Ferroptosis

Regulated cell death is a fundamental physiological process that ensures cell integrity and homeostasis. Apoptosis is arguably the most well-studied form of cell death, but relatively recently, a study by Dixon et al. described an iron-dependent form of cell death associated with an accumulation of lipid peroxides, which they termed ferroptosis [1]. Ferroptosis is distinct morphologically, genetically and biochemically from other forms of cell death, including apoptosis, as it can be inhibited by iron chelation and lipophilic antioxidants [25]. Cells undergoing ferroptosis have a characteristic "ballooning phenotype" with an enlarged, empty cytoplasm, in contrast to the small, shrunken appearance of apoptotic cells with distinct membrane blebbing that precedes apoptotic body formation [26,27]. Ferroptotic cells also lack key morphological changes associated with other forms of programmed cell death, such as apoptotic bodies or the autophagosomes associated with apoptosis and autophagy, respectively [26]. Other features of ferroptosis, including reduced mitochondrial volume, increased mitochondrial membrane density and the absence of mitochondrial cristae, can also be observed using transmission microscopy [1].

Since its discovery, ferroptosis has been associated with many biological processes involved in cellular homeostasis, iron and amino acid regulation and the metabolism of polyunsaturated fatty acids [2]. In the context of cancer, induction of ferroptosis has the potential to be a novel treatment strategy, particularly for patients who relapse with drug-resistant disease following treatment with standard therapies. As cancer cells generally have higher levels of reactive oxygen species (ROS) due to increased metabolic and growth rates, cell death mechanisms such as ferroptosis that further elevate ROS levels may be a particularly effective and specific approach for the treatment of a range of cancers [28]. In addition to the aforementioned morphological changes, ferroptosis can be distinguished from other forms of cell death by monitoring the accumulation of lipid peroxides, using fluorescently labelled fatty acid analogues (i.e., C11-BODIPY), and through inhibition of cell death by either iron chelation (i.e., deferoxamine, DFO) or lipophilic antioxidants (liproxstatin-1, ferrostatin-1 or vitamin E) [29]. Furthermore, ferroptosis cannot be prevented by inhibitors of apoptosis, necroptosis or autophagy (i.e., z-VAD-FMK, necrostatin-1s and chloroquine, respectively) [1].

5.1. The Role of Iron in Ferroptosis

Iron is essential for cellular homeostasis [30], with key roles in oxygen transport, oxidative phosphorylation and DNA biosynthesis [31]. As iron chelation inhibits ferroptosis, this form of cell death is also clearly an iron-dependent process [1]. Intracellular iron levels are primarily regulated by the iron-storage protein ferritin and the transferrin receptor (TfR), which shuttles transferrin-bound iron into the cell through receptor-mediated endocytosis. The level of non-protein bound iron (labile iron pool) has implications in ferroptosis as labile iron reacts with hydrogen peroxide inside cells, yielding highly reactive hydroxyl radicals in a process known as the Fenton reaction [32]. These radicals indiscriminately damage all surrounding organic material within a range of a few nanometres, resulting in cellular damage (Figure 1) [32]. Iron also plays a role in ferroptosis through its actions on a group of iron-containing enzymes that mediate lipid peroxidation, known as lipoxygenases (LOXs) [2,33]. The key role of these enzymes is demonstrated by the LOX inhibitor, zileuton, which confers resistance to ferroptotic cell death in HT22 neuronal cells [34]. Furthermore, genetic knockdown or pharmacological inhibition of arachidonate lipoxygenases (ALOXs) protects cells against ferroptosis induced by erastin [3].

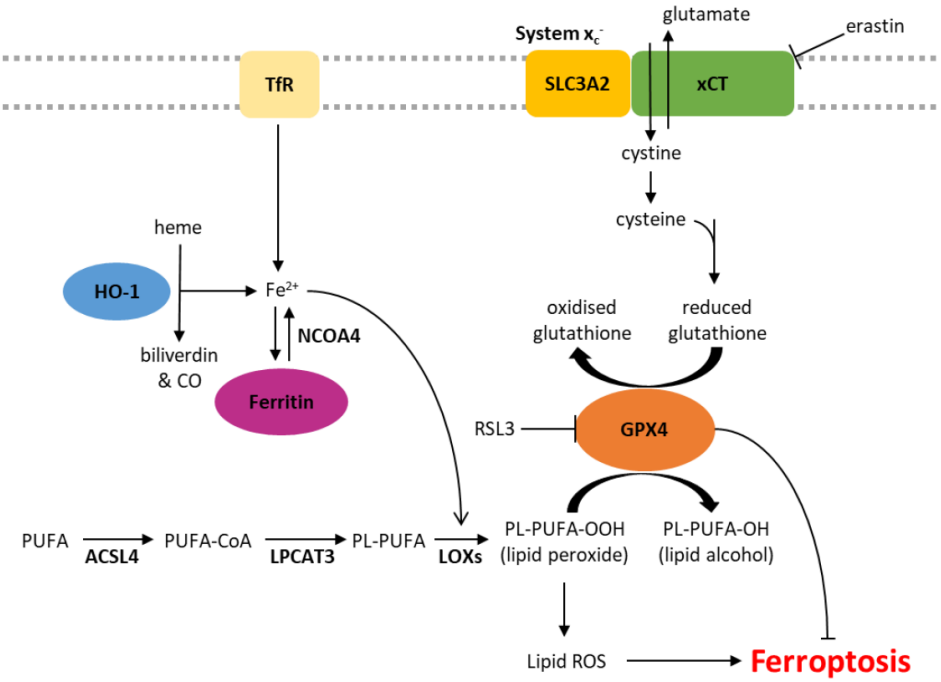

Figure 1. Biochemical pathways involved in the regulation of ferroptosis. ACSL4, acyl-CoA synthetase long-chain family member 4; CO, carbon monoxide; Fe^{2+}, ferrous iron; GPX4, glutathione peroxidase 4; HO-1, heme oxygenase 1; LOXs, lipoxygenases; LPCAT3, lysophosphatidylcholine acyltransferase 3; NCOA4, nuclear receptor coactivator 4; PL, phospholipid; PUFA, polyunsaturated fatty acid; ROS, reactive oxygen species; TfR, transferrin receptor.

5.2. Lipid Peroxidation

Lipid peroxidation is a characteristic feature of ferroptosis, distinguishing it from other forms of programmed cell death. Phospholipid peroxidation results in the oxidative degradation of lipids, the formation of peroxyl radicals and damage to the plasma membrane (Figure 1) [35,36]. Sensitivity to ferroptosis is associated with the degree of lipid saturation, the cellular location of the phospholipids and the number of phospholipids containing polyunsaturated fatty acids (PUFA) relative to those containing monounsaturated fatty acids (MUFA) [2]. Phospholipids containing PUFAs are more readily oxidised, and therefore, supplementation with PUFAs such as arachidonic acid (AA) and linoleic acid (LA) increases the sensitivity of cancer cells to ferroptosis [3,37,38]. Other studies support this notion that cellular sensitivity to ferroptosis is associated with their lipidomic profile, demonstrating that the incorporation of MUFAs into phospholipids reduces the generation of lipid ROS in membranes and therefore protects against ferroptosis [3,39]. MUFAs can also displace PUFAs from intracellular phospholipids, including in the plasma membrane, reducing the potential for lipid ROS accumulation [39].

5.3. System x_c− and GPX4

xCT, encoded by the *SLC7A11* gene, is a major part of the system x_c- cystine/glutamate antiporter. The regulatory component, SLC3A2, is involved in many other solute transporter systems, and so, xCT has been the focus of much of the work into system x_c-. Glutamate is pumped out of the cell in exchange for cystine, which is rapidly reduced to cysteine [40]. Cysteine is a rate-limiting factor in the production of glutathione (GSH), an important antioxidant due to its role as a cofactor of glutathione peroxidase 4 (GPX4) [41].

GPX4 is the primary enzyme that reduces phospholipid hydroperoxides into their corresponding alcohols, inhibiting lipid peroxidation and subsequent ferroptosis [2,42]. When the activity of GPX4 is inhibited, either directly or through GSH depletion, and lipid peroxidation exceeds tolerable levels, ferroptotic cell death is initiated (Figure 1) [2,43].

Class 1 ferroptosis inducers deplete cellular GSH by inhibiting xCT, therefore preventing cystine uptake (e.g., erastin) or interfering with GSH synthesis (e.g., buthionine sulfoximine, BSO). In vivo studies of erastin have been limited by its pharmacokinetics and poor solubility, but its more soluble analogue, imidazole ketone erastin (IKE), is metabolically stable and 100× more effective than erastin in some cell lines [44,45]. (1S,3R)-RSL3 (hereafter referred to as RSL3) was first described as a ferroptosis inducer in 2008 and shown to induce a similar phenotype to erastin via GSH-independent mechanisms [46]. In addition to RSL3, another frequently described class 2 ferroptosis inducer is ML162 [47,48]. Both RSL3 and ML162 are covalent inhibitors of GPX4 that bind and inhibit the protein directly [49].

5.4. Ferroptosis Suppressor Protein 1 and the Mevalonate Pathway

Ferroptosis has also been observed independent of GPX4 inhibition, likely due to the presence of other intracellular antioxidant systems. Recently, apoptosis-inducting factor mitochondrial 2 (AIFM2), which has since been renamed ferroptosis suppressor protein 1 (FSP1), has been implicated in resistance to ferroptosis [50,51]. A study by Doll et al. demonstrated that knockout of *FSP1* increased the sensitivity of melanoma (MDA-MD-435S), colorectal cancer (SW620), glioblastoma (U-373), lung cancer (A549 and NCI-H1437) and breast cancer (MDA-MB-436) cells to RSL3 [51]. Furthermore, resistance to RSL3 could be restored by re-expression of mouse *FSP1* in MDA-MB-436 breast cancer cells [51]. *FSP1* knockout in an osteosarcoma cell line (U-2 OS) did not affect GSH levels, suggesting its mechanism of action is independent of xCT or GSH synthesis [50]. The mechanism by which FSP1 mediates resistance to ferroptosis is thought to involve coenzyme Q_{10} (CoQ, also known as ubiquinone), generated by the mevalonate pathway. The mevalonate pathway is a multifaceted biological pathway that leads to the production of isopentenyl pyrophosphate (IPP) as well as CoQ (Figure 2). IPP is involved in the maturation of selenocysteine, an amino acid required for GPX4 translation [25,52]. IPP can also be converted to farnesyl pyrophosphate, which is an important upstream substrate in the generation of CoQ [53]. CoQ is a naturally occurring quinone that is vital to cell and tissue health in most aerobic organisms [54]. Studies have shown that FSP1 reduces CoQ to CoQ_{10}-H_2 (ubiquinol), which is a radical-trapping antioxidant that prevents the accumulation of lipid peroxides associated with ferroptosis (Figure 2) [50,51].

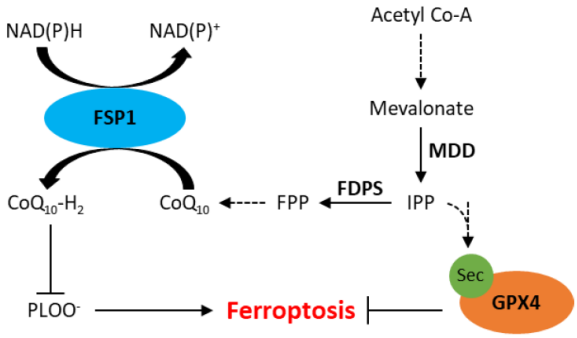

Figure 2. Schematic representation of the mevalonate pathway and its role in inhibition of ferroptosis. CoQ_{10}, ubiquinone; CoQ_{10}-H_2, ubiquinol; FDPS, farnesyl diphosphate synthase; FPP, farnesyl phosphate; FSP1, ferroptosis suppressor protein 1; GPX4, glutathione peroxidase 4; IPP, isopentenyl phosphate; MDD, mevalonate diphosphate decarboxylase; PLOO−, lipid peroxyl radicals; Sec, selenocysteine. Dotted arrows represent multiple steps within a pathway.

6. Clinical Applications of Ferroptosis

6.1. Ferroptosis in MM

Studies have already shown that treating MM cells with high concentrations of iron induces cell death, and this can be rescued by the ferroptosis inhibitor ferrostatin-1 [55]. Despite this, MM cells were shown to be more resistant to erastin-induced ferroptosis compared to another B-cell malignancy, DLBCL, and further investigation into this variation in sensitivity is required [43]. A recent study demonstrated that levels of GPX4 and xCT are higher in MM plasma cells than their healthy counterparts, suggesting MM plasma cells may be utilising this antioxidant pathway to withstand elevations in ROS levels [56]. Increased expression of these two proteins and their crucial roles in ferroptosis suggests they may represent drug targets for the treatment of MM. Furthermore, high expression of ferroptosis suppressor genes was correlated with reduced progression-free and overall survival in MM patients [57]. A number of groups have recently developed ferroptosis-related gene signatures that can be used to predict MM patient prognosis [58], high-risk patients [59] and/or drug sensitivity [60]. Fu et al. went on to show that erastin and doxorubicin synergistically reduced NCI-H929 and RPMI-8226 MM cell viability via GPX4 degradation and subsequent ROS generation [58]. Similarly, ferroptosis induced by GPX4 inhibition (RSL3 or ML162) synergistically decreased proliferation when combined with bortezomib or lenalidomide in RPMI-8226 MM cells [60]. Taken together, it can be seen that genes involved in ferroptosis may be a useful tool to prognosticate MM patients, while ferroptosis-inducing drugs have promise as agents to enhance existing chemotherapies used in the clinic.

The synthetic amino acid BSO has been found to reduce GSH levels in MM cells by inhibiting glutamate–cysteine ligase (GCL), the first enzyme in the GSH synthesis pathway, and increase the efficacy of bortezomib [61]. In bladder carcinoma cells, expression of xCT was found to be upregulated following bortezomib treatment in an Nrf2- and ATF-dependent manner [62]. Since the expression of both Nrf2 and ATF4 transcription factors is associated with poor prognosis and drug resistance in patients with bladder cancers, inhibition of xCT may represent an effective treatment to increase the efficacy of proteasome inhibitors [62]. Further supporting this, GSH degradation by omega-3 fatty acids increased the effects of bortezomib in OPM2 MM cells, and transcriptomic pathway analyses of the treated cells revealed changes in several gene pathways, including ferroptosis [63]. High-dose iron (600 μM ferric ammonium citrate) has also been shown to induce MM cell death and increase the efficacy of bortezomib in vitro and the bortezomib, melphalan and prednisone regimen in a MM mouse model [55]. These effects were again shown to involve ferroptosis in vitro, with increased production of the lipid oxidation by-product MDA and inhibition of cell death by ferrostatin-1 [55].

Lipidomic analyses have shown that AA levels are decreased in the plasma cells of patients with preclinical and early-stage MM [64]. This was confirmed in another analysis showing that although MM patients had higher levels of n-6 PUFAs compared to healthy controls, overall AA levels were reduced [65]. An earlier study, which utilised fluorescently-tagged AA, demonstrated that this fatty acid is readily taken up by MM cells and is primarily incorporated into triglycerides and phospholipids but that this uptake had no effect on proliferation [66]. The mode of transport has since been described to involve fatty acid transporters (FATPs) [67]. More recently, the addition of exogenous AA was associated with dose- and caspase-dependent apoptotic cell death in three MM lines but not healthy human peripheral blood mononuclear cells (PBMCs) [68]. Culturing cells in the presence of AA has also been shown to induce ferroptosis, which could be reversed by ferrostatin-1; the addition of physiological concentrations of AA was shown to decrease the proliferation and viability of primary MM cells and cell lines, with a concomitant decrease in GPX4 expression [69]. It is important to note that while high concentrations of AA can induce death in MM cells, low concentrations have been shown to promote their proliferation. In fact, MM cells induce lipolysis in bone marrow adipocytes and upregulate FATPs in the presence of free FAs [67]. This highlights the need to better understand the

physiological concentrations of AA that are required to induce cell death and improve delivery systems to ensure levels do not drop below the threshold such that cancer cell proliferation is promoted.

With the advent of large-scale, high-throughput drug screening technologies, there has been a rapid increase in the number of drugs that are now known to induce ferroptosis. FTY720 was first developed by structurally modifying the antibiotic myriocin and is now approved by the FDA for the treatment of multiple sclerosis [56]. Initial studies of FTY720 in MM suggested that this compound induces apoptosis and autophagy [70]; however, a more recent study showed that cell death in MM cells following treatment with FTY720 is associated with an accumulation of ROS and can, at least partially, be inhibited by ferrostatin-1 [56]. Furthermore, the study showed that FTY720 reduced expression of GPX4 and xCT in vitro, both at the mRNA and protein levels and concluded that the drug likely induces ferroptosis and autophagy, mediated by the protein phosphatase 2A/AMP-activated protein kinase pathway [56]. The naturally occurring flavone, apigenin and extracts from the plants *Thymus vulgaris*, *Arctium lappa*, *Fumaria officinalis* L. and *Lithospermum erythrorhizon* were also shown to induce cell death in a range of MM cell lines [71–74]. Cell death could be at least partially inhibited with ferrostatin-1, liproxstatin-1 or deferoxamine in all cases, suggesting ferroptosis was involved in the observed response and indicating that naturally derived plant extracts may be useful tools to induce ferroptosis in MM cells.

Recent research in MM has also uncovered a link between ferroptosis and subsequent DNA changes [75]. Induction of ferroptosis in MM results in the upregulation of a multitude of key genes involved in cellular stress, cell death, inflammation and fatty acid metabolism, including the ferritin heavy chain 1 (*FTH1*), ferritin light chain (*FTL*), *HO-1* and *SLC7A11* genes [75]. Of 616 differentially expressed genes identified in MM cells undergoing ferroptosis, the upregulation of 95 genes was inhibited by pre-treating cells with ferrostatin-1 [75]. The 95 genes identified included those that encode zinc finger proteins and genes with roles in metal binding, nuclear receptor signalling and chromatin remodelling [75].

Taken together, these findings demonstrate that MM cells have the capacity to undergo ferroptosis; however, further studies are required to identify combinations and concentrations of ferroptosis-inducing agents that are achievable in vivo to harness the potential of ferroptosis as a clinical strategy.

6.2. Ferroptosis in Lymphoma

DLBCL cells have been shown to be significantly more sensitive to erastin-induced growth inhibition compared to MM and AML cells [43]. This may be explained by the dependence of DLBCL cells on xCT for cysteine uptake, as they are unable to synthesise cysteine from methionine via the transsulfuration pathway [44]. Furthermore, a number of ferroptosis gene signatures, including genes such as *FTH1*, *GPX4*, *STEAP3*, *LPCAT3* and others, have been developed to predict prognosis and overall survival in patients with DLBCL [76–78]. Specifically, the expression of GPX4 was shown to be an independent marker of poor prognosis in DLBCL [79]. Immunohistochemistry was used to examine GPX4 expression in samples from 93 DLBCL patients, and the GPX4 positive group (35%) had significantly lower overall and progression-free survival rates [79]. Interestingly, no significant changes in GPX4 mRNA were observed, suggesting that GPX4 protein expression is regulated by post-transcriptional modification [79]. These findings support the idea that GPX4 may confer a survival advantage on DLBCL cells, possibly through oxidant tolerance and decreased sensitivity to ferroptosis, and that inhibition of GPX4 may represent a potential therapeutic target for patients with high-risk DLBCL disease. A recent study found that treatment of DLBCL cells with dimethyl fumarate depletes the cells of GSH and retards their proliferation and that these effects were potentiated by inhibition of FSP1 [80]. However, significantly higher levels of lipid peroxidation were observed

in DLBCL cells classified as GBC than ABC following treatment with dimethyl fumarate, which may be due to elevated levels of 5-lipoxygenase in the GCB sub-type [80].

Propolis, a resinous product from Western honeybees, has been shown to have anti-tumour properties in a range of cancer types. Recently, extracts from Chinese propolis were shown to induce cell death in the SU-DHL-2 DLBCL cell line, and proteomic changes following drug incubation revealed ferroptosis as the most differentially expressed pathway [81]. The propolis ethanol extract was analysed by ultra-performance liquid chromatography–electrospray ionization mass spectrometry (UPLC-ESI-MS) and determined to contain a variety of flavonoids, phenolic compounds, acylated glycerol and fatty acids. Included in the list of compounds was apigenin which has previously been shown to induce ferroptosis on its own or as a compound in other plant extracts in MM and leukaemic cell lines [71–73]. Another natural compound kayadiol, which is extracted from the pulp of a Japanese tree (*Torreya nucifera*), induced death in extranodal natural killer/T-cell lymphoma (NKTCL) cell lines and peripheral blood lymphocytes (PBLs) extracted from NKTCL patients but not healthy donor PBLs [82].

Sensitivity to ferroptosis varies between different DLBCL cell lines, with the IC_{50} of the erastin analogue, IKE, ranging from 1 nM to almost 100 μM [44]. Consistent with ferroptosis, cell death induced by IKE was associated with a significant increase in levels of lipid peroxidation and MDA and could be inhibited by pre-treating cells with ferrostatin-1 [44]. Similar effects were also observed in a mouse lymphoma model and were associated with a decrease in GSH levels from as early as 4 h after IKE dosing [44]. Decreased tumour volume in mice treated with IKE was consistent with increased MDA levels, which is indicative of lipid peroxidation and suggestive of ferroptosis as a mechanism of cell death. As single agents, the PUFAs AA, eicosapentaenoic acid (EPA) and γ-linolenic acid all caused a decrease in cell viability in the ferroptosis-sensitive DLBCL cell line SU-DHL-6 at high concentrations approaching 100 μM, whereas a lower concentration of 10 μM was sufficient to sensitise the cells to IKE [44]. Conversely, the addition of the MUFAs, oleic acid or palmitoleic acid protected the cells from ferroptosis, which is consistent with earlier reports demonstrating that addition of oleic acid to ferroptosis-sensitive BJeLR (human skin tissue), HT-1080 (fibrosarcoma) and G-401 (rhabdoid kidney tumour) cell lines can prevent RSL3-induced ferroptosis [3,44].

As discussed earlier, iron homeostasis plays a critical role in ferroptosis, and therefore targeting pathways that regulate iron levels may represent an effective treatment approach. A recent study in DLBCL with the small lysosomal iron-targeting molecule, ironomycin, demonstrated that the drug sequesters iron within lysosomes, which leads to the generation of lysosomal ROS, dysfunction of lysosomes and cell death [83]. The observed mechanism of cell death was suspected to be ferroptosis, as levels of cellular GSH were depleted, and the cell death was partially prevented by ferrostatin-1 but not by the necroptosis or apoptosis inhibitors, necrostatin-1 or z-VAD-FMK [83,84], respectively.

Recent studies demonstrate that the cytotoxicity of APR-246 (eprenetapopt), a prodrug that binds mutant *TP53*, is iron-dependent and can be prevented by iron chelators or inhibitors of lipid peroxidation, but not necroptosis, pyroptosis or apoptosis inhibitors in DLBCL cells [85]. Interestingly, the autophagy inhibitor chloroquine was able to prevent APR-246-induced death in OCI-Ly7 cells with mutant *TP53* (missense in exon 7) but not any other DLBCL cell lines. The binding of APR-246 to mutant *TP53* restores the ability of the transcription factor to interact with target genes and, as a result, induces ferritinophagy. APR-246 is also effective at inducing ferroptosis in cells with WT *TP53* through mechanisms thought to be independent of *TP53* [85]. In *Eμ-Myc* mouse lymphoma cells, APR-246 induces apoptosis regardless of *TP53* status but was, however, more effective in WT cells. Ferroptosis was not observed in these cells following APR-246 treatment, but Fer-1 could partially prevent cell death in histiocytic lymphoma cells (BAX/BAK/MLKL KO U937 cells) [86]. Other cancer cell lines and cell death mechanisms were investigated in this study leading to the conclusion that APR-246 can induce a variety of cell death types, including ferroptosis, regardless of *TP53* status [86].

Using computational and experimental approaches, altretamine, an FDA-approved anti-cancer drug used to treat ovarian cancer, was shown to have a similar mechanism of action as the drug sulfasalazine [87]. Unlike sulfasalazine, however, altretamine did not deplete GSH levels in the U2932 DLBCL cell line but did induce a significant increase in oxidised phospholipids, implicating GPX4 as a target of this drug [87]. Artesunate, a derivate of the plant extract artemisinin, is approved by the FDA for malaria treatment and its anticancer effects have been explored and recently revealed to involve ferroptosis. In Burkitt's lymphoma cells, only inhibitors of ferroptosis but not necroptosis or apoptosis could prevent artesunate-induced cytotoxicity. Furthermore, artesunate activity was associated with an increase in general ROS and lipid peroxidation and was revealed to involve the ATF4-CHOP-CHAC1 pathway [88]. Similarly, adult T-cell leukaemia/lymphoma (ATLL) cells in vitro and in a mouse xenograft model underwent ferroptosis as well as caspase-dependent apoptosis and cell cycle arrest following treatment with artesunate [89]. In a panel of DLBCL cell lines and a xenograft mouse model, artesunate induced apoptosis, autophagy and ferroptosis through inhibiting STAT3 signalling, an important pro-survival pathway in cancer cells [90]. Further investigation of already FDA-approved drugs, such as altretamine and artesunate, is warranted, given their involvement in ferroptosis and already known safety and pharmacokinetic profiles.

6.3. Ferroptosis in Leukaemia

6.3.1. Acute Lymphoblastic Leukaemia

ALL cells were shown to undergo ferroptosis following treatment with RSL3 or erastin in combination with the Smac mimetic BV6, which binds proteins that inhibit apoptosis [91]. It has also been shown that lipoxygenases play an important role in ferroptosis in ALL cells, as the lipoxygenase inhibitors, Baicalein, NDGA, Zileuton or PD146176, prevent RSL3-induced cell death [92]. The sensitivity of ALL cells to ferroptosis may be explained by hypermethylation of *FSP1* and downregulation of FSP1 expression at both the mRNA and protein level, which has been shown in several ALL cell lines and patient samples [93]. Furthermore, elevated *FSP1* expression was correlated with significantly worse overall survival in AML but has not yet been demonstrated in ALL [93]. Recent studies have shown that ferroptosis may also be involved in the efficacy of a number of natural plant extracts against ALL cells that are resistant to standard therapeutic agents and difficult-to-treat T-ALL cells [94–97].

6.3.2. Acute Myeloid Leukaemia

There are extensive studies focusing on the potential role of ferroptosis in the treatment of AML. These include investigating the effects of combining erastin with chemotherapy drugs [98] or the ferroptotic effects of other agents, such as the antimalarial drug dihydroartemisinin [99,100], a novel all-trans retinoic acid derivative [101] and the circRNAs circKDM4C, which upregulates ferroptosis [102] and circZBTB46 which prevents ferroptosis [103]. Natural derivatives with ferroptosis-inducing potential in AML have also been identified including a pollen flavonoid extract, typhaneoside [104], a monoterpenoid plant extract, perillaldehyde [105], or the diterpenoid epoxide plant extract, triptolide, which induces ferroptosis to sensitise AML and CML cells to doxorubicin [97]. Inhibitors of aldehyde dehydrogenase 3a2 and GPX4 have also been shown to synergise and induce cell death via ferroptosis in AML cells, both in vitro and in vivo [106].

As discussed earlier, APR-246 induces ferroptosis in DLBCL cells, and this has also been demonstrated in AML cells, independent of *TP53* mutational status [85,107]. Through several methods, using various cell death inhibitors and measuring markers of necroptosis (MLKL phosphorylation) and apoptosis (caspase cleavage), it was determined that APR-246 only induced ferroptosis in AML cells [107]. Furthermore, APR-246 synergised with other ferroptosis inducers in vitro, and while it was ineffective as a single agent in vivo, it effectively reduced tumour burden in mice engrafted with *SLC7A11* KD AML cells [107]. A number of phase II and III clinical trials have investigated APR-246 in combination with

azacitidine for patients with AML or myelodysplastic syndromes (MDS) and mutated p53 (Phase Ib/II Clinical Trials Identifiers: NCT03072043 and NCT03588078, Phase III Clinical Trials identifier: NCT03745716). While ferroptosis was not specifically investigated in these clinical trials, the drugs were well tolerated, and APR-246 enhanced the anti-tumour effects of azacytidine [108–110].

A study by Akiyama et al. demonstrated that high expression of the *SLC7A11* or *GPX4* genes is associated with significantly shorter overall survival rates in AML patients [111]. Zhong et al. also found that along with other ferroptosis-related genes found to be differentially expressed in AML patients, *GPX4* overexpression was again associated with poor prognosis in other publicly available cohorts [112]. This overexpression of GPX4 in AML patients highlighted a potentially efficacious drug target in this cancer, and both studies found that inhibition of GPX4 with ML210 or RSL3 induced the death of AML cells in vitro [111,112]. This is supported by other studies, which have also shown that higher expression of *SLC7A11*, *GPX4* and *LPCAT3* is associated with a worse prognosis in AML, while overexpression of *TFRC*, which encodes the transferrin receptor, was found to protect cells against ferroptosis [113,114]. In children with non-M3 AML, *FTH1* expression is associated with a poor prognosis and is upregulated during the proliferation of AML cell lines [115]. Numerous publications have identified other ferroptosis-related gene signatures, eluding to the relevance of ferroptosis in AML but also indicating the dataset used and other factors may contribute to what genes can be used to predict both prognosis and ferroptosis-sensitivity in AML [116–121].

6.3.3. Chronic Lymphocytic Leukaemia

Primary CLL cells express low levels of xCT and rely on cysteine produced by bone marrow stromal cells to reduce levels of intracellular ROS [122]. The cysteine taken up by CLL cells fuels the production of GSH, which protects the cells from the cytotoxic effects of fludarabine and oxaliplatin. Inhibitors of xCT or depletion of GSH significantly increased the sensitivity of CLL cells to both fludarabine and oxaliplatin [122]. Although the study by Zhang et al. was conducted prior to the description of ferroptosis, the effects of the xCT inhibitor and GSH depletion on cell viability strongly suggest that the cytotoxic effects observed involved ferroptosis. More recently, a study on primary CLL cells and cell lines also showed that treating cells with iron in combination with Bruton's tyrosine kinase (Btk) inhibitor, ibrutinib or the BCL-2 inhibitor, venetoclax, led to a significant accumulation of MDA and death of leukemic, but not healthy, cells [123]. Although apoptosis is understood to be the predominant mechanism of action of both ibrutinib and venetoclax, ferroptosis may also play an important role and potentiate the efficacy of these drugs. A study of a small cohort of 36 patients with CLL identified a ferroptosis-related prognostic score whereby nine genes were associated with worse overall and treatment-free survival [124]. Further mechanistic studies are required to understand whether these genes have a ferroptosis-related function in CLL patients on top of their prognostic value.

6.3.4. Chronic Myeloid Leukaemia

Cysteine depletion in an imatinib-resistant CML cell line (K562/G01) but not WT parental cells (K562) induces ferroptosis [125]. This ferroptosis was associated with the upregulation of the gene encoding thioredoxin reductase 1 (TXNRD1) in K562/G01 cells, a member of the thioredoxin (Trx) system, an important antioxidant and redox regulator [125]. Despite an increase in gene expression, the activity of TXNRD1 was decreased, which was thought to be a result of negative feedback regulation [125]. These findings led the researchers to investigate a shRNA-mediated knockdown of TXNRD1 in WT K562 cells. In these knockdown cells, cysteine depletion caused a decrease in viability which could be prevented by Fer-1, as well as increased ROS and MDA and morphological changes consistent with ferroptotic cell death [125]. The effect of TXNRD1 KD on increasing sensitivity to cysteine depletion suggests the Trx system may play a role in regulating ferroptosis. The drug tetrandrine citrate kills CML cells in vitro and reduces tumour

growth in an imatinib-resistant mouse xenograft model [126], and while ferroptosis was not confirmed as the mechanism of cell death, subsequent studies have shown that tetrandrine citrate does induce ferroptosis in breast cancer cells [127].

7. Potential Nanotechnologies for Induction of Ferroptosis

Emerging nanotechnologies have the potential to significantly improve the targeting, delivery and pharmacokinetic behaviour of drugs while reducing toxicities [128]. Drug delivery is an important determinant of efficacy in the treatment of cancer and has been a limiting factor in the development of therapeutic options, including those that target the ferroptosis pathway. Large molecules pose many issues in drug delivery, including poor solubility, poor absorption, off-target binding and in vivo instability. In the context of ferroptosis, primarily only in vitro studies of erastin and RSL3 have been possible due to poor solubility and toxicities in vivo [41,129]. Although cancer cells are generally more sensitive to ferroptosis, effects against healthy tissue have also been significant. To harness ferroptosis as an approach for cancer therapy, we must develop new means of specifically targeting the tumour cells [130]. Ferroptosis-inducing nanotechnologies have been investigated in cancers of the breast, colon and lung, as well as for neuroblastoma and hepatocellular carcinoma [131–139]. These studies primarily include the use of nanotechnologies such as dendritic mesoporous silica nanoparticles, iron oxide nanoparticles, micelles and liposomes (Figure 3). An important property to consider when designing nanotechnologies, particularly for the treatment of central nervous system (CNS) lymphoma, is their ability to cross the blood–brain barrier (BBB). This is a complex process and depends on nanoparticle size, shape and surface charge, amongst other factors [140]. Overall, in terms of size, nanoparticles up to approximately 20 nm are large enough to avoid renal excretion while being small enough to penetrate the BBB. Moreover, those nanoparticles with a negative (or relatively lower) zeta potential show greater transport through the BBB [140].

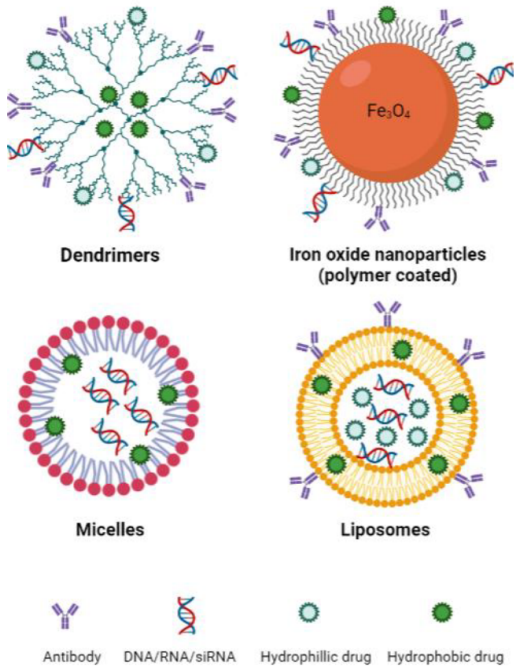

Figure 3. Basic structure of common nanotechnologies used to induce ferroptosis. Sizes: dendrimers 1–10 nm [141], iron oxide nanoparticles 10–20 nm [142], micelles 10–100 nm [143], liposomes 30 nm to several microns [143]. Created with BioRender.com (accessed on 22 March 2023).

Dendrimers are a type of spherical synthetic polymer that has a structure comprised of repeated branching chains expanding from a central core that typically contains exterior functional groups (Figure 3) [143]. Therapeutic cargo can then be encapsulated within the inner space of the dendrimer or bound to the functional groups on the exterior of the polymer. These characteristics make dendrimers highly bioavailable and biodegradable, both of which are important qualities for an efficient drug delivery system [143]. The application of dendrimers in the context of ferroptosis was investigated in pancreatic carcinoma with promising results [144]. Generation 5 poly(amidoamine) (PAMAM) dendrimers were loaded with ferric iron by chelation to hydroxyquinoline-2-carboxylic acid (8-HQC) and plasmid DNA encoding p53. Gold nanoparticles were then entrapped within the inner space of the dendrimer, as this was previously shown to enhance gene delivery efficiency [144]. The dendrimers showed efficacy both in vitro and in vivo, effectively decreasing cell viability and proliferation. Furthermore, they were able to enhance p53 expression and trigger apoptosis while simultaneously inducing ferroptosis by inhibiting xCT and increasing ROS generation through the Fenton reaction [144].

Iron oxide nanoparticles (IONs) are iron-based structures most commonly synthesised through co-precipitation whereby ferric and ferrous iron are mixed at high temperatures at a molar ratio of 1:2 in highly basic solutions to obtain the nanoparticles Fe_3O_4 or γ-Fe_2O_3 [145]. IONs have traditionally been used as drug carriers and contrast agents for both clinical and pre-clinical purposes; however, they have also been used as iron supplements for patients with iron deficiency [146]. The simplistic nature of IONs yields many benefits, notably physical and chemical stability, biocompatibility and environmental safety [142]. The coating of IONs is also common practice, with outer shells, ranging from polymers to bioactive molecules, employed for functionalisation of the nanoparticle, improving stability, biodistribution and pharmacokinetics [142]. An example of an FDA-approved ION is ferumoxytol, used for iron replacement in anaemic patients, which has recently been investigated as an anti-tumour agent [146,147]. The involvement of ferroptosis in the mechanism of action of ferumoxytol is discussed further below.

Micelles, in their most basic form, are amphiphilic molecules (surfactants) arranged spherically in aqueous solutions [148]. Surfactants are classified according to the chemical nature of their polar head and typically contain long hydrocarbon, fluorocarbon or siloxane chains as their hydrophobic tail [148]. The versatility of micelles makes them fantastic for biomedical applications, particularly as drug delivery systems [148]. The two unmatched advantages of micelles when compared to other drug delivery systems are their size and the feasibility of large-scale manufacturing [149]. Gao et al. encapsulated RSL3 in micelles rich in unsaturated FAs, thereby supplementing cells with this known ferroptosis substrate while simultaneously delivering a ferroptosis-inducing agent [150]. The micelles were shown to be more effective at reducing tumour volume in doxorubicin-resistant human ovarian adenocarcinoma-bearing mice compared to drugs administered by more conventional means, and no adverse side effects were observed in mice treated with the micelles [150]. Another group demonstrated that electron-accepting RSL3-loaded micelles were able to reduce intracellular NADPH levels and induce ferroptosis effectively in vitro and in vivo [151]. The combination of electron-accepting micelles and RSL3 induced synergistic NADPH depletion and significantly decreased tumour mass in 4T1 tumour-bearing mice [151].

Liposomes are spherical nanoparticles that range in size from 30 nm to a few microns [143]. Liposomes consist of lipids that form a bilayer resembling that of the plasma membrane and represent a relatively safe and effective method of drug delivery [152,153]. The hydrophobic nature of the lipid bilayer in liposomal nanoparticles enables the incorporation of a wide variety of hydrophilic agents within the aqueous core (Figure 4).

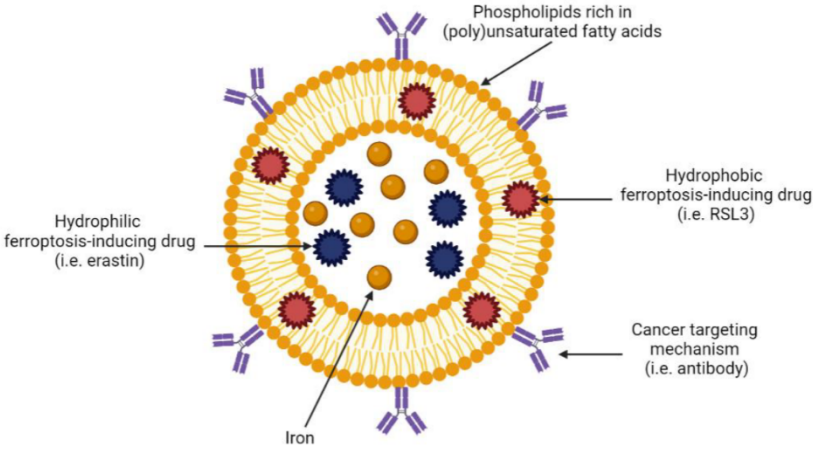

Figure 4. Example of a tumour-targeting, ferroptosis-inducing liposome. Created with BioRender.com (accessed on 27 March 2023).

Liposomes are incredibly versatile as they can be modified with polymers, antibodies or proteins that determine specificity and uptake. For example, liposomes can be coated with antibodies against receptors that are known to be overexpressed on specific cancer cells, thus targeting drug delivery to a specific tumour site and sparing healthy tissue. In the context of ferroptosis, liposomes are particularly appealing as they can be manufactured from specific lipids and fatty acids that are involved in ferroptosis. Table 2 summarises the published literature on ferroptosis-inducing liposomes in solid tumours. Due to a paucity of ferroptosis-inducing, liposome-based nanotechnologies in haematological malignancies, we discuss ferroptosis-inducing nanotechnologies more broadly for these cancers below.

Table 2. Summary of recent liposome technologies aimed at inducing ferroptosis in non-haematological cancers.

Liposome Functionalisation/Contents	Malignancy	Findings	Ferroptosis Measure	Ref.
Folate-modified LPs encapsulating erastin and MT1DP (lncRNA that represses antioxidation) (E/M@FA-LPs)	Human NSCLC	E/M@FA-LPs more effective than erastin and MT1DP alone—decreased cell viability in vitro and reduced tumour volume/weight in vivo.	GSH depletion in vitro and increased MDA in vitro and in vivo.	[154]
Unsaturated fatty acid-rich phosphatidylcholine LPs loaded with ferric ammonium citrate (LPOgener)	Human breast cancer and murine mammary carcinoma	LPOgener effectively killed breast cancer cells, with some toxicity to normal liver cells, while FAC and empty LPs had no effect. A similar trend was seen in a mouse model, and no damage to any organs was observed.	Small mitochondria with condensed membranes in vitro. Increase in oxidised C11-BODIPY in vitro and in vivo.	[155]
MMP2-activated and $ATB^{0,+}$-targeted LP containing sorafenib (inhibits xCT) and DOX (DS@MA-LS)	Murine mammary carcinoma cells (in vitro and in vivo)	DS@MA-LS decreased tumour weight more effectively in vivo compared to free-drug treatment groups. Accumulation of LPs in the liver was not associated with liver injury.	Decrease in GPX4 protein and increase in MDA in vitro.	[156]
LP rich in unsaturated lipids, containing iron and GSH-responsive DOX prodrug (LipoDSSSD)	Murine melanoma	LipoDSSSD effectively killed tumour cells, but not healthy cells in vitro; more effective than other treatment groups at reducing tumour volume/weight in mice.	Increase in oxidised C11-BODIPY and depletion of GSH in vitro.	[157]
Protoporphyrin IX (PpIX) sonosensitiser and ferumoxytol co-loaded LPs (Lipo-PpIX@Ferumoxytol)	Murine mammary carcinoma (in vitro and in vivo)	Lipo-PpIX@Ferumoxytol induced dual ferroptotic and apoptotic cell death in cancer cell lines. The single components of the LP did not induce significant toxicity in cancer cells. Synergistic cell death was also observed in in vivo, as seen by reduced tumour weight and increased survival.	Increases in ROS were observed using DCFH-DA in vitro.	[158]
Ultrasmall active catalysts (UACs, $Cu_xFe_{3-x}O_4$), camptothecin and DOX coated with pH-sensitive LP (LFCCD)	Murine colorectal cancer (in vitro and in vivo)	Ferroptosis induced by UACs synergised with apoptosis induced by the two chemotherapeutic agents resulting in inhibited tumour growth in mice.	Increase in oxidised C11-BODIPY and depletion of GSH in vitro.	[159]

Table 2. *Cont.*

Liposome Functionalisation/Contents	Malignancy	Findings	Ferroptosis Measure	Ref.
CuO_2 & artemisinin loaded LP (Lipo-ART@CPNs)	Murine lung cancer	Lipo-ART@CPNs significantly reduced tumour burden compared to control and when combined with ultrasound irradiation and was the most effective treatment group.	Increase in oxidised C11-BODIPY in vitro. GPX4 protein downregulation in vitro and in vivo.	[160]
PDGFB-targeted, iron-platinum nanoLP containing glucose oxidase (pLFePt-GOx)	Triple-negative breast cancer	The pLFePt-GOx treatment group exhibited the lowest tumour volume in a mouse xenograft model.	Decreased GPX4 expression, increased ROS production in vitro.	[161]
LPs loaded with nanoprobes and superparamagnetic iron oxide (L1/C-Lipo/DS), and LPs with GOx and DOX (L2/C-Lipo/GD)	Murine mammary carcinoma	The combination of the two LPs had a great anti-tumour effect in a metastatic breast cancer mouse model compared to other treatment groups.	Increase in oxidised C11-BODIPY and cell death prevented by Fer-1 in vitro.	[162]
Inhalable biomineralized LP loaded with DHA and pH-responsive calcium phosphate (LDM)	Human lung cancer (in vitro and in vivo)	LDM induced ferroptosis and apoptosis, whereas empty LPs and DHA-only LPs did not. LDM suppressed tumour growth in vivo and did not induce histopathological changes in other organs.	Elevated ROS (DCFH-DA) and alleviation of cell death by Fer-1 and NAC in vitro. Reduced GPX4 expression in vitro and in vivo.	[163]
GSH-triggered LPs rich in unsaturated soybean phospholipids encapsulating ferric ammonium citrate (FC-SPC-lipo)	Murine mammary carcinoma (in vitro and in vivo)	FC-SPC-lipo induced significant lipid ROS and ferroptosis in 4T1 cells and accumulated in tumour tissues in vivo. FC-SPC-lipo reduced tumour volume compared to saline in vivo, whereas empty LPs, free FAC and saturated LPs (FC-HSPC-lipo) did not.	Increase in oxidised C11-BODIPY and decreased GPX4 expression in vitro and in vivo.	[164]
PEGylated LPs loaded with a ferrocene, a Fenton catalyst (Fc-Lp-PEG)	Murine mammary carcinoma (in vitro and in vivo) and glioma in vivo.	Fc-Lp-PEG induced lipid peroxidation and cytotoxicity in cancerous but not normal cell lines. Free Fc and Fc-Lp-PEG showed high tumour inhibition ratio (45.5% and 71%, respectively) and reduced tumour volume in vivo with minimal side effects.	Increased oxidised C11-BODIPY and MDA, decrease in GPX4 and GSH, and morphological changes consistent with ferroptosis by TEM in vitro. Increased MDA in vivo.	[165]
LPs embedded with PEGylated 3 nm γ-Fe_2O_3 nanoparticles (Lp-IO)	Murine mammary carcinoma (in vitro and in vivo)	Lp-IO induced significant lipid peroxidation and ferroptotic cell death in cancer cell lines, while LPs and iron oxide nanoparticles individually did not. Lp-IO inhibited tumour growth in a mouse model and synergised with DOX.	Increase in oxidised C11-BODIPY in vitro and in vivo. Cell death prevented by Fer-1 and Lip-1 in vitro.	[166]
LP containing pH-triggered amphiphilic dendrimer releasing sorafenib and hemin (SH-AD-L)	Human liver cancer (in vitro and in vivo)	SH-AD-L induced ferroptotic cell death in vitro with mild cytotoxic effects in normal liver cells. At high concentrations, S-AD-L (no hemin) induced a slight decrease in cell viability. SH-AD-L treatment decreased tumour growth in vivo.	Increase in oxidised C11-BODIPY and MDA, and cytotoxicity alleviated by Fer-1 in vitro.	[167]

$ATB^{0,+}$, amino acid transporter $B^{0,+}$; DOX, doxorubicin; FAC, ferric ammonium citrate; Fer-1, ferrostatin-1; GSH, glutathione; Lip-1, liproxstatin-1; lncRNA, long non-coding RNA; LP, liposome; MDA, malondialdehyde; MMP2, matrix metalloproteinase 2; MT1DP, metallothionein 1D pseudogene; NAC, N-acetyl-l-cysteine; NSCLC, non-small cell lung cancer PDGFB, platelet-derived growth factor subunit B; TEM, transmission electron microscopy; WT, wild type.

8. Ferroptosis Nanotechnologies in Haematological Malignancies

While there are a limited number of studies that examine the potential of nanotechnologies as a means of inducing ferroptosis in haematological malignancies, there are, however, numerous studies reporting the efficacy of non-ferroptotic nanotechnologies in these cancers, suggesting their utility in this area. One example is pegylated liposomal doxorubicin, or DOXIL, which was the first FDA-approved nanotherapeutic drug for cancer therapy [168]. DOXIL outperformed conventional doxorubicin in terms of clinical efficacy, pharmacokinetics, biodistribution, toxicity and overall improvement in patient quality of life [168]. While no studies to date have examined ferroptosis-targeting nanotechnologies in MM, other nanotechnologies, as well as DOXIL, have shown promise in this malignancy, for example, liposomes containing bortezomib [168–171].

Unlike MM, there are a number of papers investigating ferroptosis-inducing nanotherapies in lymphoma. Zhang et al. showed the effects of the erastin analogue, IKE, on the viability of DLBCL cell lines varied, with IC_{50}s ranging from 1 nM to 100 μM, and that cell death and lipid oxidation following treatment with IKE could be prevented with ferrostatin-1 in SU-DHL-6 cells [44]. IKE was then encapsulated in polyethylene glycol-poly (lactic-co-glycolic acid) (PEG-PLGA) nanoparticles and used to treat mice bearing an SU-DHL-6 xenograft [44]. Although similar effects of free IKE and IKE-containing

nanoparticles were observed on tumour size, weight loss which was used as a measure of toxicity, was only observed in mice treated with free IKE and not in mice treated with IKE nanoparticles. This toxicity was thought to be due to the precipitation of the drug in the peritoneal cavity, while IKE nanoparticles appeared to accumulate mainly in the tumour tissue rather than in the plasma [44].

Nanoparticles may also have the capacity to aid in the induction of ferroptosis by mechanisms other than through drug delivery. For example, a recent study demonstrated that high-density lipoprotein (HDL)-like nanoparticles resulted in cell death of cell lines and primary B-cells of Burkitt's lymphoma, DLBCL and T cell–rich B cell lymphoma through mechanisms consistent with ferroptosis [172]. These HDL-like nanoparticles were manufactured to specifically target scavenger receptor type B1 (SCARDB1), a receptor that mediates cholesterol uptake and results in a compensatory increase in de novo cholesterol synthesis [172]. Consequently, increased cholesterol levels depleted the cells of GPX4 and initiated ferroptosis, which was confirmed using C11-BODIPY as a sensor of lipid ROS and with the ferroptosis inhibitor, ferrostatin-1 [172].

Ferumoxytol is an FDA-approved polyglucose sorbitol carboxymethyl ether-coated ION used for iron replacement which has recently been reported to have anti-tumour activity. Ferumoxytol inhibited cell proliferation in DLBCL cell lines while also inducing a dose-dependent reduction in cell viability, which was originally described as apoptosis. Upon further research, it was determined that ferumoxytol treatment induced an increase in phospholipid ROS by LiperFluo staining, suggesting that ferroptosis contributed to the observed cell death [146]. The mechanism of action of ferumoxytol involves the release of ferrous and ferric iron once the IONs are within macrophages in the liver, spleen and bone marrow, triggering the Fenton reaction and production of ROS [173]. Ferumoxytol treatment in DLBCL mice models inhibited the growth of tumours by inducing ferroptosis in a dose-independent manner, with no significant differences in mice body weight between treatments. Electron microscopy analysis of in vivo samples revealed mitochondrial membrane rupture and reduced mitochondrial cristae, suggestive of ferroptosis [146]. Similar to DLBCL, ferumoxytol induces oxidative stress and cell death in AML cells in vitro [147]. While ferumoxytol has only been approved by the FDA for the treatment of patients with chronic kidney disease and anaemia, the results of this study highlight the potential of ferroptosis-inducing IONs as a treatment for haematological malignancies.

Recently, nanoparticles loaded with a drug that targets N^6-methyl-adenosine (m^6a) RNA methylation were shown to be effective against AML cells both in vitro and in vivo [174]. These nanoparticles were modified to deplete AML cells of GSH and to target the leukaemic cells by conjugation to a peptide that recognises C-type lectin-like molecule-1 (CLL-1), which is overexpressed on AML blasts and stem cells. Cell death was associated with reduced GPX4 activity and increased levels of lipid peroxidation, suggesting ferroptosis was a key mechanism of action of these nanoparticles [174]. A similar approach was taken by Yu et al., who found that AML cells had higher GSH levels and GSH/GSSG ratio than normal haematopoietic cells in a mouse model [175]. They developed a GSH-responsive cysteine polymer-based ferroptosis-inducing nanomedicine (GCFN) and found that the nanomedicine caused GSH depletion through oxidation of GSH through the disulphide group in the cysteine polymer. An increase in MDA, BODIPY-C11 staining and the ability of Fer-1 to prevent death and cell proliferation inhibition indicated the involvement of ferroptosis. Furthermore, GCFN specifically targeted the bone marrow and spleen of an AML mouse model where leukemic cells are most abundantly found, while uptake in WT mice was mostly localised to the liver. In the bone marrow specifically, 97.6% leukaemic stem cells and 84.6% AML cells took up fluorescently labelled GCFN, while of the haematopoietic stem and progenitor cells (HSPCs) and other immune cell populations, less than 15% took up the nanomedicine. While this nanomedicine was not specifically generated to target leukaemic cells, it was thought that their proclivity for cysteine uptake was behind this cancer-targeting quality [175].

9. Conclusions

Haematological malignancies affect thousands of people worldwide every year, and despite many therapeutic advances, a significant proportion of patients will relapse with the drug-refractory disease. Ferroptosis represents a potential approach for treating a range of cancers, particularly those that do not respond to standard chemotherapies, which generally induce apoptosis. The ever-growing number of studies on ferroptosis since first being described in 2012 has greatly increased our understanding of this mechanism of cell death. However, further work is required to define how ferroptosis is regulated and determine why there is such variability in sensitivity between different cancers and sometimes even within the same cancer. This is crucial for the development of novel treatment approaches that harness the potential of ferroptosis.

The main factors limiting pre-clinical and clinical trials of ferroptosis-mediated therapies are the poor pharmacokinetics and toxicities associated with bona fide ferroptosis inducers. Nanotechnologies designed to target and precisely deliver drugs to tumour cells specifically may be one approach to improving specificity and increasing bioavailability. We have discussed many of the studies to date that have described different nanotechnologies that may be applicable in this context, including liposomes, which enable the targeted delivery of relevant lipids and encapsulated ferroptosis-inducing compounds to tumour cells. Combinations of ferroptosis-inducing compounds with current chemotherapies that are predominantly inducers of apoptosis have also been shown to have potent anti-tumour effects. This suggests that low doses of ferroptosis-inducing compounds may be effective when used in conjunction with existing chemotherapeutic regimens, possibly reducing toxicities and the development of drug resistance. It is envisaged that with further research, a class of ferroptosis-inducing, anti-cancer nanotherapeutics will find its place alongside other novel cancer drug classes, including monoclonal antibodies, antibody-drug conjugates and CAR-T cells.

Author Contributions: R.L.M., A.H., O.G.B. and C.T.W.-G. each undertook reviews of the scientific literature and contributed to the writing of the manuscript. All authors have read and agreed to the published version of the manuscript.

Funding: This work was supported by an Australian Government Research Training Scholarship (RLM), Jane Ramsey, Ph.D. Scholarship in Multiple Myeloma Research (AH), Flinders Foundation Cancer Seed Grant (OGB and CWG), Cancer Council SA Beat Cancer Project Clinical Investigator Award (CWG), and a Servier Staff Research Establishment Fellowship from the Royal Australasian College of Physicians (CWG).

Data Availability Statement: Data sharing not applicable.

Conflicts of Interest: The authors declare no conflict of interest.

References

1. Dixon, S.J.; Lemberg, K.M.; Lamprecht, M.R.; Skouta, R.; Zaitsev, E.M.; Gleason, C.E.; Patel, D.N.; Bauer, A.J.; Cantley, A.M.; Yang, W.S.; et al. Ferroptosis: An iron-dependent form of nonapoptotic cell death. *Cell* **2012**, *149*, 1060–1072. [CrossRef] [PubMed]
2. Stockwell, B.R.; Friedmann Angeli, J.P.; Bayir, H.; Bush, A.I.; Conrad, M.; Dixon, S.J.; Fulda, S.; Gascon, S.; Hatzios, S.K.; Kagan, V.E.; et al. Ferroptosis: A Regulated Cell Death Nexus Linking Metabolism, Redox Biology, and Disease. *Cell* **2017**, *171*, 273–285. [CrossRef] [PubMed]
3. Yang, W.S.; Kim, K.J.; Gaschler, M.M.; Patel, M.; Shchepinov, M.S.; Stockwell, B.R. Peroxidation of polyunsaturated fatty acids by lipoxygenases drives ferroptosis. *Proc. Natl. Acad. Sci. USA* **2016**, *113*, E4966–E4975. [CrossRef] [PubMed]
4. Wallington-Beddoe, C.T.; Mynott, R.L. Prognostic and predictive biomarker developments in multiple myeloma. *J. Hematol. Oncol.* **2021**, *14*, 151. [CrossRef]
5. Ebert, L.M.; Vandyke, K.; Johan, M.Z.; DeNichilo, M.; Tan, L.Y.; Myo Min, K.K.; Weimann, B.M.; Ebert, B.W.; Pitson, S.M.; Zannettino, A.C.W.; et al. Desmoglein-2 expression is an independent predictor of poor prognosis patients with multiple myeloma. *Mol. Oncol.* **2022**, *16*, 1221–1240. [CrossRef]
6. Palumbo, A.; Chanan-Khan, A.; Weisel, K.; Nooka, A.K.; Masszi, T.; Beksac, M.; Spicka, I.; Hungria, V.; Munder, M.; Mateos, M.V.; et al. Daratumumab, Bortezomib, and Dexamethasone for Multiple Myeloma. *N. Engl. J. Med.* **2016**, *375*, 754–766. [CrossRef]

7. Kumar, S.K.; Harrison, S.J.; Cavo, M.; de la Rubia, J.; Popat, R.; Gasparetto, C.; Hungria, V.; Salwender, H.; Suzuki, K.; Kim, I.; et al. Venetoclax or placebo in combination with bortezomib and dexamethasone in patients with relapsed or refractory multiple myeloma (BELLINI): A randomised, double-blind, multicentre, phase 3 trial. *Lancet Oncol.* **2020**, *21*, 1630–1642. [CrossRef]
8. Liu, Q.; Zhao, Y.; Zhou, H.; Chen, C. Ferroptosis: Challenges and opportunities for nanomaterials in cancer therapy. *Regen. Biomater.* **2023**, *10*, rbad004. [CrossRef]
9. Rajkumar, S.V.; Kumar, S. Multiple Myeloma: Diagnosis and Treatment. *Mayo Clin. Proc.* **2016**, *91*, 101–119. [CrossRef]
10. Australian Institute of Health and Welfare. Cancer data in Australia. Available online: https://www.aihw.gov.au/reports/cancer/cancer-data-in-australia/contents/summary (accessed on 1 September 2022).
11. Kumar, S.K.; Rajkumar, S.V.; Dispenzieri, A.; Lacy, M.Q.; Hayman, S.R.; Buadi, F.K.; Zeldenrust, S.R.; Dingli, D.; Russell, S.J.; Lust, J.A.; et al. Improved survival in multiple myeloma and the impact of novel therapies. *Blood* **2008**, *111*, 2516–2520. [CrossRef]
12. Kazandjian, D.; Landgren, O. A new era of novel immunotherapies for multiple myeloma. *Lancet* **2021**, *398*, 642–643. [CrossRef]
13. Mynott, R.L.; Wallington-Beddoe, C.T. Drug and Solute Transporters in Mediating Resistance to Novel Therapeutics in Multiple Myeloma. *ACS Pharmacol. Transl. Sci.* **2021**, *4*, 1050–1065. [CrossRef] [PubMed]
14. Lewis, W.D.; Lilly, S.; Jones, K.L. Lymphoma: Diagnosis and Treatment. *Am. Fam. Physician* **2020**, *101*, 34–41. [PubMed]
15. Shanbhag, S.; Ambinder, R.F. Hodgkin lymphoma: A review and update on recent progress. *CA Cancer J. Clin.* **2018**, *68*, 116–132. [CrossRef]
16. Sehn, L.H.; Salles, G. Diffuse Large B-Cell Lymphoma. *N. Engl. J. Med.* **2021**, *384*, 842–858. [CrossRef] [PubMed]
17. Li, S.; Young, K.H.; Medeiros, L.J. Diffuse large B-cell lymphoma. *Pathology* **2018**, *50*, 74–87. [CrossRef]
18. Kim, H.; Kim, H.J.; Kim, S.H. Diagnostic Approach for Double-Hit and Triple-Hit Lymphoma Based on Immunophenotypic and Cytogenetic Characteristics of Bone Marrow Specimens. *Ann. Lab. Med.* **2020**, *40*, 361–369. [CrossRef]
19. Petrich, A.M.; Gandhi, M.; Jovanovic, B.; Castillo, J.J.; Rajguru, S.; Yang, D.T.; Shah, K.A.; Whyman, J.D.; Lansigan, F.; Hernandez-Ilizaliturri, F.J.; et al. Impact of induction regimen and stem cell transplantation on outcomes in double-hit lymphoma: A multicenter retrospective analysis. *Blood* **2014**, *124*, 2354–2361. [CrossRef]
20. Riedell, P.A.; Smith, S.M. Double hit and double expressors in lymphoma: Definition and treatment. *Cancer* **2018**, *124*, 4622–4632. [CrossRef]
21. Chennamadhavuni, A.; Lyengar, V.; Shimanovsky, A. *Leukemia*; StatPearls: Treasure Island, FL, USA, 2022.
22. Beckmann, K.; Kearney, B.A.; Yeung, D.; Hiwase, D.; Li, M.; Roder, D.M. Changes in five-year survival for people with acute leukaemia in South Australia, 1980—2016. *Med. J. Aust.* **2022**, *216*, 296–302. [CrossRef]
23. Gong, H.; Li, H.; Yang, Q.; Zhang, G.; Liu, H.; Ma, Z.; Peng, H.; Nie, L.; Xiao, X.; Liu, J. A Ferroptosis Molecular Subtype-Related Signature for Predicting Prognosis and Response to Chemotherapy in Patients with Chronic Lymphocytic Leukemia. *BioMed Res. Int.* **2022**, *2022*, 5646275. [CrossRef] [PubMed]
24. Granatowicz, A.; Piatek, C.I.; Moschiano, E.; El-Hemaidi, I.; Armitage, J.D.; Akhtari, M. An Overview and Update of Chronic Myeloid Leukemia for Primary Care Physicians. *Korean J. Fam. Med.* **2015**, *36*, 197–202. [CrossRef] [PubMed]
25. Yang, W.S.; Stockwell, B.R. Ferroptosis: Death by Lipid Peroxidation. *Trends Cell Biol.* **2016**, *26*, 165–176. [CrossRef] [PubMed]
26. Battaglia, A.M.; Chirillo, R.; Aversa, I.; Sacco, A.; Costanzo, F.; Biamonte, F. Ferroptosis and Cancer: Mitochondria Meet the "Iron Maiden" Cell Death. *Cells* **2020**, *9*, 1505. [CrossRef]
27. Tang, H.M.; Tang, H.L. Cell recovery by reversal of ferroptosis. *Biol. Open* **2019**, *8*, bio043182. [CrossRef]
28. Chiang, S.-K.; Chen, S.-E.; Chang, L.-C. A Dual Role of Heme Oxygenase-1 in Cancer Cells. *Int. J. Mol. Sci.* **2018**, *20*, 39. [CrossRef]
29. Cao, J.Y.; Dixon, S.J. Mechanisms of ferroptosis. *Cell Mol. Life Sci.* **2016**, *73*, 2195–2209. [CrossRef]
30. Dev, S.; Babitt, J.L. Overview of iron metabolism in health and disease. *Hemodial. Int.* **2017**, *21* (Suppl. 1), S6–S20. [CrossRef]
31. MacKenzie, E.L.; Iwasaki, K.; Tsuji, Y. Intracellular iron transport and storage: From molecular mechanisms to health implications. *Antioxid Redox Signal* **2008**, *10*, 997–1030. [CrossRef]
32. Ayala, A.; Munoz, M.F.; Arguelles, S. Lipid peroxidation: Production, metabolism, and signaling mechanisms of malondialdehyde and 4-hydroxy-2-nonenal. *Oxid. Med. Cell Longev.* **2014**, *2014*, 360438. [CrossRef]
33. Shintoku, R.; Takigawa, Y.; Yamada, K.; Kubota, C.; Yoshimoto, Y.; Takeuchi, T.; Koshiishi, I.; Torii, S. Lipoxygenase-mediated generation of lipid peroxides enhances ferroptosis induced by erastin and RSL3. *Cancer Sci.* **2017**, *108*, 2187–2194. [CrossRef] [PubMed]
34. Liu, J.; Zhang, C.; Wang, J.; Hu, W.; Feng, Z. The Regulation of Ferroptosis by Tumor Suppressor p53 and its Pathway. *Int J Mol Sci* **2020**, *21*, 8387. [CrossRef]
35. Gaschler, M.M.; Stockwell, B.R. Lipid peroxidation in cell death. *Biochem. Biophys. Res. Commun.* **2017**, *482*, 419–425. [CrossRef] [PubMed]
36. Conrad, M.; Kagan, V.E.; Bayir, H.; Pagnussat, G.C.; Head, B.; Traber, M.G.; Stockwell, B.R. Regulation of lipid peroxidation and ferroptosis in diverse species. *Genes Dev.* **2018**, *32*, 602–619. [CrossRef] [PubMed]
37. Beatty, A.; Singh, T.; Tyurina, Y.Y.; Tyurin, V.A.; Samovich, S.; Nicolas, E.; Maslar, K.; Zhou, Y.; Cai, K.Q.; Tan, Y.; et al. Ferroptotic cell death triggered by conjugated linolenic acids is mediated by ACSL1. *Nat. Commun.* **2021**, *12*, 2244. [CrossRef] [PubMed]
38. Kagan, V.E.; Mao, G.; Qu, F.; Angeli, J.P.; Doll, S.; Croix, C.S.; Dar, H.H.; Liu, B.; Tyurin, V.A.; Ritov, V.B.; et al. Oxidized arachidonic and adrenic PEs navigate cells to ferroptosis. *Nat. Chem. Biol.* **2017**, *13*, 81–90. [CrossRef] [PubMed]

39. Magtanong, L.; Ko, P.J.; To, M.; Cao, J.Y.; Forcina, G.C.; Tarangelo, A.; Ward, C.C.; Cho, K.; Patti, G.J.; Nomura, D.K.; et al. Exogenous Monounsaturated Fatty Acids Promote a Ferroptosis-Resistant Cell State. *Cell Chem. Biol.* **2019**, *26*, 420–432.e429. [CrossRef]
40. Koppula, P.; Zhang, Y.; Zhuang, L.; Gan, B. Amino acid transporter SLC7A11/xCT at the crossroads of regulating redox homeostasis and nutrient dependency of cancer. *Cancer Commun.* **2018**, *38*, 12. [CrossRef]
41. Jiang, X.; Stockwell, B.R.; Conrad, M. Ferroptosis: Mechanisms, biology and role in disease. *Nat. Rev. Mol. Cell Biol.* **2021**, *22*, 266–282. [CrossRef]
42. Seibt, T.M.; Proneth, B.; Conrad, M. Role of GPX4 in ferroptosis and its pharmacological implication. *Free Radic Biol. Med.* **2019**, *133*, 144–152. [CrossRef]
43. Yang, W.S.; SriRamaratnam, R.; Welsch, M.E.; Shimada, K.; Skouta, R.; Viswanathan, V.S.; Cheah, J.H.; Clemons, P.A.; Shamji, A.F.; Clish, C.B.; et al. Regulation of ferroptotic cancer cell death by GPX4. *Cell* **2014**, *156*, 317–331. [CrossRef] [PubMed]
44. Zhang, Y.; Tan, H.; Daniels, J.D.; Zandkarimi, F.; Liu, H.; Brown, L.M.; Uchida, K.; O'Connor, O.A.; Stockwell, B.R. Imidazole Ketone Erastin Induces Ferroptosis and Slows Tumor Growth in a Mouse Lymphoma Model. *Cell Chem. Biol.* **2019**, *26*, 623–633.e629. [CrossRef] [PubMed]
45. Sato, M.; Kusumi, R.; Hamashima, S.; Kobayashi, S.; Sasaki, S.; Komiyama, Y.; Izumikawa, T.; Conrad, M.; Bannai, S.; Sato, H. The ferroptosis inducer erastin irreversibly inhibits system xc− and synergizes with cisplatin to increase cisplatin's cytotoxicity in cancer cells. *Sci. Rep.* **2018**, *8*, 968. [CrossRef] [PubMed]
46. Yang, W.S.; Stockwell, B.R. Synthetic lethal screening identifies compounds activating iron-dependent, nonapoptotic cell death in oncogenic-RAS-harboring cancer cells. *Chem. Biol.* **2008**, *15*, 234–245. [CrossRef]
47. Feng, H.; Stockwell, B.R. Unsolved mysteries: How does lipid peroxidation cause ferroptosis? *PLoS Biol.* **2018**, *16*, e2006203. [CrossRef]
48. Yu, H.; Guo, P.; Xie, X.; Wang, Y.; Chen, G. Ferroptosis, a new form of cell death, and its relationships with tumourous diseases. *J. Cell Mol. Med.* **2017**, *21*, 648–657. [CrossRef]
49. Moosmayer, D.; Hilpmann, A.; Hoffmann, J.; Schnirch, L.; Zimmermann, K.; Badock, V.; Furst, L.; Eaton, J.K.; Viswanathan, V.S.; Schreiber, S.L.; et al. Crystal structures of the selenoprotein glutathione peroxidase 4 in its apo form and in complex with the covalently bound inhibitor ML162. *Acta Cryst. D Struct. Biol.* **2021**, *77*, 237–248. [CrossRef]
50. Bersuker, K.; Hendricks, J.M.; Li, Z.; Magtanong, L.; Ford, B.; Tang, P.H.; Roberts, M.A.; Tong, B.; Maimone, T.J.; Zoncu, R.; et al. The CoQ oxidoreductase FSP1 acts parallel to GPX4 to inhibit ferroptosis. *Nature* **2019**, *575*, 688–692. [CrossRef]
51. Doll, S.; Freitas, F.P.; Shah, R.; Aldrovandi, M.; da Silva, M.C.; Ingold, I.; Goya Grocin, A.; Xavier da Silva, T.N.; Panzilius, E.; Scheel, C.H.; et al. FSP1 is a glutathione-independent ferroptosis suppressor. *Nature* **2019**, *575*, 693–698. [CrossRef]
52. Warner, G.J.; Berry, M.J.; Moustafa, M.E.; Carlson, B.A.; Hatfield, D.L.; Faust, J.R. Inhibition of selenoprotein synthesis by selenocysteine tRNA[Ser]Sec lacking isopentenyladenosine. *J. Biol. Chem.* **2000**, *275*, 28110–28119. [CrossRef]
53. Turunen, M.; Olsson, J.; Dallner, G. Metabolism and function of coenzyme Q. *Biochim. Biophys. Acta* **2004**, *1660*, 171–199. [CrossRef] [PubMed]
54. Saini, R. Coenzyme Q10: The essential nutrient. *J. Pharm. Bioallied Sci.* **2011**, *3*, 466–467. [CrossRef] [PubMed]
55. Bordini, J.; Morisi, F.; Cerruti, F.; Cascio, P.; Camaschella, C.; Ghia, P.; Campanella, A. Iron Causes Lipid Oxidation and Inhibits Proteasome Function in Multiple Myeloma Cells: A Proof of Concept for Novel Combination Therapies. *Cancers* **2020**, *12*, 970. [CrossRef]
56. Zhong, Y.; Tian, F.; Ma, H.; Wang, H.; Yang, W.; Liu, Z.; Liao, A. FTY720 induces ferroptosis and autophagy via PP2A/AMPK pathway in multiple myeloma cells. *Life Sci.* **2020**, *260*, 118077. [CrossRef] [PubMed]
57. Su, Q.; Li, Q.; Zhang, W.; Li, B.; Zhuang, W. Integrative analysis of enrichment and prognostic value of ferroptosis-related genes and pathways in multiple myeloma. *Carcinogenesis* **2022**, *43*, 1050–1058. [CrossRef]
58. Fu, B.; Shao, R.; Wang, H.; Chen, G.; Bai, S.; Wang, H. Integrated assessment of the clinical and biological value of ferroptosis-related genes in multiple myeloma. *Cancer Cell Int.* **2022**, *22*, 326. [CrossRef]
59. Qin, J.; Sharma, A.; Wang, Y.; Tobar-Tosse, F.; Dakal, T.C.; Liu, H.; Liu, H.; Ke, B.; Kong, C.; Liu, T.; et al. Systematic discrimination of the repetitive genome in proximity of ferroptosis genes and a novel prognostic signature correlating with the oncogenic lncRNA CRNDE in multiple myeloma. *Front. Oncol.* **2022**, *12*, 1026153. [CrossRef]
60. Gao, D.; Liu, R.; Lv, Y.; Feng, Y.; Hong, F.; Xu, X.; Hu, J.; He, A.; Yang, Y. A novel ferroptosis-related gene signature for predicting prognosis in multiple myeloma. *Front. Oncol.* **2023**, *13*, 999688. [CrossRef]
61. Nerini-Molteni, S.; Ferrarini, M.; Cozza, S.; Caligaris-Cappio, F.; Sitia, R. Redox homeostasis modulates the sensitivity of myeloma cells to bortezomib. *Br. J. Haematol.* **2008**, *141*, 494–503. [CrossRef]
62. Ye, P.; Mimura, J.; Okada, T.; Sato, H.; Liu, T.; Maruyama, A.; Ohyama, C.; Itoh, K. Nrf2- and ATF4-dependent upregulation of xCT modulates the sensitivity of T24 bladder carcinoma cells to proteasome inhibition. *Mol. Cell Biol.* **2014**, *34*, 3421–3434. [CrossRef]
63. Chen, J.; Zaal, E.A.; Berkers, C.R.; Ruijtenbeek, R.; Garssen, J.; Redegeld, F.A. Omega-3 Fatty Acids DHA and EPA Reduce Bortezomib Resistance in Multiple Myeloma Cells by Promoting Glutathione Degradation. *Cells* **2021**, *10*, 2287. [CrossRef] [PubMed]
64. Panaroni, C.; Fulzele, K.; Soucy, R.; Siu, K.T.; Mukaihara, K.; Huang, C.; Chattopadhyay, S.; Raje, N. Arachidonic Acid Induces Ferroptosis-Mediated Cell-Death in Multiple Myeloma. *Blood* **2018**, *132*, 4498. [CrossRef]

65. Jurczyszyn, A.; Czepiel, J.; Gdula-Argasińska, J.; Paśko, P.; Czapkiewicz, A.; Librowski, T.; Perucki, W.; Butrym, A.; Castillo, J.J.; Skotnicki, A.B. Plasma fatty acid profile in multiple myeloma patients. *Leuk. Res.* **2015**, *39*, 400–405. [CrossRef] [PubMed]
66. Desplat, V.; Dulery, C.; Praloran, V.; Denizot, Y. Incorporation and Effect of Arachidonic Acid on the Growth of Human Myeloma Cell Lines. *Mediat. Inflamm.* **1999**, *8*, 968415. [CrossRef]
67. Panaroni, C.; Fulzele, K.; Mori, T.; Siu, K.T.; Onyewadume, C.; Maebius, A.; Raje, N. Multiple myeloma cells induce lipolysis in adipocytes and uptake fatty acids through fatty acid transporter proteins. *Blood* **2022**, *139*, 876–888. [CrossRef]
68. Abdi, J.; Garssen, J.; Faber, J.; Redegeld, F.A. Omega-3 fatty acids, EPA and DHA induce apoptosis and enhance drug sensitivity in multiple myeloma cells but not in normal peripheral mononuclear cells. *J. Nutr. Biochem.* **2014**, *25*, 1254–1262. [CrossRef]
69. Panaroni, C.; Fulzele, K.; Soucy, R.; Huang, C.; Mukaihara, K.; Chattopadhyay, S.; Raje, N.S. Polyunsaturated Fatty Acid (PUFA) Signaling Induces Ferroptosis-Mediated Cell-Death in Multiple Myeloma. *Blood* **2019**, *134*, 3108. [CrossRef]
70. Liao, A.; Hu, R.; Zhao, Q.; Li, J.; Li, Y.; Yao, K.; Zhang, R.; Wang, H.; Yang, W.; Liu, Z. Autophagy induced by FTY720 promotes apoptosis in U266 cells. *Eur. J. Pharm. Sci.* **2012**, *45*, 600–605. [CrossRef]
71. Adham, A.N.; Hegazy, M.E.F.; Naqishbandi, A.M.; Efferth, T. Induction of Apoptosis, Autophagy and Ferroptosis by Thymus vulgaris and Arctium lappa Extract in Leukemia and Multiple Myeloma Cell Lines. *Molecules* **2020**, *25*, 5016. [CrossRef]
72. Adham, A.N.; Abdelfatah, S.; Naqishbandi, A.M.; Mahmoud, N.; Efferth, T. Cytotoxicity of apigenin toward multiple myeloma cell lines and suppression of iNOS and COX-2 expression in STAT1-transfected HEK293 cells. *Phytomedicine* **2021**, *80*, 153371. [CrossRef]
73. Adham, A.N.; Naqishbandi, A.M.; Efferth, T. Cytotoxicity and apoptosis induction by Fumaria officinalis extracts in leukemia and multiple myeloma cell lines. *J. Ethnopharmacol.* **2021**, *266*, 113458. [CrossRef] [PubMed]
74. Li, W.; Fu, H.; Fang, L.; Chai, H.; Gao, T.; Chen, Z.; Qian, S. Shikonin induces ferroptosis in multiple myeloma via GOT1-mediated ferritinophagy. *Front. Oncol.* **2022**, *12*, 1025067. [CrossRef] [PubMed]
75. Logie, E.; Van Puyvelde, B.; Cuypers, B.; Schepers, A.; Berghmans, H.; Verdonck, J.; Laukens, K.; Godderis, L.; Dhaenens, M.; Deforce, D.; et al. Ferroptosis Induction in Multiple Myeloma Cells Triggers DNA Methylation and Histone Modification Changes Associated with Cellular Senescence. *Int. J. Mol. Sci.* **2021**, *22*, 12234. [CrossRef] [PubMed]
76. Weng, J.; Chen, L.; Liu, H.; Yang, X.-P.; Huang, L. Ferroptosis Markers Predict the Survival, Immune Infiltration, and Ibrutinib Resistance of Diffuse Large B cell Lymphoma. *Inflammation* **2022**, *45*, 1146–1161. [CrossRef] [PubMed]
77. Chen, X.; Hu, S.; Han, Y.; Cai, Y.; Lu, T.; Hu, X.; Chu, Y.; Zhou, X.; Wang, X. Ferroptosis-related STEAP3 acts as predictor and regulator in diffuse large B cell lymphoma through immune infiltration. *Clin. Exp. Med.* **2023**, 1–17. [CrossRef]
78. Wu, H.; Zhang, J.; Fu, L.; Wu, R.; Gu, Z.; Yin, C.; He, K. Identification and Development of a 4-Gene Ferroptosis Signature Predicting Overall Survival for Diffuse Large B-Cell Lymphoma. *Technol. Cancer Res. Treat.* **2023**, *22*, 15330338221147772. [CrossRef]
79. Kinowaki, Y.; Kurata, M.; Ishibashi, S.; Ikeda, M.; Tatsuzawa, A.; Yamamoto, M.; Miura, O.; Kitagawa, M.; Yamamoto, K. Glutathione peroxidase 4 overexpression inhibits ROS-induced cell death in diffuse large B-cell lymphoma. *Lab. Investig.* **2018**, *98*, 609–619. [CrossRef]
80. Schmitt, A.; Xu, W.; Bucher, P.; Grimm, M.; Konantz, M.; Horn, H.; Zapukhlyak, M.; Berning, P.; Brandle, M.; Jarboui, M.A.; et al. Dimethyl fumarate induces ferroptosis and impairs NF-kappaB/STAT3 signaling in DLBCL. *Blood* **2021**, *138*, 871–884. [CrossRef]
81. Liu, X.; Tian, Y.; Yang, A.; Zhang, C.; Miao, X.; Yang, W. Antitumor Effects of Poplar Propolis on DLBCL SU-DHL-2 Cells. *Foods* **2023**, *12*, 283. [CrossRef]
82. He, C.; Wang, C.; Liu, H.; Shan, B. Kayadiol exerted anticancer effects through p53-mediated ferroptosis in NKTCL cells. *BMC Cancer* **2022**, *22*, 724. [CrossRef]
83. Devin, J.; Caneque, T.; Lin, Y.L.; Mondoulet, L.; Veyrune, J.L.; Abouladze, M.; Garcia De Paco, E.; Karmous Gadacha, O.; Cartron, G.; Pasero, P.; et al. Targeting Cellular Iron Homeostasis with Ironomycin in Diffuse Large B-cell Lymphoma. *Cancer Res.* **2022**, *82*, 998–1012. [CrossRef] [PubMed]
84. Mai, T.T.; Hamai, A.; Hienzsch, A.; Caneque, T.; Muller, S.; Wicinski, J.; Cabaud, O.; Leroy, C.; David, A.; Acevedo, V.; et al. Salinomycin kills cancer stem cells by sequestering iron in lysosomes. *Nat. Chem.* **2017**, *9*, 1025–1033. [CrossRef] [PubMed]
85. Hong, Y.; Ren, T.; Wang, X.; Liu, X.; Fei, Y.; Meng, S.; Han, X.; Sun, C.; Shen, H.; Li, L.; et al. APR-246 triggers ferritinophagy and ferroptosis of diffuse large B-cell lymphoma cells with distinct TP53 mutations. *Leukemia* **2022**, *36*, 2269–2280. [CrossRef]
86. Wang, Z.; Hu, H.; Heitink, L.; Rogers, K.; You, Y.; Tan, T.; Suen, C.L.W.; Garnham, A.; Chen, H.; Lieschke, E.; et al. The anti-cancer agent APR-246 can activate several programmed cell death processes to kill malignant cells. *Cell Death Differ.* **2023**, *30*, 1033–1046. [CrossRef] [PubMed]
87. Woo, J.H.; Shimoni, Y.; Yang, W.S.; Subramaniam, P.; Iyer, A.; Nicoletti, P.; Rodríguez Martínez, M.; López, G.; Mattioli, M.; Realubit, R.; et al. Elucidating Compound Mechanism of Action by Network Perturbation Analysis. *Cell* **2015**, *162*, 441–451. [CrossRef]
88. Wang, N.; Zeng, G.-Z.; Yin, J.-L.; Bian, Z.-X. Artesunate activates the ATF4-CHOP-CHAC1 pathway and affects ferroptosis in Burkitt's Lymphoma. *Biochem. Biophys. Res. Commun.* **2019**, *519*, 533–539. [CrossRef]
89. Ishikawa, C.; Senba, M.; Mori, N. Evaluation of artesunate for the treatment of adult T-cell leukemia/lymphoma. *Eur. J. Pharmacol.* **2020**, *872*, 172953. [CrossRef]
90. Chen, Y.; Wang, F.; Wu, P.; Gong, S.; Gao, J.; Tao, H.; Shen, Q.; Wang, S.; Zhou, Z.; Jia, Y. Artesunate induces apoptosis, autophagy and ferroptosis in diffuse large B cell lymphoma cells by impairing STAT3 signaling. *Cell. Signal.* **2021**, *88*, 110167. [CrossRef]

91. Dächert, J.; Schoeneberger, H.; Rohde, K.; Fulda, S. RSL3 and Erastin differentially regulate redox signaling to promote Smac mimetic-induced cell death. *Oncotarget* **2016**, *7*, 63779–63792. [CrossRef]
92. Probst, L.; Dächert, J.; Schenk, B.; Fulda, S. Lipoxygenase inhibitors protect acute lymphoblastic leukemia cells from ferroptotic cell death. *Biochem. Pharmacol.* **2017**, *140*, 41–52. [CrossRef]
93. Pontel, L.B.; Bueno-Costa, A.; Morellato, A.E.; Carvalho Santos, J.; Roue, G.; Esteller, M. Acute lymphoblastic leukemia necessitates GSH-dependent ferroptosis defenses to overcome FSP1-epigenetic silencing. *Redox Biol* **2022**, *55*, 102408. [CrossRef] [PubMed]
94. Mbaveng, A.T.; Fotso, G.W.; Ngnintedo, D.; Kuete, V.; Ngadjui, B.T.; Keumedjio, F.; Andrae-Marobela, K.; Efferth, T. Cytotoxicity of epunctanone and four other phytochemicals isolated from the medicinal plants Garcinia epunctata and Ptycholobium contortum towards multi-factorial drug resistant cancer cells. *Phytomedicine* **2018**, *48*, 112–119. [CrossRef] [PubMed]
95. Mbaveng, A.T.; Ndontsa, B.L.; Kuete, V.; Nguekeu, Y.M.M.; Çelik, İ.; Mbouangouere, R.; Tane, P.; Efferth, T. A naturally occuring triterpene saponin ardisiacrispin B displayed cytotoxic effects in multi-factorial drug resistant cancer cells via ferroptotic and apoptotic cell death. *Phytomedicine* **2018**, *43*, 78–85. [CrossRef] [PubMed]
96. Lou, S.; Hong, H.; Maihesuti, L.; Gao, H.; Zhu, Z.; Xu, L.; Tian, S.; Kai, G.; Huang, G.; Zhao, H. Inhibitory effect of hydnocarpin D on T-cell acute lymphoblastic leukemia via induction of autophagy-dependent ferroptosis. *Exp. Biol. Med.* **2021**, *246*, 1541–1553. [CrossRef]
97. Wu, X.; Chen, S.; Huang, K.; Lin, G. Triptolide promotes ferroptosis by suppressing Nrf2 to overcome leukemia cell resistance to doxorubicin. *Mol. Med. Rep.* **2023**, *27*, 17. [CrossRef]
98. Yu, Y.; Xie, Y.; Cao, L.; Yang, L.; Yang, M.; Lotze, M.T.; Zeh, H.J.; Kang, R.; Tang, D. The ferroptosis inducer erastin enhances sensitivity of acute myeloid leukemia cells to chemotherapeutic agents. *Mol. Cell Oncol.* **2015**, *2*, e1054549. [CrossRef]
99. Du, J.; Wang, T.; Li, Y.; Zhou, Y.; Wang, X.; Yu, X.; Ren, X.; An, Y.; Wu, Y.; Sun, W.; et al. DHA inhibits proliferation and induces ferroptosis of leukemia cells through autophagy dependent degradation of ferritin. *Free Radic Biol. Med.* **2019**, *131*, 356–369. [CrossRef]
100. Grignano, E.; Cantero-Aguilar, L.; Tuerdi, Z.; Chabane, T.; Vazquez, R.; Johnson, N.; Zerbit, J.; Decroocq, J.; Birsen, R.; Fontenay, M.; et al. Dihydroartemisinin-induced ferroptosis in acute myeloid leukemia: Links to iron metabolism and metallothionein. *Cell Death Discov.* **2023**, *9*, 97. [CrossRef]
101. Du, Y.; Bao, J.; Zhang, M.-j.; Li, L.-l.; Xu, X.-L.; Chen, H.; Feng, Y.-b.; Peng, X.-q.; Chen, F.-h. Targeting ferroptosis contributes to ATPR-induced AML differentiation via ROS-autophagy-lysosomal pathway. *Gene* **2020**, *755*, 144889. [CrossRef]
102. Dong, L.-h.; Huang, J.-j.; Zu, P.; Liu, J.; Gao, X.; Du, J.-w.; Li, Y.-f. CircKDM4C upregulates P53 by sponging hsa-let-7b-5p to induce ferroptosis in acute myeloid leukemia. *Environ. Toxicol.* **2021**, *36*, 1288–1302. [CrossRef]
103. Long, F.; Lin, Z.; Long, Q.; Lu, Z.; Zhu, K.; Zhao, M.; Yang, M. CircZBTB46 Protects Acute Myeloid Leukemia Cells from Ferroptotic Cell Death by Upregulating SCD. *Cancers* **2023**, *15*, 459. [CrossRef] [PubMed]
104. Zhu, H.Y.; Huang, Z.X.; Chen, G.Q.; Sheng, F.; Zheng, Y.S. Typhaneoside prevents acute myeloid leukemia (AML) through suppressing proliferation and inducing ferroptosis associated with autophagy. *Biochem. Biophys. Res. Commun.* **2019**, *516*, 1265–1271. [CrossRef] [PubMed]
105. Catanzaro, E.; Turrini, E.; Kerre, T.; Sioen, S.; Baeyens, A.; Guerrini, A.; Bellau, M.L.A.; Sacchetti, G.; Paganetto, G.; Krysko, D.V.; et al. Perillaldehyde is a new ferroptosis inducer with a relevant clinical potential for acute myeloid leukemia therapy. *Biomed. Pharmacother.* **2022**, *154*, 113662. [CrossRef] [PubMed]
106. Yusuf, R.; Saez, B.; Sharda, A.; van Gastel, N.; Yu, V.W.C.; Baryawno, N.; Scadden, E.; Acharya, S.; Chattophadhyay, S.; Huang, C.; et al. Aldehyde dehydrogenase 3a2 protects AML cells from oxidative death and the synthetic lethality of ferroptosis inducers. *Blood* **2020**, *136*, 1303–1316. [CrossRef] [PubMed]
107. Birsen, R.; Larrue, C.; Decroocq, J.; Johnson, N.; Guiraud, N.; Gotanegre, M.; Cantero-Aguilar, L.; Grignano, E.; Huynh, T.; Fontenay, M.; et al. APR-246 induces early cell death by ferroptosis in acute myeloid leukemia. *Haematologica* **2021**, *107*, 403–416. [CrossRef]
108. Sallman, D.A.; DeZern, A.E.; Garcia-Manero, G.; Steensma, D.P.; Roboz, G.J.; Sekeres, M.A.; Cluzeau, T.; Sweet, K.L.; McLemore, A.; McGraw, K.L.; et al. Eprenetapopt (APR-246) and Azacitidine in TP53-Mutant Myelodysplastic Syndromes. *J. Clin. Oncol.* **2021**, *39*, 1584–1594. [CrossRef]
109. Cluzeau, T.; Sebert, M.; Rahmé, R.; Cuzzubbo, S.; Lehmann-Che, J.; Madelaine, I.; Peterlin, P.; Bève, B.; Attalah, H.; Chermat, F.; et al. Eprenetapopt Plus Azacitidine in TP53-Mutated Myelodysplastic Syndromes and Acute Myeloid Leukemia: A Phase II Study by the Groupe Francophone des Myélodysplasies (GFM). *J. Clin. Oncol.* **2021**, *39*, 1575–1583. [CrossRef]
110. Mishra, A.; Tamari, R.; DeZern, A.E.; Byrne, M.T.; Gooptu, M.; Chen, Y.B.; Deeg, H.J.; Sallman, D.; Gallacher, P.; Wennborg, A.; et al. Eprenetapopt Plus Azacitidine After Allogeneic Hematopoietic Stem-Cell Transplantation for TP53-Mutant Acute Myeloid Leukemia and Myelodysplastic Syndromes. *J. Clin. Oncol.* **2022**, *40*, 3985–3993. [CrossRef]
111. Akiyama, H.; Zhao, R.; Rahhal, A.; Nishida, Y.; Ayoub, E.; Ostermann, L.B.; Andreeff, M.; Ishizawa, J. Therapeutic Targeting of Ferroptosis Pathway in Combination with Mitochondrial Oxidative Stress Induction in Acute Myeloid Leukemia. *Blood* **2021**, *138*, 1162. [CrossRef]
112. Zhong, F.-M.; Yao, F.-Y.; Liu, J.; Zhang, H.-B.; Zhang, J.; Zhang, N.; Lin, J.; Li, S.-Q.; Li, M.-Y.; Jiang, J.-Y.; et al. Ferroptosis-related molecular patterns reveal immune escape, inflammatory development and lipid metabolism characteristics of the tumor microenvironment in acute myeloid leukemia. *Front. Oncol.* **2022**, *12*, 888570. [CrossRef]

113. Wei, J.; Xie, Q.; Liu, X.; Wan, C.; Wu, W.; Fang, K.; Yao, Y.; Cheng, P.; Deng, D.; Liu, Z. Identification the prognostic value of glutathione peroxidases expression levels in acute myeloid leukemia. *Ann. Transl. Med.* **2020**, *8*, 678. [CrossRef] [PubMed]
114. Wei, J.; Nai, G.Y.; Dai, Y.; Huang, X.J.; Xiong, M.Y.; Yao, X.Y.; Huang, Z.N.; Li, S.N.; Zhou, W.J.; Huang, Y.; et al. Dipetidyl peptidase-4 and transferrin receptor serve as prognostic biomarkers for acute myeloid leukemia. *Ann. Transl. Med.* **2021**, *9*, 1381. [CrossRef] [PubMed]
115. Zhang, J.; Liu, L.; Wei, J.; Wu, X.; Luo, J.; Wei, H.; Ning, L.; He, Y. High expression level of the FTH1 gene is associated with poor prognosis in children with non-M3 acute myeloid leukemia. *Front. Oncol.* **2023**, *12*, 1068094. [CrossRef] [PubMed]
116. Zhu, K.; Lang, Z.; Zhan, Y.; Tao, Q.; Yu, Z.; Chen, L.; Fan, C.; Jin, Y.; Yu, K.; Zhu, B.; et al. A novel 10-gene ferroptosis-related prognostic signature in acute myeloid leukemia. *Front. Oncol.* **2022**, *12*, 1023040. [CrossRef]
117. Shao, R.; Wang, H.; Liu, W.; Wang, J.; Lu, S.; Tang, H.; Lu, Y. Establishment of a prognostic ferroptosis-related gene profile in acute myeloid leukaemia. *J. Cell Mol. Med.* **2021**, *25*, 10950–10960. [CrossRef]
118. Huang, X.; Zhou, D.; Ye, X.; Jin, J. A novel ferroptosis-related gene signature can predict prognosis and influence immune microenvironment in acute myeloid leukemia. *Bosn. J. Basic Med. Sci.* **2022**, *22*, 608–628. [CrossRef]
119. Zhou, F.; Chen, B. Prognostic significance of ferroptosis-related genes and their methylation in AML. *Hematology* **2021**, *26*, 919–930. [CrossRef]
120. Ke, P.; Bao, X.; Liu, C.; Zhou, B.; Huo, M.; Chen, Y.; Wang, X.; Wu, D.; Ma, X.; Liu, D.; et al. LPCAT3 is a potential prognostic biomarker and may be correlated with immune infiltration and ferroptosis in acute myeloid leukemia: A pan-cancer analysis. *Transl. Cancer Res.* **2022**, *11*, 3491–3505. [CrossRef]
121. Guo, X.; Zhou, X. Risk stratification of acute myeloid leukemia: Assessment using a novel prediction model based on ferroptosis-immune related genes. *Math. Biosci. Eng.* **2022**, *19*, 11821–11839. [CrossRef]
122. Zhang, W.; Trachootham, D.; Liu, J.; Chen, G.; Pelicano, H.; Garcia-Prieto, C.; Lu, W.; Burger, J.A.; Croce, C.M.; Plunkett, W.; et al. Stromal control of cystine metabolism promotes cancer cell survival in chronic lymphocytic leukaemia. *Nat. Cell Biol.* **2012**, *14*, 276–286. [CrossRef]
123. Bordini, J.L.C.; Toscani, L.; Ranghetti, P.; Perotta, E.; Scarfò, L.; Ghia, P.; Campanella, A. High dose iron impairs malignant B-cell viability in chronic lymphocytic leukemia. *HemaSphere* **2022**, *6*, 496–497. [CrossRef]
124. Pan, B.; Li, Y.; Xu, Z.; Miao, Y.; Yin, H.; Kong, Y.; Zhang, X.; Liang, J.; Xia, Y.; Wang, L.; et al. Identifying a novel ferroptosis-related prognostic score for predicting prognosis in chronic lymphocytic leukemia. *Front. Immunol.* **2022**, *13*, 962000. [CrossRef] [PubMed]
125. Liu, S.; Wu, W.; Chen, Q.; Zheng, Z.; Jiang, X.; Xue, Y.; Lin, D. TXNRD1: A Key Regulator Involved in the Ferroptosis of CML Cells Induced by Cysteine Depletion In Vitro. *Oxid. Med. Cell Longev.* **2021**, *2021*, 7674565. [CrossRef] [PubMed]
126. Xu, X.H.; Gan, Y.C.; Xu, G.B.; Chen, T.; Zhou, H.; Tang, J.F.; Gu, Y.; Xu, F.; Xie, Y.Y.; Zhao, X.Y.; et al. Tetrandrine citrate eliminates imatinib-resistant chronic myeloid leukemia cells in vitro and in vivo by inhibiting Bcr-Abl/β-catenin axis. *J. Zhejiang Univ. Sci. B* **2012**, *13*, 867–874. [CrossRef]
127. Yin, J.; Lin, Y.; Fang, W.; Zhang, X.; Wei, J.; Hu, G.; Liu, P.; Niu, J.; Guo, J.; Zhen, Y.; et al. Tetrandrine Citrate Suppresses Breast Cancer via Depletion of Glutathione Peroxidase 4 and Activation of Nuclear Receptor Coactivator 4-Mediated Ferritinophagy. *Front Pharm.* **2022**, *13*, 820593. [CrossRef]
128. Onoue, S.; Yamada, S.; Chan, H.K. Nanodrugs: Pharmacokinetics and safety. *Int. J. Nanomed.* **2014**, *9*, 1025–1037. [CrossRef]
129. Zhao, Y.; Li, Y.; Zhang, R.; Wang, F.; Wang, T.; Jiao, Y. The Role of Erastin in Ferroptosis and Its Prospects in Cancer Therapy. *Onco Targets* **2020**, *13*, 5429–5441. [CrossRef]
130. Zhao, J.; Xu, B.; Xiong, Q.; Feng, Y.; Du, H. Erastininduced ferroptosis causes physiological and pathological changes in healthy tissues of mice. *Mol. Med. Rep.* **2021**, *24*, 12352. [CrossRef]
131. Yang, R.; Li, Y.; Wang, X.; Yan, J.; Pan, D.; Xu, Y.; Wang, L.; Yang, M. Doxorubicin loaded ferritin nanoparticles for ferroptosis enhanced targeted killing of cancer cells. *RSC Adv.* **2019**, *9*, 28548–28553. [CrossRef]
132. Liang, X.; Chen, M.; Bhattarai, P.; Hameed, S.; Tang, Y.; Dai, Z. Complementing Cancer Photodynamic Therapy with Ferroptosis through Iron Oxide Loaded Porphyrin-Grafted Lipid Nanoparticles. *ACS Nano* **2021**, *15*, 20164–20180. [CrossRef]
133. Liu, R.; Rong, G.; Liu, Y.; Huang, W.; He, D.; Lu, R. Delivery of apigenin-loaded magnetic Fe2O3/Fe3O4@mSiO2 nanocomposites to A549 cells and their antitumor mechanism. *Mater. Sci. Eng. C* **2021**, *120*, 111719. [CrossRef] [PubMed]
134. Zhang, J.; Yang, J.; Zuo, T.; Ma, S.; Xokrat, N.; Hu, Z.; Wang, Z.; Xu, R.; Wei, Y.; Shen, Q. Heparanase-driven sequential released nanoparticles for ferroptosis and tumor microenvironment modulations synergism in breast cancer therapy. *Biomaterials* **2021**, *266*, 120429. [CrossRef]
135. Han, W.; Duan, X.; Ni, K.; Li, Y.; Chan, C.; Lin, W. Co-delivery of dihydroartemisinin and pyropheophorbide-iron elicits ferroptosis to potentiate cancer immunotherapy. *Biomaterials* **2022**, *280*, 121315. [CrossRef] [PubMed]
136. Ji, P.; Wang, X.; Yin, J.; Yao, Y.; Du, W. Amplification of ferroptosis with a liposomal nanoreactor cooperates with low-toxicity doxorubicin apoptosis for enhanced tumor chemotherapy. *Biomater. Sci.* **2022**, *10*, 1544–1553. [CrossRef] [PubMed]
137. Wu, F.; Du, Y.; Yang, J.; Shao, B.; Mi, Z.; Yao, Y.; Cui, Y.; He, F.; Zhang, Y.; Yang, P. Peroxidase-like Active Nanomedicine with Dual Glutathione Depletion Property to Restore Oxaliplatin Chemosensitivity and Promote Programmed Cell Death. *ACS Nano* **2022**, *16*, 3647–3663. [CrossRef] [PubMed]
138. Yu, M.; Yu, J.; Yi, Y.; Chen, T.; Yu, L.; Zeng, W.; Ouyang, X.-k.; Huang, C.; Sun, S.; Wang, Y.; et al. Oxidative stress-amplified nanomedicine for intensified ferroptosis-apoptosis combined tumor therapy. *J. Control Release* **2022**, *347*, 104–114. [CrossRef]

139. Zhang, K.; Ma, Z.; Li, S.; Wu, Y.; Zhang, J.; Zhang, W.; Zhao, Y.; Han, H. Disruption of dual homeostasis by a metal-organic framework nanoreactor for ferroptosis-based immunotherapy of tumor. *Biomaterials* **2022**, *284*, 121502. [CrossRef]
140. Miao, Y.-B.; Zhao, W.; Renchi, G.; Gong, Y.; Shi, Y. Customizing delivery nano-vehicles for precise brain tumor therapy. *J. Nanobiotechnol.* **2023**, *21*, 32. [CrossRef]
141. Liaw, K.; Zhang, F.; Mangraviti, A.; Kannan, S.; Tyler, B.; Kannan, R.M. Dendrimer size effects on the selective brain tumor targeting in orthotopic tumor models upon systemic administration. *Bioeng. Transl. Med.* **2020**, *5*, e10160. [CrossRef]
142. Arias, L.S.; Pessan, J.P.; Vieira, A.P.M.; Lima, T.M.T.; Delbem, A.C.B.; Monteiro, D.R. Iron Oxide Nanoparticles for Biomedical Applications: A Perspective on Synthesis, Drugs, Antimicrobial Activity, and Toxicity. *Antibiotics* **2018**, *7*, 46. [CrossRef]
143. Sim, S.; Wong, N.K. Nanotechnology and its use in imaging and drug delivery (Review). *Biomed. Rep.* **2021**, *14*, 42. [CrossRef] [PubMed]
144. Ma, W.; Gao, Y.; Ouyang, Z.; Fan, Y.; Yu, H.; Zhan, M.; Wang, H.; Shi, X.; Shen, M. Apoptosis-enhanced ferroptosis therapy of pancreatic carcinoma through PAMAM dendrimer-iron(III) complex-based plasmid delivery. *Sci. China Chem.* **2022**, *65*, 778–788. [CrossRef]
145. Wu, W.; He, Q.; Jiang, C. Magnetic iron oxide nanoparticles: Synthesis and surface functionalization strategies. *Nanoscale Res. Lett.* **2008**, *3*, 397–415. [CrossRef]
146. Huang, Q.T.; Hu, Q.Q.; Wen, Z.F.; Li, Y.L. Iron oxide nanoparticles inhibit tumor growth by ferroptosis in diffuse large B-cell lymphoma. *Am. J. Cancer Res.* **2023**, *13*, 498–508.
147. Trujillo-Alonso, V.; Pratt, E.C.; Zong, H.; Lara-Martinez, A.; Kaittanis, C.; Rabie, M.O.; Longo, V.; Becker, M.W.; Roboz, G.J.; Grimm, J.; et al. FDA-approved ferumoxytol displays anti-leukaemia efficacy against cells with low ferroportin levels. *Nat. Nanotechnol.* **2019**, *14*, 616–622. [CrossRef]
148. Guerrero-Hernández, L.; Meléndez-Ortiz, H.I.; Cortez-Mazatan, G.Y.; Vaillant-Sánchez, S.; Peralta-Rodríguez, R.D. Gemini and Bicephalous Surfactants: A Review on Their Synthesis, Micelle Formation, and Uses. *Int. J. Mol. Sci.* **2022**, *23*, 1798. [CrossRef]
149. Lu, Y.; Zhang, E.; Yang, J.; Cao, Z. Strategies to improve micelle stability for drug delivery. *Nano Res* **2018**, *11*, 4985–4998. [CrossRef]
150. Gao, M.; Deng, J.; Liu, F.; Fan, A.; Wang, Y.; Wu, H.; Ding, D.; Kong, D.; Wang, Z.; Peer, D.; et al. Triggered ferroptotic polymer micelles for reversing multidrug resistance to chemotherapy. *Biomaterials* **2019**, *223*, 119486. [CrossRef] [PubMed]
151. Guo, X.; Liu, F.; Deng, J.; Dai, P.; Qin, Y.; Li, Z.; Wang, B.; Fan, A.; Wang, Z.; Zhao, Y. Electron-Accepting Micelles Deplete Reduced Nicotinamide Adenine Dinucleotide Phosphate and Impair Two Antioxidant Cascades for Ferroptosis-Induced Tumor Eradication. *ACS Nano* **2020**, *14*, 14715–14730. [CrossRef]
152. Olusanya, T.O.B.; Haj Ahmad, R.R.; Ibegbu, D.M.; Smith, J.R.; Elkordy, A.A. Liposomal Drug Delivery Systems and Anticancer Drugs. *Molecules* **2018**, *23*, 907. [CrossRef]
153. Bozzuto, G.; Molinari, A. Liposomes as nanomedical devices. *Int. J. Nanomed.* **2015**, *10*, 975–999. [CrossRef] [PubMed]
154. Gai, C.; Liu, C.; Wu, X.; Yu, M.; Zheng, J.; Zhang, W.; Lv, S.; Li, W. MT1DP loaded by folate-modified liposomes sensitizes erastin-induced ferroptosis via regulating miR-365a-3p/NRF2 axis in non-small cell lung cancer cells. *Cell Death Dis.* **2020**, *11*, 751. [CrossRef] [PubMed]
155. He, Y.-J.; Liu, X.-Y.; Xing, L.; Wan, X.; Chang, X.; Jiang, H.-L. Fenton reaction-independent ferroptosis therapy via glutathione and iron redox couple sequentially triggered lipid peroxide generator. *Biomaterials* **2020**, *241*, 119911. [CrossRef] [PubMed]
156. Kou, L.; Sun, R.; Jiang, X.; Lin, X.; Huang, H.; Bao, S.; Zhang, Y.; Li, C.; Chen, R.; Yao, Q. Tumor Microenvironment-Responsive, Multistaged Liposome Induces Apoptosis and Ferroptosis by Amplifying Oxidative Stress for Enhanced Cancer Therapy. *ACS Appl. Mater. Interfaces* **2020**, *12*, 30031–30043. [CrossRef]
157. Yang, Y.; Zuo, S.; Li, L.; Kuang, X.; Li, J.; Sun, B.; Wang, S.; He, Z.; Sun, J. Iron-doxorubicin prodrug loaded liposome nanogenerator programs multimodal ferroptosis for efficient cancer therapy. *Asian J. Pharm. Sci.* **2021**, *16*, 784–793. [CrossRef]
158. Zhou, L.; Dong, C.; Ding, L.; Feng, W.; Yu, L.; Cui, X.; Chen, Y. Targeting ferroptosis synergistically sensitizes apoptotic sonodynamic anti-tumor nanotherapy. *Nano Today* **2021**, *39*, 101212. [CrossRef]
159. Li, Q.; Gao, W.; Zhang, C.; Wang, P.; Wang, X.; Yan, M.; Jiang, W.; Wu, Z.; Wei, P.; Tian, G.; et al. A Biodegradable High-Efficiency Magnetic Nanoliposome Promotes Tumor Microenvironment-Responsive Multimodal Tumor Therapy Along with Switchable T2 Magnetic Resonance Imaging. *ACS Appl. Mater. Interfaces* **2022**, *14*, 24160–24173. [CrossRef]
160. Li, Z.; Wang, C.; Dai, C.; Hu, R.; Ding, L.; Feng, W.; Huang, H.; Wang, Y.; Bai, J.; Chen, Y. Engineering dual catalytic nanomedicine for autophagy-augmented and ferroptosis-involved cancer nanotherapy. *Biomaterials* **2022**, *287*, 121668. [CrossRef]
161. Zhang, C.; Leng, Z.; Wang, Y.; Ran, L.; Qin, X.; Xin, H.; Xu, X.; Zhang, G.; Xu, Z. PDGFB targeting biodegradable FePt alloy assembly for MRI guided starvation-enhancing chemodynamic therapy of cancer. *J. Nanobiotechnol.* **2022**, *20*, 264. [CrossRef]
162. Zhang, N.; Shu, G.; Qiao, E.; Xu, X.; Shen, L.; Lu, C.; Chen, W.; Fang, S.; Yang, Y.; Song, J.; et al. DNA-Functionalized Liposomes In Vivo Fusion for NIR-II/MRI Guided Pretargeted Ferroptosis Therapy of Metastatic Breast Cancer. *ACS Appl. Mater. Interfaces* **2022**, *14*, 20603–20615. [CrossRef]
163. Fu, F.; Wang, W.; Wu, L.; Wang, W.; Huang, Z.; Huang, Y.; Wu, C.; Pan, X. Inhalable Biomineralized Liposomes for Cyclic Ca^{2+}-Burst-Centered Endoplasmic Reticulum Stress Enhanced Lung Cancer Ferroptosis Therapy. *ACS Nano* **2023**, *17*, 5486–5502. [CrossRef] [PubMed]
164. Fu, J.J.; Liu, C.C.; Feng, G.N.; Li, S.P.; Yu, Y.Y.; Du, L.R.; Zhang, J.Y.; Zhang, Y.; Lei, X.P.; Dai, X.; et al. Activatable unsaturated liposomes increase lipid peroxide of cell membrane and inhibit tumor growth. *Biomater. Adv.* **2023**, *147*, 213323. [CrossRef]

165. Liu, Y.; Chen, J.; He, Z.; Luo, H.; Liu, X.; Sun, Y.; Ge, D.; Liu, X.; Shi, W. Ferrocene-liposome-PEG: A robust OH/lipid peroxide nano-converter for inducing tumor ferroptosis. *Biomater. Sci.* **2023**, *11*, 542–553. [CrossRef] [PubMed]
166. Liu, Y.; Quan, X.; Li, J.; Huo, J.; Li, X.; Zhao, Z.; Li, S.; Wan, J.; Li, J.; Liu, S.; et al. Liposomes embedded with PEGylated iron oxide nanoparticles enable ferroptosis and combination therapy in cancer. *Natl. Sci. Rev.* **2023**, *10*, nwac167. [CrossRef]
167. Su, Y.; Zhang, Z.; Lee, L.T.O.; Peng, L.; Lu, L.; He, X.; Zhang, X. Amphiphilic Dendrimer Doping Enhanced pH-Sensitivity of Liposomal Vesicle for Effective Co-delivery toward Synergistic Ferroptosis-Apoptosis Therapy of Hepatocellular Carcinoma. *Adv. Health Mater.* **2023**, *12*, e2202663. [CrossRef] [PubMed]
168. Barenholz, Y. Doxil(R)–the first FDA-approved nano-drug: Lessons learned. *J. Control Release* **2012**, *160*, 117–134. [CrossRef]
169. Braham, M.V.; Deshantri, A.K.; Minnema, M.C.; Öner, F.C.; Schiffelers, R.M.; Fens, M.H.; Alblas, J. Liposomal drug delivery in an in vitro 3D bone marrow model for multiple myeloma. *Int. J. Nanomed.* **2018**, *13*, 8105–8118. [CrossRef]
170. Deshantri, A.K.; Fens, M.H.A.M.; Ruiter, R.W.J.; Metselaar, J.M.; Storm, G.; Mandhane, S.N.; Graat, G.H.M.; Lentjes, E.G.W.; Yuan, H.; de Bruijn, J.D.; et al. Complete Tumor Regression by Liposomal Bortezomib in a Humanized Mouse Model of Multiple Myeloma. *HemaSphere* **2020**, *4*, e463. [CrossRef]
171. Federico, C.; Alhallak, K.; Sun, J.; Duncan, K.; Azab, F.; Sudlow, G.P.; de la Puente, P.; Muz, B.; Kapoor, V.; Zhang, L.; et al. Tumor microenvironment-targeted nanoparticles loaded with bortezomib and ROCK inhibitor improve efficacy in multiple myeloma. *Nat. Commun.* **2020**, *11*, 6037. [CrossRef]
172. Rink, J.S.; Lin, A.Y.; McMahon, K.M.; Calvert, A.E.; Yang, S.; Taxter, T.; Moreira, J.; Chadburn, A.; Behdad, A.; Karmali, R.; et al. Targeted reduction of cholesterol uptake in cholesterol-addicted lymphoma cells blocks turnover of oxidized lipids to cause ferroptosis. *J. Biol. Chem.* **2021**, *296*, 100100. [CrossRef]
173. Pai, A.B.; Garba, A.O. Ferumoxytol: A silver lining in the treatment of anemia of chronic kidney disease or another dark cloud? *J. Blood Med.* **2012**, *3*, 77–85. [CrossRef] [PubMed]
174. Cao, K.; Du, Y.; Bao, X.; Han, M.; Su, R.; Pang, J.; Liu, S.; Shi, Z.; Yan, F.; Feng, S. Glutathione-Bioimprinted Nanoparticles Targeting of N6-methyladenosine FTO Demethylase as a Strategy against Leukemic Stem Cells. *Small* **2022**, *18*, e2106558. [CrossRef] [PubMed]
175. Yu, Y.; Meng, Y.; Xu, X.; Tong, T.; He, C.; Wang, L.; Wang, K.; Zhao, M.; You, X.; Zhang, W.; et al. A Ferroptosis-Inducing and Leukemic Cell-Targeting Drug Nanocarrier Formed by Redox-Responsive Cysteine Polymer for Acute Myeloid Leukemia Therapy. *ACS Nano* **2023**, *17*, 3334–3345. [CrossRef] [PubMed]

Publication 2

International Journal of Molecular Sciences

MDPI

Article

Novel (1S,3R)-RSL3-Encapsulated Polyunsaturated Fatty Acid Rich Liposomes Sensitise Multiple Myeloma Cells to Ferroptosis-Mediated Cell Death

Ali Habib [1], Rachel L. Mynott [1], Oliver G. Best [1], Isabella A. Revesz [2], Clive A. Prestidge [2] and Craig T. Wallington-Gates [1,3,4,5,*]

1 College of Medicine and Public Health, Flinders University, Bedford Park, SA 5042, Australia; ali.habib@flinders.edu.au (A.H.); rachel.mynott@flinders.edu.au (R.L.M.); giles.best@flinders.edu.au (O.G.B.)
2 Clinical Health Sciences, University of South Australia, Adelaide, SA 5005, Australia; isabella.revesz@unisa.edu.au (I.A.R.); clive.prestidge@unisa.edu.au (C.A.P.)
3 School of Health, University of the Sunshine Coast, Sippy Downs, QLD 4556, Australia
4 School of Medicine and Dentistry, Griffith University, Birtinya, QLD 4575, Australia
5 Department of Haematology, Sunshine Coast University Hospital, Birtinya, QLD 4575, Australia
* Correspondence: craig.wallington-gates@health.qld.gov.au

Abstract

Multiple myeloma (MM) is an incurable malignancy of plasma cells that accounts for 10% of all haematological malignancies diagnosed worldwide. The poor outcome of patients with MM highlights the ongoing need for novel treatment strategies. Ferroptosis is a recently characterised form of non-apoptotic programmed cell death. Phospholipids (PLs) containing polyunsaturated fatty acids (PUFAs) play a crucial role as ferroptosis substrates when oxidised to form toxic lipid reactive oxygen species (ROS). Using a range of scientific techniques, we demonstrate a strong correlation between the PL profile of MM and diffuse large B cell lymphoma (DLBCL) cells with their sensitivity to ferroptosis. Using this PL profiling, we manufacture liposomes that are themselves composed of PL-PUFA ferroptosis substrates relatively deficient in MM cells, with and without the GPX4 inhibitor, RSL3, for investigation of their ferroptosis-inducing potential. PL-PUFAs were more abundant in DLBCL than MM cell lines, consistent with greater ferroptosis sensitivity. In contrast, MM cells generally contained a significantly higher proportion of PLs containing monounsaturated fatty acids. Altering the lipid composition of MM cells through exogenous supplementation with PL-PUFAs induced ferroptosis-mediated cell death and further sensitised these cells to RSL3. Liposomes predominantly comprising PL-PUFAs were subsequently manufactured and loaded with RSL3. Uptake, cytotoxicity and lipid ROS studies demonstrated that these novel liposomes were readily taken up by MM cells. Those containing RSL3 were more effective at inducing ferroptosis than empty liposomes or free RSL3, resulting in IC_{50} values an average 7.1-fold to 14.5-fold lower than those for free RSL3, from the micromolar to nanomolar range. We provide a better understanding of the mechanisms associated with ferroptosis resistance of MM cells and suggest that strategies such as liposomal delivery of relatively deficient ferroptosis-inducing PL-PUFAs together with other targeted agents could harness ferroptosis for the personalised treatment of MM and other cancers.

Keywords: cancer; haematology; multiple myeloma; ferroptosis; phospholipids; fatty acids; saturated; unsaturated; nanotechnology; nanoparticles; liposomes

Academic Editors: Emanuela Grassilli and Maria Grazia Cerrito

Received: 5 June 2025
Revised: 2 July 2025
Accepted: 3 July 2025
Published: 9 July 2025

Citation: Habib, A.; Mynott, R.L.; Best, O.G.; Revesz, I.A.; Prestidge, C.A.; Wallington-Gates, C.T. Novel (1S,3R)-RSL3-Encapsulated Polyunsaturated Fatty Acid Rich Liposomes Sensitise Multiple Myeloma Cells to Ferroptosis-Mediated Cell Death. *Int. J. Mol. Sci.* **2025**, *26*, 6579. https://doi.org/10.3390/ijms26146579

1. Background

Multiple myeloma (MM) is the second most common haematological malignancy worldwide and is characterised by the clonal proliferation of plasma cells in the bone marrow [1,2]. Despite advances in treatment, MM is still considered incurable. Between 2016 and 2020, the 5-year survival rate for patients with MM in Australia was 59.5%, with 10,848 people living with the disease at the end of 2020 who were diagnosed between 2011 and 2020 [3]. Although survival rates among MM patients are predicted to improve with the advent of recent therapeutic advances [4,5], there remains an ongoing need for novel treatment approaches. This is particularly important for the significant proportion of patients who relapse or develop disease that is resistant to standard therapies.

The efficacy of many cancer therapies, including those used to treat MM patients, is dependent on their ability to induce apoptosis-mediated cell death. However, tumorigenesis and disease evolution are often associated with resistance to many of the current treatment options [6,7]. Relatively recently, an iron-dependent form of programmed cell death (PCD), termed ferroptosis, was described [8]. Ferroptosis is characterised by lipid peroxidation, which leads to breakdown of cell membranes and disruption of cellular homeostasis. Given that the intracellular signalling pathways involved in ferroptosis are distinct from other forms of PCD [8–10], induction of ferroptosis may represent a promising therapeutic strategy for targeting apoptosis-resistant cells with the potential to significantly improve outcomes for cancer patients, including those with MM.

Phospholipids (PLs) play crucial roles in many cellular processes and are the main constituent of cellular membranes [11]. The peroxidation of certain PLs, specifically glycerophospholipids, is also crucial for the initiation and propagation of ferroptosis [11–14]. PLs consist of a polar phosphate head region and two nonpolar fatty acid chains linked by a glycerol backbone [11,15,16]. PLs are characterised according to the head group as this largely dictates the chemical properties, structure, function, and membrane localisation of the lipid [11,15,16]. The fatty acids (FAs) that make up the acyl chains within PLs are carboxylic acids with an aliphatic chain. FAs can be categorised into three distinct classes: saturated fatty acids (SFAs), monounsaturated fatty acids (MUFAs) and polyunsaturated fatty acids (PUFAs). Unlike SFA and MUFA, PUFAs are readily oxidised and represent important substrates for lipid peroxidation [12].

Phosphatidylethanolamine (PE) lipids predominantly comprise PUFAs and are abundant in the inner leaflet of the plasma membrane [12]. The susceptibility of PE lipids to oxidation means they are important substrates for ferroptosis [12], although other PLs, including phosphatidylcholine (PC) and phosphatidylserine (PS), are also readily oxidised [12,14,17]. In addition to the class of PL, the degree of unsaturation also affects how readily lipids are oxidised [12].

The lipid peroxidation that occurs during ferroptosis is associated with the formation of potent oxidising agents, particularly hydroxyl radicals, via the Fenton reaction [8]. Hydroxyl radicals remove a bis-allylic hydrogen atom from PL-PUFAs, forming carbon-centred PLs, which react with oxygen molecules to form highly potent PL peroxyl radicals that trigger ferroptotic cell death [14]. Regulation of lipid peroxidation is complex and involves several key molecules, including the antioxidant glutathione peroxidase 4 (GPX4) [9,18]. GPX4 is a selenoprotein which converts toxic lipid peroxides into neutral alcohols and, in doing so, inhibits lipid peroxidation and ferroptosis [19,20]. Given the role of lipid peroxidation in ferroptosis, lipid-based nanostructures, e.g., liposomes, may represent a promising means of delivering therapeutic agents and ferroptosis substrates to cells that may otherwise be relatively insensitive to this form of cell death.

Liposomes are extremely versatile spherical vesicles that primarily consist of lipids and range in size from 30 nm to a few micrometres [21]. The lipid-rich nature of these

nanoparticles enables hydrophilic agents to be encapsulated within the aqueous core, which is surrounded by the hydrophobic lipid bilayer. Although small vesicles such as liposomes are typically taken up by cells via endocytosis, uptake can be modified and improved by controlling their lipid composition [22]. The versatility of liposomes lies in the ability to modify their surface with polymers, antibodies and proteins. Adding components or surface functionalising liposomes may significantly expand their possible therapeutic applications by enabling the delivery of macromolecular drugs or genetic therapies (e.g., siRNA) in a highly targeted manner.

The use of nanotechnologies aimed at inducing ferroptosis in cancer cells has grown exponentially in recent years, with studies in non-small lung cancer, breast cancer, colon cancer, colorectal cancer, ovarian cancer and skin cancers [23–28]. Many of these studies focused on nanotechnologies other than liposomes, capable of delivering iron to the cells. However, two recent studies in which both ferroptosis- and apoptosis-inducing compounds were encapsulated within liposomes demonstrate the potential of these nanoparticles as a means of overcoming drug resistance [29,30].

MM cells are inherently less sensitive to ferroptosis-inducing compounds than diffuse large B cell lymphoma (DLBCL) cells, as shown in the study by Yang et al., who tested the efficacy of the cysteine antiporter X_C^- inhibitor, erastin [9]. Despite their relative insensitivity to erastin, it is apparent that MM cells can undergo ferroptosis [31,32]. However, realising the potential of ferroptosis as a novel approach for the treatment of haematological malignancies [18] requires a better understanding of the mechanisms related to ferroptosis sensitivity in these cancers.

In the current study, we performed lipidomic analyses which identified a strong association between cellular lipid composition and the ferroptosis sensitivity of MM and DLBCL cells. Liposome nanoparticles were then manufactured from ferroptosis-inducing PL-PUFAs, identified in the lipidomic analyses to be relatively deficient in MM cells, and loaded with the GPX4 inhibitor, RSL3. Functional studies demonstrate that the liposomes were rapidly taken up by MM cells and that the delivery of PL-PUFAs as ferroptosis substrates and RSL3 in a liposomal formulation was significantly more potent than exogeneous PL-PUFAs in combination with free RSL3 at inducing ferroptosis-mediated cell death.

The findings of this study highlight the importance of cellular lipid composition in relation to ferroptosis sensitivity and provide a proof-of-principle that liposomal nanoparticles, themselves composed of PL-PUFA ferroptosis substrates and containing other targeted therapeutics, may represent an effective means of inducing ferroptosis in MM and other cancer cells that are less sensitive to this form of programmed cell death. Moreover, this research suggests there is enormous potential for developing precision or personalised lipid nanoparticle therapeutics for induction of ferroptosis.

2. Results

2.1. MM Cells Are Less Sensitive to the GPX4 Inhibitor, RSL3, than DLBCL Cells

The glutathione peroxidase 4 (GPX4) enzyme catalyses the reduction of PL hydroperoxides into their corresponding alcohols, which decreases levels of lipid ROS and inhibits ferroptosis [33]. Indirect inhibition of GPX4 with erastin has been shown to induce ferroptosis in DLBCL, but not MM, cell lines [9]. We demonstrated similar effects in MM and DLBCL cells using RSL3, a small molecule inhibitor that directly inhibits GPX4 by binding to the catalytic selenocysteine residue of the enzyme (Figure 1A). Cell death was observed in all the DLBCL cell lines with an average IC_{50} value of 354.41 $\pm$ 170.04 nM. With the exception of OPM-2 cells, the MM lines were much less sensitive to RSL3, with and average IC_{50} value of 4722.50 $\pm$ 1741.65 nM (excluding the OPM-2 MM cell line) (Figure 1A). Western blot analysis of whole cell lysates from the MM and DLBCL cell lines suggested

differences in the sensitivity to RSL3 between the lines were not due to varying expression of its target, GPX4 (Figure 1B,C). Ferroptosis is associated with characteristic changes in cell morphology, including a "ballooning" phenotype due to an enlarged cytoplasm. Using an IncuCyte® S3 Live-Cell Analysis System, we observed morphological changes that are consistent with ferroptosis in both the MM and DLBCL cells, with the RSL3 sensitive OPM-2 cell line displaying ferroptotic morphology when cultured with 200 nM RSL3 for 24 h (Figure 1D). The effects of RSL3 on cell morphology were inhibited by the synthetic antioxidant, liproxstatin-1, which supports the assertion that the changes observed were associated with ferroptosis.

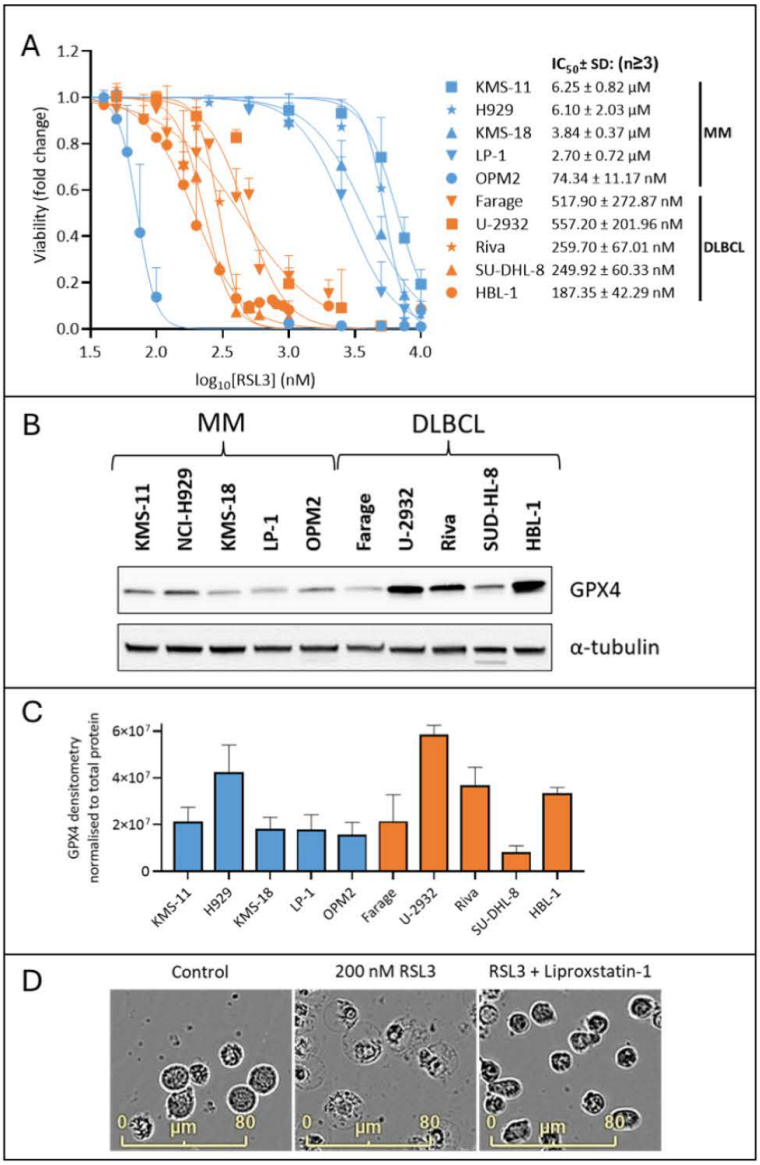

Figure 1. MM cells are generally less sensitive to RSL3 induced cell death compared to DLBCL cells. (**A**) Cell viability was assessed by annexin V/PI staining and flow cytometry in MM and DLBCL

cell lines treated with RSL3 for 24 h. Dual annexin V/PI negative cells were considered viable. The mean ± standard deviation of duplicate measurements are shown from at least 3 independent experiments. (**B**) Western blot for GPX4 expression in untreated MM and DLBCL cells. Alpha tubulin expression was assessed as a loading control. (**C**) Western blot densitometry data are mean (normalised to total protein) ± standard deviation from a minimum of three independent experiments. (**D**) Untreated OPM-2 cells, OPM-2 cells cultured with 200 nM RSL3, and OPM-2 cells cultured with RSL3 200 nM and 2 μM liproxstatin-1, for 24 h. Images were captured at 20× magnification using an IncuCyte® S3 Live-Cell Analysis System and v2023A software. MM, multiple myeloma; DLBCL, diffuse large B cell lymphoma, GPX4, glutathione peroxidase 4; RSL3, (1S,3R)-RSL3.

To further demonstrate that ferroptosis is the major mechanism of cell death in MM cell lines cultured with RSL3, MM cells were cultured with bortezomib that is known to induce apoptosis in MM cells [34] with and without the pan-caspase inhibitor Z-VAD-FMK or liproxstatin-1, and compared to similar cell cultures using RSL3 (Supplementary Figure S1A). Z-VAD-FMK was able to prevent the majority of cell death induced by bortezomib but not with RSL3, which was near completely prevented by liproxstatin-1. Moreover, we observed morphological changes that are consistent with either apoptosis or ferroptosis when OPM2 cells were cultured with either bortezomib or RSL3, respectively (Supplementary Figure S1B). The possibility that another form of cell death, known as necroptosis, was involved in the effects of RSL3 against MM cells was investigated using the receptor-interacting serine/threonine-protein kinase 1 (RIPK1) inhibitor necrostatin-1s (Nec-1s). In necroptosis, RIPK1 and RIPK3 form a necrosome complex, resulting in a signalling cascade that ends in phosphorylation of mixed lineage kinase domain-like protein (MLKL) and execution of necroptosis [35]. Nec-1s did not prevent RSL3-induced cell death or lipid oxidation, indicating that necroptosis does not play a role in the toxicity of RSL3 against MM cells (Supplementary Figure S2A,B). Furthermore, Western blotting showed that none of the MM cell lines express RIPK3, which is a protein that is crucial for activation of necroptosis (Supplementary Figure S2C).

2.2. *MM Cells Generally Contain Higher Proportions of PL-MUFA than DLBCL Cell Lines*

Studies show that PLs containing PUFAs represent important substrates for ferroptosis, [12] and that the peroxidation of these lipids is a crucial step in ferroptosis [36]. To investigate this, the PL profiles of the MM ($n = 5$) and DLBCL cell lines ($n = 5$) were analysed by liquid chromatography–mass spectrometry (LC-MS).

To examine the acyl chains within the PLs in more detail, the PLs were grouped as follows: (1) PLs with completely saturated acyl chains (SFA), (2) PLs containing a combination of SFA and MUFA (MUFA), (3) PLs containing both MUFA and PUFA (MUFA/PUFA), or (4) PLs containing a combination of SFA and PUFA (PUFA). Due to their low abundance, phospholipids containing SFA/MUFA or MUFA/MUFA were grouped together and those containing SFA/PUFA or PUFA/PUFA were also grouped together. PLs typically contain a SFA in the *sn1* position, whereas the *sn2* position can contain SFA, MUFA or PUFA [37]. Analysis of the data revealed that MM cell lines had a higher proportion of PLs containing MUFAs than the DLBCL cell lines (Figure 2A). In contrast, DLBCL cell lines contained a higher proportion of PLs containing PUFAs than MUFAs (Figure 2A). Studies suggest that MUFAs play a role in protecting cells against ferroptosis by preventing accumulation of toxic lipid ROS and reducing the amount of PUFAs that are incorporated into PLs [12,38,39].

The most notable difference between the two cancer types appears to be in the proportions of PLs containing PUFA or MUFA (Figure 2A). The DLBCL cell lines were found to contain significantly ($p < 0.01$) higher levels of PL-PUFA (38.52% ± 2.72% of the total phospholipidome) in comparison to the MM cell lines (33.76% ± 6.20%) (Figure 2A). In

contrast, the MM cell lines had significantly ($p < 0.0001$) higher levels of PL-MUFA, which constituted up to 49.36% ± 7.58% of their total PL content, compared to 39.35 ± 6.62% in the DLBCL cells (Figure 2A). There was also a significant ($p < 0.001$) difference between DLBCL and MM lines in the levels of PLs containing SFA only, however SFA levels were under 10% in both cancers (Figure 2A). There was no significant difference between the MUFA/PUFA groups when comparing MM and DLBCL (Figure 2A). In addition to distinct differences between the two cancers, differences in the PL composition between each of the cell lines were also observed (Supplementary Figure S3).

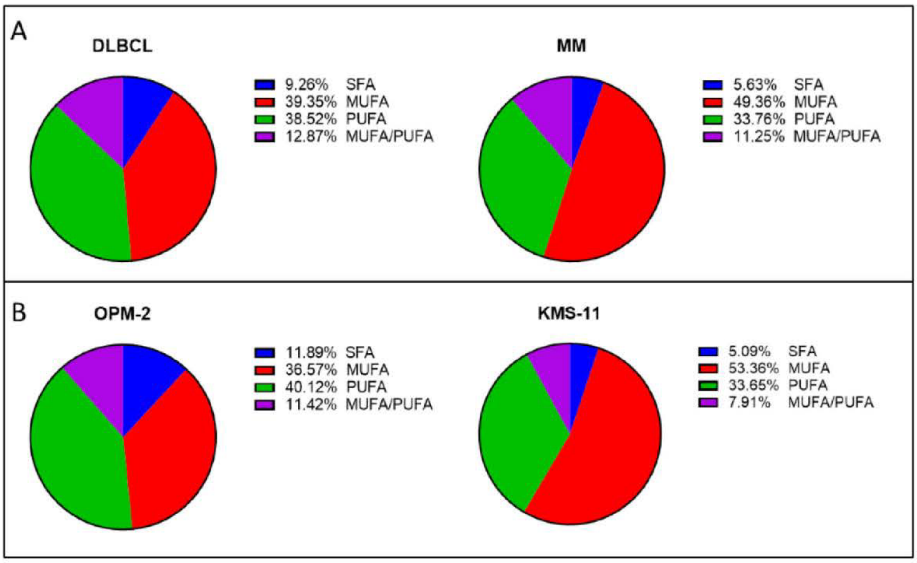

Figure 2. Distinct differences in the phospholipid composition of MM and DLBCL cells. (**A**) Analysis of data pooled from the MM (excluding ferroptosis-sensitive OPM-2) and DLBCL lines showing the proportions of each PL acyl chain. Proportions were calculated as the peak area of each acyl chain relative to the total PL peak area by LC-MS. Data are the mean from a minimum of 4 biological replicates per cell line. (**B**) PL composition in the OPM-2 and KMS-11 MM lines showing the proportions of each PL acyl chain. Data are the mean from a minimum of 12 biological replicates per cell line. All statistical analyses (see text) were performed using Student's *t*-test using a minimum of 4 biological replicates. MM, multiple myeloma; DLBCL, diffuse large B cell lymphoma; MUFA, monounsaturated fatty acid; PUFA, polyunsaturated fatty acid; SFA, saturated fatty acid.

Next, we compared the phospholipidome of the ferroptosis sensitive and resistant MM cell lines, OPM-2 and KMS-11, respectively (Figure 2B). A higher proportion (40.12% ± 8.44%) of PUFA were identified in the OPM-2 cells compared to MUFA (36.57 ± 11.91%) (Figure 2B). In contrast, the lipid profile of KMS-11 cells was almost the reverse, with the largest proportion of lipids identified as MUFAs (53.36 ± 4.20%), with a significantly ($p < 0.0001$) smaller proportion of PUFAs (33.65 ± 2.62%) (Figure 2B). There was also a statistically significant difference in MUFA ($p < 0.001$) and PUFA ($p < 0.05$) between the two cell lines (Figure 2B). Interestingly, the OPM-2 cell line had significantly greater proportions of SFA ($p < 0.01$) and MUFA/PUFA ($p < 0.001$) than the KMS-11 cell line (Figure 2B). Some studies suggest that SFA plays a role in promoting ferroptosis induction [40,41], while others suggest that they play a protective role [42], indicating that the effects of SFAs may be context dependent. The role of PLs containing both MUFA and PUFA has yet to be fully elucidated in the literature but may influence ferroptosis sensitivity.

2.3. Exogenous PL-PUFA Induces Ferroptosis in MM Cells Proportional to the Degree of Acyl Chain Saturation

Given that PUFA but not MUFA are readily oxidised leading to accumulation of lipid ROS and ferroptosis [12], we hypothesised that the ratio of PL-PUFA to PL-MUFA may dictate the sensitivity of MM cells to ferroptosis. OPM-2 and KMS-11 MM cells were cultured with four PE lipids with different degrees of acyl chain saturation, that were identified from the lipidomic analysis and from the literature (Figure 3B, Supplementary Figure S3) [38,43]. Both cell lines demonstrated the capacity to take up the four lipids studied, as demonstrated by the significant increase in the levels of these lipids in cell lysates analysed by LC-MS (Figure 3A). However, uptake of the lipids varied between the two cell lines. The addition of PE (16:0_16:0) resulted in an 80.1 ± 31.4-fold increase in the intracellular levels of PL in the OPM-2 cell line, while a fold change increase of 540.3 ± 156.9 was observed in KMS-11 cells (Figure 3A). Uptake of PE (16:0_18:2) was observed in both cell lines, with a 95.4 ± 34.8-fold increase observed in OPM-2 cells and a 65.5 ± 38.1-fold increase in KMS-11 cells (Figure 3B). The uptake of PE (16:0_20:4) was also observed in the two lines, with fold changes of 39.3 ± 33.3 and 58.8 ± 26.0 in the OPM-2 and KMS-11 cells, respectively. Following the addition of PE (16:0_22:6), we observed a 248.2 ± 41.0-fold increase in this lipid in OPM-2 cells, compared to a 439.3 ± 161.4-fold change in KMS-11 cells (Figure 3A).

PE (16:0_20:4) and PE (16:0_22:6) induced cell death of both cell lines, with IC_{50} values of 53.61 ± 5.62 μM and 33.99 ± 15.34 μM for OPM-2 cells, and 54.19 ± 2.51 μM and 37.33 ± 9.03 μM for KMS-11 cells, respectively (Figure 3B). The cytotoxic effects of these lipids in both cell lines were inhibited by the synthetic antioxidant, liproxstatin-1, suggesting the cell death observed was due to ferroptosis (Figure 3B). In contrast, no cytotoxic effects induced by PE (16:0_16:0) or PE (16:0_18:2) were observed.

Treatment of OPM-2 and KMS-11 cells with PL-PUFA increased lipid ROS levels, as demonstrated by changes in the levels of oxidised C11 BODIPY; statistically significant fold changes of >2 relative to unmanipulated cells were observed in both OPM-2 and KMS-11 cell lines following treatment with 40 μM PE (16:0_20:4) or PE (16:0_22:6) (Figure 3C). A statistically significant increase in oxidised C11 BODIPY, without a decrease in cell viability, was also observed in OPM-2 when cultured with PE (16:0_18:2). The KMS-11 cells displayed a smaller, non-significant, fold change increase in oxidised C11 BODIPY following treatment with PE (16:0_18:2) (Figure 3C). Treatment with PE (16:0_16:0) had no significant effect on lipid ROS or cell viability in either cell line (Figure 3C). In all cases, the increases in lipid ROS levels were prevented by liproxstatin-1, consistent with induction of ferroptosis (Figure 3C).

Interestingly, both OPM-2 and KMS-11 cells were found to contain significantly higher levels of the lysophospholipids, lysophosphatidylethanolamine (LPE) (16:0) and LPE (22:6), following treatment with PE (16:0_22:6) (Figure 3D). Lysophospholipids are characterised by a polar head group and a singular carbon chain and are typically a minor component of the total lipid composition of cells [44]. However, studies have shown that levels of lysophospholipids significantly increase during ferroptosis, with a concomitant decrease in the corresponding PUFA-containing PL [9,45]. In OPM-2 cells, LPE (16:0) and LPE (22:6) increased 65.9 ± 17.0 and 4.9 ± 1.3-fold, respectively, while in KMS-11 cells, the same lipids increased by 45.2 ± 12.4 and 2.9 ± 0.6-fold, respectively (Figure 3D). No significant change in the levels of these lysophospholipids was observed in either cell line following culture with the other lipids. These findings indicate that PE (16:0_22:6) may be consumed during ferroptosis, resulting in the formation of the corresponding lysophospholipids.

Next, we examined the effects of the lipids on the morphology of MM cells. OPM-2 cells were cultured with PE (16:0_22:6) and images captured over a 24 h time frame using an IncuCyte S3 instrument (Figure 3E). The images show that the cells underwent

morphological changes characteristic of ferroptosis, including cytoplasmic "ballooning", in response to addition of the lipid (Figure 3E) [46]. These changes were evident in cells treated with the lipid from 8 h onwards; an additional movie file shows this in more detail (see Supplementary File S1).

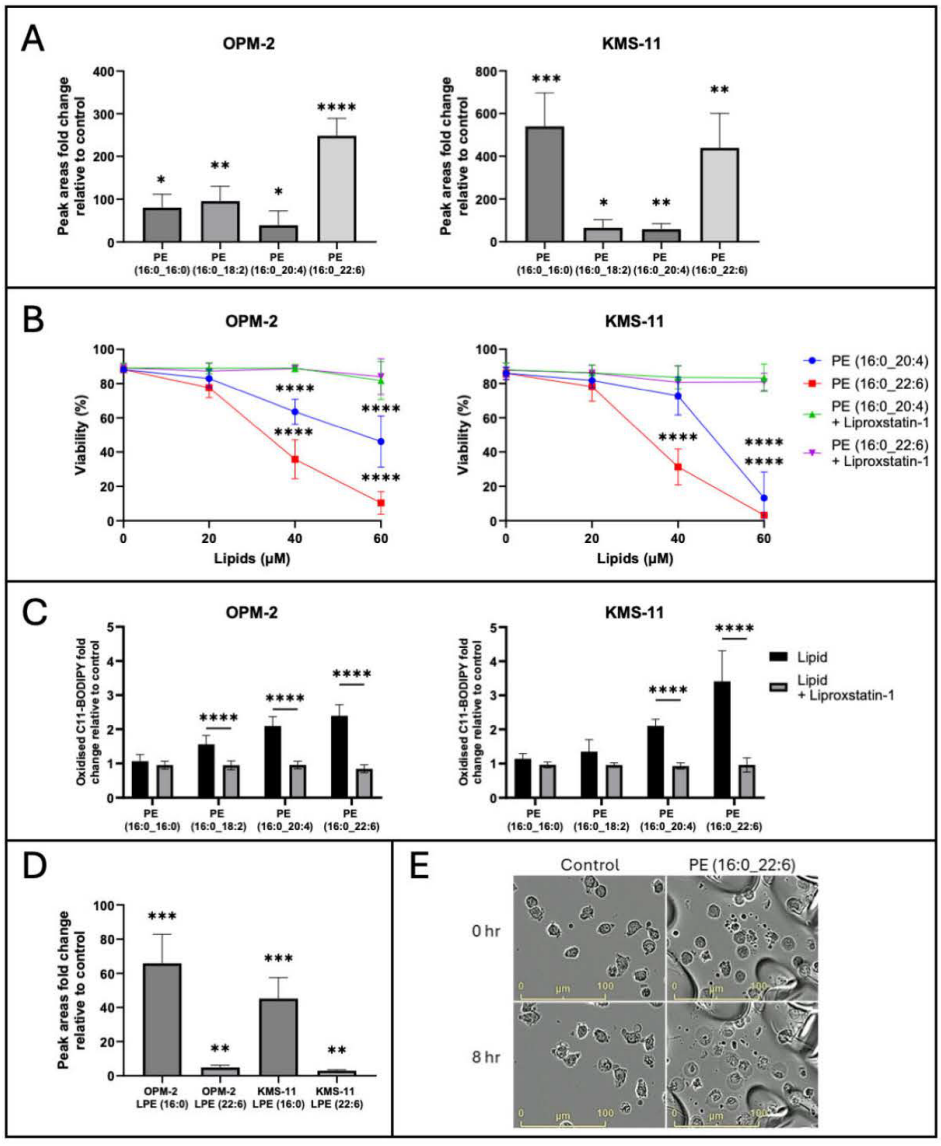

Figure 3. Ferroptosis induced by exogenous PL-PUFA correlates with the degree of acyl chain saturation. (**A**) OPM-2 and KMS-11 cells were cultured with 20 μM of the lipids indicated. Lipid uptake was assessed by LC-MS. Data are presented as mean fold changes relative to unmanipulated cell lines ± standard deviation from 3 independent experiments and statistical analyses performed using Student's *t*-test for statistical analysis (* $p < 0.05$, ** $p < 0.01$, *** $p < 0.001$, **** $p < 0.0001$). (**B**) OPM-2 and KMS-11 MM cells were cultured with the indicated concentrations of the PE lipids. Cell viability was assessed by flow cytometry following staining with annexin V and PI. Dual annexin V/PI negative cells were considered viable. Data are the mean ± standard deviation of duplicate measurements from

3 independent experiments using two-way ANOVA for statistical analysis (**** $p < 0.0001$). (**C**) OPM-2 and KMS-11 MM cells were cultured with 40 μM of the PE lipids, ± liproxstatin-1, as indicated. Lipid ROS levels were assessed by flow cytometry in cells stained with C11 BODIPY. Data are the mean ± standard deviation of duplicate measurements from 3 independent experiments using two-way ANOVA for statistical analysis (**** $p < 0.0001$). (**D**) OPM-2 and KMS-11 MM cells were cultured with 20 μM PE (16:0_22:6) for 4 h. LPE levels were determined by LC-MS. Data are presented as mean fold changes ± standard deviation from 3 independent experiments and statistical analyses performed using Student's *t*-test for statistical analysis (** $p < 0.01$, *** $p < 0.0001$). (**E**) OPM-2 cells were cultured with or without 60 μM PE (16:0_22:6). Images were acquired at the 0 and 8 h time points using an IncuCyte S3 live cell analysis system at 20× magnification. LPE, lysophosphatidylethanolamine; PE, phosphatidylethanolamine.

2.4. Exogenous PL-PUFA and RSL3 Synergise, Inducing Ferroptosis-Mediated Cell Death

Having determined that addition of exogenous PL-PUFA alters the lipidome of MM cells (Figure 3A) and can induce ferroptotic cell death (Figure 3B), we hypothesised that altering the lipid composition of MM cells may also sensitise these cells to ferroptosis induced by the GPX4 inhibitor, RSL3. Combinations of RSL3 and PE (16:0_20:4) or PE (16:0_22:6) were synergistic in OPM-2 MM cells; in combination with PE (16:0_20:4) or PE (16:0_22:6) the IC_{50} values for RSL3 were 43.59 ± 5.24 nM and 34.11 ± 6.54 nM, respectively, compared to an IC_{50} of 74.34 ± 11.17 nM for RSL3 alone (Figures 1A and 4A). In the KMS-11 cells PE (16:0_20:4) and PE (16:0_22:6) significantly increased the sensitivity of the cells to RSL3; IC_{50} values for RSL3 in combination with the lipids were 4.86 ± 2.05 μM and 2.13 ± 0.69 μM, respectively, while the IC_{50} value for RSL3 alone was 6.25 ± 0.82 μM (Figures 1A and 4A). Synergistic cell death with RSL3 was observed for both PE (16:0_20:4) and PE (16:0_22:6), with fractional products of −0.3 and −0.75 for the two lipids, respectively (Figure 4A, fractional products of <−0.1 are indicative of synergy [47]). In both OPM-2 and KMS-11 cells, addition of liproxstatin-1 prevented the cell death induced by combinations of RSL3 and the lipids, consistent with a ferroptosis-mediated mechanism of cell death (Supplementary Figure S4A).

While PL-PUFA are substrates for ferroptosis, high proportions of PL-MUFA are thought to protect cells from this form of programmed cell death [12,39]. To explore this possibility in the context of MM, OPM-2 and KMS-11 cell lines were treated with RSL3 in combination with either PE (16:0_16:0) or PE (16:0_18:1) (Figure 4B). Addition of PE (16:0_18:1) to OPM-2 cells inhibited both ferroptosis-mediated cell death and the accumulation of lipid ROS in response to RSL3, similar to the effects observed with liproxstatin-1 (Figure 4B,C). In contrast, PE (16:0_16:0) had no significant effect on the response of OPM-2 cells to RSL3 (Figure 4B). Given 5 μM RSL3 did not induce cell death in KMS-11 cells, the addition of either PE (16:0_16:0) or PE (16:0_18:1) had no effect on the sensitivity of these cells to RSL3 (Figure 4B).

Combining RSL3 and PE (16:0_22:6) augmented lipid ROS generation in both the OPM-2 and KMS-11 cell lines (Figure 4C), suggesting that increasing cellular PL-PUFA content increases the availability of substrates for lipid ROS generation. The increase in lipid ROS generation when PE (16:0_22:6) was added to RSL3 was also inhibited by liproxstatin-1 in both cell lines (Figure 4C and Supplementary Figure S4B). Furthermore, the increase in lipid ROS levels induced by RSL3 was prevented by PE (16:0_18:1) in both cell lines (Figure 4C).

Interestingly, LC-MS analysis did not show a significant increase in PE (16:0_18:1) in cells treated with this lipid. However, it appeared that levels of other oleic acid (18:1)-containing PLs were increased throughout the phospholipidome of both OPM-2 and KMS-11, while the proportion of PL-PUFA decreased (Supplementary Figure S5). Cells

can metabolise exogenous PLs, such as PE (16:0_18:1), breaking them down into free fatty acids and thus allowing them to be incorporated into other PLs [38,48]. This may explain why oleic acid, but not specifically PE (16:0_18:1) levels increased in the treated samples, however further experiments would be required to determine the fate of this lipid.

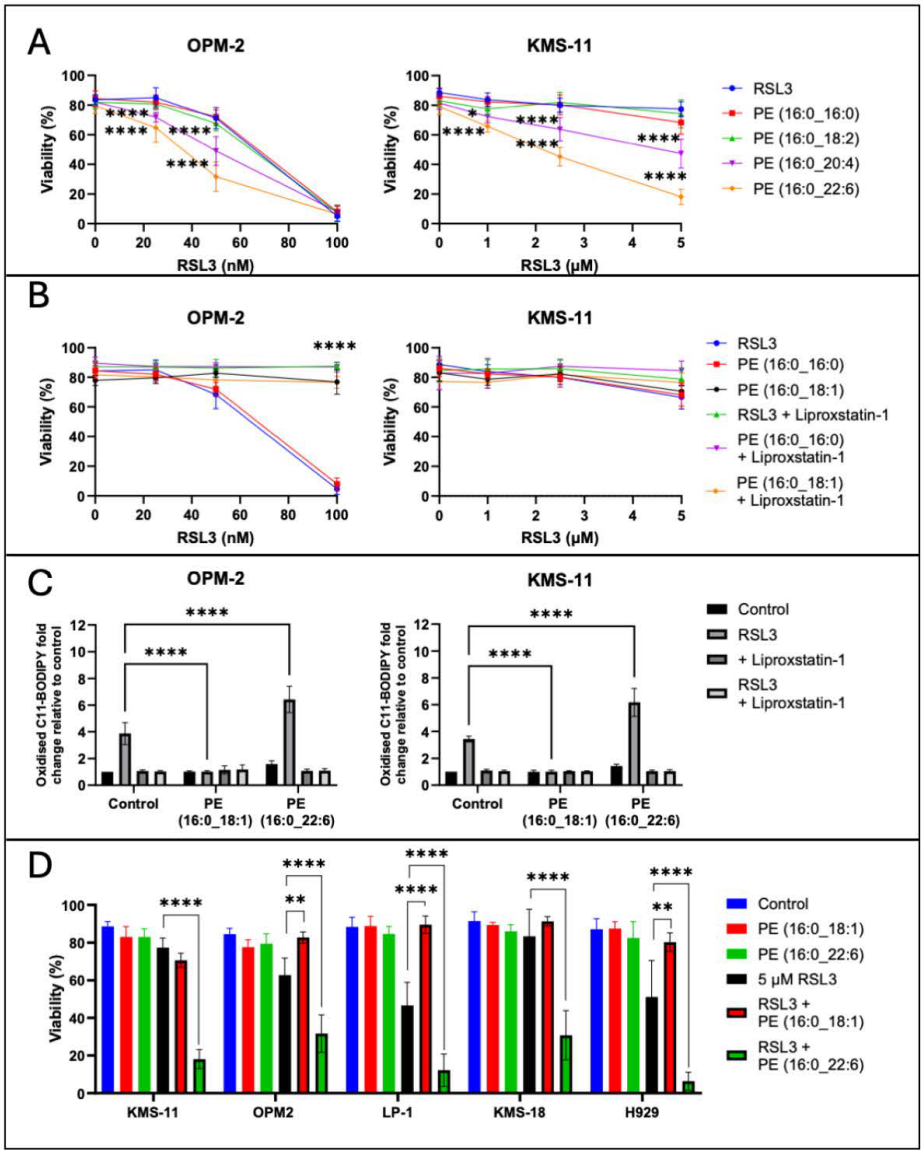

Figure 4. PL-PUFA and RSL3 induce synergistic, ferroptosis-mediated cell death while PL-MUFA protect cells from ferroptosis. (**A**) OPM-2 and KMS-11 cells were cultured with 20 μM PE (16:0_20:4) or PE (16:0_22:6) and the concentrations of RSL3 indicated. Cell viability was assessed using annexin V/PI staining and flow cytometry. Dual annexin V/PI negative cells were considered viable. (**B**) OPM-2 and KMS-11 cells were cultured with 20 μM PE (16:0_16:0) or PE (16:0_18:1) and RSL3. Cell viability was assessed by flow cytometry using annexin V/PI and flow cytometry. (**C**) OPM-2 and KMS-11 were cultured with PE (16:0_22:6) or PE (16:0_18:1) and RSL3 ± liproxstatin-1. Lipid ROS levels were assessed by flow cytometry in cells stained with C11 BODIPY. Data are fold change

relative to untreated control. (**D**) MM cell lines were cultured with 1 μM (KMS-11, LP-1, KMS-18, H929) or 50 nM (OPM-2) RSL3 for 24 h, with or without 20 μM PE (16:0_18:1) or PE (16:0_22:6). Cell viability was assessed by flow cytometry following staining with annexin V and PI. All data are the mean ± standard deviation of duplicate measurements from 3 independent experiments using two-way ANOVA for statistical analysis (* $p < 0.05$, ** $p < 0.01$, **** $p < 0.0001$).

To study the effects of specific PE lipids on MM cells more broadly, three additional MM cell lines were treated with RSL3 and either PE-PUFA or PE-MUFA (Figure 4D). Consistent with our findings from the OPM-2 and KMS-11 cell lines, treatment of LP-1 and H929 MM cell lines with RSL3 in combination with PE (16:0_18:1), led to a significant reduction in cell death (Figure 4D). However, this effect was not observed in the KMS-18 cell line. Also consistent with our earlier findings, we observed synergy between RSL3 and PE (16:0_22:6) in all five of the MM cell lines, suggesting this is not a cell line dependent effect (Figure 4D).

2.5. Induction of Ferroptosis in MM Cells by PL-PUFA-Rich Liposomes

The lipidomic data presented was used to inform the manufacture of novel liposomes, predominantly composed of PE (16:0_22:6) (98%), which induced ferroptosis-mediated cell death when added exogenously to the MM cells (Figure 3B). The remaining 2% was a pegylated saturated fatty acid, DSPE-PEG2000, which was added to stabilise the liposomes [49]. The mean diameter of the synthesised liposomes was 135 nm with a polydispersity index (PDI) of 0.06 and neutral charge of −2 mV. PDI represents the size distribution of liposomes, with values under 0.30 suggesting nanoparticles of uniform size. To assess their stability, liposomes were stored for 2 weeks at 4 °C after synthesis; the mean diameter of the liposomes after 2 weeks was 131 nm with a PDI of 0.18, confirming they were stable within this time frame.

Initially, liposomes, which included the fluorescently tagged lipid PE (18:1) (lissamine rhodamine B sulfonyl)-conjugated at a 1 in 1000 dilution, were synthesised to enable their cellular uptake to be assessed. OPM-2 and KMS-11 cells were cultured with varying amounts of the liposomes for 24 h and levels of the fluorescently tagged lipid in the cells were assessed by flow cytometry. Liposome uptake was similar in both the OPM-2 and the KMS-11 cells, with >80% of the cells analysed identified as containing the fluorescent lipid after the addition of 15 μg/mL of the liposomes to cell cultures for 24 h (Figure 5A).

Next, varying amounts of the liposomes were added to OPM-2 and KMS-11 MM cells for 24 h, with dose dependent cell death observed in both lines (Figure 5B). The IC_{50} values for the liposomes against the OPM-2 and KMS-11 cells were 36.80 ± 14.53 μg/mL and 33.28 ± 4.89 μg/mL, respectively (Figure 5B). A concomitant increase in levels of lipid ROS was also observed in cells treated with the liposomes, with a 1.6 ± 0.2-fold increase in the OPM-2 and a 1.7 ± 0.3-fold increase in the KMS-11 cells in response to a 15 μg/mL dose of the liposomes (Figure 5C). Addition of liproxstatin-1 prevented both the cell death and lipid ROS accumulation induced by the liposomes (Figure 5B,C).

Consistent with the results obtained using exogenous lipids and RSL3, addition of free RSL3 in combination with the liposomes significantly increased the cytotoxic effects of the nanoparticles. In combination with 50 nM or 2.5 μM RSL3, the IC_{50} values for the liposomes against the OPM-2 and KMS-11 cells were reduced to 10.61 ± 2.91 μg/mL and 8.44 ± 2.73 μg/mL, respectively (Figure 5B). Synergy between 15 μg/mL of the liposomes and RSL3 was confirmed, with fractional products of −0.54 for the OPM-2 cell line and −0.33 for the KMS-11 cell line (Figure 5B). RSL3 also significantly increased the levels of ROS induced by the liposomes in both cell lines; 15 μg/mL of liposomes in combination

with RSL3 resulted in an 8.4 ± 1.1-fold increase in lipid ROS in the OPM-2 cells and a 15.8 ± 3.6-fold increase in the KMS-11 cells (Figure 5C).

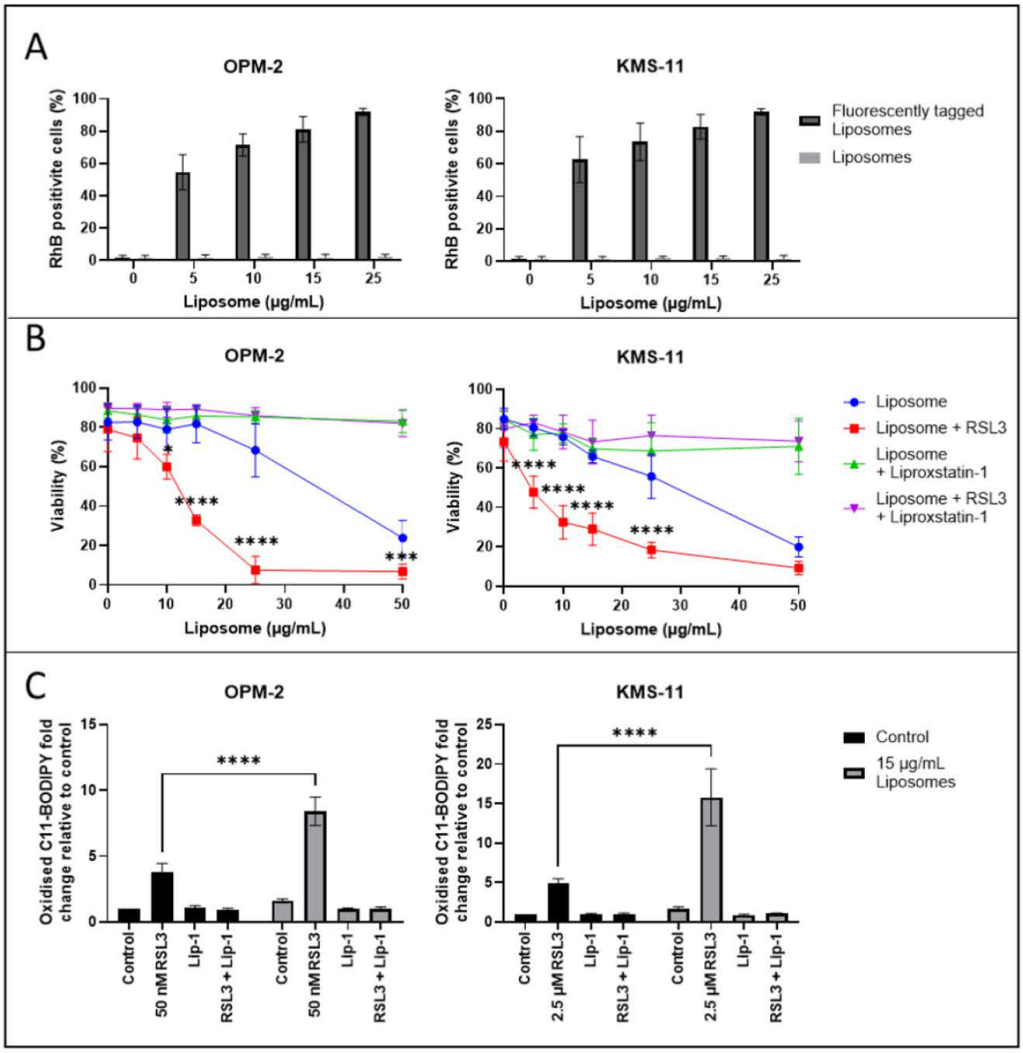

Figure 5. Liposomes composed of PE (16:0_22:6) combined with free RSL3 induce synergistic ferroptosis-mediated cell death of MM cells. (**A**) OPM-2 and KMS-11 cells were cultured for 24 h with increasing concentrations of liposomes, which did or did not contain PE (18:1) (lissamine rhodamine B sulfonyl)-conjugated lipid at a 1 in 1000 dilution. The percentage of cells containing the fluorescently tagged lipid was assessed by flow cytometry. (**B**) OPM-2 and KMS-11 cells were cultured with increasing concentrations of liposomes, with or without 50 nM (OPM-2) or 2.5 µM (KMS-11) free RSL3 with or without liproxstatin-1. Cell viability was assessed using annexin V/PI staining and flow cytometry. (**C**) OPM-2 and KMS-11 cells were cultured with 15 µg/mL liposomes, plus 50 nM or 2.5 µM RSL3, respectively, ± liproxstatin-1. Lipid ROS levels were assessed by flow cytometry in cells stained with C11 BODIPY. All Data are the mean ± standard deviation of duplicate measurements from 3 independent experiments using two-way ANOVA for statistical analyses (*** $p < 0.001$, **** $p < 0.0001$).

2.6. PL-PUFA-Rich Liposomes Containing RSL3 Induce Ferroptosis-Mediated Cell Death of MM Cells

Next, RSL3 was encapsulated within the liposomes tested in Figure 5. In total, 50 µg/mL (113.41 µM) RSL3 was incorporated into the liposomes, corresponding to ~5% of the total liposome mass at assembly. RSL3 is a lipophilic molecule, which means it is likely to localise to the lipid bilayer of the liposomes. The mean diameter of the synthesised liposomes containing RSL3 was 135 nm with a PDI of 0.24 and a near neutral charge (zeta potential of −2 mV). A HPLC method for quantifying the concentration of RSL3 within the liposomes was developed based on the manufacturer's guidelines for RSL3 purification and assessment (personal communication to A. Habib from Selleck Chemicals LLC). Increasing concentrations of RSL3 were prepared to generate standard curves (Figure 6A). RSL3 encapsulation efficiency was assessed using this methodology and was determined to be approximately 67%.

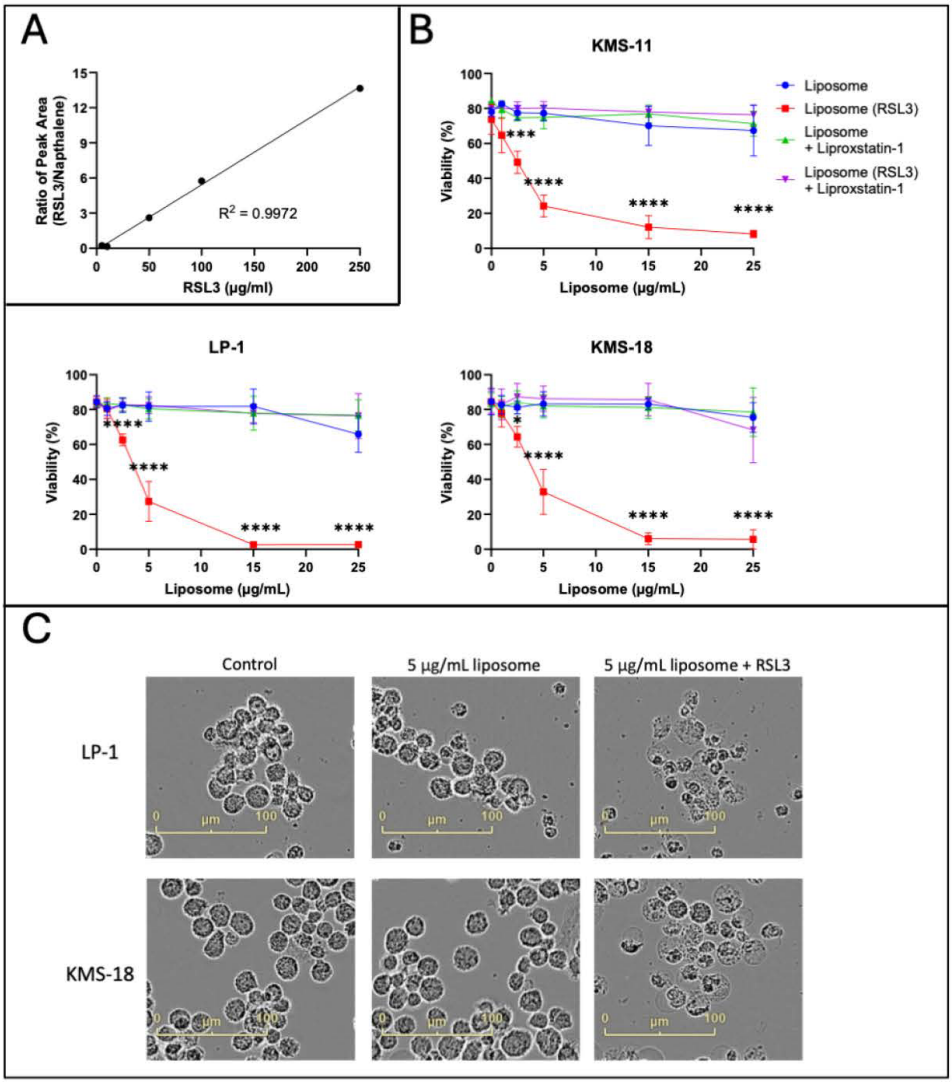

Figure 6. Liposomes encapsulating RSL3 are highly effective at inducing ferroptosis-mediated death of MM cells. (**A**) Representative standard curve generated for assessing RSL3 incorporation efficiency

into liposomes, generated using peak areas from HPLC. (**B**) KMS-11, LP-1 and KMS-18 cells were cultured with increasing concentrations of liposomes that either did or did not contain RSL3 and with or without addition of free liproxstatin-1. Cell viability was assessed using annexin V/PI staining and flow cytometry. Data are the mean ± standard deviation of duplicate measurements from 3 independent experiments using two-way ANOVA for statistical analyses (*** $p < 0.001$, **** $p < 0.0001$). (**C**) MM cells were cultured for 24 h with 5 µg/mL liposomes that either did or did not contain RSL3. Images were acquired at 24 h using an IncuCyte S3 live cell analysis system at 20× magnification.

KMS-11, LP-1 and KMS-18 MM cell lines were cultured for 24 h with increasing concentrations of liposomes, which did or did not contain RSL3. The IC_{50} values for the RSL3-encapsulated liposomes in the aforementioned cell lines were 3.80 ± 0.67 µg/mL, 3.35 ± 0.70 µg/mL and 4.05 ± 1.51 µg/mL, respectively, which are equivalent to RSL3 concentrations of 430.39 ± 76.13 nM (KMS-11), 379.84 ± 79.25 nM (LP-1) and 459.47 ± 171.52 nM (KMS-18) (Figure 6B). In comparison, the IC_{50} values for free RSL3 against these lines were 6.25 ± 0.82 µM, 2.70 ± 0.72 µM, and 3.84 ± 0.37 µM, respectively (Figure 1A), consistent with an average 7.1-fold to 14.5-fold decrease in the IC_{50}s by the RSL3-encapsulated liposomes from the micromolar to the nanomolar range. Morphological changes consistent with ferroptosis were observed in the MM cell lines after 24 h of treatment with the RSL3-containing liposomes (Figure 6C) and both the morphological changes and cell death were prevented by co-administration of liproxstatin-1 (Supplementary Figure S6 and Figure 6B). Additionally, increases in lipid ROS were also observed in the MM cells when cultured with these liposomes containing RSL3 in all three cell lines (Supplementary Figure S7). These increases in lipid ROS were preventable with liproxostatin-1, indicative of ferroptosis (Supplementary Figure S7). The effects of the RSL3-encapsulated liposomes were not assessed against OPM-2 MM cells due to their sensitivity to RSL3 and because the RSL3 concentrations that would be required in liposomes for this cell line were below the limit of detection of the HPLC assay.

3. Discussion

Conventional cancer therapies, particularly chemotherapeutic regimens, typically induce tumour cell death by triggering apoptotic pathways. However, the significant proportion of cancer patients who are initially treatment-resistant or who relapse with drug-resistant disease highlights the pressing need for the development of new and improved therapeutic approaches.

Despite advances in the treatment of MM, it is still considered an incurable disease. Ferroptosis may represent a new avenue for treatment of this and other forms of cancer. However, it is apparent from the current study (Figure 1A) and that of Yang et al. [9], that MM cells are relatively insensitive to ferroptosis-mediated cell death induced either by direct (RSL3) or indirect (erastin) inhibition of GPX4, compared to DLBCL cells. The current study was undertaken to explore the role of PLs in enhancing the sensitivity of MM cells to ferroptosis and whether manipulation of the lipidome of these cells using novel liposomes represents an approach for harnessing this form of programmed cell death.

Unlike the other 5 MM lines investigated in this work, OPM-2 cells were significantly more sensitive to the GPX4 inhibitor, RSL3 (Figure 1A). This was apparent as cell death and characteristic morphological changes were induced by relatively low concentrations of the drug and both effects were inhibited by the synthetic antioxidant, liproxstatin-1. In comparison, IC_{50} values for RSL3 in the other MM lines were up to 95 times higher. Although we observed significant variation in GPX4 expression between the different lines (Figure 1B,C), no correlation between their sensitivity to RSL3 and expression of

its target, GPX4, or trends in GPX4 expression between the MM and DLBCL lines, were apparent (Figure 1).

PLs play a pivotal role in ferroptosis, particularly lipids containing PUFA [12]. By performing a lipidomic analysis of MM and DLBCL cells, we showed that the MM cells studied generally contained a significantly lower proportion of PLs containing PUFAs, and a higher proportion of MUFA, than DLBCL cells (Figure 2A). The exception were the OPM-2 MM cells, which in terms of their proportions of PUFA and MUFA, were similar to DLBCL cells rather than the other MM lines (Figure 2B). Furthermore, OPM-2 cells, like DLBCL cells, were sensitive to RSL3 with IC_{50} values in a nanomolar range (Figure 1A). Overall, in the cell lines studied, the data demonstrated a strong link between the proportion of PUFA-containing PLs and the sensitivity of cells to RSL3.

The importance of the balance between PUFA and MUFA content is further highlighted by our finding that uptake of PUFAs is sufficient to induce ferroptosis (Figure 3B) and sensitise MM cells to RSL3 (Figure 4A). Our observation that OPM-2 and KMS-11 cells were significantly more sensitive to PE (16:0_22:6) than to PE (16:0_20:4) (Figure 3B,C), in terms of both ferroptosis-mediated cell death and lipid oxidation, is consistent with a previous study, suggesting that the degree of PL acyl chain saturation relates to ferroptosis sensitivity [12]. Oxidation of PUFAs during ferroptosis is known to result in their degradation, with a concomitant increase in levels of lysophospholipid species [9,45]. Accordingly, we observed an increase in the proportion of lysophospholipids in both OPM-2 and KMS-11 MM cells following culture with non-cytotoxic concentrations of PE (16:0_22:6) (Figure 3D). This finding indicates that even at low concentrations, addition of lipid substrates is sufficient to induce an increase in acyl chain oxidation and may prime normally ferroptosis-insensitive cells to this form of cell death. This is supported by the synergy observed between unsaturated PE lipids and RSL3 (Figure 4), where a non-cytotoxic dose of lipids significantly decreased the IC_{50} value for RSL3 in KMS-11 and OPM-2 MM cells. The effects of exogenous PUFAs on ferroptosis-resistant MM cells reinforce the notion that these cells do inherently express the machinery to undergo ferroptosis, but may lack sufficient endogenous ferroptosis substrates required to initiate this cell death process [31,32].

The contrasting effects of MUFA supplementation on the RSL3 sensitivity of OPM-2 cells (Figure 4B) further illustrates the strong association between fatty acid composition and the ferroptosis sensitivity of MM cells. Under basal conditions, OPM-2 cells had a significantly higher proportion of PUFAs than KMS-11 cells. The addition of exogenous MUFA to OPM-2 cells raised the intracellular proportion of this lipid and possibly displaced PUFAs from the lipidome, thereby significantly reducing the sensitivity of these cells to RSL3. Similar effects of MUFAs have been observed in human epithelial cells and mouse fibroblasts suggesting that the anti-ferroptotic effects of MUFAs are not limited to MM cells [38,50].

Iron is essential for cellular homeostasis [51], with key roles in oxygen transport, oxidative phosphorylation and DNA biosynthesis [52]. As iron chelation inhibits ferroptosis, this form of cell death is also clearly an iron-dependent process [8]. Intracellular iron levels are primarily regulated by the iron-storage protein ferritin, and the transferrin receptor (TfR) which shuttles transferrin-bound iron into the cell through receptor-mediated endocytosis. The level of non-protein bound iron (labile iron pool) has implications in ferroptosis as labile iron reacts with hydrogen peroxide inside cells, yielding highly reactive hydroxyl radicals in a process known as the Fenton reaction [53]. These radicals indiscriminately damage all surrounding organic material within a range of a few nanometres, resulting in cellular damage [53]. Iron also plays a role in ferroptosis through its actions on a group of iron-containing enzymes that mediate lipid peroxidation, known as lipoxygenases (LOXs) [19,54]. The key role of these enzymes is demonstrated by the LOX inhibitor,

zileuton, which confers resistance to ferroptotic cell death in HT22 neuronal cells [55]. Furthermore, genetic knockdown or pharmacological inhibition of arachidonate lipoxygenases (ALOXs) protects cells against ferroptosis induced by erastin [56]. While labile iron and LOX expression or activity were not investigated in the current study, our focus on PLs remains mechanistically valid due to the observed dependence of RSL3-induced MM cell death on lipid ROS and prevention by ferroptosis inhibitors such as liproxstatin-1.

The ability to encapsulate drugs or to bind molecules, such as antibodies, to the surface of liposomes, means they represent an extremely versatile form of nanoparticles. We were able to show that liposomes manufactured from specific lipids, identified from the lipidomic screen of MM and DLBCL cells, were readily taken up by MM cells, leading to lipid ROS accumulation and ferroptosis-mediated cell death (Figure 5). This further demonstrates the crucial role of PUFAs as ferroptosis substrates and important determinants of MM cell sensitivity to this form of cell death. Moreover, this highlights the potential of ferroptosis-inducing liposomes as personalised or "precision" therapeutics, as it is conceivable that liposomes could be manufactured for specific patients, based on the lipidome of their tumour cells. As observed with exogenous PUFAs and free RSL3, liposomal delivery of PUFA combined with free RSL3 also exhibited a high degree of synergy against OPM-2 and KMS-11 MM cells, in terms of lipid ROS accumulation and ferroptosis-mediated cell death (Figure 5). While previous studies have used liposomes to deliver ferroptosis-inducing compounds to cancer cells, few have shown that the lipids used to manufacture the liposomes themselves are alone sufficient to induce ferroptosis or that this effect can be further enhanced by encapsulating RSL3 within the liposomes [23–28].

The current study demonstrated that it is possible to encapsulate RSL3 at concentrations of approximately 113 μM, a level that represented around 5% of the mass of the liposomes. Subsequent treatment of three MM cell lines showed that RSL3 delivered in this liposomal formulation was on average 7.1-fold to 14.5-fold more effective than free RSL3, represented by a decrease in the IC_{50}s for cell viability from the micromolar to the nanomolar range (Figures 1A and 6B). Furthermore, significantly fewer RSL3-encapsulated liposomes than empty liposomes were required to induce a similar degree of ferroptosis-mediated cell death (Figures 5B and 6B). Future development of our liposomes will include external functionalisation with a monoclonal antibody against a MM-specific cell surface protein such as B cell maturation protein (BCMA), for tumour-directed cell death and sparing of healthy tissues, in preparation for in vivo testing. Such in vivo models include the syngeneic immunocompetent model utilising murine MM 5TGM1 cells in C57BL/KaLwRij mice [34] and human MM xenografts using NOD scid gamma (NSG) mice [57]. Finally, the challenges of translating liposome therapeutics for in vivo use are substantial and include stability, clearance, opsonisation and deactivation, and off-target effects [58]. Some of these have been considered in our ex vivo developmental process including liposome size and charge, inclusion of DSPE-PEG2000 and external functionalisation with a tumour-specific monoclonal antibody; however, until such in vivo experimentation is undertaken, it is difficult to predict how successful our liposomes will be, despite their encouraging in vitro efficacy presented herein.

4. Methods

4.1. Drugs, Chemicals, and Other Reagents

(1S,3R)-RSL3 (RSL3), bortezomib, liproxstatin-1, Z-VAD-FMK and necrostatin-1s were purchased from Selleck Chemicals (Houston, TX, USA). The lipids, 16:0 PE, 16:0-18:1 PE, 16:0-18:2 PE, 16:0-20:4 PE and 16:0-22:6 PE were purchased from Sigma-Aldrich (St. Louis, MO, USA). FITC-conjugated Annexin V and Annexin V Binding Buffer were purchased from Becton Dickinson Biosciences (Franklin Lakes, NJ, USA). Propidium iodide was

purchased from Sigma-Aldrich. BODIPY^{TM} 581/591 C11 (D3861) was purchased from Thermo Fisher Scientific (Waltham, MA, USA). Anti-GPX4 and anti-RIP3 rabbit monoclonal antibodies were purchased from Cell Signalling Technology (Danvers, MA, USA). Anti-actin mouse monoclonal antibody was purchased from Millipore (Burlington, MA, USA). Peroxidase-conjugated, goat anti-rabbit and goat anti-mouse secondary antibodies were purchased from Invitrogen (Waltham, MA, USA).

4.2. Cell Culture

The human MM cell line, RPMI-8226 (ATC CCL-155), was purchased from the American Type Culture Collection (ATCC, Manassas, VA, USA). The KMS-11 (JCRB1179) human MM cell line was purchased from CellBank Australia (Sydney, Australia). The LP-1 (ACC 41) and OPM-2 (ACC 50) human MM cell lines were purchased from the Leibniz Institute DSMZ—German Collection of Microorganisms and Cell Cultures GmbH (Braunschweig, Germany). The NCI-H929 line was kindly provided by Prof. Andrew Spencer (Monash University, Melbourne, VIC, Australia), and KMS-18 cells were kindly provided by Prof. Junia Melo (South Australia Pathology, Adelaide, Australia). The DLBCL cell lines SU-DHL-8, OCI-Ly19, Farage, U-2932 and HBL-1 were supplied by Dr Giles Best (Adelaide, Australia). All cells were cultured in RPMI-1640 (Gibco, Waltham, MA, USA) supplemented with 10% foetal bovine serum, 50 units/mL penicillin, 0.25 mg/mL streptomycin, 2 mM L-glutamine and 15 mM HEPES buffer (all Gibco). Cells were maintained at 37 °C in 5% CO_2. All cell lines were genetically authenticated by the Australian Genome Research Facility (AGRF; Adelaide, Australia) and determined mycoplasma-free using the MycoStrip^{TM}—Mycoplasma Detection Kit (InvivoGen, San Diego, CA, USA). For cell culture, viable cells were enumerated by mixing 10 µL of cell suspension in a 1:1 ratio with 0.4% trypan blue (Invitrogen) and counted using a haemocytometer (Adelab, Adelaide, Australia).

4.3. Assessment of Cell Viability

Cells were initially cultured at a cell density of 3×10^5 cells/mL with or without treatment for up to 24 h. Cells were washed in phosphate-buffered saline (PBS, Gibco, Waltham, MA, USA) and stained with 0.27 µg/mL FITC-conjugated Annexin V and 0.4 µg/mL propidium iodide (PI) in 1X Annexin V Binding Buffer for 10 min in the dark at room temperature. Intact cells were gated based on their size (forward scatter, FSC) and internal complexity (side scatter, SSC). Doublets were excluded by area scaling of the FSC area and height properties. Data from a minimum of 10,000 intact single cells was acquired either on a CytoFLEX S or CytoFlex SRT flow cytometer (Beckman Coulter, Brea, CA, USA), with analysis performed using CytExpert Software v2.4 or CytExpert SRT Software v1.0 (Beckman Coulter), respectively. Cells negative for both Annexin V and propidium iodide were considered viable. For cell death inhibition experiments, cells were preincubated in 200 µM Z-VAD-FMK for 45 min to inhibit apoptosis prior to the addition of RSL3 or bortezomib whereas 2 µM liproxstatin-1 to inhibit ferroptosis or 1 µM necrostatin-1s to inhibit necroptosis were added at the same time, prior to assessing cell viability by flow cytometry.

4.4. Assessment of Lipid ROS

Cells were cultured with or without treatment for 24 h at 37 °C. 30 min prior to the end of the incubation, a final concentration of 400 nM C11 BODIPY-FITC was added to relevant wells before a further 15 min incubation. Cells were then washed twice with PBS and re-suspended in fresh PBS prior to analysis by flow cytometry, as described above.

4.5. Sample Preparation for Lipidomic Analyses

Cells were cultured at a density of 3×10^5 cells/mL with or without treatment for 4 h. Cell suspensions were washed in PBS and stored at −80 °C before processing. Subsequent sample processing and analysis by liquid chromatography/mass spectrometry was performed in the Lipidomics and Metabolomics core facility at the South Australian Health and Medical Research Institute (SAHMRI, Adelaide, Australia). All samples were prepared in duplicate and protein concentrations determined using the bicinchoninic acid (BCA) assay (Thermo Fisher Scientific), as per the manufacturer's instructions. An extraction buffer consisting of acetonitrile/isopropanol/splash mix (99:99:2, *v*/*v*) was made fresh and 100 µL added to the equivalent of 10 µg of protein from each sample. Samples were then sonicated for 10 min and incubated at −20 °C for one hour. Samples were centrifuged at 16,000× *g* for 15 min and the supernatant transferred to a glass vial. A pooled quality control sample was prepared by combining 10 µL of supernatant from all samples in a glass vial. Samples were then run on a XEVO G2-XS QTOF liquid chromatography/mass spectrometer (Waters Corporation, Milford, MA, USA) according to a lipidomics assay protocol established at SAHMRI [59]. Sample data were processed and analysed using Skyline Targeted Mass Spec Environment v23.1 [60], MetaboAnalyst v5.0 and v6.0 (Wishart Research Group, Alberta, Canada) and Microsoft Excel v16.96. Heatmaps and Volcano plots were generated using MetaboAnalyst. Data were normalised to the median, $\log_{10}$ transformed, auto-scaled (mean-centred) and divided by the standard deviation of each variable.

4.6. Live Cell Imaging

50 µL poly-L-ornithine (Sigma-Aldrich) was added to each well of a 96 well plate and incubated for 1 h at room temperature. Excess solution was then removed from the wells and the plates were dried for 1 h. 5000–10,000 cells, with or without treatment, were added to each well. Images were obtained every hour for up to 24 h using an IncuCyte® S3 Live-Cell Analysis System and software v2023A (Sartorius Australia, Victoria, Australia) at 20× magnification.

4.7. Western Blotting

3 to 5 million cells were lysed in 10 mM Tris/HCl (pH 7.4), 137 mM NaCl containing 10% glycerol, 1% NP40, 10 mM β-glycerophosphate, 2 mM sodium fluoride and complete EDTA-free protease inhibitor cocktail (Sigma-Aldrich). The samples were kept on ice for 10 min before centrifugation at 14,000× *g* to clarify the lysate. Equal amounts of protein were loaded onto a Mini-PROTEAN TGX Precast Gel (Bio-Rad, Hercules, CA, USA) and transferred onto nitrocellulose membranes using a Trans-Blot Turbo Transfer System (Bio-Rad). Membranes were then blocked in 5% non-fat dairy milk powder in 50 mM Tris (pH 7.4), 154 mM NaCl and 1% Tween20 at room temperature for two hours. Primary and secondary antibodies were used as per the manufacturers' instructions and membranes were imaged on a ChemiDoc MP system (Bio-Rad) after incubation in Clarity Western ECL Substrate (Bio-Rad). GPX4, RIP3 and anti-actin primary antibodies were used at a dilution of 1:1000, 1:1000 and 1:5000, respectively, and HRP-conjugated secondary antibodies were used at a dilution of 1:15,000. Image Lab Software v6.1 (Bio-Rad) was used for densitometric analysis of Western blot images.

4.8. Liposome Preparation

4.8.1. Micro-Fluidics Synthesis

A NanoAssemblr® Ignite system (Precision Nanosystems, Vancouver, BC, Canada) was used to prepare all formulations using the following parameters: total flow rate = 12 mL/min,

flow ratio = 3:1 (aqueous: organic), total volume = 4mL, start and end waste = 0.01 mL. Lipids were dissolved in 1mL of ethanol as the organic phase to produce a final lipid concentration of 1 mg/mL. Drug free liposomes were prepared using PBS (pH = 7.4) as the aqueous phase. Liposomes were prepared in an organic phase consisting of PE (16:0_22:6): DSPE-PEG2000 at ratios of 98:2 (*w*/*w*%). Synthesised liposomes were dried under N_2 gas to remove excess solvent. Liposomes containing a Rhodamine B-conjugated lipid at a concentration of 1 µg/mL were also synthesised to enable liposome uptake to be assessed by flow cytometry.

4.8.2. Liposome Characterisation

The various liposome formulations were characterised by dynamic light scattering (DLS) using a Malvern Zetasizer Nano ZS at 25 °C and Zetasizer Nano software v3.30 (Malvern Panalytical, Worcestershire, UK). Samples were diluted 10-fold with Milli-Q ultrapure water (Merck Millipore, Burlington, MA, USA) for all size measurements. Results were reported as a mean hydrodynamic diameter ± standard deviation, and polydispersity index (PDI). Zeta potential was also measured using the Malvern Zetasizer. Undiluted samples were used for zeta potential measurements, with results reported as the average zeta potential ± standard deviation.

4.8.3. Assessment of Liposome Uptake

Cells were cultured, with or without, liposomes containing the PE (18:1) (lissamine rhodamine B sulfonyl)-conjugated lipid (approximately 1 µg/mL in 1 mg/mL liposome concentration) at concentrations of up to 50 µg/mL, for 24 h at 37 °C. Cells were then washed with PBS and resuspended in fresh PBS. The proportion of cells containing the fluorochrome-tagged lipid was determined by flow cytometry, as described above.

4.8.4. Assessment of Liposome RSL3 Encapsulation

Liposomes were prepared, with or without, varying concentrations of RSL3. Ultrafiltration using an Ultracell Ultrafiltration system fitted with a PES 5 kDa membrane filter (Merk Millipore, Burlington, MA, USA) was then used to remove free RSL3. The liposome solutions were weighed before and after filtration to account for volume lost during filtration before dilution at a 1:1 ratio in the mobile phase and analysis as described below.

4.8.5. High-Performance Liquid Chromatography

High-performance liquid chromatography (HPLC—Shimadzu Nexera XR) and a Phenomenex Luna 5 µm C18(2) 100 Å, LC Column 250 × 4.6 mm (Phenomenex, Torrance, CA, USA) HPLC column were used to determine the concentration of RSL3 encapsulated within the liposomes. Conditions were as per manufacturer's instructions and are described below, with alterations to account for equipment variability. The column oven was set to 25 °C, with a wavelength of 280 nm and flow rate of 0.8 mL/min. Mobile phase A consisted of H_2O and 0.1% trifluoroacetic acid (TFA), mobile phase B was composed of acetonitrile and 0.1% TFA. Naphthalene was used as an internal standard at a concentration of 100 µg/mL. The injection volume was 10 µL and the isocratic method used was 10% mobile phase A/90% mobile phase B. RSL3 standards, ranging from 5 µg/mL–250 µg/mL, and unknown samples were prepared in mobile phase B. Peaks were detected at a retention time of 1.9 min. All samples were measured in triplicate with a minimum of three biological replicates.

4.9. Statistical Analyses

Statistical analyses were performed by Student's *t*-test for two-group comparisons and two-way ANOVA for comparing more than two groups, using GraphPad Prism software v10.2.0 (Boston, MA, USA). A p-value < 0.05 was considered statistically sig-

nificant, with differing degrees of statistical significance indicated as follows: * $p < 0.05$, ** $p < 0.01$, *** $p < 0.001$, **** $p < 0.0001$. The fractional product method was used to determine synergistic, additive or antagonistic effects of drug combinations, with values of <0.1 indicative of synergy [47]. GraphPad Prism was used to fit 4-parameter logistic (4PL) sigmoidal dose–response models for cell viability data to determine IC_{50} values.

5. Conclusions

Collectively, the results of this study demonstrate a significant link between the polyunsaturated and monounsaturated fatty acid composition of MM cells and their sensitivity to ferroptosis. By manipulating the intracellular PL composition, we demonstrate that it is possible to markedly sensitise MM cells to ferroptosis induced by GPX4 inhibition. Our liposomes manufactured from PL-PUFAs that are relatively deficient in MM cells and loaded with RSL3 provide strong proof-of-principle evidence that lipid nanoparticles may represent a highly effective mechanism for delivering both ferroptosis substrates and ferroptosis-inducing agents to cancer cells. Moreover, by manufacturing liposomes with specific PL-PUFAs that are less abundant in MM cells compared to ferroptosis-sensitive cancers, and by extension, less abundant in MM cells from a given MM patient compared to another MM patient, personalised or precision ferroptosis-inducing liposomes could be developed. These findings support further research and development of therapeutics that induce ferroptosis as a novel treatment approach for MM and other forms of cancer, and particularly for overcoming resistance to more conventional apoptosis-inducing therapies.

Supplementary Materials: The following supporting information can be downloaded at: https://www.mdpi.com/article/10.3390/ijms26146579/s1.

Author Contributions: A.H., O.G.B., C.A.P. and C.T.W.-G. designed the experiments; A.H., R.L.M., O.G.B. and I.A.R. performed the experiments; A.H., O.G.B., C.A.P. and C.T.W.-G. performed the data analysis; A.H., O.G.B. and C.T.W.-G. wrote the manuscript; A.H., O.G.B., C.A.P. and C.T.W.-G. edited the manuscript. All authors have read and agreed to the published version of the manuscript.

Funding: A.H. was funded by a Jane Watson Ramsey Myeloma Research PhD Scholarship. R.L.M. was funded by an Australian Government Research Training Program (RTP) Scholarship and Margaret Fay Fuller Foundation Scholarship Top-Up. C.W.G was funded by a Cancer Council SA Clinical Investigator Grant and Flinders Foundation Cancer Seed Grant.

Institutional Review Board Statement: Not applicable.

Informed Consent Statement: The authors give full consent to publishing this work in the International Journal of Molecular Sciences.

Data Availability Statement: The datasets used and/or analysed during the current study are available from the corresponding author on reasonable request.

Acknowledgments: The authors would like to acknowledge Martin Snel and Paul Trim from the Lipidomics Facility at the South Australian Health and Medical Research Institute for technical assistance with all lipidomics analyses and Kara Paxton from the Nanostructure and Drug Delivery Group at the University of South Australia for technical analysis with nanoparticle formation and HPLC.

Conflicts of Interest: The authors declare no conflict of interest.

List of Abbreviations

DLBCL	Diffuse large B cell lymphoma
FA	Fatty acid
GPX4	Glutathione peroxidase 4

HPLC	High-performance liquid chromatography
LC-MS	Liquid chromatography–mass spectrometry
LIP-1	Liproxstatin-1
LOX	Lipooxygenase
LPC	Lysophosphatidylcholine
LPE	Lysophosphatidylethanolamine
MM	Multiple myeloma
MUFA	Monounsaturated fatty acid
NEC-1	Necrostatin-1
PC	Phosphatidylcholine
PCD	Programmed cell death
PDI	Polydispersity index
PE	Phosphatidylethanolamine
PI	Propidium iodide
PL	Phospholipid
PS	Phosphatidylserine
PUFA	Polyunsaturated fatty acid
RIPK	Receptor-interacting protein kinase
ROS	Reactive oxygen species
RSL3	(1S,3R)-RSL3
SFA	Saturated fatty acid

References

1. Rasche, L.; Chavan, S.S.; Stephens, O.W.; Patel, P.H.; Tytarenko, R.; Ashby, C.; Bauer, M.; Stein, C.; Deshpande, S.; Wardell, C.; et al. Spatial genomic heterogeneity in multiple myeloma revealed by multi-region sequencing. *Nat. Commun.* **2017**, *8*, 268. [CrossRef]
2. Cowan, A.J.; Green, D.J.; Kwok, M.; Lee, S.; Coffey, D.G.; Holmberg, L.A.; Tuazon, S.; Gopal, A.K.; Libby, E.N. Diagnosis and Management of Multiple Myeloma: A Review. *JAMA* **2022**, *327*, 464–477. [CrossRef]
3. Australian Institute of Health and Welfare. Cancer Data in Australia. Available online: https://www.aihw.gov.au/reports/cancer/cancer-data-in-australia/contents/survival (accessed on 20 March 2025).
4. Shah, U.A.; Mailankody, S. Emerging immunotherapies in multiple myeloma. *BMJ* **2020**, *370*, 3176. [CrossRef]
5. Kazandjian, D.; Landgren, O. A look backward and forward in the regulatory and treatment history of multiple myeloma: Approval of novel-novel agents, new drug development, and longer patient survival. *Semin. Oncol.* **2016**, *43*, 682–689. [CrossRef] [PubMed]
6. Al-Odat, O.S.; Guirguis, D.A.; Schmalbach, N.K.; Yao, G.; Budak-Alpdogan, T.; Jonnalagadda, S.C.; Pandey, M.K. Autophagy and Apoptosis: Current Challenges of Treatment and Drug Resistance in Multiple Myeloma. *Int. J. Mol. Sci.* **2022**, *24*, 644. [CrossRef]
7. Safa, A.R. Drug and apoptosis resistance in cancer stem cells: A puzzle with many pieces. *Cancer Drug Resist.* **2022**, *5*, 850–872. [CrossRef]
8. Dixon, S.J.; Lemberg, K.M.; Lamprecht, M.R.; Skouta, R.; Zaitsev, E.M.; Gleason, C.E.; Patel, D.N.; Bauer, A.J.; Cantley, A.M.; Yang, W.S.; et al. Ferroptosis: An iron-dependent form of nonapoptotic cell death. *Cell* **2012**, *149*, 1060–1072. [CrossRef] [PubMed]
9. Yang, W.S.; SriRamaratnam, R.; Welsch, M.E.; Shimada, K.; Skouta, R.; Viswanathan, V.S.; Cheah, J.H.; Clemons, P.A.; Shamji, A.F.; Clish, C.B.; et al. Regulation of ferroptotic cancer cell death by GPX4. *Cell* **2014**, *156*, 317–331. [CrossRef]
10. Yang, W.S.; Stockwell, B.R. Ferroptosis: Death by Lipid Peroxidation. *Trends Cell Biol.* **2016**, *26*, 165–176. [CrossRef]
11. Ahmed, S.; Shah, P.; Ahmed, O. *Biochemistry, Lipids*; StatPearls: Treasure Island, FL, USA, 2022.
12. Rodencal, J.; Dixon, S.J. A tale of two lipids: Lipid unsaturation commands ferroptosis sensitivity. *Proteomics* **2023**, *23*, e2100308. [CrossRef]
13. Forcina, G.C.; Dixon, S.J. GPX4 at the Crossroads of Lipid Homeostasis and Ferroptosis. *Proteomics* **2019**, *19*, e1800311. [CrossRef]
14. Hassannia, B.; Van Coillie, S.; Vanden Berghe, T. Ferroptosis: Biological Rust of Lipid Membranes. *Antioxid. Redox Signal* **2021**, *35*, 487–509. [CrossRef] [PubMed]
15. Henneberry, A.L.; Wright, M.M.; McMaster, C.R. The major sites of cellular phospholipid synthesis and molecular determinants of Fatty Acid and lipid head group specificity. *Mol. Biol. Cell* **2002**, *13*, 3148–3161. [CrossRef]
16. Fahy, E.; Cotter, D.; Sud, M.; Subramaniam, S. Lipid classification, structures and tools. *Biochim. Biophys. Acta* **2011**, *1811*, 637–647. [CrossRef] [PubMed]
17. Mortensen, M.S.; Ruiz, J.; Watts, J.L. Polyunsaturated Fatty Acids Drive Lipid Peroxidation during Ferroptosis. *Cells* **2023**, *12*, 804. [CrossRef] [PubMed]

18. Mynott, R.L.; Habib, A.; Best, O.G.; Wallington-Gates, C.T. Ferroptosis in Haematological Malignancies and Associated Therapeutic Nanotechnologies. *Int. J. Mol. Sci.* **2023**, *24*, 7661. [CrossRef]
19. Stockwell, B.R.; Friedmann Angeli, J.P.; Bayir, H.; Bush, A.I.; Conrad, M.; Dixon, S.J.; Fulda, S.; Gascon, S.; Hatzios, S.K.; Kagan, V.E.; et al. Ferroptosis: A Regulated Cell Death Nexus Linking Metabolism, Redox Biology, and Disease. *Cell* **2017**, *171*, 273–285. [CrossRef]
20. Seibt, T.M.; Proneth, B.; Conrad, M. Role of GPX4 in ferroptosis and its pharmacological implication. *Free Radic. Biol. Med.* **2019**, *133*, 144–152. [CrossRef]
21. Sim, S.; Wong, N.K. Nanotechnology and its use in imaging and drug delivery (Review). *Biomed. Rep.* **2021**, *14*, 42. [CrossRef]
22. Alshehri, A.; Grabowska, A.; Stolnik, S. Pathways of cellular internalisation of liposomes delivered siRNA and effects on siRNA engagement with target mRNA and silencing in cancer cells. *Sci. Rep.* **2018**, *8*, 3748. [CrossRef]
23. Akiyama, H.; Zhao, R.; Rahhal, A.; Nishida, Y.; Ayoub, E.; Ostermann, L.B.; Andreeff, M.; Ishizawa, J. Therapeutic Targeting of Ferroptosis Pathway in Combination with Mitochondrial Oxidative Stress Induction in Acute Myeloid Leukemia. *Blood* **2021**, *138*, 1162. [CrossRef]
24. Koppula, P.; Lei, G.; Zhang, Y.; Yan, Y.; Mao, C.; Kondiparthi, L.; Shi, J.; Liu, X.; Horbath, A.; Das, M.; et al. A targetable CoQ-FSP1 axis drives ferroptosis- and radiation-resistance in KEAP1 inactive lung cancers. *Nat. Commun.* **2022**, *13*, 2206.
25. Wu, F.; Du, Y.; Yang, J.; Shao, B.; Mi, Z.; Yao, Y.; Cui, Y.; He, F.; Zhang, Y.; Yang, P. Peroxidase-like Active Nanomedicine with Dual Glutathione Depletion Property to Restore Oxaliplatin Chemosensitivity and Promote Programmed Cell Death. *ACS Nano* **2022**, *16*, 3647–3663. [CrossRef] [PubMed]
26. Li, Q.; Gao, W.; Zhang, C.; Wang, P.; Wang, X.; Yan, M.; Jiang, W.; Wu, Z.; Wei, P.; Tian, G.; et al. A Biodegradable High-Efficiency Magnetic Nanoliposome Promotes Tumor Microenvironment-Responsive Multimodal Tumor Therapy Along with Switchable T2 Magnetic Resonance Imaging. *ACS Appl. Mater. Interfaces* **2022**, *14*, 24160–24173. [CrossRef] [PubMed]
27. Gao, M.; Deng, J.; Liu, F.; Fan, A.; Wang, Y.; Wu, H.; Ding, D.; Kong, D.; Wang, Z.; Peer, D.; et al. Triggered ferroptotic polymer micelles for reversing multidrug resistance to chemotherapy. *Biomaterials* **2019**, *223*, 119486. [CrossRef]
28. Cao, Y.; Li, Y.; He, C.; Yan, F.; Li, J.R.; Xu, H.Z.; Zhuang, J.F.; Zhou, H.; Peng, Y.C.; Fu, X.J.; et al. Selective Ferroptosis Inhibitor Liproxstatin-1 Attenuates Neurological Deficits and Neuroinflammation After Subarachnoid Hemorrhage. *Neurosci. Bull.* **2021**, *37*, 535–549. [CrossRef]
29. Kou, L.; Sun, R.; Jiang, X.; Lin, X.; Huang, H.; Bao, S.; Zhang, Y.; Li, C.; Chen, R.; Yao, Q. Tumor Microenvironment-Responsive, Multistaged Liposome Induces Apoptosis and Ferroptosis by Amplifying Oxidative Stress for Enhanced Cancer Therapy. *ACS Appl. Mater. Interfaces* **2020**, *12*, 30031–30043. [CrossRef] [PubMed]
30. Ji, P.; Wang, X.; Yin, J.; Yao, Y.; Du, W. Amplification of ferroptosis with a liposomal nanoreactor cooperates with low-toxicity doxorubicin apoptosis for enhanced tumor chemotherapy. *Biomater. Sci.* **2022**, *10*, 1544–1553. [CrossRef]
31. Panaroni, C.; Fulzele, K.; Soucy, R.; Siu, K.T.; Mukaihara, K.; Huang, C.; Chattopadhyay, S.; Raje, N. Arachidonic Acid Induces Ferroptosis-Mediated Cell-Death in Multiple Myeloma. *Blood* **2018**, *132*, 4498. [CrossRef]
32. Bordini, J.; Morisi, F.; Cerruti, F.; Cascio, P.; Camaschella, C.; Ghia, P.; Campanella, A. Iron Causes Lipid Oxidation and Inhibits Proteasome Function in Multiple Myeloma Cells: A Proof of Concept for Novel Combination Therapies. *Cancers Basel* **2020**, *12*, 970. [CrossRef]
33. Toyokuni, S.; Ito, F.; Yamashita, K.; Okazaki, Y.; Akatsuka, S. Iron and thiol redox signaling in cancer: An exquisite balance to escape ferroptosis. *Free Radic. Biol. Med.* **2017**, *108*, 610–626. [CrossRef] [PubMed]
34. Wallington-Beddoe, C.T.; Bennett, M.K.; Vandyke, K.; Davies, L.; Zebol, J.R.; Moretti, P.A.B.; Pitman, M.R.; Hewett, D.R.; Zannettino, A.C.W.; Pitson, S.M. Sphingosine kinase 2 inhibition synergises with bortezomib to target myeloma by enhancing endoplasmic reticulum stress. *Oncotarget* **2017**, *8*, 43602–43616. [CrossRef] [PubMed]
35. Morgan, M.J.; Kim, Y.-S. Roles of RIPK3 in necroptosis, cell signaling, and disease. *Exp. Mol. Med.* **2022**, *54*, 1695–1704. [CrossRef]
36. Kagan, V.E.; Mao, G.; Qu, F.; Angeli, J.P.; Doll, S.; Croix, C.S.; Dar, H.H.; Liu, B.; Tyurin, V.A.; Ritov, V.B.; et al. Oxidized arachidonic and adrenic PEs navigate cells to ferroptosis. *Nat. Chem. Biol.* **2017**, *13*, 81–90. [CrossRef]
37. Manni, M.M.; Tiberti, M.L.; Pagnotta, S.; Barelli, H.; Gautier, R.; Antonny, B. Acyl chain asymmetry and polyunsaturation of brain phospholipids facilitate membrane vesiculation without leakage. *eLife* **2018**, *7*, e34394. [CrossRef] [PubMed]
38. Magtanong, L.; Ko, P.J.; To, M.; Cao, J.Y.; Forcina, G.C.; Tarangelo, A.; Ward, C.C.; Cho, K.; Patti, G.J.; Nomura, D.K.; et al. Exogenous Monounsaturated Fatty Acids Promote a Ferroptosis-Resistant Cell State. *Cell Chem. Biol.* **2019**, *26*, 420–432. [CrossRef]
39. Das, U.N. Saturated Fatty Acids, MUFAs and PUFAs Regulate Ferroptosis. *Cell Chem. Biol.* **2019**, *26*, 309–311. [CrossRef]
40. Wang, N.; Ma, H.; Li, J.; Meng, C.; Zou, J.; Wang, H.; Liu, K.; Liu, M.; Xiao, X.; Zhang, H.; et al. HSF1 functions as a key defender against palmitic acid-induced ferroptosis in cardiomyocytes. *J. Mol. Cell Cardiol.* **2021**, *150*, 65–76. [CrossRef]
41. Kuang, H.; Sun, X.; Liu, Y.; Tang, M.; Wei, Y.; Shi, Y.; Li, R.; Xiao, G.; Kang, J.; Wang, F.; et al. Palmitic acid-induced ferroptosis via CD36 activates ER stress to break calcium-iron balance in colon cancer cells. *FEBS J.* **2023**, *290*, 3664–3687. [CrossRef]
42. Miao, S.; Zhang, Q.; Ding, W.; Hou, B.; Su, Z.; Li, M.; Yang, L.; Zhang, J.; Chang, W.; Wang, J. Platelet Internalization Mediates Ferroptosis in Myocardial Infarction. *Arterioscler. Thromb. Vasc. Biol.* **2023**, *43*, 218–230. [CrossRef]

f

43. Dierge, E.; Debock, E.; Guilbaud, C.; Corbet, C.; Mignolet, E.; Mignard, L.; Bastien, E.; Dessy, C.; Larondelle, Y.; Feron, O. Peroxidation of n-3 and n-6 polyunsaturated fatty acids in the acidic tumor environment leads to ferroptosis-mediated anticancer effects. *Cell Metab.* **2021**, *33*, 1701–1715. [CrossRef] [PubMed]
44. Meyer zu Heringdorf, D. Lysophospholipids. In *Encyclopedia of Molecular Pharmacology*; Springer: Berlin/Heidelberg, Germany, 2008; pp. 710–716. [CrossRef]
45. Bersuker, K.; Hendricks, J.M.; Li, Z.; Magtanong, L.; Ford, B.; Tang, P.H.; Roberts, M.A.; Tong, B.; Maimone, T.J.; Zoncu, R.; et al. The CoQ oxidoreductase FSP1 acts parallel to GPX4 to inhibit ferroptosis. *Nature* **2019**, *575*, 688–692. [CrossRef]
46. Battaglia, A.M.; Chirillo, R.; Aversa, I.; Sacco, A.; Costanzo, F.; Biamonte, F. Ferroptosis and Cancer: Mitochondria Meet the "Iron Maiden" Cell Death. *Cells* **2020**, *9*, 1505. [CrossRef] [PubMed]
47. Webb, J.L. Effect of more than one inhibitor. In *Enzymes and Metabolic Inhibitors*; Hochster, R., Quastel, J., Eds.; Academic Press: New York, NY, USA, 1963; Volume 1, pp. 487–512.
48. Tian, H.; Zhao, X.; Zhang, Y.; Xia, Z. Abnormalities of glucose and lipid metabolism in myocardial ischemia-reperfusion injury. *Biomed. Pharmacother.* **2023**, *163*, 114827. [CrossRef]
49. Nosova, A.S.; Koloskova, O.O.; Nikonova, A.A.; Simonova, V.A.; Smirnov, V.V.; Kudlay, D.; Khaitov, M.R. Diversity of PEGylation methods of liposomes and their influence on RNA delivery. *Medchemcomm* **2019**, *10*, 369–377. [CrossRef] [PubMed]
50. Xin, S.; Mueller, C.; Pfeiffer, S.; Kraft, V.A.N.; Merl-Pham, J.; Bao, X.; Feederle, R.; Jin, X.; Hauck, S.M.; Schmitt-Kopplin, P.; et al. MS4A15 drives ferroptosis resistance through calcium-restricted lipid remodeling. *Cell Death Differ.* **2022**, *29*, 670–686. [CrossRef]
51. Dev, S.; Babitt, J.L. Overview of iron metabolism in health and disease. *Hemodial. Int.* **2017**, *21* (Suppl. 1), S6–S20. [CrossRef]
52. MacKenzie, E.L.; Iwasaki, K.; Tsuji, Y. Intracellular iron transport and storage: From molecular mechanisms to health implications. *Antioxid. Redox Signal* **2008**, *10*, 997–1030. [CrossRef]
53. Ayala, A.; Munoz, M.F.; Arguelles, S. Lipid peroxidation: Production, metabolism, and signaling mechanisms of malondialdehyde and 4-hydroxy-2-nonenal. *Oxid. Med. Cell Longev.* **2014**, *2014*, 360438. [CrossRef]
54. Shintoku, R.; Takigawa, Y.; Yamada, K.; Kubota, C.; Yoshimoto, Y.; Takeuchi, T.; Koshiishi, I.; Torii, S. Lipoxygenase-mediated generation of lipid peroxides enhances ferroptosis induced by erastin and RSL3. *Cancer Sci.* **2017**, *108*, 2187–2194. [CrossRef]
55. Liu, J.; Zhang, C.; Wang, J.; Hu, W.; Feng, Z. The Regulation of Ferroptosis by Tumor Suppressor p53 and its Pathway. *Int. J. Mol. Sci.* **2020**, *21*, 8387. [CrossRef]
56. Yang, W.S.; Kim, K.J.; Gaschler, M.M.; Patel, M.; Shchepinov, M.S.; Stockwell, B.R. Peroxidation of polyunsaturated fatty acids by lipoxygenases drives ferroptosis. *Proc. Natl. Acad. Sci. USA* **2016**, *113*, E4966. [CrossRef]
57. Zeissig, M.N.; Hewett, D.R.; Mrozik, K.M.; Panagopoulos, V.; Wallington-Gates, C.T.; Spencer, A.; Dold, S.M.; Engelhardt, M.; Vandyke, K.; Zannettino, A.C.W. Expression of the chemokine receptor CCR1 decreases sensitivity to bortezomib in multiple myeloma cell lines. *Leuk. Res.* **2024**, *139*, 107469. [CrossRef] [PubMed]
58. Moosavian, S.A.; Bianconi, V.; Pirro, M.; Sahebkar, A. Challenges and pitfalls in the development of liposomal delivery systems for cancer therapy. *Semin. Cancer Biol.* **2021**, *69*, 337–348. [CrossRef] [PubMed]
59. White, J.B.; Trim, P.J.; Salagaras, T.; Long, A.; Psaltis, P.J.; Verjans, J.W.; Snel, M.F. Equivalent Carbon Number and Interclass Retention Time Conversion Enhance Lipid Identification in Untargeted Clinical Lipidomics. *Anal. Chem.* **2022**, *94*, 3476–3484. [CrossRef]
60. Pino, L.K.; Searle, B.C.; Bollinger, J.G.; Nunn, B.; MacLean, B.; MacCoss, M.J. The Skyline ecosystem: Informatics for quantitative mass spectrometry proteomics. *Mass. Spectrom. Rev.* **2020**, *39*, 229–244. [CrossRef]

Publication 3

Habib *et al. Discover Oncology* (2025) 16:1612
https://doi.org/10.1007/s12672-025-03444-9

Discover Oncology

REVIEW Open Access

The instrumental role of lipids in governing the sensitivity of multiple myeloma to ferroptosis

Ali Habib[1], Oliver G. Best[1], Charlotte E. Toomes[1] and Craig T. Wallington-Gates[1,2,3,4*]

*Correspondence:
Craig T. Wallington-Gates

craig.wallington-gates@health.qld.gov.au
[1]College of Medicine and Public Health, Flinders University, Bedford Park, SA 5042, Australia
[2]School of Health, University of the Sunshine Coast, Sippy Downs, QLD 4556, Australia
[3]School of Medicine and Dentistry, Griffith University, Birtinya, QLD 4575, Australia
[4]Department of Haematology, Sunshine Coast University Hospital, Birtinya, QLD 4575, Australia

Abstract

Multiple myeloma (MM) is a malignancy characterised by the uncontrolled proliferation of clonal plasma cells, primarily within the bone marrow, and is still considered incurable. A significant proportion of patients relapse with drug-refractory disease, necessitating the development of novel therapeutic approaches. Ferroptosis is a recently-characterised form of non-apoptotic programmed cell death, linked to phospholipid peroxidation, that represents a promising approach for the treatment of MM and other cancers, that are refractory to more conventional apoptosis-inducing regimens. A better understanding of the relationship between cellular lipid composition and ferroptosis sensitivity is key to harnessing this form of programmed cell death as a therapeutic approach. In addition to the cellular proportions of phospholipids containing poly- and monounsaturated fatty acids, studies to date indicate that cholesterol levels impact not only the onset and progression of haematological malignancies but also the sensitivity of a variety of different cancers to ferroptosis. Therefore, manipulating the uptake and metabolism of lipids, including glycerophospholipids and cholesterol, may be an effective means of sensitising MM cells to ferroptosis. Findings from the limited number of studies concerning ferroptosis in MM and compelling evidence from other malignancies, provide a strong rationale for further investigation of ferroptosis as a novel therapeutic approach for MM.

Keywords Cancer, Haematology, Multiple myeloma, Ferroptosis, Lipids, Phospholipids, Cholesterol, Fatty acids, Saturated, Unsaturated

1 Background

Multiple myeloma (MM) is a malignancy characterised by the uncontrolled proliferation of clonal plasma cells, primarily within the bone marrow, and is still considered incurable [1, 2]. MM is the second most common haematological malignancy after non-Hodgkin lymphoma, with >175,000 new cases diagnosed annually worldwide [3], including approximately 2,600 Australians [4]. Clinical features of MM include hypercalcaemia, renal insufficiency, anaemia, bone lesions, and bone marrow failure. Until the turn of the century, 5-year survival rates among MM patients were as low as 25% [5] and despite advances in treatment, the 5-year survival rate remains around 50%, with a median overall survival of 5.5 years [6]. Furthermore, the 5-year progression-free

survival rate is only 17% for patients deemed to have high-risk disease [7] and survival among older MM patients (>65 years) has stagnated over the last 20 years [6]. Novel therapeutic approaches are urgently needed to improve outcomes for MM patients.

The median age of diagnosis for MM is 70 years and therefore, frailty and the presence of comorbidities often limit the use of intensive therapies [4]. There is also an increasing awareness of patients with 'functional high-risk' myeloma who exhibit poor responses to therapy or experience rapid relapses that are independent of genetic risk factors. Over the past two decades, the standard of care for MM patients has moved beyond conventional chemotherapy to include proteasome inhibitors (PIs - bortezomib, carfilzomib, ixazomib, etc.), immunomodulatory drugs (IMiDs - thalidomide, lenalidomide, pomalidomide, etc.) and monoclonal antibodies (mAbs – daratumumab (anti-CD38), isatuximab (anti-CD38), elotuzumab (anti-SLAMF7), etc.). Other immune and cell-based therapeutic approaches are also emerging, including bi-specific antibodies (BsAbs – teclistamab, elranatamab, etc.), antibody-drug conjugates (ADCs – belantamab mafodotin) and chimeric antigen receptor T cell therapies (CAR-T – ciltacabtagene autoleucel (cilta-cel), idecabtagene vicleucel (ide-cel)) [8].

The efficacy of many of the cancer therapy regimens currently in use rely on the induction of cell death. Cell death is a fundamental biological process that ensures that the integrity and function of cells and tissues are maintained, thereby preventing tumorigenesis. Cell death can generally be classified as either unprogrammed or programmed cell death (PCD) [9]. Unprogrammed cell death occurs in a non-regulated manner, typically in response to overwhelming chemical or physical stimuli [9, 10]. In contrast, PCD is a tightly regulated process that is essential for tissue homeostasis and protection against viruses and disease [10]. Various mechanisms of PCD have been identified, including apoptosis, autophagy, pyroptosis, necroptosis and ferroptosis [10]. This review will focus on our current knowledge regarding ferroptosis, its emerging role as an important PCD mechanism, its association with lipids, and how ferroptosis may represent a novel approach for the treatment of MM.

1.1 Ferroptosis

Ferroptosis is an iron-dependent, non-apoptotic form of PCD, characterised by lipid peroxidation [11]. Ferroptosis is distinct from other forms of PCD in terms of the morphological changes that occur and molecular mechanisms that drive cell death, illustrated by evidence that inhibitors of apoptosis have little or no effect on ferroptosis-mediated cell death [11]. Interest in ferroptosis-mediated therapeutic strategies has grown significantly in recent years, as these may represent a means of overcoming resistance to more conventional therapies that are generally reliant on apoptosis.

Lipid peroxidation is a hallmark of ferroptosis and is characterised by reactions that result in the oxidative degradation of lipids, yielding highly toxic peroxyl radicals (ROO•) [12]. Oxidation and subsequent degradation of lipids, which is catalysed by lipoxygenase enzymes (Fig. 1), results in the formation of peroxyl radicals that irreversibly compromise the integrity of cellular membranes leading to cell death [13]. However, cancer cells adapt and can develop mechanisms to buffer the harmful effects of lipid peroxidation and reactive oxygen species (ROS) that accumulate due to the high metabolic demands and rapid proliferation of the tumour.

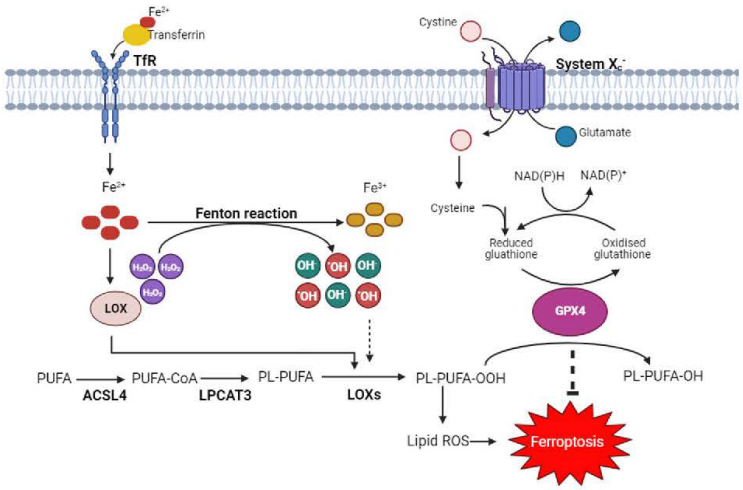

Fig. 1 Ferroptosis, driven by lipid peroxidation, is inhibited by system X_c^- and GPX4.

Iron is an important co-factor for lipoxygenases and is essential for the initiation and promotion of lipid peroxidation via the Fenton reaction [14]; the importance of iron and lipid peroxidation in ferroptosis is demonstrated by evidence that both iron chelators (deferoxamine) and synthetic antioxidants (e.g. liproxstatin-1 and ferrostatin-1) can inhibit this form of cell death by binding free iron and scavenging free radicals, respectively [15].

ACSL4, acyl-CoA synthetase long-chain family member 4; Fe^{2+}, ferrous iron; Fe^{3+}, ferric iron; GPX4, glutathione peroxidase 4; H_2O_2, hydrogen peroxide; LOXs, lipoxygenases; LPCAT3, lysophosphatidylcholine acyltransferase 3; OH^-, hydroxide ion; .OH, hydroxyl radical; PL, phospholipid; PL-PUFA-OH, phospholipid alcohol; PL-PUFA-OOH, phospholipid hydroperoxides; PUFA, polyunsaturated fatty acid; ROS, reactive oxygen species; TfR, transferrin receptor. Created with BioRender.com.

1.2 Inhibition of ferroptosis

1.2.1 System X_c^- and glutathione peroxidase 4 (GPX4)

Plasma membrane-bound system X_c^- is an important regulator of ferroptosis. This antiporter system facilitates the exchange of intracellular glutamate for extracellular cystine, which is then rapidly converted to cysteine by the thioredoxin reductase 1 (TXNRD1) enzyme (Fig. 1) [16]. Cysteine is the rate limiting step in the biosynthesis of the antioxidant and enzyme substrate, glutathione (GSH). GSH activates the catalytic domain of the selenoprotein, glutathione peroxidase 4 (GPX4) [16], which converts toxic lipid peroxides into neutral alcohols, thereby inhibiting lipid peroxidation and ferroptosis (Fig. 1) [16, 17].

1.3 The role of antioxidants in modulating ferroptosis via FSP1 and the mevalonate pathway

GPX4-independent antioxidant systems also play an important role in suppressing ferroptosis. One such system is the ferroptosis suppressor protein 1 (FSP1)/mevalonate

pathway [18], which is involved in the production of isopentenyl pyrophosphate (IPP) and coenzyme Q10 (CoQ10) (Fig. 2). This involves the reduction of acetyl-CoA to mevalonate and subsequent conversion to IPP [19], which in turn is converted to the CoQ10 substrate, farnesyl pyrophosphate [19]. Farnesyl pyrophosphate is also involved in the maturation of selenocysteine, an amino acid required for translation of GPX4 [20, 21]. CoQ10 is a naturally occurring quinone that is vital to cell and tissue health in most aerobic organisms [22]. CoQ10 is primarily involved in the mitochondrial electron transport chain, where it functions as a high-energy transfer molecule [22]. The biosynthesis of CoQ10 begins and ends in the mitochondria and is facilitated by a complex of proteins, which have not yet been fully elucidated [23].

CoQ10 is comprised of a benzoquinone ring derived from the amino acid tyrosine, which is chemically linked to 10 isoprenoid units and synthesised by the mevalonate pathway [24]. Ferroptosis suppressor protein 1 (FSP1) catalyses the regeneration of CoQ10 into its reduced form, CoQ_{10}-H_2 (ubiquinol), which functions to trap radicals (Fig. 2) [18]. FSP1 is not involved in the canonical ferroptosis pathway but does protect cells against ferroptosis-inducing agents [18]; expression of FSP1 has been shown to correlate with sensitivity to ferroptosis-inducing compounds, including RSL3, while genetic knockdown of *FSP1* has been shown to sensitise a range of different cancer cell lines to ferroptosis-inducing compounds [18]. Furthermore, FSP1 does not protect cells against pro-apoptotic agents and is not regulated by the tumour suppressor protein, TP53.

7-DHC, 7-Dehydrocholesterol; Acetyl-CoA, acetyl coenzyme A; CoQ10, ubiquinone; CoQ10-H2, ubiquinol; FPP, farnesyl phosphate; FSP1, ferroptosis suppressor protein 1; GGPP, geranylgeranyl pyrophosphate; GPX4, glutathione peroxidase 4; HMG-CoA, 3-hydroxy-3-methylglutaryl-coenzyme A; IPP, isopentenyl phosphate; ROS, reactive oxygen species. Dotted arrows represent multiple steps within a pathway. Created with BioRender.com.

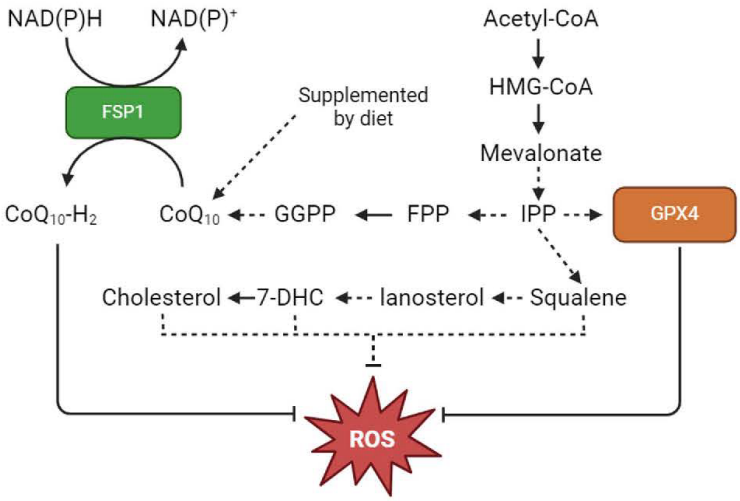

Fig. 2 Biochemical pathways of the mevalonate pathway in the inhibition of ferroptosis.

1.4 The role of lipids in ferroptosis

1.4.1 Glycerophospholipids

Lipids are a diverse group of organic molecules that are essential building blocks of life; they make up the structural composition of cell membranes, play important roles as signalling molecules and are a critical source of energy [25]. Lipids can be loosely categorised into fatty acids (FAs), glycerides, non-glyceride lipids and complex lipids. In the context of ferroptosis, phospholipids (PLs), specifically glycerophospholipids, play important roles in the initiation and propagation of lipid peroxidation (Fig. 1) [25].

FAs are carboxylic acids with an aliphatic chain, comprised of oxygen, carbon, and hydrogen atoms. They can be categorised into three distinct groups, saturated fatty acids (SFA), monounsaturated fatty acids (MUFA) and polyunsaturated fatty acids (PUFA) [26, 27]. PLs, particularly those that are comprised of PUFAs, are pivotal in ferroptosis, since they are more readily oxidised than other lipids. Emerging research in the ferroptosis space has also suggested that the degree of PL acyl chain saturation correlates with ferroptosis sensitivity [28]. The intracellular mechanisms that inhibit ferroptosis once lipid peroxidation has been initiated are complex and several pathways are now known to be involved, including the antioxidant systems coordinated by FSP1 and GPX4 [29].

There is a growing body of literature concerning the role of PL-PUFA in ferroptosis, highlighting the association between the lipid composition of different cell types and their sensitivity to ferroptosis. Several studies have examined the effects of exogenous PUFAs, including arachidonic (AA), eicosapentaenoic and docosahexaenoic acid, on cancer cells or cardiomyocytes in vitro (Table 1). Recent research has demonstrated that t(4;14)-positive MM models, a poor prognostic abnormality in MM, are sensitive to ferroptosis induced by class II ferroptosis inducers in vitro and in vivo [30]. The study found that the upregulation of MM SET domain-containing protein (MMSET) in these models resulted in the upregulation of ACSL4 (acyl-CoA synthetase long-chain family member 4), in turn increasing cellular PUFA levels [30]. A study published by our group has demonstrated that delivering PUFA to MM cells via liposomes, which are lipid-based nanoparticles, can sensitise them to the GPX4 inhibitor RSL3 [31]. These studies demonstrate that by increasing the intracellular proportion of these FAs, cells can be sensitised to ferroptosis and that in some cell types, this alone was sufficient to induce ferroptosis [27, 32, 33]. In contrast, increased levels of PLs containing MUFA (PL-MUFA) or other less readily oxidised lipid species (PL-SFA) within the lipidome have been shown to increase the resistance of cells to ferroptosis (Table 1) [16, 21, 34]. Furthermore, there is evidence that MUFAs can displace PUFAs from PLs in the lipid membrane and other subcellular regions [34].

There is also evidence that SFAs may play a role in ferroptosis, but the findings of these studies are inconsistent, with some studies suggesting that SFAs play an important role in lipotoxicity, and not ferroptosis [35]. However, another study suggested that the SFA, palmitic acid, is actively involved in lipid ROS production and ferroptosis in insulin-producing β-cells [36]. GPX4 overexpression and ferrostatin-1 were able to partially prevent cell death, while co-treatment of the cells with the MUFA, oleic acid, protected β-cells from lipid peroxidation induced by palmitic acid [36]. Magtanong et al.., also found that culturing cells with exogenous MUFA, but not treatment with ferrostatin-1, was protective against palmitic acid-induced cell death, suggesting that ferroptosis may not be the primary mechanism of cell death [34].

Table 1 Lipids and their role in ferroptosis.

Lipid	Cancer/Cell Type	Effects	Mechanism	References
Arachidonic acid (PUFA)	Multiple myeloma, colorectal cancer, cervical cancer, hypopharyngeal cancer, melanoma, mouse melanoma and Lewis lung cancer	Promotes ferroptotic cell death	Serve as fuel for lipid peroxidation, due to ability to be readily oxidised by ROS and potent radicals	[58–60]
Docosahexaenoic acid (PUFA)	Multiple myeloma, prostate cancer, colorectal cancer, cervical cancer, hypopharyngeal cancer and liver cancer	Promotes ferroptotic cell death	Serve as fuel for lipid peroxidation, due to ability to be readily oxidised by ROS and potent radicals	[31, 32, 60, 61]
Eicosapentaenoic acid (PUFA)	Colon cancer, colorectal adenocarcinoma, cervical cancer, hypopharyngeal cancer, melanoma, carcinoma, osteosarcoma, Multiple Myeloma and hepatoma	Promotes ferroptotic cell death	Serve as fuel for lipid peroxidation, due to ability to be readily oxidised by ROS and potent radicals	[60–63]
Linoleic acid (PUFA)	Pancreatic cancer, melanoma, carcinoma ovarian cancer and hepatoma	Promotes ferroptotic cell death	Serve as fuel for lipid peroxidation, due to ability to be readily oxidised by ROS and potent radicals	[62, 64]
Oleic acid (MUFA)	Melanoma and ovarian cancer	Protects against ferroptosis	Less susceptible to oxidation and can displace PUFA in the lipid membrane	[65, 66]
Palmitoleic acid (MUFA)	Oesophageal squamous cell carcinoma and ovarian cancer	Protects against ferroptosis	Less susceptible to oxidation and can displace PUFA in the lipid membrane	[66, 67]
Stearic acid (SFA)	Cardiomyocytes	Protects against ferroptosis	Less susceptible to oxidation	[39]
Palmitic (SFA)	Colon cancer and cardiomyocytes	Promotes ferroptotic cell death	Induces ferroptosis via CD36, activating ER stress and breaking calcium-iron balance	[37, 38]
Coenzyme Q10 (Ubiquinone)	Colon, breast, lung, pancreas, brain, liver, kidney, skin and intestinal cancer cell lines	Prevents cellular accumulation of ROS and ferroptotic cell death	Powerful antioxidant that can inhibit lipid peroxidation	[18, 24]
Squalene	Anaplastic large cell lymphoma, fibrosarcoma and renal adenocarcinoma	Prevents cellular accumulation of ROS and ferroptotic cell death	Free radical scavenger and actively involved in cholesterol biosynthesis as a precursor	[46, 49]
Cholesterol	Multiple myeloma, fibrosarcoma, mouse liver and renal adenocarcinoma	Protects against ferroptosis	Important in maintaining cellular membrane integrity while also inhibiting lipid peroxidation	[46, 47]

Two other studies of cardiomyocytes and colorectal cancer cell lines support the finding that palmitic acid can induce lipid peroxidation but suggest that this effect, and subsequent ferroptosis, is dependent on expression of the lipid transporter, CD36, in the plasma membrane [37, 38]. In a similar study, Kuang et al.., suggested the effects of palmitic acid on ferroptosis in colon cancer cells were due to induction of non-canonical ferroptosis via CD36, leading to an increase in ER stress, endocytosis of transferrin and an increase in intracellular ferrous iron levels [38]. In contrast, another study showed that the SFA, stearic acid, can protect cardiomyocytes from ferroptosis, which may be due to the fact this FA is less readily oxidised than the PUFAs it displaces in the lipidome [39]. Collectively, these studies suggest that the role(s) of SFAs in ferroptosis are

complex and probably context-dependent and although SFAs may have more significant roles in lipotoxicity, there is evidence that SFAs can act as either inhibitors or promoters of ferroptosis.

1.4.2 Lysophospholipids

Lysophospholipids (LPL) represent a relatively minor component of the total lipid composition in cells and are characterised by a polar head group and a single carbon (acyl) chain. The lysolipid structure within LPLs confers hydrophilicity and versatility, which facilitates their many tissue specific functions [40]. LPLs are recognised as extracellular, and in some cases intracellular, signalling mediators [40]. LPLs are commonly formed when the ester bonds of PLs are enzymatically hydrolysed by phospholipase A, producing LPL and a free fatty acid chain [41].

LPL levels have been found to be significantly elevated in cells undergoing ferroptosis, with a concomitant decrease in the corresponding PL-PUFA [42, 43]. This is thought to be due to oxidised acyl chains being the preferred substrate for specific lipases, particularly phospholipase A [43]. Inhibition of phospholipase A can rescue GPX4 null cells from ferroptosis, suggesting cleaved and oxidised PUFAs are actively involved in ferroptosis-associated membrane damage and cell death [43]. These results also suggest that increased levels of LPL may be an indication of ferroptosis-mediated cell death.

1.5 Cholesterol

Cholesterol is a major component of cell membranes and is comprised of a hydrocarbon tail, a central sterol nucleus, and a hydroxyl group [44]. Cholesterol provides membrane stability and fluidity, is important for the formation of lipid rafts, and is a crucial precursor in the synthesis of steroid hormones, vitamin D and bile acids [44]. Cholesterol may also play an important role in cancer progression by promoting proliferation, invasion, and migration [45], and may impact the sensitivity of tumour cells to ferroptosis [46, 47]. Elevated levels of intracellular cholesterol have been shown to reduce the sensitivity of human epithelial cells to ferroptosis by increasing squalene and CoQ10, with effects similar to those observed with ferrostatin-1 [46]. This study went on to demonstrate that cholesterol inhibits ferroptosis in induced liver injury in mice [46]. Squalene is a lipophilic metabolite formed during the conversion of farnesyl pyrophosphate to either cholesterol through the mevalonate pathway or oxysterol via the squalene dioxide pathway [48]. Squalene protects cells from oxidative stress by altering the intracellular lipid composition and reducing ROS levels [48, 49]. Given the roles of squalene, the enzyme squalene synthase is now recognised as a potential therapeutic target for inducing ferroptosis [48].

A recent study revealed that long-term hematopoietic stem cells (HSCs) from C57BL/6 mice fed a high-cholesterol diet had significantly lower levels of lipid peroxidation and Fe^{2+} and increased levels of glutathione compared to controls [50]. Consistent with these changes, the cells were significantly less sensitive to erastin ex vivo. Elevated levels of IL-3 and GM-CSF induced by the high cholesterol diet al.so increased activity of the mTOR-mediated signalling pathway and subsequent upregulation of SLC7A11/GPX4 expression in the HSCs [50].

Cholesterol is also crucial for the formation of lipid rafts which are important components of the plasma membrane, coordinating cell signalling and import and export

from the cell, in addition to regulating membrane fluidity and organisation [51]. Lipid rafts also impact the sensitivity of cells to ferroptosis [52]. A study found that cholesterol accumulation protects different cell types from ferroptosis by increasing the number of lipid rafts and by reducing the effects of lipid peroxidation on membrane fluidity and permeability [51]. RSL3 treatment in human melanoma and renal cancer cell lines resulted in an increase in lipid raft formation, while the combination of LDL and RSL3 yielded the densest membrane rafts, representing a dynamic shift in the lipidome in response to ROS build up [51]. Conversely, cholesterol depletion increased the sensitivity of the cells to ferroptosis-mediated cell death by decreasing lipid rafts and increasing membrane fluidity [51]. Similar results were also observed in vivo in a melanoma mouse model treated with GPX4 inhibitor, ML210, with a concomitant increase in lipid raft formation in xenograft derived cells post-treatment [51]. In a subsequent study, Zhao et al., determined that the increase in lipid raft density in response to GPX4 inhibition was mediated by ACSL4 (acyl-CoA synthetase long-chain family member 4) and that this was associated with a reduction in the efficacy of platinum-based drugs [53]. These results suggest that cancer cells can increase ferroptosis resistance through active modulation of the plasma membrane, in response to GPX4 inhibition.

In a study by Bai et al.., nanozymes capable of depleting cholesterol and disrupting lipid rafts were tested against a breast cancer cell line resulting in an increase in membrane fluidity and ferroptosis sensitivity of the cancer cells, via a mechanism involving downregulation of both GPX4 and FSP1 [54]. Similar results were observed in vivo, with evidence suggesting the efficacy of the nanozymes was mediated by both ferroptosis and anti-tumour immune responses [54].

Statins, a class of medications that inhibit 3-hydroxy-3-methylglutaryl-coenzyme A (HMG-CoA) reductase (a key enzyme in cholesterol synthesis) thereby reducing cholesterol synthesis, have also been implemented in ferroptosis [55]. A study in tripe-negative breast cancer has demonstrated that simvastatin containing nanoparticles could induce ferroptosis in vitro and could significantly reduce tumour volume in MDA-MB-231 tumour-bearing mice [56]. Another study has shown that simvastatin can induce ferroptosis in gastric cancer cells by inhibiting programmed cell death ligand 1 [57]. These results were further supported in nude mice, where simvastatin induced ferroptotic cell death, reducing both the weight and proliferation of subcutaneous tumours [57]. These studies suggest that statins, which are amongst the most frequently prescribed medications worldwide, can be used to combat cancer through the induction of ferroptosis.

1.6 The role of the cholesterol synthesis pathway in ferroptosis: implications for therapy of cancers, including multiple myeloma

Despite significant advances in the treatment of many cancers, disease relapse and drug resistance remain the most challenging aspects of patient management. Since the efficacy of many current therapies relies on apoptosis-mediated cell death, induction of ferroptosis may represent an effective alternate therapeutic approach [68, 69]. However, the role of ferroptosis in the pathobiology of cancers and the mechanisms related to the sensitivity of cancers to this form of programmed cell death, are yet to be fully elucidated [70]. Given growing evidence that cholesterol and its precursors are important modulators of ferroptosis, the various pathways involved in lipid metabolism, including the cholesterol biosynthesis pathway, have been proposed as promising targets for

ferroptosis-mediated therapeutics [46, 50]71– [75]. The next section of this review will focus on studies concerning the impact of cholesterol biosynthesis on the ferroptosis sensitivity of cancer cells, with a focus on MM.

1.7 Cholesterol

Cholesterol has long been linked to tumorigenesis, cancer progression and treatment resistance [76–78]. MM patients have been reported to have significantly lower levels of serum cholesterol compared to healthy individuals and low cholesterol levels have been associated with a higher risk of MM onset [79]. The importance of lipids in ferroptosis suggests that cholesterol also likely impacts the sensitivity of MM cells to this form of cell death. However, further studies are required to more clearly elucidate the relationship between cholesterol levels and ferroptosis sensitivity in MM.

A population study of 3,500,000 individuals found that low levels of high-density lipoprotein cholesterol (HDL-C) were associated with an increased risk of MM [79]. The study proposed that the anti-inflammatory properties of HDL-C may protect against MM tumorigenesis and that low serum levels of HDL-C may be due to increased uptake and metabolic changes within the malignant plasma cells [79]. However, contrary to previous studies [75, 80], the data suggested that total serum cholesterol levels were similar between MM and healthy individuals. Another study of 502,507 participants in the United Kingdom found that higher levels of total cholesterol, HDL-C, and low-density lipoprotein cholesterol (LDL-C) were associated with a decreased risk of MM and other plasma cell neoplasms [81].

Both studies were conducted on peripheral blood plasma and levels of cholesterol in plasma cells were not assessed. Therefore, it is not possible to ascertain from these studies whether the decreased plasma cholesterol levels among the MM patients were associated with increased uptake into the tumour cells. Another study investigating apoptosis in MM found that addition of exogenous LDL to MM cells cultured in delipidated serum, increased their viability, while cholesterol depletion triggered an increase in the expression of LDL receptors [82]. The anti-apoptotic effects of cholesterol were also evident in primary MM cells, but not their healthy counterpart [82]. While the focus of the study by Tirado-Velez et al. [82]. , was apoptosis rather than ferroptosis, it does suggest that uptake and utilisation of cholesterol, and possibly other lipids, may play an important role in the survival of MM cells.

1.8 Lanosterol

The bone marrow microenvironment (BMME) is an interactive dynamic system that regulates myeloma cell behaviour through different mechanisms. Bone marrow stromal cells (BMSCs) are key components of the BMME, and produce factors, including interleukin-6, B-cell activating factor (BAFF) and a proliferation-inducing ligand (APRIL), that can promote the survival, proliferation and migration of MM cells, thereby contributing to drug resistance [83]. The BMME, especially BMSCs, has been shown to drive ferroptosis resistance through GPX4 deSUMOylation, protecting MM cells from labile iron triggered ferroptosis [84]. A study published in 2024 suggested that BMSCs may also play an important role in the sensitivity of MM plasma cells to ferroptosis through regulation of lanosterol biosynthesis [85]. Lanosterol is a precursor for sterols (including cholesterol) and is readily oxidised, forming ROS in MM cells (Fig. 2) [85, 86].

Co-culture of MM cells with BMSCs sensitised the tumour cells to RSL3 through upregulation of transferrin and iron levels, resulting in iron overload, and lanosterol and cholesterol accumulation [85]. The study also showed that addition of exogenous lanosterol, but not cholesterol, sensitised MM cells to RSL3, while cholesterol alone had minimal effect on RSL3 IC_{50} in their MM cell lines [85]. These results were obtained using MM cells co-cultured with BMSCs, which may explain the difference in cholesterol's effects observed in this study compared to others that describe cholesterol as an inhibitor of ferroptosis (Table 1).

Importantly, the effects of BMSCs on MM cells were shown to be dependent on cell-to-cell contact and to be mediated by CD40 and its ligand (CD154), as sensitivity to RSL3 was blocked by anti-CD40 antibodies, in both the in vitro and in vivo models studied [85]. This study highlights the important role that sterols may play in the sensitivity of cancer cells to ferroptosis and may represent a potential means of sensitising MM cells to ferroptosis induced by GPX4 inhibition. Interestingly, the study by Jian et al. found that the ferroptosis inhibiting function of BMSCs was also CD40 dependant, suggesting that direct contact between the cells is required to influence ferroptosis [84]. The multifaceted role of the BMME in ferroptosis is complex, and BMSCs may both drive and inhibit ferroptosis in MM.

1.9 Leukocyte immunoglobulin-like receptor B1 (LILBR1)

A recent study identified the leukocyte immunoglobulin-like receptor B1 (LILRB1) as a marker of poor prognosis and a potential target for therapy of MM [47]. Increased expression of LILRB1 is known to play a role in immune suppression [87], but its role in tumour biology has yet to be fully defined. A study by Xian et al.., found that LILRB1-knockdown (KD) in MM cells was associated with an upregulation of oxidative phosphorylation and downregulation of the sirtuin and semaphoring neuronal signalling and antioxidant pathways, which protect cells from oxidative stress [47]. LILRB1 KD also resulted in increased expression of genes involved in fatty acid metabolism and induction of ferroptosis, and decreased expression of genes associated with ferroptosis inhibition [47]. Consistent with these changes, LILRB1 KD significantly increased the sensitivity of MM cells to RSL3, erastin and the ferroptosis-inducer, Fin56, with significantly higher levels of lipid peroxidation observed following treatment [47]. In contrast, MM cells overexpressing LILRB1 were less sensitive to the three compounds, with concomitantly lower levels of lipid peroxidation.

LILRB1 has also been shown to play a significant role in ferroptosis and disease progression in a MM mouse model [47]. LILRB1 KD suppressed disease progression, which was reversed by treatment with the synthetic antioxidant, liproxstatin-1, and RSL3 was effective at reducing tumour burden in a LILRB1 KD, but not control, MM mouse models. Higher levels of lipid ROS were observed both at baseline and following treatment with the GPX4 inhibitor in the LILRB1 KD cells [47]. Consistent with the role of LILRB1 in cholesterol uptake [47], subsequent analysis of LILRB1 KD MM cells from the mice confirmed they contained lower levels of intracellular LDL-cholesterol than MM cells from the control mice [47]. Decreased cholesterol levels in the MM cells from LILRB1 KD mice were consistent with decreased tumour burden, while overexpression resulted in significantly greater tumour burden [47].

1.10 7-dehydrocholesterol

The precursor, 7-dehydrocholesterol (7-DHC) is converted into cholesterol by 7-dehydrocholesterol reductase (Fig. 2). While there are no studies that investigate 7-DHC in MM, a recent study found that the cholesterol biosynthesis pathway and 7-DHC play important roles in another aggressive B cell malignancy, Burkitt's lymphoma, as well as neuroblastoma [72]. Contrary to previous research suggesting that 7-DHC is toxic due to its potential to undergo autoxidation, this study found that 7-DHC has pro-survival functions in cancer cells by 'shielding' lipids from oxidation, thus preventing ferroptotic cell death [72]. 7-DHC accumulation in Burkitt's lymphoma xenografts resulted in a more aggressive, ferroptosis-resistant cancer. Addition of free cholesterol to this disease model reduced the protective effects of 7-DHC, suggesting that the balance between cholesterol and its precursors may determine their impact on the sensitivity of cells to ferroptosis. To study the effects of 7-DHC on PL autoxidation in more detail, unilamellar (single lipid bilayer) liposomes loaded with 7-DHC were developed [72]. Using the fluorescence-enabled inhibited autoxidation (FENIX) assay, the authors found that liposomes containing 7-DHC, but not cholesterol, suppressed lipid peroxidation in a dose dependent manner [72, 88]. Furthermore, PL species generated as products of lipid peroxidation were found to be key mediators of ferroptosis [72], which at high levels are also known to activate the intrinsic apoptosis cascade [89]. A separate study of hypoxia-ischemia in the neonatal brain found that elevating 7-DHC levels can suppress ferroptosis and protect against tissue injury caused by an accumulation of ROS [71].

In summary, it is apparent that the cholesterol biosynthesis pathway and levels of the cholesterol pre-cursor, 7-DHC, can modulate the sensitivity of cells to ferroptosis. In addition to 7-DHC, the C27 cholesterol intermediate, desmosterol, has been identified as having anti-ferroptosis properties in human fibrosarcoma and renal adenocarcinoma cell lines [46]. Both cholesterol and desmosterol were found to elevate levels of CoQ10 and squalene, which in turn inhibit lipid peroxidation and protect against ferroptosis (Fig. 2). These effects were also demonstrated in response to treatment with doxorubicin and ischemia-reperfusion induced liver injury in mice [46]. While these studies do not specifically investigate 7-DHC in MM, they do highlight how 7-DHC levels and 7-dehydrocholesterol reductase activity may be associated with prognosis and could be targeted for the treatment of cancers.

1.11 27-hydroxycholesterol

Perturbations in cholesterol homeostasis have been associated with an increased risk of several cancers, including MM [77, 90]. The cholesterol metabolite, 27-hydroxycholesterol (27HC), has been shown to support tumour cell growth in models of estrogen receptor positive luminal breast cancer [91] and increase metastatic activity in mouse models of breast cancer [92]. Interestingly, tumour burden and the high metabolic activity of the tumour cells in the latter study were shown to be dependent upon inhibition of ferroptosis through sustained expression of GPX4 [92]. This study also concluded that increased survival rates among post-menopausal breast cancer patients receiving statins were also attributable to decreased levels of 27HC [92].

1.12 Sterol regulatory element binding proteins (SREBPs)

Sterol regulatory element binding proteins (SREBPs) are membrane bound transcription factors involved in cholesterol and lipid biosynthesis. SREB2 has been shown to inhibit ferroptosis in melanoma by reducing the labile iron pool and reducing lipid peroxidation by inducing transferrin transcription [93]. A study published investigating artesunate, an anti-malaria drug, has demonstrated promising efficacy in inducing ferroptosis in MM cell lines. Artesunate was able to prevent the nuclear localisation of SREBP2, while GPX4 and IPP were downregulated following treatment, inducing ferroptosis in MM cell lines [94]. ACSL4 levels increased following treatment, which would suggest an increase in PL-PUFA, key cellular substrates of ferroptosis [94]. These results were recapitulated through silencing of SREBP2 using siRNA, which resulted in a decrease in cell viability, an increase in lipid ROS and lipid peroxidation in the MM cell lines [94]. A study by Cai et al.., found that treatment of glioblastoma cells with the SREBP inhibitor, fatostatin, resulted in ferroptosis-mediated cell death via accumulation of lipid ROS and decreased levels of glutathione and GPX4 [95]. Similar results were also observed in a mouse model of glioblastoma using nanoparticles containing fatostatin [95].

B7H3 (also known as CD276) regulates ferroptosis sensitivity in colorectal cancer (CRC) cells by downregulating SREBP2 expression [73]. The knockdown of B7H3 decreased intracellular cholesterol levels, thereby significantly increasing the sensitivity of CRC cells to RSL3 [73]. In contrast, overexpression of B7H3 protects CRC cells against RSL3-induced ferroptosis [73]. The effects of B7H3 knockdown on the sensitivity of the CRC cells to RSL3 were inhibited by addition of exogenous cholesterol. Similar effects were observed in mouse models of CRC [73]. These studies further illustrate the importance of cholesterol and its substrates in determining the sensitivity of cancer cells to ferroptosis.

1.13 Harnessing lipids as a novel therapeutic approach for multiple myeloma

Although ferroptosis was first characterised in 2012 [11], studies that predate this discuss findings that we now know may be attributable to this form of cell death. One such study found that serum levels of the LPLs, lysophosphatidic acid (LPA) and lysophosphatidylcholine (LPC), are significantly elevated in MM patients compared to healthy controls, while levels of lipids containing AA and linoleic acid were found to be lower [96]. AA has been shown to directly induce ferroptosis in MM cells [60], while linoleic acid has been shown to sensitise cancer cells to ferroptosis (studies summarised in Table 1).

Lipid supplementation, particularly with PUFAs, has been investigated in the context of ferroptosis in multiple disease models, including MM and other haematological malignancies (Table 1) [29]. Research has demonstrated that MM cells from patients with specific molecular subsets such as t(4;14) may be susceptible to ferroptosis induction via direct GPX4 inhibition [30]. This study also found that ACLS4 knockdown led to a reduction in PUFA levels and decreased the sensitivity of MM cells to ferroptosis, but that supplementation with even low doses of PUFA (AA or adrenic acid) significantly increased their sensitivity [30]. This study suggests that some high-risk chromosomal abnormalities in MM may respond favourably to ferroptosis induction, warranting further research into other high-risk subtypes such as 1q gain or amplification, and TP53 gene mutation or deletion.

Another study found that supplementing MM cells with either eicosapentaenoic or docosahexaenoic acid, increased cell death via ferroptosis and necroptosis [61]. Interestingly, this study also found that pre-treatment of MM cells with docosahexaenoic acid increased the cytotoxic effects of the proteasome inhibitor, bortezomib, by decreasing cellular glutathione levels [61] These studies suggest that therapeutic approaches targeting multiple cell death mechanisms may be effective in MM.

The cholesterol biosynthesis pathway, involving the substrates lanosterol, 7-DHC, cholesterol, and 27-hydroxycholesterol, are critical determinants of ferroptosis sensitivity in cancer cells (Fig. 2; Table 1). While lanosterol has emerged as a driver of ferroptosis in MM, levels of 7-DHC, cholesterol and 27-hydroxycholesterol have been shown to protect a range of other cancer cells from ferroptosis-mediated cell death (Table 1). As discussed earlier in this review, recent studies have shown that LILRB1, a key regulator of cholesterol metabolism, protects MM cells from ferroptosis by maintaining cholesterol homeostasis [47], while expression of SREBPs are associated with decreased ferroptosis sensitivity in other malignancies [47, 73, 95]. Although the exact roles of SREBPs, which function as transcription factors, and LILRB1, an immune inhibitory receptor, in MM remain unclear, expression of both LILRB1 and SREBPs may decrease the sensitivity of MM cells to ferroptosis by increasing their ability to take up cholesterol [47, 73, 95]. The sensitivity of MM cells to RSL3 following knockdown of these proteins highlights the potential of LILRB1 and SREBPs and the cholesterol biosynthesis pathway as therapeutic targets for MM [47, 73, 95]. However, the published literature concerning the factors that dictate sensitivity of MM cells to ferroptosis, including the role of the BMME, is currently limited. Recent studies suggest that the interaction of MM cells with bone marrow stromal cells [84, 85] and changes in the cellular composition of lipids, including cholesterol [85], that are facilitated by the BMME, play important roles in determining the sensitivity of MM cells to ferroptosis.

Dysregulation of cholesterol metabolism and/or increased uptake into MM cells have been proposed as underlying reasons for the hypocholesterolemia and low serum LPL levels [96], observed in MM patients [75, 80]. This likely plays a significant role in the pathobiology of the disease as low serum cholesterol levels [80] have been associated with an increased risk of MM development [76, 79, 82]. These findings highlight the need for a better understanding of how cholesterol levels are regulated in MM and how this may impact the efficacy of novel, ferroptosis-dependent therapeutic approaches.

In summary, there is growing evidence that ferroptosis has potential as a novel approach for the treatment of MM and a range of other cancers, particularly for patients who develop resistance to apoptosis-dependent regimens. However, there will be significant challenges, including the development of targeted drug delivery mechanisms, before the research findings discussed can be translated into the clinic. Recent advances in nanotechnology-based delivery mechanisms (reviewed in [29]), capable of significantly improving the pharmacokinetics and bioavailability of drugs, have shown promising results. Identifying factors associated with ferroptosis resistance, such as increased levels of 7-DHC or cholesterol, may help to increase the specificity of novel treatment approaches and tailor therapies to individual patients.

2 Conclusions

Multiple myeloma is the second most common haematological malignancy in Australia and worldwide. The management of MM patients is challenging due to clinical and biological heterogeneity between patients and, despite advances in therapy over the past few decades, it is still considered incurable. A significant proportion of patients will relapse with drug-refractory disease, necessitating the development of novel therapeutic approaches. Ferroptosis, a relatively recently defined mechanism of programmed cell death, represents a promising approach for the treatment of MM and other cancers, that are refractory to apoptosis-mediated regimens.

However, a better understanding of the relationship between cellular lipid composition and ferroptosis sensitivity is key to harnessing this form of programmed cell death as a therapeutic approach. Studies to date indicate that cholesterol levels impact not only the onset and progression of haematological malignancies but also the sensitivity of a variety of different cancers to ferroptosis. Therefore, targeting the metabolism and uptake of lipids, including glycerophospholipids and cholesterol may be an effective means of sensitising tumour cells to ferroptosis-inducing drugs and could offer new strategies to treat patients who are resistant to more conventional, apoptosis-dependent treatments. Findings from the limited number of studies concerning ferroptosis in MM and compelling evidence from other malignancies, provide a strong rationale for further investigation of ferroptosis as a novel therapeutic approach for MM.

Abbreviations

27HC	27-hydroxycholesterol
7-DHC	7-Dehydrocholesterol
AA	Arachidonic acid
Acetyl-CoA	Acetyl coenzyme A
ACSL4	acyl-CoA synthetase long-chain family member 4
BMME	Bone marrow microenvironment
BMSC	Bone marrow stromal cell
CoQ10	Ubiquinone
CoQ10-H2	Ubiquinol
FA	Fatty acid
FPP	Farnesyl phosphate
FSP1	Ferroptosis suppressor protein 1
GGPP	Geranylgeranyl pyrophosphate
GPX4	Glutathione peroxidase 4
H_2O_2	Hydrogen peroxide
HDL	High-density lipoprotein
IPP	Isopentenyl phosphate
HMG-CoA	3-hydroxy-3-methylglutaryl-coenzyme A
LDL	Low-density lipoprotein
LILRB1	Leukocyte immunoglobulin-like receptor B1
LOX	Lipoxygenases
LPC	Lysophosphatidylcholine
LPCAT3	Lysophosphatidylcholine acyltransferase 3
LPE	Lysophosphatidylethanolamine
LPL	Lysophospholipids
MM	Multiple myeloma
MMSET	MM SET domain-containing protein
MUFA	Monounsaturated fatty acid
OH^-	Hydroxide ion
PC	Phosphatidylcholine
PCD	Programmed cell death
PE	Phosphatidylethanolamine
PL	Phospholipid
PL-PUFA-OH	Phospholipid alcohol
PL-PUFA-OOH	Phospholipid hydroperoxide
PS	Phosphatidylserine
PUFA	Polyunsaturated fatty acid
ROS	Reactive oxygen species
RSL3	(1S,3R)-RSL3

SFA	Saturated fatty acid
SREBP	Sterol regulatory element binding protein

Acknowledgements
There are no acknowledgements beyond the contributions of the authors.

Author contributions
A.H., O.G.B., C.E.T. and C.W.G. reviewed the literature and wrote the manuscript.

Funding
A.H. was funded by a Jane Watson Ramsey Myeloma Research PhD Scholarship. C.W.G was funded by a Cancer Council SA Clinical Investigator Grant and Flinders Foundation Cancer Seed Grant.

Data availability
No datasets were generated or analysed during the current study.

Declarations

Availability of data and materials
There is nothing to declare.

Ethics approval
There is nothing to declare.

Consent to participate
The authors give full consent to participate.

Consent for publication
The authors give full consent to publishing this work in Discover Oncology.

Competing interests
The authors declare no competing interests.

Received: 1 June 2025 / Accepted: 18 August 2025
Published online: 25 August 2025

References

1. Rasche L, Chavan SS, Stephens OW, Patel PH, Tytarenko R, Ashby C, et al. Spatial genomic heterogeneity in multiple myeloma revealed by multi-region sequencing. Nat Commun. 2017;8(1):268.
2. Cowan AJ, Green DJ, Kwok M, Lee S, Coffey DG, Holmberg LA, et al. Diagnosis and management of multiple myeloma: A review. JAMA. 2022;327(5):464–77.
3. Huang J, Chan SC, Lok V, Zhang L, Lucero-Prisno DE 3rd, Xu W, et al. The epidemiological landscape of multiple myeloma: a global cancer registry estimate of disease burden, risk factors, and Temporal trends. Lancet Haematol. 2022;9(9):e670–7.
4. Australian_Institute_of_Health_and_Welfare. Cancer data in Australia 2025 [Available from: https://www.aihw.gov.au/reports/cancer/cancer-data-in-australia/contents/survival
5. Shah UA, Mailankody S. Emerging immunotherapies in multiple myeloma. BMJ. 2020;370:m3176.
6. Turesson I, Bjorkholm M, Blimark CH, Kristinsson S, Velez R, Landgren O. Rapidly changing myeloma epidemiology in the general population: increased incidence, older patients, and longer survival. Eur J Haematol. 2018.
7. D'Agostino M, Cairns DA, Lahuerta JJ, Wester R, Bertsch U, Waage A, et al. Second revision of the international staging system (R2-ISS) for overall survival in multiple myeloma: A European myeloma network (EMN) report within the HARMONY project. J Clin Oncol. 2022;40(29):3406–18.
8. Dima D, Jiang D, Singh DJ, Hasipek M, Shah HS, Ullah F et al. Multiple Myeloma Therapy: Emerg Trends Challenges Cancers [Internet]. 2022; 14(17).
9. Cui J, Zhao S, Li Y, Zhang D, Wang B, Xie J, et al. Regulated cell death: discovery, features and implications for neurodegenerative diseases. Cell Commun Signal. 2021;19(1):120.
10. Hu XM, Li ZX, Lin RH, Shan JQ, Yu QW, Wang RX, et al. Guidelines for regulated cell death assays: A systematic summary, A categorical comparison, A prospective. Front Cell Dev Biol. 2021;9:634690.
11. Dixon SJ, Lemberg KM, Lamprecht MR, Skouta R, Zaitsev EM, Gleason CE, et al. Ferroptosis: an iron-dependent form of nonapoptotic cell death. Cell. 2012;149(5):1060–72.
12. Gaschler MM, Stockwell BR. Lipid peroxidation in cell death. Biochem Biophys Res Commun. 2017;482(3):419–25.
13. Conrad M, Kagan VE, Bayir H, Pagnussat GC, Head B, Traber MG, et al. Regulation of lipid peroxidation and ferroptosis in diverse species. Genes Dev. 2018;32(9–10):602–19.
14. Hassannia B, Vandenabeele P, Vanden Berghe T. Targeting ferroptosis to iron out cancer. Cancer Cell. 2019;35(6):830–49.
15. Angeli JPF, Shah R, Pratt DA, Conrad M. Ferroptosis inhibition: mechanisms and opportunities. Trends Pharmacol Sci. 2017;38(5):489–98.
16. Stockwell BR, Friedmann Angeli JP, Bayir H, Bush AI, Conrad M, Dixon SJ, et al. Ferroptosis: A regulated cell death nexus linking metabolism, redox biology, and disease. Cell. 2017;171(2):273–85.
17. Seibt TM, Proneth B, Conrad M. Role of GPX4 in ferroptosis and its Pharmacological implication. Free Radic Biol Med. 2019;133:144–52.
18. Doll S, Freitas FP, Shah R, Aldrovandi M, da Silva MC, Ingold I, et al. FSP1 is a glutathione-independent ferroptosis suppressor. Nature. 2019;575(7784):693–8.
19. Turunen M, Olsson J, Dallner G. Metabolism and function of coenzyme Q. Biochim Biophys Acta. 2004;1660(1–2):171–99.

20. Warner GJ, Berry MJ, Moustafa ME, Carlson BA, Hatfield DL, Faust JR. Inhibition of Selenoprotein synthesis by selenocysteine tRNA[Ser]Sec lacking isopentenyladenosine. J Biol Chem. 2000;275(36):28110–9.
21. Yang WS, Stockwell BR. Ferroptosis: death by lipid peroxidation. Trends Cell Biol. 2016;26(3):165–76.
22. Saini R. Coenzyme Q10: the essential nutrient. J Pharm Bioallied Sci. 2011;3(3):466–7.
23. Acosta MJ, Vazquez Fonseca L, Desbats MA, Cerqua C, Zordan R, Trevisson E, et al. Coenzyme Q biosynthesis in health and disease. Biochim Biophys Acta. 2016;1857(8):1079–85.
24. Kaymak I, Maier CR, Schmitz W, Campbell AD, Dankworth B, Ade CP, et al. Mevalonate pathway provides ubiquinone to maintain pyrimidine synthesis and survival in p53-Deficient cancer cells exposed to metabolic stress. Cancer Res. 2020;80(2):189–203.
25. Ahmed S, Shah P, Ahmed O, Biochemistry. Lipids. StatPearls. Treasure Island (FL)2022.
26. Calder PC, Grimble RF. Polyunsaturated fatty acids, inflammation and immunity. Eur J Clin Nutr. 2002;56(Suppl 3):S14–9.
27. Beatty A, Singh T, Tyurina YY, Tyurin VA, Samovich S, Nicolas E, et al. Ferroptotic cell death triggered by conjugated linolenic acids is mediated by ACSL1. Nat Commun. 2021;12(1):2244.
28. Rodencal J, Dixon SJ. A Tale of two lipids: lipid unsaturation commands ferroptosis sensitivity. Proteomics. 2023;23(6):e2100308.
29. Mynott RL, Habib A, Best OG, Wallington-Gates CT. Ferroptosis in haematological malignancies and associated therapeutic nanotechnologies. Int J Mol Sci. 2023;24(8).
30. Zhang J, Liu Y, Zuo L, Fan F, Yan H, Zhao F, et al. Class II ferroptosis inducers are a novel therapeutic approach for t(4;14)-positive multiple myeloma. Blood Adv. 2024;8(19):5022–38.
31. Habib A, Mynott RL, Best OG, Revesz IA, Prestidge CA, Wallington-Gates CT, Novel. (1S,3R)-RSL3-Encapsulated polyunsaturated fatty acid rich liposomes sensitise multiple myeloma cells to Ferroptosis-Mediated cell death. Int J Mol Sci. 2025;26(14):6579.
32. Shan K, Feng N, Zhu D, Qu H, Fu G, Li J et al. Free docosahexaenoic acid promotes ferroptotic cell death via Lipoxygenase dependent and independent pathways in cancer cells. Eur J Nutr. 2022.
33. Kagan VE, Mao G, Qu F, Angeli JP, Doll S, Croix CS, et al. Oxidized arachidonic and adrenic PEs navigate cells to ferroptosis. Nat Chem Biol. 2017;13(1):81–90.
34. Magtanong L, Ko PJ, To M, Cao JY, Forcina GC, Tarangelo A, et al. Exogenous monounsaturated fatty acids promote a Ferroptosis-Resistant cell state. Cell Chem Biol. 2019;26(3):420–32. e9.
35. Das UN. Saturated fatty acids, MUFAs and PUFAs regulate ferroptosis. Cell Chem Biol. 2019;26(3):309–11.
36. Krümmel B, von Hanstein A-S, Plötz T, Lenzen S, Mehmeti I. Differential effects of saturated and unsaturated free fatty acids on ferroptosis in rat β-cells. J Nutr Biochem. 2022;106:109013.
37. Wang N, Ma H, Li J, Meng C, Zou J, Wang H, et al. HSF1 functions as a key defender against palmitic acid-induced ferroptosis in cardiomyocytes. J Mol Cell Cardiol. 2021;150:65–76.
38. Kuang H, Sun X, Liu Y, Tang M, Wei Y, Shi Y, et al. Palmitic acid-induced ferroptosis via CD36 activates ER stress to break calcium-iron balance in colon cancer cells. Febs J. 2023;290(14):3664–87.
39. Miao S, Zhang Q, Ding W, Hou B, Su Z, Li M et al. Platelet Internalization Mediates Ferroptosis in Myocardial Infarction. Arteriosclerosis, Thrombosis, and Vascular Biology. 2023;43(2):218 – 30.
40. Heringdorf, DMz. Lysophospholipids. Encyclopedia of molecular Pharmacology. Berlin, Heidelberg: Springer; 2008.
41. Spickett CM. Formation of oxidatively modified lipids as the basis for a cellular epilipidome. Front Endocrinol (Lausanne). 2020;11:602771.
42. Bersuker K, Hendricks JM, Li Z, Magtanong L, Ford B, Tang PH, et al. The CoQ oxidoreductase FSP1 acts parallel to GPX4 to inhibit ferroptosis. Nature. 2019;575(7784):688–92.
43. Yang WS, SriRamaratnam R, Welsch ME, Shimada K, Skouta R, Viswanathan VS, et al. Regulation of ferroptotic cancer cell death by GPX4. Cell. 2014;156(1–2):317–31.
44. Craig M, Yarrarapu SNS, Dimri M, Biochemistry. Cholesterol. StatPearls. Treasure Island (FL)2024.
45. White AM, Best OG, Hotinski AK, Kuss BJ, Thurgood LA. The role of cholesterol in chronic lymphocytic leukemia development and pathogenesis. Metabolites. 2023;13:7.
46. Sun Q, Liu D, Cui W, Cheng H, Huang L, Zhang R, et al. Cholesterol mediated ferroptosis suppression reveals essential roles of coenzyme Q and squalene. Commun Biol. 2023;6(1):1108.
47. Xian M, Wang Q, Xiao L, Zhong L, Xiong W, Ye L, et al. Leukocyte immunoglobulin-like receptor B1 (LILRB1) protects human multiple myeloma cells from ferroptosis by maintaining cholesterol homeostasis. Nat Commun. 2024;15(1):5767.
48. Picón DF, Skouta R. Unveiling the therapeutic potential of squalene synthase: Deciphering its biochemical mechanism, disease implications, and intriguing ties to ferroptosis. Cancers (Basel). 2023;15(14).
49. Garcia-Bermudez J, Baudrier L, Bayraktar EC, Shen Y, La K, Guarecuco R, et al. Squalene accumulation in cholesterol auxotrophic lymphomas prevents oxidative cell death. Nature. 2019;567(7746):118–22.
50. Liu C, Liao W, Chen J, Yu K, Wu Y, Zhang S, et al. Cholesterol confers ferroptosis resistance onto myeloid-biased hematopoietic stem cells and prevents irradiation-induced myelosuppression. Redox Biol. 2023;62:102661.
51. Zhao X, Lian X, Xie J, Liu G. Accumulated cholesterol protects tumours from elevated lipid peroxidation in the microenvironment. Redox Biol. 2023;62:102678.
52. Michel V, Bakovic M. Lipid rafts in health and disease. Biol Cell. 2007;99(3):129–40.
53. Zhao X, Zhao Z, Li B, Huan S, Li Z, Xie J, et al. ACSL4-mediated lipid rafts prevent membrane rupture and inhibit Immunogenic cell death in melanoma. Cell Death Dis. 2024;15(9):695.
54. Bai T, Xue P, Shao S, Yan S, Zeng X. Cholesterol Depletion-Enhanced ferroptosis and immunotherapy via engineered nanozyme. Adv Sci (Weinh). 2024;11(38):e2405826.
55. Sizar O, Khare S, Patel P, Talati R. Statin medications. StatPearls. Treasure Island (FL): StatPearls publishing copyright © 2025. StatPearls Publishing LLC.; 2025.
56. Yao X, Xie R, Cao Y, Tang J, Men Y, Peng H, et al. Simvastatin induced ferroptosis for triple-negative breast cancer therapy. J Nanobiotechnol. 2021;19(1):311.
57. Sun D, Cui X, Yang W, Wei M, Yan Z, Zhang M, et al. Simvastatin inhibits PD-L1 via ILF3 to induce ferroptosis in gastric cancer cells. Cell Death Dis. 2025;16(1):208.
58. Panaroni C, Fulzele K, Soucy R, Siu KT, Mukaihara K, Huang C, et al. Arachidonic acid induces Ferroptosis-Mediated Cell-Death in multiple myeloma. Blood. 2018;132:4498.

59. Liao P, Wang W, Wang W, Kryczek I, Li X, Bian Y, et al. CD8(+) T cells and fatty acids orchestrate tumor ferroptosis and immunity via ACSL4. Cancer Cell. 2022;40(4):365–e786.
60. Dierge E, Debock E, Guilbaud C, Corbet C, Mignolet E, Mignard L, et al. Peroxidation of n-3 and n-6 polyunsaturated fatty acids in the acidic tumor environment leads to ferroptosis-mediated anticancer effects. Cell Metab. 2021;33(8):1701–e155.
61. Chen J, Zaal EA, Berkers CR, Ruijtenbeek R, Garssen J, Redegeld FA. Omega-3 fatty acids DHA and EPA reduce bortezomib resistance in multiple myeloma cells by promoting glutathione degradation. Cells. 2021;10(9).
62. Suda A, Umaru BA, Yamamoto Y, Shima H, Saiki Y, Pan Y, et al. Polyunsaturated fatty acids-induced ferroptosis suppresses pancreatic cancer growth. Sci Rep. 2024;14(1):4409.
63. Zhang Y, Shen G, Meng T, Lv Z, Li X, Li J, et al. Eicosapentaenoic acid enhances the sensitivity of osteosarcoma to cisplatin by inducing ferroptosis through the DNA-PKcs/AKT/NRF2 pathway and reducing PD-L1 expression to attenuate immune evasion. Int Immunopharmacol. 2023;125:111181.
64. Chen Y, Liao X, Jing P, Hu L, Yang Z, Yao Y, et al. Linoleic Acid-Glucosamine hybrid for endogenous Iron-Activated ferroptosis therapy in High-Grade serous ovarian cancer. Mol Pharm. 2022;19(9):3187–98.
65. Ubellacker JM, Tasdogan A, Ramesh V, Shen B, Mitchell EC, Martin-Sandoval MS, et al. Lymph protects metastasizing melanoma cells from ferroptosis. Nature. 2020;585(7823):113–8.
66. Tesfay L, Paul BT, Konstorum A, Deng Z, Cox AO, Lee J, et al. Stearoyl-CoA desaturase 1 protects ovarian cancer cells from ferroptotic cell death. Cancer Res. 2019;79(20):5355–66.
67. Luo H, Wang X, Song S, Wang Y, Dan Q, Ge H. Targeting stearoyl-coa desaturase enhances radiation induced ferroptosis and Immunogenic cell death in esophageal squamous cell carcinoma. Oncoimmunology. 2022;11(1):2101769.
68. Chen X, Kang R, Kroemer G, Tang D. Broadening horizons: the role of ferroptosis in cancer. Nat Rev Clin Oncol. 2021;18(5):280–96.
69. Roh JL, Kim EH, Jang HJ, Park JY, Shin D. Induction of ferroptotic cell death for overcoming cisplatin resistance of head and neck cancer. Cancer Lett. 2016;381(1):96–103.
70. Liu MR, Zhu WT, Pei DS. System Xc(-): a key regulatory target of ferroptosis in cancer. Invest New Drugs. 2021;39(4):1123–31.
71. Genaro-Mattos TC, Korade Z, Sahar NE, Angeli JPF, Mirnics K, Peeples ES. Enhancing 7-dehydrocholesterol suppresses brain ferroptosis and tissue injury after neonatal hypoxia-ischemia. Sci Rep. 2024;14(1):7924.
72. Freitas FP, Alborzinia H, dos Santos AF, Nepachalovich P, Pedrera L, Zilka O, et al. 7-Dehydrocholesterol is an endogenous suppressor of ferroptosis. Nature. 2024;626(7998):401–10.
73. Jin H, Zhu M, Zhang D, Liu X, Guo Y, Xia L, et al. B7H3 increases ferroptosis resistance by inhibiting cholesterol metabolism in colorectal cancer. Cancer Sci. 2023;114(11):4225–36.
74. Rink JS, Lin AY, McMahon KM, Calvert AE, Yang S, Taxter T, et al. Targeted reduction of cholesterol uptake in cholesterol-addicted lymphoma cells blocks turnover of oxidized lipids to cause ferroptosis. J Biol Chem. 2021;296:100100.
75. Liu X, Xu P, Wang L, Zhang C, Wang M, Ouyang J et al. Cholesterol levels provide prognostic information in patients with multiple myeloma. Clin Lab. 2020;66(4).
76. Ding X, Zhang W, Li S, Yang H. The role of cholesterol metabolism in cancer. Am J Cancer Res. 2019;9(2):219–27.
77. Halimi H, Farjadian S, Cholesterol. An important actor on the cancer immune scene. Front Immunol. 2022;13:1057546.
78. Jiang W, Jin WL, Xu AM. Cholesterol metabolism in tumor microenvironment: cancer hallmarks and therapeutic opportunities. Int J Biol Sci. 2024;20(6):2044–71.
79. Choi T, Choi IY, Han K, Jeong SM, Yoo JE, Rhee SY et al. Lipid level, lipid variability, and risk of multiple myeloma: A nationwide Population-Based study of 3,527,776 subjects. Cancers (Basel). 2021;13(3).
80. Yavasoglu I, Tombuloglu M, Kadikoylu G, Donmez A, Cagirgan S, Bolaman Z. Cholesterol levels in patients with multiple myeloma. Ann Hematol. 2008;87(3):223–8.
81. Li L, Yu Z, Ren J, Niu T. Low cholesterol levels are associated with increasing risk of plasma cell neoplasm: A UK biobank cohort study. Cancer Med. 2023;12(22):20964–75.
82. Tirado-Velez JM, Benitez-Rondan A, Cozar-Castellano I, Medina F, Perdomo G. Low-density lipoprotein cholesterol suppresses apoptosis in human multiple myeloma cells. Ann Hematol. 2012;91(1):83–8.
83. Fotiou D, Katodritou E. From biology to clinical practice: the bone marrow microenvironment in multiple myeloma. J Clin Med. 2025;14(2):327.
84. Jiang H, Li Q, Yang X, Jia L, Cheng H, Wang J, et al. Bone marrow stromal cells protect myeloma cells from ferroptosis through GPX4 desumoylation. Cancer Lett. 2025;611:217388.
85. Jiang H, Wang L, Zhang Q, Wang S, Jia L, Cheng H, et al. Bone marrow stromal cells dictate lanosterol biosynthesis and ferroptosis of multiple myeloma. Oncogene. 2024;43(21):1644–53.
86. Kushiro T, Ebizuka Y. 1.18 - Triterpenes. In: Liu H-W, Mander L, editors. Comprehensive natural products II. Oxford: Elsevier; 2010. pp. 673–708.
87. Zeller T, Münnich IA, Windisch R, Hilger P, Schewe DM, Humpe A, et al. Perspectives of targeting LILRB1 in innate and adaptive immune checkpoint therapy of cancer. Front Immunol. 2023;14:1240275.
88. Shah R, Farmer LA, Zilka O, Van Kessel ATM, Pratt DA, Beyond DPPH. Use of Fluorescence-Enabled inhibited autoxidation to predict oxidative cell death rescue. Cell Chem Biol. 2019;26(11):1594–e6077.
89. McIntyre TM. Bioactive oxidatively truncated phospholipids in inflammation and apoptosis: formation, targets, and inactivation. Biochim Biophys Acta. 2012;1818(10):2456–64.
90. Gámez B, Whipp D, Rao S, Morris EV, Park YE, Kaya Z et al. High cholesterol increases myeloma tumour burden and promotes resistance to bortezomib. BioRxiv. 2025:2025.01.21.633916.
91. Nelson ER, Wardell SE, Jasper JS, Park S, Suchindran S, Howe MK, et al. 27-Hydroxycholesterol links hypercholesterolemia and breast cancer pathophysiology. Science. 2013;342(6162):1094–8.
92. Liu W, Chakraborty B, Safi R, Kazmin D, Chang CY, McDonnell DP. Dysregulated cholesterol homeostasis results in resistance to ferroptosis increasing tumorigenicity and metastasis in cancer. Nat Commun. 2021;12(1):5103.
93. Hong X, Roh W, Sullivan RJ, Wong KHK, Wittner BS, Guo H, et al. The lipogenic regulator SREBP2 induces transferrin in Circulating melanoma cells and suppresses ferroptosis. Cancer Discov. 2021;11(3):678–95.
94. Liang L, Liu Y, Wu X, Chen Y. Artesunate induces ferroptosis by inhibiting the nuclear localization of SREBP2 in myeloma cells. Int J Med Sci. 2023;20(12):1535–50.

95. Cai J, Ye Z, Hu Y, Ye L, Gao L, Wang Y, et al. Fatostatin induces ferroptosis through Inhibition of the AKT/mTORC1/GPX4 signaling pathway in glioblastoma. Cell Death Dis. 2023;14(3):211.
96. Sasagawa T, Okita M, Murakami J, Kato T, Watanabe A. Abnormal serum lysophospholipids in multiple myeloma patients. Lipids. 1999;34(1):17–21.

Publisher's note

BIBLIOGRAPHY

1. Cowan AJ, Green DJ, Kwok M, Lee S, Coffey DG, Holmberg LA, et al. Diagnosis and Management of Multiple Myeloma: A Review. JAMA. 2022;327(5):464-77.
2. Ludwig H, Novis Durie S, Meckl A, Hinke A, Durie B. Multiple Myeloma Incidence and Mortality Around the Globe; Interrelations Between Health Access and Quality, Economic Resources, and Patient Empowerment. Oncologist. 2020;25(9):e1406-e13.
3. Australian_Institute_of_Health_and_Welfare. Multiple myeloma in Australia statistics 2024 [Available from: https://www.aihw.gov.au/.
4. Lee JY, Hong SH. Hematopoietic Stem Cells and Their Roles in Tissue Regeneration. Int J Stem Cells. 2020;13(1):1-12.
5. Giebel B, Bruns I. Self-renewal versus differentiation in hematopoietic stem and progenitor cells: a focus on asymmetric cell divisions. Curr Stem Cell Res Ther. 2008;3(1):9-16.
6. Khodadadi L, Cheng Q, Radbruch A, Hiepe F. The Maintenance of Memory Plasma Cells. Front Immunol. 2019;10:721.
7. Corso A, Mangiacavalli S. Non-Secretory Myeloma: Ready for a new Definition? Mediterr J Hematol Infect Dis. 2017;9(1):e2017053.
8. Katzmann JA, Clark RJ, Abraham RS, Bryant S, Lymp JF, Bradwell AR, et al. Serum reference intervals and diagnostic ranges for free kappa and free lambda immunoglobulin light chains: relative sensitivity for detection of monoclonal light chains. Clin Chem. 2002;48(9):1437-44.
9. Kaseb H, Annamaraju P, Babiker HM. Monoclonal Gammopathy Of Undetermined Significance. StatPearls. Treasure Island (FL)2022.
10. Rajkumar SV, Landgren O, Mateos MV. Smoldering multiple myeloma. Blood. 2015;125(20):3069-75.
11. Inc MFoA. Gather Round Breakfast - Myeloma Fast Facts: Myeloma Australia; 2025 [Available from: https://myeloma.org.au/gather-round-breakfast.
12. Mateos MV, Kumar S, Dimopoulos MA, Gonzalez-Calle V, Kastritis E, Hajek R, et al. International Myeloma Working Group risk stratification model for smoldering multiple myeloma (SMM). Blood Cancer J. 2020;10(10):102.
13. Rasche L, Kortum KM, Raab MS, Weinhold N. The Impact of Tumor Heterogeneity on Diagnostics and Novel Therapeutic Strategies in Multiple Myeloma. Int J Mol Sci. 2019;20(5).
14. Pawlyn C. High-risk myeloma: a challenge to define and to determine the optimal treatment. Lancet Haematol. 2021;8(1):e4-e6.
15. Li Y, Wang X, Zheng H, Wang C, Minvielle S, Magrangeas F, et al. Classify hyperdiploidy status of multiple myeloma patients using gene expression profiles. PLoS One. 2013;8(3):e58809.
16. Ankathil R, Foong E, Siti-Mariam I, Norhidayah R, Nazihah MY, Sangeetha V, et al. Hyperdiploid Multiple Myeloma with Novel Complex Structural Chromosome Abnormalities Associated with Poor Prognosis : A Rare Case Report. Int J Hematol Oncol Stem Cell Res. 2021;15(3):199-205.
17. Kumar S, Fonseca R, Ketterling RP, Dispenzieri A, Lacy MQ, Gertz MA, et al. Trisomies in multiple myeloma: impact on survival in patients with high-risk cytogenetics. Blood. 2012;119(9):2100-5.
18. Chretien ML, Corre J, Lauwers-Cances V, Magrangeas F, Cleynen A, Yon E, et al. Understanding the role of hyperdiploidy in myeloma prognosis: which trisomies really matter? Blood. 2015;126(25):2713-9.
19. Avet-Loiseau H, Attal M, Moreau P, Charbonnel C, Garban F, Hulin C, et al. Genetic abnormalities and survival in multiple myeloma: the experience of the Intergroupe Francophone du Myélome. Blood. 2007;109(8):3489-95.
20. McAuley N, Cymer I, McAvera R, Hopkins AM, Glavey SV. Chromosome 1 Alterations in Multiple Myeloma: Considerations for Precision Therapy. Eur J Haematol. 2025;114(3):400-10.
21. Flynt E, Bisht K, Sridharan V, Ortiz M, Towfic F, Thakurta A. Prognosis, Biology, and Targeting of TP53 Dysregulation in Multiple Myeloma. Cells. 2020;9(2).
22. Tang X, Chen Y. Identification and prognostic analysis of metabolic genes associated with TP53 mutation in multiple myeloma. Hematology. 2024;29(1):2377850.

23. Singh C, Panakkal V, Sreedharanunni S, Jandial A, Jain A, Lad D, et al. Presentation and Impact of Double and Triple hit Cytogenetics in Patients With Multiple Myeloma in the Real World. Clinical Lymphoma Myeloma and Leukemia. 2022;22(8):e685-e90.
24. Rasche L, Chavan SS, Stephens OW, Patel PH, Tytarenko R, Ashby C, et al. Spatial genomic heterogeneity in multiple myeloma revealed by multi-region sequencing. Nat Commun. 2017;8(1):268.
25. Weinhold N, Ashby C, Rasche L, Chavan SS, Stein C, Stephens OW, et al. Clonal selection and double-hit events involving tumor suppressor genes underlie relapse in myeloma. Blood. 2016;128(13):1735-44.
26. Bolli N, Avet-Loiseau H, Wedge DC, Van Loo P, Alexandrov LB, Martincorena I, et al. Heterogeneity of genomic evolution and mutational profiles in multiple myeloma. Nat Commun. 2014;5:2997.
27. Keats JJ, Chesi M, Egan JB, Garbitt VM, Palmer SE, Braggio E, et al. Clonal competition with alternating dominance in multiple myeloma. Blood. 2012;120(5):1067-76.
28. Rasche L, Schinke C, Maura F, Bauer MA, Ashby C, Deshpande S, et al. The spatio-temporal evolution of multiple myeloma from baseline to relapse-refractory states. Nature Communications. 2022;13(1):4517.
29. Schavgoulidze A, Cazaubiel T, Perrot A, Avet-Loiseau H, Corre J. Multiple Myeloma: Heterogeneous in Every Way. Cancers (Basel). 2021;13(6).
30. Salomon-Perzyński A, Jamroziak K, Głodkowska-Mrówka E. Clonal Evolution of Multiple Myeloma-Clinical and Diagnostic Implications. Diagnostics (Basel). 2021;11(9).
31. Fotiou D, Katodritou E. From Biology to Clinical Practice: The Bone Marrow Microenvironment in Multiple Myeloma. Journal of Clinical Medicine. 2025;14(2):327.
32. Paiva B, Azpilikueta A, Puig N, Ocio EM, Sharma R, Oyajobi BO, et al. PD-L1/PD-1 presence in the tumor microenvironment and activity of PD-1 blockade in multiple myeloma. Leukemia. 2015;29(10):2110-3.
33. Diaz-Tejedor A, Lorenzo-Mohamed M, Puig N, Garcia-Sanz R, Mateos MV, Garayoa M, et al. Immune System Alterations in Multiple Myeloma: Molecular Mechanisms and Therapeutic Strategies to Reverse Immunosuppression. Cancers (Basel). 2021;13(6).
34. Augustson BM, Begum G, Dunn JA, Barth NJ, Davies F, Morgan G, et al. Early mortality after diagnosis of multiple myeloma: analysis of patients entered onto the United kingdom Medical Research Council trials between 1980 and 2002--Medical Research Council Adult Leukaemia Working Party. J Clin Oncol. 2005;23(36):9219-26.
35. Blimark C, Holmberg E, Mellqvist UH, Landgren O, Bjorkholm M, Hultcrantz M, et al. Multiple myeloma and infections: a population-based study on 9253 multiple myeloma patients. Haematologica. 2015;100(1):107-13.
36. Shah UA, Mailankody S. Emerging immunotherapies in multiple myeloma. BMJ. 2020;370:m3176.
37. D'Agostino M, Cairns DA, Lahuerta JJ, Wester R, Bertsch U, Waage A, et al. Second Revision of the International Staging System (R2-ISS) for Overall Survival in Multiple Myeloma: A European Myeloma Network (EMN) Report Within the HARMONY Project. J Clin Oncol. 2022;40(29):3406-18.
38. Turesson I, Bjorkholm M, Blimark CH, Kristinsson S, Velez R, Landgren O. Rapidly changing myeloma epidemiology in the general population: Increased incidence, older patients, and longer survival. Eur J Haematol. 2018.
39. Kazandjian D, Landgren O. A look backward and forward in the regulatory and treatment history of multiple myeloma: Approval of novel-novel agents, new drug development, and longer patient survival. Semin Oncol. 2016;43(6):682-9.
40. Holstein SA, McCarthy PL. Immunomodulatory Drugs in Multiple Myeloma: Mechanisms of Action and Clinical Experience. Drugs. 2017;77(5):505-20.
41. Ito S. Proteasome Inhibitors for the Treatment of Multiple Myeloma. Cancers (Basel). 2020;12(2).
42. Facon T, Lee JH, Moreau P, Niesvizky R, Dimopoulos M, Hajek R, et al. Carfilzomib or bortezomib with melphalan-prednisone for transplant-ineligible patients with newly diagnosed multiple myeloma. Blood. 2019;133(18):1953-63.
43. Dimopoulos MA, Goldschmidt H, Niesvizky R, Joshua D, Chng WJ, Oriol A, et al. Carfilzomib or bortezomib in relapsed or refractory multiple myeloma (ENDEAVOR): an interim

overall survival analysis of an open-label, randomised, phase 3 trial. Lancet Oncol. 2017;18(10):1327-37.
44. Sana MK, Abdullah SM, Javed S, Ehsan H, Faizan U, Khalid F, et al. Efficacy of Ixazomib and Bortezomib with Lenalidomide Combination Regimens for Multiple Myeloma: A Systematic Review. Blood. 2020;136(Supplement 1):40-1.
45. Burwick N, Sharma S. Glucocorticoids in multiple myeloma: past, present, and future. Ann Hematol. 2019;98(1):19-28.
46. Wudhikarn K, Wills B, Lesokhin AM. Monoclonal antibodies in multiple myeloma: Current and emerging targets and mechanisms of action. Best Pract Res Clin Haematol. 2020;33(1):101143.
47. Lu RM, Hwang YC, Liu IJ, Lee CC, Tsai HZ, Li HJ, et al. Development of therapeutic antibodies for the treatment of diseases. J Biomed Sci. 2020;27(1):1.
48. Lonial S, Weiss BM, Usmani SZ, Singhal S, Chari A, Bahlis NJ, et al. Daratumumab monotherapy in patients with treatment-refractory multiple myeloma (SIRIUS): an open-label, randomised, phase 2 trial. Lancet. 2016;387(10027):1551-60.
49. Lokhorst HM, Plesner T, Laubach JP, Nahi H, Gimsing P, Hansson M, et al. Targeting CD38 with Daratumumab Monotherapy in Multiple Myeloma. N Engl J Med. 2015;373(13):1207-19.
50. Dimopoulos MA, Oriol A, Nahi H, San-Miguel J, Bahlis NJ, Usmani SZ, et al. Daratumumab, Lenalidomide, and Dexamethasone for Multiple Myeloma. N Engl J Med. 2016;375(14):1319-31.
51. Palumbo A, Chanan-Khan A, Weisel K, Nooka AK, Masszi T, Beksac M, et al. Daratumumab, Bortezomib, and Dexamethasone for Multiple Myeloma. N Engl J Med. 2016;375(8):754-66.
52. Frampton JE. Isatuximab: A Review of Its Use in Multiple Myeloma. Target Oncol. 2021;16(5):675-86.
53. Grosicki S, Bednarczyk M, Barchnicka A, Grosicka O. Elotuzumab in the treatment of relapsed and refractory multiple myeloma. Future Oncol. 2021;17(13):1581-91.
54. Magen H, Muchtar E. Elotuzumab: the first approved monoclonal antibody for multiple myeloma treatment. Ther Adv Hematol. 2016;7(4):187-95.
55. Herrera M, Pretelli G, Desai J, Garralda E, Siu LL, Steiner TM, et al. Bispecific antibodies: advancing precision oncology. Trends in Cancer. 2024;10(10):893-919.
56. Firestone R, Lesokhin AM, Usmani SZ. An Embarrassment of Riches: Three FDA-Approved Bispecific Antibodies for Relapsed Refractory Multiple Myeloma. Blood Cancer Discov. 2023;4(6):433-6.
57. Chau CH, Steeg PS, Figg WD. Antibody-drug conjugates for cancer. Lancet. 2019;394(10200):793-804.
58. Kleber M, Ntanasis-Stathopoulos I, Terpos E. BCMA in Multiple Myeloma-A Promising Key to Therapy. J Clin Med. 2021;10(18).
59. Mukhopadhyay P, Abdullah HA, Opalinska JB, Paka P, Richards E, Weisel K, et al. The clinical journey of belantamab mafodotin in relapsed or refractory multiple myeloma: lessons in drug development. Blood Cancer Journal. 2025;15(1):15.
60. Lam N, Trinklein ND, Buelow B, Patterson GH, Ojha N, Kochenderfer JN. Anti-BCMA chimeric antigen receptors with fully human heavy-chain-only antigen recognition domains. Nat Commun. 2020;11(1):283.
61. Johnson KB, Wei WQ, Weeraratne D, Frisse ME, Misulis K, Rhee K, et al. Precision Medicine, AI, and the Future of Personalized Health Care. Clin Transl Sci. 2021;14(1):86-93.
62. Inam S, Ross JA, Touzeau C, Moreau P, Kumar SK, Harrison SJ. Paving the way to precision medicine in multiple myeloma. Expert Rev Hematol. 2021;14(4):323-7.
63. Kumar S, Kaufman JL, Gasparetto C, Mikhael J, Vij R, Pegourie B, et al. Efficacy of venetoclax as targeted therapy for relapsed/refractory t(11;14) multiple myeloma. Blood. 2017;130(22):2401-9.
64. Nicholson LB. The immune system. Essays Biochem. 2016;60(3):275-301.
65. Aziz M, Iheanacho F, Hashmi MF. Physiology, Antibody. StatPearls. Treasure Island (FL)2022.
66. Justiz Vaillant AA, Jamal Z, Ramphul K. Immunoglobulin. StatPearls. Treasure Island (FL)2022.

67. Lipman NS, Jackson LR, Trudel LJ, Weis-Garcia F. Monoclonal versus polyclonal antibodies: distinguishing characteristics, applications, and information resources. ILAR J. 2005;46(3):258-68.
68. F.Stills H. Polyclonal Antibody Production. The Laboratory Rabbit, Guinea Pig, Hamster, and Other Rodents. American College of Laboratory Animal Medicine2012.
69. Berger M, Shankar V, Vafai A. Therapeutic applications of monoclonal antibodies. Am J Med Sci. 2002;324(1):14-30.
70. Cho SF, Anderson KC, Tai YT. Targeting B Cell Maturation Antigen (BCMA) in Multiple Myeloma: Potential Uses of BCMA-Based Immunotherapy. Front Immunol. 2018;9:1821.
71. Coquery CM, Erickson LD. Regulatory roles of the tumor necrosis factor receptor BCMA. Crit Rev Immunol. 2012;32(4):287-305.
72. Roy P, Sarkar UA, Basak S. The NF-kappaB Activating Pathways in Multiple Myeloma. Biomedicines. 2018;6(2).
73. Seckinger A, Delgado JA, Moser S, Moreno L, Neuber B, Grab A, et al. Target Expression, Generation, Preclinical Activity, and Pharmacokinetics of the BCMA-T Cell Bispecific Antibody EM801 for Multiple Myeloma Treatment. Cancer Cell. 2017;31(3):396-410.
74. GlaxoSmithKline. Blenrep combinations accepted for review by the US FDA for the treatment of relapsed/refractory multiple myeloma 2024 [Available from: https://www.gsk.com/en-gb/media/press-releases/blenrep-combinations-accepted-for-review-by-the-us-fda-for-the-treatment-of-relapsedrefractory-multiple-myeloma/.
75. Puertas B, Mateos MV, Gonzalez-Calle V. Anti-BCMA CAR T-cell Therapy: Changing the Natural History of Multiple Myeloma. Hemasphere. 2022;6(3):e691.
76. Friedman KM, Garrett TE, Evans JW, Horton HM, Latimer HJ, Seidel SL, et al. Effective Targeting of Multiple B-Cell Maturation Antigen-Expressing Hematological Malignances by Anti-B-Cell Maturation Antigen Chimeric Antigen Receptor T Cells. Hum Gene Ther. 2018;29(5):585-601.
77. Sheykhhasan M, Ahmadieh-Yazdi A, Vicidomini R, Poondla N, Tanzadehpanah H, Dirbaziyan A, et al. CAR T therapies in multiple myeloma: unleashing the future. Cancer Gene Therapy. 2024;31(5):667-86.
78. Nawaz W, Xu S, Li Y, Huang B, Wu X, Wu Z. Nanotechnology and immunoengineering: How nanotechnology can boost CAR-T therapy. Acta Biomater. 2020;109:21-36.
79. Li W, Liang L, Liao Q, Li Y, Zhou Y. CD38: An important regulator of T cell function. Biomedicine & Pharmacotherapy. 2022;153:113395.
80. Matalonga J, Glaria E, Bresque M, Escande C, Carbó JM, Kiefer K, et al. The Nuclear Receptor LXR Limits Bacterial Infection of Host Macrophages through a Mechanism that Impacts Cellular NAD Metabolism. Cell Reports. 2017;18(5):1241-55.
81. de Weers M, Tai YT, van der Veer MS, Bakker JM, Vink T, Jacobs DC, et al. Daratumumab, a novel therapeutic human CD38 monoclonal antibody, induces killing of multiple myeloma and other hematological tumors. J Immunol. 2011;186(3):1840-8.
82. Overdijk MB, Verploegen S, Bogels M, van Egmond M, Lammerts van Bueren JJ, Mutis T, et al. Antibody-mediated phagocytosis contributes to the anti-tumor activity of the therapeutic antibody daratumumab in lymphoma and multiple myeloma. MAbs. 2015;7(2):311-21.
83. Overdijk MB, Jansen JHM, Nederend M, Lammerts van Bueren JJ, Groen RWJ, Parren PWHI, et al. The Therapeutic CD38 Monoclonal Antibody Daratumumab Induces Programmed Cell Death via Fcγ Receptor–Mediated Cross-Linking. The Journal of Immunology. 2016;197(3):807-13.
84. van der Veer MS, de Weers M, van Kessel B, Bakker JM, Wittebol S, Parren PW, et al. Towards effective immunotherapy of myeloma: enhanced elimination of myeloma cells by combination of lenalidomide with the human CD38 monoclonal antibody daratumumab. Haematologica. 2011;96(2):284-90.
85. Cui J, Zhao S, Li Y, Zhang D, Wang B, Xie J, et al. Regulated cell death: discovery, features and implications for neurodegenerative diseases. Cell Commun Signal. 2021;19(1):120.
86. Hu XM, Li ZX, Lin RH, Shan JQ, Yu QW, Wang RX, et al. Guidelines for Regulated Cell Death Assays: A Systematic Summary, A Categorical Comparison, A Prospective. Front Cell Dev Biol. 2021;9:634690.
87. Elmore S. Apoptosis: a review of programmed cell death. Toxicol Pathol. 2007;35(4):495-516.

88. Papathanassoglou ED, Moynihan JA, Ackerman MH. Does programmed cell death (apoptosis) play a role in the development of multiple organ dysfunction in critically ill patients? a review and a theoretical framework. Crit Care Med. 2000;28(2):537-49.
89. Man SM, Karki R, Kanneganti TD. Molecular mechanisms and functions of pyroptosis, inflammatory caspases and inflammasomes in infectious diseases. Immunol Rev. 2017;277(1):61-75.
90. Dhuriya YK, Sharma D. Necroptosis: a regulated inflammatory mode of cell death. J Neuroinflammation. 2018;15(1):199.
91. Battaglia AM, Chirillo R, Aversa I, Sacco A, Costanzo F, Biamonte F. Ferroptosis and Cancer: Mitochondria Meet the "Iron Maiden" Cell Death. Cells. 2020;9(6).
92. Lee D, Kim IY, Saha S, Choi KS. Paraptosis in the anti-cancer arsenal of natural products. Pharmacol Ther. 2016;162:120-33.
93. Kroemer G, Levine B. Autophagic cell death: the story of a misnomer. Nat Rev Mol Cell Biol. 2008;9(12):1004-10.
94. Khalid N, Azimpouran M. Necrosis. StatPearls. Treasure Island (FL)2022.
95. Mlynarczuk-Bialy I, Dziuba I, Sarnecka A, Platos E, Kowalczyk M, Pels KK, et al. Entosis: From Cell Biology to Clinical Cancer Pathology. Cancers (Basel). 2020;12(9).
96. Dixon SJ, Lemberg KM, Lamprecht MR, Skouta R, Zaitsev EM, Gleason CE, et al. Ferroptosis: an iron-dependent form of nonapoptotic cell death. Cell. 2012;149(5):1060-72.
97. Gaschler MM, Stockwell BR. Lipid peroxidation in cell death. Biochem Biophys Res Commun. 2017;482(3):419-25.
98. Conrad M, Kagan VE, Bayir H, Pagnussat GC, Head B, Traber MG, et al. Regulation of lipid peroxidation and ferroptosis in diverse species. Genes Dev. 2018;32(9-10):602-19.
99. Angeli JPF, Shah R, Pratt DA, Conrad M. Ferroptosis Inhibition: Mechanisms and Opportunities. Trends Pharmacol Sci. 2017;38(5):489-98.
100. Stockwell BR, Friedmann Angeli JP, Bayir H, Bush AI, Conrad M, Dixon SJ, et al. Ferroptosis: A Regulated Cell Death Nexus Linking Metabolism, Redox Biology, and Disease. Cell. 2017;171(2):273-85.
101. Seibt TM, Proneth B, Conrad M. Role of GPX4 in ferroptosis and its pharmacological implication. Free Radic Biol Med. 2019;133:144-52.
102. Sui X, Zhang R, Liu S, Duan T, Zhai L, Zhang M, et al. RSL3 Drives Ferroptosis Through GPX4 Inactivation and ROS Production in Colorectal Cancer. Front Pharmacol. 2018;9:1371.
103. Dong S, Li X, Jiang W, Chen Z, Zhou W. Current understanding of ferroptosis in the progression and treatment of pancreatic cancer. Cancer Cell Int. 2021;21(1):480.
104. Wu S, Zhu C, Tang D, Dou QP, Shen J, Chen X. The role of ferroptosis in lung cancer. Biomark Res. 2021;9(1):82.
105. Doll S, Freitas FP, Shah R, Aldrovandi M, da Silva MC, Ingold I, et al. FSP1 is a glutathione-independent ferroptosis suppressor. Nature. 2019;575(7784):693-8.
106. Turunen M, Olsson J, Dallner G. Metabolism and function of coenzyme Q. Biochim Biophys Acta. 2004;1660(1-2):171-99.
107. Warner GJ, Berry MJ, Moustafa ME, Carlson BA, Hatfield DL, Faust JR. Inhibition of selenoprotein synthesis by selenocysteine tRNA[Ser]Sec lacking isopentenyladenosine. J Biol Chem. 2000;275(36):28110-9.
108. Yang WS, Stockwell BR. Ferroptosis: Death by Lipid Peroxidation. Trends Cell Biol. 2016;26(3):165-76.
109. Saini R. Coenzyme Q10: The essential nutrient. J Pharm Bioallied Sci. 2011;3(3):466-7.
110. Acosta MJ, Vazquez Fonseca L, Desbats MA, Cerqua C, Zordan R, Trevisson E, et al. Coenzyme Q biosynthesis in health and disease. Biochim Biophys Acta. 2016;1857(8):1079-85.
111. Kaymak I, Maier CR, Schmitz W, Campbell AD, Dankworth B, Ade CP, et al. Mevalonate Pathway Provides Ubiquinone to Maintain Pyrimidine Synthesis and Survival in p53-Deficient Cancer Cells Exposed to Metabolic Stress. Cancer Res. 2020;80(2):189-203.
112. Dev S, Babitt JL. Overview of iron metabolism in health and disease. Hemodial Int. 2017;21 Suppl 1:S6-S20.
113. Toyokuni S, Ito F, Yamashita K, Okazaki Y, Akatsuka S. Iron and thiol redox signaling in cancer: An exquisite balance to escape ferroptosis. Free Radic Biol Med. 2017;108:610-26.
114. Chen Y, Li X, Wang S, Miao R, Zhong J. Targeting Iron Metabolism and Ferroptosis as Novel Therapeutic Approaches in Cardiovascular Diseases. Nutrients. 2023;15(3).

115. Shah R, Shchepinov MS, Pratt DA. Resolving the Role of Lipoxygenases in the Initiation and Execution of Ferroptosis. ACS Cent Sci. 2018;4(3):387-96.
116. Shintoku R, Takigawa Y, Yamada K, Kubota C, Yoshimoto Y, Takeuchi T, et al. Lipoxygenase-mediated generation of lipid peroxides enhances ferroptosis induced by erastin and RSL3. Cancer Sci. 2017;108(11):2187-94.
117. Ahmed S, Shah P, Ahmed O. Biochemistry, Lipids. StatPearls. Treasure Island (FL)2022.
118. Montealegre C, Verardo V, Luisa Marina M, Caboni MF. Analysis of glycerophospho- and sphingolipids by CE. Electrophoresis. 2014;35(6):779-92.
119. Hishikawa D, Hashidate T, Shimizu T, Shindou H. Diversity and function of membrane glycerophospholipids generated by the remodeling pathway in mammalian cells. J Lipid Res. 2014;55(5):799-807.
120. PubChem Pathway Summary for Pathway WP2533, Glycerophospholipid biosynthetic pathway [Internet]. 2022 [cited 25/11/2022].
121. van der Veen JN, Kennelly JP, Wan S, Vance JE, Vance DE, Jacobs RL. The critical role of phosphatidylcholine and phosphatidylethanolamine metabolism in health and disease. Biochimica et Biophysica Acta (BBA) - Biomembranes. 2017;1859(9, Part B):1558-72.
122. Vance JE. Phospholipid synthesis and transport in mammalian cells. Traffic. 2015;16(1):1-18.
123. Uphoff A, Hermansson M, Haimi P, Somerharju P. Chapter 11 - Analysis of complex lipidomes. In: Vékey K, Telekes A, Vertes A, editors. Medical Applications of Mass Spectrometry. Amsterdam: Elsevier; 2008. p. 223-49.
124. Brindley DN, Pilquil C, Sariahmetoglu M, Reue K. Phosphatidate degradation: phosphatidate phosphatases (lipins) and lipid phosphate phosphatases. Biochim Biophys Acta. 2009;1791(9):956-61.
125. Calder PC, Grimble RF. Polyunsaturated fatty acids, inflammation and immunity. Eur J Clin Nutr. 2002;56 Suppl 3:S14-9.
126. Beatty A, Singh T, Tyurina YY, Tyurin VA, Samovich S, Nicolas E, et al. Ferroptotic cell death triggered by conjugated linolenic acids is mediated by ACSL1. Nat Commun. 2021;12(1):2244.
127. Hassannia B, Van Coillie S, Vanden Berghe T. Ferroptosis: Biological Rust of Lipid Membranes. Antioxid Redox Signal. 2021;35(6):487-509.
128. Ayala A, Munoz MF, Arguelles S. Lipid peroxidation: production, metabolism, and signaling mechanisms of malondialdehyde and 4-hydroxy-2-nonenal. Oxid Med Cell Longev. 2014;2014:360438.
129. Jiang X, Stockwell BR, Conrad M. Ferroptosis: mechanisms, biology and role in disease. Nat Rev Mol Cell Biol. 2021;22(4):266-82.
130. Shan K, Feng N, Zhu D, Qu H, Fu G, Li J, et al. Free docosahexaenoic acid promotes ferroptotic cell death via lipoxygenase dependent and independent pathways in cancer cells. Eur J Nutr. 2022.
131. Kagan VE, Mao G, Qu F, Angeli JP, Doll S, Croix CS, et al. Oxidized arachidonic and adrenic PEs navigate cells to ferroptosis. Nat Chem Biol. 2017;13(1):81-90.
132. Magtanong L, Ko PJ, To M, Cao JY, Forcina GC, Tarangelo A, et al. Exogenous Monounsaturated Fatty Acids Promote a Ferroptosis-Resistant Cell State. Cell Chem Biol. 2019;26(3):420-32 e9.
133. Heringdorf DMz. Lysophospholipids. Encyclopedia of Molecular Pharmacology. Berlin, Heidelberg: Springer; 2008.
134. Spickett CM. Formation of Oxidatively Modified Lipids as the Basis for a Cellular Epilipidome. Front Endocrinol (Lausanne). 2020;11:602771.
135. Bersuker K, Hendricks JM, Li Z, Magtanong L, Ford B, Tang PH, et al. The CoQ oxidoreductase FSP1 acts parallel to GPX4 to inhibit ferroptosis. Nature. 2019;575(7784):688-92.
136. Yang WS, SriRamaratnam R, Welsch ME, Shimada K, Skouta R, Viswanathan VS, et al. Regulation of ferroptotic cancer cell death by GPX4. Cell. 2014;156(1-2):317-31.
137. Craig M, Yarrarapu SNS, Dimri M. Biochemistry, Cholesterol. StatPearls. Treasure Island (FL)2024.
138. Sun Q, Liu D, Cui W, Cheng H, Huang L, Zhang R, et al. Cholesterol mediated ferroptosis suppression reveals essential roles of Coenzyme Q and squalene. Commun Biol. 2023;6(1):1108.

139. Garcia-Bermudez J, Baudrier L, Bayraktar EC, Shen Y, La K, Guarecuco R, et al. Squalene accumulation in cholesterol auxotrophic lymphomas prevents oxidative cell death. Nature. 2019;567(7746):118-22.
140. Liu C, Liao W, Chen J, Yu K, Wu Y, Zhang S, et al. Cholesterol confers ferroptosis resistance onto myeloid-biased hematopoietic stem cells and prevents irradiation-induced myelosuppression. Redox Biol. 2023;62:102661.
141. Shimada K, Hayano M, Pagano NC, Stockwell BR. Cell-Line Selectivity Improves the Predictive Power of Pharmacogenomic Analyses and Helps Identify NADPH as Biomarker for Ferroptosis Sensitivity. Cell Chem Biol. 2016;23(2):225-35.
142. Ingold I, Conrad M. Selenium and iron, two elemental rivals in the ferroptotic death process. Oncotarget. 2018;9(32):22241-2.
143. Chen X, Kang R, Kroemer G, Tang D. Broadening horizons: the role of ferroptosis in cancer. Nat Rev Clin Oncol. 2021;18(5):280-96.
144. Roh JL, Kim EH, Jang HJ, Park JY, Shin D. Induction of ferroptotic cell death for overcoming cisplatin resistance of head and neck cancer. Cancer Lett. 2016;381(1):96-103.
145. Liu MR, Zhu WT, Pei DS. System Xc(-): a key regulatory target of ferroptosis in cancer. Invest New Drugs. 2021;39(4):1123-31.
146. Bordini J, Morisi F, Cerruti F, Cascio P, Camaschella C, Ghia P, et al. Iron Causes Lipid Oxidation and Inhibits Proteasome Function in Multiple Myeloma Cells: A Proof of Concept for Novel Combination Therapies. Cancers (Basel). 2020;12(4).
147. Zhong Y, Tian F, Ma H, Wang H, Yang W, Liu Z, et al. FTY720 induces ferroptosis and autophagy via PP2A/AMPK pathway in multiple myeloma cells. Life Sci. 2020;260:118077.
148. Logie E, Van Puyvelde B, Cuypers B, Schepers A, Berghmans H, Verdonck J, et al. Ferroptosis Induction in Multiple Myeloma Cells Triggers DNA Methylation and Histone Modification Changes Associated with Cellular Senescence. Int J Mol Sci. 2021;22(22).
149. Rink JS, Lin AY, McMahon KM, Calvert AE, Yang S, Taxter T, et al. Targeted reduction of cholesterol uptake in cholesterol-addicted lymphoma cells blocks turnover of oxidized lipids to cause ferroptosis. J Biol Chem. 2021;296:100100.
150. Freedman A, Jacobsen E. Follicular lymphoma: 2020 update on diagnosis and management. Am J Hematol. 2020;95(3):316-27.
151. Vakiti A, Mewawalla P. Acute Myeloid Leukemia. StatPearls. Treasure Island (FL)2022.
152. Welfare AIoHa. ACUTE MYELOID LEUKAEMIA. Australia 2017. p. https://www.acrf.com.au/support-cancer-research/types-of-cancer/acute-myeloid-leukaemia/.
153. Yusuf R, Saez B, Sharda A, van Gastel N, Yu VWC, Baryawno N, et al. Aldehyde dehydrogenase 3a2 protects AML cells from oxidative death and the synthetic lethality of ferroptosis inducers. Blood. 2020;136.
154. Akiyama H, Zhao R, Rahhal A, Nishida Y, Ayoub E, Ostermann LB, et al. Therapeutic Targeting of Ferroptosis Pathway in Combination with Mitochondrial Oxidative Stress Induction in Acute Myeloid Leukemia. Blood. 2021;138(Supplement 1):1162-.
155. Birsen R, Larrue C, Decroocq J, Johnson N, Guiraud N, Gotanegre M, et al. APR-246 induces early cell death by ferroptosis in acute myeloid leukemia. Haematologica. 2021;107(2):403-16.
156. Starek-Swiechowicz B, Budziszewska B, Starek A. Endogenous estrogens-breast cancer and chemoprevention. Pharmacol Rep. 2021;73(6):1497-512.
157. Lee N, Carlisle AE, Peppers A, Park SJ, Doshi MB, Spears ME, et al. xCT-Driven Expression of GPX4 Determines Sensitivity of Breast Cancer Cells to Ferroptosis Inducers. Antioxidants (Basel). 2021;10(2).
158. Wen Y, Chen H, Zhang L, Wu M, Zhang F, Yang D, et al. Glycyrrhetinic acid induces oxidative/nitrative stress and drives ferroptosis through activating NADPH oxidases and iNOS, and depriving glutathione in triple-negative breast cancer cells. Free Radic Biol Med. 2021;173:41-51.
159. Mai TT, Hamai A, Hienzsch A, Caneque T, Muller S, Wicinski J, et al. Salinomycin kills cancer stem cells by sequestering iron in lysosomes. Nat Chem. 2017;9(10):1025-33.
160. Iida Y, Okamoto-Katsuyama M, Maruoka S, Mizumura K, Shimizu T, Shikano S, et al. Effective ferroptotic small-cell lung cancer cell death from SLC7A11 inhibition by sulforaphane. Oncol Lett. 2021;21(1):71.

161. Bebber CM, Thomas ES, Stroh J, Chen Z, Androulidaki A, Schmitt A, et al. Ferroptosis response segregates small cell lung cancer (SCLC) neuroendocrine subtypes. Nature Communications. 2021;12(1):2048.
162. Xia Y, Liu S, Li C, Ai Z, Shen W, Ren W, et al. Discovery of a novel ferroptosis inducer-talaroconvolutin A-killing colorectal cancer cells in vitro and in vivo. Cell Death Dis. 2020;11(11):988.
163. Arvelo F, Sojo F, Cotte C. Biology of colorectal cancer. Ecancermedicalscience. 2015;9:520.
164. Gyles C. Nanotechnology. Can Vet J. 2012;53(8):819-22.
165. Silva GA. Introduction to nanotechnology and its applications to medicine. Surg Neurol. 2004;61(3):216-20.
166. Mishra S. Nanotechnology in medicine. Indian Heart J. 2016;68(3):437-9.
167. Soares S, Sousa J, Pais A, Vitorino C. Nanomedicine: Principles, Properties, and Regulatory Issues. Front Chem. 2018;6:360.
168. Onoue S, Yamada S, Chan HK. Nanodrugs: pharmacokinetics and safety. Int J Nanomedicine. 2014;9:1025-37.
169. Patra JK, Das G, Fraceto LF, Campos EVR, Rodriguez-Torres MDP, Acosta-Torres LS, et al. Nano based drug delivery systems: recent developments and future prospects. J Nanobiotechnology. 2018;16(1):71.
170. Sim S, Wong NK. Nanotechnology and its use in imaging and drug delivery (Review). Biomed Rep. 2021;14(5):42.
171. He H, Pham-Huy LA, Dramou P, Xiao D, Zuo P, Pham-Huy C. Carbon nanotubes: applications in pharmacy and medicine. Biomed Res Int. 2013;2013:578290.
172. Gai C, Liu C, Wu X, Yu M, Zheng J, Zhang W, et al. MT1DP loaded by folate-modified liposomes sensitizes erastin-induced ferroptosis via regulating miR-365a-3p/NRF2 axis in non-small cell lung cancer cells. Cell Death Dis. 2020;11(9):751.
173. Yang Y, Zuo S, Li L, Kuang X, Li J, Sun B, et al. Iron-doxorubicin prodrug loaded liposome nanogenerator programs multimodal ferroptosis for efficient cancer therapy. Asian J Pharm Sci. 2021;16(6):784-93.
174. Li Z, Wang C, Dai C, Hu R, Ding L, Feng W, et al. Engineering dual catalytic nanomedicine for autophagy-augmented and ferroptosis-involved cancer nanotherapy. Biomaterials. 2022;287:121668.
175. Zhang K, Ma Z, Li S, Wu Y, Zhang J, Zhang W, et al. Disruption of dual homeostasis by a metal-organic framework nanoreactor for ferroptosis-based immunotherapy of tumor. Biomaterials. 2022;284:121502.
176. Li Q, Gao W, Zhang C, Wang P, Wang X, Yan M, et al. A Biodegradable High-Efficiency Magnetic Nanoliposome Promotes Tumor Microenvironment-Responsive Multimodal Tumor Therapy Along with Switchable T2 Magnetic Resonance Imaging. ACS Appl Mater Interfaces. 2022;14(21):24160-73.
177. He YJ, Liu XY, Xing L, Wan X, Chang X, Jiang HL. Fenton reaction-independent ferroptosis therapy via glutathione and iron redox couple sequentially triggered lipid peroxide generator. Biomaterials. 2020;241:119911.
178. Zhang C, Leng Z, Wang Y, Ran L, Qin X, Xin H, et al. PDGFB targeting biodegradable FePt alloy assembly for MRI guided starvation-enhancing chemodynamic therapy of cancer. J Nanobiotechnology. 2022;20(1):264.
179. Alshehri A, Grabowska A, Stolnik S. Pathways of cellular internalisation of liposomes delivered siRNA and effects on siRNA engagement with target mRNA and silencing in cancer cells. Sci Rep. 2018;8(1):3748.
180. Filipczak N, Pan J, Yalamarty SSK, Torchilin VP. Recent advancements in liposome technology. Adv Drug Deliv Rev. 2020;156:4-22.
181. Zinger A, Cvetkovic C, Sushnitha M, Naoi T, Baudo G, Anderson M, et al. Humanized Biomimetic Nanovesicles for Neuron Targeting. Adv Sci (Weinh). 2021;8(19):e2101437.
182. Koppula P, Lei G, Zhang Y, Yan Y, Mao C, Kondiparthi L, et al. A targetable CoQ-FSP1 axis drives ferroptosis- and radiation-resistance in KEAP1 inactive lung cancers. Nat Commun. 2022;13(1):2206.

183. Wu F, Du Y, Yang J, Shao B, Mi Z, Yao Y, et al. Peroxidase-like Active Nanomedicine with Dual Glutathione Depletion Property to Restore Oxaliplatin Chemosensitivity and Promote Programmed Cell Death. ACS Nano. 2022;16(3):3647-63.
184. Gao M, Deng J, Liu F, Fan A, Wang Y, Wu H, et al. Triggered ferroptotic polymer micelles for reversing multidrug resistance to chemotherapy. Biomaterials. 2019;223:119486.
185. Cao Y, Li Y, He C, Yan F, Li JR, Xu HZ, et al. Selective Ferroptosis Inhibitor Liproxstatin-1 Attenuates Neurological Deficits and Neuroinflammation After Subarachnoid Hemorrhage. Neurosci Bull. 2021;37(4):535-49.
186. Kou L, Sun R, Jiang X, Lin X, Huang H, Bao S, et al. Tumor Microenvironment-Responsive, Multistaged Liposome Induces Apoptosis and Ferroptosis by Amplifying Oxidative Stress for Enhanced Cancer Therapy. ACS Appl Mater Interfaces. 2020;12(27):30031-43.
187. Ji P, Wang X, Yin J, Yao Y, Du W. Amplification of ferroptosis with a liposomal nanoreactor cooperates with low-toxicity doxorubicin apoptosis for enhanced tumor chemotherapy. Biomater Sci. 2022;10(6):1544-53.
188. Wang S, Konorev EA, Kotamraju S, Joseph J, Kalivendi S, Kalyanaraman B. Doxorubicin induces apoptosis in normal and tumor cells via distinctly different mechanisms. intermediacy of H(2)O(2)- and p53-dependent pathways. J Biol Chem. 2004;279(24):25535-43.
189. Webb JL. Effect of more than one inhibitor.1963.
190. Liang D, Minikes AM, Jiang X. Ferroptosis at the intersection of lipid metabolism and cellular signaling. Mol Cell. 2022;82(12):2215-27.
191. Rodencal J, Dixon SJ. A tale of two lipids: Lipid unsaturation commands ferroptosis sensitivity. Proteomics. 2023;23(6):e2100308.
192. Yuan H, Li X, Zhang X, Kang R, Tang D. Identification of ACSL4 as a biomarker and contributor of ferroptosis. Biochem Biophys Res Commun. 2016;478(3):1338-43.
193. Cui J, Wang Y, Tian X, Miao Y, Ma L, Zhang C, et al. LPCAT3 Is Transcriptionally Regulated by YAP/ZEB/EP300 and Collaborates with ACSL4 and YAP to Determine Ferroptosis Sensitivity. Antioxid Redox Signal. 2023;39(7-9):491-511.
194. Liao P, Wang W, Wang W, Kryczek I, Li X, Bian Y, et al. CD8(+) T cells and fatty acids orchestrate tumor ferroptosis and immunity via ACSL4. Cancer Cell. 2022;40(4):365-78.e6.
195. Zhang J, Liu Y, Li Q, Zuo L, Zhang B, Zhao F, et al. ACSL4: a double-edged sword target in multiple myeloma, promotes cell proliferation and sensitizes cell to ferroptosis. Carcinogenesis. 2023;44(3):242-51.
196. Liang D, Feng Y, Zandkarimi F, Wang H, Zhang Z, Kim J, et al. Ferroptosis surveillance independent of GPX4 and differentially regulated by sex hormones. Cell. 2023;186(13):2748-64 e22.
197. Das UN. Saturated Fatty Acids, MUFAs and PUFAs Regulate Ferroptosis. Cell Chem Biol. 2019;26(3):309-11.
198. Krummel B, von Hanstein AS, Plotz T, Lenzen S, Mehmeti I. Differential effects of saturated and unsaturated free fatty acids on ferroptosis in rat beta-cells. J Nutr Biochem. 2022;106:109013.
199. Miao S, Zhang Q, Ding W, Hou B, Su Z, Li M, et al. Platelet Internalization Mediates Ferroptosis in Myocardial Infarction. Arteriosclerosis, Thrombosis, and Vascular Biology. 2023;43(2):218-30.
200. Mynott R. Investigating ferroptosis as an approach to treating multiple myeloma: Flinders University, College of Medicine and Public Health; 2025.
201. Zou Y, Henry WS, Ricq EL, Graham ET, Phadnis VV, Maretich P, et al. Plasticity of ether lipids promotes ferroptosis susceptibility and evasion. Nature. 2020;585(7826):603-8.
202. Manni MM, Tiberti ML, Pagnotta S, Barelli H, Gautier R, Antonny B. Acyl chain asymmetry and polyunsaturation of brain phospholipids facilitate membrane vesiculation without leakage. Elife. 2018;7.
203. Battaglia AM, Sacco A, Perrotta ID, Faniello MC, Scalise M, Torella D, et al. Iron Administration Overcomes Resistance to Erastin-Mediated Ferroptosis in Ovarian Cancer Cells. Front Oncol. 2022;12:868351.
204. Dierge E, Debock E, Guilbaud C, Corbet C, Mignolet E, Mignard L, et al. Peroxidation of n-3 and n-6 polyunsaturated fatty acids in the acidic tumor environment leads to ferroptosis-mediated anticancer effects. Cell Metab. 2021;33(8):1701-15 e5.

205. Chen J, Zaal EA, Berkers CR, Ruijtenbeek R, Garssen J, Redegeld FA. Omega-3 Fatty Acids DHA and EPA Reduce Bortezomib Resistance in Multiple Myeloma Cells by Promoting Glutathione Degradation. Cells. 2021;10(9).
206. Panaroni C, Fulzele K, Soucy R, Siu KT, Mukaihara K, Huang C, et al. Arachidonic Acid Induces Ferroptosis-Mediated Cell-Death in Multiple Myeloma. Blood. 2018;132:4498.
207. Suda A, Umaru BA, Yamamoto Y, Shima H, Saiki Y, Pan Y, et al. Polyunsaturated fatty acids-induced ferroptosis suppresses pancreatic cancer growth. Scientific Reports. 2024;14(1):4409.
208. Zhang Y, Shen G, Meng T, Lv Z, Li X, Li J, et al. Eicosapentaenoic acid enhances the sensitivity of osteosarcoma to cisplatin by inducing ferroptosis through the DNA-PKcs/AKT/NRF2 pathway and reducing PD-L1 expression to attenuate immune evasion. International Immunopharmacology. 2023;125:111181.
209. Chen Y, Liao X, Jing P, Hu L, Yang Z, Yao Y, et al. Linoleic Acid-Glucosamine Hybrid for Endogenous Iron-Activated Ferroptosis Therapy in High-Grade Serous Ovarian Cancer. Mol Pharm. 2022;19(9):3187-98.
210. Li Z, Ji BW, Dixit PD, Tchourine K, Lien EC, Hosios AM, et al. Cancer cells depend on environmental lipids for proliferation when electron acceptors are limited. Nature Metabolism. 2022;4(6):711-23.
211. Torcasio R, Gallo Cantafio ME, Ikeda RK, Ganino L, Viglietto G, Amodio N. Lipid metabolic vulnerabilities of multiple myeloma. Clin Exp Med. 2023;23(7):3373-90.
212. Tian H, Zhao X, Zhang Y, Xia Z. Abnormalities of glucose and lipid metabolism in myocardial ischemia-reperfusion injury. Biomedicine & Pharmacotherapy. 2023;163:114827.
213. Liu S, Yang W, Li Y, Sun C. Fetal bovine serum, an important factor affecting the reproducibility of cell experiments. Sci Rep. 2023;13(1):1942.
214. Yang WS, Stockwell BR. Synthetic lethal screening identifies compounds activating iron-dependent, nonapoptotic cell death in oncogenic-RAS-harboring cancer cells. Chem Biol. 2008;15(3):234-45.
215. Henry WS, Muller S, Yang JS, Innes-Gold S, Das S, Reinhardt F, et al. Ether lipids influence cancer cell fate by modulating iron uptake. bioRxiv. 2024.
216. Sokol KH, Lee CJ, Rogers TJ, Waldhart A, Ellis AE, Madireddy S, et al. Lipid availability influences ferroptosis sensitivity in cancer cells by regulating polyunsaturated fatty acid trafficking. Cell Chemical Biology. 2024.
217. Qiu B, Zandkarimi F, Bezjian CT, Reznik E, Soni RK, Gu W, et al. Phospholipids with two polyunsaturated fatty acyl tails promote ferroptosis. Cell. 2024;187(5):1177-90.e18.
218. Naowarojna N, Wu TW, Pan Z, Li M, Han JR, Zou Y. Dynamic Regulation of Ferroptosis by Lipid Metabolism. Antioxid Redox Signal. 2023;39(1-3):59-78.
219. Wang N, Ma H, Li J, Meng C, Zou J, Wang H, et al. HSF1 functions as a key defender against palmitic acid-induced ferroptosis in cardiomyocytes. J Mol Cell Cardiol. 2021;150:65-76.
220. Kuang H, Sun X, Liu Y, Tang M, Wei Y, Shi Y, et al. Palmitic acid-induced ferroptosis via CD36 activates ER stress to break calcium-iron balance in colon cancer cells. Febs j. 2023;290(14):3664-87.
221. Krümmel B, von Hanstein A-S, Plötz T, Lenzen S, Mehmeti I. Differential effects of saturated and unsaturated free fatty acids on ferroptosis in rat β-cells. The Journal of Nutritional Biochemistry. 2022;106:109013.
222. Newell M, Baker K, Postovit LM, Field CJ. A Critical Review on the Effect of Docosahexaenoic Acid (DHA) on Cancer Cell Cycle Progression. Int J Mol Sci. 2017;18(8).
223. Panaroni C, Fulzele K, Mori T, Siu KT, Onyewadume C, Maebius A, et al. Multiple myeloma cells induce lipolysis in adipocytes and uptake fatty acids through fatty acid transporter proteins. Blood. 2022;139(6):876-88.
224. Ubellacker JM, Tasdogan A, Ramesh V, Shen B, Mitchell EC, Martin-Sandoval MS, et al. Lymph protects metastasizing melanoma cells from ferroptosis. Nature. 2020;585(7823):113-8.
225. Tesfay L, Paul BT, Konstorum A, Deng Z, Cox AO, Lee J, et al. Stearoyl-CoA Desaturase 1 Protects Ovarian Cancer Cells from Ferroptotic Cell Death. Cancer Res. 2019;79(20):5355-66.
226. Luo H, Wang X, Song S, Wang Y, Dan Q, Ge H. Targeting stearoyl-coa desaturase enhances radiation induced ferroptosis and immunogenic cell death in esophageal squamous cell carcinoma. Oncoimmunology. 2022;11(1):2101769.

227. Usmani SZ, Nahi H, Plesner T, Weiss BM, Bahlis NJ, Belch A, et al. Daratumumab monotherapy in patients with heavily pretreated relapsed or refractory multiple myeloma: final results from the phase 2 GEN501 and SIRIUS trials. Lancet Haematol. 2020;7(6):e447-e55.
228. Palumbo A, Chanan-Khan A, Weisel K, Nooka AK, Masszi T, Beksac M, et al. Daratumumab, Bortezomib, and Dexamethasone for Multiple Myeloma. New England Journal of Medicine. 2016;375(8):754-66.
229. Suvannasankha A, Bahlis N, Trudel S, Weisel K, Koenecke C, Oriol A, et al. Safety and efficacy of belantamab mafodotin with pembrolizumab in patients with relapsed or refractory multiple myeloma. Cancer. 2024;130(15):2629-41.
230. Yu B, Jiang T, Liu D. BCMA-targeted immunotherapy for multiple myeloma. Journal of Hematology & Oncology. 2020;13(1):125.
231. Tai YT, Acharya C, An G, Moschetta M, Zhong MY, Feng X, et al. APRIL and BCMA promote human multiple myeloma growth and immunosuppression in the bone marrow microenvironment. Blood. 2016;127(25):3225-36.
232. Xu X, Narni-Mancinelli E, Cantoni C, Li Y, Guia S, Gauthier L, et al. Structural Insights into the Inhibitory Mechanism of an Antibody against B7-H6, a Stress-Induced Cellular Ligand for the Natural Killer Cell Receptor NKp30. Journal of Molecular Biology. 2016;428(22):4457-66.
233. Rose N, Pinho-Nascimento CA, Ruggieri A, Favuzza P, Tamborrini M, Roth H, et al. Generation of monoclonal antibodies against native viral proteins using antigen-expressing mammalian cells for mouse immunization. BMC Biotechnology. 2016;16(1):83.
234. Peng S, Chen G, Yu KN, Feng Y, Zhao L, Yang M, et al. Synergism of non-thermal plasma and low concentration RSL3 triggers ferroptosis via promoting xCT lysosomal degradation through ROS/AMPK/mTOR axis in lung cancer cells. Cell Commun Signal. 2024;22(1):112.
235. Braham MV, Deshantri AK, Minnema MC, Oner FC, Schiffelers RM, Fens MH, et al. Liposomal drug delivery in an in vitro 3D bone marrow model for multiple myeloma. Int J Nanomedicine. 2018;13:8105-18.
236. Deshantri AK, Fens M, Ruiter RWJ, Metselaar JM, Storm G, Mandhane SN, et al. Complete Tumor Regression by Liposomal Bortezomib in a Humanized Mouse Model of Multiple Myeloma. Hemasphere. 2020;4(5):e463.
237. Zhang Y, Tan H, Daniels JD, Zandkarimi F, Liu H, Brown LM, et al. Imidazole Ketone Erastin Induces Ferroptosis and Slows Tumor Growth in a Mouse Lymphoma Model. Cell Chem Biol. 2019;26(5):623-33 e9.
238. Šturm L, Poklar Ulrih N. Basic Methods for Preparation of Liposomes and Studying Their Interactions with Different Compounds, with the Emphasis on Polyphenols. Int J Mol Sci. 2021;22(12).
239. Carugo D, Bottaro E, Owen J, Stride E, Nastruzzi C. Liposome production by microfluidics: potential and limiting factors. Sci Rep. 2016;6:25876.
240. Wang R, Xiao R, Zeng Z, Xu L, Wang J. Application of poly(ethylene glycol)-distearoylphosphatidylethanolamine (PEG-DSPE) block copolymers and their derivatives as nanomaterials in drug delivery. Int J Nanomedicine. 2012;7:4185-98.
241. Briuglia ML, Rotella C, McFarlane A, Lamprou DA. Influence of cholesterol on liposome stability and on in vitro drug release. Drug Deliv Transl Res. 2015;5(3):231-42.
242. Riaz MK, Riaz MA, Zhang X, Lin C, Wong KH, Chen X, et al. Surface Functionalization and Targeting Strategies of Liposomes in Solid Tumor Therapy: A Review. Int J Mol Sci. 2018;19(1).
243. Gbian DL, Omri A. Lipid-Based Drug Delivery Systems for Diseases Managements. Biomedicines. 2022;10(9).
244. Abucayon EG, Sweeney S, Matyas GR. A Reliable Quantification of Cholesterol and 25-Hydroxycholesterol in Liposomal Adjuvant Formulation by Liquid Chromatography High-Resolution Tandem Mass Spectrometry. ACS Omega. 2024;9(17):19637-44.
245. Nosova AS, Koloskova OO, Nikonova AA, Simonova VA, Smirnov VV, Kudlay D, et al. Diversity of PEGylation methods of liposomes and their influence on RNA delivery. Medchemcomm. 2019;10(3):369-77.
246. Zhao X, Lian X, Xie J, Liu G. Accumulated cholesterol protects tumours from elevated lipid peroxidation in the microenvironment. Redox Biol. 2023;62:102678.
247. Xian M, Wang Q, Xiao L, Zhong L, Xiong W, Ye L, et al. Leukocyte immunoglobulin-like receptor B1 (LILRB1) protects human multiple myeloma cells from ferroptosis by maintaining cholesterol homeostasis. Nat Commun. 2024;15(1):5767.

248. Freitas FP, Alborzinia H, dos Santos AF, Nepachalovich P, Pedrera L, Zilka O, et al. 7-Dehydrocholesterol is an endogenous suppressor of ferroptosis. Nature. 2024;626(7998):401-10.
249. Cauzzo J, Nystad M, Holsæter AM, Basnet P, Škalko-Basnet N. Following the Fate of Dye-Containing Liposomes In Vitro. Int J Mol Sci. 2020;21(14).
250. Eugster R, Luciani P. Liposomes: Bridging the gap from lab to pharmaceuticals. Current Opinion in Colloid & Interface Science. 2025;75:101875.
251. Liu P, Chen G, Zhang J. A Review of Liposomes as a Drug Delivery System: Current Status of Approved Products, Regulatory Environments, and Future Perspectives. Molecules. 2022;27(4).
252. Bian J, Girotti J, Fan Y, Levy ES, Zang N, Sethuraman V, et al. Fast and versatile analysis of liposome encapsulation efficiency by nanoParticle exclusion chromatography. Journal of Chromatography A. 2022;1662:462688.
253. Weissig V. Liposomes Came First: The Early History of Liposomology. In: D'Souza GGM, editor. Liposomes: Methods and Protocols. New York, NY: Springer New York; 2017. p. 1-15.
254. Nisini R, Poerio N, Mariotti S, De Santis F, Fraziano M. The Multirole of Liposomes in Therapy and Prevention of Infectious Diseases. Front Immunol. 2018;9:155.
255. Zhang Y, Tan H, Daniels JD, Zandkarimi F, Liu H, Brown LM, et al. Imidazole Ketone Erastin Induces Ferroptosis and Slows Tumor Growth in a Mouse Lymphoma Model. Cell Chem Biol. 2019;26(5):623-33.e9.
256. Yu Y, Meng Y, Xu X, Tong T, He C, Wang L, et al. A Ferroptosis-Inducing and Leukemic Cell-Targeting Drug Nanocarrier Formed by Redox-Responsive Cysteine Polymer for Acute Myeloid Leukemia Therapy. ACS Nano. 2023;17(4):3334-45.
257. Craig M, Yarrarapu SNS, Dimri M. Biochemistry, Cholesterol. StatPearls. Treasure Island (FL)2025.
258. White AM, Best OG, Hotinski AK, Kuss BJ, Thurgood LA. The Role of Cholesterol in Chronic Lymphocytic Leukemia Development and Pathogenesis. Metabolites. 2023;13(7).
259. Liu C, Liao W, Chen J, Yu K, Wu Y, Zhang S, et al. Cholesterol confers ferroptosis resistance onto myeloid-biased hematopoietic stem cells and prevents irradiation-induced myelosuppression. Redox Biology. 2023;62:102661.
260. Nsairat H, Khater D, Sayed U, Odeh F, Al Bawab A, Alshaer W. Liposomes: structure, composition, types, and clinical applications. Heliyon. 2022;8(5):e09394.
261. Perona JS. Membrane lipid alterations in the metabolic syndrome and the role of dietary oils. Biochimica et Biophysica Acta (BBA) - Biomembranes. 2017;1859(9, Part B):1690-703.
262. Mills TT, Huang J, Feigenson GW, Nagle JF. Effects of cholesterol and unsaturated DOPC lipid on chain packing of saturated gel-phase DPPC bilayers. Gen Physiol Biophys. 2009;28(2):126-39.
263. Andar AU, Hood RR, Vreeland WN, DeVoe DL, Swaan PW. Microfluidic Preparation of Liposomes to Determine Particle Size Influence on Cellular Uptake Mechanisms. Pharmaceutical Research. 2014;31(2):401-13.
264. Tang M, Yarragudi SB, Pan P, Yang K, Kanamala M, Wu Z. Effect of size and pH-sensitivity of liposomes on cellular uptake pathways and pharmacokinetics of encapsulated gemcitabine. Journal of Liposome Research. 2024:1-11.
265. Kolter M, Wittmann M, Köll-Weber M, Süss R. The suitability of liposomes for the delivery of hydrophobic drugs – A case study with curcumin. European Journal of Pharmaceutics and Biopharmaceutics. 2019;140:20-8.
266. Wallace SJ, Li J, Nation RL, Boyd BJ. Drug release from nanomedicines: Selection of appropriate encapsulation and release methodology. Drug Deliv Transl Res. 2012;2(4):284-92.
267. Vakili-Ghartavol R, Rezayat SM, Faridi-Majidi R, Sadri K, Jaafari MR. Optimization of Docetaxel Loading Conditions in Liposomes: proposing potential products for metastatic breast carcinoma chemotherapy. Scientific Reports. 2020;10(1):5569.
268. Xie Y, Shao N, Jin Y, Zhang L, Jiang H, Xiong N, et al. Determination of non-liposomal and liposomal doxorubicin in plasma by LC–MS/MS coupled with an effective solid phase extraction: In comparison with ultrafiltration technique and application to a pharmacokinetic study. Journal of Chromatography B. 2018;1072:149-60.
269. Milano G, Innocenti F, Minami H. Liposomal irinotecan (Onivyde): Exemplifying the benefits of nanotherapeutic drugs. Cancer Sci. 2022;113(7):2224-31.

270. Berg EA, Fishman JB. Labeling Antibodies Using a Maleimido Dye. Cold Spring Harb Protoc. 2019;2019(3).
271. Berg EA, Fishman JB. Labeling Antibodies Using N-Hydroxysuccinimide (NHS)-Fluorescein. Cold Spring Harb Protoc. 2019;2019(3).
272. Marques AC, Costa PC, Velho S, Amaral MH. Lipid Nanoparticles Functionalized with Antibodies for Anticancer Drug Therapy. Pharmaceutics. 2023;15(1).
273. Abdolahpour S, Toliyat T, Omidfar K, Modjtahedi H, Wong AJ, Rasaee MJ, et al. Targeted delivery of doxorubicin into tumor cells by nanostructured lipid carriers conjugated to anti-EGFRvIII monoclonal antibody. Artificial Cells, Nanomedicine, and Biotechnology. 2018;46(1):89-94.
274. Potter DA, Gorschboth CM, Schneider PD. Liposome uptake by melanoma: in vitro comparison with hepatocytes. J Surg Res. 1985;39(2):157-63.
275. Zalba S, Ten Hagen TL. Cell membrane modulation as adjuvant in cancer therapy. Cancer Treat Rev. 2017;52:48-57.
276. Abumanhal-Masarweh H, da Silva D, Poley M, Zinger A, Goldman E, Krinsky N, et al. Tailoring the lipid composition of nanoparticles modulates their cellular uptake and affects the viability of triple negative breast cancer cells. J Control Release. 2019;307:331-41.
277. Alavi M, Hamidi M. Passive and active targeting in cancer therapy by liposomes and lipid nanoparticles. Drug Metabolism and Personalized Therapy. 2019;34(1).
278. Alavi M, Hamidi M. Passive and active targeting in cancer therapy by liposomes and lipid nanoparticles. Drug Metab Pers Ther. 2019;34(1).
279. Saraf S, Jain A, Tiwari A, Verma A, Panda PK, Jain SK. Advances in liposomal drug delivery to cancer: An overview. Journal of Drug Delivery Science and Technology. 2020;56:101549.
280. Szczepanowicz K, Bzowska M, Kruk T, Karabasz A, Bereta J, Warszynski P. Pegylated polyelectrolyte nanoparticles containing paclitaxel as a promising candidate for drug carriers for passive targeting. Colloids and Surfaces B: Biointerfaces. 2016;143:463-71.
281. Ravar F, Saadat E, Gholami M, Dehghankelishadi P, Mahdavi M, Azami S, et al. Hyaluronic acid-coated liposomes for targeted delivery of paclitaxel, in-vitro characterization and in-vivo evaluation. Journal of Controlled Release. 2016;229:10-22.
282. Wang D, Yating S, Yange L, Fanchao M, and Lee RJ. Clinical translation of immunoliposomes for cancer therapy: recent perspectives. Expert Opinion on Drug Delivery. 2018;15(9):893-903.
283. Canato E, Grigoletto A, Zanotto I, Tedeschini T, Campara B, Quaglio G, et al. Anti-HER2 Super Stealth Immunoliposomes for Targeted-Chemotherapy. Adv Healthc Mater. 2023;12(29):e2301650.
284. Cheng WW, Allen TM. The use of single chain Fv as targeting agents for immunoliposomes: an update on immunoliposomal drugs for cancer treatment. Expert Opin Drug Deliv. 2010;7(4):461-78.
285. Jin BK, Odongo S, Radwanska M, Magez S. NANOBODIES®: A Review of Diagnostic and Therapeutic Applications. Int J Mol Sci. 2023;24(6).
286. Hama S, Sakai M, Itakura S, Majima E, Kogure K. Rapid modification of antibodies on the surface of liposomes composed of high-affinity protein A-conjugated phospholipid for selective drug delivery. Biochemistry and Biophysics Reports. 2021;27:101067.
287. Mafra A, Laversanne M, Marcos-Gragera R, Chaves HVS, McShane C, Bray F, et al. The global multiple myeloma incidence and mortality burden in 2022 and predictions for 2045. J Natl Cancer Inst. 2025;117(5):907-14.
288. Yang WC, Lin SF. Mechanisms of Drug Resistance in Relapse and Refractory Multiple Myeloma. Biomed Res Int. 2015;2015:341430.
289. Li P, Lyu T. Research Progress on Ferroptosis in Multiple Myeloma. Curr Treat Options Oncol. 2024;25(10):1276-82.
290. Zhang W, Li Q, Zhang Y, Wang Z, Yuan S, Zhang X, et al. Multiple myeloma with high expression of SLC7A11 is sensitive to erastin-induced ferroptosis. Apoptosis. 2024;29(3-4):412-23.
291. Ni Z, Angelidou G, Hoffmann R, Fedorova M. LPPtiger software for lipidome-specific prediction and identification of oxidized phospholipids from LC-MS datasets. Scientific Reports. 2017;7(1):15138.
292. Zeng Z, Chen J, Lin J, Wang S. Pegylated liposomal doxorubicin for multiple myeloma. Cochrane Database Syst Rev. 2016;2016(10).

293. Hao W, Sun N, Fan Y, Chen M, Liu Q, Yang M, et al. Targeted Ferroptosis-Immunotherapy Synergy: Enhanced Antiglioma Efficacy with Hybrid Nanovesicles Comprising NK Cell-Derived Exosomes and RSL3-Loaded Liposomes. ACS Applied Materials & Interfaces. 2024;16(22):28193-208.
294. Yu N, Zhang Y, Li J, Gu W, Yue S, Li B, et al. Daratumumab Immunopolymersome-Enabled Safe and CD38-Targeted Chemotherapy and Depletion of Multiple Myeloma. Adv Mater. 2021;33(39):e2007787.
295. Schriewer L, Schütze K, Petry K, Hambach J, Fumey W, Koenigsdorf J, et al. Nanobody-based CD38-specific heavy chain antibodies induce killing of multiple myeloma and other hematological malignancies. Theranostics. 2020;10(6):2645-58.
296. Kozik V, Pentak D, Paździor M, Zięba A, Bąk A. From Design to Study of Liposome-Driven Drug Release Part 1: Impact of Temperature and pH on Environment. Int J Mol Sci. 2023;24(14).
297. Medina-Herrera A, Sarasquete ME, Jiménez C, Puig N, García-Sanz R. Minimal Residual Disease in Multiple Myeloma: Past, Present, and Future. Cancers (Basel). 2023;15(14).
298. Sarfraz M, Afzal A, Yang T, Gai Y, Raza SM, Khan MW, et al. Development of Dual Drug Loaded Nanosized Liposomal Formulation by A Reengineered Ethanolic Injection Method and Its Pre-Clinical Pharmacokinetic Studies. Pharmaceutics. 2018;10(3).